INFORMATION TO USERS

This manuscript has been reproduced from the microfilm master. UMI films the text directly from the original or copy submitted. Thus, some thesis and dissertation copies are in typewriter face, while others may be from any type of computer printer.

The quality of this reproduction is dependent upon the quality of the copy submitted. Broken or indistinct print, colored or poor quality illustrations and photographs, print bleedthrough, substandard margins, and improper alignment can adversely affect reproduction.

In the unlikely event that the author did not send UMI a complete manuscript and there are missing pages, these will be noted. Also, if unauthorized copyright material had to be removed, a note will indicate the deletion.

Oversize materials (e.g., maps, drawings, charts) are reproduced by sectioning the original, beginning at the upper left-hand corner and continuing from left to right in equal sections with small overlaps. Each original is also photographed in one exposure and is included in reduced form at the back of the book.

Photographs included in the original manuscript have been reproduced xerographically in this copy. Higher quality 6" x 9" black and white photographic prints are available for any photographs or illustrations appearing in this copy for an additional charge. Contact UMI directly to order.

UMI

A Bell & Howell Information Company
300 North Zeeb Road, Ann Arbor MI 48106-1346 USA
313/761-4700 800/521-0600

STRUCTURAL CONTROL AND ANISOTROPY OF MINERALIZATION WITHIN THE CHUQUICAMATA PORPHYRY COPPER DEPOSIT, NORTHERN CHILE

by

Darryl Desment Lindsay

Submitted in partial fulfilment of the requirements
for the degree of
Doctor of Philosophy

at

Dalhousie University
Halifax, Nova Scotia
December 1997

DALHOUSIE UNIVERSITY

FACULTY OF GRADUATE STUDIES

The undersigned hereby certify that they have read and recommend to the Faculty of Graduate Studies for acceptance a thesis entitled "Structural Control and Anisotropy of Mineralization Within the Chuquicamata Porphyry Copper Deposit, Northern Chile"

by Darryl D. Lindsay

in partial fulfillment of the requirements for the degree of Doctor of Philosophy.

Dated: September 9, 1997

External Examiner

Research Supervisor

Examining Committee

DALHOUSIE UNIVERSITY

Date: December 4, 1997

AUTHOR: Darryl Desment Lindsay

TITLE: Structural Control and Anisotrophy of Mineralization Within the Chuquicamata Porphyry Copper Deposit, Northern Chile

DEPARTMENT OR SCHOOL: Department of Earth Sciences

DEGREE: Ph.D. CONVOCATION: May YEAR: 1997

Permission is herewith granted to Dalhousie University to circulate and to have copies for non-commercial purposes, at its discretion, the above title upon request of individuals or institutions.

Signature of Author

Table of Contents

List of Illustrations

List of Tables

List of Plates

Abstract

Chuquicamata, one of the world's largest porphyry copper type deposits, is located in the Domeyko Cordillera in the Antofagasta region of northern Chile. The giant deposit is the largest of several situated within the strands of the West Fault System, a regional north-south strike-slip shear system paralleling the Late Cretaceous-Oligocene magmatic arc. The strike-slip system developed in response to plate tectonic interaction between the subducting Nazca and South American plates and reflects variable rates and angles of convergence with the concomitant generation of porphyry magma bodies, some of which, like Chuquicamata, may have been emplaced into an active shear system.

Did the evolving structure play a significant role in ore control, making Chuquicamata a giant? Is there evidence of ductile deformation and of exhumation of the mineralizing system through to a brittle regime? Can the structural evolution of the deposit be linked with regional tectonics? These are some of the questions addressed during this project, taking advantage of the superb exposure afforded by a 4.5 x 3.0 x 0.7 km deep open pit. Detailed structural mapping and measuring of veinlet systems, fault systems and vein arrays within and around the mine during an 18 month period, were supplemented by study of drillcore, polished slabs, oriented polished thin sections, and limited geochronology

The examination and analysis of ductile deformational features, mineralized stockwork systems, and vein arrays indicate the emplacement and mineralization at Chuquicamata developed within an active dextral strike-slip fault zone that was exhumed through time. 1) Ductile deformation fabrics indicate top-to-the-SSW for reverse faults and dextral strike-slip for steeply dipping shear zones. Geometrical relationships between these fault sets are consistent with a strike-slip system that parallels the NNE-trend of the host porphyry complex. Examination of the porphyry stockwork system at the scale of the deposit scale suggests a disseminated nature to mineralization, however, within sectors of the mine defined at structural domain scale, individual veinlets of the mineralized stockwork system show preferential orientations. The preferred orientations, representative of domains in the deposit, are N-S to NNE-SSW, NE-SW and WNW-ESE. 2) At the deposit scale, vein arrays associated with molybdenite, pyrite and enargite mineralization and syn- and post-mineralization fault system events crosscut the copper-bearing stockwork. The preferred orientations have a marked influence on the anisotropy of metal grade distribution within the deposit and are therefore of strategic importance to the operation. Mineralization of the vein arrays is related to fault slip and renewed magmato-hydrothermal activity. Fault systems and vein arrays define seven structural domains within the deposit that suggest at least two distinct deformational events. Domains of syn-mineralization fault-vein systems indicate continued mineralization within a dextral strike-slip deposit setting. 3) Domains of brittle post-mineralization fault systems indicate an inversion of the strike-slip deformation zone from dextral to sinistral and a concentration of deformation and displacement along the regional West Fault.

Acknowledgements

I must first thank my advisor, Dr. Marcos Zentilli, who with enthusiasm, encouragement and perseverance, propped open the door for this study of a world-class Andean porphyry deposit. For this opportunity, I thank Milton C. Graves, Cuesta Research Ltd. and Francisco Camus, Corporacion Nacional del Cobre de Chile, who provided a means of entry to Chuquicamata.

I am very grateful to Guillermo Ossandon, Roberto Freraut and Juan Palluata, successive Superintendents of Geology at the CODELCO- Division Chuquicamata, who acknowledged the contribution of this study and provided considerable logistical support. The sampling and field examination of the Chuquicamata deposit was directed and assisted by Jose Rojas de la Rivera, CODELCO-Chuquicamata staff geologist, and assisted by Fernando Ramierez (CODELCO-Chuqui), Victorino Moyano (CODELCO-Chuqui) and Patricio East (Contract geologist). Thanks to these and the rest of the geology and geomechanics mine personnel who provided many hours of fruitful discussions on Chuquicamata and other deposits of the district, in the process teaching me Spanish.

A special thanks to Andrew Tomlinson for his discussions on the regional structural geology, his thorough critical reviews of the initial drafts of this thesis, and his and his family's much appreciated hospitality while we were in Santiago. Deserving of a heartfelt thanks is Renée Cheng for her patience, companionship in the field, editorial skills, and assistance in bringing this thesis to a close.

Thanks to: Lewis Gustafson for illustrating for me the vigour that is needed to examine these enormous ore deposits in the detail required for understanding and knowledge, and Dr. John Dilles for discussions concerning the Fortuna Intrusive Complex as it appears outside of the open pit. Dr. Peter Reynolds, Keith Taylor and Dr. Casey Ravenhurst are acknowledged for keeping me in touch with the art of $^{40}Ar/^{39}Ar$ geochronology. Thanks for the patience of Dr. Dorothy Godfrey-Smith, Pat Scallion and Dr. Don Arnold (Dalhousie Chemistry) concerning my meddling in the art of Electron Spin Resonance and Alexander Grist who gratefully allowed me use of the Dalhousie Fission Track Laboratory facilities for sample preparation and computational needs. Departmental Administrative staff: Darlene Van de Rijt and Norma Keeping and CODELCO-Chuquicamata secretarial staff: Nina Lopez L., Luis Morgado, Juan Olcay are gratefully thanked for their display of juggling skills in effort to keep me present (on paper) in both the northern and southern hemispheres.

Financial support for this thesis was provided by Dr. Marcos Zentilli through NSERC operating grants, CODELCO-Chuquicamata and Cuesta Research Ltd. Additional support was through a Dalhousie University Graduate Scholarship (1992-1997), a Hugh E. McKinstry Fund award of the Society of Economic Geologists Foundation, Inc (1993), and travel grants from IGCP #342 "Age and Isotopes of Andean Ore Deposits".

Chapter 1. Introduction

1.1 Introductory Statement

The occurrence of large-tonnage, low-grade porphyry-type deposits, which are genetically related to volcano-plutonic activity and located along, or near, regional scale fault systems, such as many of those deposits in the Central Andes of northern Chile, implies a genetic link between continental deformation, igneous activity/intrusive emplacement, and porphyry-style alteration and mineralization. Chuquicamata is one such deposit located within the regional Domeyko Fault System in northern Chile. This thesis investigates and documents the structural evolution of one of the largest porphyry copper deposits of the world, Chuquicamata in northern Chile. Based on extensive field mapping and associated laboratory study, a relative sequence of structural, alteration and mineralization events has been established, which can be ascribed to two main pulses with $^{40}Ar/^{39}Ar$ ages of 33.4 and 31 Ma. The study quantifies the preferred orientations of mineralized structures and their spatial distribution in different domains, which impart anisotropy to ore grade distribution at the deposit scale. The detailed observations in the large open pit allow to critically assess the validity of tectonic hypotheses proposed by others in the regional context of the Central Andes.

1.1.1 Aims and Purpose of this Thesis

The principal aims of this thesis were threefold: 1) to establish a relative structural history of the Chuquicamata mineralized system and relate this history to mineralization events, thus assisting in better assessing the distribution of ore types and reserves; 2) to ascertain whether and in what ways the protracted structural deformation of the mineralizing system is responsible for its giant size, and 3) to use the exceptional artificial outcrop provided by the open pit in the measurement of deposit-scale fault orientations and kinematics, supported by modern geochronological techniques such as $^{40}Ar/^{39}Ar$, to test regional tectonic hypotheses proposed by regional studies of others (e.g. Maksaev and Zentilli, 1988; Maksaev, 1990; Reutter et al., 1991, 1996; Scheuber and Reutter, 1992;

Tomlinson and Blanco, 1997a,b), and at the same time establish links between the structural evolution of the mineralized system, with plate tectonic models applicable to the western margin of the Central Andes. An important subordinate goal of the study was to assist in the ore reserve calculations by quantifying the anisotropy of the different operational rock units.

1.2 Current Model Parameters for Porphyry-type Copper Deposits

1.2.1 Porphyry Copper Deposits

The term porphyry copper deposit (PCD) refers to a large volume of rock, which has been mineralized by copper sulfide and copper-iron-sulfide minerals (American Geological Institute, 1966). Although now superseded, the most accepted porphyry deposit model is that of Lowell and Guilbert (1970). This model, which proposes recognizable concentric variations in alteration and mineralization assemblages, depicts the final product of a complex set of processes resulting from the epizonal emplacement of a porphyritic intrusion, associated heating, cooling and fluid flow (Titley, 1993). Variations between individual deposits (eg. Gustafson and Hunt, 1975; Eastoe, 1983; Dilles and Einaudi, 1992; Gustafson and Quiroga, 1995; Zvezdov et al., 1993) essentially result from a difference in setting or rock types (Titley, 1993; McMillan et al., 1995; Thompson, 1995). For a summary and discussion of various models the reader is referred to McMillan and Panteleyev (1980), Titley (1993) and McMillan et al. (1995). As stated by Gustafson and Hunt (1975), the detailed study of a specific deposit conforms to generally accepted model components and may be considered a variation of a theme. In the case of Chuquicamata, extreme structural control and telescoping of successive magmato-hydrothermal events may make this deposit one of the most atypical in terms of alteration and mineralization *zonation*. However, the generalized alteration and mineralization assemblages at the Chuquicamata deposit are consistent with the generally accepted models.

In general, porphyry copper deposits are shallowly emplaced (depths of 1 to 5 km from the surface) mineralized systems defined as having low grades (ca.1% Cu), high tonnage ($>100*10^6$ tonnes), and concentrations of Fe, Cu and Mo sulfides localized in the highly fractured upper parts of felsic intrusive rocks or adjacent country rocks (Titley and

Beane, 1981). Alteration and mineralization zonation is genetically related to, and spatially centred on the intrusive body. This chapter is a review of the general characteristics of porphyry copper deposits in terms of setting, porphyry emplacement, alteration, mineralization, and supergene enrichment. In Chapter 3, a description of the Chuquicamata porphyry copper deposit is presented as a comparison to the accepted porphyry copper deposit models.

1.2.1.1 Setting

Almost all porphyry deposits are found at non-collisional convergent plate margins associated with island-arc or continental-arc settings, as such an often implied genetic relationship between subduction, magmatism and porphyry deposits is generally accepted (Sillitoe, 1972; Hollister, 1978; Sillitoe and Bonham, 1984). Emplacement setting and rock type are commonly used to classify porphyry deposits (McMillan and Panteleyev, 1980; McMillan et al., 1995).

1.2.1.2 Source and Emplacement

Burnham (1979) discussed the potential sources of magmas available to produce porphyry copper deposits. These are summarized as: (1) the melting of subducting oceanic crust with an expected derivation of hydrous, calc-alkaline magmas with the requisite properties for volcanic arc and porphyry deposit formation, and (2) relatively anhydrous mafic magmas rising from the upper mantle into the lower continental crust having the capacity to generate granitic to dioritic, H_2O-bearing melts by anatexis and assimilation (Burnham, 1979). Once these magmas are emplaced in upper crustal levels where porphyry-type alteration and mineralization may form, the proposed models again diverge based on the evolution and interaction of fluids.

From the perspective of fluids, end-member models have been proposed based on fluid inclusion studies, isotopic signatures, and their relation to alteration and mineralization assemblages. These end-member porphyry models are the orthomagmatic model, where high temperature (750°-400°C) and salinity (>15%by wt. NaCl) fluids transport the ore

components and are generated from within the intruding body (Burnham, 1979; Phillips, 1973) and the convective model, where the intruding pluton acts as an energy source to drive low temperature (450°-250°C) and salinity (<15% by wt. NaCl) ground water convection cells with flow through the subsolidus pluton. These fluids scavenge ore components both from the pluton and country rock (see Norton and Cathles, 1979; White, 1968). A general consensus exists supporting the overlap of these end-member systems to varying degrees for individual deposits (eg. Gustafson and Hunt, 1975; Zvezdov et al., 1993). Further suggestions concerning the mineralizing fluids involves the evolution of a single (plume model of Henley and McNabb, 1978), or two independently evolved fluids (White, 1974). These various interpretations of fluid generation and interaction accommodate the results of numerous fluid inclusion studies (eg. Roedder, 1971; Chivas and Wilkins, 1977). Current literature, based on fluid, gas and melt inclusions in primary magmatic and stockwork quartz heavily favours the orthomagmatic model of metal source for porphyry formation (Bodnar, 1995; Hedenquist, 1995; Graney and Kesler, 1995; Lowenstern, 1995) as do stable isotope (Weihed and Fallick, 1994) and radiogenic isotopic (Zentilli et al., 1988) studies.

1.2.1.3 Alteration

Lowell and Guilbert (1970) provide the most accepted conceptual porphyry-type deposit model comprising concentric variations in alteration and mineralization assemblages (Fig. 1.1A). Since the proposal of this model many porphyry deposits have been studied in great detail, resulting in the separation of events and the refining of alteration and mineralization sequences and assemblages (eg. Eastoe, 1983; Dilles and Einaudi, 1992; Gustafson and Quiroga, 1995; Zvezdov et al., 1993). It is acknowledged that the complete model alteration sequence is rarely developed or preserved, with variations in the assemblages being controlled by host rock composition and pre-ore structures (Guilbert and Lowell, 1974). However, the generalized characteristics of the four typical alteration zones, potassic, sericitic, argillic and propylitic, summarized in Table 1.1, are found in the majority of porphyry-type deposits.

1.2.1.4 Hypogene Mineralization

Due to their low metal grade and very large volume, porphyry-type deposits are described as "disseminated". However, at a small scale, mineralization is, to a great extent, controlled by fractures (Fig. 1.1C). Estimates put greater then 90% of mineralization in or adjacent to fractures and veins (Beane and Titley, 1981).

As summarized by Lowell and Guilbert (1970), Henley and McNabb (1978) and McMillan and Panteleyev (1980), hypogene mineralization generally consists of varying amounts of pyrite, chalcopyrite, bornite and molybdenite within fracture fillings or quartz-bearing veinlets. A typical ore zonation includes: a central barren or weakly mineralized zone containing pyrite (<2%), chalcopyrite, molybdenite and minor bornite. Outwards from the core there are enrichments in molybdenite, chalcopyrite and pyrite. Enclosing the ore zones is a pyrite-rich halo (10-15%) with variable amounts of chalcopyrite and molybdenite (Fig. 1.1B). Base and precious metal bearing veins may occur peripheral to the porphyry mineralization in associated fractures (McMillan and Panteleyev, 1980). Other metallic minerals that may be present include magnetite, usually characteristic of more mafic host rocks and gold-rich porphyry systems (Clark and Arancibia, 1995; Guilbert and Lowell, 1974), and chalcocite (or digenite) that may be found from the central ore zones to the outer peripheral areas in the upper levels of the deposit.

Table 1.1. General characteristics of alteration zones associated with porphyry copper deposits (after Lowell and Guilbert, 1970; Edwards and Atkinson, 1985).

	Propylitic	Potassic	Phyllic	Argillic
		metasomatism leaching Ca, Na	sericitic alteration leaches Mg,Ca,Na	intermediate(I) and advanced(A)
Characteristic assemblage	Chlorite, epidote, calcite, sericite	biotite, orthoclase, quartz	quartz, sericite	I- montmorillonite, illite, chlorite, kaolinite A- kaolinite, diaspore, quartz, amorphous silica
Accessory Minerals	apatite, anhydrite, ankerite	albite, sericite, anhydrite, apatite	alunite	pyrophyllite andalusite, corundum
Mineralization	hematite	magnetite, chalcopyrite, bornite, pyrite	pyrite >> chalcopyrite	pyrite, (chalcopyrite, bornite)

Fig. 1.1 Schematic cross-sectional diagram of the Lowell and Guilbert porphyry copper model illustrating the spatial relationships and zonation of (A) alteration and (B) mineralization. In B, the mineralization within the ore shell is approximated by 1% pyrite, 1-3% chalcopyrite and 0.03% molybdenite and that within the pyrite shell by 10% pyrite, 0-3% chalcopyrite and trace amounts of molybdenite. (C) indicates the dominant style of mineralization. After Lowell and Guilbert (1970).

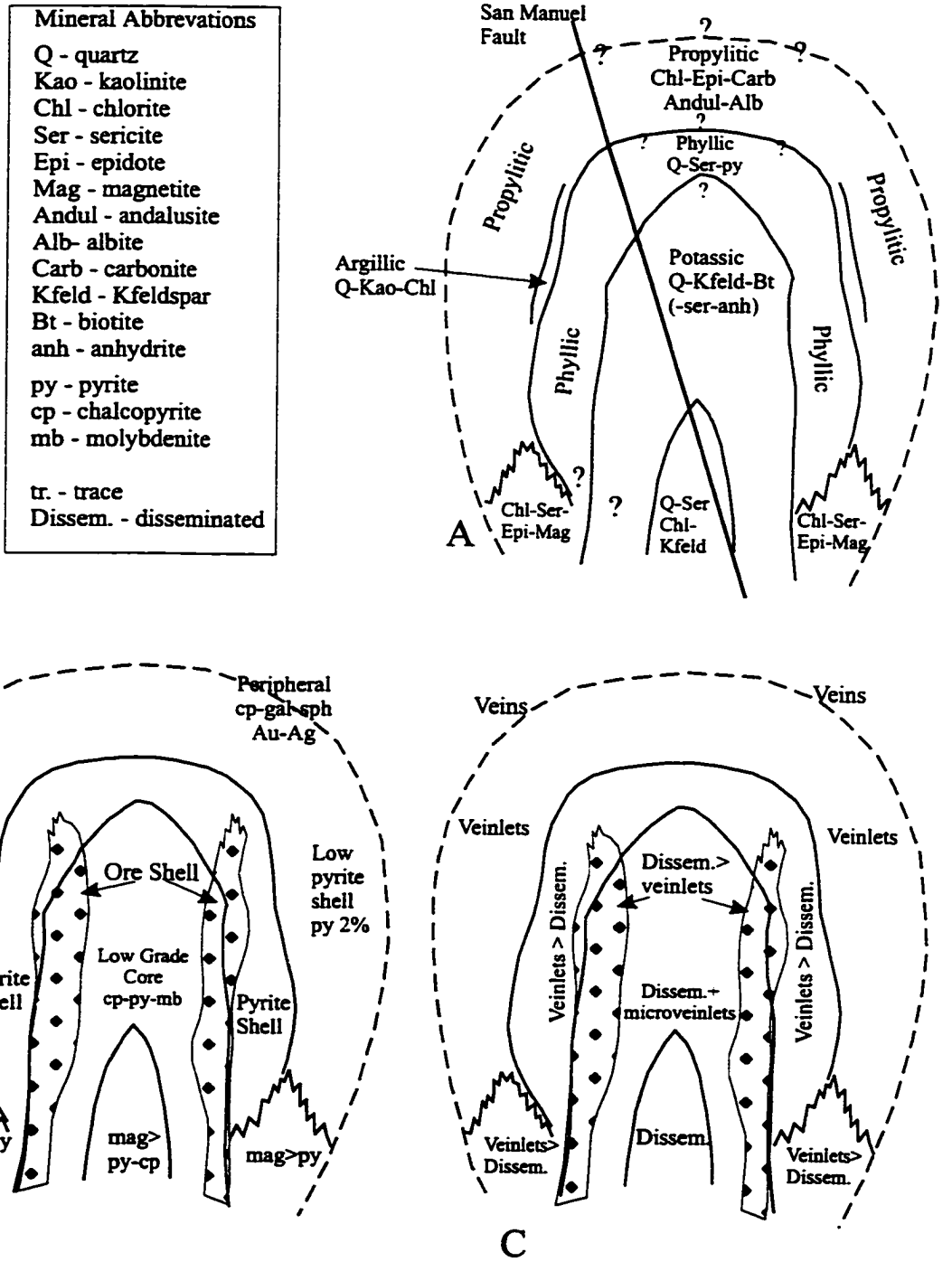

1.2.1.5 Supergene Enrichment

Supergene enrichment is important in porphyry copper deposits, often determining if the deposit will be economic. Leaching of copper from hypogene mineralization by hydrochemical weathering processes from above the water table and precipitation of the copper from solution at the water table and below it forms a secondary enrichment blanket. This process changes a vertical hypogene mineral zonation into a horizontally stratified supergene zonation (Titley, 1994; Ague and Brimhall, 1989). Copper minerals found within the supergene blanket may include chalcocite, djurleite, digenite, covellite and small amounts of native copper. Ague and Brimhall (1989) summarize the chemical processes involved in the formation of this enrichment zone and Titley (1994) outlines expected mineral assemblages.

1.2.1.6 Summary of Porphyry-type Copper Deposits

Emplacement of porphyry copper deposits are common within volcano-plutonic complexes associated with convergent plate margins in either island-arc or continental settings. Lower crustal-upper mantle magma sources are generally accepted as potential porphyry-forming magmas. However, the need for and extent of magma mixing, fractionation, and/or assimilation on ascent for the formation and emplacement of the porphyries is still debated. Many detailed, deposit-specific alteration and mineralization studies have been undertaken to examine PCD modelling. However, Lowell and Guilbert's generalized alteration and mineralization distribution model is still the most accepted model for this deposit type. Evidence from fluid, gas and melt inclusion studies on porphyry copper deposits indicate the presence of magmatic fluids capable of transporting all ore components. Stable-isotope studies on late-stage phyllic alteration assemblages suggest that meteoric fluids do not contribute to main-stage mineralization having little, if any, ore component input. The extent of secondary mineral re-concentration, as evidenced by supergene alteration processes often influences the economic viability of porphyry mineralization. Structural control, or the utilization of structural features such as fault and fracture systems, may play an important role in many of the essential steps in the generation of a porphyry deposit from

a regional tectonic control on magma generation, rise and emplacement, to the circulation of hydrothermal fluids through fracture systems and the displacement of volumes of mineralized rock.

1.2.2 PCDs and Regional Fault Zones

Several authors have noted the association of regional scale faults with the emplacement of igneous complexes (e.g. Guineberteau et al., 1987; Hutton et al., 1990; Scheuber and Reutter, 1992; D'Lemos et al., 1992; Tikoff and Teyssier, 1992; Morand, 1992; Karlstrom et al., 1993; Brown, 1994) and the presence of porphyry-type deposits (e.g. Seraphim and Hollister, 1976; Hollister, 1978; Titley and Beane, 1981; Maksaev, 1990). These and other authors support the probability of a tectonic component in the generation and/or emplacement of PCDs (Guilbert, 1981; Sillitoe, 1981; Thompson, 1995; Sasso et al., 1995; Skewes and Stern, 1995). However, identifying specific structural controls that have guided the emplacement of PCDs has not been successful (Hunt, 1991). A possible exception are those PCDs in northern Chile, where structural relations indicate a contemporaneity of deformation and the emplacement of plutons with (Maksaev, 1990; Mpodozis et al., 1994; Tomlinson, 1994; Lindsay et al., 1995) and without porphyry-type mineralization (Grocott et al., 1994), and where a regional structural control to mineralization processes probably exists but latest fault motion has obscured the relation by dissection of the PCD (Reutter et al., 1993,1996).

1.2.3 Stockwork Systems

The generation of the mineralized fracture systems in porphyry type deposits is a function of fluid saturation within the cooling host intrusion and the rupture of the pluton and surrounding country rocks (Burnham, 1979; Henley and McNabb, 1978; Phillips, 1973; Knapp and Norton, 1981; Koide and Bhattachaji, 1975). As a shallowly emplaced intrusion cools, an outer crystallized carapace forms and acts as an impermeable barrier to volatiles and to a crystallizing H_2O-saturated interstitial melt (Burnham, 1979). Cooling of this carapace and the underlying melt give rise to increased vapour pressures which may result

in resurgent, or second boiling, and the release of mechanical energy (Phillips, 1975; Burnham, 1979). The energy release may hydraulically rupture the carapace, releasing pressures and mineralizing fluids (Phillips, 1975; Burnham, 1979, 1985; Sillitoe, 1985). Resealing of the fracture system by mineral crystallization and continued generation of elevated supralithostatic fluid pressures by feldspar crystallization, will lead to renewed hydraulic fracturing. The result is a release of hydrothermal fluids into a highly fractured, permeable host rock, a consequence of which is widespread fracture-controlled alteration and mineralization in what is denominated a "stockwork".

At the district to deposit scales, the importance of mineralized stockwork systems has been previously noted by Hollister (1978) and with this importance comes the observation that porphyry-type deposits have definable sets of veinlets (Hunt, 1991; Gustafson and Hunt, 1975; Hollister, 1978, Sillitoe, 1985). Original work by Rehrig and Heidrick (1972) and Haynes and Titley (1980) shows that fracture and dike patterns are related to the emplacement and cooling of host rocks and porphyries and that these patterns, as well as fractures related to later regional stresses, can be identified and quantified as regional vein/fracture densities.

Recently, work has focussed on prevalent vein, veinlet and fracture trends within porphyries (Casselman et al., 1995; Heberlein, 1995). Few studies, however, have attempted to separate the discrete mineralization events, in terms of fractures formed by either local magmatic stresses or by regional tectonic stresses, opting instead for the simplified classification of vein sets into "A", "B" and "D" type veins (see Gustafson and Hunt, 1975; Gustafson and Quiroga, 1995). Although veins and veinlets described within this study in general fit the model classification scheme of Gustafson and Hunt (1975), at Chuquicamata it became obvious that we were dealing with a multicycle process. In order to maintain objectivity, in this thesis the mineralized veins and veinlets are presented and discussed as individual features to test for independent directional trends. In this way, any changes in the fracture control of the mineralizing system can be detected.

1.2.4 Porphyry Copper Deposits, Faults and Stockwork Systems

It is one of the purposes of this thesis to understand the role that structural control plays in ore emplacement through multiple mineralization events. It is generally accepted that mineralization within PCDs is disseminated seeming to imply that sulphides are randomly distributed as particles with the body of the igneous rock. As indicated above, this is a misconception, not only in the case of Chuquicamata but in most PCDs, where 80-90% of ore mineralogies are contained in veins and veinlets (Lopez, 1939; Hollister, 1978; Beane and Titley, 1981). Chuquicamata may be described arbitrarily at three distinct mineralization scales, as: (i) a disseminated deposit where copper-bearing sulfides are irregularly distributed in the granodioritic host rock, (ii) a deposit of mineralized stockwork or sheeted veinlet systems where mineralization is contained in thin veinlets, and (iii) a deposit of large vein systems that contain irregular amounts of copper-bearing sulfides and large molybdenum concentrations. The potential extent of structural control within porphyry-type deposits is therefore exemplified by the various systems at Chuquicamata, which serves as a field laboratory for structurally controlled porphyry deposits.

Mineralization within the veins and veinlets at Chuquicamata are shown not to be chaotic, as might be expected in an evolving magmato-hydrothermal system, but instead, structurally controlled at the scale of mineralization where distinct veinlets representing separate mineralizing pulses have preferred orientations.

1.2.5 Scope of the present study

The work in this thesis was carried out as the initial phase of an ongoing Dalhousie University-CODELCO-Chile research project, whose goal was and is to characterize and define the multitude of processes associated with giant, multiple event, magmato-hydrothermal systems. The principal focus of this thesis is to characterize the structural aspects of the deposit and to assign a first order identification of the sequence of alteration-mineralization events. This thesis forms the basis for continuing geochronological, mineralogical and fluid evolution studies within the Chuquicamata system and should provide a baseline structural sequence for comparison in other fault-related magmato-

hydrothermal systems in the Andes.

1.3 History and Previous Work at Chuquicamata

1.3.1 History of Mining at Chuquicamata

The Chuquicamata porphyry copper deposit is located in the province of El Loa, Antofagasta Region, Chile (22°17' S latitude; 68°55' W longitude), at an altitude of 2800 metres above sea level in the Cordillera de Domeyko (Fig. 1.2). It is one of the largest and richest porphyry copper deposits in the world and is found within a specialized copper metallogenic province that stretches from southern Peru to central Chile along the western flank of the Central Andes (e.g. Maksaev, 1990).

Archeologists and historians believe descendants of the native Atacamenians were the first to use the copper of this region for the fabrication of arms and domestic utensils (Marcosson, 1957; Campos et al., 1979). It is also believed that in 1535 the troops of Spanish conquistador Diego de Almagro used copper from Chuquicamata to replace the horseshoes of their horses.

Small scale modern mining started after the War of the Pacific (1879-1882), exploiting the high-grade vein deposits that gave way at depth to increased concentrations of pyrite. These workings included the Zaragoza, Balmaceda, Lerida and San Antonio veins that existed at the northeastern periphery of the present Chuquicamata open pit and the llampera, or oxidized body at its centre (Wroth, 1917).

The first time an interest was taken in Chuquicamata as a large scale deposit was in 1910, when A. Burrage interested the Guggenheim brothers in an investment partnership (Campos et al., 1979). They organized the "Chile Exploration Company" and initiated one of the first comprehensive geological studies by W. Lindgren in 1912, encompassing the Chuquicamata district. At this time an evaluation of the deposit indicated reserves (154 million tonnes @ 2.43% Cu, (Lopez, 1939)) that justified mining development. The Chile Copper Company began mining operations in 1915 with the extraction of oxide mineralization, principally atacamite, antlerite, brochantite and kroenkite, at grades of about 1.75% Cu (Campos et al., 1979). The mine was operated as an open pit by the Anaconda

Copper Mining Company from 1923 until 1971 after which the Corporacíon del Cobre de Chile oversaw the deposit until the culmination of nationalization in 1976. This resulted in the creation of the Corporacíon Nacional del Cobre (CODELCO), the present owners and operators of Chuquicamata.

Since 1952, sulphides, primarily supergene chalcocite and covellite, have been extracted. Presently, an average grade of ~1% Cu is being mined from mixed ores that are composed of chalcocite, covellite, enargite, digenite, bornite and chalcopyrite. By-product ores also extracted include molybdenum, rhenium, selenium and doré, an amalgam of precious metals.

1.3.2 Previous Work

As expected for a mine with a production history of greater than 80 years, there have been many internal studies updating the immediate geology of the deposit, but there are very few published studies, the last comprehensive papers in the international literature date from the 1940s. The most recent publications attempt to relate the PCD to the magmato-tectonic and structural evolution of northern Chile (Lindsay et al., 1995; Reutter et al., 1993, 1996). Tables 1.2 and 1.3 summarize the main topics of published and unpublished geological studies undertaken in and around Chuquicamata.

Fig. 1.2 Location of the Chuquicamata porphyry deposit in the Domeyko Cordillera, with respect to the Domeyko Fault System, and the physiographic zones of the Antofagasta region of northern Chile after Maksaev (1990).

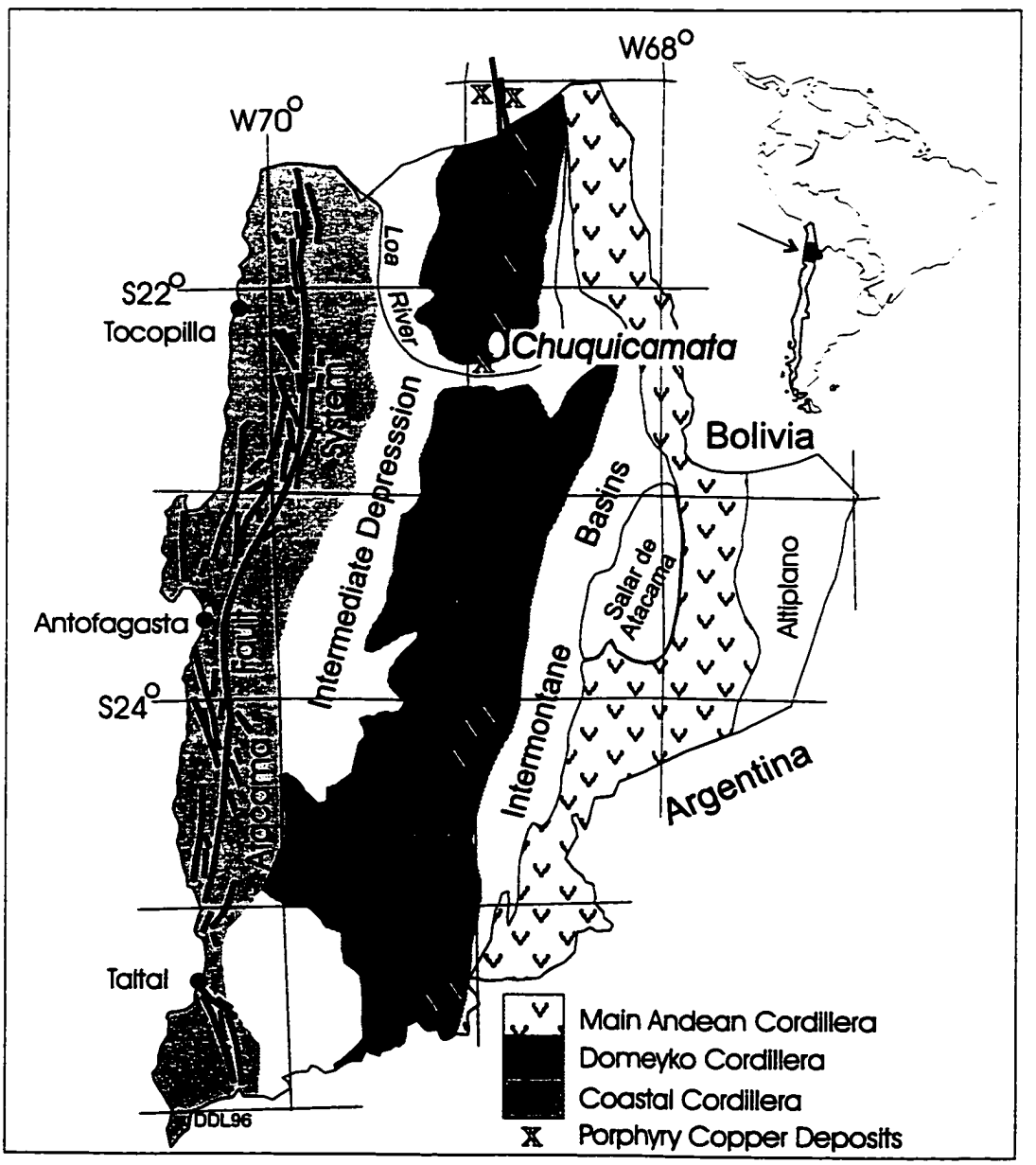

Table 1.2 Summary of all published materials involving studies at Chuquicamata. Complete references are listed at the end of the thesis.

Published materials	Year	Author(s)
General Geology	1916	P. Yeatman
	1952	V. D. Perry
	1980	O. Alvarez, J. Miranda and P. Guzman
Mineralization	1939	V. M. Lopez
	1942	V. M. Lopez
	1944	O. W. Jarrell
Rock Properties	1980	M. Munoz and M. Araneda
Petrology and Alteration	1985	C. O. Alvarez and I. Aracena
	1987	M. A. Parada, I. Aracena and H. Tanaka
Hypogene alteration and mineralization	1985	O. Alvarez and R. Flores
Regional Radiometric Geochronology	1972	G. S. Quirt
	1988 a 1988 b	V. Maksaev, R. Boric, M. Zentilli and P. H. Reynolds
	1994	M. Zentilli, T. E. Krough, V. Maksaev and C. E. Alpers
Isotopes	1988	M. Zentilli, B. R. Doe, C. E. Hedge, O. Alvarez, E. Tidy and J. A. Daroca
Model for PCDs	1988	V. Maksaev and M. Zentilli
Supergene	1985	R. Flores
Dating Supergene	1996	R. Sillitoe and E. H. McKee

Table 1.3 Summary of unpublished studies undertaken by university students.

Degree and Author	Univ.	Year	Topic Relating to the Chuquicamata PCD
Ph.D.: B. L. Renzetti	Ind.	1957	Geology and petrogenesis
Ph.D.: W. J. Ambrus	Sal.	1979	PCD models and regional correlations
Ph.D.: H. M. Soto	Sal.	1979	Alteration and primary mineralization
Ph.D.: V. Maksaev	Dal.	1990	Regional geology and geochronology
M.Sc. M. Lewis	Dal.	1996	Hypogene covellite assemblages
Memoria: P. Guzman	Chile	1983	Reserve calculations
Memoria: J. Pallauta	Chile	1982	Slope stability and rock quality
Memoria: I. Aracena	Chile	1981	Lithogeochemistry and alteration
Memoria: M. Vega	UCN	1982	Fluid inclusions in quartz veins
Memoria: F. Ramierez	UCN	1993	Structural and geomechanical study

Ind. = University of Indiana, USA
Sal. = Universidad de Salamanca, Salamanca, Spain
Dal. = Dalhousie University, Halifax, NS, Canada
Chile = Universidad de Chile, Santiago, Chile
UCN = Universidad Catolica del Norte, Antofagasta, Chile

1.4 This Work and its Significance to Porphyry Copper Deposit Models

This thesis was initiated in 1993 as a more traditional structural geology study to unravel the tectonic controls and the history of emplacement and deformation of the Chuquicamata deposit. However, this was also a time of administrative change within CODELCO- Chuquicamata and it became clear that the company would not sponsor a purely academic study, but would be interested instead in an applied study which would assist production, exploration for new reserves, and prediction of ore grade. Therefore, the project had to be modified to satisfy this dual purpose.

During 1994, under a new Superintendent of Geology (G. Ossandón), the original project was reproposed and accepted as an integral contribution towards the development of a new geological model. This project provided a detailed structural database on which economic mineral reserve calculations could be made.

Mapping at various scales and sampling was undertaken over four field seasons for a total of 18 months. Twelve of these months were spent working as a member of the geological staff for CODELCO-Chuquicamata. Perhaps not in the most efficient way in terms of research, this work, which included remapping the surface distributions of alteration, mineralization and structural features, within and adjacent to the open pit, and a project mapping and describing the West Fault, constitutes the basis for the description and discussion of the structural evolution of the Chuquicamata porphyry copper deposit.

The significance of this study is related to several aspects of mineral deposit studies. First, it examines in detail the main scales of mineralization for one of the world's most important yet under-studied porphyry-type copper deposits. These distinct scales of mineralization are the veinlet-scale stockwork system, composed of mineralized fractures usually <10 mm in width, some of which bear alteration halos adjacent to the veinlet, and the vein-array scale of mineralization. The vein-array scale is largely composed of quartz-molybdenite veins that have widths exceeding 1 metre and are spatially and probably temporally coincident with the development of deposit-scale fault systems. This change in scale of mineralization is related to the vertical extension of separate but overlapping magmato-hydrothermal systems. This study provides detail to the accepted alteration and

mineralization model for porphyry systems and establishes a discrimination by scale of mineralization, which is a concept that may be applied to other giant ore deposits. Secondly, this study documents the important control exerted by local- and regional-scale structural systems on the emplacement of host intrusions and throughout the alteration and mineralization processes of a giant ore system. There have been studies relating regional fracture systems to mineral deposit centres in the much better studied porphyry copper districts of the southwestern United States by Titley et al., (1986), but this is the first one to examine a mineralized porphyry within a magmatic arc that was undergoing deformation throughout its emplacement and mineralization history. On a regional scale this study proposes a style of structural control on porphyry deposit formation for northern Chile as compared to the models developed from the porphyry districts of the southwestern United States. Finally, this study provides an indispensable and superb framework from which further detailed studies on alteration, mineralization and fluid evolution may be developed.

1.4.1 Approach and Methods

This thesis focuses on structurally based studies at two different scales. First, at the veinlet scale (Chapter 5), or scale of mineralization, where structural sampling was completed within stockwork zones. Structural sampling consisted of characterizing individual veinlets, with minimum lengths of 10 cm, by noting mineralogy, associated alteration, relative timing, or crosscutting relationships, widths and orientation. This resulted in a data set where veinlet sets were formed and orientations were analysed using stereographic procedures. Although this project was established to assist the mine production geologist, and thereby requiring observation solely at the hand sample scale, numerous samples were collected and examined in thin section and polished thin section. Second, at the deposit scale (Chapter 6), where faults and veins were mapped according to an established set of criteria, including fault/vein filling, mineralogical and alteration associations, widths, orientations and displacement sense. These features were located within the Chuquicamata coordinate system using a Total Station topographic instrument. Structural features were traced from bench to bench in the field and in areas where bench access was

not permitted, previous geological mapping was used to establish continuity and structural relationships.

1.4.2 Limitations

Limitations of this study can be ascribed to either company (CODELCO) criteria or project specific criteria. Company restrictions are chiefly administrative barriers to mine accessibility and safety liability concerns within the active mining environment. Both restrictions impact on the time allotted for mapping in the field and the locations of the mine open to field study. Limitations specific to the collection of structural data at both fault-vein (Chapter 6) and veinlet (Chapter 5) scales are related to the method and style of open pit mining, which destroy points of observation as mining progresses. Both Chapters 5 and 6 deal with the directional trends of structural features, which within a porphyry-type deposit environment are predominantly vertical. A bias is therefore inherent in the mapping of vertical bench faces, which limit the exposure of those features trending parallel or sub-parallel to the bench face. However, similar studies of small sites across a regional area have suggested that although measurement of horizontal sites was preferred, there was no significant difference between vertical and horizontal study sites (Titley et al., 1986). Confirmation of the similarities between horizontal and vertical study sites could not be established at Chuquicamata due to the mining method, which left no exposed horizontal surfaces within the mine, and the extensive gravel cover of the Chuquicamata units outside of the mine. In light of numerical models that suggest horizontal fractures and veins may become prevalent at deeper structural levels within and adjacent to porphyry systems (Knapp and Norton (1981), vertical surfaces within a porphyry deposit may be preferable as exposed vein orientations may assist in estimating a depth of exposure. As indicated, the reproducibility of measurements from the same sites studied is hampered since the bench face exposures have a limited lifetime as a result of active mining. Finally, the data sets collected represent distinct scales of structural data. The data may be somewhat biased due to collection methodology in the system being studied. However, this methodology was the best attainable and effort was made to locate study sites on a bench faces of different

orientations. Consistency across large areas and local variations explainable by the presence of higher-order structures indicate the methodology is valid.

1.5 Summary of Thesis Chapters

This thesis is organized into three parts with a total of eight chapters. Part I includes an introduction to the study and a general history of the Chuquicamata deposit in Chapter 1. A description of the district and regional geology, a summary of the tectonic evolution for the district, and an introduction to the West Fault System, a structural control on the emplacement and mineralization of the Chuquicamata porphyry copper deposit are presented in Chapter 2. Based on the present state of knowledge and taking a mine geologist's view, documentation of the geology of the Chuquicamata deposit is presented in Chapter 3.

Part II begins with a documentation of pre-mineralization, ductile-brittle structural features exposed within the Chuquicamata Intrusive Complex, in Chapter 4. This is followed by a description of veinlets in the structural sampling data set and a discussion of control of fracture orientation and mineralization in Chapter 5. Chapter 6 provides a description of the deposit-scale structures, a classification of these structures into domains of similar character, a proposal of deformational events and a discussion on the probable geological setting that gave rise to their formation. Post-mineralization displacements and the West Fault are addressed in Chapter 7.

Part III, presents a conceptual model sequence of structural events and their control on stages of mineralization from veinlet to deposit scales for the Chuquicamata deposit in Chapter 8.

Chapter 2. Lithostratigraphy of the Chuquicamata District

To place this study into a geological framework, the lithostratigraphy outcropping within and surrounding the Chuquicamata open pit is presented in this chapter. The described area is restricted to the region located within the Chuquicamata district, which includes the Chuquicamata Hills to the east, the Fortuna Hills to the west and the Radomiro Tomic and Mina Sur mines to the north and south respectively (Fig. 2.1). This area is located within the Domeyko Cordillera, a rugged, longitudinal mountain range with maximum altitudes of 4500 metres. The Domeyko Cordillera is one of six north-south trending physiographic units occurring within the Antofagasta region of northern Chile (Fig. 1.2). To the north, the Domeyko Cordillera joins the high Andes. At the latitude of Chuquicamata it is separated from the main Andean chain by the Loa River Valley and further south by the Salar de Atacama Basin. Previous mapping in the district of Chuquicamata and its surrounding region includes 1:50000 scale by Tomlinson et al. (in prep.), 1:1000000 scale by Reutter et al.(1994), 1:500000 scale by Boric et al. (1990), 1:50000 scale by Chong and Pardo (1993, proprietary) and 1:250000 scale by Marinovic and Lahsen (1984).

Within this thesis, relative and absolute ages are presented for the Chuquicamata deposit, which correspond to cooling ages for lithologic units and alteration-mineralization events that occur between ca. 34-30 Ma. The reader should refer to the revised Cenozoic time scale of Berggren et al.(1995a), which is the basis for the Cenozoic era presented by Gradstein and Ogg (1996), to become familiar with the Eocene - Oligocene boundary ages. For all other geochronological units see Berggren et al. (1995b).

Fig. 2.1 Illustration of the area described in Chapter 2 as the Chuquicamata District. This includes the Fortuna Hills of the Sierra del Medio, the Chuquicamata Hills, and the Mina Sur, Chuquicamata and Radomiro Tomic deposits. A generalized distribution of rock types is shown in the shaded areas, which represent outcrop. (UTM coordinate system).

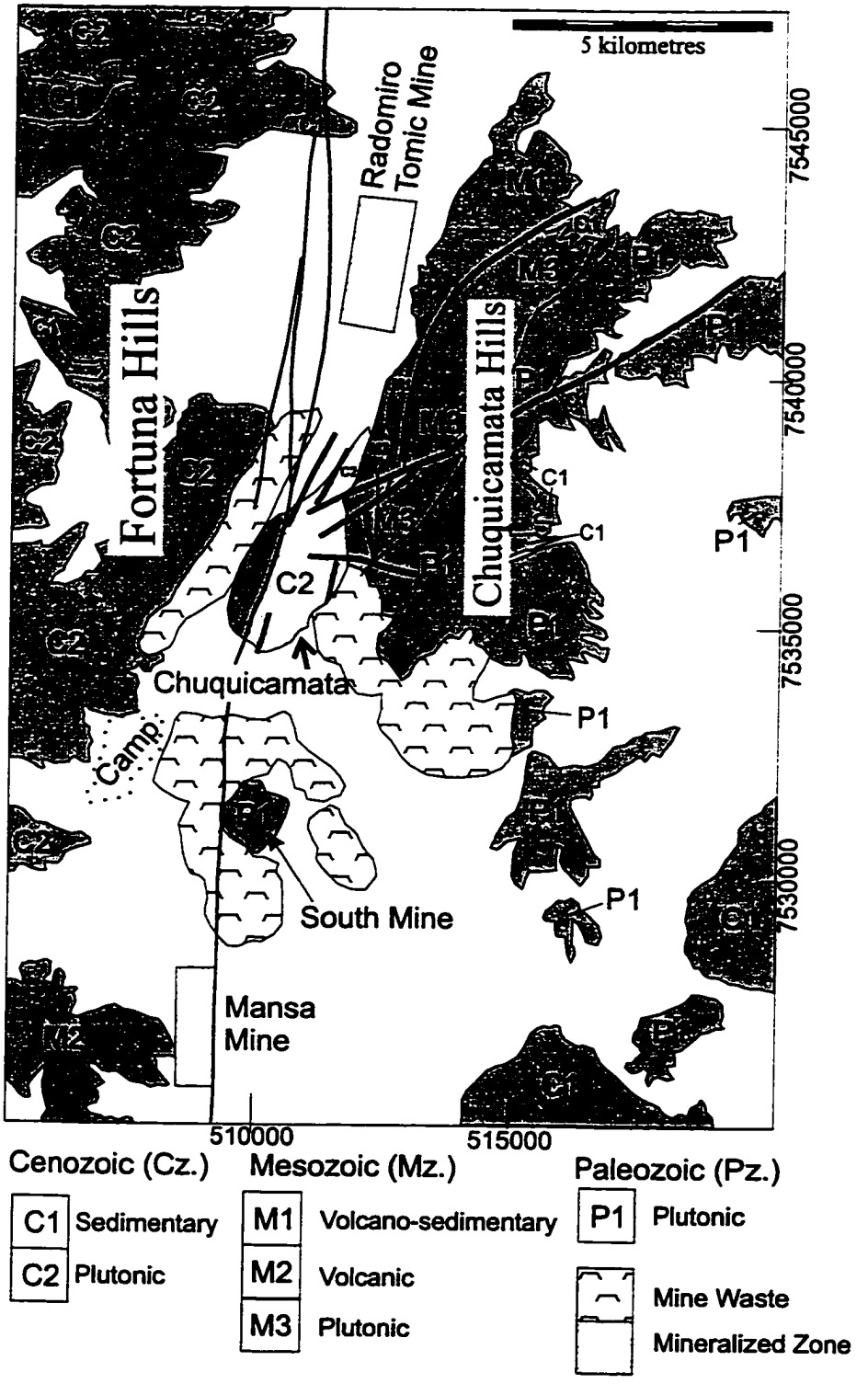

2.1 Paleozoic

The Paleozoic geology in the immediate Chuquicamata area, located in the Chuquicamata Hills (Fig. 2.2), is poorly understood due to the lack of detailed mapping internal to the Paleozoic units. The complexity of these units and the lack of petrology, geochemical and geochronological studies have left many of these units undifferentiated to a great extent. Chong and Pardo (1993) attribute undifferentiated metamorphic sequences to the Precambrian and/or Paleozoic, although recent mapping and geochronological studies indicate that the majority of units in the district are Carboniferous to Permian in age (Tomlinson et al., in prep.).

2.1.1 Igneo-Metamorphic Complex of Chuquicamata (CIMC)

CIMC is an informal name for the Igneo-Metamorphic Complex of Chuquicamata unit, proposed by Marinovic and Lahsen (1984). Chong and Pardo (1993) divide the CIMC into two sub-units comprised of (a) dioritic-gabbroic gneisses and weakly to moderately foliated micaceous schists and (b) diorites, microdiorites and rare metamorphosed tonalites (Renzetti, 1957; Ambrus, 1979; Marinovic and Lahsen, 1984; Chong and Pardo, 1993). Tomlinson et al. (in prep) on the other hand, consider the CIMC a single unit; stating that the amphibolites and schists are gradational with meta-diorites, which intrude the upper Paleozoic Mesa Granite. The meta-diorites are fine-grained amphibole-plagioclase porphyritic to coarse-grained equigranular rocks, whose outcrops trend NNE-SSW to NE-SW and are emplaced to the west of and intruding the Mesa Granite. Phenocrysts of acicular amphibole (5-7%, up to 5 mm) and blocky feldspar (7-10%, 1-2 mm) are hosted in a plagioclase-rich matrix and an assemblage of chlorite-calcite-muscovite was produced by alteration.

Radiometric, K/Ar, dates for the diorites give Permian ages of 273±9 Ma (hornblende) and 267±6 Ma (biotite) (Tomlinson et al., in prep.). The diorite, meta-diorite and tonalite unit intrudes the upper Paleozoic Mesa Granite (Chapter 2.1.2), suggesting that the Mesa Granite is the oldest unit in the area.

Fig. 2.2 Distribution of the Paleozoic Mesa Granite and diorite, meta-diorite and tonalite units outcropping in the Chuquicamata district. These units form the bulk of the Chuquicamata Hills to the east of the Chuquicamata and Radomiro Tomic deposits. The exotic oxide ore of the South Mine is hosted by metadiorite and amphibolite units.

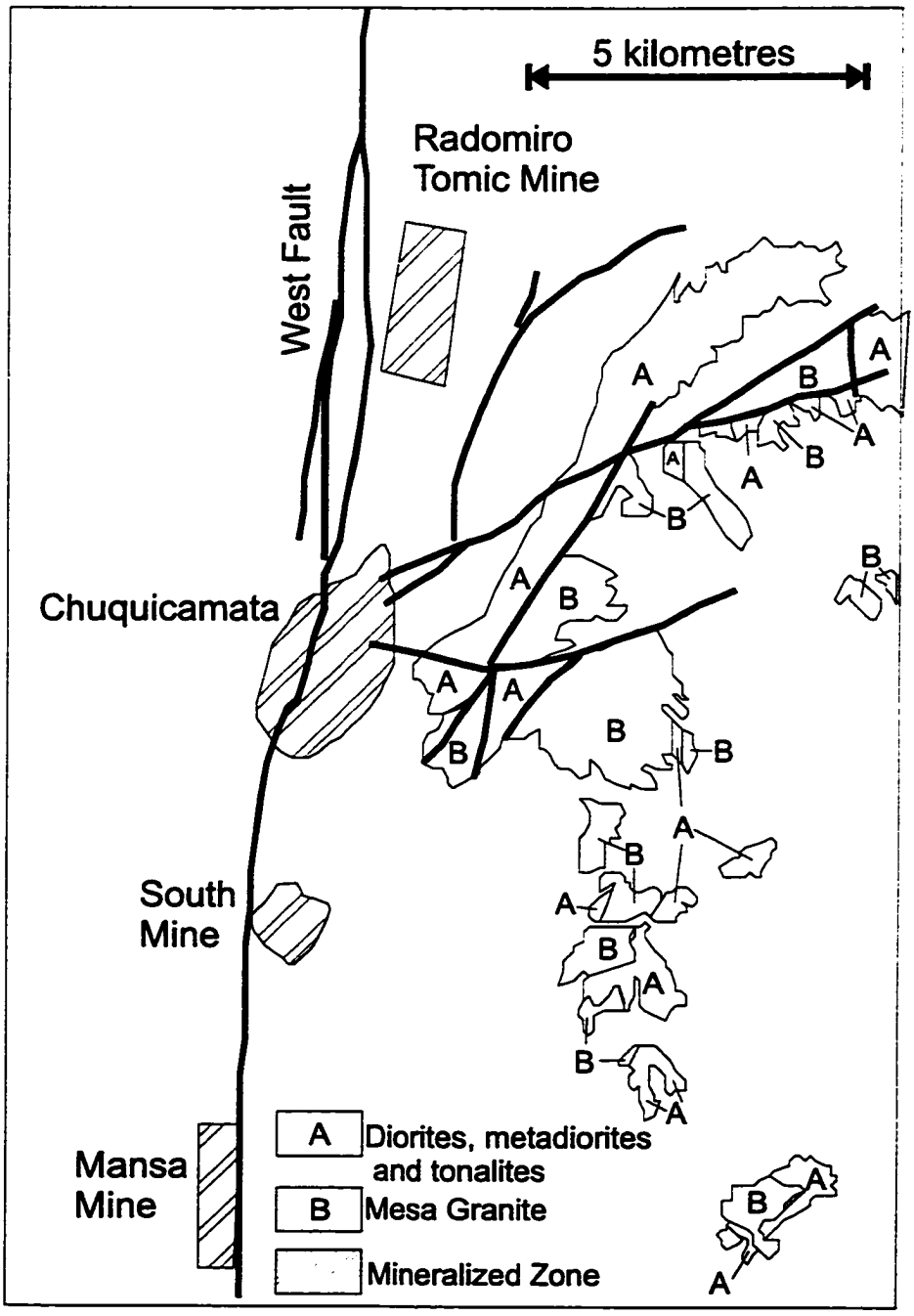

2.1.2 Mesa Granite

Renzetti (1957) defines this unit as having a variety of textural phases from coarse grained to porphyritic containing quartz, partially sericitized plagioclase, K-feldspar, chloritized biotite, and epidote, magnetite and titanite as accessories minerals. Deformation ranges from intergranular fractures and undulatory extinction in quartz to strongly foliated proto-mylonitic fabrics (Tomlinson et al., in prep.). This unit is variably intruded by andesitic and porphyritic rhyolite dikes oriented N-S to NE-SW (Chong and Pardo, 1993) and dioritic to amphibolitic units previously thought to be lower Paleozoic in age (Tomlinson et al., in prep).

Results of K/Ar dating indicate the Mesa Granite to be Permo-Carboniferous in age (305± 4 Ma, in biotite, Marinovic and Lahsen, 1984). Other K/Ar ages, 196±6 Ma and 189±6 Ma (whole rock) are interpreted as minimum ages, as this unit is intruded by Permian diorites (Tomlinson et al., in prep.). The K/Ar whole rock ages may also be the result of a Lower Jurassic alteration event (Tomlinson et al., in prep.).

2.1.3 Paleozoic Summary

The two main units of the Paleozoic terrain, previously comprising the CIMC, are the Mesa Granite and an unnamed unit consisting of diorites, metadiorites and tonalites. The variable textured and deformed Carboniferous-Permian Mesa Granite is intruded by the Permian diorite/meta-diorite unit (Tomlinson et al., in prep.). Andesitic to rhyodacitic dikes within these units may represent feeder systems to younger, probably Cretaceous to Tertiary, volcanic systems related to the Domeyko magmatic arc.

2.2 Mesozoic

Mesozoic units consist of Triassic volcanic and plutonic units and Upper Triassic to Jurassic back-arc sedimentary sequences. The back-arc sequences are associated with the formation of the Jurassic volcano-plutonic arc (Coastal Cordillera) to the west (Fig. 1.2). Chong and Pardo (1993) conclude that the Paleozoic plutono-metamorphic units described in the previous section (Chapter 2.1) were exposed during the Triassic-Jurassic, forming the

bedrock to the basin and providing sedimentary input from further east.

The Jurassic meta-sedimentary units are deformed and are in fault contact with older Triassic East Granodiorite (Chapter 2.2.1.2) and younger Tertiary Chuquicamata Complex (Chapter 2.3.1.3) intrusive units. This thin discontinuous belt of outcrops trends north-north-east and is located to the east of the Chuquicamata and Radomiro Tomic open pits, forming the lower western slopes of the Chuquicamata Hills (Fig. 2.3).

2.2.1 Triassic

2.2.1.1 Agua Dulce Formation

Chong and Pardo (1993) describe the upper Triassic sequence, known as the Agua Dulce Formation (Garcia (1967) *in* Marinovic and Lahsen, 1984) or Tuina Group (Flint et al.,1983) within the Chuquicamata district, as having an angular discordance with underlying Permo-Triassic volcanic rocks. This discordance is not observed in the study area but is represented by fault contacts. The siliciclastic to volcaniclastic sequence is dominated by conglomerate and breccia with beds of siltstones and sandstones intercalated with calc-alkaline lavas and pyroclastic deposits. The sequence fines upward into and is overlain by dolomitic limestones (Chong and Pardo, 1993). Capping this Triassic sequence and grading into Jurassic sediments are shales and calcareous muds that outside of the study area, bear upper Triassic ammonites (Choristoceras, Chong and Pardo, 1993). These sedimentary units are in fault contact with the Middle Triassic Elena and East Granodiorite units.

A series of andesitic to microdioritic metre scale dikes outcrop to the east and northeast of the Chuquicamata open pit. Two populations are present one trending NE-SW and the other NW-SE, both being concentrated in Carboniferous to Triassic plutonic units (Chong and Pardo, 1993; Tominson et al., in prep). These dikes are suggested to be feeder systems to the Late Triassic Agua Dulce Formation (Tomlinson et al., in prep).

Fig. 2.3 Distribution of the Mesozoic units in the Chuquicamata district. Upper Triassic volcanic to siliciclastic and Middle Jurassic calcareous marine sedimentary units are transported south along NNE trending fault systems. These units form the lower slopes of the Chuquicamata Hills to the east and are exposed within the Chuquicamata open pit.

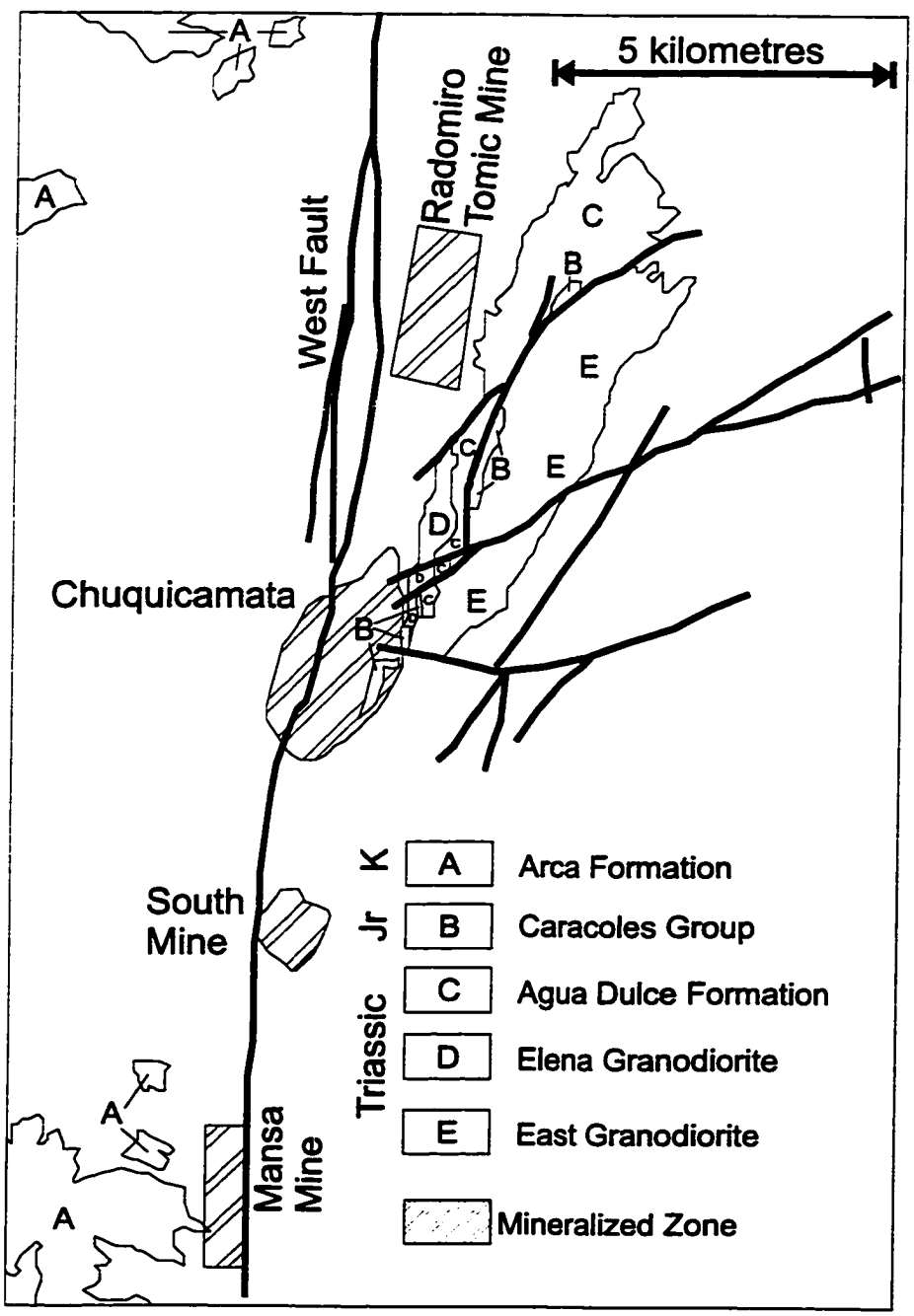

2.2.1.2 East Granodiorite

The most prominent Triassic feature in the district is the large East Granodiorite trending NNE from the Chuquicamata open pit. It is medium to coarse grained hornblende-biotite equigranular granodiorite. Mafic minerals are partially to totally altered to chlorite and plagioclase feldspars are weakly to partially saussuritized.

This unit maintains fault contacts with Triassic-Jurassic sedimentary sequences and intrusive contacts with Permian diorites (Chong and Pardo, 1993). Mafic xenoliths are abundant and may represent remnants or fragments of the Permian units, whose foliation it cuts (Tomlinson et al., in prep.). Similar to the Paleozoic units, this granodiorite is intruded by porphyritic dacite and andesite dikes, which vary in orientation from north-south to northeast-southwest in parallel to the Messabi Fault (Tomlinson and Blanco, 1997a).

^{40}Ar / ^{39}Ar radiometric dating of the East Granodiorite gives ages of 204 ±3 Ma (hornblende, Zentilli, unpublished data), while U/Pb dating of zircons indicate an age of 229 ±2 Ma (Tomlinson et al., in prep). Thus, the radiometric dating indicates that this unit is Triassic rather then the previously suggested Paleozoic (Renzetti, 1957; Ambrus, 1979; Soto, 1979; Marinovic and Lahsen, 1984; Maksaev, 1990; Chong and Pardo, 1993). The argon ages probably represent partially thermally reset ages by the spatially adjacent Messabi shear zone and/or the emplacement of the Chuquicamata intrusive complex.

2.2.1.3 Elena Granodiorite

This granodioritic unit, which outcrops to the east of the Chuquicamata open pit, is in fault contact with Mesozoic meta-sedimentary units (Chong and Pardo, 1993). These authors also describe weak mafic mineral orientations along contacts and attribute these to metamorphic or tectonic processes. Drillcore evaluation shows several metre scale zones of strongly foliated granodioritic units near the granodiorite-metasediment contact (C. Ulriksen, pers.comm., 1995; Zentilli, pers. comm., 1996). These sheared contacts are rarely observed in surface outcrops. The Tertiary Chuquicamata Complex intrudes the Elena Granodiorite having gradational and diffuse contacts.

The Elena Granodiorite was originally described by Renzetti (1957) as having an

equigranular to porphyritic texture with interstitial matrix minerals. The granodiorite is composed of orthoclase, plagioclase (An_{25}-An_{30}), quartz, hornblende, biotite, chlorite, and accessory minerals. There has been some debate over the association of this unit. Some authors have suggested that it is equivalent to the East Porphyry (Chapter 2.3.1.3.1) (Ambrus, 1979). Other authors have equated it with the Triassic East Granodiorite (Aracena, 1981; Tapia, 1980). Mapping during this study showed no distinct contact relationships, other than gradational, between the East Porphyry and Elena Granodiorite. Complicating the contact zone are the faulted blocks of Mesozoic meta-sedimentary units and abundant xenoliths of meta-sedimentary, dioritic, gneissic and quartz vein that are found dominantly within the East Porphyry. However, surface mapping and mapping of the initial open pit by Waterman (1951) concluded that although the contact between East porphyry and Elena appears gradational, Chuquicamata rocks intrude the Elena Granodiorite.

K/Ar and $^{40}Ar/^{39}Ar$ radiometric dates for this unit are inconclusive. Munizaga (1976) reports an age of 125±3.8 Ma (recalculated), Tapia (1980) an age of 38.1±1.5 Ma, and Zentilli (unpublished data, Cu881) an $^{40}Ar/^{39}Ar$ age of 30.8±1.3 Ma. Aracena (1981) and Tapia (1980) interpret the radiometric ages as reset Mesozoic ages by the intrusion of the Chuquicamata porphyry suite. This interpretation has been confirmed by Tomlinson et al.'s (in prep.) U/Pb zircon age of 227±2 Ma.

2.2.2 Jurassic

2.2.2.1 Caracoles Group

The Caracoles Group (Ramirez and Gardeweg, 1982), a marine transgressive sequence, which is concordant over the Upper Triassic Agua Dulce Formation, consists of minor basal conglomerates and sandstones, fossiliferous limestones and calcareous muds, sandstones and shales (Chong and Pardo, 1993). The upper contact is gradational from strictly marine into mixed marine fine grained sediments, topped by the Estratos de San Lorenzo red beds, which marks the transition from marine Jurassic to continental Cretaceous (Chong and Pardo, 1993; Marinovic and Lahsen, 1984). In the study area, only the Middle to Late Jurassic (Bajocian and Oxfordian)section is observed (Chong and Pardo, 1993;

Thomas, 1978). Fault bound sections of this sequence outcrops along the Messabi Fault and are exposed within the Chuquicamata open pit.

Outside the study area, this sequence exhibits open to tight folds that are locally overturned and reverse faulted (Maksaev, 1990; Scheuber and Reutter, 1992; Marinovic and Lahsen, 1984). Fold axes trend NW-SE and N-S to NE-SW. Scheuber and Reutter (1992) indicate that deformation of the Jurassic marine sequence was accommodated by bedding parallel slip that concentrated in steeper fold limbs of anticlines cored by Paleozoic basement and that strike-slip faults initiated along these fold limbs.

2.2.3 Cretaceous

Chong and Pardo (1993) assign a transitional series of marine to continental sedimentary units to the "Tithonian-Neocomian" including the San Salvador Formation (Lira, 1989), the Estratos de San Lorenzo (Marinovic and Lahsen, 1984) and the red beds of Chug-Chug (Chong and Pardo, 1993) indicating that these units do not occur within the vicinity of the Chuquicamata deposit. Red agglomerates located along the lower slopes of the Chuquicamata Hills, which were previously classified as Cretaceous in age (Vega and Bordones, 1981) are now thought to be Triassic (Agua Dulce Formation) (Tomlinson et al., in prep.; Chong and Pardo, 1993).

2.3 Cenozoic

The Early Cenozoic is an important era in the geology of northern Chile, since igneous complexes and associated porphyry copper mineralization were emplaced at this time. Presently outcropping in the Chuquicamata open pit are two Eocene-Oligocene intrusive complexes, the Fortuna and the Chuquicamata (Fig. 2.4). Recent regional mapping (eg. Tomlinson et al., in prep) indicate that correlatable coeval extrusive units associated with these intrusive complexes are not observed in the Chuquicamata District. The association of coeval extrusive units with intrusive complexes hosting porphyry style deposits are proposed for some porphyry models (compare Sillitoe and Bonham, 1984; Gustafson and Hunt, 1975). A period of rapid uplift, erosion and exhumation, as proposed by Maksaev and Zentilli

(1988), may have removed coeval extrusive units. This erosion and exhumation may be evidenced by fluvial deposits with intercalated strata of volcanic ash (30.15±0.26 Ma, May et al., 1996) found within the Calama basin, 20 km to the south and southeast of Chuquicamata, which indicates volcanic activity in the region approximately at the time of one of the mineralization phases at Chuquicamata. Substantial uplift and erosion during and following the intrusion of the Chuquicamata Complex generated thick sequences of Miocene and younger gravels, which cover the Chuquicamata Complex bedrock to the north.

2.3.1 Paleogene

2.3.1.1 Los Picos Diorite

Originally described by Thomas (1978) and further summarized by Vega and Bordones (1981) and Chong and Pardo (1993), this diorite to quartz-monzonite unit is best known 7 km to the west of the Chuquicamata district, where it forms the wall rock to the Fortuna Complex (J. Dilles in Tomlinson et al., in prep.). Diorites of this unit are also observed as roof-pendants in the Fortuna Granodiorite (Chong and Pardo, 1993). K/Ar dates for the Los Picos unit (43.4±1.2 Ma, biotite, Tomlinson et al., in prep.; 45.1±1.8 Ma, biotite, Thomas, 1978) indicate an Eocene age.

2.3.1.2 Fortuna Intrusive Complex

Units within the Fortuna Complex were first described by Renzetti (1957). However, detailed regional mapping by J. Dilles (in Tomlinson et al., in prep.) and mapping completed in this study of the open pit exposures (Fig. 2.5) have redefined the original units. This complex is comprised of four units, three of which, the Fiesta Granodiorite, Tetera and San Lorenzo Porphyries, outcrop in the open pit. The nomenclature used here is that proposed by J. Dilles during the course of his mapping in a SERNAGEOMIN (Chilean Geological Survey) - CODELCO sponsored project (Tomlinson et al., in prep.). Pending formal peer review and publication by those authors it is best to consider this nomenclature as preliminary and informal. An Eocene age for the intrusive suite is based on numerous radiometric ages for Fortuna Complex samples (Table 2.1).

2.3.1.2.1 Antena Granodiorite

This unit, defined by Ambrus (1979), is not exposed in the open pit, but is distinguished from the Fiesta Granodiorite by having a greater abundance of biotite in comparison to amphibole as well as a medium grained equigranular texture. Radiometric age data, which is summarized in Table 2.1, indicates an Eocene age for this granodiorite. Maksaev (1990) presents a similar age for a ductile shear zone found within this unit.

2.3.1.2.2 Fiesta Granodiorite

Initially known as Fortuna Granodiorite (senso stricto Ambrus, 1979), the Eocene-Oligocene (Table 2.1) Fiesta Granodiorite is a medium to coarse grained crowded porphyritic rock with 5-25% matrix. Pale to medium green amphiboles (up to 2 cm), containing inclusions of plagioclase, biotite and magnetite, are characteristic of this unit that is composed of plagioclase, K-feldspar and quartz in a similar groundmass with biotite and magnetite.

2.3.1.2.3 Tetera Porphyry

This unit generally occurs as aplitic dike-like bodies with the wider (>1m) dikes tending towards a more porphyritic texture with <40% plagioclase phenocrysts in an aplitic feldspar-quartz matrix. When associated with the San Lorenzo Porphyry, these aplitic dikes are mineralized with molybdenite near fractured and sheared contacts. Radiometric $^{40}Ar/^{39}Ar$ data (Table 2.1) give Late Eocene ages of 35.5±04 Ma.

Fig. 2.4 Distribution of Cenozoic units in the Chuquicamata district. Chuquicamata Complex units are known to form the bedrock to Neogene gravel sequences, which overlie the Radomiro Tomic deposit. The West Fault forms the contact between the Chuquicamata and Fortuna intrusive complexes.

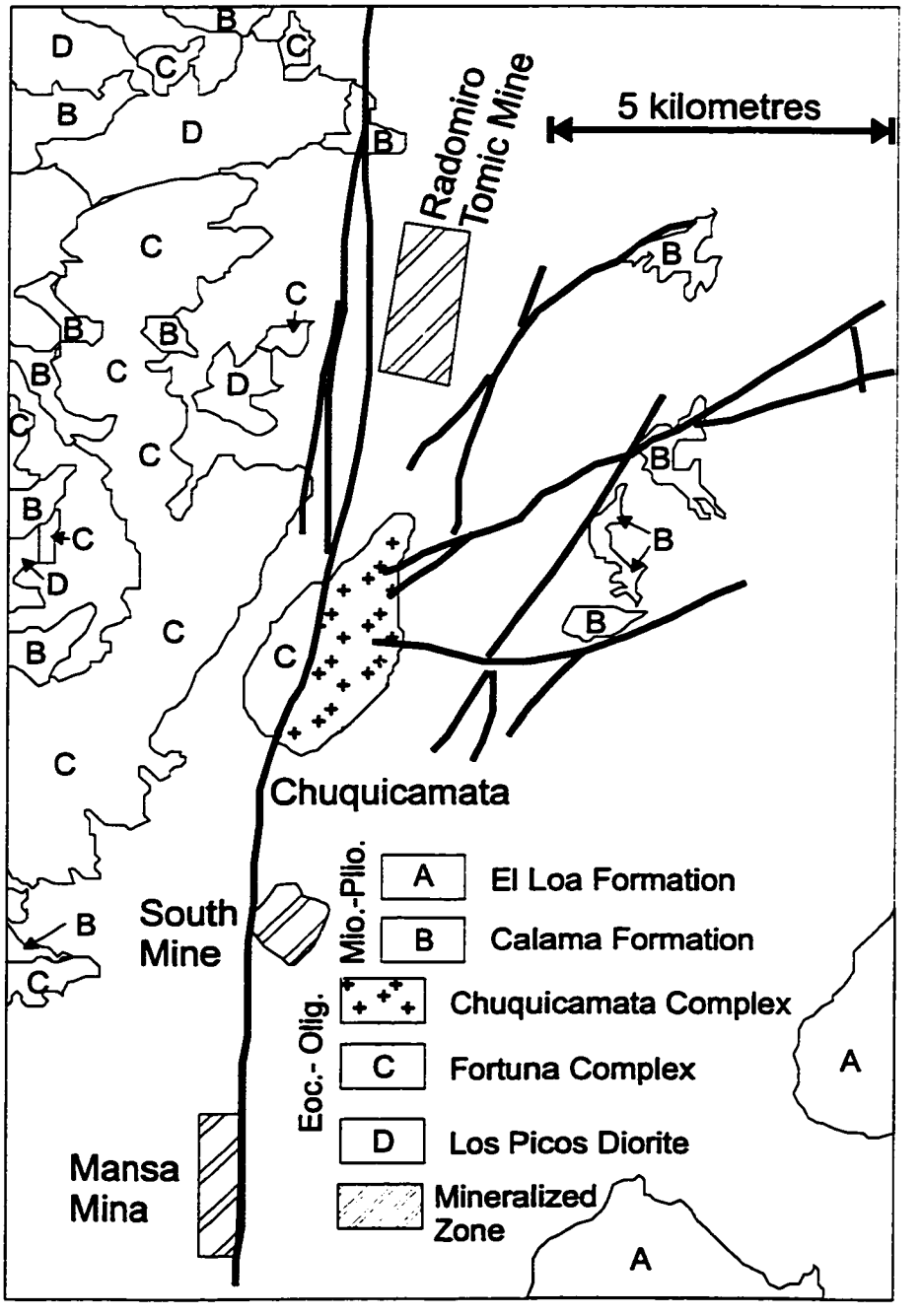

Fig. 2.5 The Fortuna Complex is dominated by the Fiesta Granodiorite, which hosts small bodies of Tetera and San Lorenzo porphyritic units. The porphyritic units are exposed at deeper exposures of the open pit, although thin dikes are present closer to the surface. The West Fault juxtaposes the Fortuna Complex against the Chuquicamata Complex to the east. Faults in unmapped areas are compiled from the Chuquicamata Geomechanics base map.

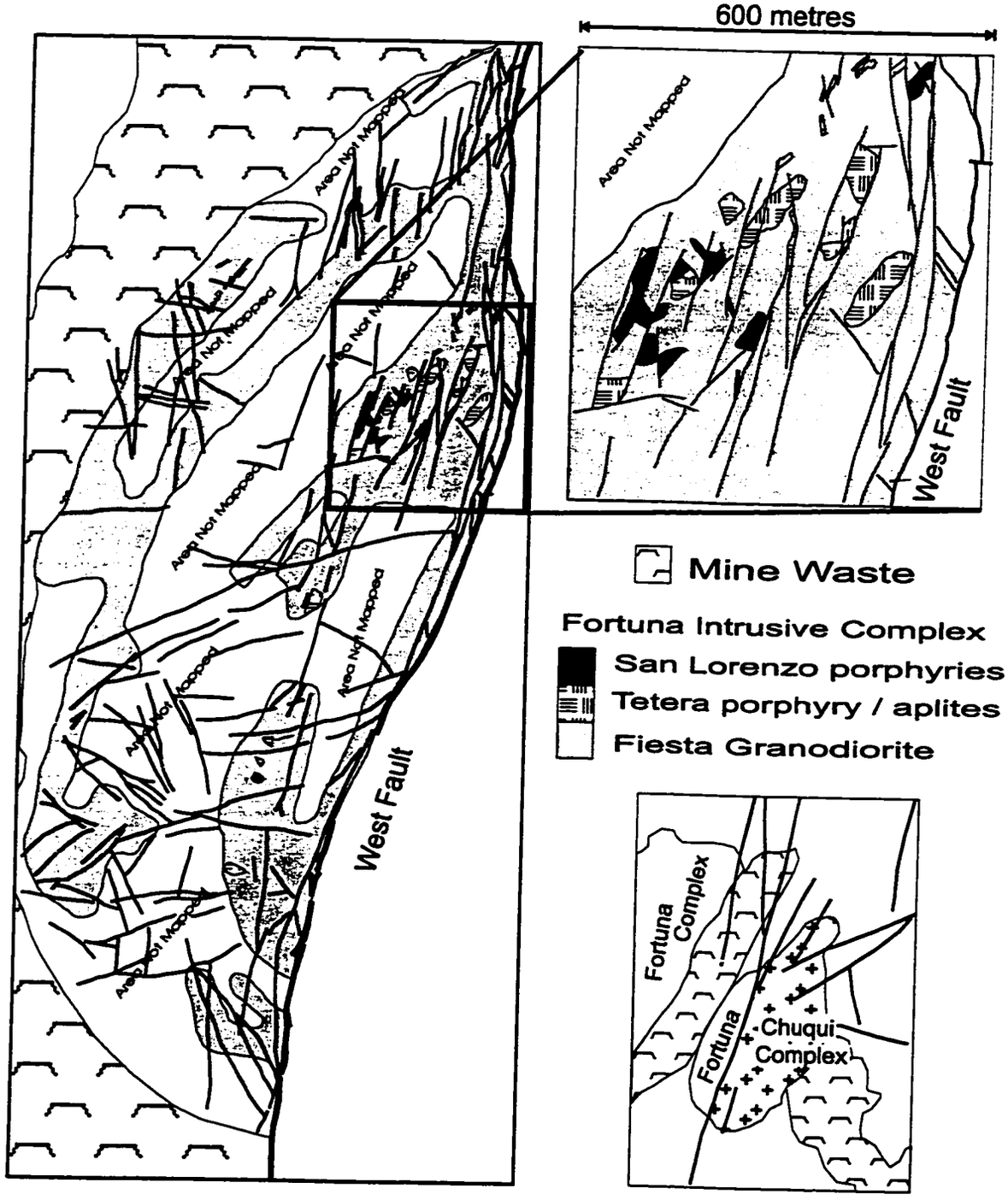

2.3.1.2.4 San Lorenzo Granodiorite Porphyry

This porphyritic granodiorite with a felsic matrix is related to and probably intruded earlier then the more mafic San Lorenzo Quartz-monzodiorite (Chapter 2.3.1.2.5). J. Dilles (pers. comm., 1995) describes this unit as containing 45-60% phenocrysts of plagioclase, biotite, amphibole, quartz, K-feldspar, magnetite and sphene in a light-grey aplitic matrix. This unit is not observed within the open pit.

2.3.1.2.5 San Lorenzo Quartz Monzodiorite

This unit was previously described by Vega (1986) as a porphyritic dacite. It contains 30-50% phenocrysts of plagioclase, amphibole, biotite, magnetite and rare quartz in a fine grained dark grey groundmass. This unit has sharp contacts with the Fiesta and Tetera units which it intrudes.

Mineralization is associated with this unit as the following assemblages: weakly disseminated chalcopyrite throughout the matrix, bornite-chalcopyrite-pyrite replacing biotite and amphibole, and molybdenite- pyrite in veinlets. These assemblages are also found in a halo of undetermined extent around the San Lorenzo intrusion within the Fiesta and Tetera units. The unit appears fresh, although zones of biotitized and chloritized amphiboles and saussauritized plagioclase are present. An Eocene age for this unit was determined by $^{40}Ar/^{39}Ar$ radiometric analyses (Table 2.1).

Table 2.1 Summary of radiometric ages for the Fortuna intrusive suite. TGA= Total gas age.

Lithological Unit	**Age ± 2sigma**	**Method / Mineral**	**Source**
Antena Granodiorite	36.2±1.4	K/Ar Biotite	Ambrus, 1979
	39.5±1.1	K/Ar Biotite	Maksaev et al., 1988b
	39.0±1.2	K/Ar Biotite	Maksaev et al., 1988b
	35.6±1.0	$^{40}Ar/^{39}Ar$ TGA Biotite	Maksaev, 1990
(foliated)	34.8±1.6	$^{40}Ar/^{39}Ar$ TGA Biotite	Maksaev, 1990
	40.6±1.2	K/Ar Biotite	Tomlinson et al., in prep.
	39.6±1.2	K/Ar Biotite	Tomlinson et al., in prep.
	36.3±1.1	K/Ar Biotite	Tomlinson et al., in prep.
Fiesta Granodiorite	37.8±1.2	K/Ar Biotite	Quirt, 1972
	35.9±1.0	K/Ar Biotite	Ruiz et al., 1965 in Ambrus, 1979
	39.0±3.0	K/Ar Biotite	Geochron, 1977 in Ambrus, 1979
	37.3±1.2	K/Ar Biotite	Tomlinson et al., in prep.
	39.5±0.5	$^{40}Ar/^{39}Ar$ Hornblende	Cuesta Research, unpublished.
	36.4±0.3	$^{40}Ar/^{39}Ar$ Biotite	Cuesta Research, unpublished.
	35.3±0.3	$^{40}Ar/^{39}Ar$ K-feldspar	Cuesta Research, unpublished.
	36.9±0.3	$^{40}Ar/^{39}Ar$ TGA Biotite	Cuesta Research, unpublished.
	34.9±0.3	$^{40}Ar/^{39}Ar$ K-feldspar	Cuesta Research, unpublished.
	38.4±0.5	$^{40}Ar/^{39}Ar$ Hornblende	Cuesta Research, unpublished.
	35.9±0.3	$^{40}Ar/^{39}Ar$ TGA Biotite	Cuesta Research, unpublished.
	36.1±0.4	$^{40}Ar/^{39}Ar$ K-feldspar	Zentilli, unpublished data
Tetera Aplitic Porphyry	35.5±0.4	$^{40}Ar/^{39}Ar$ K-feldspar	Zentilli, unpublished data
San Lorenzo Porphyry	38.5±1.1	K/Ar Biotite	Tomlinson et al., in prep.
	37.1±0.9	K/Ar Biotite	Tomlinson et al., in prep.
		$^{40}Ar/^{39}Ar$ Hornblende	Zentilli, unpublished data

2.3.1.3 Chuquicamata Intrusive Complex (CIC)

The CIC is a 14 km long by 0.5-2 km wide intrusive complex that extends in a NNE direction. Except for a series of deeply weathered outcrops exposed along the western edge of the Chuquicamata Hills, it is buried beneath Miocene gravels. The only good exposures are found within the Chuquicamata and Radomiro Tomic open pit mines and an extensive collection of drillcore. It is in fault and intrusive contact with Mesozoic igneous and metamorphosed volcano-sedimentary sequences to the east and is bound to the west by the West Fault. Based on textural variations, the granodioritic intrusion is composed of three main phases: the East Porphyry, the West Porphyry and the Banco Porphyry (Renzetti, 1957; Ambrus, 1979; Aracena, 1981; Parada et al., 1987; Martin et al., 1993).

The complex is weakly mineralized throughout its entire length (0.3% Cu, Ambrus, 1979) having at least two economic ore concentrations. One is the Chuquicamata deposit (Chapter 3.0), located in the southernmost exposure of the CIC, and the other is the Radomiro Tomic deposit located approximately 5 km to the north, a possible extension of Chuquicamata.

For further lithological descriptions, the reader is referred to Chapter 3 where the details of the Chuquicamata Intrusive Complex and the associated porphyry copper deposit are presented.

2.3.2 Neogene

Neogene stratigraphy (Fig. 2.6) in and around the Chuquicamata district is represented by at least three sedimentary units with intercalated tuffs and ignimbrites: the Oligocene Calama Formation, the Miocene-Pliocene El Loa Formation and the yet unnamed Miocene to Recent gravels (Naranjo and Paskoff, 1981; Tomlinson et al., in prep.). Work by May et al. (1996) in the Calama Basin, east and south of the Chuquicamata district, has defined five unconformable sedimentary successions ranging in age from Oligocene to Quaternary.

The lower gravel unit of the Oligocene Calama Formation, defined as alluvial braidplain conglomerates by May et al. (1996), is equivalent to those gravels described by

Soto (1979) as bearing clasts of metamorphic, andesitic and granitic compositions, and Munchmeyer and Urqueta's (1974) unit comprising fragments of porphyritic rocks and clasts of the Fortuna Granodiorite. An intercalated ash at the top of this unit has been dated at 30.15+/-0.26 Ma (May et al., 1996).

Discordantly overlying the Calama Formation is the El Loa Formation. This formation is composed of a well-bedded basal section of diatomites containing gastropods and root casts, topped by red shales and an upper sequence of ignimbrites overlain by calcarenites and limestones (Chong and Pardo, 1993; Naranjo and Paskoff, 1981; 1982). Naranjo and Paskoff (1981) propose a period of intense erosion prior to the deposition of the El Loa Formation, while May et al. (1996) suggest a cessation of sedimentation associated with the regional climate change to hyper-arid conditions as proposed by Alpers and Brimhall (1988).

Unconformably overlying the previous formations are unnamed Miocene units of sorted and stratified gravels having diorite, amphibolite, leached and altered porphyry and Mesa Granite clasts, which are cemented by gypsum and copper oxides (Munchmeyer and Urqueta, 1974). In the Mansa Mina shaft, weakly sulphate-cemented gravels of andesitic and granodioritic compositions are observed (Chong and Pardo, 1993). Moving basinward, south and east, gravel strata becomes dominated by fluvial and playa sediments which are topped by gypcrete (May et al., 1996). Ash layers within the sediments give an age of 19.62±0.36 Ma ($^{40}Ar/^{39}Ar$; May et al., 1996). A Miocene-Pliocene upper unit of alluvial to lacustrine sediments with intercalated ignimbrites and ash tuffs within the uppermost gravels at Mina Sur (8.6±0.4 Ma, K/Ar, biotite, Hunt, 1970) is unconformably overlain by fluvial, lacustrine and palustrine carbonate facies dated between 6 and 3 Ma (May et al., 1996). The youngest unit of this Neogene sequence is an ash tuff of latest Pliocene age (2.8±0.7 Ma, $^{40}Ar/^{39}Ar$, amphibole, M. Zentilli, unpublished data) that unconformably overlies Triassic andesitic agglomerates to the north-east of the Chuquicamata open pit.

2.4 Quaternary

Fluvio-lacustrine deposits with minor associated salts (Depositos de Playas), salars of mixed salts and carbonates, and alluvial-colluvial deposits are the dominant Quaternary sedimentary units in the Chuquicamata district (Chong and Pardo, 1993; May et al.,1996).

Fig. 2.6 Paleogene to Neogene stratigraphy from in and around the Chuquicamata district from May et al. (1996). These authors also indicate the relationship of folding phases and motions on the West Fault (stippled areas in respective columns) to the Calama Formation, the El Loa Formation and the overlying Miocene-Pliocene gravels. Radiometric ages are from May et al., (1996).

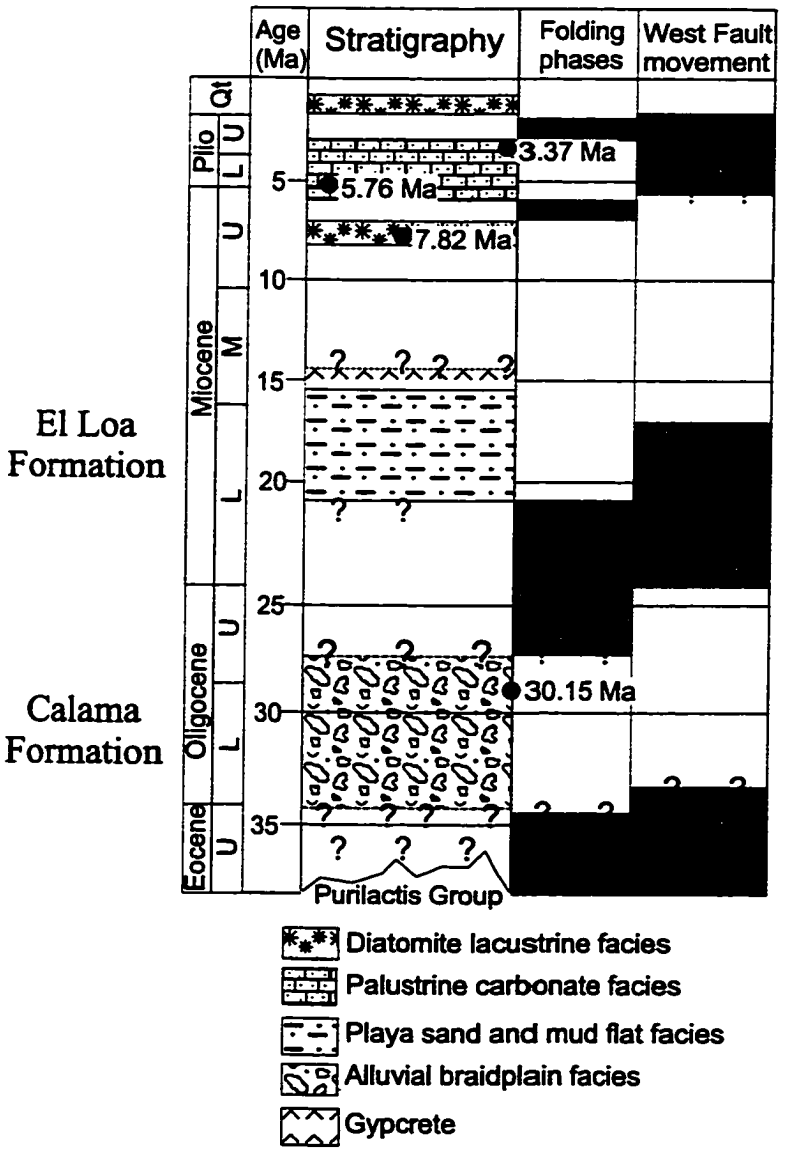

2.5 Tectonic Evolution of the Domeyko Area

In Andean tectonics, two main orogenic cycles are evoked: the Paleozoic Hercynic (Coira et al., 1982) or Gondwana (Mpodozis and Ramos, 1989) cycle, during which the development of magmatic arcs and accretion of micro-continental blocks caused lateral growth (westward) of the South American margin and the Mesozoic-Cenozoic Andean cycle, during which subduction-related tectono-magmatic arcs developed over late Paleozoic basement (Coira et al.,1982; Mpodozis and Ramos, 1989). During the Andean cycle, the magmatic arcs and associated mineralization intermittently, yet progressively, migrated eastwards through time (Maksaev et al., 1988; Maksaev and Zentilli, 1988; Maksaev, 1990; Boric et al, 1990; Scheuber and Reutter, 1992).

2.5.1 Gondwana Tectonic Cycle

During the Cambrian to Ordovician, the Domeyko region would have been located at the southeastern edge of the Precambrian Arequipa Massif within a region of localized magmatic arc development. This Precambrian landmass eroded into a probable open ocean to the west and a narrow sea to the east, depositing sediments over oceanic basement (Mpodozis and Ramos, 1989). Accretion of the Arequipa Massif to the central-western South American margin created a topographic high that provided sediments to the Domeyko area over continental basement, and to the west over proposed oceanic basement (Mpodozis and Ramos, 1989).

The development of a magmatic arc within the accreted terranes during the Carboniferous to middle Triassic, follows the initiation of eastwards directed subduction (Mpodozis and Ramos, 1989; Coira et al., 1982; Maksaev, 1990 and references therein). Kay et al. (1989) and Bahlburg et al. (1988) suggest this Carboniferous to Triassic magmatic arc displays a continental rift to within plate magmatic arc affinity based on geochemical data. In the Domeyko region, this arc is represented by the Permo-Carboniferous Mesa Granite, the Triassic East and Elena Granodiorites and volcano- sedimentary units of the Agua Dulce Formation. Maksaev (1990) summarizes that the Carboniferous to Triassic magmatic arc, the Gondwana magmatic arc of Ramos et al. (1986), followed the middle to late Carboniferous

Chanic tectonic event, and represents a static magmatic front over a stable convergent subduction system at the plate margin of Gondwana.

2.5.2 Andean Cycle

During the early Mesozoic, a major westward shift of the magmatic arc from the Domeyko region to the present day coast was the result of major crustal movements during the Middle to Late Triassic (Maksaev, 1990; Coria et al., 1982; Mpodozis and Ramos, 1989). Maksaev (1990) referred to this as the Atacamenian tectonic event, which he hypothesized may relate to the accretion of an exotic terrane, or the subduction of an oceanic ridge, that resulted in the establishment of a subduction zone further west. This tectonic event is recorded by an unconformity at the base of Upper Triassic strata outside of the study area (Maksaev, 1990).

Late Triassic igneous activity continued through the Middle Jurassic - Early Cretaceous along the coast, culminating with the emplacement of plutonic rocks within an extensional magmatic arc setting (Grocott et al., 1993; Scheuber and Reutter, 1992). According to Mpodozis and Ramos (1989) and Coria et al. (1982), a Late Triassic marine transgression initiated an ensialic back-arc (Tarapaca) basin in the Domeyko area, in which basin subsidence was controlled by extensional tectonics associated with the coastal arc (Grocott et al., 1993). Sediments, derived in part from the coastal arc and from the east of the Domeyko region, accumulated in the back-arc Tarapaca Basin from Late Triassic (terrestrial and marine) through Jurassic (calcareous marine) to middle Cretaceous (red beds) (Chong and Pardo, 1993; Naranjo and Paskoff, 1982; Maksaev, 1990; Mpodozis and Ramos, 1989; Coria et al., 1982). The termination of the coastal arc activity in the Early Cretaceous was accompanied by a change to transpressional strike-slip tectonics (Grocott et al., 1993).

A plate tectonic reorganization, from high angle sinistral convergence of the Aluk plate to smaller angle dextral convergence of the Farallon plate, during the middle to Late Cretaceous imposed a compressional tectonic regime (Peruvian tectonic event) on the South American margin. This event inverted the Triassic through Cretaceous back-arc basin, forming open to tight folds with NW-SE and N-S to NE-SW fold axes (Maksaev, 1990;

Marinovic and Lahsen, 1984; Scheuber and Reutter 1992; Chong and Pardo, 1993). Following the Peruvian tectonic phase, magmatism migrated eastwards towards the Domeyko region (Scheuber and Reutter, 1992; Maksaev et al., 1988).

Magmatism in the Domeyko arc continued from the Late Cretaceous through to the Oligocene with uplift and magmatism peaking in the central Domeyko Cordillera during the Eocene-Oligocene, following the Eocene Incaic tectonic event (38.5 Ma, Scheuber and Reutter, 1992; Maksaev, 1979). Multiple magmato-hydrothermal systems were emplaced along a reactivated(?) strike-slip fault system following this event, forming the porphyry copper deposits found within the Chuquicamata district (Scheuber and Reutter, 1992; Maksaev et al., 1988a, 1988b; Maksaev, 1989, 1990; Boric et al., 1990; Mpodozis and Ramos, 1989).

Subsequently, a Miocene change in plate kinematics caused a reversal of the strike-slip system of the Domeyko Cordillera and a shift of the magmatic arc eastwards to its present location in the Main Andean Ranges. This deformation phase is known as the Quechua tectonic event (Maksaev, 1990).

2.5.3 The Domeyko Fault System

The intra-arc, Domeyko Fault System, an approximately 40 km wide zone of distributed deformation, is generally contained within the north-south trending Late Cretaceous to late Paleogene, Domeyko Cordillera in northern Chile (Fig. 1.2). Initiation and growth of this fault system is associated with Eocene shortening that can be related to a period of oblique convergence of the Nazca plate beneath the South American plate (Scheuber and Reutter, 1992; Reutter, et al., 1994, 1996; Maksaev, 1990; Sillitoe, 1972). The fault system bounds several upper Paleozoic crustal blocks that were uplifted along high angle reverse faults during the Cretaceous (Tomlinson and Blanco, 1997a) and displaces Paleogene volcanic units (Maksaev, 1990). Tomlinson and Blanco (1997a) have constrained the initial post-Paleozoic activity of this fault system to the middle Eocene (~44 Ma). The Eocene shortening continued until approximately 37 Ma (Reutter et al., 1996; Tomlinson and Blanco, 1997a). During which time transcurrent fault activity began to concentrate along the

West Fault System, a dominant segment of the Domeyko Fault System.

2.5.3.1 The West Fault System

In the Antofagasta region, the intra-arc Domeyko Fault System includes a dominant eastern segment known as the West Fault System. This fault system, which may continue into southern Peru (Clark, 1993), is associated with numerous world class porphyry-type deposits in northern Chile and includes: the Sulfato Fault near Copaquire (Hollister and Bernstein, 1975), the Sierra Castillo Fault at El Salvador-Potrerillos (Tomlinson et al., 1993; Tomlinson, 1994) and the West Fault at Chuquicamata (Perry, 1952; Taylor, 1935; Sillitoe, 1973; Lindsay et al., 1995; Reutter et al., 1995)(Fig. 2.7). Thus the importance of the West Fault System is not confined to its dissection of the Chuquicamata porphyry copper deposit (see Reutter et al., 1995), but is important as an intra-continental boundary for plate and regional tectonics, magma emplacement and fluid mobilization, as well as being a control on the localization of a great number of world class porphyry deposits.

Despite the importance of the West Fault System, it has had until recently little study in terms of domain extent, magnitude and sense of displacement, characterization of physical and chemical properties, or evaluation of activity. Many of these topics are of a regional nature, outside the research bounds of this thesis, and are being completed by Tomlinson et al., (in prep). However, excavation of the open pit at Chuquicamata allows an unprecedented 3-dimensional exposure of several branches of the West Fault System including its centerpiece, the West Fault, an early pre-cursor, the Messabi Fault, and other important faults related to the mineralization at Chuquicamata that are characterized in later chapters. The field data derived from in and around this unique exposure allows a detailed study of the structural evolution of magmatic-arc tectonics and the control of emplacement and mineralization of the Chuquicamata deposit.

As the West Fault is also known as the West Fissure (Lopez, 1939, 1942; Perry, 1952; Taylor, 1935; Maksaev, 1990; Reutter et al.,1993, 1996), it is proposed here that the term West Fault System be reserved to describe the regional fault system, the central strike-slip segment of the Domeyko Fault System, and that West Fault be used in the historical

sense as that gouge-bearing fault zone limiting differing lithologies, alteration and mineralization assemblages found within the Chuquicamata porphyry copper deposit and district.

2.6 Summary

Eastward migration of the deformation and magmatic front to the Domeyko Cordillera in the late Cretaceous is related to plate tectonic adjustments. Convergence rates and directions were substantially modified (Pilger, 1984; Pardo-Casas and Molnar, 1987), changing from low relative velocity, strongly oblique convergence, resulting in crustal extension during the latest Mesozoic (see Grocott et al., 1993, 1994), to high relative velocity, intermediate-angle oblique convergence, resulting in crustal transpression and the initiation of the Domeyko Fault System during the early Cenozoic (Scheuber and Reutter, 1992; Reutter et al., 1993, 1996).

Deformation and uplift associated with the Eocene Incaic tectonic event was followed by the emplacement of Eocene-Oligocene plutonic complexes, within which multiple magmato-hydrothermal porphyry copper systems developed. Deformation and displacement along the West Fault System continued periodically during and following the emplacement of the porphyry copper systems. Uplift, extreme erosion and exhumation of Permo-Carboniferous to Tertiary units, during the Quechua tectonic event, deposited Miocene-Pliocene conglomeratic gravels into intermontane basins flanking the Domeyko Cordillera. A stabilization of uplift and exhumation during the late Tertiary and a substantial climate change to one of super-aridity (Alpers and Brimhall, 1988) allowed for the preservation of several economic mineral deposits, including Chuquicamata in northern Chile.

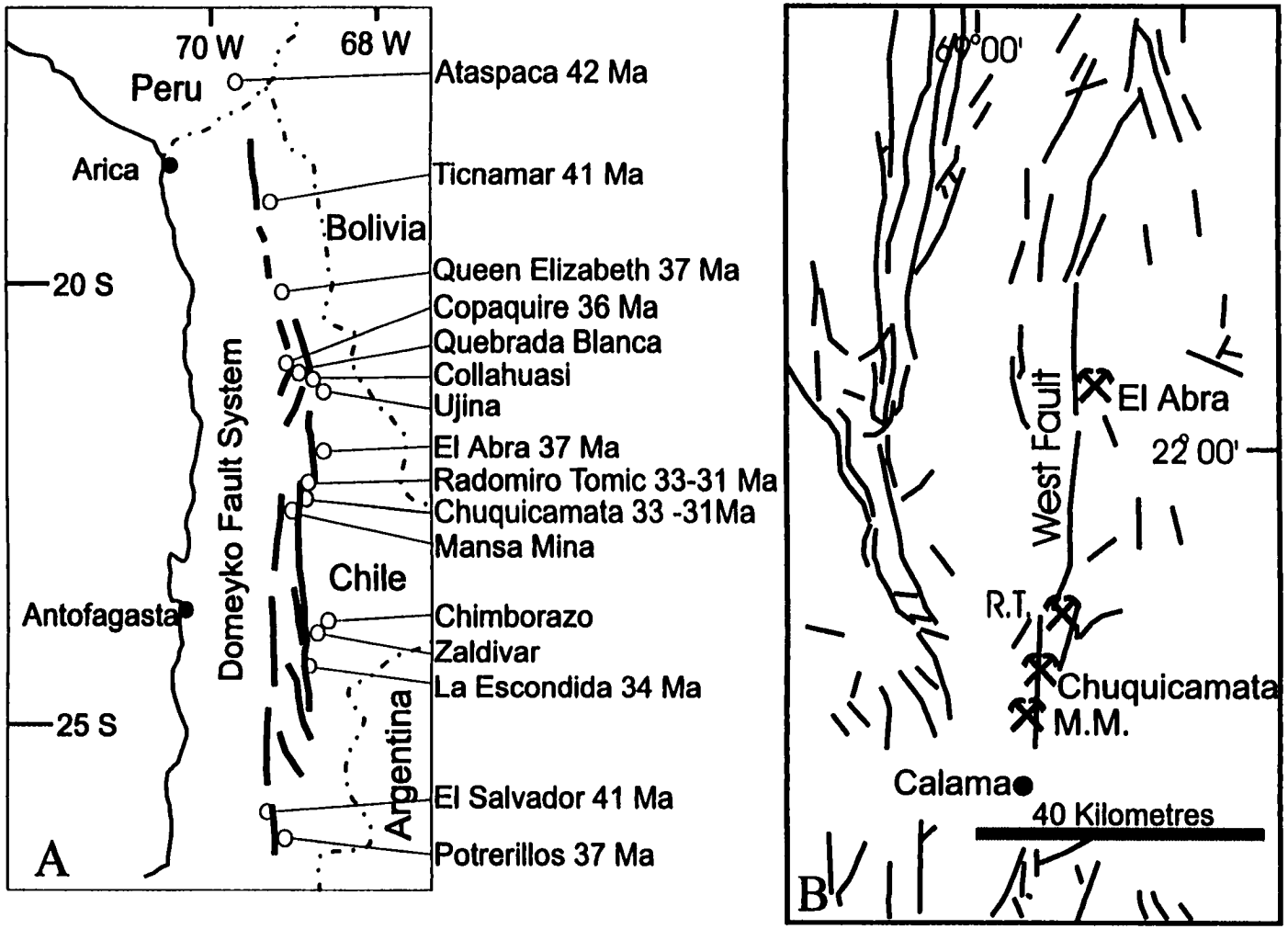

Fig. 2.7 A) The Domeyko Fault System is illustrated with its numerous associated porphyry copper deposits (compiled from Maksaev, 1990; Clark, 1993). (B) The West Fault System, comprised of numerous fault segments, is the easternmost part of the Domeyko System in the Antofagasta region. These fault systems are associated with a number of world class porphyry copper deposits including Chuquicamata.

Chapter 3. The Chuquicamata Porphyry Copper Deposit

This chapter introduces the Chuquicamata porphyry deposit study area through a description of the deposit geology. General geological aspects of the deposit's host lithologies, the main alteration facies and sub-facies, and the main sulphide mineral stages and assemblages are presented. Structural aspects of the deposit are briefly mentioned in this chapter and are described and discussed in more detail in subsequent chapters that form the main focus of this study. The reader is referred to the following chapters that focus on the deformational stages observable within the Chuquicamata deposit: Chapter 4-pre-mineralization deformation, Chapter 5-stockwork mineralization, Chapter 6-syn-mineralization fault systems and vein arrays, and Chapter 7-post mineralization deformation.

3.1 Introduction to the Study Area

Chuquicamata district (Fig. 2.1), is located within the Domeyko Cordillera, a rugged, longitudinal mountain range with maximum altitudes of 4500 m. The Domeyko Cordillera is one of six north-south trending physiographic units located within the Antofagasta region of northern Chile (Fig. 1.1).

Regional geology (already detailed in Chapter 2.0) includes Carboniferous through Middle Triassic plutonic rocks, remnants of a late Paleozoic magmatic arc upon which the Tertiary arc was built. Folded Jurassic meta-sedimentary units, that represent an inverted back-arc basin that formed during the Late Cretaceous Peruvian tectonic phase. These Paleozoic and Mesozoic units were subsequently intruded by Eocene plutons of the Tertiary magmatic arc. Following the Eocene Incaic tectonic phase, magmatism renewed in the Oligocene with the emplacement of plutonic complexes which generated multiple magmato-hydrothermal systems resulting in porphyry copper deposits. Strong uplift, erosion and exhumation, initiated during the Eocene, continued into the Miocene, resulting in the deposition of thick gravel sequences into basins along the flanks of the Domeyko Cordillera until the Pliocene.

3.2 Chuquicamata Host Rock Lithologies

The mineralization of the Chuquicamata porphyry copper deposit is contained within three textural phases of the Chuquicamata Intrusive Complex (CIC) (Fig. 3.1). The following descriptions of the East Porphyry, West Porphyry and Banco Porphyry are based on field observations by the author and those of previous studies (Renzetti, 1957; Langerfeldt, 1964; Ambrus, 1979; Soto, 1979; Aracena, 1981; Alvarez et al., 1980; Martin et al., 1993). An age of intrusion, or emplacement, for this intrusive complex has yet to be established (Zentilli et al., 1994b). Prior to absolute age dating, it is suggested that further petrological studies be undertaken to identify and characterize each textural phase and any sub-phase, as well as to clearly identify contact relationships between phases.

3.2.1 East Porphyry

The most extensive unit in the Chuquicamata complex, the East Porphyry, is characterized by a crowded porphyritic texture where phenocrysts are in corner or edge contact. This unit is very light in colour, almost whitish, due to the abundant plagioclase phenocrysts. Phenocrystic phases (>65%) include subhedral to euhedral plagioclase laths 2-4 mm in length, poikilitic K-feldspar megacrysts up to 5 cm in length that enclose grains of plagioclase, quartz and biotite, biotite booklets 2-5 mm in diameter, irregular to oblate quartz eyes 2-10 mm in diameter and rare amphibole phenocrysts approximately 3-5 mm in length. Quartz, K-feldspar and lesser amounts of plagioclase compose the medium-grain groundmass. This unit is classified as a matrix-poor monzogranitic porphyry with an interstitial matrix (<15%). The East Porphyry is distinguished from the other textural phases by its crowded texture and the presence of amphibole, or the biotite pseudomorphs of amphibole. The Banco and West Porphyries have a lesser volume of phenocrysts and greater proportions of groundmass. The East Porphyry has gradational contacts with the West Porphyry and sharp to gradational contacts with the Banco Porphyry which intrudes it. This unit intrudes and hosts xenoliths or roof pendant remnants of the Mesozoic metasedimentary sequence (Chapter 2.2). Least altered samples of the East Porphyry give radiometric ages of 34-36 Ma (Table 3.1) (Reynolds et al., in press; Zentilli et al., 1995).

3.2.2 West Porphyry

Exposure of this unit is restricted to the uppermost benches of the north wall in the Chuquicamata open pit (Fig. 3.1). The light pink West Porphyry has an open porphyritic texture with phenocrysts (10-15%) that are rarely in contact. Phenocrystic phases comprise 15-30% of this matrix-dominated porphyry and include euhedral plagioclase feldspar laths 1-3 mm in length, zoned poikilitic K-feldspar megacrysts up to 5 cm in length, rounded quartz eyes 5-10 mm in diameter and biotite booklets 1-3 mm in diameter. The surrounding aplitic groundmass is composed of quartz, K-feldspar, minor plagioclase and biotite. This unit is classified as a monzogranite. The West Porphyry is distinguished from the East Porphyry by its increased proportion of matrix, open texture, or uncommon contact between phenocrysts, and lack of amphibole phenocrysts and from the Banco Porphyry by its colour, single phenocryst size population and aplitic matrix. The West Porphyry has gradational contacts with the East Porphyry and is not observed to be in contact with the Banco Porphyry. Ambrus (1979) indicates a probable reset age of 31.8±0.9 Ma for this unit (Table 3.1).

Fig. 3.1 (A) Surface distribution map of the East Porphyry, the West Porphyry and the Banco Porphyry textural units of the Chuquicamata Complex mapped during this study within the 1995 open pit. (B) Surface distribution of the same units compiled by B. Applegate within the 1966 open pit. Comparison of the distributions shows the downward pinching-out of the West Porphyry unit, the vertical nature of the Banco Porphyry and a thinning of the quartz-sericite zone against the West Fault. The difference in elevation between A and B is approximately 300m. Chuquicamata grid coordinates, N5000 and E4000 are shown for correlation purposes. Both maps are illustrated at the same scale.

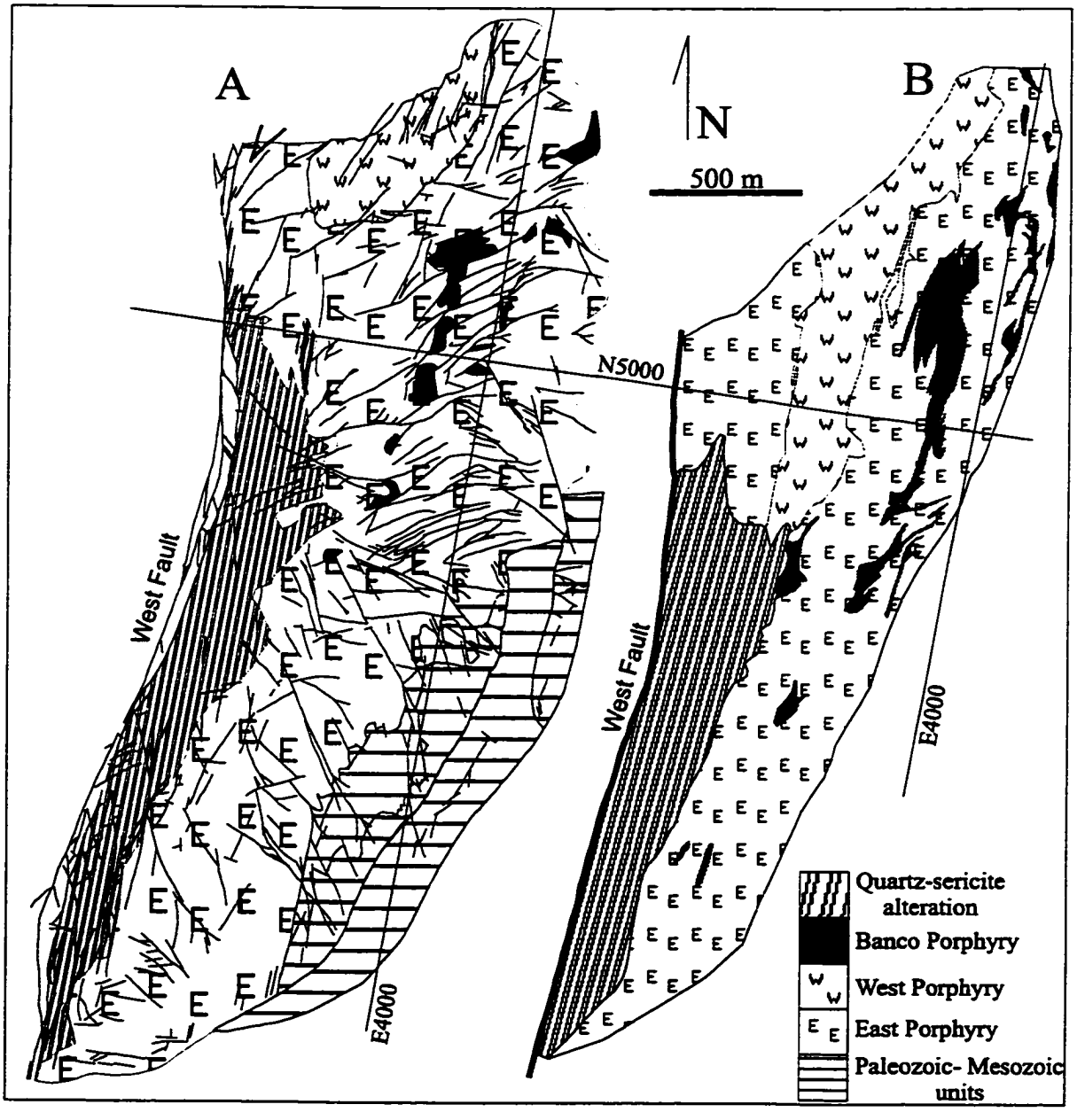

3.2.3 Banco Porphyry

The Banco Porphyry outcrops as a series of NNE trending dike-like bodies, up to 150 m wide, intruding the East Porphyry in the northern sector of the open pit and to the northeast of the mine (Fig. 3.1). This light- to medium-grey unit has an open porphyritic texture with phenocrysts (30%) that are commonly in point or edge contact within an aphanitic groundmass. It is commonly referred to as the 'double porphyry' due to a bimodal population of euhedral-subhedral plagioclase phenocrysts (3-4 mm and 1-2 mm). Other phenocrystic phases include K-feldspar megacrysts up to 5 cm in length, rounded to flattened quartz eyes (up to 1 cm) and rare biotite (1-2 mm) contained in an aphanitic quartz-biotite-(K-feldspar) matrix. This unit is classified as a monzodioritic porphyry. The Banco Porphyry is easily distinguished from the West Porphyry by the darker colour of its groundmass and from the East Porphyry by its colour and open uncrowded porphyritic texture. Intrusive contacts with the East Porphyry are sharp to gradational. The Banco Porphyry has not been observed in contact with the West Porphyry. Least altered samples give ages of approximately 33 Ma (Table 3.1) (Reynolds et al., in press).

Table 3.1 Compilation of available age data for least altered Chuquicamata units. Ages from Reynolds et al.(in press) are plateau ages except where total gas ages (TGA) are indicated. The indicated age of the West Porphyry is likely the result of later thermal resetting.

Lithological Unit	Age± (2sigma)	Method / Mineral	Source
East Porphyry	34.2±0.68	$^{40}Ar/^{39}Ar$, K-feldspar	Reynolds et al., in press
	33.4±0.66	$^{40}Ar/^{39}Ar$, K-feldspar	Reynolds et al., in press
	33.7±1.0	$^{40}Ar/^{39}Ar$, TGA Biotite concentrate	Reynolds et al., in press
	35.0±1.0	$^{40}Ar/^{39}Ar$, TGA Biotite single crystal	Reynolds et al., in press
West Porphyry	31.8±0.9	K/Ar biotite	Ambrus, 1979
Banco Porphyry	33.8±1.3	K/Ar biotite	Alvarez et al. 1980
	33.1±0.2	$^{40}Ar/^{39}Ar$, K-feldspar	Reynolds et al., in press

3.2.4 Lithologic Distribution and Contact Relationships

The East, West and Banco porphyries are the most common textural types in the Chuquicamata Intrusive Complex with the East Porphyry being the dominant unit making up approximately 80% of the exposure at the deposit. The West and Banco porphyries make up approximately 5% each with the remaining 10% belonging to a strongly altered quartz-sericitic rock whose protolith unit is unclear (Chapter 3.3.3). All of the porphyritic units follow the NNE trend of the intrusive complex.

The West Porphyry, restricted to northern exposures in the Chuquicamata open pit, parallels the NNE orientation of the CIC. Prior lithologic distributions compiled by Applegate (1966) shows this unit occupying up to one quarter of the past exposure (Fig 3.1B). Applegate's (1966) map pattern compared with that interpreted from surface mapping undertaken by this study indicates that the dike-like unit has pinched out at depth. The elevation difference between surface maps is greater than 300 metres.

The Banco porphyry occurs as a series of dikes with interpreted lengths on the order of several hundreds of metres and variable widths generally less then 100 m. The Banco dikes parallel the NNE CIC trend along the eastern side of the open pit. Comparison of past and present surface maps shows that the Banco dikes maintain a vertical to sub-vertical continuity (Fig. 3.1 A and B). Drillcore mapping by mine geologists indicates that the Banco Porphyry continues at depth in the eastern sector of the mine.

The East and Banco porphyries commonly show a sharp contact relation, which is often obscured by the presence of thick veins parallelling the apparent contact, and an uncommon gradational contact relation. Similarly, the East and West Porphyries have a gradational contact relationship where the amount of matrix material gradually increases over tens to several tens of metres. Contact relationships between the Banco and West Porphyry units are not expected to be observed in the Chuquicamata open pit owing to their spatial separation and parallel trends. The contact relationships may be observable in the Radomiro Tomic open pit further north.

The East Porphyry is the only unit that maintains contact relationships with rock units outside of the Chuquicamata Complex. Thin, <30 cm, medium grained quartz-K-feldspar

apotheses of the East Porphyry intrude the Mesozoic metasedimentary sequence (Chapter 2.2), crosscutting stratigraphy and in some places being displaced by bedding parallel shear planes. Observable in the upper eastern benches of the open pit are angular xenoliths of metasedimentary, granitic and dioritic origins, including gneissic and massive quartz vein rock that are contained in a matrix of East Porphyry. To the east of the open pit, irregular dioritic bodies are observed within the East Porphyry, around which the abundance of ferro-magnesian minerals (biotite and amphibole) increases. These small bodies (<20 m diameters) are interpreted as amphibolites and roof pendants (Renzetti, 1957; Chong and Pardo, 1993).

3.2.5 Summary

The Chuquicamata Complex bears three textural phases: the East, West and Banco Porphyries. Of these units, the granodioritic East Porphyry makes up approximately 80% of the exposure in the Chuquicamata open pit and has the least porphyritic texture. The younger, dike-like West and Banco Porphyries are matrix dominated, with Banco being more mafic due to finely disseminated biotite in its matrix. Based on the comparison of lithological distribution maps for the open pit surface over a elevation change of 300 metres, the West Porphyry has pinched out within the East Porphyry and the Banco Porphyry maintains a vertical to sub-vertical continuity (Fig. 3.1). Radiometric ages are inconclusive with respect to emplacement events (Table 3.1). Field relationships indicate that the East Porphyry is intruded by the Banco Porphyry. Contact relationships between the East and West porphyries are gradational and the spatial separation of the West and Banco porphyries suggests that these units will not intersect within the exposure of the Chuquicamata open pit.

3.3 Alteration Zones of the Chuquicamata Deposit

The hydrothermal alteration pattern at Chuquicamata is composed of a massive quartz-sericitic zone along the deposit's western edge, discontinuous remnants of a potassic alteration zone mixed with a chloritic assemblage that outcrops along the eastern boundary of the deposit and a transitional zone of sericitic to potassic alteration (Fig. 3.2 and Fig. 3.3). An argillic alteration zone, approximated in Fig. 3.2, is mentioned here but has yet to be

clearly defined in terms of its composition and distribution at Chuquicamata. Each assemblage is briefly characterized below, using the classification scheme presently in use by the mine geologists. Thorough characterizations of the dominant alteration assemblages is being examined in a concurrent study at Dalhousie University. A summary of distribution patterns is presented and discussed in light of new radiometric age data.

3.3.1 Potassic Alteration

The potassic alteration zone at Chuquicamata preserves the texture of the host rocks that in places display cataclastitic to mylonitic deformation (Chapter 4). The characteristic assemblage is one of euhedral to subhedral poikilitic K-feldspar megacrysts, plagioclase feldspars partially altered to K-feldspar, and amphibole altered to biotite or further altered to sericite or feldspar + quartz. Biotitization may be present as finely disseminated biotite throughout the host rock, or concentrated as irregular, discontinuous veinlets (<0.5 mm), or as halos along K-feldspar (±quartz) veinlets (< 1 cm). Distribution of this assemblage is irregular owing to the transitional nature of chloritic assemblages along the eastern expanse of the deposit and by a variable sericitization throughout the deposit.

3.3.1.1 K-Silicification

A sub-zone of potassic alteration that appears to be silicified has been identified by drillcore logging and recent pit surface exposures. The alteration is characterized by microscopic cataclastic host rock textures. The matrix to the cataclasite is cryptocrystalline K-feldspar and plagioclase that has partially or wholly altered to K-feldspar and quartz. Original K-feldspar is generally light in colour and any mafic minerals, essentially biotite, occur in trace amounts or are absent. This sub-zone is called K-silicification (Ksil) due to a partial to complete cryptocrystalline silicification and a proposed K-feldspathification of the host rock (L. Gustafson, 1996, pers.comm.).

Fig. 3.2 Distribution of the most common alteration zones outcropping within the Chuquicamata open pit. Note that this is a plan view map of the open pit surface, which has an elevation change of over 400 metres between the eastern edge of the chloritic zone and the sericitic zone adjacent to the West Faut to the west. See figure 3.3 for generalized cross-sections at N3600, N4500 and N5000.

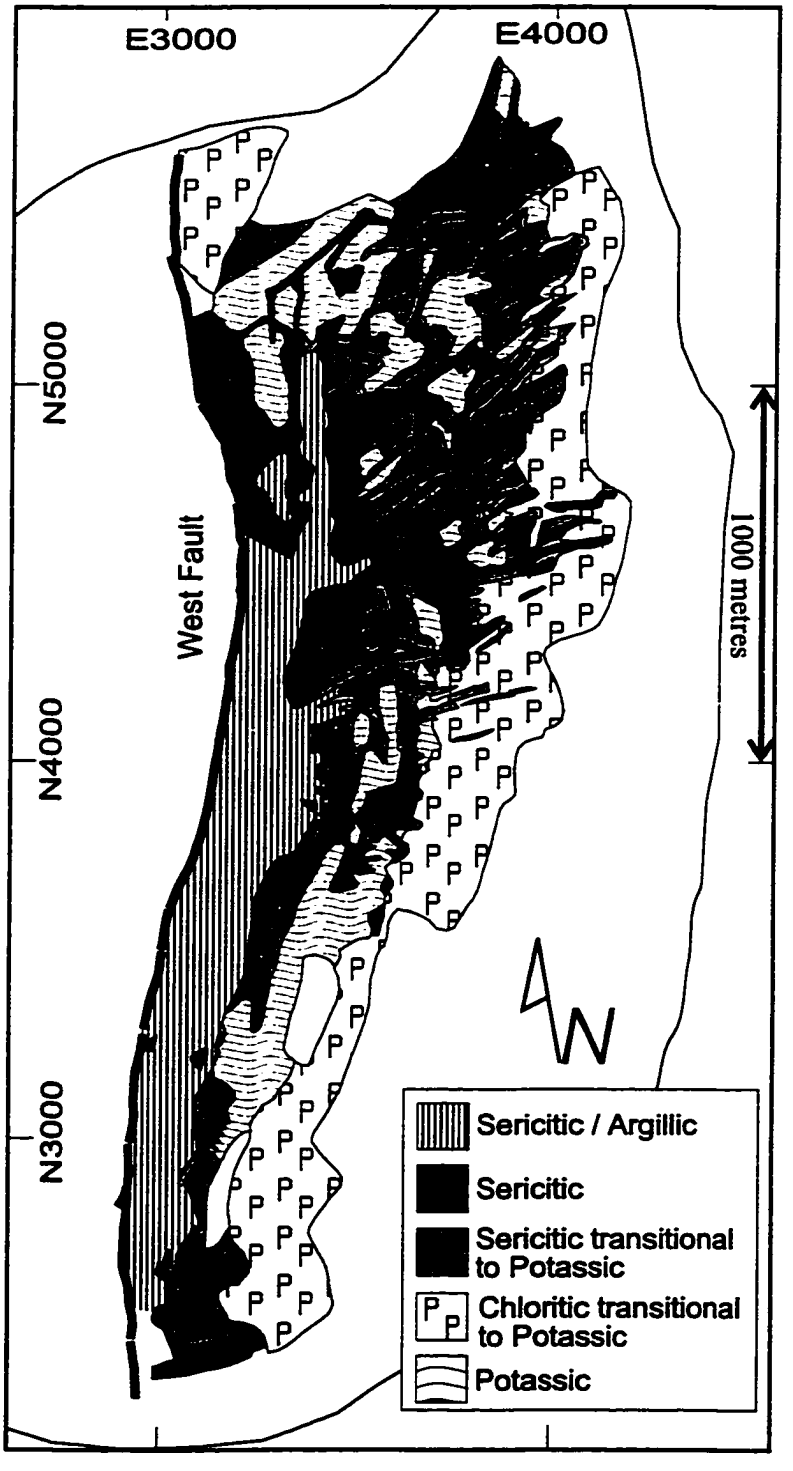

Fig. 3.3 Cross sections N3600, N4500 and N5000 showing generalized alteration zones for the Chuquicamata deposit. Note the concentration of sericitic alteration adjacent to the West Fault in the southern sections and the appearance of symmetry in the northernmost section. The November 1995 open pit outline is shown for reference. Compare these alteration patterns with those concentric patterns of the Lowell and Guilbert model (Fig. 1.1).

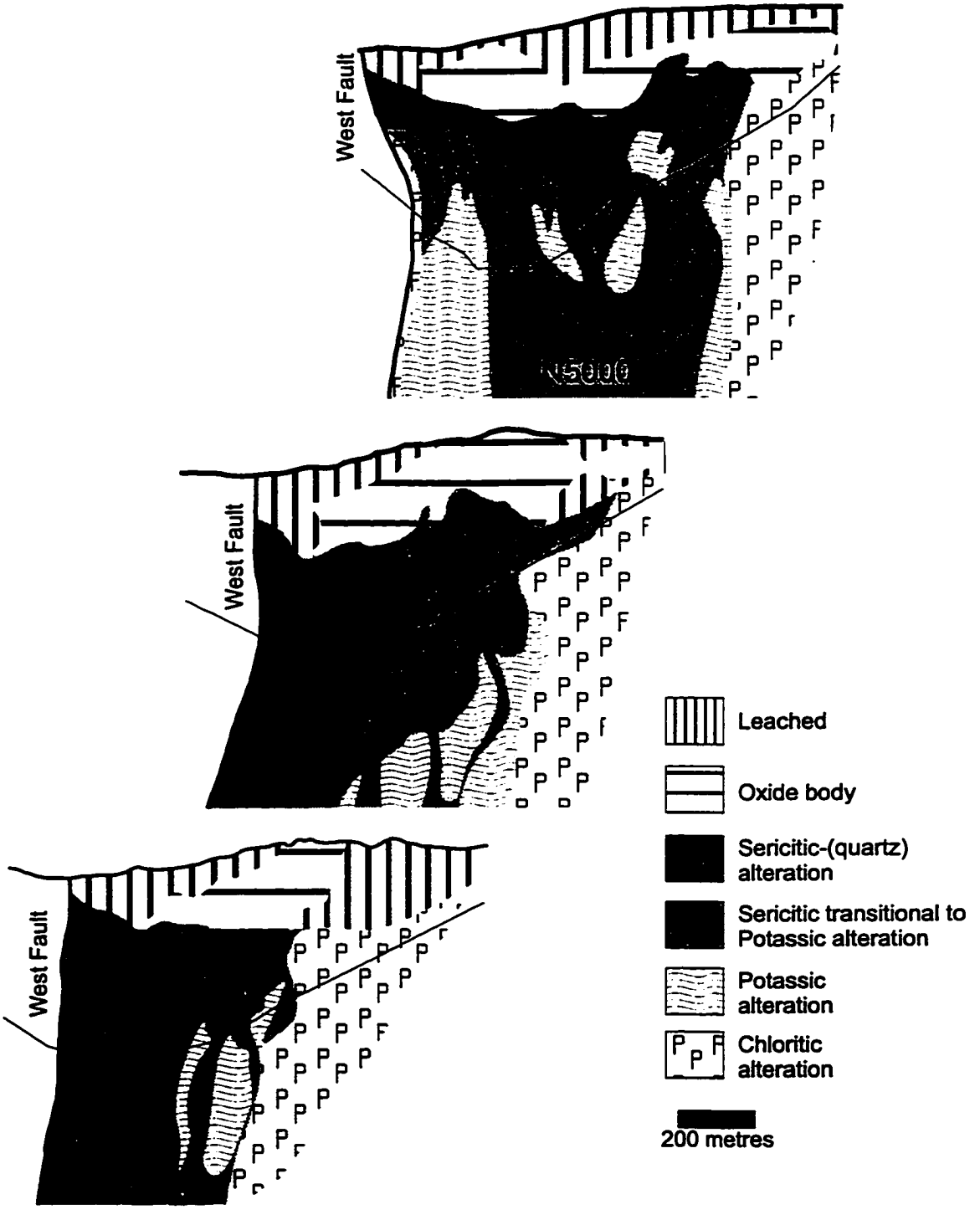

3.3.2 Chloritic (Propylitic) Alteration

This alteration zone is characterized by the abundance of chlorite-magnetite ±sericite±hematite. The chlorite replaces all original magmatic amphiboles and biotite. The presence of epidote and calcite as part of this alteration assemblage is sporadic and restricted to those areas adjacent to Mesozoic meta-sedimentary units. In general, this alteration assemblage does not outcrop within the open pit, except where Paleozoic and Mesozoic units are in contact with the CIC.

3.3.2.1 Chloritic-over-Potassic Alteration Zone

To a large extent, within the open pit, the chloritic alteration assemblage is observed transitional to potassically altered rocks. In this case, the chloritic assemblage is primarily confined to veinlets and fracture surfaces that bear the assemblage chlorite ± magnetite ± sericite leaving the potassically altered rock between fractures unaffected. This is the dominant "propylitic" alteration phase encountered in the open pit. Due to its mixed nature with the potassic alteration assemblage it is commonly referred to as the chloritic-over-potassic alteration zone.

3.3.3 Quartz - Sericitic Alteration

The quartz-sericite alteration is observed replacing large volumes of host rock lithologies as the result of hydrothermal activity. This alteration type is divided into two groups: one of pervasive alteration, where the original rock texture is completely obliterated, and the other, a "selectively" pervasive alteration, where the original rock texture is partially preserved and component feldspars and micas are altered. In both cases, all original minerals, with the exception of quartz, have been altered to a mixture of fine sericite and clay group minerals. Where rock texture is present, pseudomorphs of feldspars and biotite by sericite±clay minerals are characteristic.

3.3.3.1 Sericitic-over-Potassic Alteration

Like the propylitic alteration zone, the sericitic alteration zone also defines an

overprinting zone of sericitic-over-potassic. This zone is characterized by a host rock that retains its texture with both plagioclase and K-feldspars being weakly to partially sericitized and biotites showing some discolouration. The bulk of sericitic alteration is confined to the halos of veins and veinlets, between which the host rock maintains a potassic alteration assemblage.

3.3.4 Argillic Alteration

The composition of a proposed argillic alteration zone has yet to be characterized. However, the occurrence of kaolinite group and montmorillonite group minerals with sericite and their distribution in the central-west area of the mine indicates the presence of a mappable alteration unit. In general, this alteration type appears similar in texture to the massive quartz-sericite alteration zone with clay minerals (kaolinite, halloysite, montmorillonite and nontronite) being derived from completely altered feldspars and micas. The distribution of this zone generally coincides with the West Fault (Chapter 4.0) and is spatially associated with enargite-sphalerite vein mineralization. The relationship between this alteration and mineralization is a subject under study by CODELCO staff geologists.

3.3.5 Formation and Distribution of Alteration Zones

Alteration within porphyry-type deposit systems follows the exsolution of principally magmatic fluids from the shallowly emplaced crystallizing host pluton. These early, high temperature, >450°C, magmato-hydrothermal fluids circulate throughout the crystallizing melt and adjacent country rocks resulting in alkali (potassium) metasomatism. Fracturing by a combination of thermal, vapour and hydraulic pressures allows the influx of meteoric waters that interact with and cool the magmatic fluids resulting in low temperature, 450°-250°C, fracture-controlled phyllic alteration. For summaries and discussions of fluid evolution in relation to alteration the reader is referred to Meyer and Hemley (1967), Henley and McNabb (1978), Gustafson and Hunt (1975); Beane and Titley, 1981; Titley (1994), and Dilles and Einaudi (1992).

The distribution of (magmato-)hydrothermal alteration zones at Chuquicamata (Fig.

3.2 and 3.3) has been described by Zentilli et al. (1995) as a central quartz-sericitic, or phyllic, zone surrounded by a potassic alteration zone that subsequently gives way to an outer propylitic zone. This pattern of alteration is interpreted as the result of a younger phyllic phase superimposed over an older potassic-propylitic phase (Zentilli et al., 1995; Reynolds et al., in press). The distribution has also been attributed to displacements along intra-deposit faults (Alvarez et al., 1980). The field mapping of this study supports both of these interpretations, as the younger phyllic event is strongly controlled by fault and vein systems at the time of alteration. These systems crosscut and may offset the earlier alkali metasomatism that parallels the CIC host rock.

Based on recent radiometric age data, Zentilli et al., (1995) and Reynolds et al., (in press) propose a 2 to 4 m.y. age difference between the potassic alteration and the sericitic alteration phases, attributing these ages to hydrothermal alteration events associated with distinct intrusive episodes. Besides the multi-stage magmato-hydrothermal history, another complication distinguishing Chuquicamata from other porphyry deposits is the presence of the West Fault, which has probably displaced a portion of the Chuquicamata ore-body. The complex structural and magmato-hydrothermal history of the Chuquicamata deposit precludes the application of the simplified Lowell and Guilbert model.

3.3.6 Summary and Age Relations

Geological mapping in the open pit has confirmed the presence of the typical alteration phases associated with PCD formation. The complex alteration history and the distribution of these phases makes comparison to the Lowell and Guilbert model unwarranted. The older phases of inner potassic and outer chloritic alteration bear the expected spatial relation for a cooling magmato-hydrothermal system, conforming to the elongate, NNE, form of the Chuquicamata Intrusive Complex. The greatest influence these alteration assemblages have on the country rocks appears to be a partial chloritization of amphiboles in the intruded Elena granodiorite (Chapter 2.3.1.3.4). Nearby meta-sedimentary rocks from a variety of depositional facies have been metamorphosed to greenschist facies by a combination of the intrusion of the Chuquicamata Complex and deformation along the

Messabi Fault zone.

$^{40}Ar/^{39}Ar$ cooling ages for K-feldspar and biotite from potassically altered samples range between 32 to 34 Ma and 32 to 35 Ma respectively (Table 3.2). The wider range in age for biotite analyses may result from excess argon within the biotite mineral structure. The presence of excess argon would result in an older age, that is in this case 35 Ma. The bulk of the pervasive quartz-sericitic alteration is confined to a zone adjacent to and parallelling the West Fault, being limited in places by its associated branches. Further structural control of this hydrothermal alteration phase is demonstrated by the abundance of quartz-sericitic halos tracing fault and vein systems (Fig. 3.2). These fault systems offset potassic and propylitic assemblages (see Chapter 6). Cooling ages for sericite samples from this alteration zone range from 30 to 31 Ma (Table 3.2).

An explanation for the temporally extensive alteration has been proposed by Zentilli et al. (1994a, 1995). The model of these authors involves a multiple magmato-hydrothermal history for Chuquicamata where the observed potassic alteration phase represents the deeper and hotter part of an older magmato-hydrothermal system that had been partially exhumed before being overprinted by a younger hydrothermal system that is represented by the phyllic alteration phase, which probably formed at lower temperatures and at a shallower depth with respect to the surface.

Table 3.2. Compilation of the most recent radiometric ages for the alteration phases at Chuquicamata. All ages are from Zentilli et al. (1995) and Reynolds et al., (in press). TGA = total gas age.

Alteration Phase	**Age ±1 sigma**	**Method and Mineral**
Chloritic	33.7±0.2 Ma	$^{40}Ar/^{39}Ar$ K-feldspar
	35.2±0.2 Ma	$^{40}Ar/^{39}Ar$ TGA Biotite
	33.4±0.4 Ma	$^{40}Ar/^{39}Ar$ K-feldspar
	33.9±0.3 Ma	$^{40}Ar/^{39}Ar$ TGA Biotite
Potassic	33.4±0.2 Ma	$^{40}Ar/^{39}Ar$ K-feldspar
	32.8±0.2 Ma	$^{40}Ar/^{39}Ar$ TGA Biotite
Sericitic-over-Potassic	32.1±0.2 Ma	$^{40}Ar/^{39}Ar$ K-feldspar
	31.9±0.2 Ma	$^{40}Ar/^{39}Ar$ TGA Biotite
Quartz-Sericitic	31.4±0.4 Ma	$^{40}Ar/^{39}Ar$ TGA Sericite
	31.1±0.2 Ma	$^{40}Ar/^{39}Ar$ TGA Sericite

3.4 Generalized Sulphide Assemblages

Due to their large volume and relatively low grade, porphyry type deposits are often described as disseminated deposits. However, at the scale of mineralization, 80-90% of the sulphides are present in fractures and veinlets (Lopez, 1939), which is consistent with estimates for a number of different porphyry copper deposits that put more then 90% of mineralization in or adjacent to fractures and veins (Beane and Titley, 1981).

As summarized by Lowell and Guilbert (1970), Henley and McNabb (1978) and McMillan and Panteleyev (1980) amongst others, hypogene mineralization generally consists of varying amounts of pyrite, chalcopyrite, bornite and molybdenite within fracture fillings or quartz-bearing veinlets. A typical sulphide ore zoning is composed of a central barren or weakly mineralized zone containing pyrite (<2%), chalcopyrite, molybdenite and minor bornite. Outwards from the core are enrichments in molybdenite, chalcopyrite and pyrite and enclosing these ore zones is a pyrite-rich halo (10-15%) with variable amounts of chalcopyrite and molybdenite (Fig. 1.1). Base and precious metal bearing veins may occur peripheral to the porphyry mineralization in associated faults and fractures (Sillitoe, 1972, 1973; McMillan and Panteleyev, 1980). Other metallic minerals that may be present include magnetite, diagnostic of the deeper parts of the deposit (Guilbert and Lowell, 1974), and chalcocite that may be found from the ore zones to the outer peripheral areas in the upper levels of the deposit.

The present Chuquicamata classification scheme identifies mineralization zones based on the presence of copper-bearing minerals as either hypogene or supergene and are further categorized by their associated alteration zone (Table 3.3). The classification method was established through detailed drillcore logging by several consultants and mine staff and was applied during the surface mapping undertaken during this study.

As previously mentioned, this study focusses on observations at the hand sample scale and, as such, the reader should be aware that ongoing studies by M. Zentilli and Cuesta Research Ltd. indicate the presence of independent mineral zones bearing chalcocite, djurleiite and digenite. The identification of these minerals in the field at Chuquicamata is difficult at best and thus, are presented here as chalcocite.

3.4.1 Hypogene Mineralization

Four hypogene mineral assemblages are presently observed in the Chuquicamata deposit including (i) bornite> (digenite- chalcopyrite- covellite), (ii) chalcopyrite≥ (bornite-digenite- covellite), (iii) digenite and (iv) chalcopyrite> (pyrite, chalcocite and covellite) (Table 3.2). Within the quartz-sericitic alteration zone, both the (iii) and (iv) assemblages dominate. Bornite and/or chalcopyrite dominated assemblages, (i) and (ii), are most common in the sericite-over-potassic alteration zone. These assemblages also characterize the potassic alteration zone. Chalcopyrite is the only copper-bearing mineral in the chloritic alteration zone. These mineral assemblages may be classified into those more closely associated with magmatic fluids and those associated with hydrothermal fluids.

3.4.1.1 Magmatic Assemblages and Associations

Magmatic stage hypogene assemblages are those which are deposited in a host rock where the mineralizing fluids appear to be in equilibrium with the wallrock at outcrop to hand sample scales. The emplacement of minerals which already exist in the host rock may line the fracture, but in general there is little alteration observable along the trace of the fracture or vein. The mineralizing fluids are of magmatic origin with little or no input from meteoric or connate waters from the surrounding country rock. Mineral phases chalcocite, bornite, chalcopyrite, covellite and pyrite may be present as grains disseminated throughout the host rock occupying sites in mafic minerals (Soto, 1979; Tobey, 1971). These sulphides also are observed in quartz veinlets, K-feldspar veinlets and disseminated along healed fractures. These early veins are classified as "A-veins" according to the classification scheme of Gustafson and Hunt (1975).

A general zonation from a central bornite-chalcopyrite(-digenite) grading outwards to chalcopyrite-pyrite and further to pyrite-magnetite-hematite has been described for Chuquicamata (Tobey, 1971; Soto, 1979; Ambrus, 1979). Ambrus (1979) also describes potassic alteration assemblages associated with chalcopyrite+bornite+(digenite) bearing quartz veinlets that he observed crosscutting feldspar grains without producing alteration halos.

Table 3.3 Classification of mineralization zones within the Chuquicamata deposit based on associated alteration assemblages and the extent of supergene enrichment.
(Dg-digenite, Cc-chalcocite, Cp-chalcopyrite, Bo-bornite, Cv-covellite)

Alteration Zone	Hypogene Mineralization	Supergene Mineralization
Quartz-Sericitic	Dg Cp+(Bo)+(Dg)	Cc Cv Cv+Cp+Dg
Sericitic-over-potassic	Cp>Bo+Dg+(Cv) Bo>Dg+Cp+(Cv) Cp> others	Cc+(Cv)+(Cp)+(Dg) Cv+Cp+Dg+(Cc)
Potassic	Cp>Bo+Dg+(Cv) Bo>Dg+Cp+(Cv) Cp> others	Cc+(Cv)+(Cp)+(Dg) Cv+Cp+Dg+(Cc)
Chloritic (propylitic)	Cp> others	Cc+(Cv)+(Cp)+(Dg) Cv+Cp+Dg+(Cc)

3.4.1.2 Hydrothermal Stage

Previous studies (Ambrus, 1979; Soto, 1979; Tobey, 1971) discuss three phases of hydrothermal activity that Tobey defines as the hypogene mineralization activity in which the mineralizing fluids are not in equilibrium with the wallrock through which they pass. This chemical disequilibrium may be associated with an increasing component of meteoric water resulting in a change in acidity and a decrease in temperature of the mineralizing fluids. As a result these mineralizing fluids produce an alteration halo along the veins, the veinlets and the fractures through which they pass. These phases of the hydrothermal stage of hypogene mineralization are referred to as the transitional, or late-magmatic, the principal, or main-stage, and the late stage.

3.4.1.2.1 Transitional

This phase follows the generation of potassium-metasomatism alteration (Soto, 1979) and is characterized by abundant quartz veinlets with central sutures that may have alteration halos (Ambrus, 1979; Soto, 1979). These veinlets are also known as the 'B-vein' set of Gustafson and Hunt (1975). Molybdenite deposited in quartz veinlets is the dominant mineralization, which may have been accompanied by deposition of chalcopyrite-bornite-(digenite) and/or chalcopyrite-pyrite assemblages. These assemblages have clear associations with anhydrite, biotite and chlorite (Soto, 1979). Soto (1979) describes two occurrences of quartz-molybdenite, the first as individual veinlets (mm to cm widths) and the second as composite veins (widths in metres) comprised of numerous individual veinlets. These large quartz-molybdenite veins are also known as "Blue Veins" (Waterman, 1951).

3.4.1.2.2 Principal

Alteration halos of quartz-sericite are characteristic of the vein mineralization in this stage. Gustafson and Hunt (1975) have categorized this veinlet set as 'D-veins'. The dominant sulphide mineral phase is pyrite, that to the east of the massive quartz-sericite alteration zone is associated with a zone of bornite and bornite-chalcopyrite that grades eastwards through pyrite± chalcopyrite± enargite± sphalerite to pyrite± enargite±

tetrahedrite± chalcopyrite± sphalerite (Soto, 1979). The massive quartz-sericite zone also bears pyrite, chalcopyrite, enargite and sphalerite mineralization as "D-vein" assemblages. These D-veins crosscut the quartz, A-veins, and quartz-molybdenite veinlets of the B-vein magmatic and transitional stages respectively.

3.4.1.2.3 Late

Late stage mineralization is dominantly composed of pyrite-enargite veins having widths of up to tens of centimetres. These veins are primarily emplaced near and parallel to the West Fault within the quartz-sericite alteration zone (Tobey, 1971; Soto, 1979). Fractures in these veins hold pyrite- bornite, pyrite- covellite and pyrite- chalcocite that Soto (1979) interprets as hypogene assemblages. Sphalerite, galena, tennantite and tetrahedrite, present in lesser amounts, are also attributed to late stage mineralization. Late stage mineralization is also noted in the northeastern sector of the open pit as veins of dominantly pyrite (Tobey, 1971).

3.4.2 Supergene Mineralization

Supergene enrichment is important in porphyry copper deposits, often determining if the deposit will be economic (Guilbert and Park, 1986). Leaching of hypogene mineralization by hydro-chemical weathering processes from above the water table and precipitation at lower levels forms a secondary enrichment blanket changing the vertical hypogene mineral zonation into a horizontally stratified zonation of supergene mineralization (Titley, 1994; Ague and Brimhall, 1989). Sulphide minerals found within the supergene blanket may include chalcocite, djurleite, digenite, covellite and native copper. Ague and Brimhall (1989) summarize chemical processes involved in the formation of this enrichment zone and Titley (1994) outlines expected mineral assemblages.

Mineralization of supergene origin at Chuquicamata is best developed in the quartz-sericitic alteration zone. The enrichment blanket has the form of an elongate bowl that is divided into an upper chalcocite zone that grades into a lower covellite zone. In the chalcocite enrichment zone, chalcocite variably replaces all other mineral phases and is

present as blackish surface coatings, or rims, on pyrite and chalcopyrite. In the lower zone, covellite replaces all copper sulphide mineral phases and grades downward into the partially replaced hypogene assemblages of covellite-chalcopyrite-digenite-(bornite). The supergene assemblages of chalcocite and covellite + chalcopyrite are also present within the sericitic-over-potassic, potassic and chloritic alteration zones. Sillitoe and McKee (1996) present K/Ar radiometric dates ranging from 15 to 19 Ma for the supergene system at Chuquicamata.

3.4.3 Summary

Although the distribution of mineralization with respect to lithological unit has not been studied, mineralization is present in all units. Mine geologists indicate that the Banco Porphyry has an overall lower abundance of mineralization, leading to the suggestion the this unit may be considered an intra-mineral intrusion (see Kirkham, 1971). However, nowhere is this body observed crosscutting mineralization. The lower degree of mineralization may be due to physical or chemical properties specific to this unit, or its location, generally east of the strongly mineralized potassic stockwork system and massive quartz-sericite alteration zone.

With respect to alteration, supergene mineralization (~17 Ma, Sillitoe and McKee, 1996) composed of dominantly chalcocite and covellite, overprints all alteration zones. Quartz-sericitic alteration (~31 Ma, Zentilli et al., 1994a, 1995; Reynolds et al., in press) is dominated by pyrite-digenite-chalcopyrite assemblages and potassic alteration (~33.4 Ma Zentilli et al., 1994a, 1995; Reynolds et al, in press) zones predominantly bear molybdenite and chalcopyrite-bornite-digenite-covellite assemblages. A variety of mineralization stages are presented by Ambrus (1979), Soto (1979) and Tobey (1971) all of whom describe the mineralization as vein and veinlet hosted. This thesis examines the orientations of these vein and veinlet arrays in Chapter 5: *Mineralized veinlet systems and structural sampling* and Chapter 6: *Veins, fault systems and structural domains* and proposes a sequence of emplacement that is then evaluated in terms of the regional tectonic setting.

3.5 Chuquicamata and Ductile - Brittle Structural Features

Discussions of the structure of the Chuquicamata PCD usually begin with and focus on the West Fault and the systems of faults that crosscut the open pit (eg. Lopez, 1939; Reutter et al., 1996). This regional scale fault system is without doubt essential to the evolution of the deposit. However, numerous other structural features including mylonites, protomylonites, cataclastites and a variety of breccias, are rarely mentioned although they may be of equal importance to the evolution of the mineralized system. These fault rocks are presented and discussed within this thesis. Prior to the presentation of chapters concerning fault rocks and the mineralized structures that comprise the Chuquicamata deposit, the following clarification of fault nomenclature used in this study is offered.

3.5.1 Clarification of Fault Rock Nomenclature

Many authors mention the difficulties that exist in naming the variety of fault, or shear zone, rocks from differing structural levels (Williams et al., 1994; Bursnall, 1989; Chester et al., 1985; Wise et al., 1984; Tullis et al., 1982). This difficulty is, in part, due to the scale of observation. So, in this study, although microscopic descriptions are presented, the reader should recall that all fault rocks are discussed from the perspective of mesoscopic, or hand sample, scale using the following nomenclature.

Shear zones are relatively narrow zones of deformation across which significant zone parallel displacement is evident (Ramsey and Huber, 1987). The end-member terms brittle, where cataclastic grain-size reduction is evident in a hand sample as randomly oriented angular rock and mineral fragments, and ductile, where deformation appears to have been accommodated by flow at the hand sample scale, are used to further identify conditions of shear zone formation (Ramsey, 1980). Description of shear zone rocks as mylonitic rocks, or mylonites, which commonly display a foliation and possibly a lineation, refers to those rocks in which strain has localized into a relatively narrow planar zone within which grain-size reduction has occurred by plastic or brittle deformation mechanisms (Tullis et al., 1982; Williams et al., 1994) which can not be determined by the unaided eye. As such, the term mylonite describes shear zone rocks that have been produced in part by plastic deformation,

which implies intracrystalline creep, climb or glide of dislocations and diffusive mass transfer (Knipe, 1989; Scholz, 1987) and cataclasite describes those fault rocks produced by dominantly brittle fracture mechanisms. The determination of fault rock formation mechanisms, and thus naming of the rock as mylonite or cataclasite, would then be based on microscopy or study at submicroscopic scales of observation. For the purposes of this thesis, which focusses on the hand sample scale of observation, mylonites are those fault rocks that are foliated and cataclasites are those fault rocks with random fabrics. Mylonites may be further classified as protomylonites, where rock or mineral fragments are contained within a matrix of grain-sized reduced material that composes 10-50% of the fault rock, or ultramylonites, where the matrix composes 90-100% of the fault rock (see Sibson, 1977). The most common cataclastic fault rocks in the study area are gouge, which has <30% visible rock fragments, and breccia with >30% visible fragments. Both mylonites and cataclastites may show similar structural fabrics and shear sense indicators (Hanmer and Passchier, 1991; Lister and Snoke, 1984; Passchier and Simpson, 1986; Rutter et al., 1986; Chester and Logan, 1987; Chester et al., 1985; Tanaka, 1992).

3.5.2 Overview of Structural Systems at Chuquicamata

Bulk ductile-brittle deformation was noted by Langerfeldt (1964), who described cataclastites, as tectonically "shredded" rocks, protomylonites, or which were common in sectors beneath the cataclastites, and mylonites. Soto (1979) described the mylonites as localized along the central length of the deposit (open pit of 1970's) decreasing in intensity towards the east. These deformed rocks are also mentioned as being most abundant along the contacts of porphyritic and granitic rocks, as well as, between different phases of porphyritic rocks (Ambrus, 1979). Brittle fault systems and their relation to the regional West Fault and tectonic deformation events have been preliminarily examined in Reutter et al., (1993, 1996) and Lindsay et al., (1995, 1996).

The distribution and variety of deformational features from early formed ductile-brittle mylonitic shear zones through brittle faults and breccias, that are present in Chuquicamata, represent important components to the geological evolution of this magmato-

hydrothermal system. These features and their significance are presented and discussed in the following chapters: Chapter 4: *Pre-Mineralization Ductile and Cataclastic Structural Features*; Chapter 6: *Veins, Fault Systems and Structural Domains* and Chapter 7: *Post-Mineralization Displacement Phases*.

3.6 Geological Summary of the Chuquicamata Deposit

The Chuquicamata Complex is composed of three textural phases: the East, the West and the Banco Porphyries. Of these units, the monzogranitic East Porphyry makes up approximately 80% of the exposure in the Chuquicamata open pit and has the least porphyritic texture. The younger, dike-like monzogranitic West and monzodioritic Banco Porphyries have matrix-dominated porphyritic textures. All units can be summarized as presenting varying abundances of phenocrystic phases that include plagioclase, quartz, megacrysts of K-feldspar, biotite and rare amphibole and zircon and sphene as accessory minerals. Ages of emplacement for these units have not been evaluated in detail, although an Eocene-Oligocene age is suggested (Zentilli et al., 1994; Reynolds et al., in press).

Alteration assemblages consistent with potassic, propylitic and phyllic alteration overprint the lithological units. A veinlet associated quartz-sericitic alteration that is present in the potassic alteration zone is visibly distinct from the massive texture destructive phyllic alteration zone. The phyllic alteration, a quartz-sericite-clay? assemblage clearly crosscuts and overprints the relatively older potassic assemblage and its contained mineralization.

The distribution of mineralization with respect to lithological unit has not been studied. However, with respect to alteration, supergene mineralization (~17 Ma, Sillitoe and McKee, 1996) overprints all alteration zones. The quartz-sericitic alteration zone (~31 Ma Zentilli et al., 1994a, 1995; Reynolds et al., in press) and potassic alteration zone (~34 Ma Zentilli et al., 1994a, 1995; Reynolds et al, in press) include abundant molybdenite as well as Cu-Fe-sulphide assemblages. A variety of mineralization stages are presented by Ambrus (1979), Soto (1979) and Tobey (1971), all of whom describe the mineralization as being 80-90% vein and veinlet hosted. The metre scale vein and millimetre scale veinlet styles of mineralization suggest distinct stages, conditions of formation and processes associated with

their emplacement. The following chapters present the characteristics of the evolution of deformation at Chuquicamata and its relationship to the conditions and processes responsible for the mineralization of the porphyry copper system.

Chapter 4. Pre-Mineralization Ductile to Cataclastic Features

Within the Chuquicamata complex, ductile deformation occurs as discontinuous shear zones associated with contact zones of different porphyry phases and fault zones that were later reactivated or evolved into brittle fault systems. Inside and outside the open pit, ductile deformation is also observed within blocks of Mesozoic metasedimentary units that subsequent faulting has displaced. Deformation along the trend of the metasedimentary units is regional and is referred to as the Messabi Fault (Fig. 4.1)(Lindsay et al., 1995; Reutter et al., 1996; Tomlinson et al., in prep.). First ductile and cohesive cataclastic deformation within the CIC are described (Section 4.1) and then deformation associated with the Messabi fault is described (Section 4.2). The evidence for early, pre-mineralization deformation provides information concerning regional and local stress fields following the emplacement of the host porphyry. The relative orientations of these deformation zones are of use in proposing probable regional structural settings for the emplacement of the Chuquicamata porphyry copper deposit.

4.1 Early Features in the Chuquicamata Intrusive Complex

The dominant unit of the Chuquicamata complex, the East Porphyry, displays a variety of localized, non-penetrative foliations, which range from weakly to moderately developed planar fabrics to mylonitic shear zones. These ductile fabrics occur in two settings within the complex: 1) associated with the contact zones between different intrusive phases of the complex, and 2) associated with younger brittle fault zones that were reactivated, or evolved from ductile shear zones. The description of foliation and shear zone fabrics within the Chuquicamata deposit is not new (Langerfeldt, 1964; Ambrus, 1979; Soto, 1979). However, these features have yet to be interpreted with respect to the geological setting of the Chuquicamata deposit. These planar fabrics represent early shear zones that either have become reactivated as brittle fault structures, or have been abandoned, with all subsequent deformation being accommodated by brittle faulting and vein array formation.

Fig. 4.1 Location map indicating the general trace of the Messabi Fault. The fault trends from a NE-SW orientation in its northern trace to a N-S orientation closer to the Chuquicamata Mine. The trace is offset in a dextral sense by a series of NE-SW trending faults (Estanques Blancos and Balmaceda) and is traceable within the mine where the fault is associated with Jurassic slates and calc-silicate units. This schematic figure is generalized from maps by Tomlinson et al.(in prep) and Chong and Pardo (1993). Named principal faults are labelled.

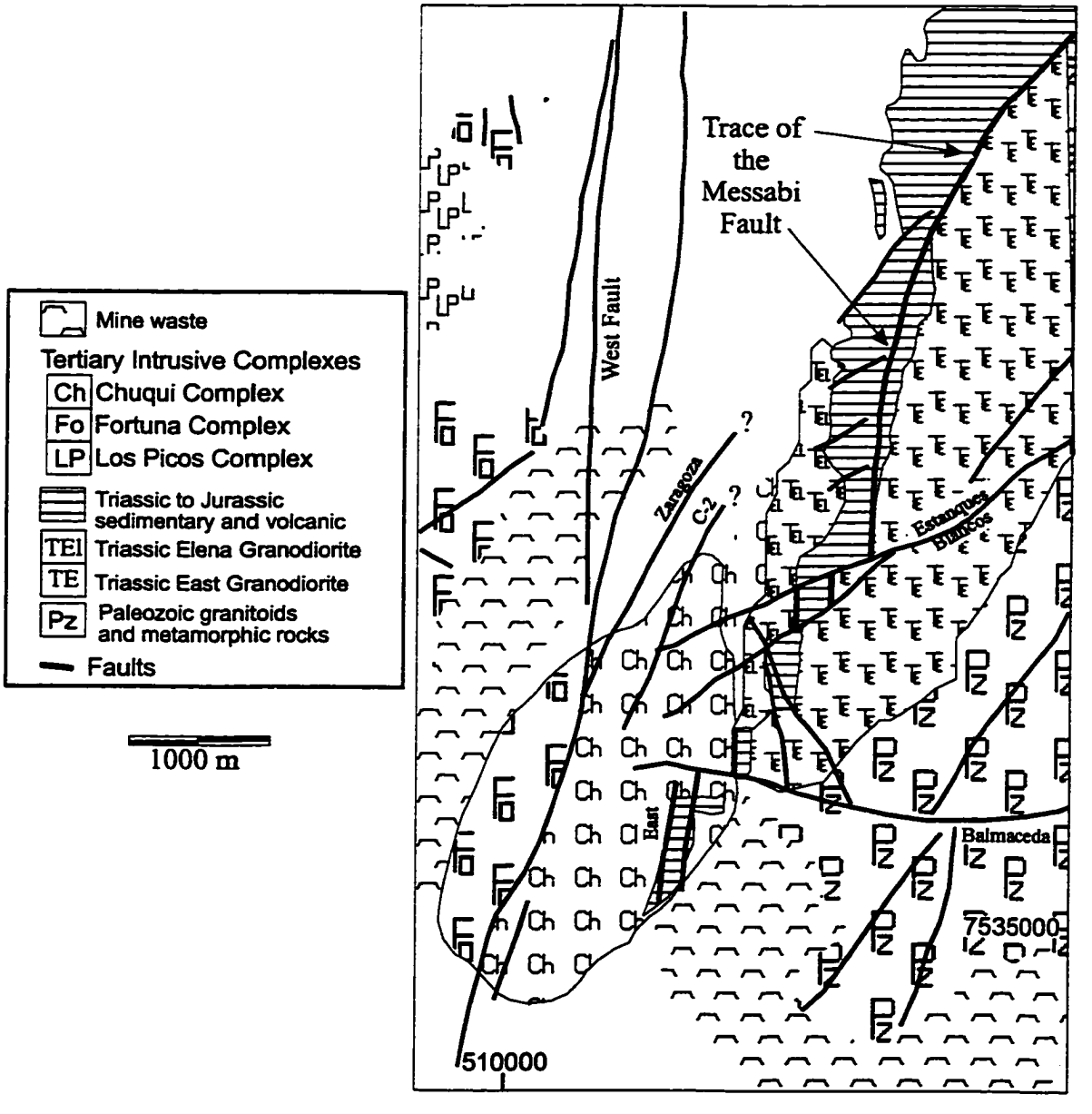

In the following sections description of the ductile and ductile-brittle structures within the CIC are divided into three groups. First those ductile structures associated with the porphyry contact zones are described, then the ductile fabrics associated with younger brittle fault systems, and finally cohesive cataclastic zones are described. Fully brittle fault zones are described in Chapter 6. It should be noted that ductile deformation zones are neither dominant nor abundant at Chuquicamata. However, these early formed fabrics, not previously considered in geological models for the emplacement and mineralization of Chuquicamata, do provide important insight into the structural setting of the host rocks prior to the episodes of alteration and mineralization.

4.1.1 Ductile fabrics associated with porphyry contact zones

During structural and alteration-mineralization mapping completed during this study, lithologic contacts were checked and updated following recent mine expansion. Mapping revealed gradational contacts between porphyritic phases of the CIC that commonly bear ductile to ductile-brittle deformation fabrics. These fabrics are described and discussed below.

4.1.1.1 Weakly developed foliations

Throughout the northeastern sector, especially in the north end of the mine (Fig. 4.2 and Fig. 6.2), where the East Porphyry contains up to 5% biotite and abundant quartz eyes, areas bear a weakly to moderately developed foliation. The intensity of the foliation is spatially related to contact zones between the East Porphyry and Banco or West porphyries.

The plane of foliation is defined by the alignment of biotite grains and subrounded quartz eyes. Perpendicular to the foliation these quartz eyes have axial ratios of 2:1 to 3:1 suggesting a 3-dimensional oblate form. With the exception of the slightly elliptical quartz eyes linear fabrics are not present on the foliation plane. In thin section the quartz eyes are composed of dynamically recrystallized grains that show weak shape-preferred orientations and have interdigitated grain boundaries. Relict, coarser grains exhibit subgrain formation and undulose extinction. The mica grain alignment and the oblate nature of the quartz eyes

indicate a weak symmetric fabric suggesting the foliation may have resulted from flattening.

Zones of ductile fabric appear to have a spatial relationship with the Banco Porphyry, which in places has foliated gradational contacts with the East Porphyry. A weak planar fabric also occurs within the gradational contact zone between the East and West Porphyries. These relationships suggest that the observed planar fabrics are associated with the intrusion of the dike-like Banco and West porphyries into the host East Porphyry. Figure 4.3A shows the small data set that suggests these planar fabrics do not maintain a consistent, or dominant orientation. Ongoing pit mapping and drillcore logging will increase the database concerning intrusive relationships between the porphyry units.

Fig. 4.2 The distribution of planar fabrics within the CIC show a spatial relationship to the contacts between porphyry units, contacts of the Chuquicamata Complex and its Mesozoic country rocks, and the trends of the principal fault traces. Bracketed and labelled (A-F) zones refer to individual segments of the Messabi Fault, which is crosscut by later brittle fault systems. The fault separated segments are discussed in chapter 4.2 and Fig. 4.5. Fault traces for brittle fault systems have been removed for clarity.

Figure 4.2

(see caption on previous page)

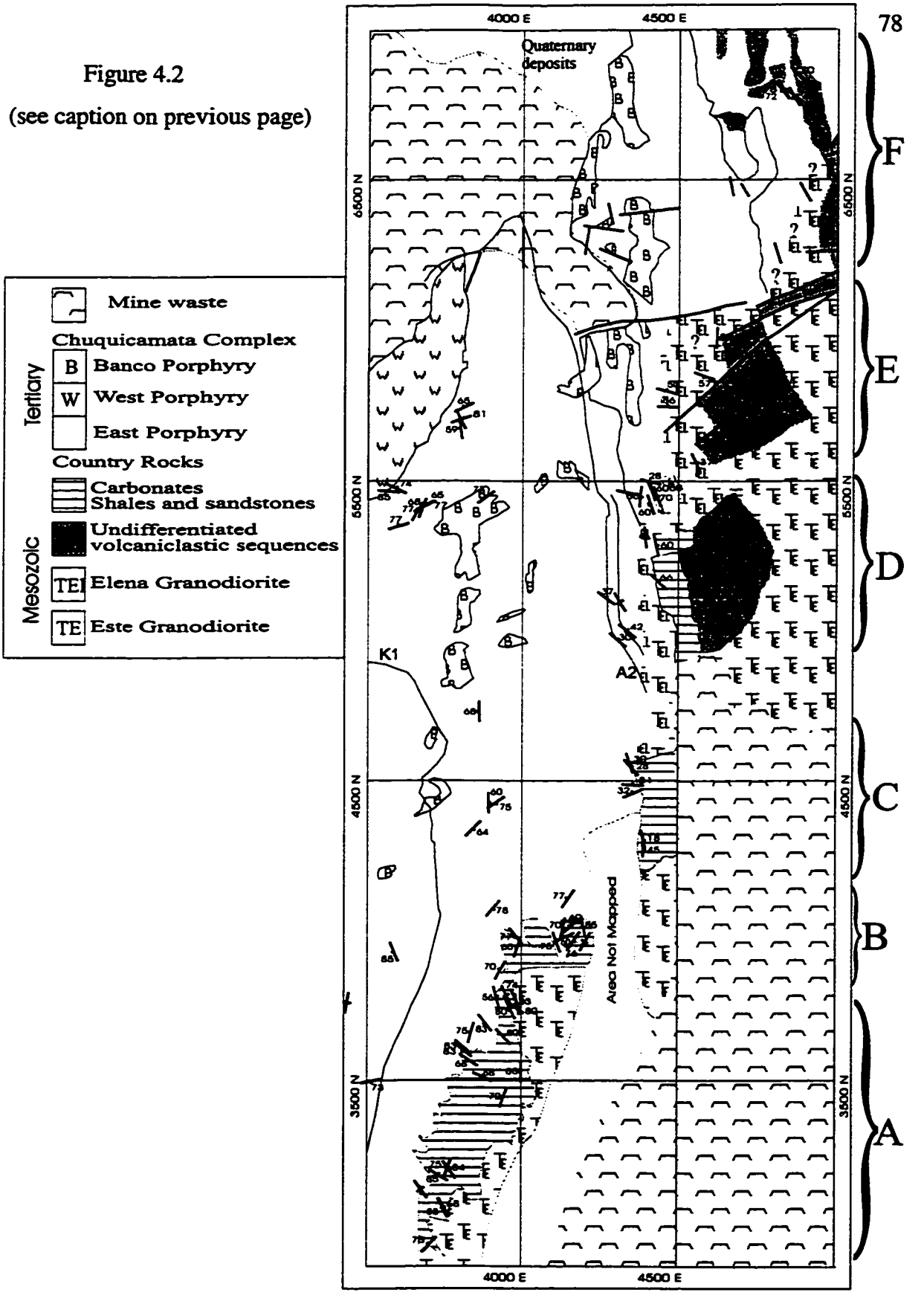

4.1.1.2 Mylonitic shear zones

Along the northern slope of the mine (ca. N5500, E3420, elev.2189), a discontinuous shear zone within the gradational contact zone between the East and West Porphyries is mylonitic in character. It is included here as its setting, being in the contact zone between two porphyries, is similar to the fabric zones described above. Other mylonitic shear zones are described in Section 4.1.2. This narrow, 10-30 cm wide, shear zone is composed of discontinuous, millimetre thick bands of quartz and feldspar that are crosscut by later quartz veinlets and fine fractures that bear sericite alteration halos. It trends approximately E-W and dips shallowly south.

In thin section, quartz shows a variety of grain sizes (<0.5 mm). The finer recrystallized grains, together with similar sized K-feldspar grains, form a matrix for anhedral perthitic feldspars (1 mm) and fragments(?) of quartz ribbons. Quartz ribbons, which contain elongate grains (>2:1), along with trails of fine granular feldspar grains, define the planar shear fabric. Large K-feldspar porphyroclasts display undulose extinction and appear to be thinly mantled by finer grains of neo-crystallized feldspar (eg. FitzGerald and Stünitz, 1993). Recrystallization along intragranular fractures within the porphyroclast is also present. Grain size reduction through both dynamic recrystallization and cataclasis is evident for the perthitic feldspar porphyroclasts that are hosted in a fine grained dynamically recrystallized quartz matrix (<0.2 mm). A plane containing a poorly defined shear direction due to a very weak mineral stretching(?) lineation, reveals sigma-type asymmetric tails on feldspar porphyroclasts indicating a dextral strike-slip component of shear. Quartz veinlets are abundant, averaging 0.4 mm in width, and show no deformation. Earliest formed veinlets, composed of coarse anhedral quartz, are oriented parallel to the shear fabric and later formed quartz - adularia veinlets crosscut the planar fabric, grading into zones of cataclasite.

Deformation conditions are difficult to determine for this shear zone due to the restricted mineral assemblage. However, based on intracrystalline deformation structures in quartz and the development of weak core and mantle structures on feldspar porphyroclasts, mid- to upper greenschist conditions for deformation are suggested (compare Simpson, 1985; Gapais, 1989; Pryer, 1993; FitzGerald and Stünitz, 1993; Passchier and Trouw, 1996).

4.1.2 Ductile fabrics associated with fault systems

4.1.2.1 Weakly developed planar fabrics

As described for the porphyry contact zones, weak to moderately developed planar fabrics are associated with the traces of principal brittle faults, usually occurring within 1-2 metres of the brittle fault and parallel to its trend. This relationship is observed for primarily the principal faults of structural domains A and B (see Chapter 6) that have been repeatedly reactivated during later deformation events with, or without, associated alteration and mineralization. Figure 4.3B shows a stereographic projection of planar ductile fabrics (203/83 and 238/88) associated with brittle fault system trends. Sigma-type porphyroclast (Hanmer and Passchier, 1991), dextral kinematic indicators are present in foliated zones trending parallel to NNE-SSW and NE-SW brittle faults. Mineralized veinlets crosscut these foliated zones at shallow angles and where the veinlets parallel the foliation the veinlets crosscut feldspar porphyroclasts. These data are confined to two principal fault systems, one is indicated by arrows on figure 4.2 the other is located off the map to the west and is present on figure 4.1 as Zaragoza. The presence of these features may reflect an important pre-mineralization displacement and/or these ductile deformation zones may have concentrated slip during later brittle faulting events.

Fig. 4.3 Schmidt lower hemisphere stereographic plots for sub-sets of measured ductile planar fabrics. A) Plot of those fabrics associated with various porphyries of the CIC. B) Fabrics associated with NE and NNE trending fault systems. These can be compared with the brittle fault system trends presented in Chapter 6. Symbols correspond to fabrics related to the NNE trending fault system (o) and the NE trending system (+). C) Distribution of steeply-dipping planar fabrics that shows no general trend probably as the result of rotation? associated with later brittle fault motions. D) Shallowly-dipping shear zones that outcrop in the northeastern sector of the mine at or near surface.

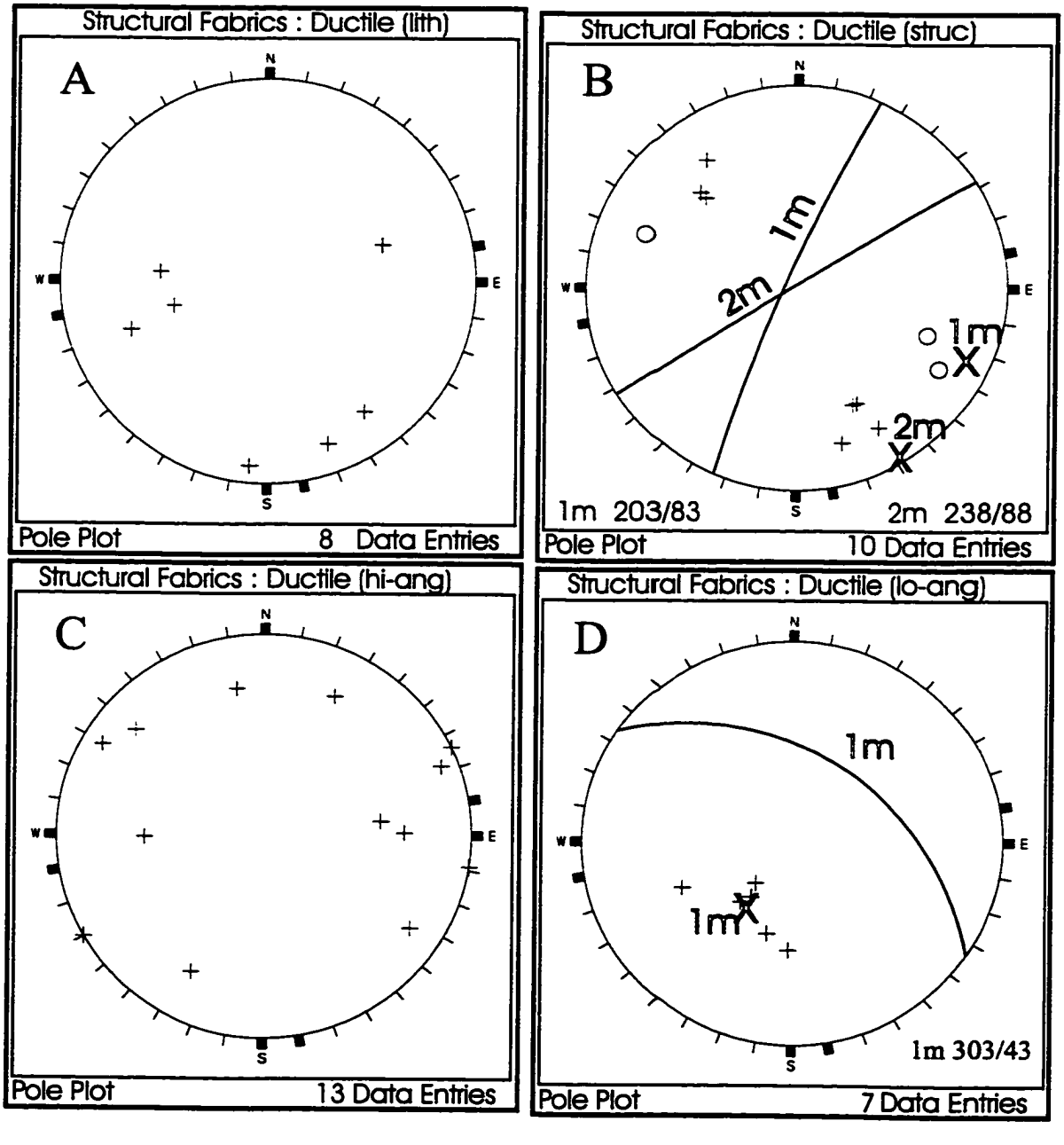

4.1.2.2 Mylonitic shear zones

Mylonitic shear zones, within the Chuquicamata Complex, in the upper benches, higher elevations, of the northeastern sector of the mine occur as a shallowly dipping set, with shear zone dips of ≤60°, whereas those on the eastern slope of the mine have greater dip angles (≥60°). The abundance of mylonitic zones increases towards the east, concentrating on where the East Porphyry comes into contact with Mesozoic metasedimentary and plutonic units along the Messabi Fault (Section 4.2).

4.1.2.2.1 Shallowly dipping shear zones

Shallowly dipping shear zones are primarily found in the uppermost northeastern benches of the mine and a single shallowly dipping shear zone is found in the central-north area of the mine (see area D in Fig. 4.2 for location). This latter shear zone is within the gradational contact between the East and West porphyries and was described in Section 4.1.1.2.

A series of shear zones, approximately 100 metres apart, along the northeastern benches, are 30-100 cm thick and trend NW-SE, dipping to the NE (Plate 4.1; Fig. 4.3D), with down-dip stretching lineations. Intermediate to these shear zones are more discrete 5-10 cm thick mylonitic shear zones that are localized along the base of sub-horizontal aplitic dikes. In hand sample these shallowly dipping shear zones are defined by wavy compositional banding consisting of chlorite - (biotite) and discontinuous quartz ribbons of less than 1 mm widths, which also define a stretching lineation. In one exposure a quartz veinlet, 3-4 mm wide, parallels the foliation and displays an intrafolial z-fold (Plate 4.2).

In thin section, the shear zones are composed of weakly elongate polygonal grains, <0.2 mm, of quartz and minor feldspar, chlorite platelets, 0.05-0.1 mm, and minor chloritized biotite, 2-3 mm, aligned subparallel to the plane of foliation (Plate 4.3). Lenticular quartz grain aggregates, 1-2 mm, have axial ratios of approximately 2:1 and are inclined to the foliation. Opaque minerals are associated with biotite/chlorite, present as fine grains (0.1 mm) within the plane of foliation.

Deformation is characterized by grain size reduction of quartz through dynamic

recrystallization processes. The coarser quartz grains and quartz grain aggregates exhibit intracrystalline deformation including subgrain formation, undulose extinction and recrystallization (Plate 4.4). The quartz grains, 2-3 mm, within veinlets show subgrain formation, deformation laminae and recrystallization, with grain boundaries inclined to the foliation. Partially chloritized biotite exhibits weak deformation bands and slip along cleavage planes. The assemblages and structures described above are characteristic of low-grade deformation conditions, forming at 300-400°C, which is consistent with contact aureole conditions around an intruding pluton (Passchier and Trouw, 1996; Simpson, 1985; Schmid and Haas, 1989; FitzGerald and Stünitz, 1993).

At the hand sample scale, shear sense is determined by S-C fabrics (Berthé et al., 1979; Lister and Snoke, 1984) and a quartz veinlet displaying an intrafolial z-fold. In thin section, shear sense is determined from chlorite platelets, that form an S-C fabric around inclined lenticular quartz grain aggregates (Plate 4.4) and alignment of dynamically recrystallized quartz grains (Passchier and Trouw, 1996; Hanmer and Passchier, 1991) in quartz bands and veinlets. These kinematic indicators define a top-to-the-SW sense of shear.

The quartz- chlorite- (biotite)- (feldspar) assemblage and the deformation character of the shear zones, dominantly intracrystalline deformation of quartz, suggest conditions consistent with greenschist metamorphism for the formation of these shear zones (Best, 1982; Simpson, 1985; cf. FitzGerald and Stunitz, 1993). Deformed biotite veinlets(?) parallel the planar shear fabric and provide a relative timing relationship between the potassic alteration stage of PCD emplacement and ductile-brittle deformation.

4.1.2.2.2 Steeply dipping shear zones

Discontinuous, steeply dipping shear zones within the East Porphyry are found sporadically along the eastern expanse of the open pit (Fig. 4.2). Widths are difficult to estimate as the shear zones are usually found with the foliation plane subparallel to the mine bench face. In general, the shear zones are within a few hundred metres of the complex, sheared intrusive contact between the East Porphyry, the Middle Jurassic metasedimentary units and the Triassic Elena Granodiorite. Although orientations of these shear zones vary

Plate 4.1 An approximately strike-parallel view, looking southeast, of a low-angle ductile deformation, mylonitic zone exposed within an upper northeastern bench-face (A2, elevation 2974m).The shear zone occurs within the subporphyritic East Porphyry unit of the Chuquicamata Complex within 200 m of its contact with the Mesozoic Elena Granodiorite. The chloritic shear zone is defined by a quartz-feldspar-mica (chloritized biotite) wavy compositional banding (308/30) on the order of 1 mm wide. Quartz-rod stretching lineations are down-dip and displacement sense is top-to-the-southwest. Low-angle shear zones have only been observed along the uppermost benches in the northeastern sector of the mine in association with the fault contact with country rocks. Hammer is 35 cm in length.

Plate 4.2 Similar view to Plate 4.1 but of a hand sample collected from the same shear zone. The sample shows a foliation-parallel quartz vein that has been deformed into a z-fold indicating a top-to-the-southwest displacement sense. This displacement sense is consistent with kinematic indicators observed in thin section. The presence of the vein suggests a quartz mineralization event prior to, or possibly during, the deformation event. Peso scale is 1 cm in diameter.

Plate 4.1 (see caption on previous page).

Plate 4.2 (see caption on previous page)

Plate 4.3 Photomicrograph illustrating a weakly chloritized biotite veinlet filling a fracture subparallel to the foliation plane within a quartzo-feldspathic band of the mylonite shown in Plate 4.1. Fine chlorite platelets are evenly distributed throughout this sample and assist in the definition of S-C fabrics. Note: the thin section is not oriented with respect to fault zone geometry. Plane polarized light, long axis of photomicrograph approximately 2.5 mm, (CU-1052b).

Plate 4.4 Photomicrograph of a lenticular quartz-grain aggregate that is inclined to the foliation. View is perpendicular to the foliation and parallel to the lineation. The asymmetric quartz porphyroclast illustrates undulose extinction, subgrain formation and recrystallization. The fine chlorite platelets and elongate quartz and feldspar grains within the matrix form an S-C fabric. These and similar kinematic indicators confirm the top-to-the-southwest sense of displacement observed at the hand-sample scale. Crossed nicols, long axis of photomicrograph approximately 2.5 mm, (CU-1052a).

Plate 4.3 (see caption on previous page)

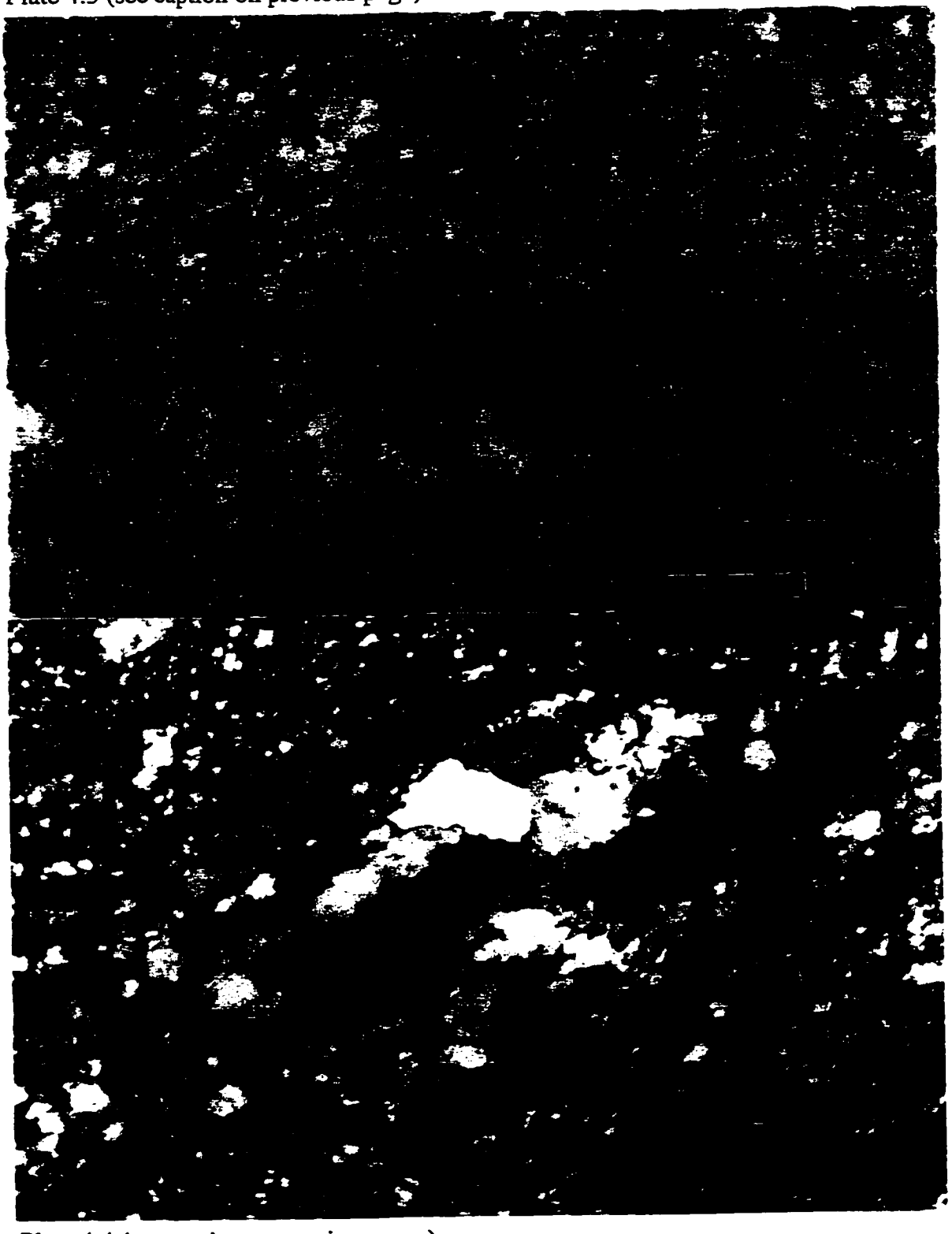

Plate 4.4 (see caption on previous page)

as a result of later brittle fault activity (Fig. 4.3C), they roughly parallel the north-south to NNE-SSW contact.

The shear zones are defined, in hand sample, by alternating bands of thin (<1 mm) quartz ribbons, stretched and flattened quartz eyes (>5:1), granular bands (1-3 mm) of plagioclase- K-feldspar and aggregates of fine grained biotite-chlorite (Plates 4.5 and 4.6). Biotite and chlorite are minor constituents aligned parallel to the plane of shear. Subhedral plagioclase and K-feldspar porphyroclasts (2-4 mm) are aligned with their long axes inclined to the plane of foliation. The planar fabric is best developed by quartz-biotite-chlorite and a poorly developed linear fabric is defined by quartz rods, granular feldspar, and micaceous aggregates. In thin section, the shear zones comprise a matrix of dynamically recrystallized quartz and cataclastically grain-size reduced feldspars (<0.1 mm). Aggregates of chlorite (biotite)-opaques parallel the foliation. Feldspar porphyroclasts are weakly to partially saussuritised.

Deformation structures are exhibited by all minerals comprising the shear zones. Porphyroclasts of plagioclase and K-feldspar show weak subgrain formation, minor intra-fracture recrystallization and undulose extinction (Plate 4.7). For the most part, the porphyroclasts are cataclastically grain-size reduced igneous phenocrysts. Quartz ribbons are dynamically recrystallized (0.05 mm), showing a preferred grain shape alignment (Plate 4.8). Coarser quartz grains exhibit subgrain formation and strong undulose extinction.

Kinematic indicators within these shear zones include sigma-type quartz-feldspar tails on subrounded to rounded quartz and feldspar porphyroclasts (Plates 4.9), grain shape alignment, through dynamic recrystallization of quartz (Plate 4.8), S-C fabric formed in part by quartz bands and inclined aggregates and book-shelf sliding of fractured feldspar porphyroclasts. The shear sense of these kinematic features is consistently dextral. In cases where lineations are not subhorizontal, a dextral-oblique slip with the western-side down is indicated.

The intracrystalline deformation features exhibited by the steeply dipping shear zones are similar in character to those described for the shallowly dipping shear zones and are therefore proposed to have formed under similar conditions.

Plate 4.5 This proto-mylonite shows a lateral variation in grain-size reduction, where the central area of the sample illustrates grain-size reduction of the medium-grained feldspar-rich East Porphyry unit. Towards the left of the photo, cataclasis has reduced the average grain size by a factor of ~10. The mylonitic fabric is composed of quartz, plagioclase, K-feldspar and fine aggregates of chlorite-biotite (wispy black laminae). Porphyroclasts of fragmented plagioclase and K-feldspar crystals within this matrix have been used to determine a dextral sense of shear for this north-south ductile-brittle fault. Millimetre scale is in the upper left corner of the photo and bottom centre is an arrow that approximates north. (CU-841).

Plate 4.6 Hand sample of a NE-SW trending deformation zone in the northeastern section of the mine, cut perpendicular to the foliation (215/70) and parallel to the subhorizontal lineation to observe kinematic indicators. Similar to the previous sample, Plate 4.5, deformation is concentrated within quartz-rich areas. Elongate quartz grains are inclined and bend into the shear plane and (sub-)rounded K-feldspar and plagioclase porphyroclasts are mantled and winged by quartz. These asymmetrically winged porphyroclasts indicate a dextral sense of shear. Also this sample, note that mafic minerals are absent and plagioclase has been partially sericitized. Most importantly, the deformation fabric of this sample is crosscut by stockwork veinlets of Cu-Fe-sulphides having associated quartz-sericitic alteration halos. Note that this sericitization associated with the veinlets is visually distinct from the sericitization of the plagioclase. (CU-848).

Plate 4.5 (see caption on previous page).

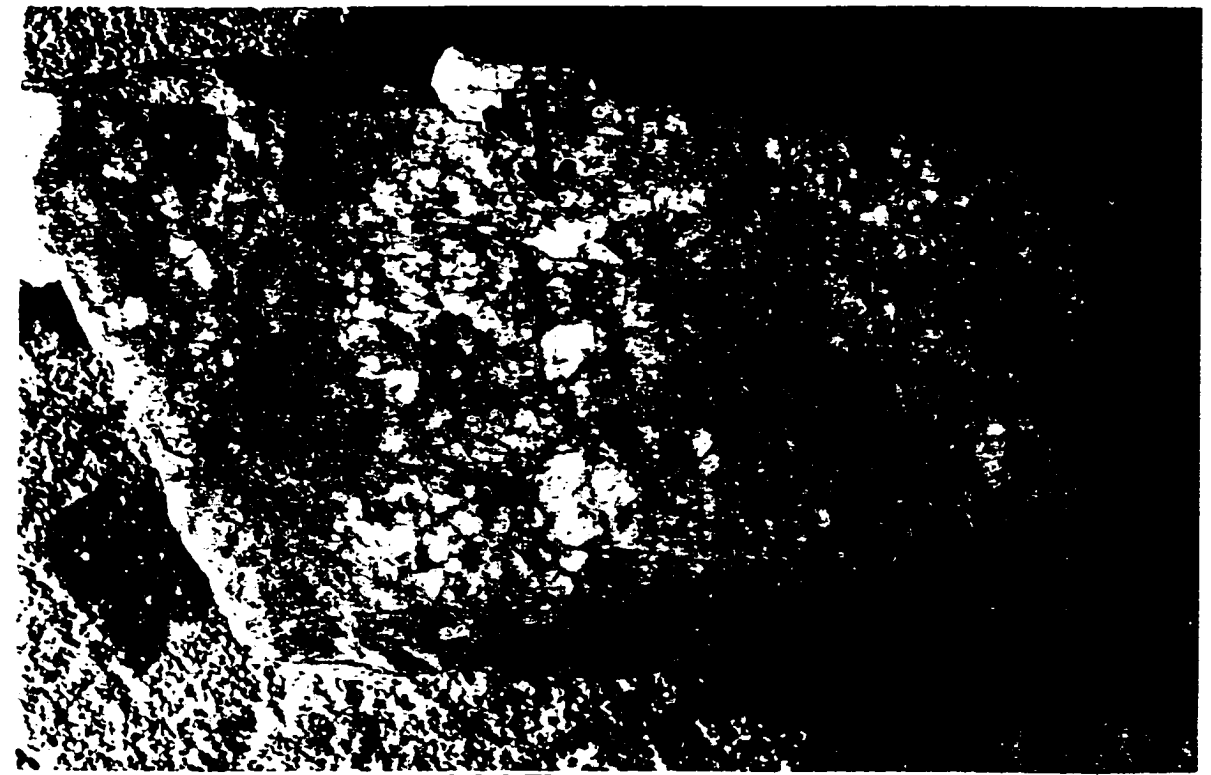

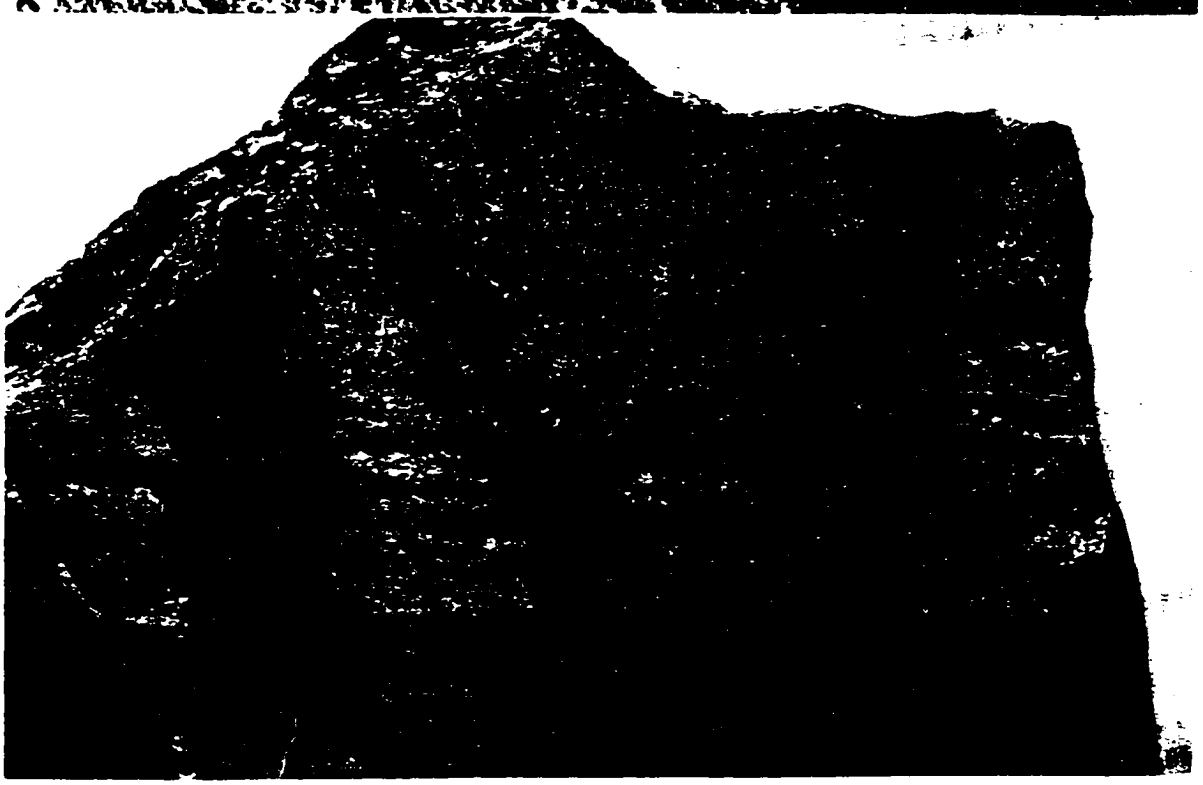

Plate 4.6 (see caption on previous page).

Plate 4.7 Photomicrograph of grain-size reduced perthitic K-feldspar porphyroclast from a deformation zone similar to that shown in Plate 4.5. The porphyroclast shows minor intracrystalline fracture and strong undulatory extinction. Foliation is defined by recrystallized quartz ribbons (see Plate 4.8) and alignment of very fine chlorite platelets. "Tails" or recrystallization of quartz within pressure shadows can be observed on the symmetrical porphyroclast. Crossed nicols, long axis of photomicrograph approximately 2.5 mm, (CU-876).

Plate 4.8 Detail of a dynamically recrystallized quartz ribbon from the same thin section as the previous photomicrograph. The ribbon, which is <0.5 mm in width, is composed of fine elongate quartz grains that are inclined towards the shear direction. The shear plane is defined by the ribbon and the s-fabric is defined by the quartz grain boundaries, in this case the shear sense is dextral. Plagioclase, lower left corner of photomicrograph, is almost completely sericitized. Crossed nicols, the long axis of photomicrograph is approximately 1.5 mm, (CU-876).

Plate 4.7 (see caption on previous page).

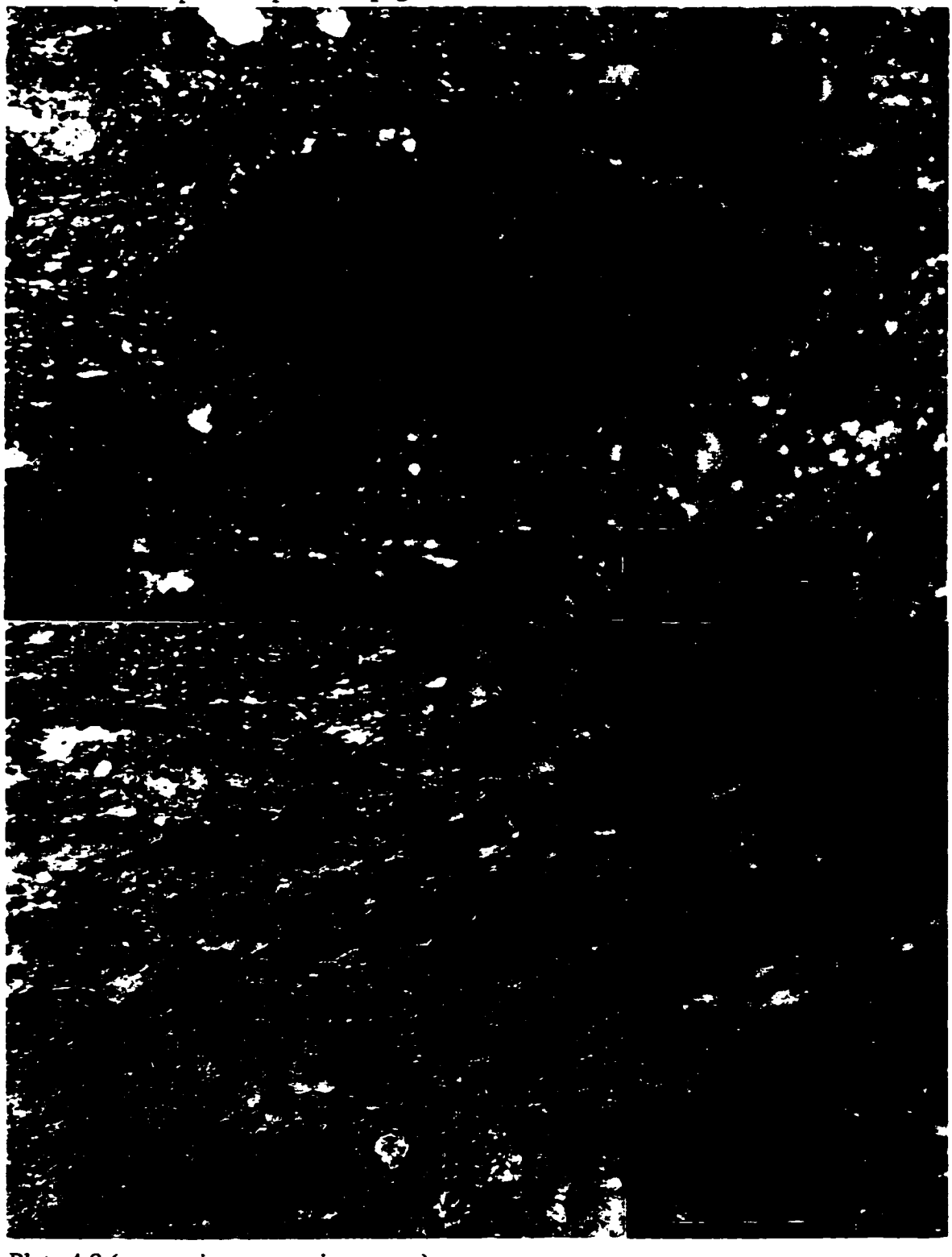

Plate 4.8 (see caption on previous page).

Plate 4.9 Photomicrograph of a rounded K-feldspar porphyroclast illustrating the development of asymmetrical, sigma-type tails composed of recrystallized quartz and cataclastically grain-size-reduced feldspars. Shear sense for this high-angle ductile deformation zone is dextral. Crossed nicols. The long axis of the photomicrograph is approximately 2.5 mm, (CU-876).

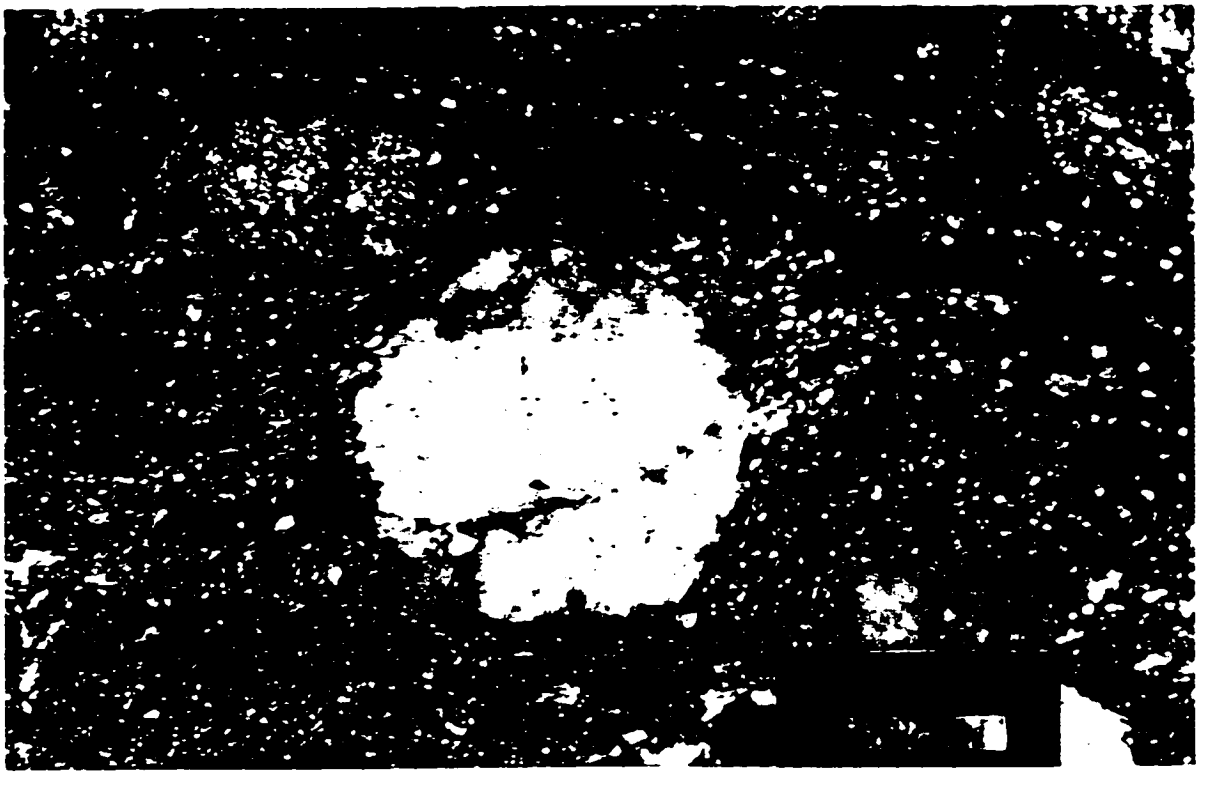

Mineralized fractures, including irregular K-feldspar, quartz-sulphide, and sulphide veinlets with sericitic alteration halos, crosscut the ductile shear zones (Plate 4.6) and clearly indicate that ductile deformation within the CIC took place prior to the formation of the veinlet systems. The sequence of stockwork mineralization is presented in Chapter 5.

4.1.3 Cataclasis and the Chuquicamata Complex

Cataclasis at Chuquicamata is most readily observed as gouge- and breccia- bearing brittle fault systems found throughout the open pit (see Chapter 6). However, cohesive cataclastic rock (see Sibson, 1977; Tullis et al., 1982) are also present in fault and fracture zones and are a pervasive texture throughout the East Porphyry.

Rare planar zones, millimetres to centimetres in width of cohesive micro-breccia in an aphanitic black matrix appear pseudotachylytic, which is inconsistent with a fluid-rich porphyry environment of formation. Rather these structures probably represent quenched melt emplaced during a magmatic hydraulic fracturing event prior to (?) mineralization. Microscopic cataclastic textures are almost ubiquitous in the East Porphyry, especially in samples from along the eastern expanse of the open pit. The texture of the cataclastic deformation is characterized by intragranular to intergranular fractures in feldspar grains that in some cases are healed by matrix minerals. Biotite grains are bent, showing an irregular wavy extinction, and quartz phenocrysts display weak to strong undulose extinction, complex interdigitating grain boundaries and intragranular fractures. The encompassing groundmass is dominantly fine grained recrystallized quartz and comminuted feldspar. These deformation characteristics suggest a bulk plastic-brittle behaviour of the East Porphyry.

Previous work has mentioned the presence of cataclastic textures and has attempted to map the extent of these textures (Langerfeldt, 1964). Soto (1979) and Ambrus (1979) describe an area (200 m X 600 m) in the southeastern part of the mine, which was outlined by Langerfeldt (1964)(Fig. 4.4), stating that cataclastic textures decrease with depth. In present exposures, this cataclastic deformation appears to be restricted between two strongly deformed zones, the Messabi Fault (Section 4.2) and a series of discontinuous shear zones within the East Porphyry (Section 4.1.2.2.2) that trend sub-parallel to the Messabi Fault.

Fig. 4.4 Distribution of the zones of megabreccia and cataclastic deformation delineated by Langerfeldt (1964) and described by Soto (1979) and Ambrus (1979). This zone is shown in relation to the 1995 open pit distribution of structural features. Compared with figures 3.1, 3.2 and 4.2 the cataclastic deformation zone coincides with chloritic to potassically altered East Porphyry and its faulted contact zone (Messabi Fault) with Mesozoic to Paleozoic country rocks. The megabreccia zone is almost wholly associated with the phyllic alteration zone. The megabreccia is projected from bench F4 (2770 m) and the cataclastic zone from H1 (2697 m).

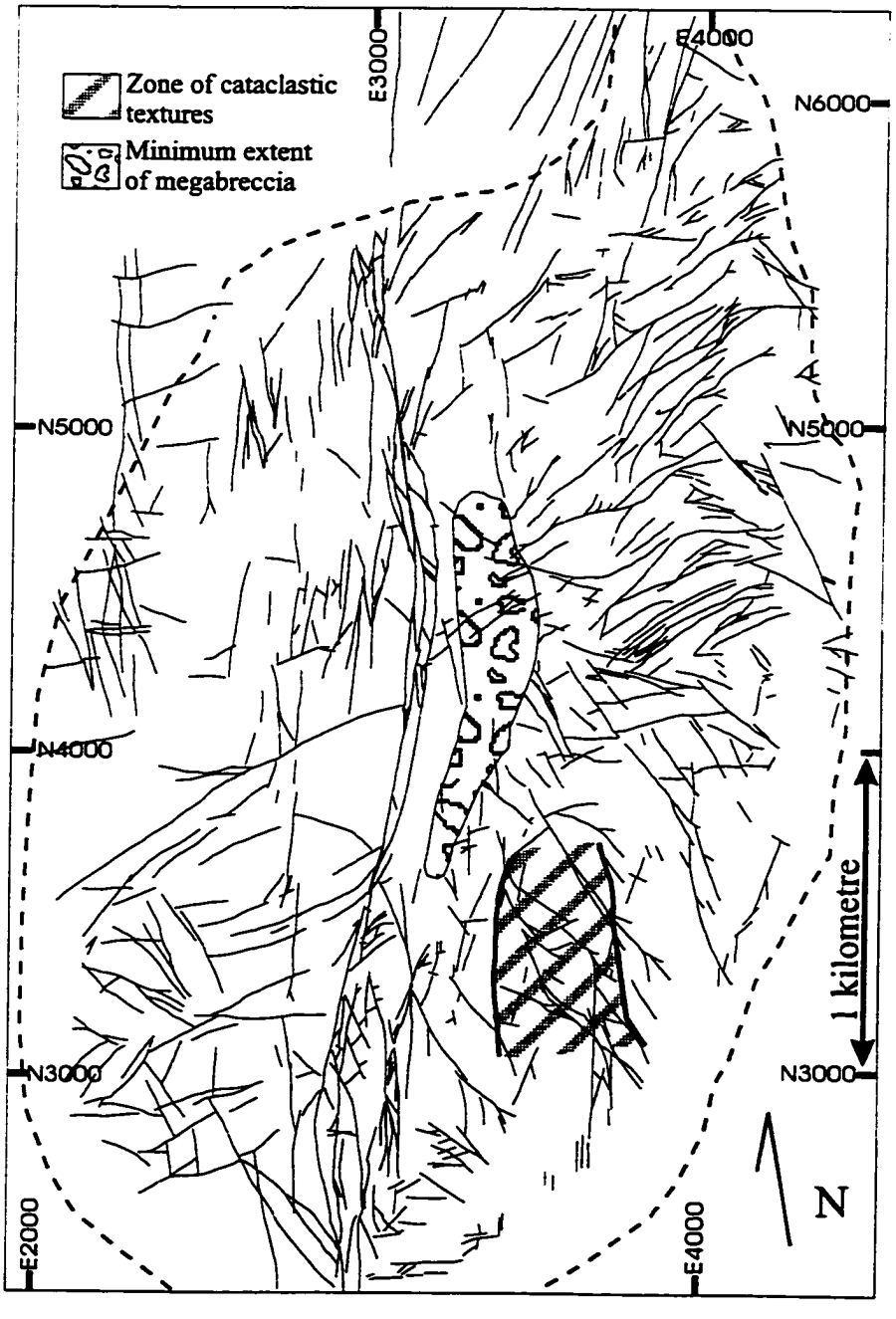

4.1.4 Importance of CIC Ductile-Brittle Structures

Ductile planar fabrics, consisting of weak foliations and mylonitic shear zones, are related to an early deformation following emplacement of the various phases of the CIC. Foliations spatially related to the Banco and West Porphyry intrusive phases, may represent syn-emplacement fabrics related to the intrusion of these porphyries into the cooling East Porphyry. The foliated and gradational contacts of the Banco and West with the East suggest the Banco and West are separate intrusive phases emplaced into the host East Porphyry, which was likely still hot, though crystallized, when the Banco and West were emplaced. This interpretation is consistent with geochronological and trace-element geochemical data that indicate the Banco and West are broadly coeval with the East Porphyry but are geochemically distinct batches of magma, even if closely related (Zentilli et al., 1995). The gradational mylonitic contact of the East and West porphyries with a dextral displacement component suggests the West Porphyry was emplaced at elevated temperatures when deviatoric stresses deformed the complex.

The shallowly dipping, NW-striking, dip-slip reverse mylonitic shear zones also indicate the presence of a deviatoric stress field while the CIC was at elevated, lower greenschist, temperatures, with NE-SW directed shortening being indicated. Steeply dipping mylonitic shear zones are oriented subparallel to the complex, intrusive and deformed contact between the East Porphyry and the older country rocks. The majority of these shear zones are located approximately 100 m from the contact, have variable mineral assemblages due to contact metamorphism and overprinting by later hydrothermal alteration, and consistently indicate a dextral to dextral-oblique sense of displacement. They are inferred to indicate that the East Porphyry was still at elevated temperatures when dextral shearing occurred along its eastern border, probably related to activity along the subparallel dextral Messabi Fault (see Section 4.2). Weak foliations, produced by dextral simple shear, trend parallel to the principal fault directions of the Zaragoza and Estanques Blancos fault systems. These and other steeply dipping shear zones are crosscut by mineralized veinlets. This relationship suggests that some of the regional scale displacement along these fault systems may be attributable to ductile deformation occurring prior to mineralization at Chuquicamata.

A cataclastically deformed area, found between the sheared intrusive contact of the Chuquicamata Complex and Mesozoic rocks, or Messabi Fault (Section 4.2), and the discontinuous exposure of steeply dipping shear zones, suggests the deformation of a cooled margin of the CIC subsequent to shear zone formation. Although the cataclastic textures of this zone would have provided a sufficient permeability network for mineralizing fluids, mineralization appears minimal and disseminated.

Within the shear zones and the cataclastically deformed area, textures and deformation styles of quartz and feldspar, which define fabric elements consistent with bulk heterogeneous shear, indicate an approximate temperature range of 300° to 500°C. The plastic-brittle deformation textures and mineral assemblages, associated with the emplacement and cooling of the host porphyry, are consistent with deformation at greenschist grade temperatures. This deformation phase is clearly pre-hypogene mineralization as mineralized veinlets crosscut the plastic-brittle shear zones.

4.2 The Messabi Fault System: Assisting CIC Emplacement?

The Messabi Fault System is composed of a band of ductile shear zones that limit the Chuquicamata Complex to the east (Fig. 4.1; Fig. 4.2). The shear zones that define the Messabi Fault are contained within a thin belt (≤300 m) of Mesozoic meta-sedimentary units (see above, Chapter 2.2). Northwards from Chuquicamata, this north-south shear zone curves to become northeast-southwest trending over a length of approximately 8 kilometres. As the fault nears Chuquicamata it is offset by a series of dextral brittle faults that displace the trend of the shear zone southwest. These displaced portions of the metasedimentary hosted shear zone are exposed in the open pit. The southern continuation of the Messabi which is located in the open pit has been reactivated as a brittle sinistral fault, known as East Fault (Fig. 4.1), and bears sericitic-argillic alteration. Southwards from the Chuquicamata open pit, the trace of the Messabi is covered by mine infrastructure and Miocene-Pliocene gravels.

Along the northern trace of the Messabi, relatively small, massive magnetite-(hematite) bodies are present (Martin et al., 1993). These authors suggest a probable fault controlled emplacement mechanism for these deposits. However, further studies of the iron-

rich deposits and their structural relationships are warranted to determine whether their origin is sedimentary (ironstones, Boggs, 1987), hydrothermal, or replacement (e.g. Mackin, 1968, in Park and MacDiarmid, 1975; Guilbert and Park, 1986), and their relation, if any, to the Chuquicamata Intrusive Complex and porphyry deposit.

The Messabi Fault is considered an associate fault of the West Fault within the West Fault System (Chapter 2.5.3.1). It is suggested to have assisted in the emplacement of the Chuquicamata Complex during a bulk non-coaxial dextral shear probably initially associated with the Middle-Late Eocene Incaic shortening phase, but outlasting that event.

The Messabi Fault zone parallels and in part forms the contact of the Chuquicamata complex (East Porphyry) with the Mesozoic metasedimentary units. The CIC-metasedimentary unit contact relationship is intrusive as evidenced by metaigneous and metasedimentary xenoliths in an East Porphyry matrix, and granitic quartz-K-feldspar apophyses of the CIC traceable into Mesozoic amphibolitic and hornfelsed units. The geometrically complex Messabi Fault has accommodated a bulk, ductile to brittle, heterogeneous shear, resulting in a finite displacement on the order of two kilometres (Tomlinson and Blancos, 1997a).

4.2.1 Displaced Blocks Bearing the Messabi Fault

Deformation of the Messabi Fault is present in a band of Mesozoic metasedimentary units of Jurassic marine sedimentary and Triassic volcanic-volcaniclastic formations. Outcrop exposures within and to the immediate northeast of the Chuquicamata open pit, comprise contact metamorphosed calcareous shales, siltstones, carbonates, tuffaceous andesitic agglomerate and porphyritic andesites. As a result of later brittle faulting, packages, or blocks, of these metasedimentary units have been offset into a southwestern stepping pattern (A through F, Figure 4.2). These individual offset, fault-bound blocks are composed of differing packages of volcano-sedimentary stratigraphy through which shear zones of the Messabi Fault pass. The complexity of the fault-bound slivers is enhanced by brittle deformation which overprints the district. In some cases, the original sedimentary features such as bedding, graded bedding and asymmetric ripple marks are preserved in fault-bound

blocks and slivers.

4.2.1.1 Blocks within the open pit

Blocks A and B are dominantly composed of fine grained, black, calcareous to carbonaceous pelites composed of a quartz- sericite- chlorite- carbonate assemblage and minor beds of black to tan, recrystallized meta-carbonates (meta-micrites). Adjacent to the CIC intrusive contact, these units are hornfelsed. Several tens of metres away from the contact, a strong planar fabric defined by micaceous and carbonaceous materials of the pelites delineate a shear zone whose total width is not exposed. Close to the CIC contact, the orientation of the planar fabric is NNW-SSE dipping subvertically westward (Fig. 4.5A and B). This orientation may be reoriented from the regional N-S to NNE-SSW trend of the Messabi fault, as a result of intrusion of the CIC into the metasedimentary block, stoping of the metasedimentary block during emplacement of the CIC, and/or small block rotation associated with numerous younger brittle faults present in this part of the mine.

Kinematic indicators within the pelites and calc-silicate units include sigma-type winged porphyroclasts (Hanmer and Passchier, 1991), S-C fabric microstructures (Berthé et al., 1979) and mesoscopic intrafolial z-type folds. The microstructures indicate a dextral sense of shear. The few observed lineations are southward trending with plunges of 20-30 degrees suggesting oblique displacements on this steeply-dipping shear zone. NNW-SSE trending, horizontal hinge lines of mesoscopic (parasitic?) folds in calc-silicate units are subparallel to the shear zone foliation suggesting fault-normal shortening across the Messabi fault or rotation of folds into the shear direction as a result of progressive shear.

Metamorphic assemblages associated with the shear zones are dominated by quartz-muscovite-chlorite-feldspar-(biotite). Although there is no apparent evidence of a static metamorphic overprint, eg. metacrysts, that might be associated with a contact aureole or the quartz-sericite hydrothermal event described in Chapter 3.3.3, very fine grained sericite-clay minerals(?) replace feldspar porphyroclasts in some of the observed thin sections. Late crosscutting veinlets include feldspar (adularia), quartz, quartz+chlorite, calcite, and calcite+chlorite.

4.2.1.2 Limited open pit exposure

The limited exposure of Block C is located along the easternmost upper benches; extending, at surface, beneath a cover of mine waste materials (sector C in Fig. 4.2). As in the previous section, the shear zones of the Messabi Fault are concentrated in metasedimentary units of quartz- muscovite- (carbonaceous materials)- (clay) pelites. The exposed section is approximately strike parallel so that strongly foliated granodiorites at the base can be seen grading into foliated metasedimentary units higher in the bench face. In contrast to the orientation of the planar fabric of blocks A and B, the fabric here is oriented NW-SE dipping at a low-angle to the NE (Fig. 4.5C compare Fig. 4.3D). Kinematic data are unavailable, but this low-angle fabric is inferred to have developed during the same event that formed the similarly oriented, low-angle, reverse-fault fabric in the CIC (see Section 4.1.2.2.1).

4.2.1.3 Surface exposures : Reconnaissance mapping

The stratigraphic package in block D differs from the previously presented pelite and calc-silicate dominated blocks. Surface mapping shows that this block is dominantly composed of reddish andesitic agglomerate, which varies northwards to a facies with a carbonate-rich matrix. The agglomerate bears rounded buff coloured meta-carbonate and sericitically altered andesitic clasts at its northernmost exposure. Along its western contact, this agglomerate is in sharp fault contact with the shear zone pelites and calc-silicates. Deformation is constrained to the pelitic units while the calcareous units do not show evidence of deformation, which may be the result of recrystallization processes following the deformation phase. The planar fabric trend in this block is oriented NNW-SSE dipping moderately eastwards (Fig. 4.5D compare 4.5A and B). The pelites show weak compositional layering composed of alternating quartz-feldspar-chlorite and chlorite-epidote-rich bands, at the millimetre scale. These bands comprise the shear fabric along with aligned chlorite and elongate aggregates of recrystallized quartz grains. A dextral shear sense is indicated by S-C fabrics. Fine chlorite group minerals, $<<0.1$ mm, define a weak secondary crenulation fabric which is not observed in hand samples.

Fig. 4.5 Schmidt lower-hemisphere stereographic projections of planar fabrics associated with the Messabi Fault. These stereoplots correspond to the bracketed areas outlined in Fig. 4.2 that encompass individual segments of the Messabi Fault that are separated by cross-cutting brittle fault systems that trend NE-SW. (+) fabrics found in igneous units; (o) fabrics found in metasedimentary rock units. These plots may be compared with those plots of fabrics found in the CIC units as presented in Fig. 4.3. See discussion in text.

Fig. 4.5 (see caption on previous page)

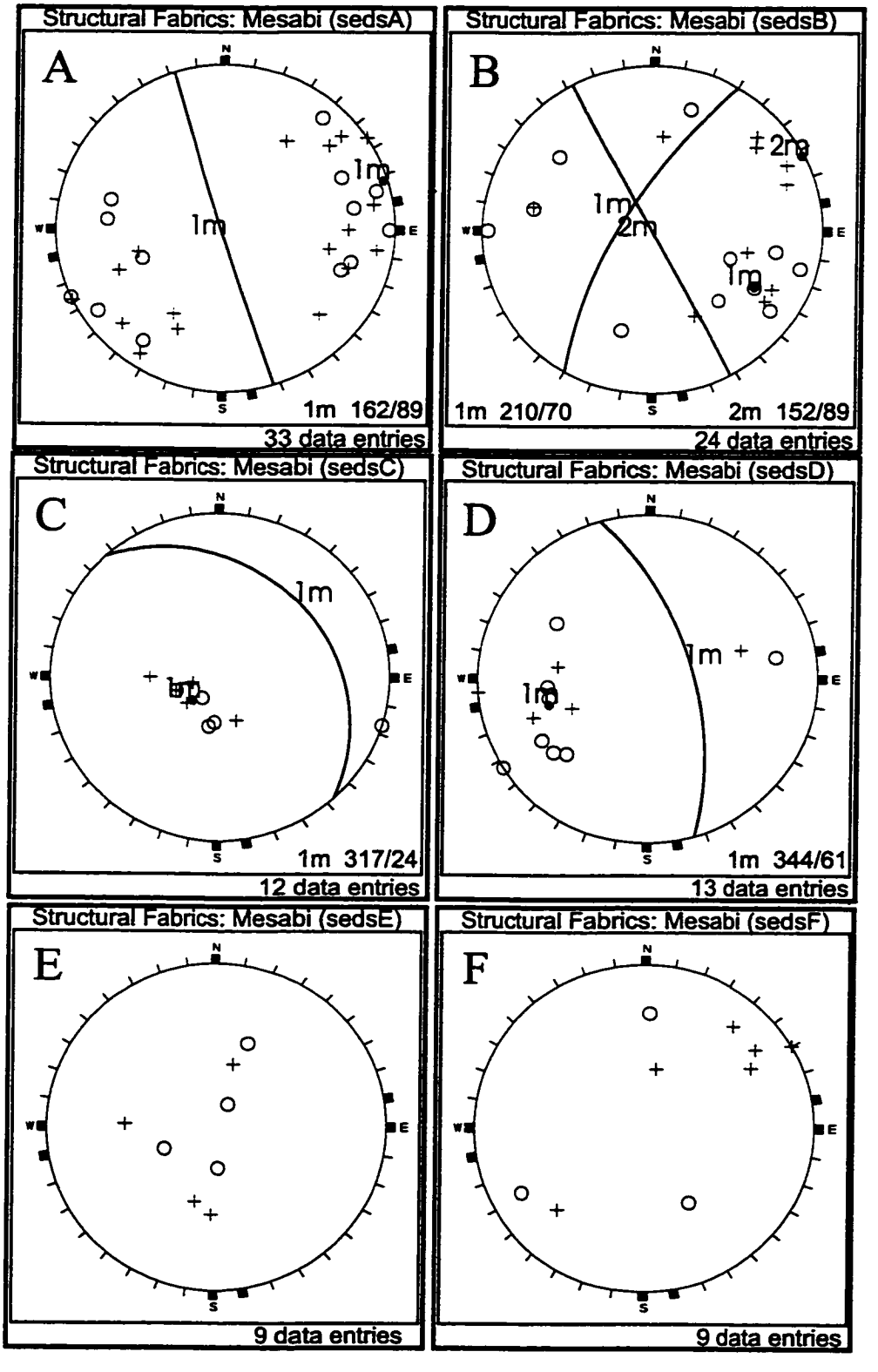

Surface exposures of blocks E and F (Fig. 4.2) are limited to shallow exploratory pits from the turn of the century. Mapping of block E indicates an undulatory nature to the meta-sedimentary units. A well-bedded, fine grained, quartzo-feldspathic-(carbonate) unit appears to underlie the carbonate facies conglomerate described previously. Sparse exposures of the conglomerate show pebble- to cobble-sized clasts that include volcanic and carbonate fragments in a medium to coarse grained matrix. Besides the primary fabric (bedding) in the (meta)siltstones no other fabrics were apparent.

Block F contains mostly hornfelsed units that occur as isolated individual, or trails of xenoliths, near and along the contact of the CIC with the Mesozoic block that trends away from the mine (Figs. 4.1 and 4.2). Reconnaissance mapping indicates a more diverse Mesozoic stratigraphic package within this block and further north. This area includes microdiorites, both massive to porphyritic dacitic to andesitic units, and meta-sedimentary units. In association with the Mesozoic units, the Chuquicamata complex units are observed to have planar fabrics that parallel the contact of the main block of meta-sedimentary units. Deformation fabrics observed in a porphyritic dacite from the Mesozoic block and an adjacent mylonite zone within the East porphyry unit are similar. Mineral assemblages of quartz-feldspar-chlorite-(biotite) define a planar fabric that is best developed in the East Porphyry. Quartz shows sub-grain formation and recrystallization, whereas rounded phenocrystic feldspars deformed by cataclastic grain-size reduction. Chlorite parallels the fabric and fills fractures. Kinematic indicators across this zone suggest a dextral sense of displacement. Lineations of the East Porphyry and a foliated porphyritic dacite pitch between 30° and 65° to the south on N- and NW-striking, westward dipping subvertical shear planes. The relationship of planar and linear fabrics suggest a high angle oblique fault with a west-side-up sense of displacement. The above deformation characteristics are similar to those presented for the ductile-brittle deformation zones in the Chuquicamata complex, suggesting deformation under similar lower greenschist metamorphic temperatures.

4.2.2 Messabi Fault Zone Summary

Ductile deformation within the Messabi Fault zone affects Paleozoic through Tertiary igneous and sedimentary rock units. The fault zone is comprised of shear zones that bound lesser deformed, or recrystallized, metasedimentary slivers. The shear zones are concentrated within pelitic and calc-silicate units of the Middle Jurassic (Chapter 2.2.2). Deformation is also localized adjacent to and along the Tertiary-Mesozoic contact where the Chuquicamata Intrusive Complex is deformed into mylonitic shear zones.

The dominant mineral assemblages of the shear zones are composed of quartz-feldspar-chlorite-(biotite) and quartz-muscovite-chlorite-(feldspar) with variable amounts of opaque minerals. Deformation character of the shear zones is characterized by plastic intracrystalline mechanisms in quartz and cataclastic, or brittle to plastic-brittle transitional, mechanisms in feldspars and micas. Kinematic indicators, present as S-C fabrics and asymmetric winged clasts, indicate dextral displacement along the shear zones comprising the Messabi Fault Zone. The mineral assemblages and deformation character of the shear zones suggest greenschist facies temperatures at the time of deformation and are likely to have formed during the cooling of the CIC.

4.3 Timing of Ductile(-brittle) Deformation

Timing of ductile deformation at Chuquicamata, both within the Chuquicamata complex and along the associated Messabi Fault, are defined by geochronological data. A lower age limit is constrained by the massive, texture destructive, sericitic alteration phase that parallels fault and vein structures which crosscut ductile deformation zones. This alteration phase occurred at about 31 Ma. An upper age limit for ductile deformation in the CIC corresponds to the age of emplacement of the CIC, which has been proposed to be ca. 34-33 Ma (Zentilli et al., in press). Ductile deformation along the Messabi Fault could be older, but given the similarities of its structures and those in the CIC and its spatial association with the CIC, it is inferred that the ductile deformation fabrics of the Messabi fault formed contemporaneously with the ductile fabrics of the CIC at ca. 34-33 Ma shortly after emplacement.

Field relationships, presented previously in this chapter, suggest that the Chuquicamata complex intruded parallel to the Messabi shear zone and is itself deformed by displacement along the Messabi shear zone. Following emplacement, the Chuquicamata complex cooled and ductile-brittle deformation processes must have been operative localizing strain in the formation of zones of planar fabrics. In attempt to establish an intrusion age for the Chuquicamata complex, Zentilli et al. (1994) present an inconclusive U-Pb zircon (lower intercept) age of 32.3 ± 5 Ma for the East Porphyry unit. $^{40}Ar/^{39}Ar$ ages of least altered (potassic and chloritic) and undeformed samples of the CIC indicate a range of ages from 33.3±0.2 to 35.2±0.2 Ma (Reynolds et al., in press). Reynolds et al. (in press) also present a sample of East Porphyry mylonite from outside of the open pit as having a slightly younger age of 32.8±0.2 Ma. An $^{40}Ar/^{39}Ar$ analysis of sericite from a quartz-muscovite schist within the Messabi Fault provides a similar 33.4±0.2 Ma age (Cuesta Research, unpublished data) most probably a reset older age resulting from the intrusion of the CIC.

The observed planar fabrics within the Chuquicamata complex are composed of mineral assemblages akin to those of potassic alteration and are crosscut by veinlet arrays that are also associated with potassic alteration. The initial interpretation of the observed relationships and available geochronological data is the absolute geochronological dates represent deformation ages reset by the high temperature (>350°C) potassic alteration phase. However, considering that potassic alteration is a high temperature alteration, associated with the final stages of crystallization, and that the intrusion was emplaced within an epizonal environment, it is suggested that the geochronological data, even if reset by potassic alteration, approximates the age of emplacement, crystallization and ductile deformation of the CIC.

4.4 Pre-mineralization (Ductile-Cataclastic) Deformation

This chapter has presented data on a characteristic set of poorly exposed ductile faults in and around the Chuquicamata complex. These faults, or mylonitic shear zones, bear deformation microstructures and mineral assemblages which indicate formation at

greenschist facies conditions. Low to medium-grade metamorphic conditions, 300-500°C, described by Passchier and Trouw (1996) are similar to those proposed by Simpson (1985) as low to mid-greenschist conditions for deformation across the ductile-brittle transition (compare Scholtz, 1988). The emplacement of the porphyry host rocks into epizonal levels precludes the metamorphic greenschist grade and brittle-ductile transition connotation of deformation depths on the order of 8-15 kilometres. Instead the heat of intrusion and magmatically derived fluids, possibly in association with pore fluids from the intruded country rock, are responsible for the alteration assemblages and deformation character of the porphyry host rock. Contact metamorphism of the metasedimentary units, within which the Messabi Fault occurs, is limited to narrow zones of hornfelsed metasedimentary units immediately adjacent to the intrusive contact of the Chuquicamata complex. The recrystallized nature of carbonate units and unstrained chlorite grains, which form S-C fabrics in pelitic units, suggest post-deformation solid-state crystallization related with a cooling thermal aureole associated with the initial intrusion, East Porphyry, or the subsequent intrusion of Banco Porphyry. This thermal aureole is reflected in the distribution of radiometric age dates, which coincide with those of the potassic alteration (34-33 Ma, Reynolds et al, in press), within the shear zones of the Chuquicamata complex and for schists associated with the Messabi Fault. However, deformation continued, as microstructures within quartz eyes and ribbons of the East Porphyry shear zones do not show complete recovery. The development of a wide cataclastic zone within the East Porphyry, adjacent to the Messabi Fault, supports continued deformation at low temperatures. The characteristics of the deformation and metamorphism are consistent with an epizonal emplacement for the Chuquicamata complex (Sillitoe, 1973) and suggest the mylonitic shear zones formed in this otherwise brittle environment because of the heat supplied by the CIC. Mylonitic shear zones formed during emplacement, crystallization and cooling with progressively more brittle conditions being produced as the complex cooled, probably ending with the development of the fully brittle fault systems.

Although this is a limited exposure of the magmato-tectonic arc, in which the CIC resides, the data of early, localized ductile deformation is compatible with the regionally

based, subduction-driven, dextral strike-slip to transpression model (Reutter et al., 1991, 1996; Scheuber and Reutter, 1992; Scheuber et al., 1994; Tomlinson and Blanco, 1997). The orientation of shallowly dipping reverse faults and steeply dipping dextral strike-slip to oblique-slip faults concur with structures expected to form in dextral strike-slip settings (Fig. 4.6; Woodcock and Schubert, 1994; Sanderson and Marchini, 1984).

Scheuber and Reutter (1992), from a regional perspective, propose that shortening of the Late Cretaceous-Late Eocene magmatic arc into N-S trending Paleozoic basement cored anticlines with steep to overturned limbs of Mesozoic sequences preceded and overlapped with dextral transcurrent deformation. In contrast, Tomlinson and Blanco (1997) propose a regional-scale sinistral strike-slip event associated with the Messabi Fault, citing evidence from the map-scale structure of Permian and Triassic granitoids and meta-granitoids in the Chuquicamata Hills, preceding the observed dextral deformation (Lindsay et al., 1995, 1996; Reutter et al., 1996; Tomlinson et al., in prep). Data from this study is compatible with both regionally-based structural models. The dextral ductile deformation appears centred within Mesozoic meta-sedimentary sequences of the Messabi Fault yet is also present in the CIC suggesting synchronous formation of reverse faults and steeply-dipping strike-slip to oblique-slip faults through distributed deformation within a regional strike-slip fault system that involved the Chuquicamata Intrusive Complex. The intrusion and early deformation of the CIC represents only a portion of the total regional deformation. The evidence from this study, although it can not constrain events prior to the emplacement of the CIC, must be accommodated by regional models.

Fig. 4.6 A) Initial fault geometries, after the first increment of deformation, for the structural features that may form within dextral transtensional, wrench tectonic and transpressional strike-slip deformational settings (from Sanderson and Marchini, 1984). B) A generalization of the ductile fabrics and their geometry approximated in and around the Chuquicamata open pit. Although the orientations of these features may be modified by progressive shear and later brittle faulting, their geometrical similarity to the simple shear and transtensional geometries is inferred as a first approximation.

Fig.4.6 (see caption on previous page)

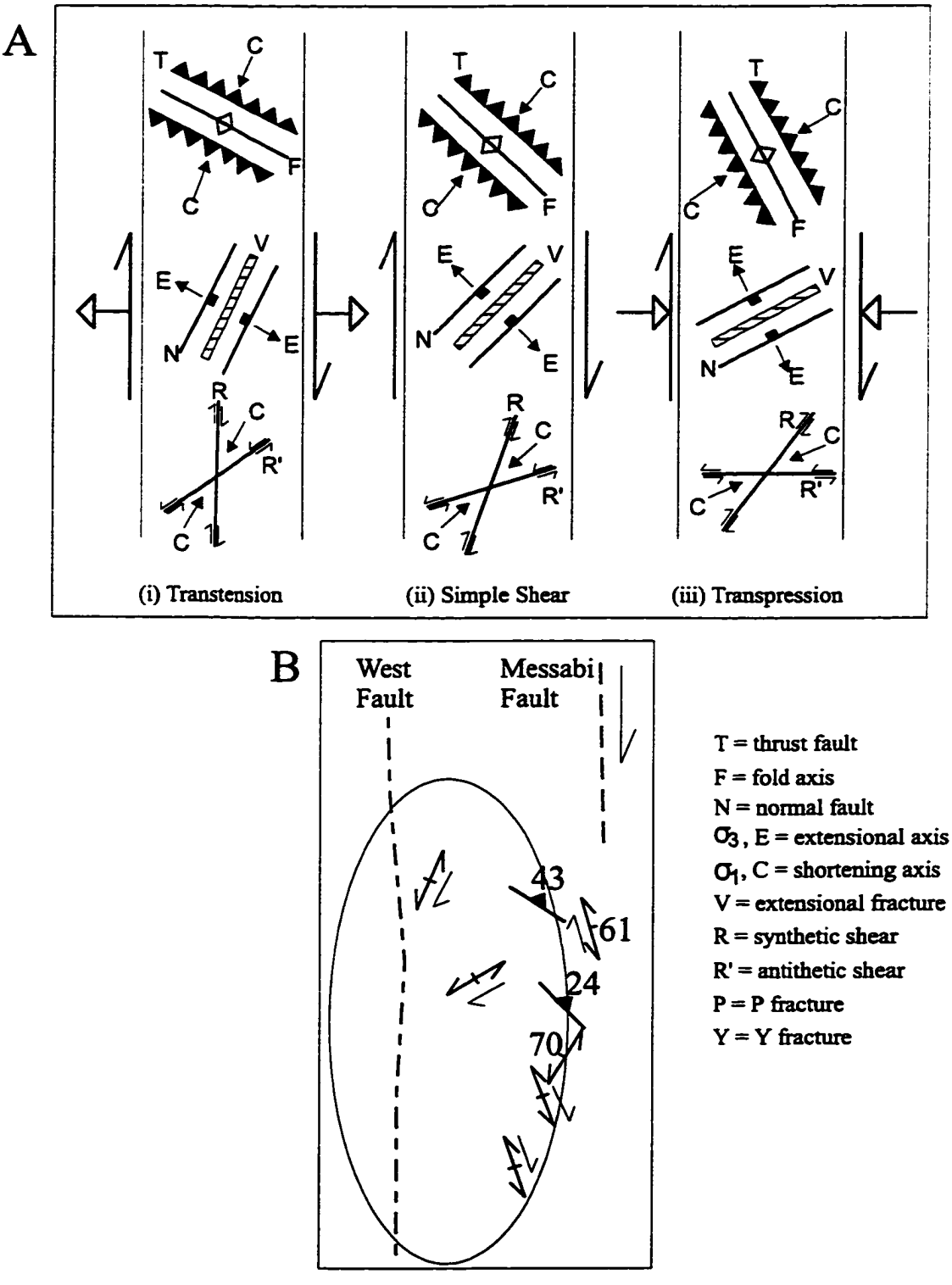

Chapter 5. Mineralized Veinlet Systems and Structural Sampling

Stockwork systems are recognized as an important control on the mineralization, alteration and fluid evolution in porphyry copper systems (Phillips, 1973; Hollister, 1978; Burnham, 1979; Gustafson and Hunt 1975; Sillitoe, 1985; Hunt 1991; Titley, 1993; Gustafson and Quiroga, 1995). Thermodynamic considerations and numerical modelling have shown that above and within the cooled carapaces of shallowly emplaced magmatic intrusions, fracture systems develop in response to magmatic cooling and fluid saturation, and as such may host porphyry-type deposits (Burnham, 1979; Koide and Bhattacharji, 1975; Knapp and Norton, 1981). This recognition of fracturing and ore potential lead to studies examining regional fracture and dike patterns and relating the patterns to intrusions, porphyry deposits, and regional stress fields (eg. Rehrig and Heidrick, 1972; Titley and Heidrick, 1978; Heidrick and Titley, 1982). Key studies have focussed on regional quantification of vein and fracture densities in the southwestern United States (Rehig and Heidrick 1972; Haynes and Titley 1980; Titley et al. 1986) and deposit-specific fracture evolution and density studies (Titley et al, 1978; Haynes and Titley, 1980; Haynes, 1984; Titley et al., 1986). These studies showed trends of increasing fracture densities as porphyry-type deposits were approached from the surrounding country rock, indicating that the intrusion-related porphyry was associated with the generation of the widespread fracture systems.

Collection of directional data for mineralized veinlet sets from *within* porphyry-type deposits is becoming an accepted practice. The focus is usually on gross vein, veinlet and fracture trends (e.g. Casselman et al. 1995; Heberlein 1995) with few studies considering the influence of domainal fault systems (e.g. Baldwin et al., 1978) on the mineralized veinlet systems and therefore on trends in ore grades (Lindsay et al., 1995).

In this chapter, directional data collected from a series of sample sites within the stockwork zone of the Chuquicamata deposit, are examined from several perspectives. First, the general characteristics of the stockwork system are presented, including distribution, veinlet types, and relative timing. Then the structural sampling data is related to the distribution of alteration zones within the deposit and summarized with respect to the

structural sectors, in which the sample sites are located. A follow-up discussion then examines the formation and controls on the stockwork system and the resulting anisotropy of ore grades at Chuquicamata.

5.1 Chuquicamata: Scale of Mineralization

The Chuquicamata deposit may be described as three distinct mineralization scales: a disseminated deposit where copper-bearing sulphides are irregularly distributed in the monzogranodioritic host rock and brecciated zones, a deposit of mineralized stockwork or sheeted veinlet systems where mineralization is contained in thin veinlets, and a deposit of a sequence of vein arrays that contain concentrations of both copper and molybdenum. Lopez (1939, 1942) indicated that the majority of ore mineral assemblages at Chuquicamata are contained in veins and veinlets. Initial descriptions of the mineralization stated the relative abundance of Cu-sulphides as decreasing from chalcocite, through enargite, covellite, tennantite-tetrahedrite, and bornite to chalcopyrite. The order of hypogene mineral deposition was described as: quartz, pyrite, enargite, chalcopyrite-bornite and tennantite-tetrahedrite in vein assemblages concentrated near the NE border of the open pit (Fig. 5.1)(Lopez, 1939, 1942). In a report on Chuquicamata, stating "...considering Cu-sulphide mineralization seems to be closely associated with many different kinds and ages of quartz veining...", Langerfeldt (1964) recommended that an emphasis be given to the study and mapping of quartz veinlets. Soto (1979) examined veinlet concentrations in drillcore and outlined zones of higher veinlet densities central to the open pit and adjacent to the West Fault (Fig. 5.2). A compilation of pit surface mapping, also showed a coincidence of copper concentrations and the abundance of quartz veinlets, and that high copper concentrations were located adjacent to, but not wholly within, the quartz-sericitic alteration zone (Fig. 5.3)(Soto, 1979).

This chapter describes the veinlet scale of mineralization, which is considered distinct from the vein scale that is presented in Chapter 6. The distinction between the scales of mineralized systems is based on rare crosscutting relationships principally between a quartz-molybdenite vein array and the underlying stockwork system that is presented here.

5.1.1 Distribution of Stockwork Systems at Chuquicamata

Sites studied within this project are representative of several alteration zones but with a bias towards sericitic and sericitic-over-potassic zones (Fig. 5.1). The bias results from the widespread overprinting of the potassic alteration zone by a sericitization of plagioclase feldspars. The majority of the study sites correspond to the zones of high veinlet concentrations outlined by Soto (1979) (Fig. 5.2). The actual extent of mineralized and quartz-bearing stockwork at Chuquicamata is restricted to the sericitic through potassic alteration zones (Fig. 5.1; cf. distribution of Lopez, 1939).

An abrupt termination in the southward extension of the stockwork system along the eastern mine slope correlates with principal fault structures (see below, Chapter 6) that have apparently displaced the veinlet systems. In the southernmost areas of the open pit, veinlet systems are limited by branches of the West Fault System. Adjacent to the West Fault, within the quartz-sericitic alteration zone, stockwork mineralization is discontinuous at best, usually observed as pervasively altered blocks of host rock containing stockwork mineralization within the massive quartz-sericite alteration zone. Adjacent to the West Fault, low-density veining (0.6 veins/m) of dominantly pyrite-enargite mineralization is common (Rojas and Lindsay, unpublished data).

5.1.2 Veinlets of the Stockwork Systems

The sampling sites of this project cover a vertical range of approximately 450 m, only a small fraction of the suggested >3-8 km vertical extension of porphyry copper systems (Lowell, 1968; Dilles and Einaudi, 1992). The stockwork systems currently exposed in the open pit show compositional variety from quartz veinlet dominated systems along the central axis of the open pit, through quartz-sulphide systems, to quartz-poor-sulphide-rich systems adjacent to the quartz-rich zone and in the central northeastern sector of the mine. Further studies, using drillcore logging, may evaluate the continuity and compositional variances in the veinlet systems at depth and with respect to other deposit characteristics.

Fig. 5.1 A) Distribution of structural sampling study sites in relation to principal fault and vein structures mapped within the Chuquicamata open pit. B) The same study sites with respect to the distribution of the alteration zones mapped within the open pit. Both A and B show the approximate extent of the stockwork, as an irregular polygon, and the projected extent of the mineralized veins discussed by Lopez (1939), as an ellipse. Black circles are locations of structural sampling sites within the stockwork system. These are discussed with the text.

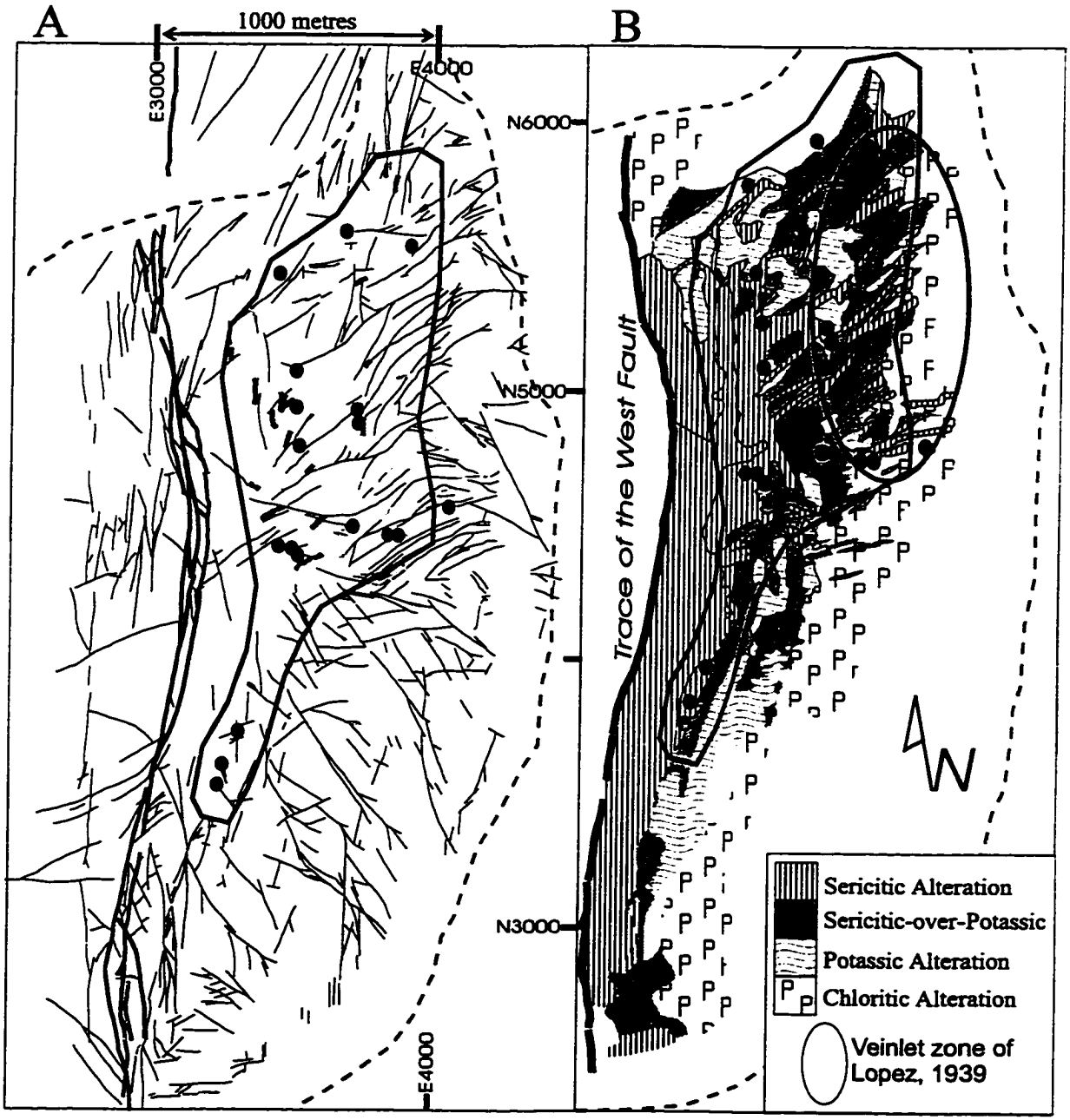

Fig. 5.2 Distribution of veinlet concentrations in cross-sections N4400 and N4900 with sample sites from this study projected into the sections. Note that the majority of study sites are adjacent to the zone of high concentration and that the current pit surface at the time of sampling is reflected by the position of the study sites. Vertical scale equals horizontal scale. Cross sections after Soto (1979).

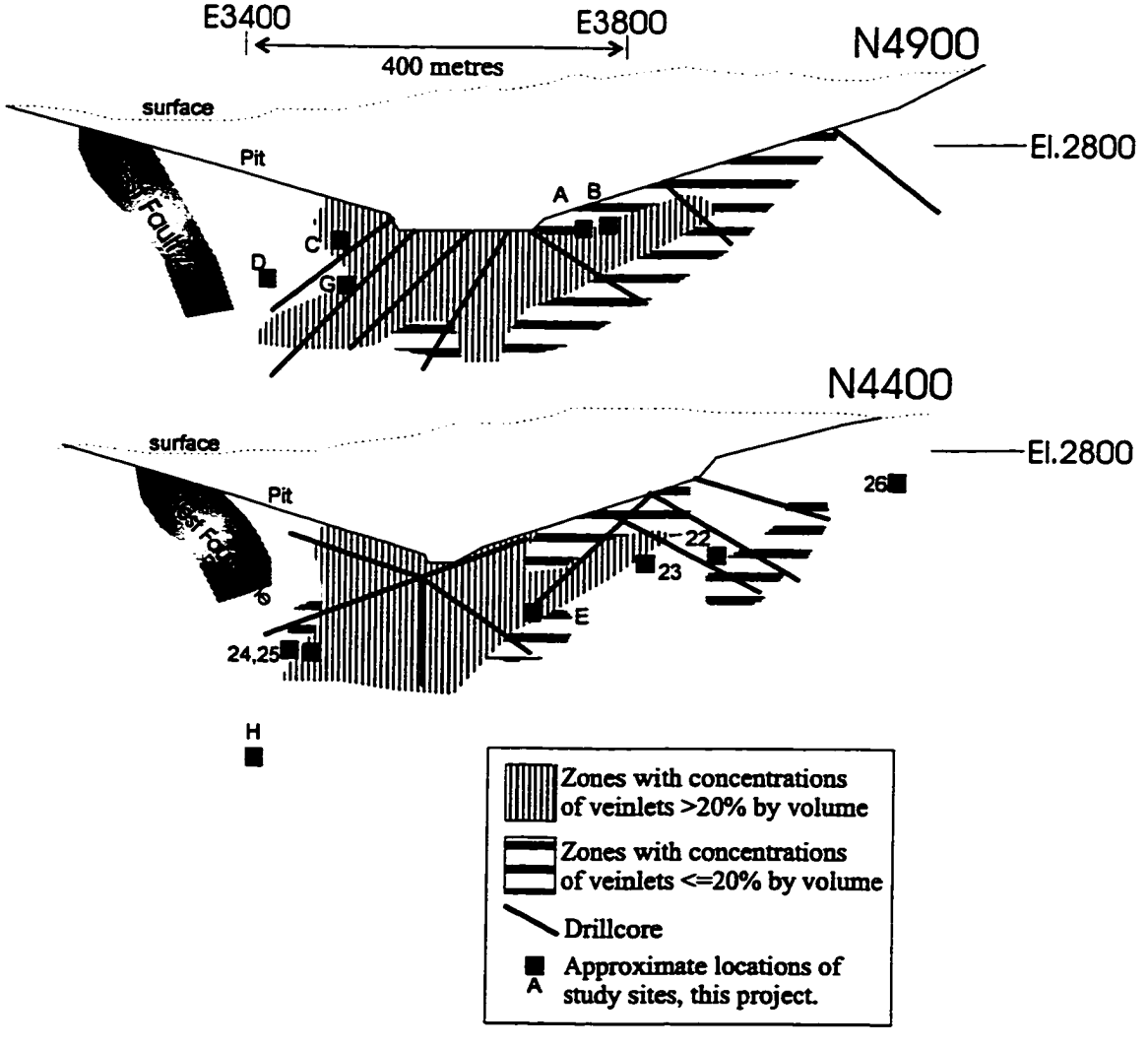

Fig. 5.3 Surface projection of the domain of quartz veining and illustrating the relationship between quartz-sericitic alteration, quartz vein distribution and the 0.5% Cu limit (after Soto, 1979).

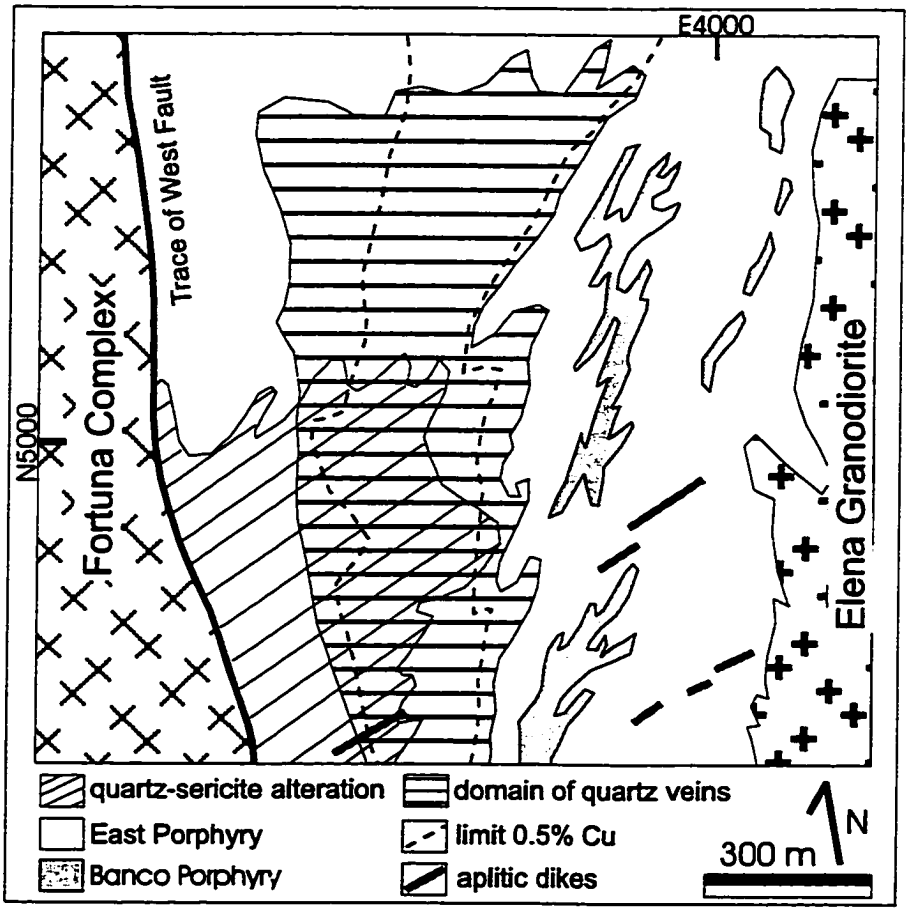

Compilation of veinlet types from all mineralized stockwork study sites allows for the establishment of seven generalized veinlet types that are used to provide a relative sequence of formation (Table 5.1). Although not all veinlet types are observed at every site, the relative timing sequence remains consistent for all sites studied. Other veinlets including, alunite, gypsum and molybdenite filled fractures were also encountered. However, these veinlets, although distinct, were not present in a majority of sites, did not show association with other veinlets observed at the site, either synchronous or crosscutting, or showed relations indicating they were the result of remobilization during some later event and therefore not associated with the emplacement of the stockwork system. The veinlets described below are consistent, in terms of vein and gangue mineralogy and comparable with respect to wallrock alteration, with the A, B, and D veinlet sets established by Gustafson and Hunt (1975) for the El Salvador porphyry deposit and may be classified as such. However, the veinlets kept as distinct sets may be a more useful approach (compare Titley, 1994) as with depth the identification of new veinlet types and relationships between those known veinlet types may become less certain as indicated by Gustafson and Quiroga (1996).

Veinlet type#1, v1 or A-type of Gustafson and Hunt (1975), quartz±K-feldspar was observed in two forms, both of which vary between 0.5 and 30 mm widths. The first is a sinuous, equigranular aplitic dikelet form, where K-feldspar dominates the assemblage and veinlet boundaries are gradational to sharp. The second form are quartz veinlets having a K-feldspar lining between the quartz and the wallrock. These two occurrences are texturally distinct, are under-represented with respect to abundance, based on bench-face mapping, and are located in mid- to upper elevations within the open pit. These veinlets have no apparent wallrock alteration halos at the outcrop and hand sample scales.

Quartz veinlets (Plate 5.1), veinlet type v2 or A-type of Gustafson and Hunt (1975), range in width from 0.5 to 35 mm, with most about 2 mm, and are white, aphanitic, having sharp contacts with the host rock and show no apparent alteration halos in the adjacent wallrock. Rare, thin, "hairline" quartz veinlets, which are not characteristic of this veinlet type but are grouped within it, crosscut all other veinlets where observed but due to their scarce distribution their relatio with all veinlet types is unclear

Quartz-molybdenite veinlets (Plate 5.2), veinlet type v3 or B-type veinlets of Gustafson and Hunt (1975), range in width from 1-20 mm, are commonly 5 mm or greater, and are a characteristic mineralization phase within the stockwork system. These veinlets are generally concentrated at lower elevations in the northern sector of the open pit. The veins show ribbon texture, where the molybdenite mineralization trends sub-parallel to the vein walls, either at the vein-wallrock interface, or more commonly internal to the quartz vein. This character is likely enhanced by the continuity of the sulphide (molybdenite) within the veinlet as compared with the discontinuous nature of the sulphides in the subsequent veinlets.

Quartz+sulphide veinlets (Plates 5.1 and 5.3), veinlet type v4, have 1-4 mm widths, crosscut the previous veinlet types and bear a combination of chalcopyrite ±pyrite ±bornite ±chalcocite ±covellite. As discussed by Lewis (1996), chalcocite (digenite) and covellite represent hypogene assemblages, at least in the potassic and probably in the sericitic-over-potassic alteration zones. The chalcocite variety, covellite and sphalerite of supergene origin commonly occur as very fine grained surface coatings on chalcopyrite-pyrite-rich assemblages making exact mineral identification extremely difficult in the field. The hypogene assemblages are observed central to the quartz veinlet, or distributed throughout the veinlet. In any case, the sulphide mineralization is contained within the quartz of the veinlet as a discontinuous trace. These veinlets would likely be classified as D-type veinlets in the Gustafson and Hunt (1975) scheme although no apparent alteration halos are observable at the hand sample scale.

Veinlet type v5, is similar to v4 without the quartz host and having a range in width between 0.1 and 4 mm, with a typical width being 0.5 mm. This veinlet type is observed as discontinuous trails of chalcopyrite and/or pyrite through the host rock. There is no apparent alteration halo associated with this veinlet type, which would be included in the D-type veinlets of Gustafson and Hunt (1975).

Plate 5.1 Hand sample illustrating crosscutting veinlet relationships for veinlet types v2, quartz, v4 quartz+sulphide and v6 sulphide(chalcopyrite+pyrite)+quartz-sericitic alteration halo. Veinlet relationships such as those observed in this photo provide the relative temporal sequence of stockwork scale alteration and mineralization events. In this case, v2 veinlets are the earliest formed at this site and that v4 and v6 veinlets are formed later. From this slab section the relationship between v4 and v6 is not clear, although, it appears that alteration associated with v6 may overprint a portion of the v4 veinlet (arrow). The East Porphyry host rock to this veinlet mineralization is potassically altered. Note that the biotite in the host rock displays a weak planar fabric that trends subparallel to elongate quartz eyes. This weak planar fabric is crosscut by all veinlet types. (CU-850).

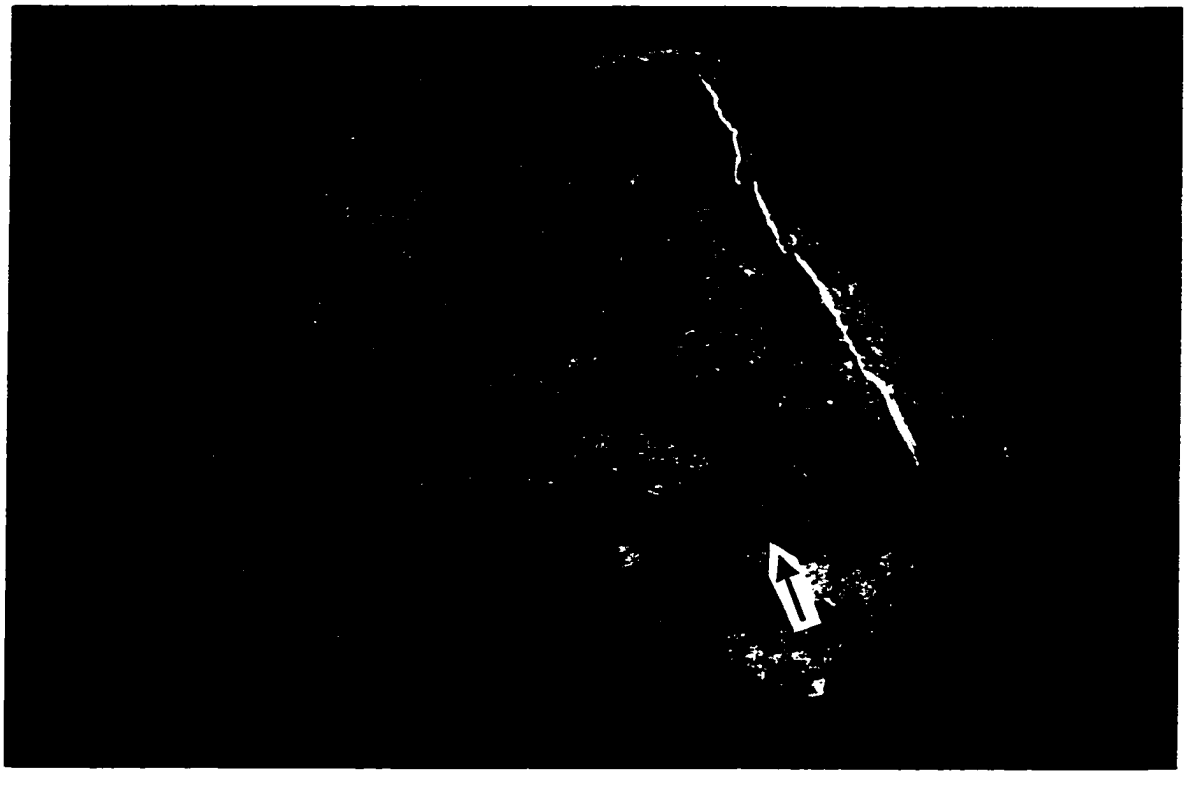

Plate 5.2 Photo showing detail of veinlet relationships at structural sampling site C (Plate 5.4). A quartz-molybdenite veinlet, v3, 1 cm in width, traverses the photo from lower left to upper right. Molybdenite forms the thin dark grey laminations that are observed adjacent and parallel to the veinlet walls. This veinlet is clearly earlier than the sulphide+sericitic alteration halo veinlets, or v6 veinlets that crosscut it. Chalcopyrite is the dominant sulphide in the v6 veinlets, but notice that the surface of the chalcopyrite is coated with fine dark brown to black "soot". This supergene coating is commonly a mixed of chalcocite+covellite and may involve sphalerite in some cases. Similar to plate 5.1 the host rock to veinlet mineralization is the East Porphyry with potassic alteration. Again notice that the sericitic halos on the v6 veinlets is a distinct greenish color.

Plate 5.3 This hand sample photo is from structural sampling site D (Plate 5.5) and illustrates the texture destructive nature of the sericitic alteration (darker) associated with the emplacement of v6 veinlets. Note that the mineralization within the veinlets is traceable, although it is discontinuous. The chalcopyrite mineralization in this sample also bears thin coatings of supergene chalcocite-covellite "soot". The East Porphyry host rock is altered to a sericitic-over-potassic phase, that is, plagioclase feldspars and biotite have been almost completely sericitized but K-feldspar remains stable. The veinlet sericitic alteration (darker) overprints and destroys a K-feldspar phenocryst (upper left of photo) and is evidently controlled by the subparallel fractures that served as channels to hydrothermal fluids.

Plate 5.2 (see caption on previous page).

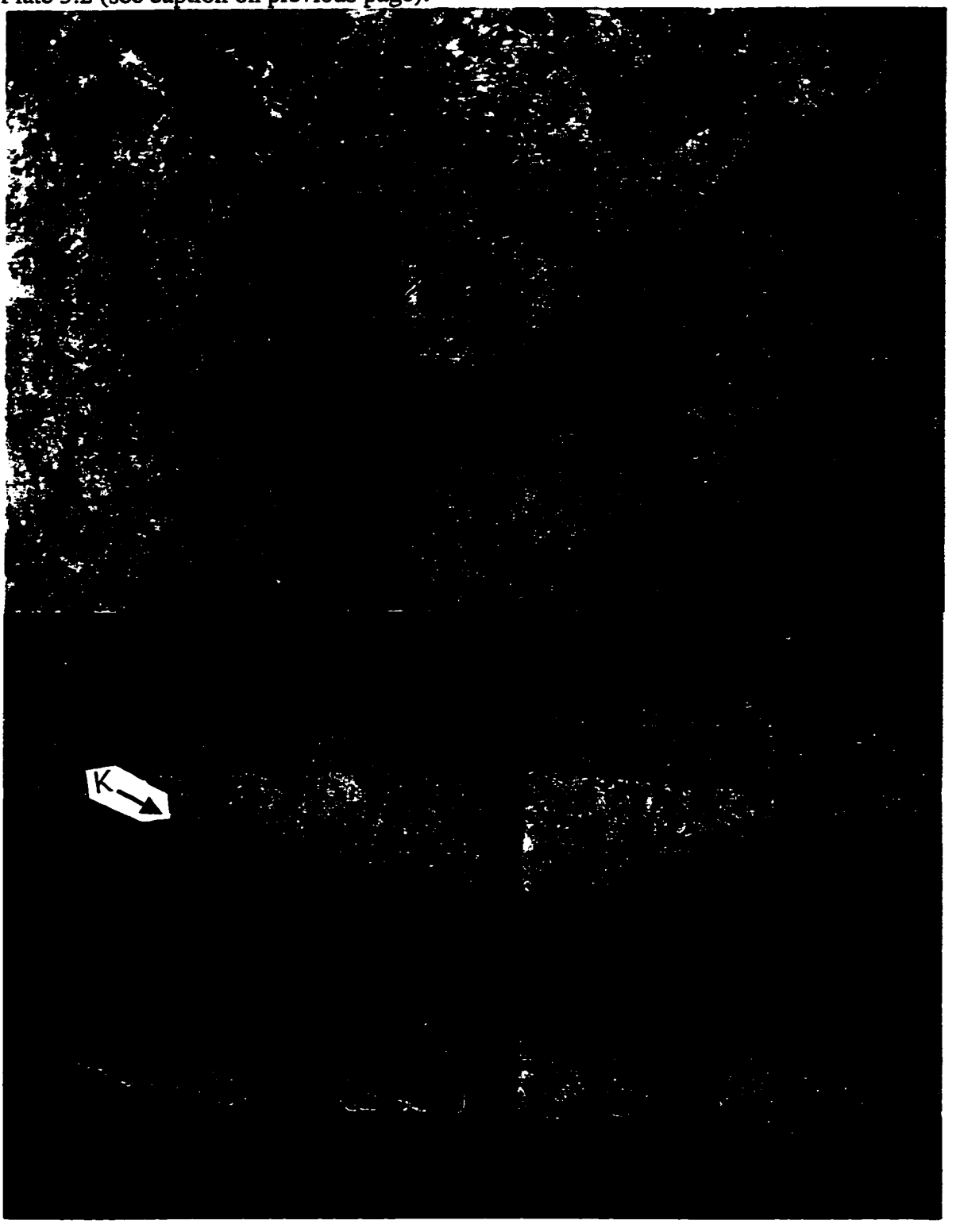

Plate 5.3 (see caption on previous page).

Veinlet type v6, which are similar to v5 except for the presence of a sericite±quartz halo (Plates 5.2 and 5.3). The alteration halo generally increases the veinlet widths to 10 mm or greater with the sulphides being central to the veinlet. These are D-type veinlets of Gustafson and Hunt (1975).

A possibly later formed quartz +sulphide veinlet type, v7, is characterised by mineralized vugs. This veinlet type was suggested by mine geologists but was not common in the studied sites. This vein type is likely equivalent to veinlet type v4.

5.1.3 Timing of Stockwork Formation

The relative timing relationships between veinlet types was established by crosscutting veinlet relations at the study sites. Within the deposit, as a whole, the relative timing of stockwork formation is indicated by the relationships of the veinlet systems with ductile deformation fabrics (Chapter 4) and mineralized fault-vein arrays (Chapter 6). Veinlet systems crosscut and in rare cases parallel fabrics associated with earlier formed ductile deformation. The ductile deformation is inferred as having occurred prior to, or contemporaneously with the potassic alteration phase at about 33.4 Ma (see above, Chapter 4; Reynolds et al., in press; Zentilli et al., 1995). Although the relationship is rarely present and for the most part obscured by pervasive alteration and later fault motions, the veinlet systems discussed in this chapter are interpreted to be crosscut by the large fault-vein arrays (see below, Chapter 6) and are therefore pre-fault-vein array formation. The fault sets and large vein arrays focus massive, texture destructive, quartz-sericitic alteration along their traces. The age of this sericitic alteration phase is approximately 31 Ma (Reynolds et al., in press; Zentilli et al., 1995). This massive whitish sericitic alteration is visually distinct from the greenish sericite-quartz veinlet alteration halos, from which **preliminary** radiometric data suggest an age of 32.1±0.3 Ma ($^{40}Ar/^{39}Ar$, sericite, Cuesta Research Ltd., unpublished data); an age which may be interpreted as consistent with hypogene mineralization associated with the late stages of stockwork mineralization that formed closely following the potassic alteration phase.

Table 5.1 This table lists a generalization of the veinlet types identified and categorized by this study. These classifications are based on outcrop and hand sample observations and samples from eighteen structural sampling sites. The veinlet types are listed in a relative timing sequence from earliest to latest emplaced based on observable crosscutting relationships.

	Veinlet Mineralogy
v1	quartz±K-feldspar; K-feldspar
v2	quartz
v3	quartz+molybdenite
v4	quartz+sulphide (pyrite, chalcopyrite, bornite, chalcocite, covellite)
v5	sulphide (chalcopyrite, pyrite, bornite, chalcocite, covellite)
v6	sulphide with quartz-sericitic halo (greenish to buff)
v7	quartz+pyrite+chalcopyrite, vug spaces, equivalent to v4?

5.2 Stockwork and Alteration

Stockwork systems, which are comprised of a series of veinlets, are found within host rocks that have been altered and now bear alteration assemblages which vary from potassic (Chapter 3.3.1) to sericitic (Chapter 3.3.3). Alteration zone refers to the alteration assemblage of the host rock within which the stockwork is contained and not the alteration associated with individual veinlets of the stockwork itself. In establishing whether the stockwork mineralization is associated with a particular alteration-mineralization episode difficulties arise. The difficulty is essentially of overprinting alteration events. For example, stockwork systems are observed to be present in rocks that have a background of potassic alteration and a background of sericitic-over-potassic alteration. In this case, it is most probable that the stockwork mineralization present in both alteration zones formed simultaneously in association, or shortly thereafter, with the potassic alteration phase, which has an age of ~33 Ma (Chapter 3). However, the texture destructive nature of the quartz-sericitic alteration phase makes the identification and separation of multiple stockwork systems impossible. It is considered that the stockwork system that is observed within the quartz-sericitic alteration zone may represent that which is observed within the potassic and sericitic-over-potassic alteration zones. Although the generation of a second stockwork associated with the formation of the quartz-sericitic alteration zone is also probable.

From the established veinlet sequence (Table 5.1), fluid evolution of the stockwork completed a typical cycle from an early, high temperature, potassium silicate alteration (K-feldspar±quartz±biotite veinlet) phase through a later, acidic, low temperature, phyllic (quartz-sericite-pyrite veinlet) alteration phase overprinting a potassium silicate altered host rock. From field mapping the sericitic-over-potassic, selectively pervasive alteration zone (Chapter 3.3.3.1), overprints the potassic zone and therefore overprints the stockwork/veinlet system. The puzzling relationship of the stockwork/veinlet system with the massive quartz-sericite alteration zone is further complicated by supergene enrichment which may be in part responsible for the sericitic-over-potassic alteration zone and has modified the veinlet assemblages to dominantly chalcocite- (covellite) and/or hypogene assemblages with thin surface coatings of supergene chalcocite±covellite±(sphalerite). It is believed that the

observed stockwork/veinlet system formed during hydrothermal activity associated with or immediately following the development of the potassic alteration of the host rock. If a subsequent stockwork system was generated by a later hydrothermal event then it is wholly contained within, or immediately adjacent to the pervasive quartz-sericitic alteration zone, or its related mineralized fault-vein features. It is expected that the study sites contained within the potassic and sericitic-over-potassic alteration zones will provide the best information concerning the development of the stockwork/veinlet system and its structural control (Fig. 5.1; Table 5.2).

Table 5.2 Distribution of veinlet study sites with respect to alteration zone (Chapter 3.3) and structural domain (Chapter 6). Benches M1,I1 and F4 are shown for reference. Q-S=quartz-sericite; S-K=sericitic-over-potassic; K=potassic; Chl-K=chloritic-over-potassic.
Structural domains A through D and G are defined in Chapter 6 (see Fig. 6.1).
Note *=sites on boundaries with other domains.

Alteration Structure	Q-S	S-K	K	Chl-(K)
Sector A		D, I, L	C	
Sector B	24, 25, H	A, B, E, M	G*, 22, 23	26
Sector D	J	N		
Sector G	K*			

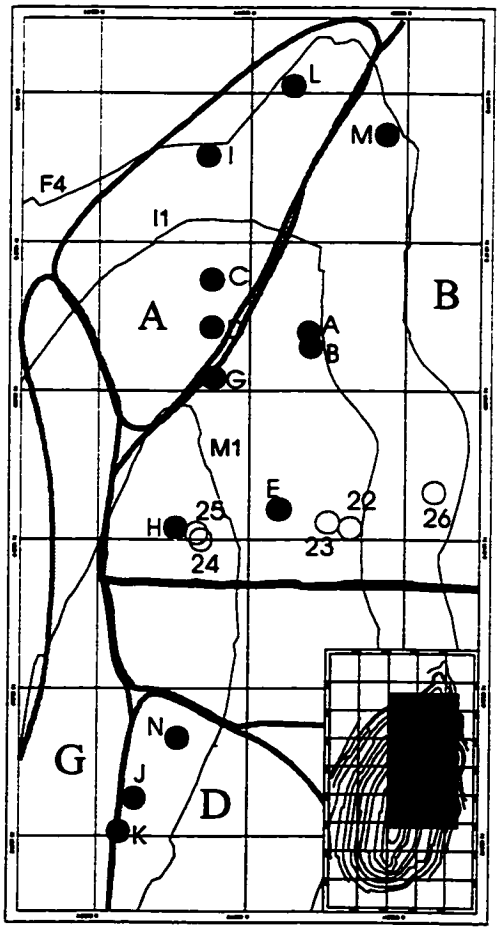

5.3 Preferred Orientations of Veinlet Systems

5.3.1 Methodology

Collection of azimuth, dip, width, mineralogy and relative timing data were used characterize the mineralized veinlet sets. A minimum 10 cm length limit was employed to limit data collection to those continuous outcrop-scale features, rather than those short discontinuous features which are better observed in drillcore studies. The collected data was transferred to a digital database (Appendix 1) for analyses and storage.

Describing the whole of the exposed ore-body in such a manner would be impossible because of the sheer size of the task. Instead, individual study sites having dimensions of 2 metres by 1.5 to 2 metres were selected and used to characterize the orientations of the veinlets comprising the stockwork system (Plates 5.4 and 5.5). Veinlet data from a total of eighteen sites were collected and analysed for preferred directional trends. Sampling sites were selected to observe any stockwork variation between the various alteration zones and to observe any variation between different levels of the deposit. In general, sites were established in sectors of the mine of interest to the mine geologists. The data collected from individual sites were used to define veinlet orientation similarities and differences amongst the other veinlets of the stockwork and to those larger scale fault-vein features defining structural sectors. The study sites of the original project, where data were weighted by continuity, are indicated by numeric labels (22-26). These sites were subdivided into a grid of nine subsections and data were collected for each veinlet that passed through each subsection of the site. The veinlets with greater continuity pass through several subsections and thus their data were recorded with greater frequency thereby weighting the data. The data collection methodology was then modified, to single measurements per continuous fracture/veinlet trace within each site, for letter labelled (A-N) sites to decrease collection time and interference with mining activities. Limitations to this style of data collection are discussed above in Chapter 1.3.5.

Data collected from individual sampling sites were examined for preferred trends in orientation by the use of stereographic plots. A PC-based computer program, DIPS, was used to produce lower hemisphere Schmidt equal-angle stereographic pole-from-plane

Plate 5.4 These photos show examples of the structural sampling sites used to collected data on the mineralized stockwork system at Chuquicamata. (A) Structural sampling site C was located within the East Porphyry unit of the Chuquicamata Intrusive Complex, as were all sampling sites. The mineralized host rock at this site is potassically altered. The site is approximately 1.2m high by 2m wide and is located on an E-W bench-face. (B) Structural sampling site D is located within a zone of sericitic-over-potassic alteration, meaning that the biotite is partially to completely altered to sericite and the K-feldspar is stable. This site has similar dimensions as the previous and is located on a N-S bench-face. The difference in alteration between the sites is reflected in the overall color. Both sites contain similarly mineralized veinlet systems, which are interpreted to have formed following, or in relation with, the hydrothermal evolution of the potassic alteration event that is represented in the host rocks to the veinlet mineralization. The sericitic alteration that affects the host rock at site D (eg. Plate 5.3) does not appear to bring more mineralization as similar stockwork systems are observed at both potassically (eg. site C) and partially sericitized (eg. site D) study sites. More importantly, sericitic alteration (darker) associated with veinlet mineralization completely alters host rock texture. This may indicate these sericitic events are distinct and that the lighter colored alteration event takes place following v6 mineralization within the stockwork system.

Plate 5.4 A (see caption on previous page).

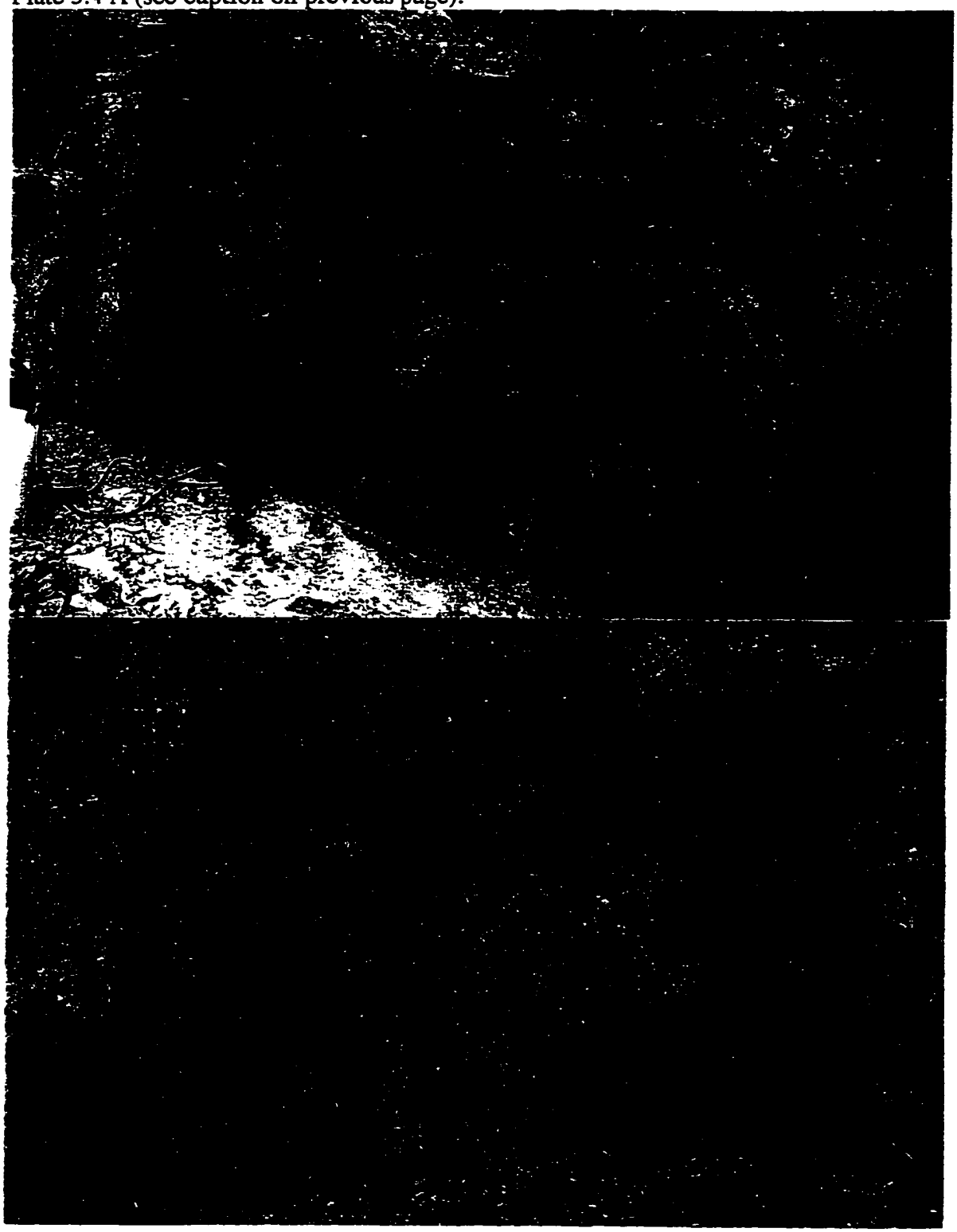

Plate 5.4 B (see caption on previous page).

projections. A counting grid of 4% of the circle radius and a count area of 1% of the total area were the settings used to produce the veinlet plots. For all plots, best-fit planes, representing the preferred orientations of the veinlets, were selected either by picking the peak maximum concentration of poles, or by selecting a window of data around the maximum concentration and allowing the software to compute an unweighted average of the selected data.

5.3.2 Individual Site Veinlet Trends

From each site, the veinlet descriptions were classified according to the generalized veinlet types listed in Table 5.1. Stereographic projections of similar veinlet types were then created for each individual site and compiled to maps of study site distribution. The stereographic plots show similar characteristics for compilations of each veinlet set. The following description and discussion is restricted to veinlet types v2, v3, v5 and v6 due to the scarcity of the other veinlet types (v1, v4, v7). Figure 5.4 shows the compilation of quartz veinlet (v2) stereoplots. Those study sites along the eastern side of the open pit (M, A, B, E) show a weak to moderate preferred NE-SW directional trend. Study sites that are located along the northern to central section of the mine (L, I, C, D) generally indicate a N-S preferred orientation. The abundance of quartz veinlets in these sites suggests a quartz-rich central corridor to the deposit. This corridor may represent a deeper expression of the northern and southern siliceous zones of Lopez (1939) and may also give way at depth to the Ksil alteration zone (see above, Chapter 3.3.1.1). Those sites within, or immediately adjacent to, the massive quartz-sericite alteration zone (H, N, J, K) suggest a NW-SE preferred orientation for the emplacement of quartz veinlets.

The first observed sulphide mineralization within the veinlet sequence is the quartz-molybdenite veinlet set, v3, (Fig. 5.5). The abundance of this veinlet set is low compared with the other veinlet sets. Despite this low abundance, dominant trends similar to those orientations of the quartz veinlet set are discernable. The sites with greatest concentrations of quartz-molybdenite veinlets are located at intermediate elevations within the open pit at its northern end. This veinlet type is low in abundance in he overall stockwork system in

comparison with the abundance of quartz-molybdenite veins in the larger vein arrays (Chapter 6).

Later stage copper-bearing mineralization, v5 veinlets, show greater abundances compared with the previous two veinlet sets. Highest veinlet concentrations are located at the deepest exposures studied and within the quartz-sericite alteration zone (Fig.5.6). The preferred trend of the veinlets at these sites (N, J, K) is a NW-SE to WNW-ESE direction. Those northernmost sites, along the central section of the mine (L, I, C, D), have few if any v5 veinlets, with the sites closest to the quartz-sericite alteration zone (G, H) indicating NE-SW orientations. Those sites along the eastern side of the open pit indicate a strongly preferred NE-SW orientation.

Figure 5.7 shows the distribution of individual study sites and stereoplots for veinlet type v6, sulphide veinlets with quartz-sericitic halos. Once again, the preferred orientations for those sites along the eastern side of the mine are NE-SW. This trend appears to swing to NNE-SSW for the northernmost site. Those sites deepest in the mine (N, J, K) indicate a NW-SE directional trend. However, these sites are located in the texture destructive quartz-sericitic alteration zone making identification of veinlets which bear halos extremely difficult. Those orientations collected indicate a weak residual quartz halo that was interpreted as representing an original quartz-sericitic halo. Directional trends for those north-central study sites vary from N-S to E-W trends.

From these individual site analyses, it is apparent that within the extents of the mineralized stockwork system, there exist sectors of preferred directional trends. These directional trends may vary between veinlet sets within the same study site (eg. Site H, D), or remain approximately constant for all those veinlets observed at the site (eg. Site N). Implications of these preferred trends include an anisotropic control on mineralization and thus ore grade within the deposit. The mechanism of formation for these veinlet systems is discussed in Chapter 5.5 : *Stockwork Formation*, and the affect of the directional controls on ore grade are presented in the following section.

Fig. 5.4 Lower hemisphere Schmidt stereographic projections for quartz veinlets, v2, for select structural sampling sites discussed in the text. Note the general north-south trend for those sites in the northern sector of the mine and weak to moderate NE-SW trends for those eastern sites. Polygons outline structural domains that are discussed in Chapter 6.

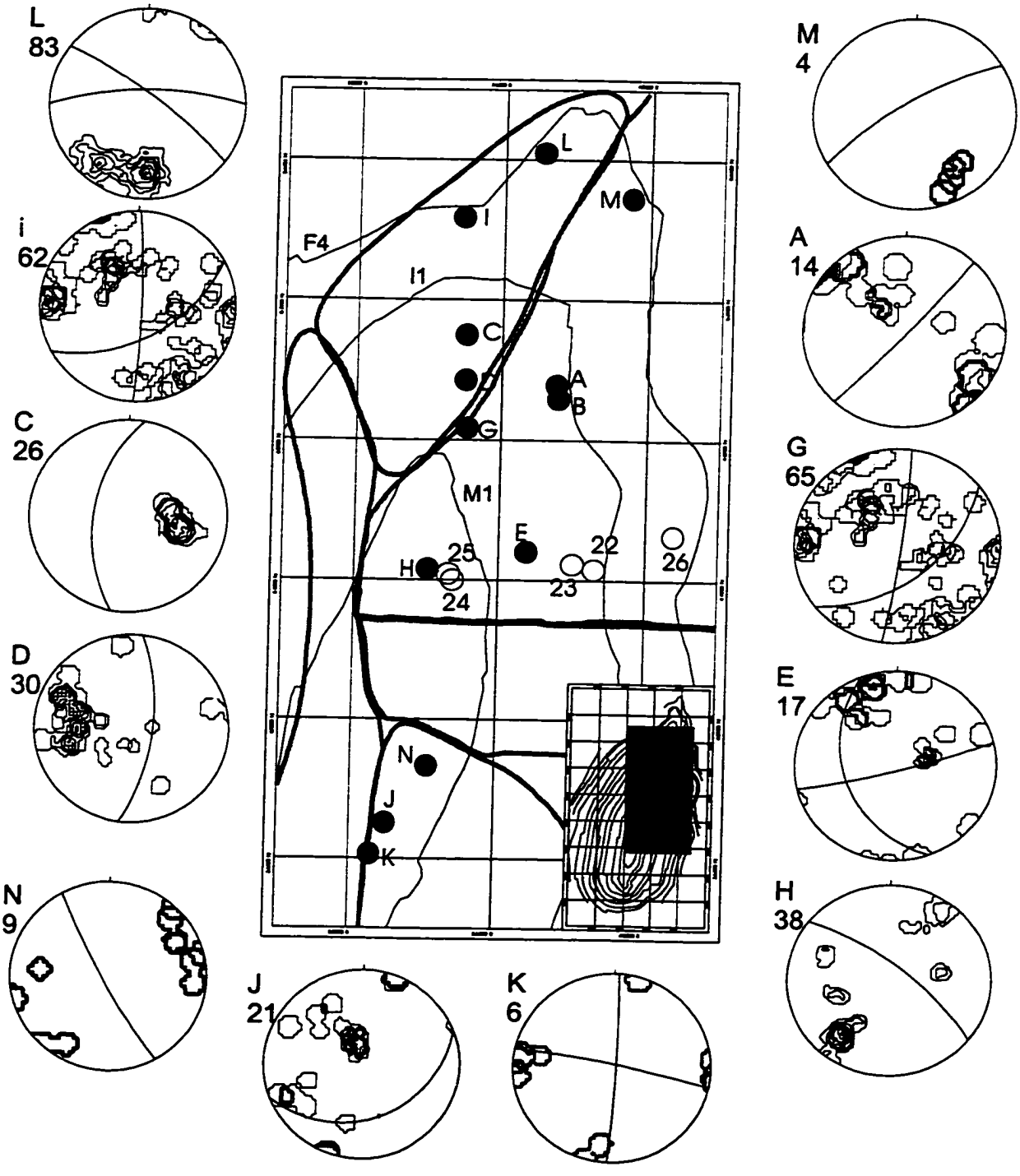

Fig. 5.5 Lower hemisphere Schmidt stereographic projections for quartz-molybdenite veinlets, v3, for select structural sampling sites discussed in the text. Note the general north-south trend for those sites in the northern sector of the mine and NE-SW trends for those eastern sites. Abundance of this veinlet type is generally low throughout the observed stockwork systems. Polygons outline structural domains that are discussed in Chapter 6.

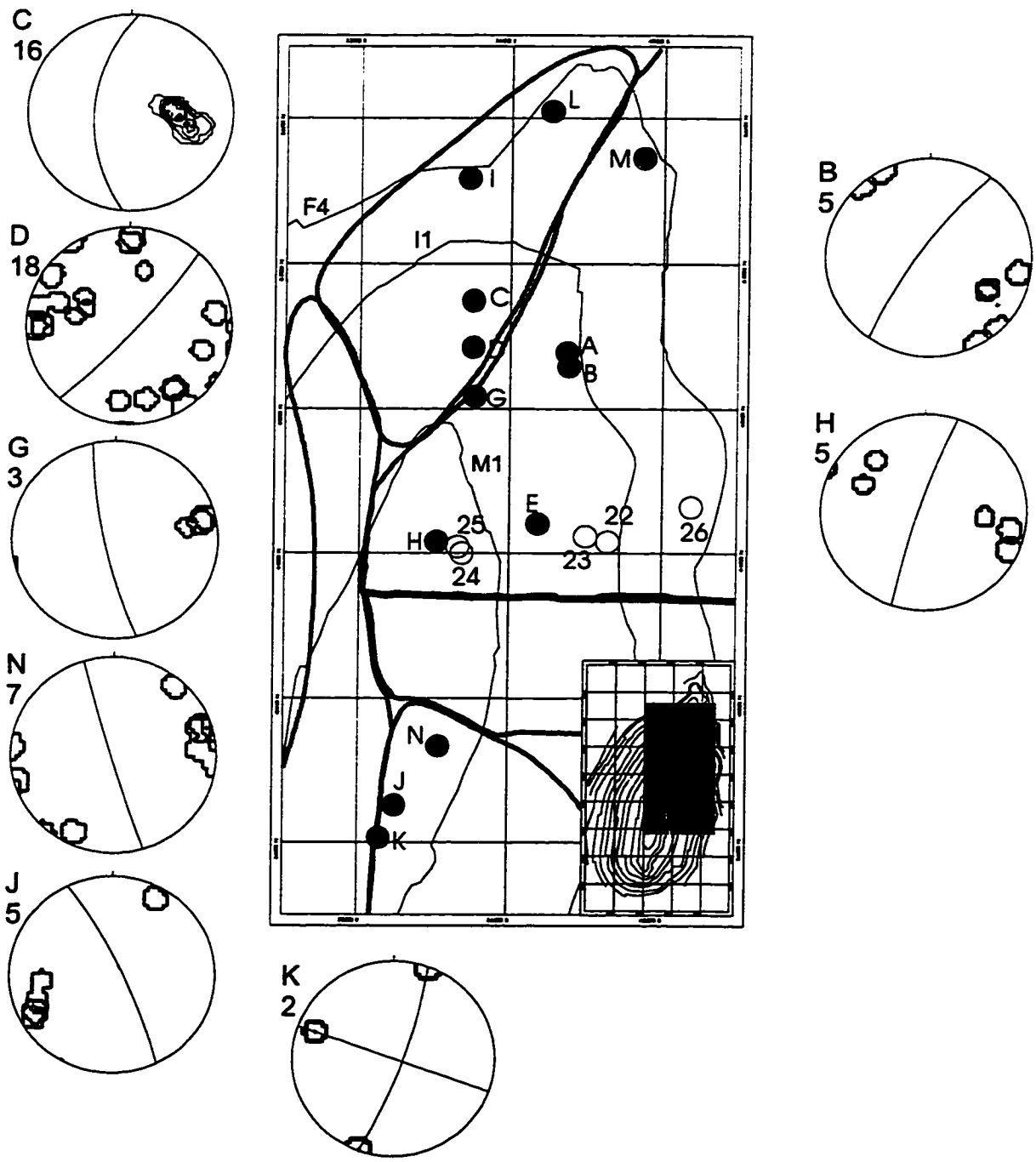

Fig. 5.6 Lower hemisphere Schmidt stereographic projections for sulphide veinlets, v5, for select structural sampling sites discussed in the text. Note the general NE-SW trend for the majority of sample sites. Sites in the southern sector of the mine indicate WNW-ESE to NW-SE trends. Polygons outline structural domains that are discussed in Chapter 6.

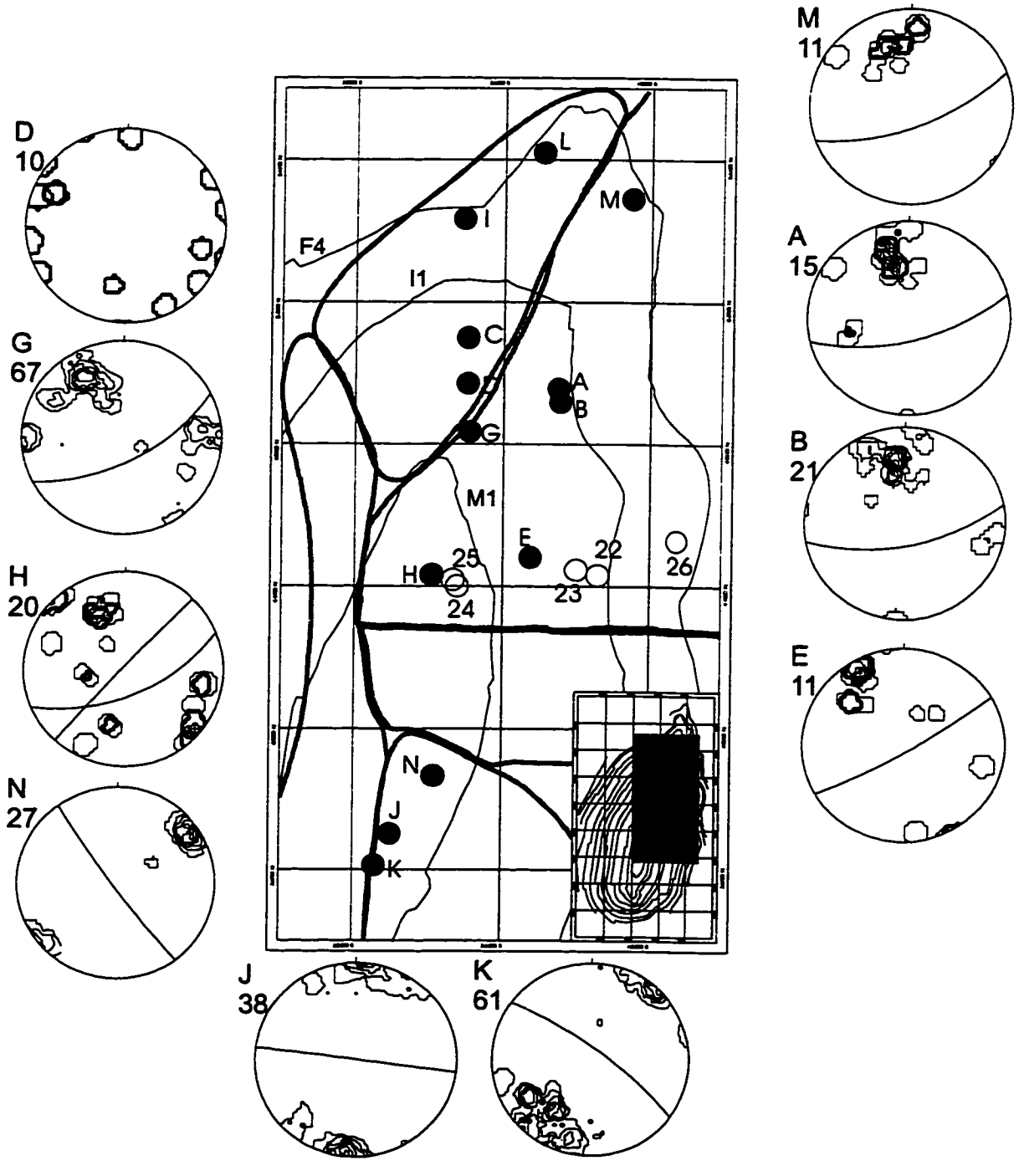

Fig. 5.7 Lower hemisphere Schmidt stereographic projections for veinlets with sericitic halos, v6, for select structural sampling sites discussed in the text. Note the variety of trends for those sites listed along the left side of the diagram and the NE-SW trends for those eastern sites. Sites in the southern sector of the mine maintain northwesterly trends. Polygons outline structural domains that are discussed in Chapter 6.

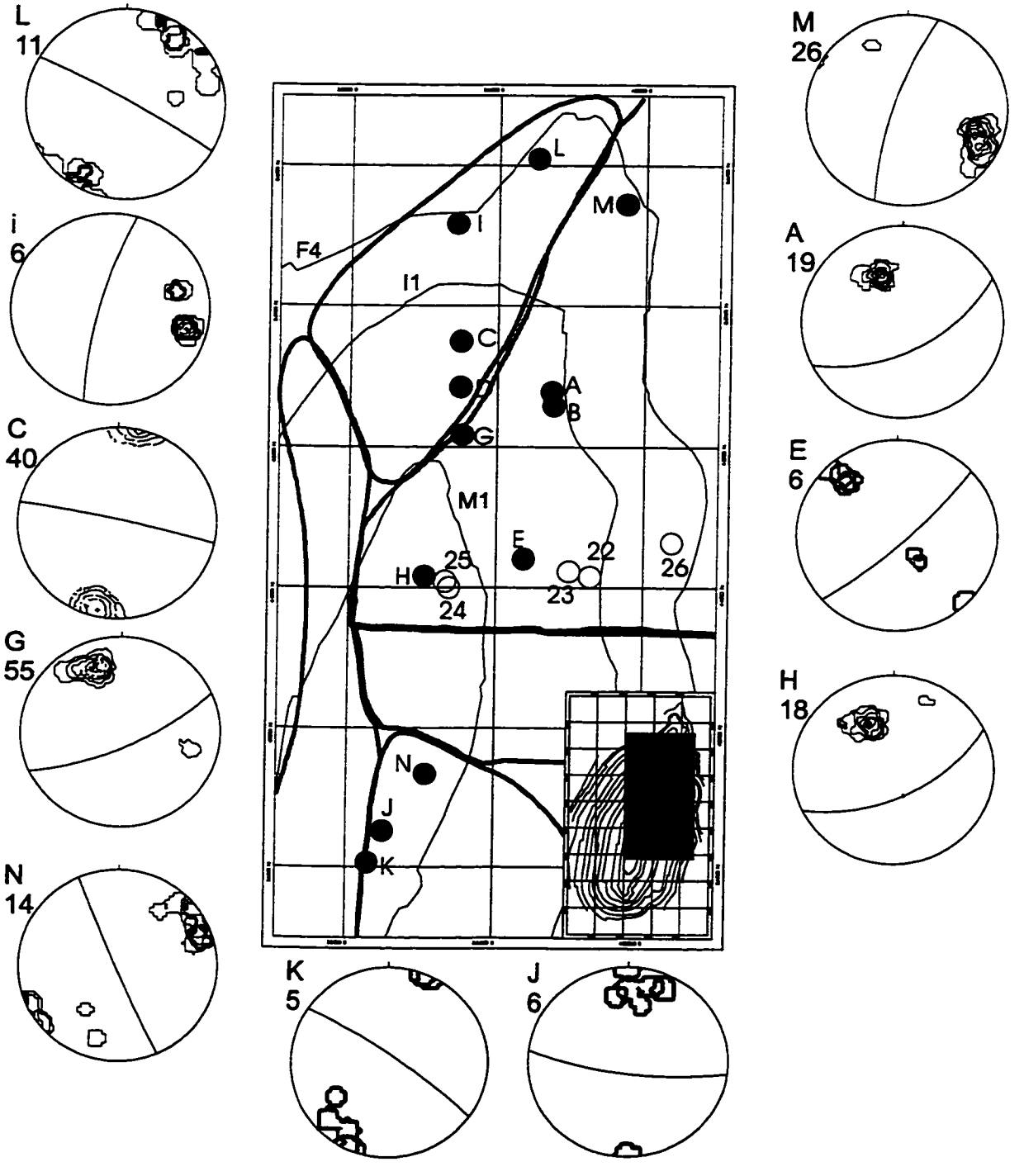

5.3.3 Sectoral Veinlet Trends and Anisotropy of Ore Grade

In the preceding section, it was demonstrated that the directional trends of individual veinlet sets were distributed such that sectors of preferred orientations could be defined within the mine. Veinlets v4 through v6 are considered the most important in this section, as these veinlets provide the majority of copper mineralization. The directional trends for these veinlet sets, illustrated as stereoplots, are summarized in Fig. 5.8 through 5.11 for the various sectors. The plots are compilations of all the individual sites that are located within the respective sector. The sectors are referred to in the present chapter as northern, northeastern, and southern. These sectors correspond to structural domains, A (Zaragoza), B (Estanques Blancos) and G (West Fault), which are defined and characterized by larger scale fault and vein systems (Lindsay et al., 1995; see below, Chapter 6 this study).

The veinlet compilation for the northern sector is contributed to by all sites with potassic to sericitic-over-potassic background alteration of the host rock. These sites are located at intermediate to lower elevations in the open pit. Those sites located on the upper benches are quartz veinlet dominated and contribute little to the compilations of mineralized veinlets (Fig. 5.4). The preferred trend of mineralized veinlets is a NNE-SSW direction, dipping at intermediate angles to the west, that varies to NE-SW and E-W directions, which tend to dip towards the southeast (Fig. 5.8). This directional variance results from the inclusion of site G, which may better correlate with the trends of the northeastern sector.

The northeastern sector has been subdivided into two groups. One compilation containing those sites which are located in potassic to sericitic-over-potassic alteration zones (Fig. 5.9), excluding sites #22 and #23, and a second group compiled of those sites in the quartz sericitic alteration zone (Fig. 5.10). This separation was done on the basis that the stockwork system in the sericitic-over-potassic is an overprinted stockwork system equivalent to that in the potassic alteration zone (Chapter 5.2) and that the same can not be ascertained for the stockwork in the pervasively altered quartz-sericitic zone. For both groups within this sector, a dominantly NE-SW trend, dipping to the southeast is evident. Compiled veinlet sets of the quartz-sericite group appear more dispersed, but their peak trends are NE-SW. If a conclusion of equivalency can be drawn based on similarities in veinlet system

trends then the veinlets within the quartz-sericite alteration zone can be considered to have formed during the same event as those observed in lesser altered zones. In any case, both groups of this sector indicate similar NE-SW veinlet directional trends.

The southern sector is dominated by sites within the quartz-sericitic zone, an exception being site N, which has a background alteration consistent with Ksil alteration (see Chapter 3.3.1.1). Nevertheless, compiled mineralized veinlet sets for this sector indicate a preferred NW-SE directional trend (Fig. 5.11). This trend is consistent for mineralized veinlets of all included sites regardless of background alteration (compare Figs. 5.6 and 5.7). This relationship, as the one proposed for the northeastern sector, suggests that the stockwork systems within both alteration zones may be considered equivalent.

As mentioned previously, the mineralization within the Chuquicamata porphyry copper deposit is principally contained within veinlets. These veinlets have been shown here to have preferred directional trends within spatial sectors of the mine. The trends are distinct for the different sectors outlined above. Using the preferred orientation data derived from this study at both veinlet and vein scales, Krige and Dunn (1995) presented initial geostatistical correlations for ore grades and reserves from Chuquicamata. These authors indicate that anisotropies of mineralization exist for sectors within the mine and that the anisotropies vary between sectors. Further, unpublished geostatistical correlations coincide with the veinlet anisotropies defined in this study (R. Freraut, pers. comm., 1995).

Fig. 5.8 Lower hemisphere Schmidt stereographic projections for the most common veinlet types, see Table 5.1, observed at the structural sampling sites (D, I, L) in the northern sector of the mine. Refer to Table 5.2 for locations and alteration relations. These sites are located in the sericitic-over-potassic alteration zone. See text for discussion.

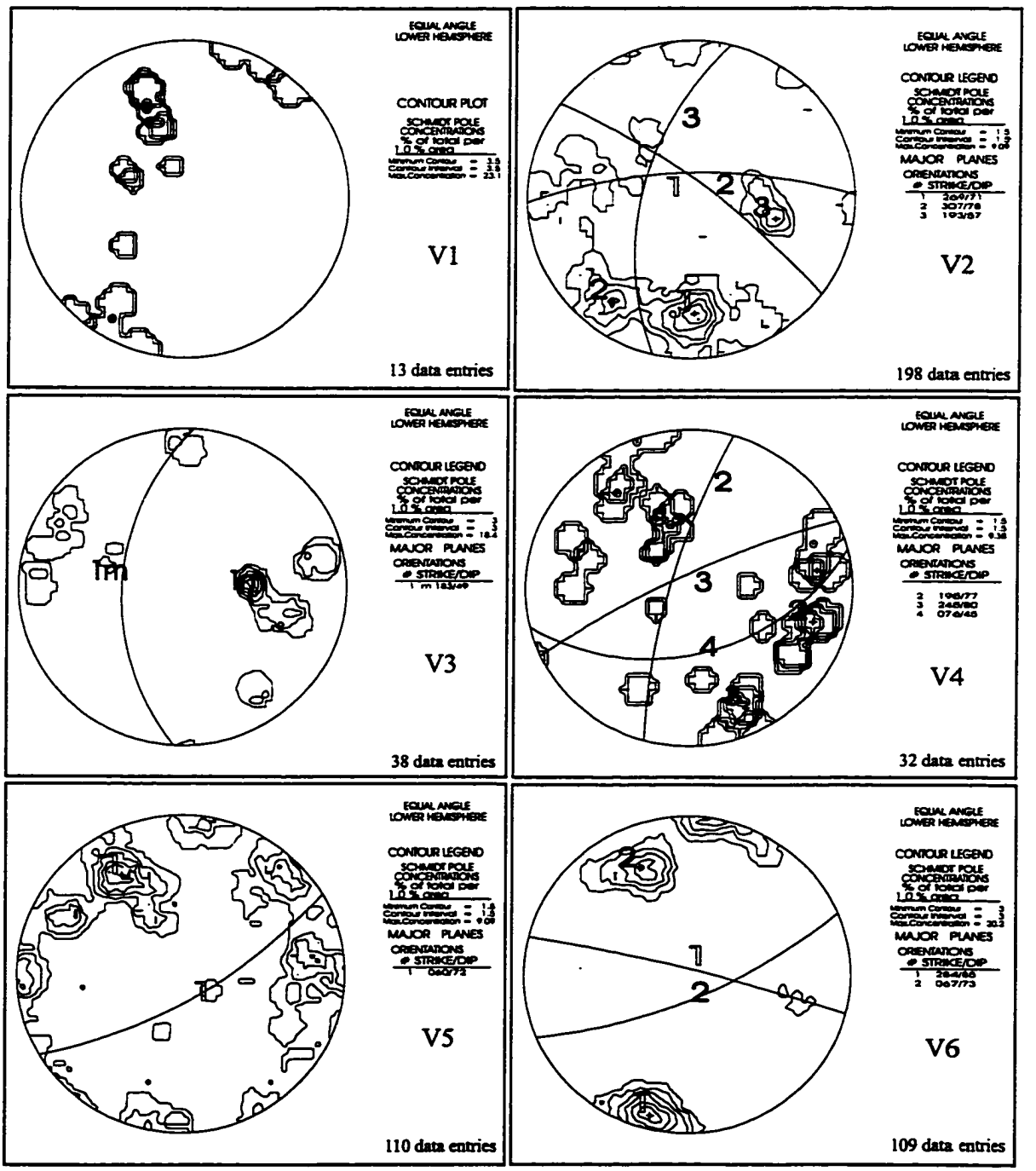

Fig. 5.9 Lower hemisphere Schmidt stereographic projections for the most common veinlet types, see Table 5.1, observed at the structural sampling sites (A, B, E, M, G) in the northeastern sector of the mine. Refer to Table 5.2 for locations and alteration relations. These sites are within the potassic and sericitic-over-potassic alteration zones. See text for discussion.

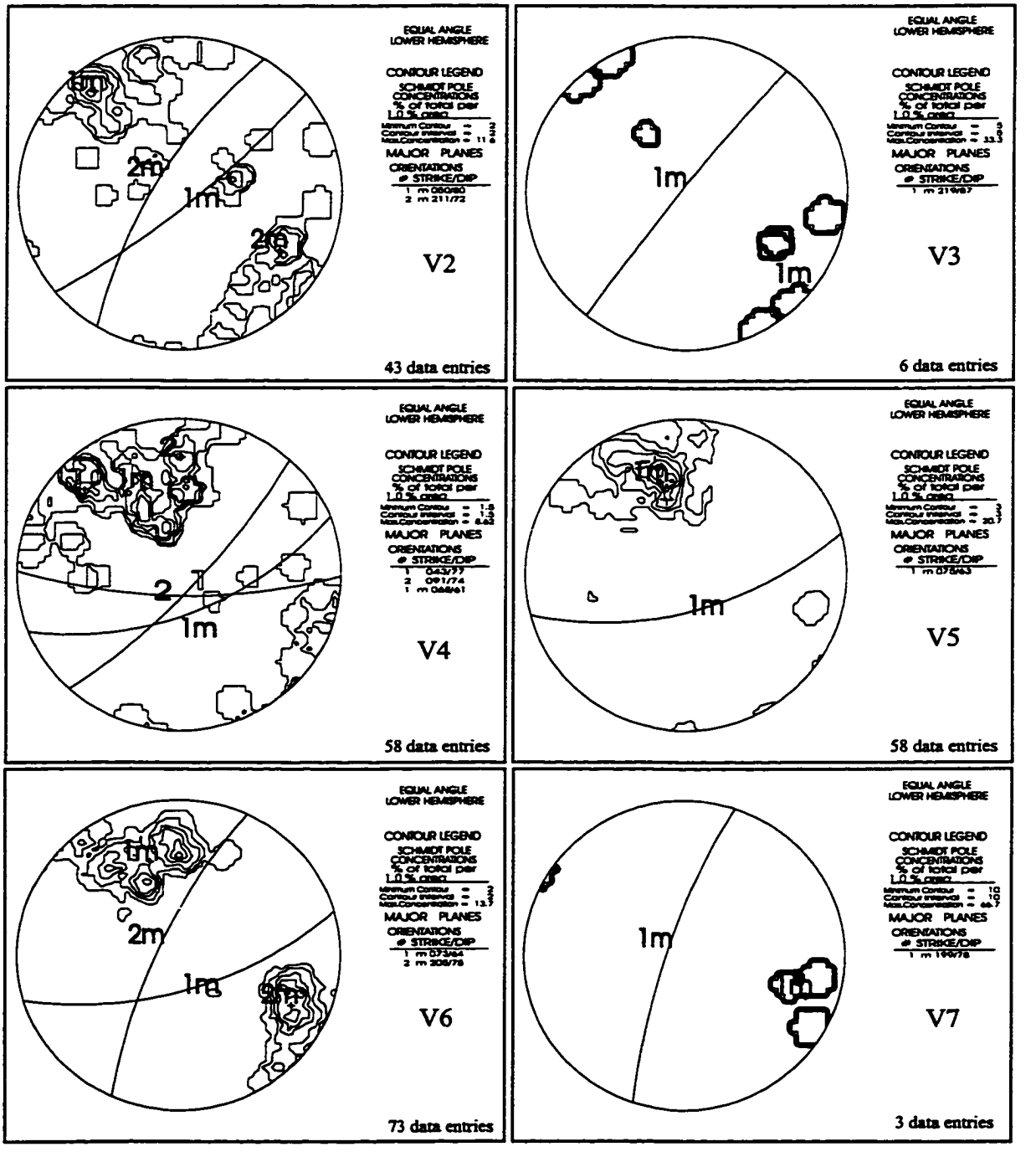

Fig. 5.10 Lower hemisphere Schmidt stereographic projections for the most common veinlet types, see Table 5.1, observed in the structural sampling sites (H, 24, 25) in the northeastern sector of the mine. Refer to Table 5.2 for locations and alteration relations. These sites are within the quartz-sericitic alteration zone. See text for discussion.

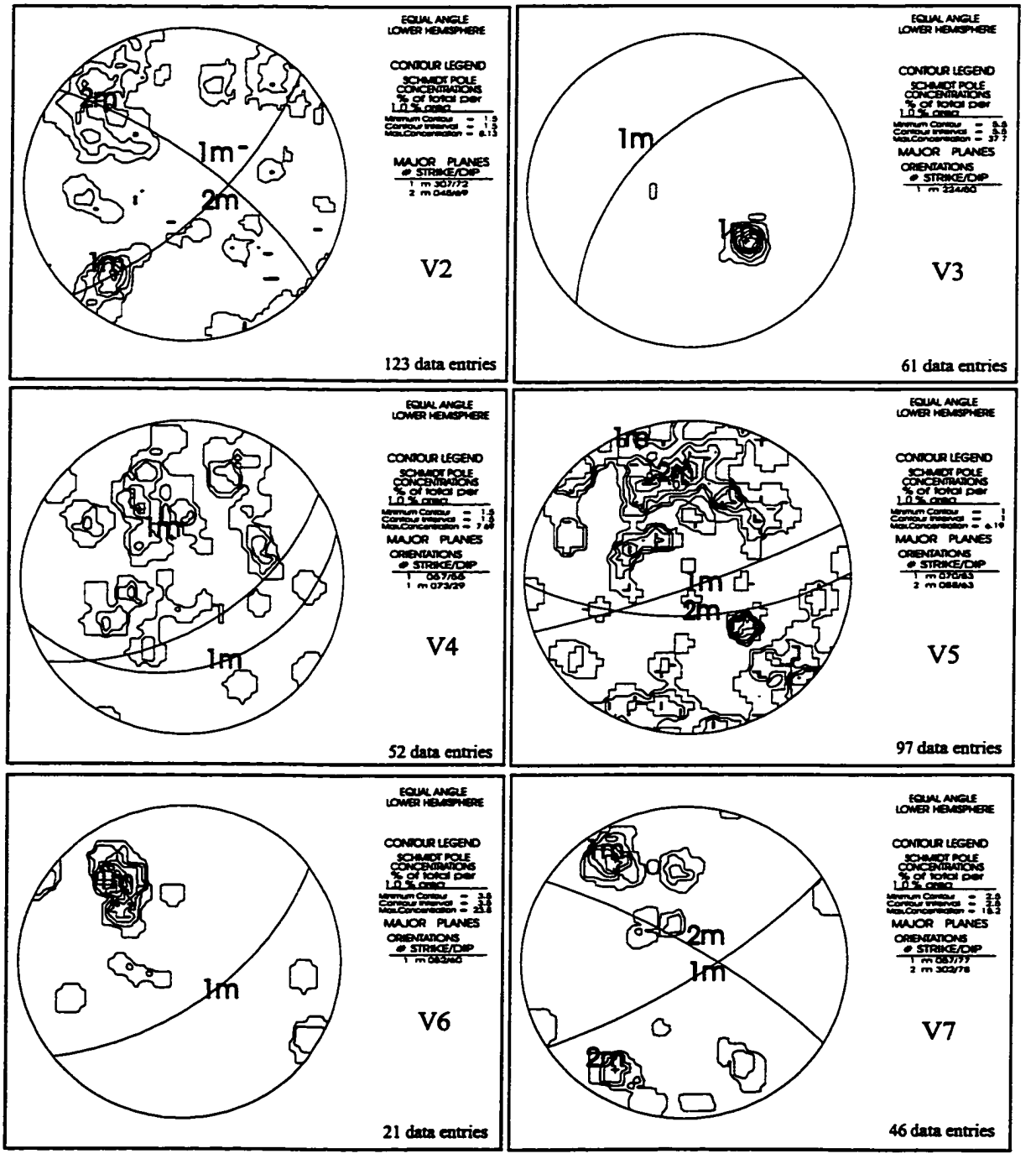

Fig. 5.11 Lower hemisphere Schmidt stereographic projections for the most common veinlet types, see Table 5.1, that were observed in the structural sampling sites (J, K) in the southern sector of the mine. Refer to Table 5.2 for locations and alteration relations. These sites are within the quartz-sericitic alteration zone. See text for discussion.

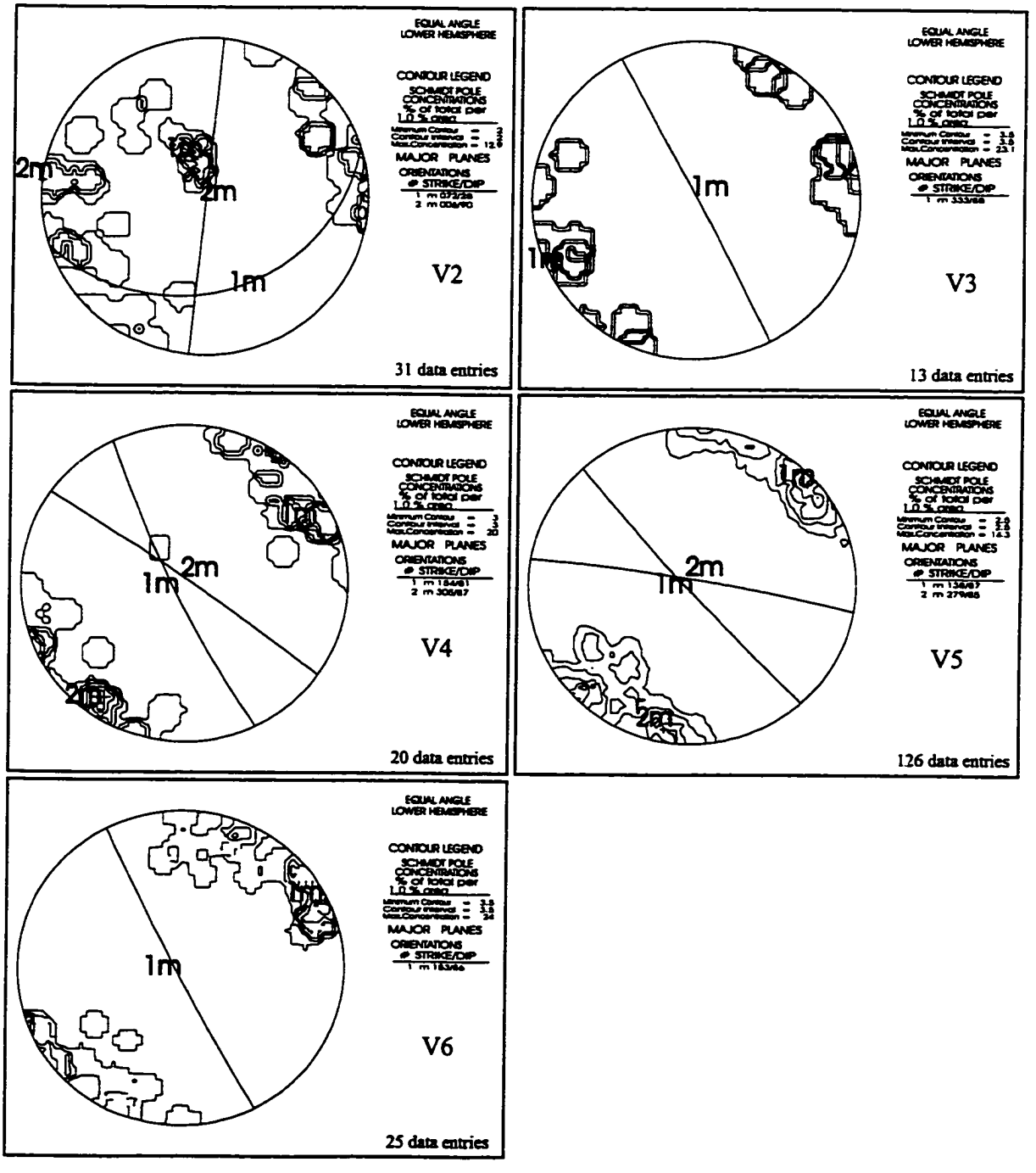

5.4 Stockwork Formation

Zones, or sectors, of directional trends of mineralized veinlet systems have been established for the Chuquicamata porphyry copper deposit. Directional trends in veinlet orientations are not unique to Chuquicamata, having been described from a number of porphyry deposits and the districts which surround them (Haynes and Titley, 1980; Titley et al., 1986; Casselman et al. 1995; Heberlein 1995). Titley et al. (1986) established, for the porphyry systems of the American southwest, a correlation between the density of veinlets and mineralized centres, and related the regionally distributed fracture patterns to tectonically induced upper crustal stress fields during and following porphyry emplacement (Rehrig and Heidrick, 1972; Heidrick and Titley, 1982). The veinlet systems within the Chuquicamata deposit, in comparison with those regional studies, represent the fracture systems as formed within the cooling carapace of the host intrusion.

Formation of fracture systems within the environment of a shallowly emplaced pluton have been presented by Burnham (1979, 1985). Aspects of fracturing in this setting have been modelled by Koide and Bhattacharji (1975) who examined fracturing relating to the actual emplacement of the igneous body neglecting the presence of fluids. Knapp and Norton (1981) following Burnham (1967, 1979) found that tensile and shear fractures, produced by thermal and fluid pressures have similar orientations within the cooling pluton and indicate that shear fractures tend to be the first formed and then become reactivated as tension fractures. These authors indicate that the fractures form simultaneously near the top of the pluton, but at depth, a maximum 0.2 m.y. lag may exist between earlier formed fluid (magma) pressure enhanced fractures and fractures formed by thermal processes. By way of numerical modelling, Knapp and Norton (1981) also indicate that fracture dips would be intermediate to vertical above and adjacent to the pluton becoming shallower at greater depth within the pluton. Although the models take place in isotropic stress fields, Burnham (1979) suggests that the orientation of the least principal stress depends on the regional stress field as dictated by the tectonic setting.

Stockwork formation is believed to be an end result of the emplacement of a fluid-saturated granodioritic stock into epizonal crustal levels. Sillitoe (1973) proposed that these

late stage stocks are subvolcanic in nature. At deeper erosional levels, stocks and their associated porphyry deposits have been related to batholiths as cupolas (Dilles and Einaudi, 1992; Henley and McNabb, 1978). The shallow emplacement of sub-volcanic stocks or cupolas may result in the formation of a stockwork system if there is a reduction in confining pressure and crystallization occurs over a restricted temperature range. The separation of crystals from the melt during crystallization leads to a relative increase in the concentration of volatile components in the residual liquid. If the melt becomes saturated with respect to fluid and crystalline phases, such that vapour pressure exceeds the confining forces retrograde, or resurgent boiling will occur with an accompanying release of mechanical energy (Burnham, 1979; Phillips, 1973). This energy release within a largely consolidated rock may overcome tensile rock strength resulting in an increase in volume (expansion) through the creation of extensive fracture systems and brecciation. These fracture systems provide an initial permeability network for fluids rising from the consolidating melt. The release of the vapour and fluid pressure causes a relative decrease in the total pressure, setting up a pressure gradient that may draw in pore fluids from depth from the intruded country rocks establishing a hydrothermal circulation system centred on the intrusion. Continued cooling and fluid migration and trapping lead to multiple episodes of hydrofracturing and mineralization resulting in a succession of crosscutting veinlets with different alteration association (Burnham, 1979).

The processes responsible for generating a fracture system and mineralized stockwork systems are not limited to resurgent boiling (Phillips, 1973) and subsequent hydraulic fracturing (Phillips, 1972), but may include fluid pumping mechanisms (Sibson, 1987, 1990, 1996) in structurally active fault zones. These processes are active until the fluid source becomes depleted or temperature and pressure gradients approach equilibrium with the regional norms causing the magmato-hydrothermal system to decay into a geothermal system.

Temperature and pressures related to the formation of stockwork systems are usually established through studies of fluid inclusions. A fluid inclusion study by Vega (1986) on veinlet quartz from B- and D-type veinlets, for a cross section within the mine (N4500),

shows that mineralizing fluids ranged in temperature from 200°-450°C and salinity from 1%-25% in weight equivalent NaCl. Calculations by Vega (1986) suggest a depth to boiling of 750-1300 metres (lithostatic) or 2000-3500 metres (hydrostatic). These fluid parameters are consistent to those described for stockwork systems of other porphyry deposits. The establishment of veinlet types and a relative timing sequence for the stockwork/veinlet system in the Chuquicamata deposit by this study will be used as a basis for the development of a comprehensive fluid inclusion study that will better constrain the evolution of mineralizing fluids and their chemistry for this complex deposit. In many porphyry systems, fluid inclusion studies of earlier formed veinlets, related to the potassic alteration phase of porphyry copper mineralization, indicate fluids of high temperature, usually greater than 350°C and high salinity. Whereas, those later formed veinlets associated with the phyllic alteration phase indicate fluids of lower temperatures, <350°C, and lower salinities (e.g. Moore and Nash, 1974; Gustafson and Hunt, 1975; Haynes and Titley, 1980; Dilles and Einaudi, 1992).

The formation of a mineralized stockwork system is an evolutionary process from magma emplacement, cooling, and fluid generation to resurgent boiling and hydraulic fracturing causing host rock rupture and fluid circulation. The circulation and interaction of magmatically derived fluids and convecting meteoric and/or connate fluids around and within the fractured pluton result in alteration and mineral precipitation. At a single level of exposure, fluid inclusions from crosscutting veinlet sets show an evolution of the mineralizing fluids from earlier high temperature- high salinity fluids to later lower temperature-lower salinity fluids. As the magmatic fluid source retreats to depth with the crystallizing melt, fracturing deepens, resulting in a complex vertically extensive, or telescoped mineralized fracture system.

5.5 The Chuquicamata Mineralized Stockwork

In the preceding sections of this chapter, the general conditions and processes for stockwork formation, and sequence of emplacement for the mineralized veinlets for Chuquicamata and porphyry deposits in general were presented. Here the preferred

orientations of the veinlets sets are reviewed and evaluated with respect to the processes and timing of fracture formation.

Fracture and veinlet formation is an end-product of the shallow emplacement of a magmatic body. Fractures result from thermal cooling and the release of mechanical energy built up from fluid-saturated melt and vapour pressures during resurgent boiling. This process is successive, as fractures become sealed by precipitating minerals and fluid and vapour pressures rise again. These dense fracture systems are located in the uppermost parts of the cooling pluton, generally in a crystallized carapace, and the adjacent country rocks. Fracture orientation is dominantly vertical, although numerical modelling suggests shallowly dipping fractures may lie along the vertical pluton-country rock contact. Magma pressures influence the conditions of fracture formation, initially causing shear fractures to form, which later become reactivated as tensile fractures. Conditions of fracture formation are also influenced by the regional tectonic setting, which may dictate where the least principal stress lies. Initially exsolved fluids are of high temperature and high salinities. Through repeated rupturing meteoric waters are drawn into the system so that later fluids are characterized by lower temperatures and salinities. This characteristic fluid evolution is known for a number of porphyry deposits.

The mineralized fracture systems at Chuquicamata developed within the subporphyritic East Porphyry syn- to post- the potassium metasomatic alteration event. This alteration event was closely associated in time with plastic-brittle reverse fault development in the East Porphyry (see above, Chapter 4), suggesting regionally imposed stress conditions on the pluton. Veinlet systems, currently outcropping at the active mining surface, reveal a limited width along a north-south central quartz-rich corridor. The trend of the stockwork system exposed in the open pit appears limited towards its southern end by NE-SW trending brittle faults.

Based on the distribution of structural sampling sites and the directional trends which each veinlet set displays at individual sites, the deposit may be divided into a minimum of three stockwork mineralized sectors. The veinlets of the northern sector display both N-S and NE-SW preferred directional trends. Those of the northeastern sector display dominantly NE-

SW orientations and those of the southern sector show NW-SE preferred orientations. The sectors that bear this mineralized stockwork are defined later as structural domains, see Chapter 6, and are characterized on the basis of deposit-scale fault and vein systems. Although the preferred hypothesis involves a regional control of maximum and minimum principal stresses, the orientations and character of the stockwork at Chuquicamata suggest a magmatic control that is represented by a fault-separated sub-radial pattern. Such a pattern would be expected above a shallowly emplaced igneous body where principal stresses were controlled by magmatic forces. In the preferred case, a NE-SW orientation for the maximum principal stress, contained in a horizontal plane with the minimum principal stress, would account for shear fractures with N-S to NNW-SSE orientations and extensional shear fractures forming in NE-SW orientations. Closest to the fluid source, magmatic pressures would dominate, preferentially forming tensile fractures, whose pattern would be dictated by the shape of the intrusion and the deeper crystallizing melt.

Chapter 6. Veins, Fault Systems and Structural Domains

This chapter describes the main fault and vein types encountered at the bench-face mapping scale (~1:400-1:2000) within the Chuquicamata open pit and which are generally depicted in geological maps (e.g. Lopez, 1939; Guilbert and Park, 1986), in contrast with the smaller features discussed in Chapter 5 that are not. These features are classified according to the presence of intra-fault material, or vein mineral assemblages. Vein sets are consistent with A-D-type vein nomenclature developed by Gustafson and Hunt (1975) except that the veins described in this chapter are of a greater scale with widths of tens to several hundreds of centimetres. Additionally, most faults and veins show interpretable features of reactivation or prolonged evolution. For veins these include: (i) crack-seal vein textures, (ii) composite veins and (iii) crosscutting mineral assemblages, and for faults: multi-generation breccias and gouges. Therefore, the conditions necessary for formation and/or reactivation of these features are discussed. Characterization and discussion of veinlets and stockwork systems, those veins have thicknesses of less then 10 cm, have been presented in Chapter 5.0 and are not included here.

The fault types established here are described in a relative timing sequence based on observed crosscutting relationships in the field. They are also used to define structural domains, which are spatial zones of the open pit that are occupied by fault and vein systems that have similar characteristics and orientations. Domain associations are then proposed based on the timing and relation of structural domain formation. Mineralization of the structural domains is discussed in light of structural settings, mineralization mechanisms and the data presented in previous chapters. All faults, including post-mineral faults are described in this chapter but discussion of post-mineralization deformation is presented in Chapter 7.

6.1 Methodology

Bench mapping was undertaken with the objective of defining the principal fault systems and structural domains occurring within the Chuquicamata open pit below bench H1 (elevation 2697 m), which mine staff defined as the economic limit of the deposit (Fig. 6.1).

Mapped structures included all faults, fault surfaces and veins that had a minimum estimated length of at least one bench face (13 metres), and in most cases, a minimum width of 10 cm. Each mapped feature was topographically located using a Total Station topographic instrument, which provided accurate northing, easting and elevation coordinates within the Chuquicamata grid system. For the mapped structural features, the following characteristics were noted where possible: azimuth, dip, width, striation, contact with host rock, intra-fault material, mineralization, alteration, vein morphology, degree of cataclasis, relative timing relationships and sense of displacement. Sense of shear was determined from shape fabrics or brittle shear criteria based on kinematic indicators and fracture relations as described and defined by Hanmer and Passchier (1991), Simpson and Schmidt (1983), Lister and Snoke (1984), Simpson (1985,1986), Passchier and Simpson (1986), Rutter et al. (1986), Chester and Logan (1987), Chester et al. (1985), Tanaka (1992), and Petit (1987). These and other notable observations were recorded on a specially designed mapping form and later entered into a digital database (Appendix 2). This database composes the data set used to establish and analyse the structural sectors presented in this chapter.

In order to check structure continuity, mapping above bench H1, on accessible benches, was undertaken periodically, using the same methodology. This methodology was also used during preliminary geological mapping of the western half of the open pit. Areas inaccessible during the project were completed by compilation of previous mapping by other workers. The compiled areas were used only to trace principal structures from the open pit to the surrounding area for purposes of regional mapping. This data was not compiled to the digital database established for this study.

Fig. 6.1 Distribution of the principal fault and vein systems mapped within the Chuquicamata open pit. Those faults below the Bench H1 reference line were topographically located within the open pit during this study. Areas above the reference line were mapped in the pit where accessible and compiled from geological archives of the Chuquicamata geological staff. Thick lines represent fault-parallel veins. The reference coordinates correspond to the Chuquicamata coordinate system.

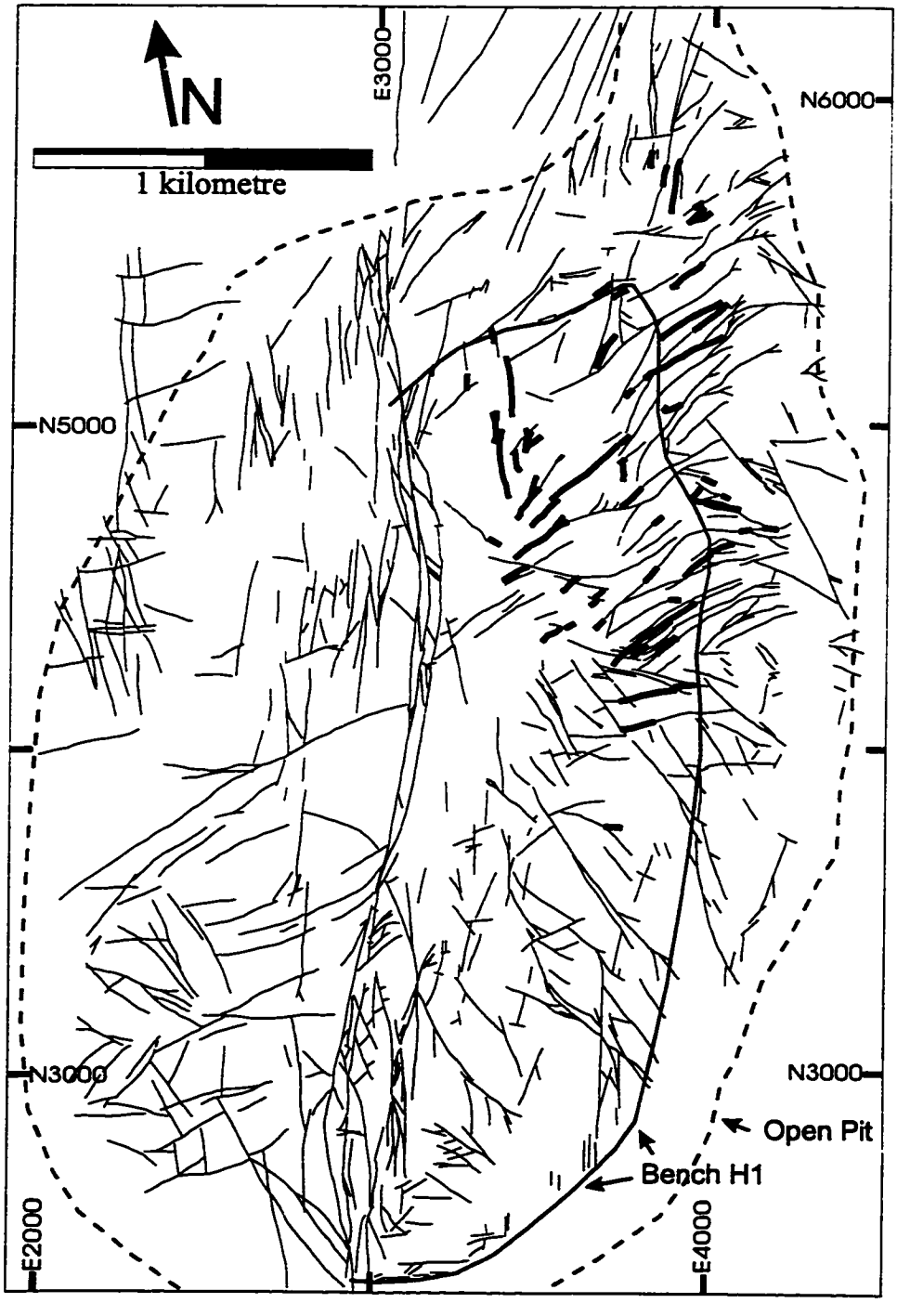

Table 6.1 General characteristics of main fault and vein types mapped at bench scale within the Chuquicamata open pit below bench H1 (elevation 2697 m). *Note () indicate number of composite veins in this group. **Note these veins also contain later mineralization not associated with the emplacement of the original vein and are discussed as composite veins. Mineral abbreviations Mo-molybdenite, Py-pyrite, En-enargite, cp-chalcopyrite, cc-chalcocite, cv-covellite, bo-bornite, sph-sphalerite, ga-galena, ten-tennentite, qtz-quartz, flds-feldspar.() in Alteration and Character columns mean that relationship is observed but not characteristic.

Structural Feature	Dominant Sulphide Mineralogy	Alteration	Character	Average Width	Total* Measured
Fault type 1 ductile shear zones			quartz: ductile feldspar: brittle	0.20 m	78
Fault type 2 gouge	py, cp, cc, cv, bo, en, sph, ten	sericitic argillic	foliated cataclastites	0.55 m	1013
Fault type 3 surfaces	mo, py and probably other mineralogies	sericitic (silicification)	straight undulating	0.05 m	729
Vein type 1 quartz	quartz **	(k-feldspar)	massive to foliated	0.30 m	78 (31)
Vein type 2 quartz-mo	quartz mo **	(sericitic) (silicification)	crack-seal	0.85 m	205 (44)
Vein type 3 pyrite	py >>cp,cc,cv,en,bo	sericitic argillic	massive granular texture	0.42 m	259 (50)
Vein type 4 Cu-Fe-Sulphides	en, py >> sph,ga,cc,cv,cp	sericitic argillic	massive (foliated?)	0.15 m	46 (17)

6.2 Dominant Fault and Vein Types

Three principal fault types and four principal vein types were recognized within the Chuquicamata open pit (Table 6.1). Veins represent distinct mineralization events, although once formed, the vein, as the brittle faults, were commonly reactivated. Relative timing relationships for faulting and mineralization are derived from crosscutting relationships, mineralization and degree of cataclasis. The vein types described below are presented in order from earliest-formed to latest-formed based on field relationships.

6.2.1 Fault Type#1 - Ductile Shear Zones

Ductile shear zones occur mainly along the eastern flank of the Chuquicamata complex within the East Porphyry (Fig. 6.2). The ductile shear zones are mesoscopically characterized by moderate to strongly developed planar fabric, defined by heterogeneously sheared quartz and aligned biotite grains. Associated with the planar fabric is a weak mineral lineation formed by elongate quartz rods, trails of biotite aggregates or grain-size reduced K-feldspar fragments. Microscopically the shear zones are characterized by subgrain formation, polygonalization and recrystallization of quartz grains in quartz eyes and ribbons. The deformed and recrystallized quartz shows grain and subgrain alignment and undulose extinction. Biotite shows kink bands, slip along cleavage planes and mineral grain alignment along shear planes. Plagioclase and K-feldspar display intragranular fractures and grain-size reduction by cataclasis. Feldspar porphyroclasts, especially K-feldspar megacrysts, have developed quartz pressure shadows that assist in defining the shear plane and to a lesser extent the stretching lineation. Further description and discussion of the ductile deformation zones encountered in the East Porphyry can be found in Chapter 4.

Locally, the shear zones are oriented sub-parallel to the main mineralized brittle faults in the deposit, indicating favourable orientations of the shear zones for reactivation and subsequent mineralization, or progressively more brittle conditions along the shear zone as it cooled. The majority of these shear zones parallel the trend of the Messabi Fault (Chapter 4.2) and are crosscut by mineralized veins and veinlets indicating a period of ductile deformation prior to mineralization. This early deformation has a minimum age of ca. 33.4

Ma (Reynolds et al., in press) and appears to be contemporaneous with deformation along the Messabi Fault. The shear zones show a variety of fault displacement types including dextral oblique-reverse, reverse and right-lateral strike-slip.

6.2.2 Fault Type#2 - Gouge-bearing

Faults bearing cataclastically derived intra-fault materials are the most common fault type at Chuquicamata and are distributed throughout the deposit (Fig. 6.1). The intra-fault materials range from breccias composed of angular rock fragments to clay-sized, matrix-dominated, fault gouges. The latter may have a moderate to strongly developed planar fabric which bear kinematic indicators reminiscent of mylonites (Plate 6.1 and 6.2)(Reutter et al., 1996; compare Chester et al., 1985 and Cladouhos, 1996a and 1996b). Rock fragments, or clasts within the gouge, are derived from the fault-bordering lithologies and include quartz vein fragments, variably altered host rock fragments and composite grains of sulphide mineral assemblages. Fragments have undergone size reduction through brittle cataclastic, or milling, processes related to multiple fault motions. The resulting grey-black matrix ranges from fine sand to clay sized. Magnitudes of displacement range from tens of metres for fragment-supported breccias to hundreds of metres for gouge-dominated by clay-sized intra-fault materials. Alteration and mineralization associated with these faults are a result of cyclical activity causing periodic increases in permeability that was open to hydrothermal fluid flow and cataclastic incorporation of laterally adjacent mineralized wall rock.

6.2.2.1 Formation and Activity

The generation of fault gouges and the presence of both early and later formed mineralization assemblages within the gouges indicates periodic increases in permeability associated with either multiple fault plane reactivation events or prolonged fault activity. These events make assessment of the relative timing and the sense of displacement difficult.

Fig. 6.2 Distribution of ductile shear zones encountered in the CIC. Shear zones located near and parallel to the Messabi Fault are shown in Fig. 4.2. Grid corresponds to the Chuquicamata coordinate system and reference benches M1, I1 and F4 are at 2437m, 2645m and 2770m elevations. The thick, approximately north to south trending line indicates the surface trace of the West Fault.

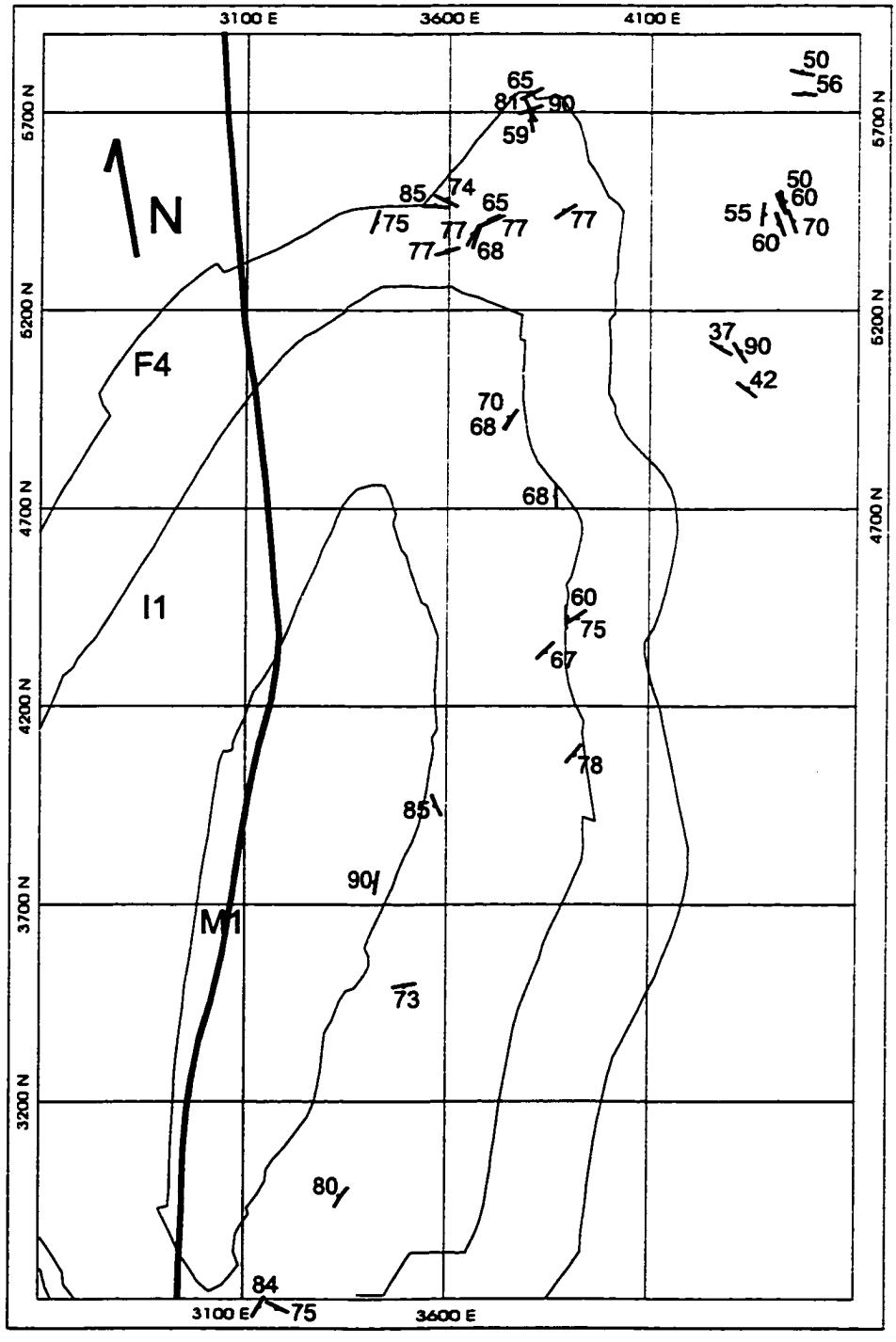

Plate 6.1 This photo illustrates a typical foliated gouge-bearing fault (C2 Fault) from the northern sector of the mine. The host rock is completely altered to a quartz-sericitic assemblage and has been brecciated and incorporated into the gouge. Finely ground pyrite imparts the black color to the gouge material. The strongly developed s-c fabric indicates a sinistral displacement for this fault. Note that sphalerite is also present within this gouge material. Scale is in centimetres. (CU834).

Plate 6.2 Displacement sense on brittle gouge-bearing faults was determined using the same types of kinematic indicators that are present in mylonitic rocks. This fine-grained foliated fault gouge bears subrounded quartz porphyroclasts that display sigma-type asymmetric tails composed of finer ground minerals, most likely derived from sericitized feldspars and mineral fragments (arrow) that define s-fabrics. This fault is part of a NE-SW trending dextral system that outcrops along the northern face of the mine. The yellow pencil is approximately 1 cm in width.

Plate 6.1 (see caption on previous page).

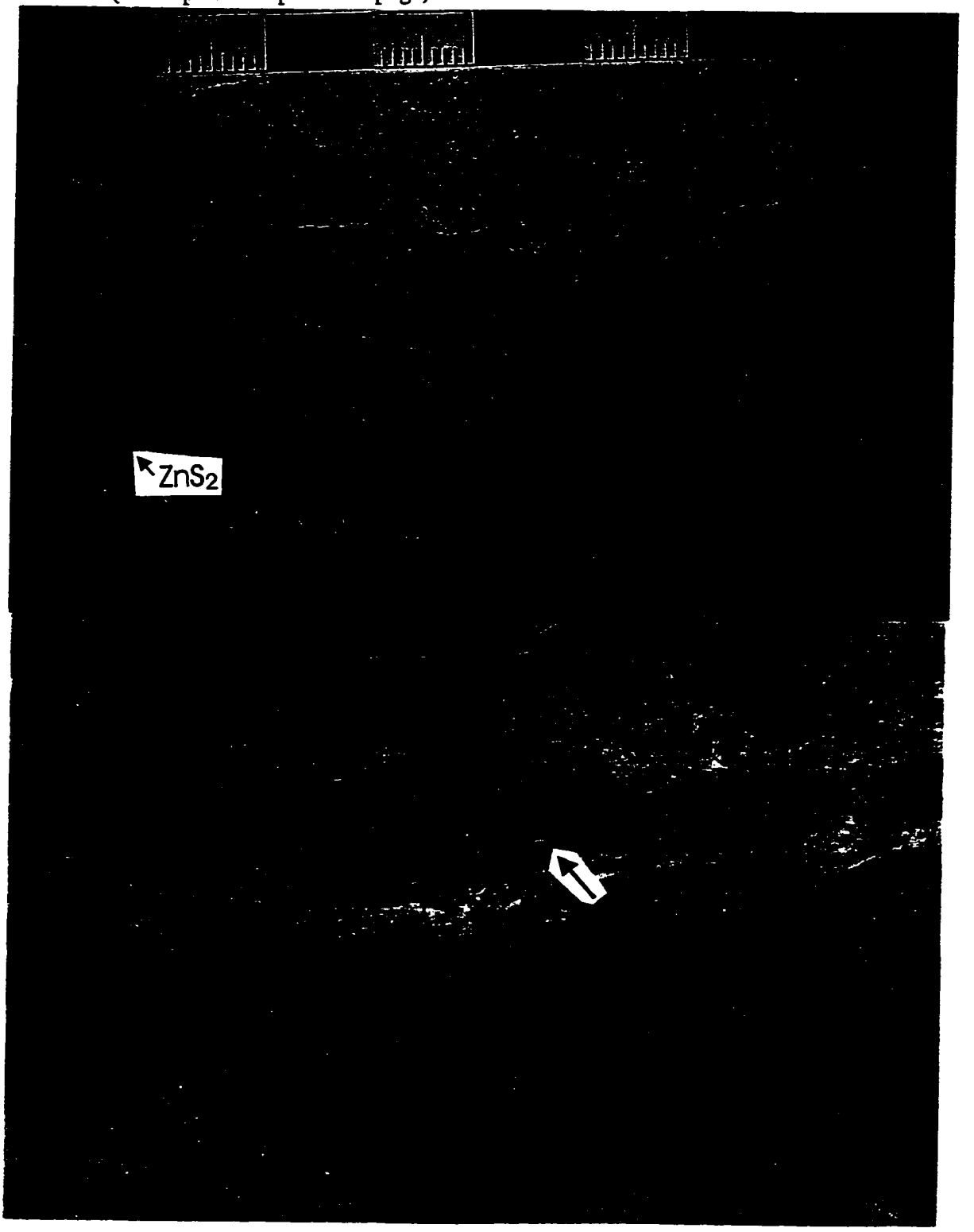

Plate 6.2 (see caption on previous page).

Fault reactivation results from an imposed far-field, regional, or local stress field on a pre-existing fault of suitable orientation. Both regional and local stresses are modified by local anisotropies and the presence of high pore-fluid pressures. The presence of high pore or fluid pressure lowers the effective confining pressure and the normal stress acting on an incipient fracture making the rock weak (Hubbert and Willis, 1957; Hubbert and Rubey, 1959; Secor, 1965; Phillips, 1972). The resistance of the rock to sliding then becomes equivalent to the sum of its cohesive shear strength and the product of its effective normal stress and the coefficient of internal friction. Once a fault or vein increment is formed the cohesive strength across this discontinuity becomes equivalent to that of the intra-fault material or the vein-rock interface, which will generally be less than that of the host rock. If so, reactivation along the existing fracture, or vein, is more likely than the formation of a new fracture in the intact rock providing the existing fracture is appropriately oriented.

Permeability related with brittle fault zones is generally several orders of magnitude greater than in intact crystalline rocks (Brace, 1980), is highly anisotropic and varies with fault activity through time (Sibson et al., 1975; Sibson, 1990, 1996; Caine et al., 1996). The permeability is related to the architecture of the fault zone, which generally comprises a central core zone surrounded by a damage zone and protolith, both of which may inhibit or enhance fluid flow along the fault (Wallace and Morris, 1986; Caine et al., 1996). Core zones comprised of clay-rich gouges (Anderson et al., 1983) or well-indurated cataclasite zones (Chester and Logan, 1986) are likely to act as fluid barriers. While adjacent damage zones, which may be composed of subsidiary faults, fractures and veins, are likely to have relatively higher permeability than the core zones (Chester and Logan, 1986; Moore et al., 1995). The permeability of fault and vein associated breccias and fractured wallrock allows the penetration of hydrothermal fluids, the latest hydrothermal event overprinting any previous event. The pervasive quartz-sericite alteration zone (Chapter 3.3.3) is a result of increased permeability along cyclically active faults. The widespread distribution of this alteration has lead some former authors to relate *all* the mineralization at Chuquicamata to the latest quartz-sericite hydrothermal alteration phase (Soto, 1979; Lopez 1939, 1942; Ramirez, 1993).

6.2.3 Fault Type#3 - Fault Surfaces

This fault type is composed of observable fault planes that generally represent either the hanging wall or footwall surface for which further data on intra-fault materials and width could only be approximated. These surfaces are the most obvious in the open pit as they control the shape of bench faces. This is the case for many of the faults in structural sectors E and F, described below, which show variably striated undulatory surfaces with irregular patches of gouge adhered to the surface. As the confidence in the intra-fault material mineralogies and width measurements is low due to exposures parallel to bench faces these faults were kept separate from the faults for which more data was available.

6.2.4 Vein Type#1 - Quartz

This vein type is distributed throughout the northern half of the open pit from the lowest elevations of the open pit, to the upper benches, close to the pre-mine surface (Fig. 6.3). These veins are comprised primarily of massive white to pinkish quartz (Plate 6.3), have variable widths, commonly 20-30 cm, and uncommonly displays millimetre to centimetre widths of K-feldspar. The K-feldspar forms a lining to the quartz-filled fracture. Soto (1979) proposed that the lack of associated alteration halo indicated that the mineralizing fluids were probably in equilibrium with the host rock. However, this relationship may also result from the rapid nature of the mineralizing event, where fluid circulation and crystallization is too rapid to allow for chemical reaction (Akande and Zentilli, 1982). Contacts with the metasomatically altered host rock are irregular to planar. In thin section, quartz textures vary from massive (sub)-equigranular (millimetre) to elongate equigranular (micrometre) strained grains suggesting post-vein emplacement deformation.

This vein type is equivalent to finer A-type *veinlets* described by Gustafson and Hunt (1975) as an early formed vein in porphyry copper evolution. Emplacement of these veins probably occurred following the early high temperature (>350°C) K-silicate alteration phase. The relationship of this vein-type with the stockwork/veinlet system has not been conclusively established. However, fractures having orientations subparallel, or oblique, to the vein orientation variably bear chlorite, epidote, pyrite, chalcopyrite, hematite, or

chalcocite, the latter being the result of a later enrichment process. These veins rarely show quartz-sericitic alteration halos. The observed alteration and mineralization associated with this vein type are likely a consequence of younger events, which may include the formation of a stockwork/veinlet system, resulting in the reactivation of the structure along which the quartz vein was emplaced and involving the circulation of hydrothermal fluids.

Fig. 6.3 Surface distribution of Type#1, massive to laminated quartz, veins within the open pit. Grid corresponds to the Chuquicamata coordinate system and reference benches M1, I1 and F4 are at 2437m, 2645m and 2770m elevations.

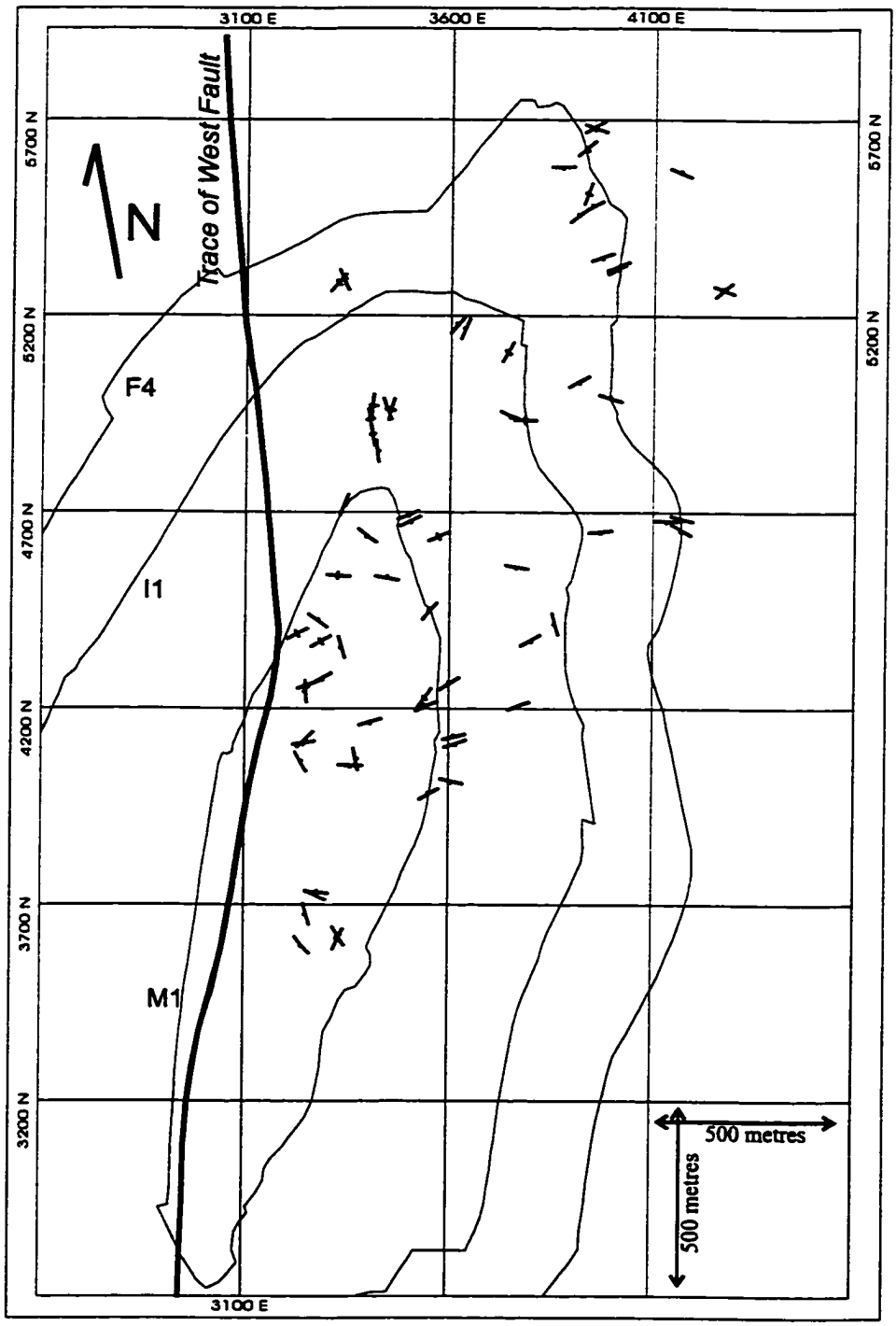

Plate 6.3 Photograph of a portion of a typical large-scale massive quartz vein. The vein contact with the host rock is sharp and just observable on the left-hand side of the sample. The host rock has been altered to a quartz-sericitic assemblage. The right-hand side of the sample approximates the central portion of the vein. For the most part, pyrite is filling open space within the fractured quartz vein. The greyish-black material in the upper central portion of the photo is supergene chalcocite-covellite "soot" that is coating the pyrite. Scale is in centimetres.

6.2.5 Vein Type#2 - Quartz-Molybdenite

This vein type is concentrated primarily in the northern sector of the mine (Fig. 6.4). Although it is likely that these veins were also generated in the southern part of the mine, but subsequent brittle deformation obscures this evidence. Fragments, or blocks, of quartz-molybdenite veins are located in the southern sector of the mine discontinuously traceable within the West Fault Zone and its associated mega-breccia zone (see below, Chapter 6.3.1.7). Individual veins are traceable for several tens of metres along both strike and dip directions, however, vein groups that define a discontinuous series are mappable over lateral and vertical distances of up to 100 metres. The quartz-molybdenite veins are up to 5 metres in width and striped in appearance, having alternating light and dark, millimetre to centimetre wide, laminations parallel to the vein walls (Plate 6.4). The colour variation is due to variable molybdenite concentrations within the veins; the darker laminae representing higher concentrations of molybdenite (Soto, 1979). In hand sample, the veins are composed of aphanitic quartz grains, <1 mm, having an overall saccharoidal-like texture with fine disseminations and very thin, ≤0.5 mm, planar laminations of molybdenite. Disseminated molybdenite imparts a blue to grey colouration to the veins (Soto, 1979). Molybdenite also concentrates along later dissolution surfaces forming asymmetric stylolites that are a result of post-mineralization deformation processes probably associated with the formation of the West Fault and its subsidiary branches. Stylolites are uncommonly observed within those veins exposed along the eastern expanse of the open pit and rarely within blocks of vein rock within the West Fault Zone and mega-breccia zone. Molybdenite is also deposited along fracture and fault surfaces that have no associated alteration halos. This molybdenite is in part remobilised, probably derived from the large quartz-molybdenite veins that show stylolitic dissolution textures.

In thin section, the quartz shows a variety of grain sizes, millimetre to micrometre, having an overall polygonal shape. Generally, these veins show strong recrystallization with subequigranular zones displaying grain boundary bulging (migration) and subgrain formation. Areas of large, 1-2 mm, columnar grains, which may represent the original texture of the veins, show strong undulose extinction, subgrain formation and recrystallization along

grain boundaries. Sericite is observed filling fracture-connected void spaces crosscutting quartz grain boundaries.

Vein contacts with the host rock are planar. Irregular widths of sericite-(clay)-quartz alteration halos parallel these veins. The permeability of these veins is indicated by the presence of a variety of fracture fillings that both cross-cut and parallel the host quartz-molybdenite vein, but whose assemblages are clearly deposited later. These assemblages include sericite, chalcocite-covellite, chalcocite-pyrite, pyrite-chalcopyrite and pyrite+/-enargite+/-sphalerite and sericite within fracture and void spaces within the vein. Although the sericite alteration appears associated with the quartz-molybdenite vein emplacement, it is interpreted as a later stage event associated with the hydrothermal system that resulted in the massive texture-destructive quartz-sericitic alteration zone (Chapter 3.3.3). Further study of sericitic alteration assemblages is underway to establish hydrothermal and magmatic affinities and characteristics. The circulation of probable later hydrothermal fluids through the permeability network of fractured quartz-molybdenite veins would result in the alteration of wallrock adjacent to the veins and the observed sericite veinlets within the veins.

6.2.5.1 Mechanism of Formation

The particular striped character of the quartz-molybdenite veins suggests a crack-seal formation mechanism (Phillips, 1972; Gretener, 1969; Ramsey, 1980; Laubach, 1988) akin to the gouge-generating reactivation process for Type#2 faults. A crack-seal mechanism suggests the Type#2 veins are mineralized hydraulic fractures formed by a series of extensional, or shear extensional events associated with fracturing by supralithostatic fluid pressures. The crack-seal texture, of these veins results from repeated fluid introduction, probably from hydrofracturing events associated with the emplacement of a magmatic body at depth. A fluid pumping mechanism may have assisted in the circulation and focussing of meteoric fluids through or near the mineral-bearing intrusion that was the heat source for fluid convection. The mechanisms involved in these hydraulic fracturing and fluid pumping process are outlined in detail by Hubbert and Willis (1957), Hubbert and Rubey (1959), Secor (1965), Phillips (1972), Ramsey (1980),Sibson et al. (1975) and Sibson (1990, 1996).

Plate 6.4 Two quartz-molybdenite veins, V2, associated with the large vein array. (A) This vein outcrops on the northern mine face in a host rock that is completely sericitized. This vein, although not observable in this photo, bears a ribbon, or crack-seal texture that is characteristic of this vein array. The vertical exposure of the vein in this photo is approximately 12 m. The width of the vein at the bottom of the photo is 40 cm. (B) This vein is located approximately 52 m below (A) within the same northern sector of the mine, but within a potassically altered host rock. There is no stockwork present adjacent to this vein. In the middle of the photo the characteristic crack-seal texture is observable as a vertical color banding. This vein is 1.5m in width at the bottom of the photo.

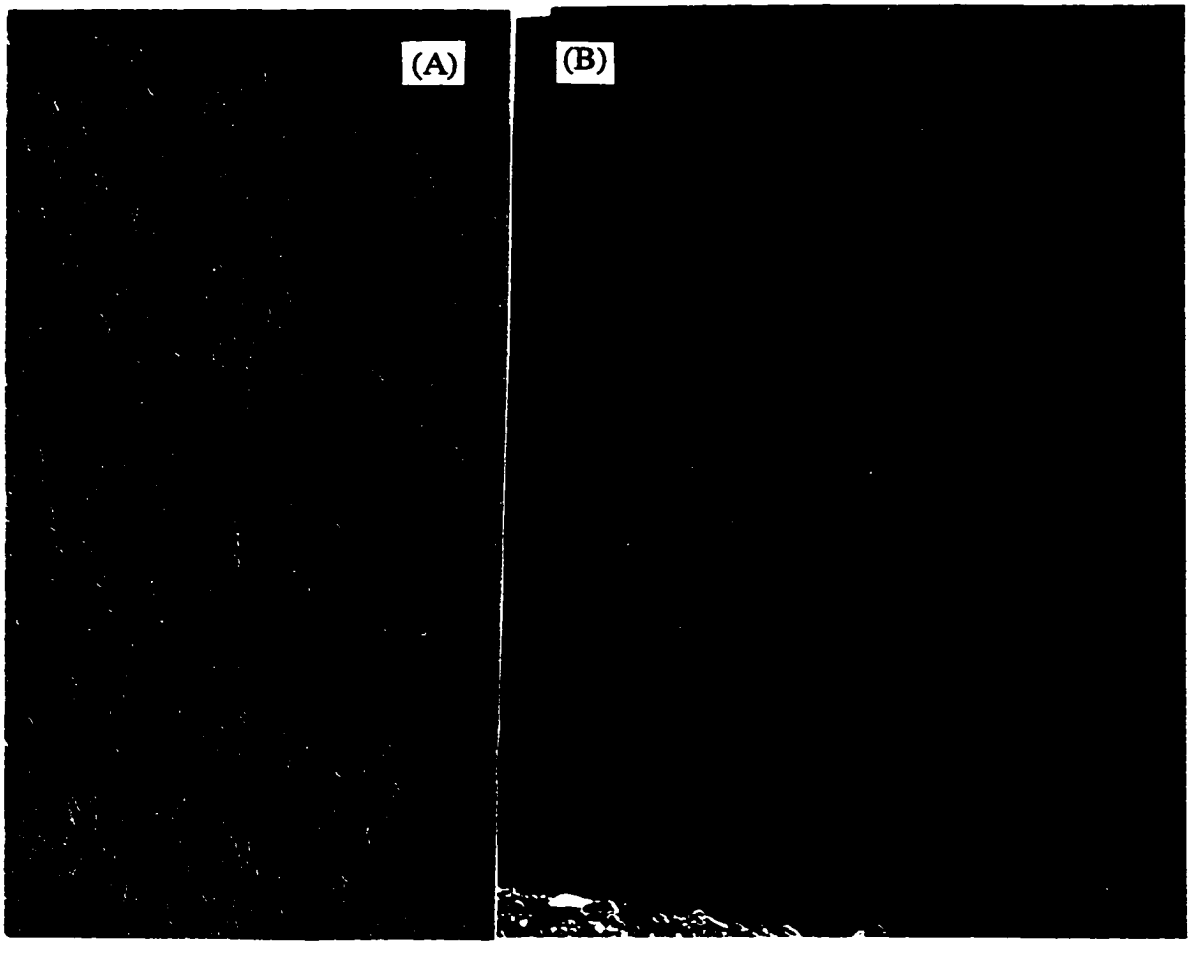

Fig. 6.4 Surface distribution of mapped Type#2, quartz-molybdenite, veins within the open pit. In the northern half of the mine (north of N4200 and above bench I1) the vein orientations suggest a radial (NW-SE through E-W) pattern that is modified by later brittle faulting. An approximate N-S trend in the southernmost section of the mine reflects a re-orientation of vein fragments within the West Fault Zone. Grid corresponds to the Chuquicamata coordinate system and reference benches M1, I1 and F4 are at 2437m, 2645m and 2770m elevations.

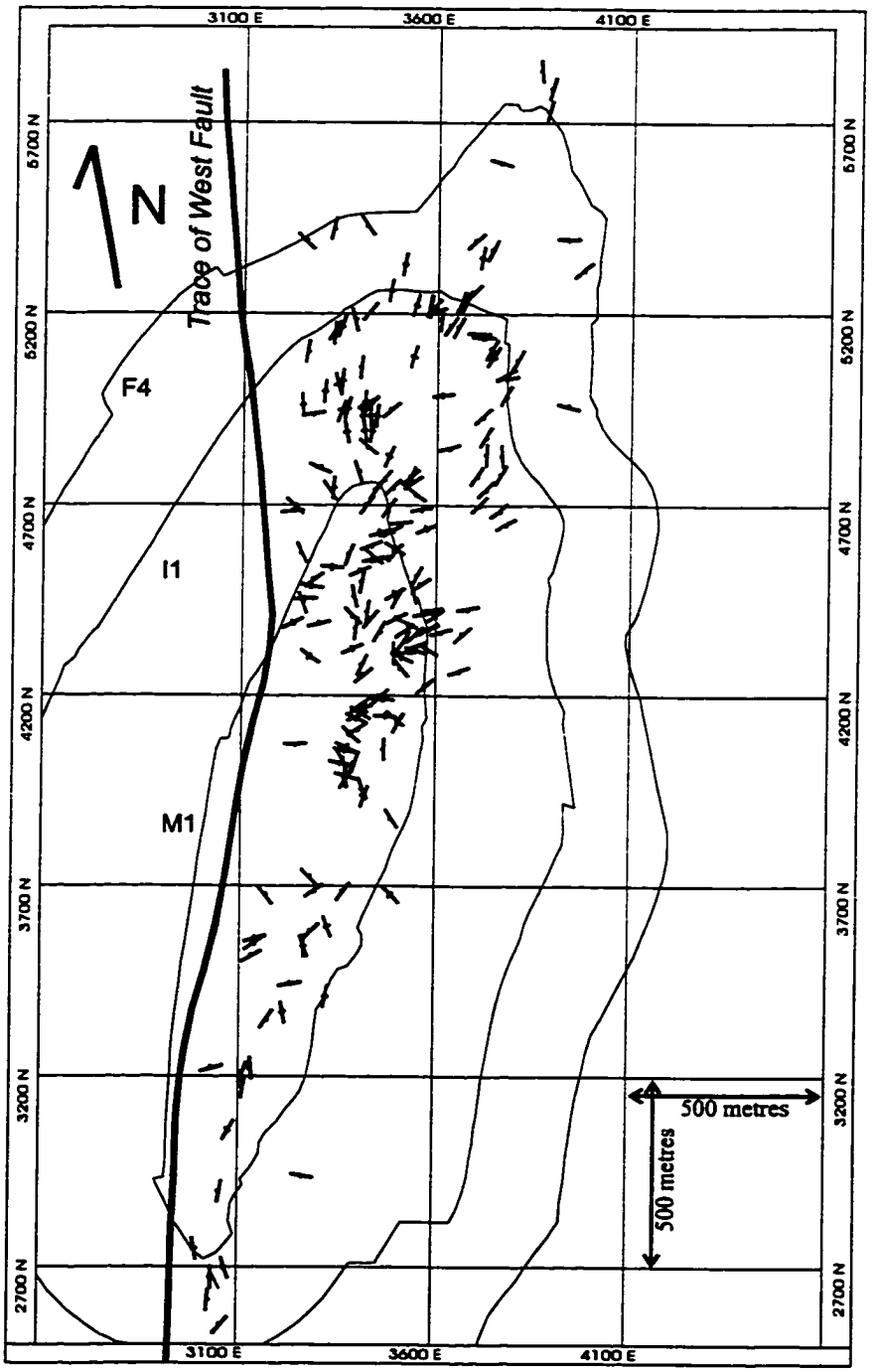

6.2.6 Vein Type#3 - Pyrite dominated

The vein mineralogy is dominated by medium to coarse grained pyrite that is associated with minor chalcopyrite, chalcocite, covellite and traces of enargite (Table 6.1). Massive pyrite-(chalcopyrite) is commonly granular in texture with chalcocite and covellite occurring as surface coatings on the grains. Some occurrences show that the massive pyrite has been brecciated, fragments of sericitized host rock incorporated within the breccia, and then cemented by a finer gouge of pyrite fragments, <<1 mm, and massive chalcocite, indicating vein parallel fault activity. Massive pyrite veins are observed to crosscut and more commonly parallel previously formed Type#1 and Type#2 veins and occur as intra-fault materials in the form of cemented breccias and gouges (Plate 6.5). This vein type is not useful as a relative time marker, since pyrite is ubiquitous, present in almost all mineralizing events in the Chuquicamata porphyry system. Also, this vein type may represent a vertical extension of vein Type#4 although a depth relationship has not been confirmed.

Contacts of pyrite-dominated veins with wall rock are obscured by intense sericitic-argillic halos (Plate 6.6). Further petrological study is required to conclude whether this alteration is associated with the emplacement of these veins, or is a spatial relationship resulting from a subsequent alteration phase. This alteration association is illustrated by chalcocite-(covellite) coated granular pyrite-chalcopyrite veins located in the massive quartz-sericitic alteration zone, which have coarsely crystalline sericite and clay minerals filling interstitial spaces between pyrite granules, suggesting a sericite-clay mineralization subsequent to pyrite formation.

Vein type#3 is distributed throughout the central and northern sectors of the open pit with a greater concentration of these pyrite veins in the central eastern sector (Fig. 6.5). Outcroppings of these massive pyrite veins in the upper northeastern benches of the open pit coincide with records of historical mine workings. However, thinner granular veins also occur in the massive quartz-sericite alteration zone deeper in the pit. The Zaragoza vein (Chapter 6.3.1.1) may be representative of this vein type, that were initially mined for copper as vein deposits. The ore consisted of copper oxides and massive supergene enrichment with chalcocite-(covellite) after enargite and pyrite. The veins became uneconomic at deeper

levels, those exposed in the open pit, showing only pyrite (Wroth, 1917).

6.2.7 Vein Type#4 - Cu- Fe-sulphide dominated

In general, this vein type is distributed in the northern sector of the open pit at deeper levels of exposure (elevations <2420 masl)(Fig. 6.6) and within or immediately adjacent to the quartz-sericite alteration zone. Type#4 are considered to have formed late in the evolution of the deposit, D-type veins according to the Gustafson and Hunt (1975) nomenclature, and include enargite- and sphalerite-dominated veins. In many cases, these veins are emplaced within a pre-existing vein, fault or fracture network and may show right angle changes in orientation at fault and fracture intersections suggesting that mineralizing fluids of this event used any accessible permeability. This vein group is dominated by enargite veins, which are massive, coarse crystalline veins that commonly include pyrite, sphalerite and unidentified clays. In many cases, a vein of massive pyrite is fractured and/or brecciated and enargite fills the interstitial space between fragments. This relationship is interpreted as a crosscutting association between vein types, yet it is probable that vein Type#3 and #4 are related by depth.

Plate 6.5 This photo illustrates the relationship between a subhorizontal quartz vein (V1) and a pair of subvertical pyrite-dominated, V3 veins. The vertical vein on the right is a massive pyrite vein that has incorporated wallrock fragments. The vein on the left is composite vein, in part massive and in part composed of a series of closely spaced pyrite veins. This exposure along the eastern expanse of the mine has been mapped as sericitic-over-potassic alteration. Hammer length is 35 cm.

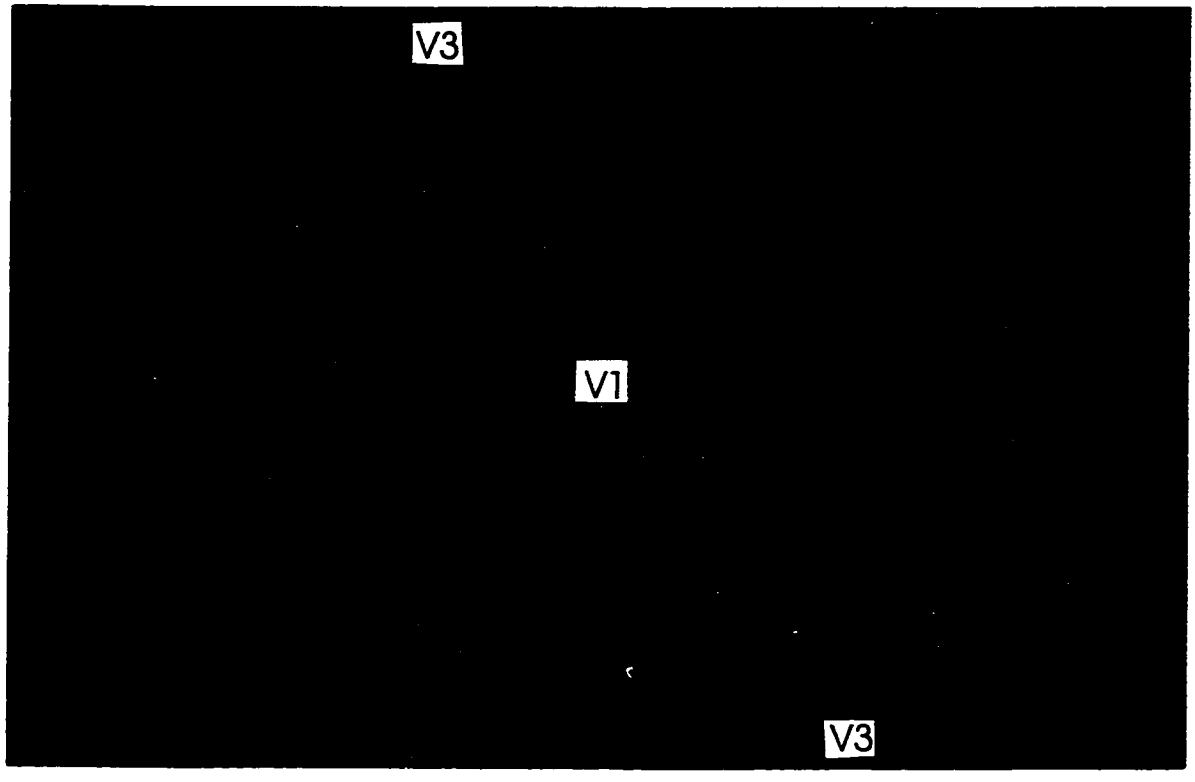

Plate 6.6 Associated with the vein arrays and fault systems in the northern half of the mine is a texture destructive quartz-sericitic alteration (lighter color) that radiates from an intensely altered zone adjacent to the West Fault along faults and veins that provided channels to circulating hydrothermal fluids. In this photo, the fault-vein-controlled quartz-sericitic alteration is shown overprinting the pre-existing potassic alteration. People are approximately 1.8m in height.

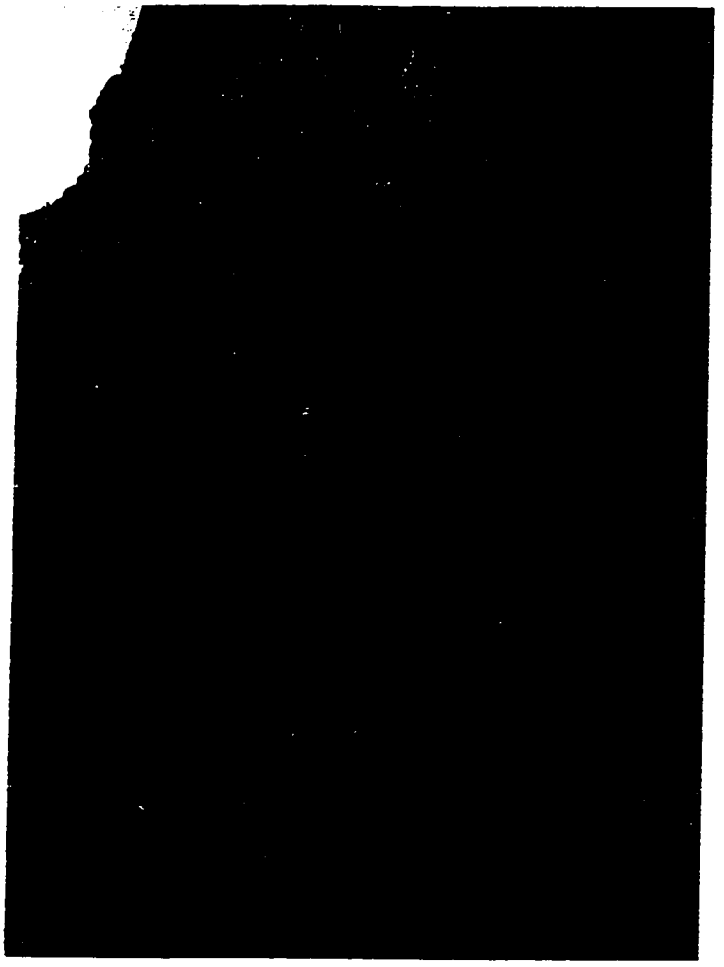

Fig. 6.5 Surface distribution of mapped Type#3, pyrite-dominated veins. These veins show a concentration in the north-central and north-eastern sectors of the mine. The traces of these veins coincide with historical vein mine workings indicating a probable vertical relationship between copper-rich vein mineralogies and pyrite-dominated veins. Grid corresponds to the Chuquicamata coordinate system. Reference benches M1, I1 and F4 at 2437m, 2645m and 2770m elevations are shown.

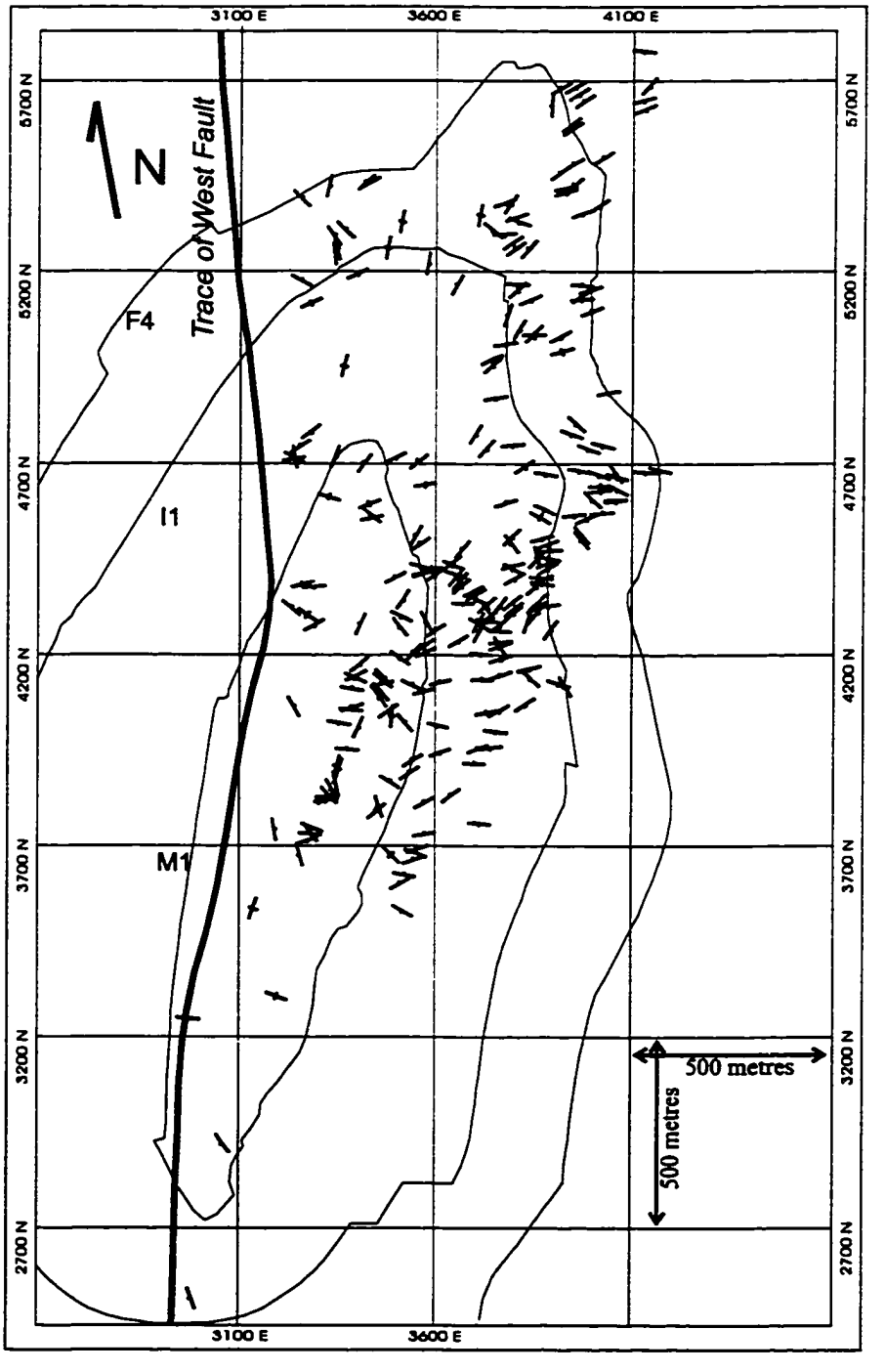

Fig. 6.6 Surface distribution of Cu-Fe sulphide Type#4 veins in the Chuquicamata open pit. These veins are concentrated within the quartz-sericite alteration zone and along the West Fault. Grid corresponds to the Chuquicamata coordinate system. Reference benches M1, I1 and F4 at 2437m, 2645m and 2770m elevations are shown.

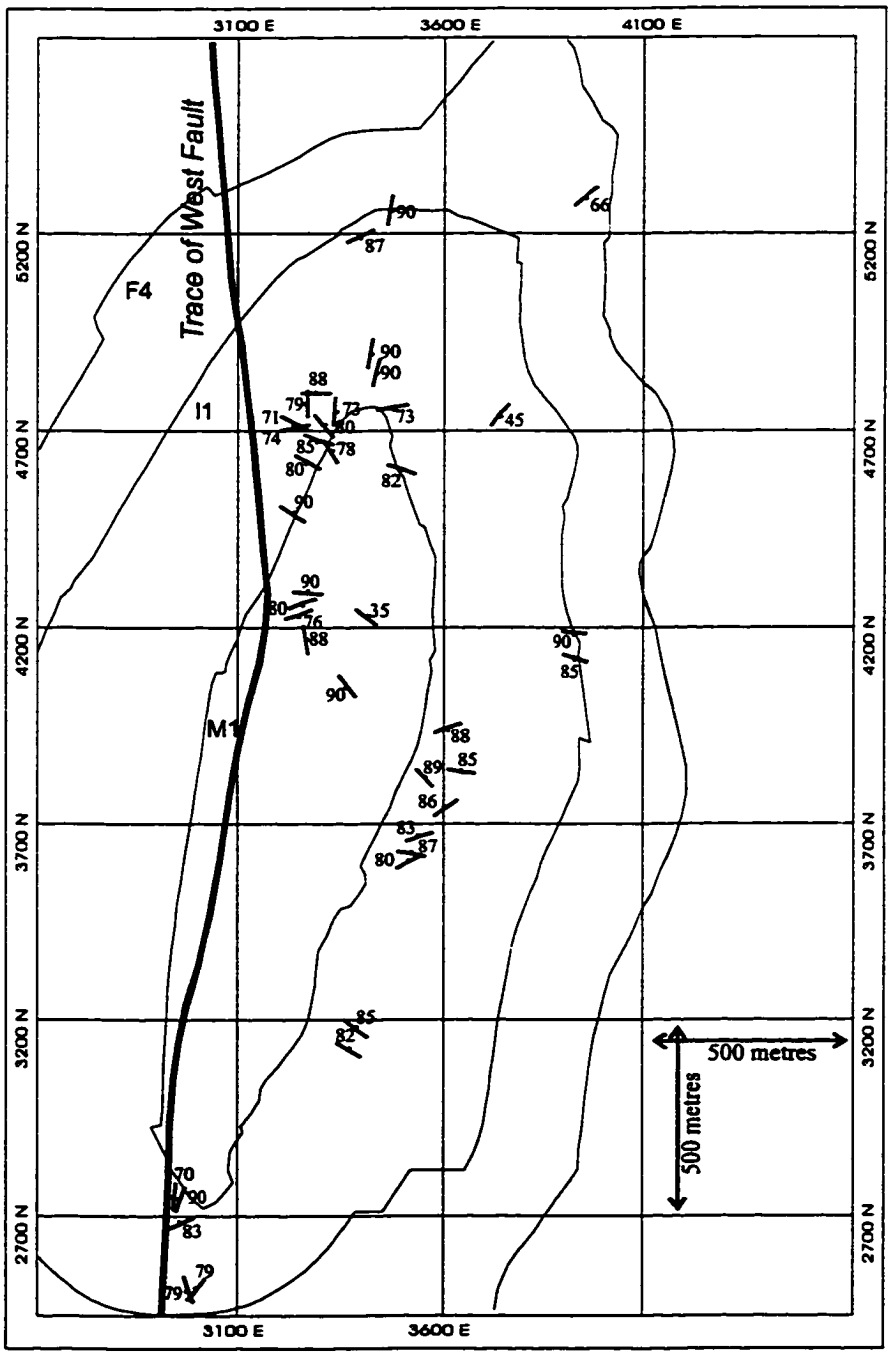

6.2.8 Faults and Vein Arrays: Relationships with Ductile Deformation and Veinlet Mineralization

The analysis of crosscutting relationships in the field and in cut slab sections leads to the following generalized relative time of formation sequence. The formation of these faults and veins represent at least three distinct episodes in the evolution of the Chuquicamata deposit. These episodes are 1) an early pre-mineralization ductile deformation; 2) brittle faulting and vein emplacement, associated with a hydrothermal alteration and mineralization sequence, and 3) subsequent brittle faulting following the hydrothermal events.

Type#1 faults showing ductile deformation are crosscut by mineralized veins and gouge-bearing Type#2 faults and therefore formed prior to the hydrothermal mineralization episodes represented by the described vein types. As discussed in Chapter 4, these zones of ductile deformation formed during the emplacement and cooling of the Chuquicamata complex. Later vein-bearing brittle faults, some of which may have initiated on pre-existing ductile shear zones, or pre-existing veinlets (see Chapter 5), offset the Banco Porphyry dikes and Messabi Fault zone indicating an initial post-intrusion phase of fluid pressure assisted deformation. Mineralization within these brittle fault zones includes quartz (Type#1), quartz-molybdenite crack-seal veins (Type#2), coarse crystalline pyrite (Type#3) and lesser Cu-Fe and Zn sulphides (Type#4).

The relationship between the quartz veins (Type#1) and the quartz-molybdenite veins (Type#2) is best observed in veins having widths of 5-10 cm, as the thicker veins are often spatially separate, or composed of several parallel vein types (composite veins), making relative timing difficult to assess. Type#1 veins are crosscut by Type#2 veins, but the relationship between these large scale veins and those of the stockwork/veinlet system described in Chapter 5 is unknown.

Type#2, quartz-molybdenite veins, on the other hand, provide a time sequence marker as they appear consistent in the formation sequence as a distinct mineralization episode. Later mineralizing events, Type#3, then used the established permeability channels provided by the quartz-molybdenite veins in depositing assemblages of dominantly pyrite.

Fault-vein relationships are more complex to evaluate in light of deformation events during and following the mineralization of the deposit. Veins and faults are commonly parallel or sub-parallel in the deposit suggesting repeated reactivations during their evolution. Emplacement of similar veins oblique to fault traces are interpreted to be associated with formation during fault slip. Disruption of the fault and vein patterns, evident at deeper exposures in the mine, adjacent to the West Fault, are the result of the formation of a wide zone of breccia, known as the "megabreccia" (Fig.4.4). This breccia contains vein fragments, up to tens of metres in length, that can be locally used as kinematic indicators along the West Fault Zone within the pervasively altered quartz-sericite zone. This megabreccia zone formed prior to, or synchronously with, the hydrothermal event responsible for the pervasive quartz-sericite alteration zone (Chapter 3.3.3). Continued deformation along existing faults and veins generated a variably developed mineralized intra-fault material. Non-altered and non-mineralized breccia- and gouge-bearing faults formed as the result of deformation following hydrothermal activity. Other than distinguishing between those faults that bear mineralized breccias or gouges and those with unmineralized breccias, the relationships between faulting and alteration-mineralization events is indistinct, which suggests that Type#2 and Type#3 faults have no relative timing significance.

The relative timing of deformation, alteration and mineralization events is further evaluated in the following section through the definition and analysis of structural domains and domain associations. The structural domains are defined by the fault and vein systems described above and domain associations are defined by those domains deforming synchronously during tectonic or faulting phases. Domain associations are considered at district to regional scales of deformation and are discussed in light of accepted regional tectonic settings.

6.3 Structural Domains

Mapping of structural features outcropping within the open pit has allowed for the characterization of eight structural domains (Table 6.2, Fig. 6.7). These domains include the ductile Messabi Fault zone, that was discussed in Chapter 4, early brittle fault-vein sectors

(A, B, C), where some faults parallel relict shear zones and provide permeability paths for mineralizing fluids, and later brittle sectors (D, E, F, G), where faults offset earlier features and bear little mineralization.

The boundaries of the structural domains are defined by the exposed spatial extents of subparallel fault sets that display similar orientation, sense of displacement, intra-fault materials and are thought to be simultaneously active (e.g. Baldwin et al., 1978; Nur et al., 1989; compare Aydin and Page, 1981). Although domains are based on fault sets (Type#2 and Type#3), data on the presence of vein type per domain is also presented as it assists in establishing relative timing relationship between the formation and activity of individual structural domains. The data set analysed for structural trends within individual domains is presented in Appendix 2.

6.3.1 Brittle Fault Domains

The domains are composed of individual or multiple brittle fault sets that occupy an area of the mapped open pit (Fig. 6.7). In several cases, only a single dominant fault set is present, in others, probably due to unfavourable orientations for reactivation, a second overprinting fault system is also present. The domains include A and B, which contain principal faults known as the Zaragoza Fault in domain A and the Estanques Blancos Fault in domain B. These principal faults displace Mesozoic units, present outside of the open pit, in a dextral sense (Fig. 4.1). Domain C, which is considered transitional between domains B and D, bears a conjugate set of faults, one of which is mineralized. This domain also contains a principal fault, the Balmaceda Fault, which offsets Paleozoic meta-igneous units outside of the open pit with a sinistral sense of displacement (A. Tomlinson, 1996, written comm.) and Mesozoic units adjacent to the open pit in a dextral sense. The unmineralized fault set is related to a temporally distinct deformation event that also formed fault systems in domains D, E and F. The regional expression of the West Fault has been characterized on the basis of its exposure in the Chuquicamata open pit (e.g. Reutter et al., 1994, 1996). Here, domain G is composed of the sinistral West Fault and its parallel associates, the Calderones and Americana faults. It is this fault set that is considered to be the throughgoing regional

master fault for which faults in domains D, E and F are associated subsidiary faults. Reconnaissance mapping of the western portion of the open pit is presented, in brief, to provide a useful comparison for the east side structures. The similarities and differences clarify the importance of the West Fault and its role in the West Fault System.

Table 6.2 Characterization of structural domains defined within the Chuquicamata open pit. () -Estimates of displacement magnitudes from district compilations. * -determined by Reutter et al. (1996). Dilation refers to extension within the sector estimated from vein abundance and breccia formation.**-A. Tomlinson, 1996, written communication.

Domain	Initial Displacement	Latest Displacement	Orientation	Mineral Relation	Dilation
Messabi	dextral	sinistral*	NNE-SSW	dextral: pre-mineral sinistral: post-mineral	low
A - Zaragoza-C2	dextral Zaragoza 700m C2 400m	Zaragoza ? C2 sinistral	NNE-SSW and NE-SW	dextral: pre- to syn-mineral	high
B - Estanques Blancos	dextral	dextral	prominent: NE-SW minor: WNW-ESE	dextral: pre-,syn-, post-mineral?	high
C - Balmaceda	sinistral **	dextral, sinistral (500 m, 300 m)	~E-W	sinistral: pre-mineral dextral: syn post?	mod-high
D - South Central	sinistral	sinistral (500 m)	~NW-SE	post	low
E - South Eastern	dextral??	sinistral	NNE-SSW	dextral: pre-mineral? sinistral: post-mineral?	low-mod
F - Southern (Banco H1)		dextral (<100 m)	ESE-WNW	post	low
G - West Fault Americana	dextral?	sinistral (35-37 km)	NNE-SSW	dextral: syn-mineral? sinistral: post-mineral	mod

Fig. 6.7 Surface distribution of the mapped faults and veins outcropping within the open pit. The similarities between individual faults was used to group them into systems within a spatial sector of the open pit. Most structural domains have one or two principal faults that characterize those faults of the sector. Bench H1, included for reference was the upper limit to mapping, above which was later infilled by mapping undertaken during this project and compilation from previous maps. Data from previous mapping is not included in the structural database, but is used to illustrate the continuity of structures to the limit of the open pit. Faults and veins are not differentiated.

Fig 6.7 (see caption on previous page)

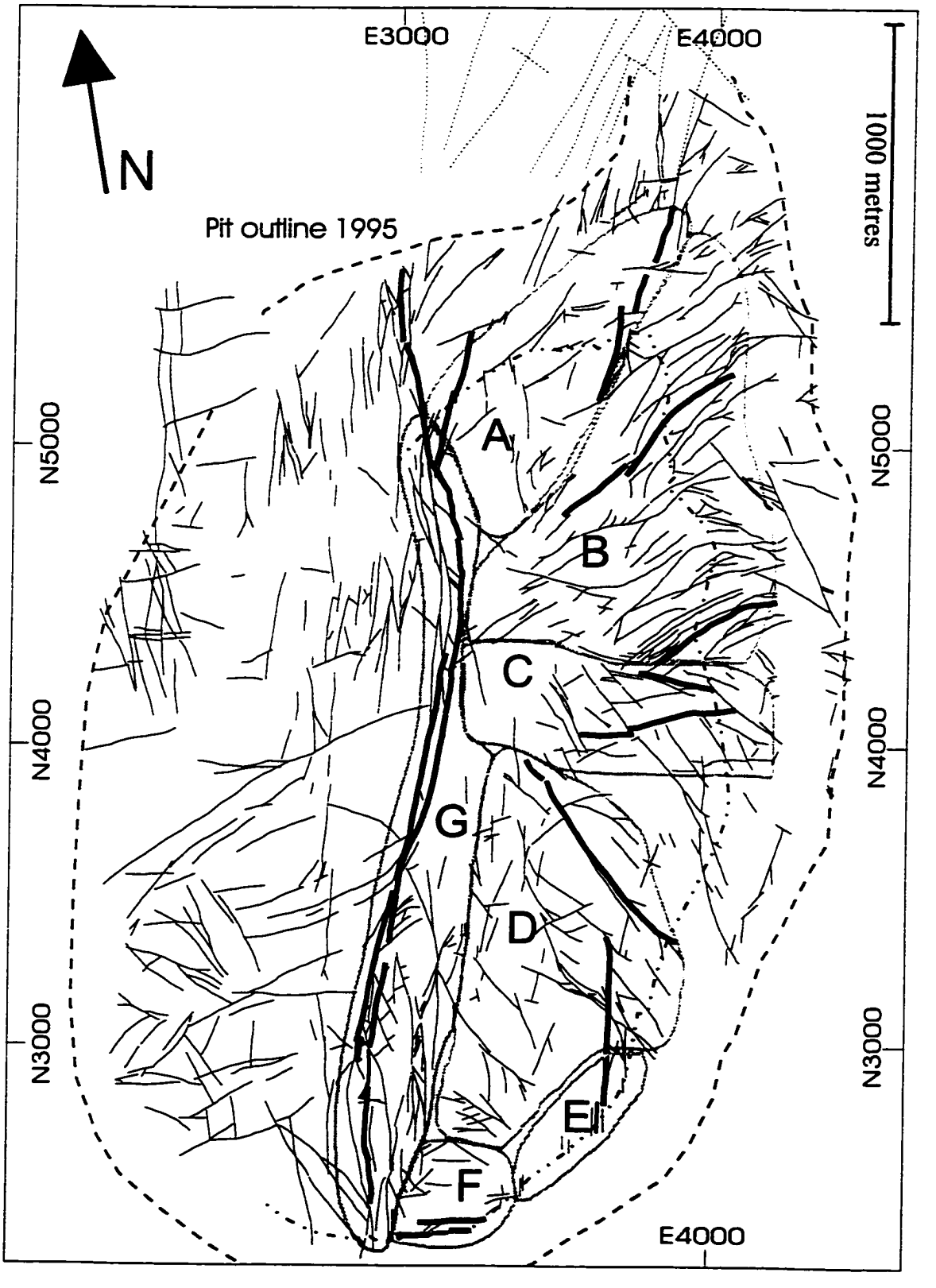

6.3.1.1 Domain A- (Zaragoza-C2)

Located in the northernmost sector of the mine, Domain A is bound to the west by the West Fault zone, Domain G, and to the east by Domain B (Estanques Blancos). This domain contains all alteration types, but is the only sector within which the West Porphyry outcrops (compare figures 3.2 and 6.7). Domain A is characterized by three dextral fault sets, a NE-SW, a NNE-SSW and a N-S system (Fig. 6.8A and B). Striae associated with gouge-bearing faults and also observed on vein surfaces are most common on NE-SW trending structures. The striae vary widely generally indicating an oblique motion for these dextral faults, however, it is impossible to correlate displacement between these faults based on striae due to the brittle nature of the deformation.

Contained within the sector are Type#1, #2, #3 veins that parallel the dominant fault orientations (Fig 6.8 C, D, E). The fault systems bear sericite and argillic halos indicating the circulation of hydrothermal fluids during or following the formation of the fault. The NNE system has two main faults known as the Zaragoza and the C2, both of which appear to either crosscut or splay from the Messabi Fault to the north of the open pit.

Ductile deformation, S-L fabrics with dextral shear sense indicators in a feldspar-quartz-chlorite-epidote assemblage, adjacent to the trace of the Zaragoza Fault in the open pit, probably indicate is was also a Type#1 fault and was a long-lived fault. Reactivation or continued activity of this dextral ductile shear zone within the brittle regime probably occurred as the result of high fluid pressures inferred to have been associated with mineralizing fluids that deposited pyrite and enargite within the Zaragoza fault as suggested by Wroth (1917). Later supergene enrichment resulted in higher grade chalcocite assemblages and Cu-oxides being deposited in the upper reaches of this fault. Mining of the enriched assemblages of this vein deposit was halted, as the vein became pyrite-rich at depth (Wroth, 1917). Regionally the Zaragoza Fault appears related to the curvature of the Messabi Fault to the north of the open pit (Fig. 4.1).

The C2 Fault hosts both quartz-molybdenite (Type#2) vein mineralization that is overprinted by massive pyrite (Type#3). Late deformation is indicated by the presence of asymmetric stylolites and a system of very fine (<1mm widths) quartz-filled extensional

fractures crosscutting the Type#2 vein along the C2 Fault. The orientation of the stylolites and veinlets corroborates sinistral shear sense indicators in foliated cataclastic fault rocks of the C2 Fault. This sinistral post-mineral shear is in contrast to the apparent dextral shear along the Messabi Fault outside of the open pit and the dextral shear sense of the Zaragoza Fault and other NNE faults comprising Domain A. The difference in shear senses confirms the reactivation of at least the C2 fault after the mineralization episodes.

Absolute displacement magnitudes for the Zaragoza and C2 faults are unknown for both initial ductile (pre-mineralization) and later brittle activities (syn- and post-mineralization), however, estimates of displacements interpreted from recent regional surface mapping by CODELCO geologists suggest approximate minimum dextral displacements of 700 metres for the Zaragoza Fault and 400 metres for the C2 Fault based on apparently offset lithological contacts. The Zaragoza and C2 faults are crosscut and offset in a dextral sense by a set of NE-SW trending faults similar to those Type#2 faults of Domain B (see below, Chapter 6.3.1.2). This NE-SW fault system in Domain A appears to have offset the NNE-SSW fault system and is therefore suggested to have formed after the NNE-SSW fault system. Relationships of the NE-SW fault system with sinistral shear along the C2 Fault are unknown. Maximum dextral displacement estimates for this NE-SW system from offset NNE-SSW faults are on the order of 150 metres.

6.3.1.1.1 Veins

Domain A contains all vein types described above with Type#2 being most abundant. Earlier formed Type#1 veins show a population average trend of 187/90 (Fig. 6.8C) with a small data cluster indicating a NNE-SSW trend. These veins are similar to the orientations, slightly NNW-SSE to NE-SW, for Type#2 veins (compare Fig. 6.8 C and D). Both of these vein sets indicate extension in an E-W to NW-SE orientation and trend parallel to the fault system trends. Similarly, Type#3 veins have a prominent N-S trend and a secondary NE-SW trend (~30% of data)(Fig.6.8E). Two trends are also observed for Type#4 veins, an approximately N-S trend (~50% of data) and an ESE-WNW (50% of data) trend (Fig 6.8F). With the exception of the ESE-trend of Type#4 veins, the prominent trends for all other veins

are similar to those trends described for the fault systems.

6.3.1.1.2 Discussion

Ductile shear zones, brittle faults and mineralized vein systems of Domain A have similar directional trends and commonly overprint each other. Fault planes may represent a favourable plane of weakness along which mineralization took place, or alternatively emplaced veins were of suitable orientation for synchronous or later fault activity. Reactivation or continued evolution of these faults and veins aided the circulation of hydrothermal fluids and deposition of late vein mineralization.

Three fault systems are evident from orientation analysis, earlier N-S and NNE-SSW trends and a later NE-SW trend. The NNE-SSW fault system displays evidence of pre-mineralization ductile deformation that relates to the cooling of the host rock soon after emplacement. This fault system hosts mineralized veins indicating reactivation of fractures during periods of high hydrothermal fluid pressures. Vein sets related to this hydrothermal activity range in orientation from NNW-SSE to NE-SW and in general parallel the fault systems. Since the faults do not appear to have a NNW-trend it is inferred that if the veins were emplaced prior to the faults, in a subradial pattern, then those veins having NNW trends were not suitably oriented for fault reactivation.

The relatively later NE-SW gouge-bearing fault system crosscuts and displaces the earlier NNE trending faults by up to 150 metres in a dextral sense. Both the earlier formed veins and fault systems and the crosscutting, predominantly gouge-bearing fault system have pervasive quartz-sericite alteration halos parallel to the fault and fault-vein traces suggesting the alteration accompanied the final phases of mineralization. Sinistral kinematic fabrics in fault gouges and dissolution features in veins along the C2 Fault indicate post-mineralization deformation associated with post-mineralization deformation and displacement concentrated along the West Fault.

Fig. 6.8 Lower hemisphere Schmidt stereographic projections for (A)Type#2 and (B) #3 faults that are used to characterise the fault systems in Domain A. Vein types are plotted in C (vein Type#1), D (vein Type#2), E (vein Type#3) and F (vein Type#4). In both fault and vein plots prominent trends are N-S, NNE-SSW and NE-SW indicating an interaction of deformation and mineralization. m= mean plane.

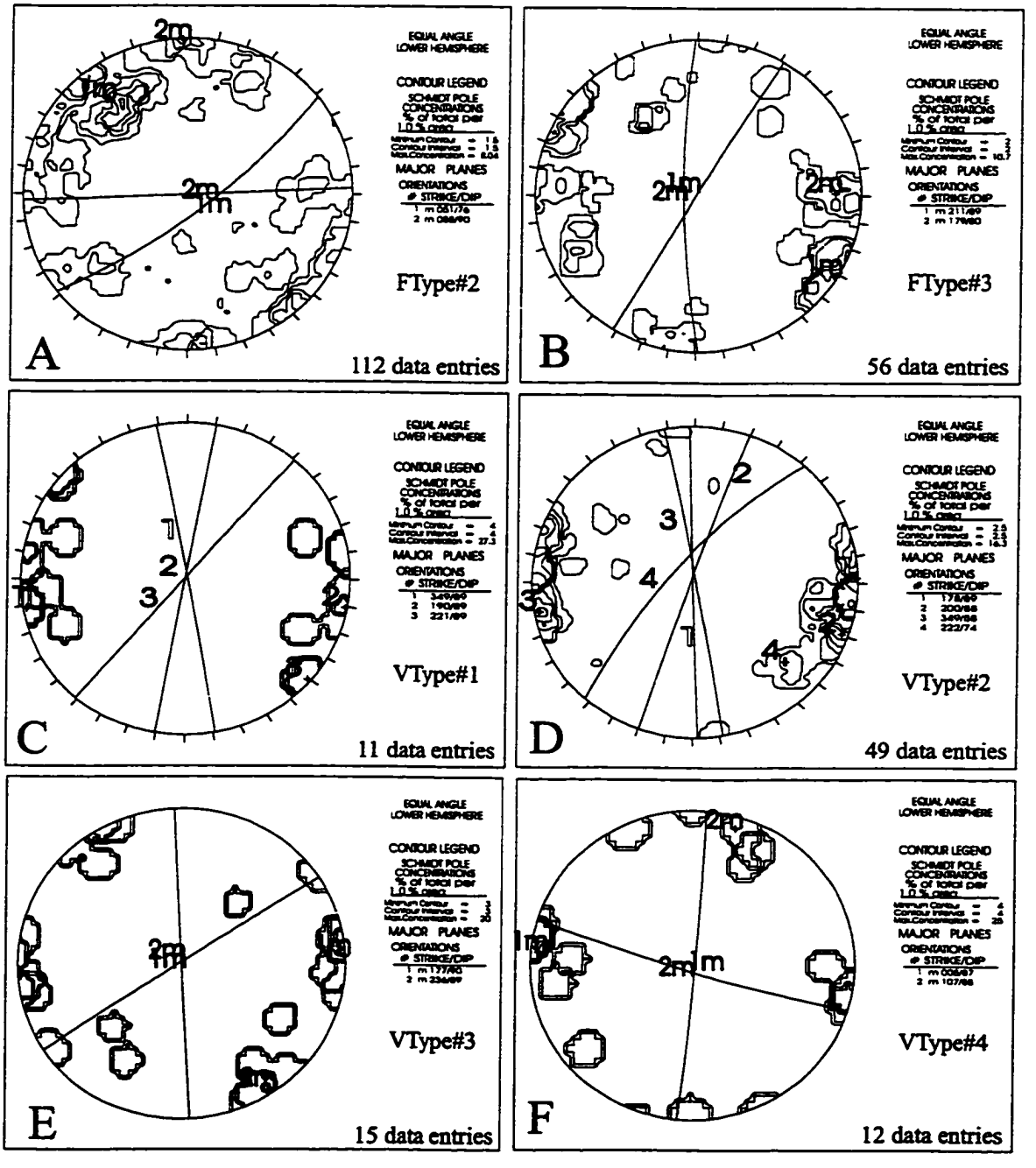

6.3.1.2 Domain B-Estanques Blancos

Located in the northeastern part of the mine, this domain is defined east of Domain A and north of Domain C (Fig. 6.7). Faults of this system trend outside of the mine to the northeast, where they offset Mesozoic and Paleozoic units and the Messabi fault zone in a dextral sense. Domain B contains all alteration types and is dominated by the East Porphyry, which is intruded by N-S trending dikes of the Banco Porphyry. This domain is characterized by a NE-SW fault system that is dominated by Type#2 faults (Fig. 6.9 A) and an ESE-WNW system of Type#3 faults (Fig. 6.9 B). Contained within the domain are ENE-trending Type#1 veins, Type#2 veins ranging from NNE-SSW to NE-SW, and NE to ENE-trending Type#3 veins (respectively Fig 6.9 C, D and E). These vein sets trend sub-parallel to the prominent fault direction and have an indistinct relationship with the NW-trending faults, which may be related to post-mineralization activity. Both fault and vein systems have sericitic-argillic alteration halos that widen towards the massive quartz-sericite alteration zone located in the SW corner of Domain B (Fig. 5.1) suggesting that the structural features acted as conduits for the circulation of late hydrothermal fluids and the massive quartz-sericite zone was the centre of this hydrothermal system. Domain B has a single named principal fault known as the Estanques Blancos, but it is made up of a series of parallel faults with important offsets.

6.3.1.2.1 Faults

The Estanques Blancos fault is the only named fault in this domain and is best known from outside the open pit from where it derives its name and displaces Mesozoic and Paleozoic units (Fig 4.2). This fault typifies those of the fault system that composes the structural domain. It is a gouge-bearing fault that has massive pyrite veins in its exposures on upper benches and quartz-molybdenite veins in its exposures at the bottom of the pit. Several fault-veins, mineralogically similar to the Zaragoza, were historically mined within this domain.

Characteristic to this domain is an NE-SW to ENE-WSW (Fig. 6.9 A and B) orientation of moderately to steeply dipping faults. A notable steepening of dip angles occurs as faults pass through the Banco Porphyry. Vertically above and below the Banco Porphyry,

the dips are between 60° and 80° toward the southeast, while within and immediately next to the Banco Porphyry the dips are vertical. This refraction most likely reflects a difference in the physical properties of the East and Banco porphyry units. A second fault population composed of dominantly Type#3 faults trends in an ESE-WNW orientation (Fig. 6.7 and Fig. 6.9B). This directional group has an unknown relationship with the northeasterly fault trend and is thought to be related with the formation of post-mineralization NW-trending structures associated with sinistral displacement of the West Fault.

The clay-sized gouge in faults of Domain B is commonly, weakly to moderately foliated and lineated and bears S-C fabrics and sigma-type mineralized porphyroclasts with asymmetric tails of sericitically altered rock fragments that indicate right-oblique normal-slip, hanging wall to the SSW displacement. This shear sense is illustrated by the displaced Mesozoic to Paleozoic units outside of the pit that have an estimated strike-slip separation of 400 metres along individual faults, and the Banco Porphyry that has an apparent right-lateral offset of approximately 200 metres. Vertical displacement components are difficult to estimate due to poor exposure of lithological contacts and inconsistent striae orientations.

Fig. 6.9 Lower hemisphere Schmidt stereographic projections for Type#2 and #3 faults that are used to characterise the fault systems, plots A (fault type#2) and B (fault type#3) in Domain B and all vein types, C (vein Type#1), D (vein Type#2), E (vein Type#3) and F (vein Type#4), that are used to interpret the relative timing of formation within and between domains. Note that NE-SW trends are significant in this domain. See text for discussion.

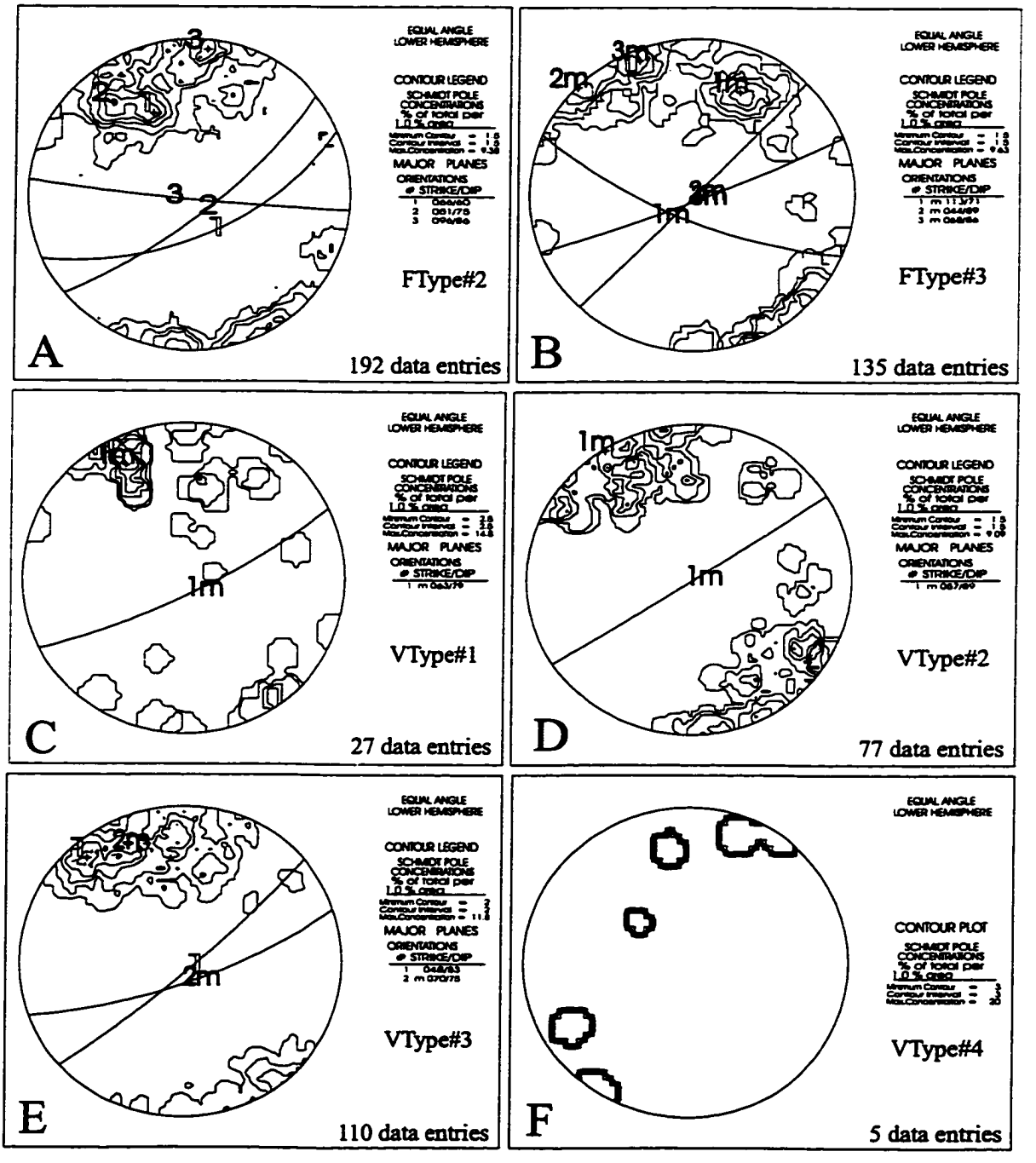

6.3.1.2.2 Veins

Domain B contains veins of Type#1 through Type#3 (Fig. 6.9 C through E). Earlier formed Type#1 veins and later formed Type#2 veins show similar preferred orientations parallel to the dominant NE-SW fault set. Quartz-molybdenite veins (Type#2) like those of Domain A have a range of orientations, generally between 030° and 090°, with an average trend of 057° (>50%) (Fig. 6.9 D). Subvertical dips vary between 60° SE and 60° NW. Both Type#1 and Type#2 veins show an NW-SE extensional component and trend sub-parallel to the dominant NE-SW direction within the domain.

This domain contains many Type#3 veins that supported old vein mines similar to the Zaragoza fault-vein in Domain A. These pyrite-dominated veins trend approximately 050/80 (11%)(Fig. 6.9 E) an average trend similar to that of Type#1 and Type#2 veins (compare Fig. 6.9 C, D and E). Type #4 veins are also present but in small numbers (Fig. 6.9 F). As mentioned previously, the emplacement of Type#4 veins was apparently within any available open space provided by fault or fracture at the time of mineralization and thus they may not be expected to have a common orientation.

6.3.1.2.3 Discussion

A dominant NE-SW to ENE-WSW and less common ESE-WNW trend exist for the fault and vein structures found within Domain B. Early ductile shear zones are parallel to later formed gouge and foliated gouge bearing fault planes (compare Fig. 4.3 B and Fig. 6.9 B). The faults of this system trend subparallel to quartz (Type#1), quartz-molybdenite (Type#2) and pyrite-dominated (Type#3) veins. The relative vertical exposures of these vein types suggests a vertical zonation (telescoping?), from eroded(?) and exploited copper-rich sulphides in their upper reaches through pyrite-rich zones to laminated quartz-molybdenite veins at their lowermost level of exposure in the open pit. Displacement sense in these fault -veins is consistently dextral with general trends of striations and cataclastic lineations suggesting an oblique, hanging wall down to the SSW, displacement. Based on interpreted contact trends across the principal faults of the domain, apparent displacement magnitudes on the order of several hundred metres are inferred based on offset interpreted contacts of the

Banco Porphyry unit and Mesozoic to Paleozoic units mapped outside the mine. The older units appear to have experienced more displacement than the Banco Porphyry. This difference in displacement can be explained by a fault splay, or horse-tail system. The Estanques Blancos outside of the mine is characterized by three or four fault principal faults, whereas within the mine there are numerous subparallel fault strands. It is probable that the apparent larger displacements shown by the principal branches of the fault system were distributed among the larger number of faults within the mine. A few of the faults within the mine may have taken up a greater share of the displacement, which is illustrated by those faults that offset the trend of the Banco Porphyry, the stockwork systems, and in places, appear to offset alteration zones (Fig.5.1). This relationship suggests a deformation history that involves the reactivation of pre-existing fabric anisotropies and fracture systems.

The faults are host to both quartz-molybdenite and pyrite-dominated vein assemblages. The permeability of the faults and veins channelled later quartz-sericite alteration from the central massive zone into the potassic and chloritic alteration zones (Fig. 5.1). Most of the Domain B faults show a moderate to strong degree of quartz-sericite alteration along their traces.

6.3.1.3 Domain C- Balmaceda

Domain C is in a transitional position, central to the N-S dimension of the open pit, between Domain B to the north and Domain D to the south (Fig. 6.7). Like the other domains, this domain contains all alteration assemblages, but differs from domains A and B by having the East Porphyry as its only lithology. Domain C has two dominant structural trends: 1) an E-W to ESE-WNW and 2) an NW-SE within a wide range of orientations from SW-trending to N-trending (Fig. 6.10 A and B) that may obscure trends of weaker systems. The NW-SE set is composed dominantly of Type#3 faults. Contained within the domain are Type#1 veins that have an ENE-WSW trend (Fig. 6.10 C), Type#2 veins which have N-S, E-W and NNE-SSW trends (Fig. 6.10 D), Type#3 veins with NE-SW, NW-SE and E-W trends, and Type#4 veins which appear to have E-W trends. Both Type#2 faults and Type#2 and #3 veins have sericitic-argillic alteration halos suggesting a circulation of late

hydrothermal fluids. A single major fault, the Balmaceda, extends to the ESE from the open pit.

6.3.1.3.1 Faults

The Balmaceda principal fault, an ESE-WNW structure crosscuts ductile deformation zones within this domain. These discontinuous ductile zones, Type#1 faults, do not parallel the principal fault, but trend roughly N-S (Fig. 4.2, Fig 6.2) (see above, Chapter 4: *Pre-Mineralization Ductile Features*). Type#2 and #3 faults have an ESE-WNW to E-W orientation dipping toward the SW (Fig. 6.10 A and B). These faults have sericitic-argillic alteration halos and uncommon asymmetrically winged porphyroclasts that are consistent with both sinistral and dextral movements. The majority of intra-fault materials in this domain are not foliated. Mesozoic units within the open pit show an apparent dextral separation of approximately 200 metres along the trace of the regional Balmaceda Fault. From regional maps the Balmaceda Fault offsets Paleozoic units approximately 250 metres in a left-lateral sense (Chong and Pardo, 1993; A. Tomlinson, 1996, written comm.). A second set of Type#3 faults of this domain have a trend of approximately 140/76 (NW-SE) and have no associated alteration halos. Shear sense of the Type#3 fault trend is dominantly sinistral, based on criteria outlined by Petite (1987), with apparent displacements of tens of metres. Type#3 faults and Type#2 faults bearing unaltered fragment-supported breccias offset gouge-bearing Type#2 faults.

6.3.1.3.2 Veins

Type#1 veins trend in an ENE-WSW direction (70%), an orientation that is oblique to the trends in the fault systems of this domain (Fig. 6.10 C). The geometry of vein Type#1 with the dominant fault trend (ESE-WNW, Fig. 6.10 A and B) is consistent with a possible vein emplacement during sinistral shear associated with the fault system, but this relationship has not been confirmed. The vein orientation is also consistent with those vein trends of Domain B with which Domain C may have been associated during the vein emplacement. Type#2 veins show a dispersed pattern (Fig. 6.10 D), however, with two probable trends, one

subparallel to the principal fault direction (E-W) and the second following an N-S direction are inferred. Pyrite-dominated veins, Type#3, are the most abundant veins in this domain and cluster into three preferred orientations (Fig 6.10 E). These veins trend NW-SE (26%), sub-parallel to the Type#3 fault direction, NE-SW (23%), an orientation similar to Domain B's dominant trend and parallel to a probable trend of Type#1 veins in Domain C, and in an E-W (20%) orientation, similar to a subordinate trend in Type#2 veins. In figure 6.5 the Type#3 veins show correlatable traces up the eastern slope of the mine in NE-SW to E-W directions with those discontinuous NW-SE trending veins located deeper in the open pit possibly associated with the quartz-sericite alteration and megabreccia zone (Fig. 4.4) and/or re-orientation by later fault motions associated with the West Fault and its subsidiary faults. The continuity of vein Types#1, #2 and#3 in E-W to NE-SW orientations (Fig. 6.3 through Fig.6.5) suggest that the emplacement of these veins is related with the emplacement of similar veins in Domain B, and that these veins in Domain C represent either the southernmost extent of mineralization at that time or that continued faulting along vein-parallel, the Estanques Blancos and Balmaceda faults offset a zone of vein and stockwork mineralization to the southwest. The few occurrences of vein Type #4 (Fig 6.10 F) parallel trends of the other vein types, which is consistent with its infilling character.

6.3.1.3.3 Discussion

Domain C is transitional between Domains B (Estanques Blancos), which bears traceable vein mineralization and D (South Central), which shows little vein mineralization. Fault types #2 and #3 show subparallel preferred orientations with Type#2 faults having ESE-WNW orientations and Type#3 faults trending in a dominantly NW-SE to WNW-ESE direction (Fig. 6.10 A and B). Alteration halos that in previously discussed domains have been associated with all structural features, appear restricted to gouge-bearing Type#2 faults and the vein sets in this domain. Sense of displacement for the dominant fault sets in Domain C also differ, with Type#2 faults showing a dextral and sinistral slip senses and those NW-SE faults showing sinistral displacements. Displacement magnitude estimates are

Fig. 6.10 Lower hemisphere Schmidt stereographic projections for Type#2 and #3 faults that are used to characterise the fault systems in Domain C and all vein types that are used to interpret the relative timing of formation within and between domains. Note that NE-SW and ESE-WNW trends are significant in this domain. See text for discussion.

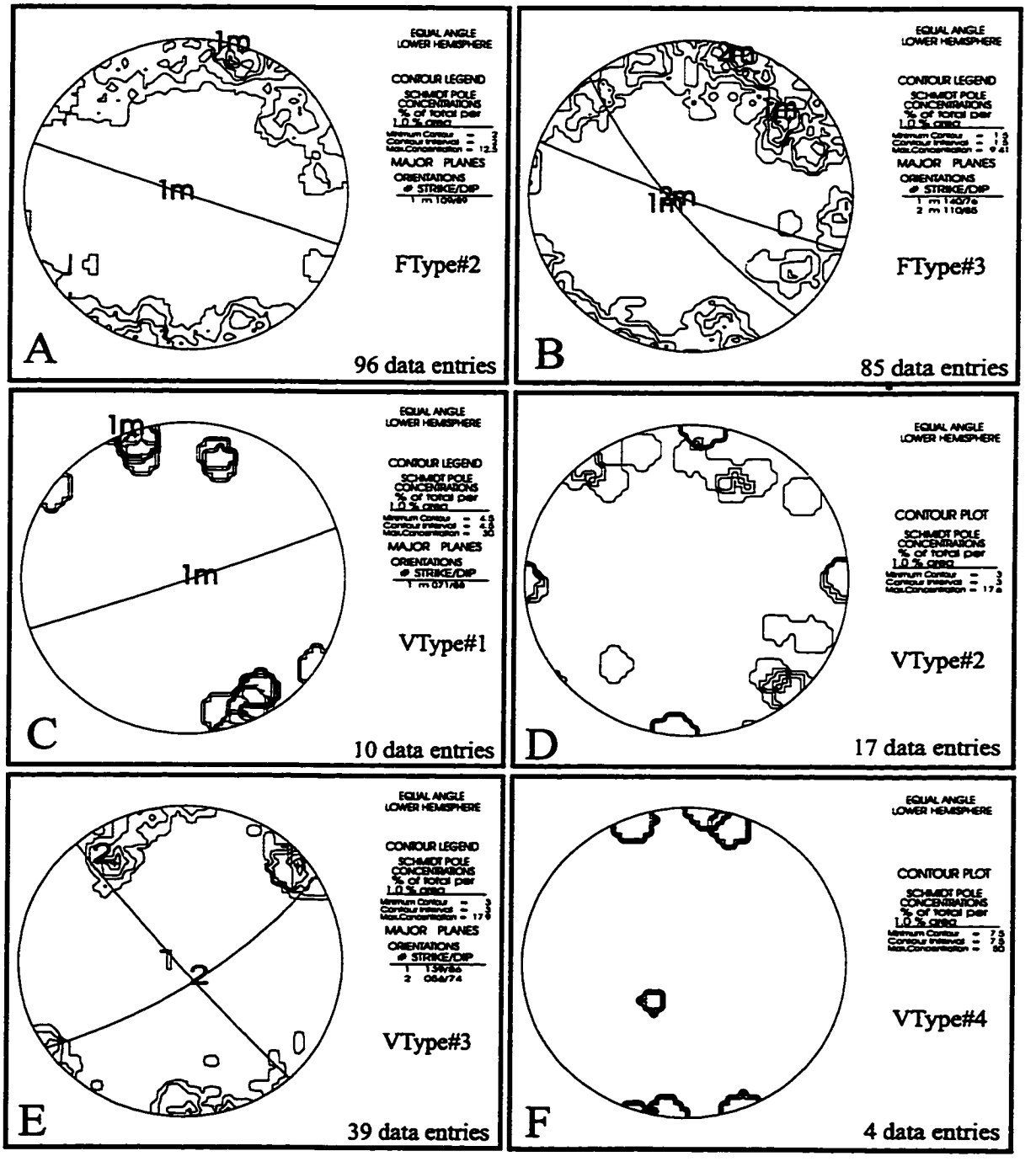

from offset Mesozoic units that range from tens of metres for Type#3 faults to several hundreds of metres for Type#2 faults including the displacement along the Balmaceda Fault. Vein orientation are similar to those established for vein sets in Domain B (Fig 6.9 C through F). The location of the veins between benches I1 and M1 and below and their trends in continuity subparallel to the Domain B veins suggests that the veins in Domain C may represent the southmost extent of the vein mineralization phase or that similar veins that were perhaps further south have been offset by principal faults as the separation of metasedimentary units indicate.

6.3.1.4 Domain D - South Central

Domain D is bound by Domain G (West Fault-Americana) to the west, Domain C to the north, and Domains E and F to the south (Fig. 6.7). Approximately 30% of Domain D contains Mesozoic and Paleozoic lithologies that were faulted into their present position by the fault systems of Domains B and C. Fault systems are dominantly NW-SE with subsidiary trends of N-S and E-W (Fig. 6.11 A and B)Type#2, #3 and #4 veins are present within the domain with types#3 and #4 being most significant (Fig. 6.11 D and E).

6.3.1.4.1 Faults

Breccia-dominated Type#2 faults trend NW-SE, as do Type#3 faults (Fig. 6.11 A and B). Secondary trends of fault Type#3 are E-W and N-S. Individual faults of the NW-SE system displace Paleozoic-Mesozoic units tens of metres in a sinistral sense, creating a jagged faulted contact between the Chuquicamata Intrusive Complex and older country rocks. These estimates of displacement are only approximate, since the intrusive contact is very irregular and difficult to trace from bench to bench within the open pit. The fragment-supported fault breccias are composed of subangular wallrock fragments in a tan to grey, unsorted matrix. N-S faults are preferentially located near the westernmost part Domain D where they trend subparallel to subsidiary faults of the West Fault in the adjacent Domain G. Slip along these N-S faults is deduced from fracture criteria outlined by Petit (1987) as sinistral. The E-W fault trend is located in the southernmost part of this domain where NW-SE

and E-W fault systems overlap. Displacement along the E-W fault set is dextral if its formation is related to that approximately E-W trend in Domain F where dextral displacement of the West Fault and quartz-sericite alteration zone are interpreted from plan section compilations from drillcore logs by Chuquicamata geologists. Together the N-S, NW-SE and E-W trends appear to compose a sinistral Riedel-type fault set with the N-S trend as the master fault, and the NW-SE and E-W trends approximating the synthetic and antithetic shears respectively (compare Fig. 6.16). The faults in this domain vary with respect to alteration halos. The majority of faults have no or a poorly developed halo, others, those closest to Domain E, appear to have argillic halos resulting from hypogene to supergene alteration.

6.3.1.4.2 Veins

Veins are not abundant in this domain (Fig. 6.11 C through E). Those observed are predominantly Type#3 veins that show a NE-SW preferred trend (241/76; 58%) (Fig. 6.11 D) and Type#4 veins that vary widely between NW-SE (315/86) to NE-SW (238/83)(Fig. 6.11 E). Type#1 veins were not observed and only 2 Type#2 veins were encountered within this domain. The veins generally have argillic alteration halos, however, silicified areas proximal to some veins were also noted.

6.3.1.4.3 Discussion

Breccia-bearing Type#2 faults dominate this domain trending NW-SE. Lithologic contacts show up to 50 metres of sinistral displacement along these faults. Together with the Type#3 faults sets, the Type#2 faults form a sinistral fault system compatible with Riedel synthetic and antithetic faults about a master fault. Type#3 veins, the most abundant in this domain, show a preferred orientation of NE-SW. This orientation corresponds to directional trends of similar veins, emplaced at higher structural levels, in Domains B and C. The similarity in orientations of type#3 veins in Domains B, C and D implies a contemporaneity to their formation. The contrast in orientations between fault systems and type#3 vein trends (compare Fig. 6.11 A and B with D) suggest that the formation of faults and veins in this

Fig. 6.11 Lower hemisphere Schmidt stereographic projections for Type#2 and #3 faults that are used to characterise the fault systems in Domain D and all vein types that are used to interpret the relative timing of formation within and between domains. Note that NW-SE trends are significant in this domain. See text for discussion.

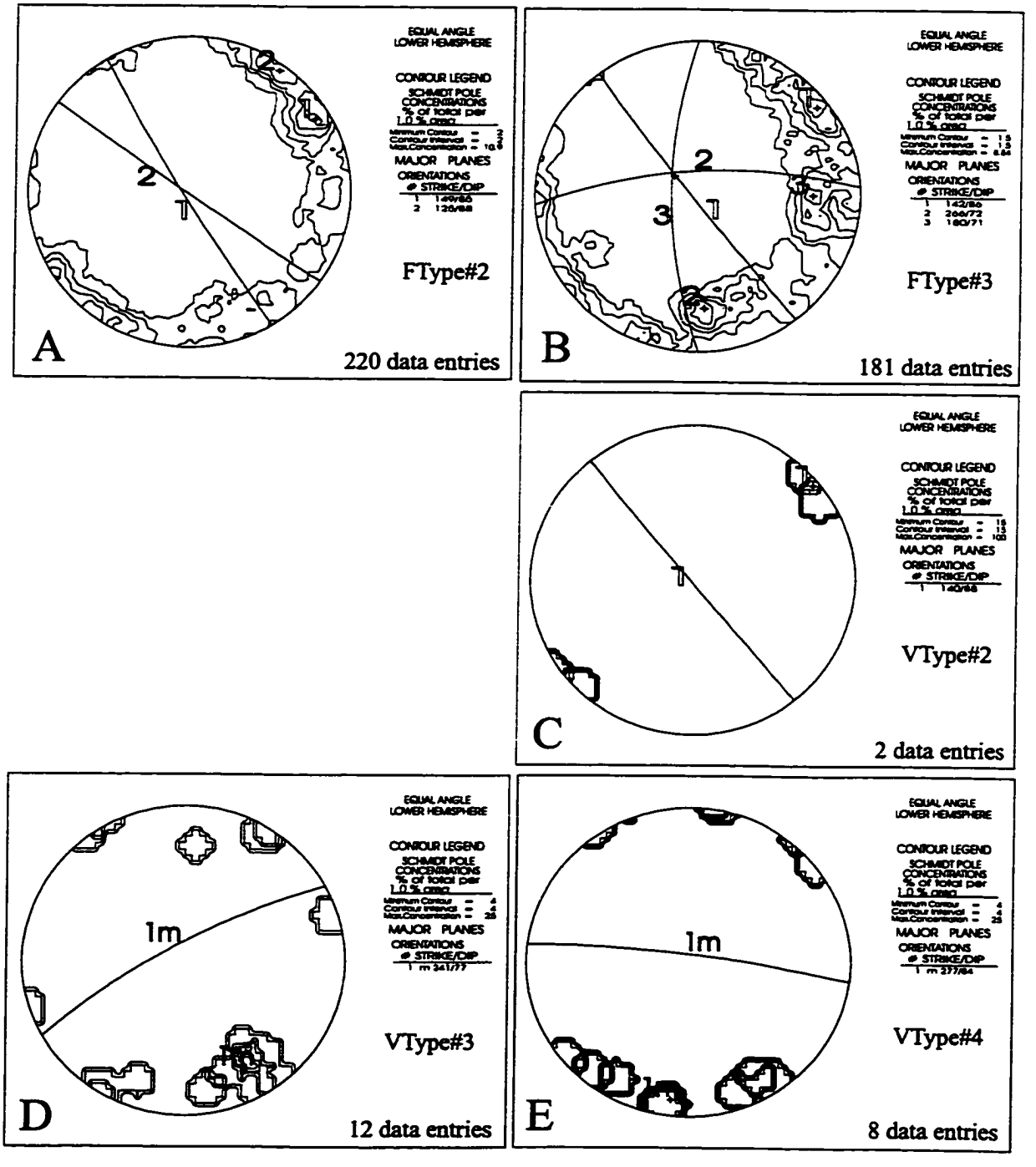

domain occurred as the result of distinct deformation events. Alteration halos on the veins also suggest their emplacement prior to the formation of the brittle unmineralized and weakly altered NW-SE fault system.

6.3.1.5 Domain E - East Fault

Domain E is located in the southeasternmost sector of the open pit (Fig. 6.7). The domain is composed of a single argillically to sericitically altered fault zone, approximately 5 metres in width, and a series of subparallel, approximately N-S trending fault surfaces (Fig. 6-12 A and B). This fault system is found next to the fault contact between the Chuquicamata complex and Mesozoic units. This fault set trends parallel to the Messabi Fault but is offset toward the west; it is interpreted as being the southern extension of the Messabi Fault (Reutter et al., 1996). The fault system trends through the southern end of the open pit beneath the mine infrastructure (crushing and mineral extraction facilities) and Miocene to Pliocene gravels.

The main zone is a breccia to gouge-bearing brittle fault zone whose fragments are strongly altered to sericitic-argillic assemblages. Asymmetric porphyroclasts within the intra-fault material of the Type#2 faults (180/82, 45%) and subsidiary fractures on the surfaces of Type#3 faults (182/85, 29%) consistently indicate sinistral kinematics. The displacement magnitude is unknown.

Fig. 6.12 Lower hemisphere Schmidt stereographic projections for Type#2 and #3 faults that are used to characterise the fault systems in Domain E and Domain F. See text for discussion.

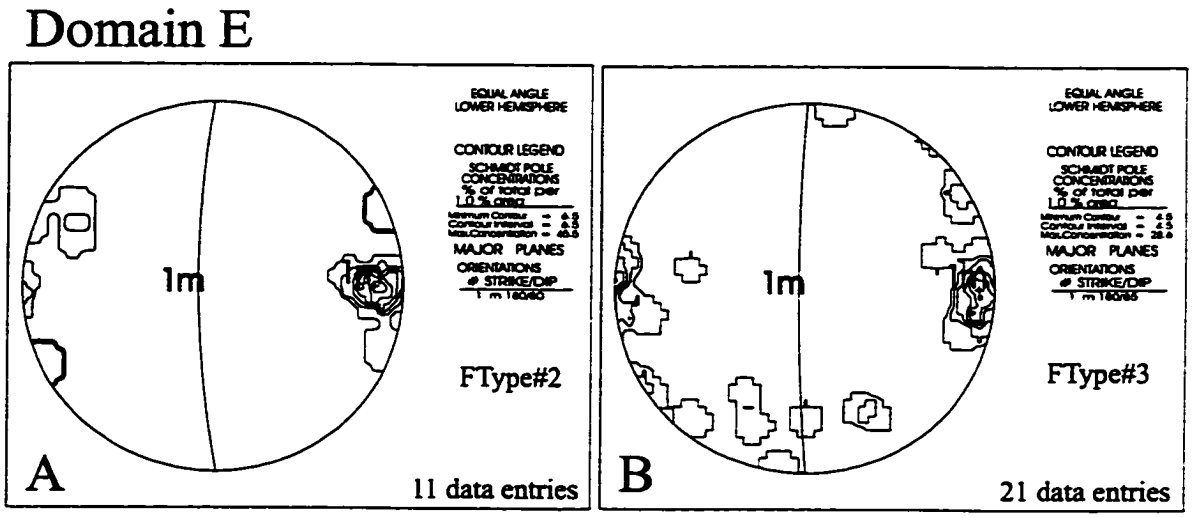

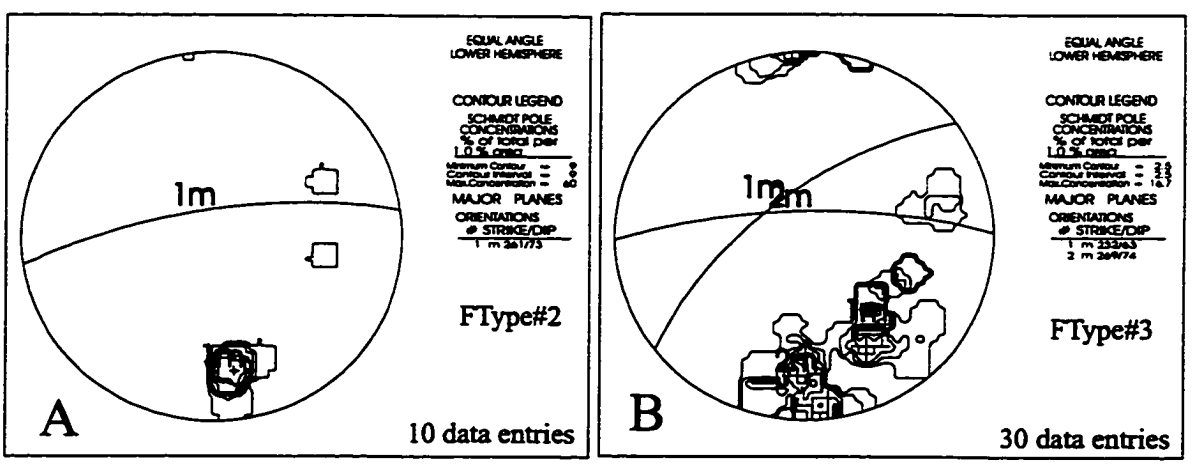

6.3.1.6 Domain F - Southern (Banco H1)

Domain F is composed of the fault system that forms the southern face of the open pit (Fig. 6.7). This dextral, E-W, fault system has crosscutting relationships with the West Fault (Domain G), in which the main fault, H1 Fault, has offset the West Fault's main branches and the adjacent quartz-sericitic alteration zones by up to 60 metres. Reactivation along the western branches of the West Fault resulted in a 30-50 metre sinistral displacement of the Domain F fault system. The relationship between this fault system and the Domain E system is unknown.

Type#2 faults have E-W orientations (262/72; 60%)(Fig. 6.12 A) subparallel to the Type#3 faults, which show two trends, one approximately E-W (266/78, 17%) and a second trending NE-SW (236/64, 17%) (Fig. 6.12 B). The second orientation represents low angle cross faults akin to compressional bridge structures (eg. Gamond, 1987) or strike-slip relays between the E-W trending faults. Available stria data (6 data) indicate a predominant strike-slip character to the cross faults with some shallow down-dip displacement, 20->051 for a cross fault and 16->079 for a principal E-W fault. These data may result from later reactivation of the faults following their initial formation resulting in a destruction of origina striae. Faults and fault planes are reddish in colour from oxidation of iron oxides. No veins outcrop in this domain.

6.3.1.7 Domain G - West Fault -Americana

Domain G comprises a fault system exposed within the Chuquicamata open pit (Fig 6.7) and to a greater extent the Chuquicamata district including the Radomiro Tomic (Chuqui Norte), Mina Sur (Exotica) and Mansa Mina properties. This structural domain places in contact the unrelated Eocene-Oligocene Chuquicamata and Fortuna intrusive complexes (Plate 6.7).

The West Fault zone includes the Americana and Calderones faults to the east and parallel to subparallel Type#2 and Type#3 fault sets several hundreds of metres to the west of the West Fault (Fig. 6.7). The parallel western fault sets, which are not included in the Domain G stereographic plots, are physically and kinematically similar to the main West

Fault branches, which have weak to strongly foliated clay-sized gouges and a sinistral sense of displacement (Plate 6.8). Gouge colour varies across the fault zone. Those faults to the east of the West Fault having grey to black gouges and those to the west have lighter coloured (tan) gouges. The gouge colour of the West Fault itself varies from whitish on its eastern side from foliated quartz-sericite rock to grey-black in its centre to tan gouge on the west side associated with grain-size reduced Fortuna Complex units. Many of the faults in Domain G limit distinct alteration - mineralization zones.

6.3.1.7.1 Faults

The main faults that comprise Domain G, as most are post-mineral faults, are described in detail in Chapter 7. Type#2 and #3 faults distributed throughout this domain trend parallel to the major faults (Figs. 6.7 and 6.13 A and B). The foliated gouge-bearing displacement zones vary between 5-10 cm up to several metres in width. Important faults in this domain besides the West Fault are the Americana, the easternmost branch of this domain, and the Calderones a central branch. Between the West Fault and the Calderones fault lies a <100 metre wide block of silicified rock, an apparent fault sliver. Further east, is the quartz-sericite alteration zone bounded between the Calderones fault and the Americana fault. Eastwards across the Americana fault are potassic and propylitic alteration assemblages that bear few veins and no apparent stockwork system. Numerous subsidiary faults crosscutting through the quartz-sericite alteration zone, display moderately to strongly foliated gouges, bearing asymmetrical porphyroclast kinematic indicators confirming sinistral displacements. Like the West Fault, the Americana shows a variety of variably coloured gouges some of which may have been injected into the fault zone (e.g. Chester and Logan, 1986; Skarmeta, 1995, pers. comm.). Directional trends average 181/85 shown by 63% of the plotted poles although the data vary between NNW and NNE trends (Type#2 faults) and Type#3 faults show a similar variation probably the result of subsidiary structures within the domain (Fig 6.7 and Fig. 6.13 A and B).

Plate 6.7 View of the southern face of the Chuquicamata open pit where the regional scale West Fault is exposed. To the left of the fault (east) lies the altered and mineralized Chuquicamata deposit and to the right (west) lies the unrelated Fortuna Complex. On the left-hand side of the photo, a branch of the Americana fault system (Calderon Fault) is observed placing sericitic alteration (east) in fault contact with a weakly mineralized silicified fault block (west). Each bench is approximately 26 m in height.

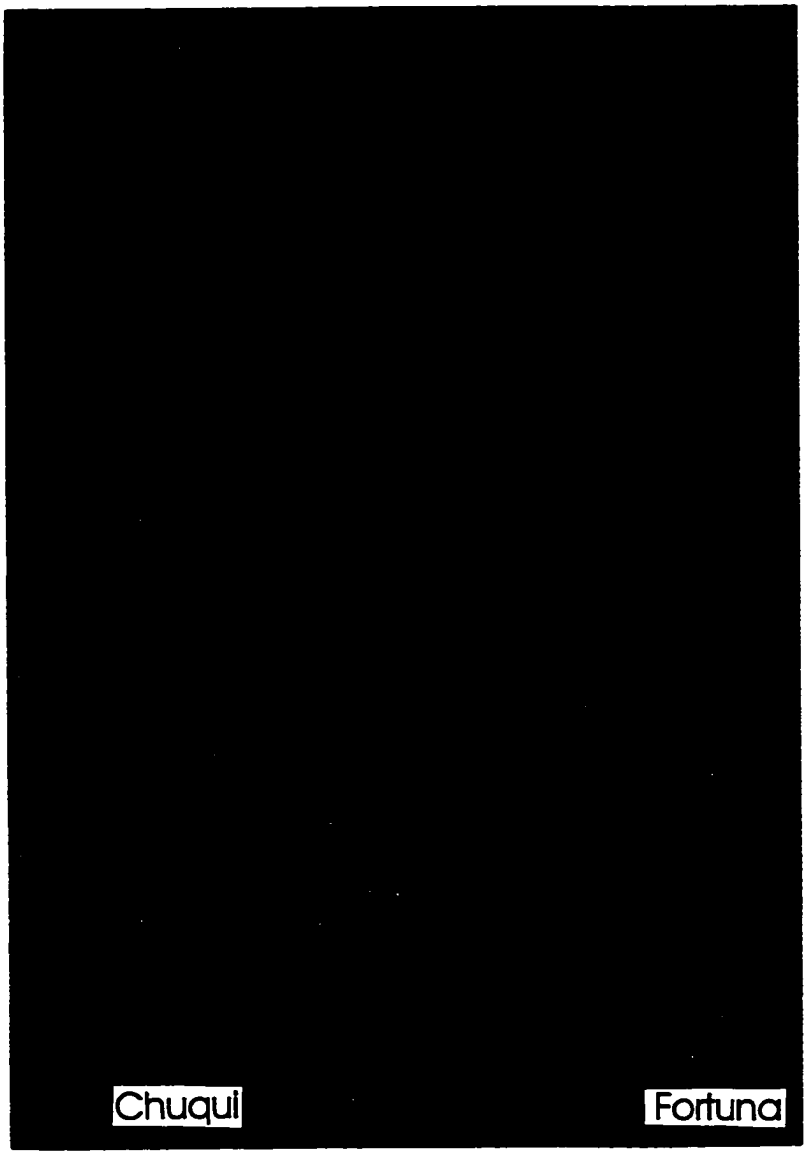

Plate 6.8 This photograph shows some detail of the West Fault's gouge. Structural fabrics in this brittle cataclastic fault rock bear sigma-type kinematic indicators and S-C fabrics. Porphyroclasts are quartz-rich fragments of the quartz-sericitic alteration zone (Fig. 3.2). Lens cap is 4 cm in diameter.

Fig. 6.13 Lower hemisphere Schmidt stereographic projections for Type#2 and #3 faults that are used to characterise the fault systems in Domain G. Post-mineralization sinistral shear along the principal faults of this domain have likely re-oriented observed veins. See text for discussion.

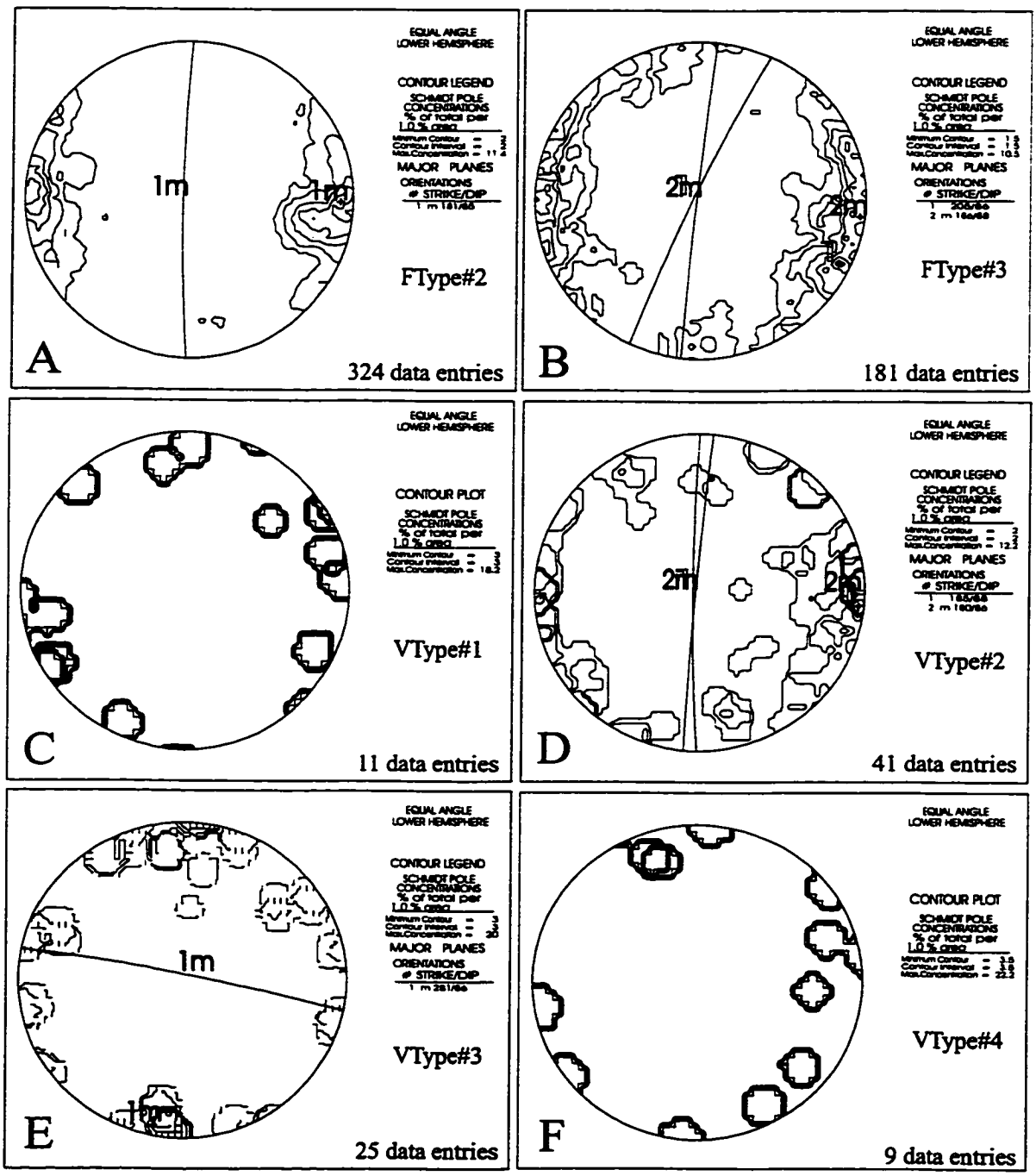

6.3.1.7.2 Veins

Most of the veins in this domain are found between the Calderones fault and the Americana fault, the eastward extension in the southern half of Domain G (Fig. 6.7). Type#1 veins show no dominant trend, appearing randomly oriented (Fig. 6.13 C), whereas 30% of the Type#2 veins are consistent with the dominant fault trend, showing a N-S to NNE-SSW preferred orientation (Fig. 6.13 D). Type#2 veins have a discontinuous distribution within this domain (Fig.6.4) occur predominately within the pervasive quartz-sericite alteration zone as vein rock fragments of mega-breccia. Type#3 veins crosscut the domain trend, having an ESE-WNW orientation (281/88; 24%) and a secondary NW-SE trend (Fig. 6.13 E). These veins are located along the easternmost edge of the domain near the Americana Fault and therefore they may relate their orientation to the sinistral West Fault-Americana shear couple. No discrete population is present for Type#4 in this domain (Fig. 6.13 F).

6.3.1.7.3 Summary

Branches of the dominant fault type in Domain G, Type#2, limit zones of distinct alteration-mineralization assemblages. The principal faults, West Fault, Americana and Calderones, trend along the borders of silicified, pervasive quartz-sericite alteration and megabreccia zones, with thinner Type#2 faults found traversing the quartz-sericitic alteration zone. Those foliated gouge-bearing Type#2 faults have subhorizontal cataclastic lineations and sinistral asymmetrical porphyroclastic kinematic indicators, which establish a sinistral strike-slip sense of displacement for this fault system.

Veins within this domain show little correlation to the dominant fault trends. Nowhere can veins be followed into faults. Blocks of Type#2 veins are traceable within the quartz-sericite zone adjacent to and parallelling the Americana fault. Type#3 veins, cluster near the C-G-D domain boundary suggesting an affinity to vein arrays of those adjacent domains. The post-alteration displacement relationship between the West Fault zone and the pervasive quartz-sericite alteration phase suggests that the orientation of any vein may not reflect its original attitude of emplacement (Lindsay et al., 1995; Reutter et al., 1996). A more detailed discussion of post-mineralization deformation and displacement associated

with the West Fault is presented in Chapter 7: *Post-mineralization Displacement Phases.*

6.3.1.8 West-side Structures

Reconnaissance mapping and compilation reveal three fault systems on the west side of the open pit, including a N-S to NNE-SSW system dipping moderately to steeply west, a E-W to ENE-WSW (220-240°) system that dips moderately toward the NW, and a uncommon NW-SE (120-150°) system dipping moderately SW to vertical that is restricted to the southwestern exposure of the open pit (Fig 6.7). Although the west side of the open pit was not the focus of this thesis, the observed fault systems are briefly presented as they provide insight toward the regional activity of Sector G fault systems.

6.3.1.8.1 Faults

Fault system kinematics are observable, but relationships between the fault systems are difficult to establish due to reactivation and brecciation. Most of the west side faults are parallel or subparallel to joint system mapped by the geotechnical staff at Chuquicamata. The gouge-bearing faults of the NNE-SSW system show small sinistral offsets of lithologic contacts and small dikes. In several cases, well-indurated cataclastic textures were observed along these trends, which are overprinted by clay-like fault gouges. The cataclastic textures may have resulted from cooling of the Fortuna Complex, as Reutter et al. (1996) proposed for ductile fabrics found within the same complex. The NNE-SSW system is an important component of the West Fault zone, which accommodates approximately 35-37 km of displacement (Dilles et al., 1997; Tomlinson and Blanco, 1997b).

The ENE-WSW to E-W fault system dominates the southwestern half of the mine and the upper western benches (Fig. 6.7). These faults commonly exhibit a range of fault breccia as intra-fault material and have widths of up to three metres. Kinematics are difficult to determine but most recent movements, reactivated by recent mining practices, show a strong N-side down, normal slip component. In places, the N-S system offsets the NE-SW system and in other localities this relationship is reversed. These displacements, whatever the sequence, are roughly metres and may result from ongoing mining practices.

The NW-SE system appears primarily in the uppermost southwestern benches. The extent and importance of this system are unknown.

6.3.1.8.2 Discussion

The western half of the Chuquicamata open pit has not been thoroughly mapped during the mine's history using geological criteria. Reconnaissance mapping during this study in the Fortuna Complex (Chapter 2.3.1.2) determined the presence of three fault systems based on directional trends, two of which are dominant. No large scale veins outcrop and only rare areas of veinlet mineralization were encountered. The dominant fault systems are a left-lateral NNE-SSW system associated with regional displacements concentrated along the West Fault, and a ENE-WSW normal-slip system that NNE-SSW system displaces in places. These faults are part of the West Fault System and support an episode of extensional (transtensional) displacement on this regional system.

6.3.2 Association of Stockwork and Structural Domain

Veinlets comprising the stockwork system that outcrops at Chuquicamata were presented in Chapter 5. The distribution of the stockwork system shows that it outcrops within the following structural domains: A in the northern part of the mine, B the northeastern part of the mine and in G, which encompasses the central and southern areas of the mine (compare Figs. 6.7 and 5.1). By examining stereoplots from these structural domains and comparing them with the preferred orientations of the veinlet sets within that structural domain, we see that the trends coincide (eg. Figs. 5.9 and 6.9). Differences between individual veinlet sets and fault and vein sets do vary, but the directional trends persist from the veinlet scale to the deposit scale. Distributions of veinlet sets and the overprinting mineralized fault-veins show that fault activity, associated with either fault-vein displacements during vein emplacement or displacements along vein-parallel faults following mineralization, apparently controls the stockwork mineralization by limiting its distribution within the deposit. This distribution of stockwork was presented in Chapter 5.1.1 and is illustrated in Figure 5.1.

As the veinlet systems and mineralized fault-vein systems are found within the same structural domains, the main hypotheses of their relationship are briefly presented. The two main hypotheses are i) that the veinlet mineralization (Table 5.1) and the mineralized deposit scale vein systems (Table 6.1) formed during the same mineralization event, and ii) that the two scales of mineralization represent distinct mineralization phases. The timing relationship between the two scales of mineralized structures is difficult to assess, due to the pervasive overprinting of late hydrothermal quartz-sericitic assemblages along the deposit scale faults and veins and post-mineralization breccia-forming fault activity. From the quartz-sericitic alteration association it is suggested the stockwork systems surrounding the large-scale faults and veins must not have been open to these late hydrothermal fluids, as alteration halos have not obscured their finer contact relationships with the host rock. This is with the exception of those veinlet systems present within the pervasive texture-destructive quartz-sericite alteration zone where the stockwork itself is difficult to identify. Within the deposit-scale veins themselves, copper-bearing mineral assemblages fill fractures. This suggests that stockwork formation took place following the emplacement of the deposit-scale veins or that a second stockwork formed within existing veins associated with the quartz-sericite alteration and thus should be contained wholly within the quartz-sericite alteration zone. If this is the case, then the fractured Type#1 and Type#2 veins would provide preferred permeability conduits and precipitation sites for later mineralizing solutions and the formation of a stockwork system in the host rock would be limited to those areas immediately adjacent to the veins. The probability of a quartz-sericite stockwork is supported by the high-temperature Cu-Fe-sulphide assemblages recognized by Lewis (1996) in this alteration zone.

Focussing on the vein character, the volumetric difference in quartz deposition that accompanies these veins needs to be accounted for. The metre scale widths of the Type#2 veins suggest the passage of large volumes of silica-bearing fluids in comparison to the millimetre to centimetre v3 veinlets of the stockwork. Soto (1979) describes the Type#2 veins as composite veins, which requires reactivation most likely by way of hydraulic fracturing. It is unlikely that the v3 veinlets of the stockwork correspond to the first-formed

veins of the composite Type#2 veins, as crosscutting v3 veinlets would be present and a hiatus in stockwork formation while Type#2 veins formed would be necessary. It is also unlikely that the v3 stockwork represents the final stage of composite vein formation before the deposition of copper-bearing phases, as the presence of the composite veins represents a preferred permeability that is likely to be active for all subsequent mineralizing events.

From the circumstantial evidence presented above, the preferred hypothesis is one of multiple hydrothermal systems. An earlier hydrothermal system developed mainly as a typical porphyry copper stockwork, including the A- through D-type veins of Gustafson and Hunt (1975). This stockwork was then overprinted by a later hydrothermal system that emplaced a larger scale of veins.

6.4 Establishing Associated Domains

This section proposes a sequence of evolution for the structural domains using relationships between the various fault and vein types and alteration phases. The purpose is to establish deformational events that distinguish between deformation timing, character and setting. These domains are then examined as a setting for the mineralization present within the vein arrays.

Similarities in the fault and vein systems making-up structural domains A and B and to a lesser extent C, suggests cause for evaluation as a single related deformation domain. The long-lived gouge-bearing faults of Domains A and B both show dextral strike-slip components and indicators of an oblique slip component, although this is more common in Sector B. The initiation of these systems as faults was most likely accomplished by the reactivation of pre-existing planar elements within the host rock as suggested by the fact that the fault systems in Domains A, B and C trend parallel or subparallel, to pre-existing planar fabrics such as ductile shear zones (Chapter 4) and veinlet systems (Chapter 5). Continued deformation in association with renewed magmato-hydrothermal activity reactivated favourably oriented fracture planes in Domains A and B, forming sets of fault-veins. Displacements along the principal faults of at least Domain B, traced into the country rock, show dextral offsets of the Messabi Fault trace (Chapter 4.2). These fault sets, NNE in

domain A, NE in domain B and ESE in domain C, were active contemporaneously with the emplacement of Type#2 vein mineralization. Incremental displacements, culminating in the observed dextral displacements, are evidenced by the crack-seal texture of the Type#2 veins. This texture in thin section exists as remnants, as the vein quartz has since been dynamically recrystallized. Domain C was probably activated toward the end of the Type#2 vein emplacement. This domain has mineralized WNW-ESE-trending structures. This fault set has sericitic-argillic alteration halos indicating the fault-vein permeability at the time of this alteration phase. Quartz-sericitic alteration parallels the fault sets in domains A and B and must have occurred during or following the reactivation of the fault system of domain B, which crosscuts and offsets structures of domain A.

Activity of domain D followed the principal alteration and mineralization events. Faults of this domain offset the alteration halo-bearing domain C faults and the supergene enrichment "basin" (Rojas and Lindsay, 1997). The dominant fault set of domain E parallels the Chuquicamata Complex-Mesozoic (Messabi) fault contact. Reactivated faults parallel to the Messabi bear no mineralization and the associated alteration may be attributed to hypogene processes. The principal faults of domain F offset branches of the West Fault (Domain G), the quartz-sericitic alteration zone and appear to limit supergene enrichment to the south. The principal ENE-WSW fault is in turn crosscut by the West Fault. These relationships establish: (i) the existence of a pre-Domain F West Fault (Domain G), (ii) post quartz-sericitic (~31 Ma, Reynolds et al., in press; Zentilli et al., 1995) and supergene mineralization (~17 Ma, Sillitoe and McKee, 1996) activity of Domain F and (iii) a reactivation of the West Fault, as a sinistral fault, sometime after 31 Ma. Domain G, bounds all sectors to the west and as such, its principal fault the West Fault, has been considered to crosscut and displace a portion of the stockwork mineralized porphyry (Maksaev and Zentilli, 1988; Lindsay et al., 1995; Reutter et al., 1996; Rojas and Lindsay, 1997), even though there have been some accounts suggesting that the West Fault was the conduit for Chuquicamata's mineralizing fluids (Lopez, 1939, 1942; Alvarez and Flores, 1985; Ramirez, 1993). The dominant activity of Domain G is associated with the formation of Domains D, E and F. Related re-activity is present on a principal fault of Domain A, the C-2 Fault, where sinistral

shear sense indicators occur in gouge-bearing sericitic alteration halos.

The relationships between fault system formation, mineralization at both stockwork and vein array scales, and pervasive alteration suggests that the deformation at Chuquicamata can be grouped into two deformational events. The earlier deformational event, or Phase I, formed the ductile fabrics discussed in Chapter 4, was associated with the stockwork development presented in Chapter 5, and the faults and veins of structural domains A, B and C. These domains are related with the multiple magmato-hydrothermal systems that provided mineralization to the stockwork and vein array systems at 34-33 Ma and ~31 Ma. Continued deformation developed the domains' principal faults into through-going deposit to district scale faults whose latest formed segments may have offset mineralized sectors of the mine.

Post-mineralization deformation resulted in the formation of a group of non-mineralized structural domains including D, E, F and G (Fig. 6.7). These fault domains comprise Phase II within which deformation resulted in the displacement and dissection of the altered and mineralized orebody.

6.5 Strike-Slip Deformation

A strike-slip deformation setting has been proposed, in one form or other, to describe the deformation and displacement along the West Fault System (Scheuber and Reutter, 1991; Boric et al., 1990; Reutter et al., 1993, 1996; Tomlinson and Blanco, 1997a, 1997b; Dilles et la., 1997) and represent the setting at the time of mineralization at Chuquicamata (Lopez, 1939; Lindsay et al., 1995; Reutter et al., 1996). In the preceding section, structural domains were associated with deformational phases in the evolution of the Chuquicamata deposit and the West Fault System. This section presents the settings and characteristics of strike-slip deformation zones, which are evaluated here in light of the observed fault and vein geometries of the proposed domains and the domain associations.

6.5.1 Strike-Slip Structural Settings

Transcurrent, or strike-slip, faults occur over a range of magnitudes (Tchalenko, 1970) and are a fault type common to obliquely convergent plate margins (Fitch, 1972;

Sylvester, 1988). The zone of deformation between rigid plates, within which a strike-slip fault system might form, has come to be known as transpressional, or transtensional, deformation following Harland (1971). Transpressional and transtensional tectonic settings are those in which deformation may be described as a combination of simple shear (wrench tectonics) and pure shear. Many studies have examined strike-slip faults from a plate tectonic perspective (Fitch, 1972; Woodcock, 1986; Woodcock and Schubert, 1994), as regional structures (Deng et al., 1986; Reutter et al., 1991), as controlling the emplacement of igneous intrusions (Murrell, 1970; Guineberteau et al., 1987; Morand, 1992; Tikoff and Teyssier, 1992; Grocott et al., 1993, 1994) and from an internal point of view of smaller scale natural systems (Granier 1985, fault tips; Woodcock and Fisher 1986, duplex structures; Gamond 1987, bridge structures; Sibson 1987, localization of mineralization; Arboleya and Engelder 1995, subsidiary structures). Analog modelling of strike-slip (simple) shear zones over single basement faults and en echelon faults identify similarities between shear zones at a variety of magnitudes including fracture and fault development and block rotation (Tchalencko, 1970; Hempton and Neher, 1986; McKenzie and Jackson, 1986; Nur et al., 1989; Schreurs, 1994). Numerical modelling of transpressional-transtensional deformation has also been advanced to examine strain paths and vorticity (Sanderson and Marchini, 1984; Fossen and Tikoff, 1993), displacement field partitioning (Tikoff and Teyssier, 1994; Teyssier et al., 1995) and their application to natural transpressional to transtensional tectonic settings. Sylvester (1988) presents a comprehensive summary of strike-slip faults systems and their settings.

6.5.2 Characteristic Features of Strike-Slip Zones

Structural features that may be present in transpressional to transtensional settings include normal faults, thrust faults, Riedel shears, veins, dykes, extension fractures and folds, whose geometries vary depending on the type of convergent tectonic setting (Fig. 6.14)(Sanderson and Marchini, 1984). The structures which develop and their orientation are primarily a function of incremental strain, pre-existing structures, and whether a strike-slip fault exists, or forms, as a single throughgoing discontinuity or as a series of en échelon

faults. The regional stress field that controls the structural geometries may be modified by the epizonal emplacement of igneous intrusions, whose modifications are reflected in associated dike or vein emplacement patterns (eg. Odé, 1957). The evaluation of vein and fault geometries of Phase I and Phase II deformation events provide important interpretive steps in establishing the controls on the mineralization and overall evolution of the deposit. From the fault and vein array patterns in the proposed domains, an influence of structural control from either regional tectonic setting, localized magmatic induced stress pattern, or some combination of these dominant features is established.

Fig. 6.14 A) A series of plan view diagrams for (i) transtensional, (ii) simple shear or wrench tectonic model, and (iii) transpression that show the orientations of fractures and faults within each system after Sanderson and Marchini (1984) compare Woodcock and Schubert (1994). These feature orientations represent those of the first increment of deformation after which the feature reacts as a material line within a shear zone. (B) Plan view diagram of geometric relations for structures of a Riedel simple shear model formed along a vertical fault, adapted from Aydin and Page (1984). For all diagrams structures are presented for dextral systems.

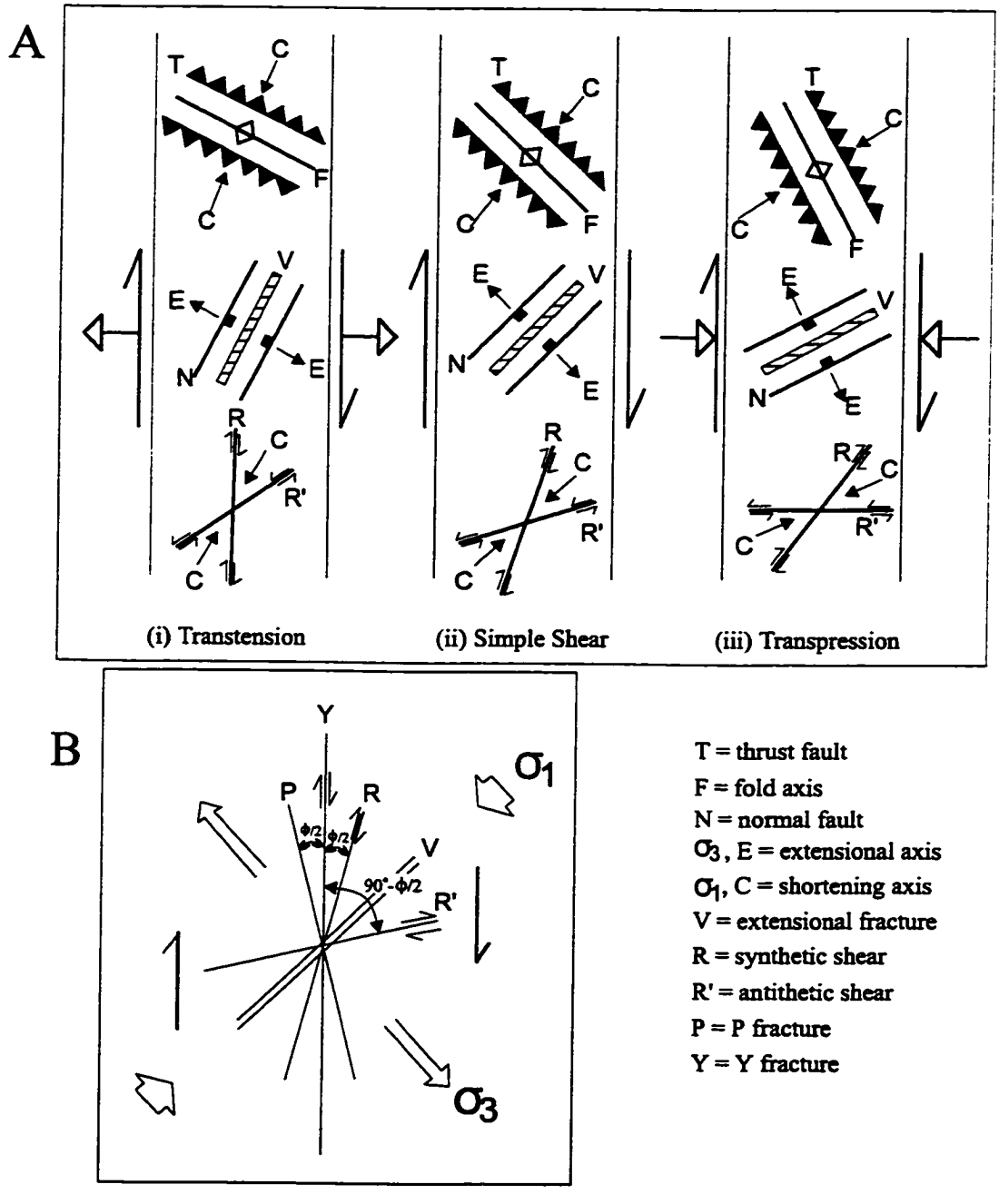

6.5.3 Deformational Phase I

Structural domains A, B, and C formed during Phase I within which mineralization and alteration are presented with respect to the formation of a fault and vein system that *overprints* the porphyry copper stockwork system. As previously suggested, Type#2 veins are considered a marker unit within the vein mineralization sequence. Domains A and B, which have the highest concentration of Type#2 veins, are considered to have formed prior to, or during this mineralization episode. Transitional domain C has a lesser quantity of Type#2 veins which follow more or less similar directional trends as those identified in domain B. Possible re-orientation of veins in domain C by the later NW-SE post-mineral fault set, which is not present in domain B may make correlation unreliable. Domain G is tentatively considered a syn-Type#2 vein domain as Type#2 veins are present, although they are observed to be large vein fragments. An assessment of early activity for domain G related with vein emplacement is difficult to make because of the large post-mineral displacement experienced by the West Fault zone (Tomlinson and Blanco, 1997b; Dilles et al., 1997), however, the presence of N-S fault-parallel type#1 and #2 veins in domain A, where post-mineral deformation is considerably less, may be supportive evidence for early N-S activity in the area including domain G. Based on the presence of Type#2 veins and by extension those mineralized structures that are directionally coincident, the structural sectors A, B, C and probably G, in some manifestation, were active syn-vein emplacement and mineral deposition.

Vein emplacement patterns associated with a magmato-hydrothermal fluid source are similar to those for dike emplacement around an intrusive centre. These patterns are typically radial and/or concentric and are modified by local and regional stress patterns (eg. Odé, 1957). Regional fracture patterns centred on porphyry intrusions have been shown to form in a pattern that is dictated by the regional tectonic setting (Rehrig and Heidrick, 1972). The vein arrays at Chuquicamata, lead by Type#2 veins, overprint the mineralized copper-bearing stockwork system and show an apparent elliptical radial vein pattern (Fig. 6.15) that is an artifact of the dimensions of the open pit. An alternative interpretation of vein emplacement within an active simple shear tectonic setting is also viable. In this scenario, it is probable

that pre-existing planes of weakness, for example the ductile planar fabrics discussed in Chapter 4 or the veinlet systems in Chapter 5 that may have extended downward from the stockwork zone as the mineralizing hydrothermal system decayed, were utilized by later hydrothermal events and through repeated activity became the quartz-molybdenite vein array observed at Chuquicamata. If the formation, or reactivation, of these fractures by magmato-hydrothermal activity was influenced by the regional tectonic setting, which is proposed to be a simple shear to transtensional setting (see Chapter 4.4), the observed vein orientations should reflect those orientations characteristic of the tectonic setting.

The geometries of the fault sets of Phase I, form angles of 010, 040 and 065, for domain A trends, 065 and 105 for domain B trends, and 120 for the preferred orientations of domain C, with respect to the overall north-south trend of the Domeyko Cordillera. Simplified, the preferred orientations domain wide are 010, 040, 065 and 115 (Fig. 6.15). The sense of slip associated with the preferred orientations is dominantly dextral for each, however, sinistral shear sense indicators are observed associated with the 115 trend. The orientations of these fault systems and their related shear sense represent a brittle dextral deformation system with the 040 being the principal displacement zone, 065 approximating the synthetic shear and 115 representing the antithetic shear. The preferred directions of faulting coincide with physically modelled and numerically derived predictions of failure within strike-slip shear zones (Tchalenko, 1970; Sanderson and Marchini, 1984; Hempton and Neher, 1986). These brittle faults coincide with those orientations, 020 and 060, of the ductile shear zones described in Chapter 4 (Fig. 4.3) and also approximate those stockwork veinlet orientations described in Chapter 5, with the exception that these latest faults crosscut the stockwork mineralization and the trend of the ductile Messabi fault. These crosscutting relationships clearly indicate that these faults although mineralized are later then the ductile faulting. The relationship of these mineralized fault-vein systems with the stockwork system is unclear. In all observed exposures of the vein arrays presented in Chapter 6, where stockwork (Chapter 5) is present, the relationship between these distinct scales of mineralization is obscured by quartz-sericitic alteration halos that are associated with the vein arrays, through which the stockwork can not be traced to the vein-alteration contact.

The dominant Type#2 vein trends are 010 and 065 with secondary trends of 040 and 100. The dispersion of vein directions about a NE orientation and the more east-west trends (see Fig. 6.5) may be accounted for by radial or sub-radial veining patterns about a magmato-hydrothermal mineralizing fluid source. The mineralization of these veins is presumed to follow the initiation of failure along the principal fault directions, that may be related to the ductile shear zones (Chapter 4) and preferred veinlet orientations (Chapter 5). Two cases concerning the control of vein Type#2 mineralization were outlined, a radial emplacement pattern due to magma pressures in isotropic confining pressures and a setting of anisotropic confining pressures where regional stress systems influence the magmato-hydrothermal related fracture patterns, where for both cases, the presence of a cyclical hydrofracturing system is necessary to produce the observed crack-seal vein textures. This hydraulic fracture system was driven by a deep magmatic source that circulated the volumes of fluid necessary for the formation of the large vein arrays (discussed by Maksaev, 1990). These mineralizing fluids, contained by an overlying stockwork sealed carapace, were overpressured and caused fracturing along preferred planes of weakness when the fluid pressures were sufficient to overcome intra-fracture, or wallrock-vein cohesion. The release of this fluid along pre-existing failure planes would have concentrated veins in NNE to NE trending extensional and shear extensional fractures, at the same time forming a subradial elliptical pattern that emphasized these trends. As previously mentioned, the veins of domain G are predominantly related to the Americana Fault in the southeastern-most part of the domain. Although there has been a concentration of post-mineralization deformation in this domain, a syn-mineralization existence of the Americana Fault can be supposed. Its position with respect to the 040, 065 and 115 trends suggests that the Americana may have been equivalent to a P-shear within the strike-slip system.

Phase I is summarized as a dextral strike-slip (transtension) fault system within which mineralization was emplaced along existing fracture systems. High fluid pressures associated with an underlying magmato-hydrothermal system reactivated existing fractures as extensional to shear extensional fractures along which mineralizing fluids flowed. Following mineralization, deformation continued forming gouge and breccia-bearing dextral faults

along the vein-wallrock contacts.

6.5.4 Deformational Phase II

Phase II formed the D, E, F and G structural domains, within which alteration and mineralization are restricted to those fault systems bordering on, or that appear to be displaced from, domains composing Phase I. The lack of mineralized vein arrays in these domains was presented in Chapter 6.3. The development sequence of these brittle fault domains is difficult to establish with no available marker units. However, the relative activity of the domains (Chapter 6.4) shows that the fault systems probably formed during the same deformation event.

The pattern of this later stage, post-mineralization faulting has a similar geometrical arrangement, except in an opposite sense, to that of Phase I (compare Fig. 6.15 and Fig 6.16).The fault sets are related to the throughgoing N-S to 010 West Fault of domain G, which is the principal displacement zone (PDZ), or master fault, to the fault systems of the other sectors. The fault set of domain D forms angles of 145 (R-shears) with respect to the approximate N-S trend of the deforming zone (Fig 6.16). Similar orientations are observed for non-altered and mineralized faults of the transitional domain C. Domain E, which is a reactivated portion of the Messabi Fault maintains a N-S to 010 trend. The ENE-WSW trending dextral fault system (R'-shears) of domain F is considered a relatively later formed member of this deformation phase based on its crosscutting relationships with the West Fault. This is consistent with some clay-box experiments that show the formation of predominantly R-shears with few R'-shears developing at a relatively later stage of deformation. The principal faults besides the West Fault in domain G, Americana and Calderones, are sub-parallel to the West Fault and may be considered Y-shears. The geometry of the fault systems making up Phase II indicates a post-mineralization sinistral transpressional deformation system at Chuquicamata (Fig. 6.16). This deformation system is compatible with the fault sets described to the west of the West Fault. Since Phase II is related to sinistral deformation and displacement associated with the West Fault as a PDZ, then it is expected that a compatible set of fault systems would have formed on either side

Fig. 6.15 Rose diagram summaries for quartz-molybdenite veins (type#2) in the defined structural sectors. Sectors A and B show the strongest directional trends. Those veins of domains C are reoriented by post-mineralization brittle fault systems. Similarly, those veins of domain G are for the most part large vein fragments within the megabreccia zone. However the vein fragment association with the Americana Fault suggests some syn-mineralization activity. A) directional trends from the structural domains with fault displacement sense. The N-S master fault is hypothetical and is not likely to have existed at the time of mineralization. B) Geometrical association of fracture and vein orientations in a dextral simple shear zone. Compare these orientations with Fig. 6.14(i) transtension, which is a deformation that is also compatible with this data.

Fig.6.15 (see caption on previous page)

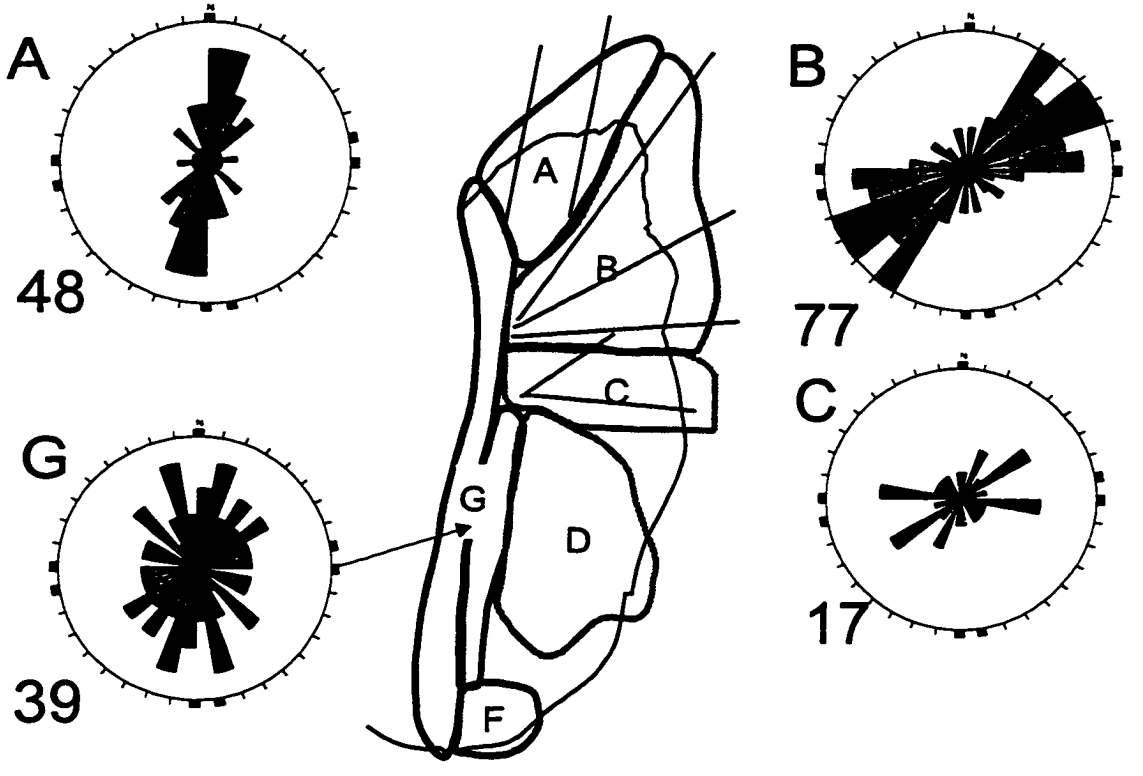

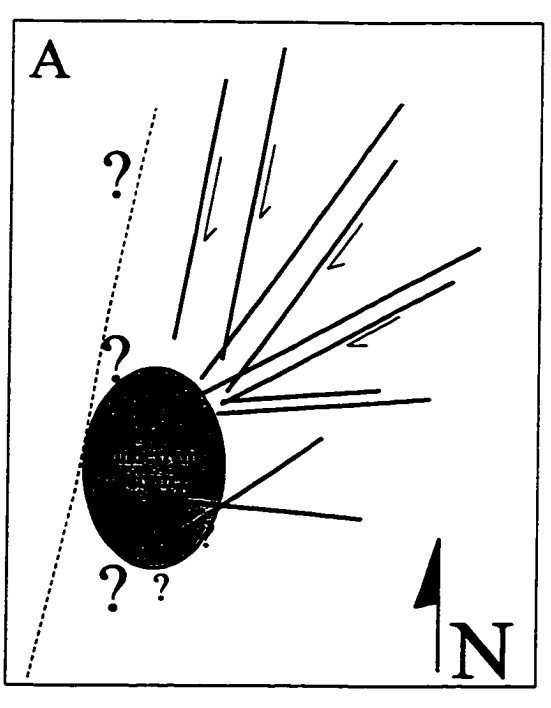

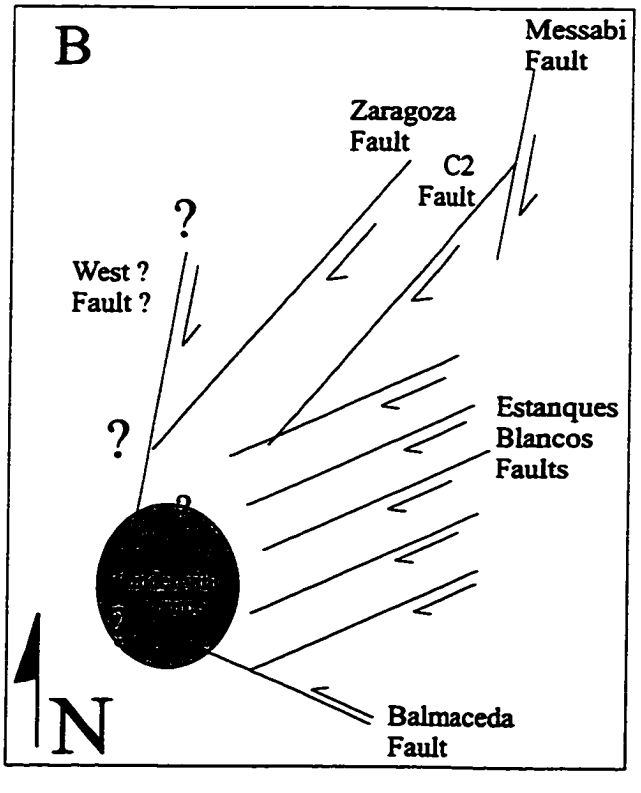

Fig. 6.16 Distribution of fault structures with post-mineralization displacements marked with shear sense indicator. Some of the principal brittle fault systems that make-up Phase II are highlighted. Inset is a schematic representation of the fault geometry that would be expected for a sinistral transpression deformation setting. See Fig. 6.14 for list of label definitions.

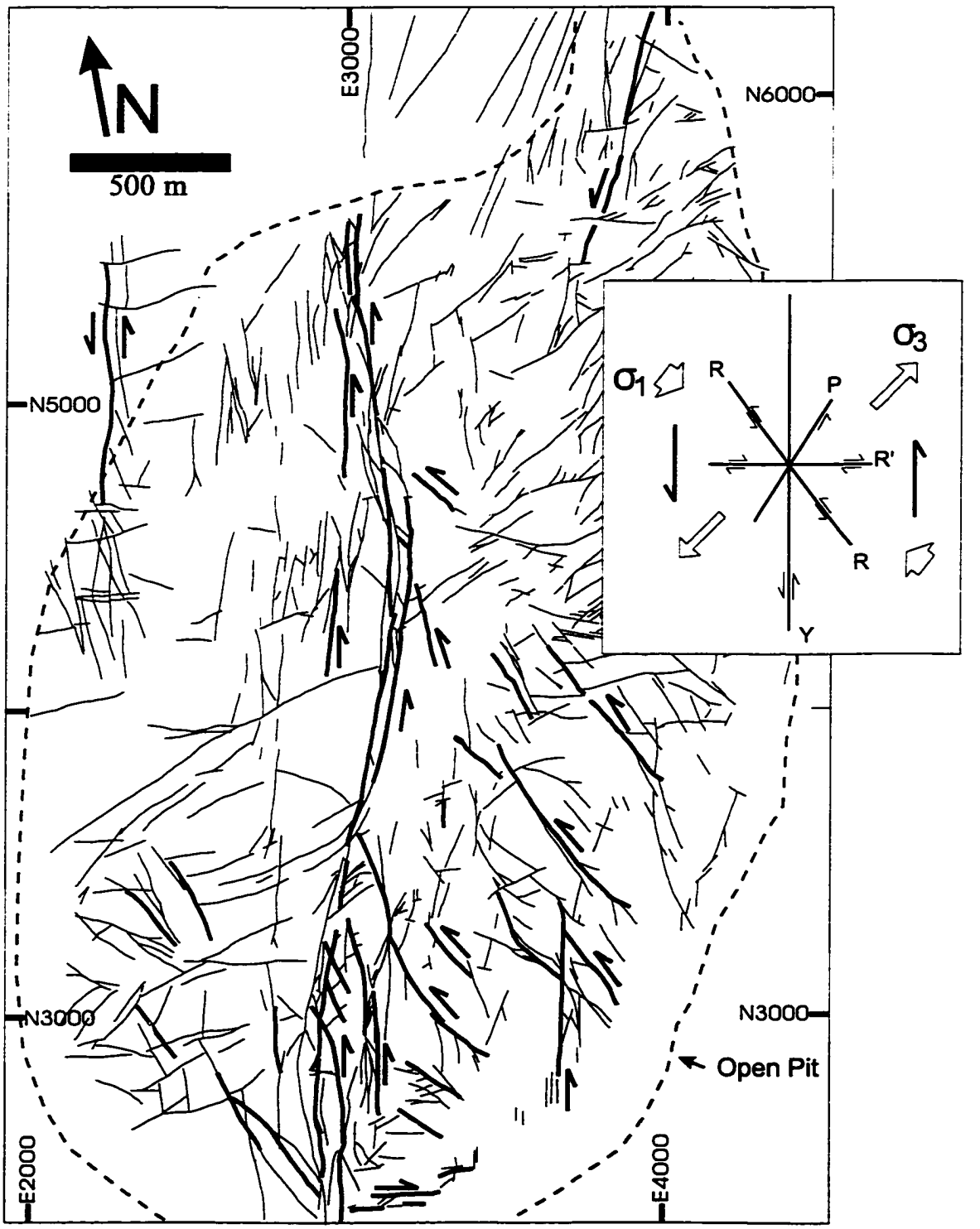

of this displacement zone. As this deformation phase is a post-mineralization event it is discussed further in Chapter 7: *Post-Mineralization Structural Features*.

6.6 Mineralization and Structural Setting

Phase I is a significant contributor to the molybdenum mineralization at the Chuquicamata deposit. Of the molybdenite-bearing structures, the most spectacular are the large Type#2 vein arrays, which parallel the dominant fault sets in individual structural domains (this chapter). The formation of these fault sets and their contained veins are a key to the structural setting of the Chuquicamata district at the time of their formation. From the observed geometries of the fault-veins, the Type#2 veins and associated mineralization formed during a transtensional to simple shear deformation event.

The geometrical relationships of the observed fault-vein systems associated with the mineralization and deformation of Phase I are similar to those which are predicted to form in transpressional to transtensional deformation systems (Sanderson and Marchini, 1984; Woodcock and Schubert, 1994; Freund, 1974). These relationships have also been described from natural systems in Iran (Tchalenko, 1970), Sumatra and California (Tikoff and Teyssier, 1994); northern Chile (Lindsay et al., 1995; Reutter et al., 1996), in granitic rocks (Granier, 1985), and at a variety of scales (Tchalenko, 1970; Hempton and Neher, 1986; Bürgmann and Pollard, 1994; Arboleya and Engelder, 1995).

The proposed mechanism of mineralization for Type#2 and related veins is one of hydraulic fracturing, where the thermal source driving the hydrothermal system is emplaced at depth within a transtensional setting. The magmato-hydrothermal system dominates the local setting utilizing and overprinting existing structures that had formed following the emplacement of the host rock unit and initial transtensional event associated with the copper-bearing stockwork system. This dextral transtension assisted mineralization pattern is in contrast to that shown by Reutter et al. (1996)(their figure 6). Although these authors do mention the mineralized trends shown in this study as secondary systems related to a N-S directed dextral shear zone. This study has shown that the mineralization phases are more likely associated with a NNE-SSW trending shear system as evidenced by the orientation of

the CIC and its contained ductile fabrics and shear zones. The data presented here correspond more closely with the transtensional system hypothesized by Maksaev and Zentilli (1988) and Maksaev (1990).

The Domeyko Cordillera is a region that has variably undergone orogen-normal and orogen-parallel deformation (Maksaev and Zentilli, 1988; Maksaev, 1990; Reutter et al., 1991; Tomlinson et al., 1994; Tomlinson and Blanco, 1997a, 1997b) and is a locally transpressional to transtensional tectonic setting. The geometries of the fault systems and vein arrays that have been presented in this chapter are representative of those geometries predicted by physical and numerical models of simple shear to transtensional systems. However, the mineralization emplaced during this event was controlled primarily by the underlying magmato-hydrothermal system and secondarily by the transtensional fault planes. Continued deformation of the Chuquicamata deposit obscures the relationships between mineralization and displacement. The post-mineralization deformation setting of Phase II shows continued activity of a strike-slip setting but with an opposite sense of shear. This inversion of the strike-slip system observed at the Chuquicamata deposit requires a fundamental change in regional tectonic controls on deformation.

Chapter 7. Post-Mineralization Displacement Phases

The Chuquicamata deposit has been subject to pre-, syn-, and post-mineralization deformation. Since the deposit comprises at least two mineralization events it may also have experienced at least two post-mineralization deformation events. In the previous chapter argument was made for two deformation domains. The first of these included all dextral deformation events and related them to a simple shear to transtensional setting within which extensional to shear extensional vein arrays were emplaced. The vein array emplacement overprinted a copper-bearing mineralized stockwork system that has previously been discussed in Chapter 5. Here the author separates the deformation that may have taken place following the stockwork emplacement and that during the vein array emplacement from that which follows the vein array formation. Both of these events, the post-stockwork and the post-vein-array, comprise Phase I. The second phase of post-mineralization deformation is associated with the formation of structural Phase II, which developed in relation to sinistral displacements of regional magnitudes along the West Fault System.

7.1 Phase One : Displacement Along Existing Structures

The post-stockwork mineralization deformation is represented by at least two generalized deformation phases. The first displaces the trend of the stockwork system (Chapter 5), potassic and chloritic alteration zone trends, and lithologic contacts in a dextral sense. The second part of this phase is more distributed and possibly lesser in magnitude and importance. The second set of displacements parallel the syn-mineralization fault motions associated with the large fault-vein structures and the development of a West Fault. This phase of deformation is concentrated in and is exposed in the northern half of the open pit.

7.1.1 Post Stockwork Displacements

In Chapter 6.5.3, the relationship of the fault-vein array systems of Phase I and stockwork system was presented. Discussion in the previous chapter suggested that the mineralization of Phase I formed in relation to a magmato-hydrothermal system associated

with pluton emplacement at depth. The crack-seal texture of the veins that crosscut the stockwork system corroborate a hydraulic fracture mechanism of formation and extensional deformation of the stockwork-bearing host porphyry. A component of fault-vein-parallel slip during mineralization is proposed to accommodate the apparent displacements of alteration contacts, lithologic contacts observed within and outside of the open pit and the apparent truncation of the stockwork system. Figure 7.1 highlights four principal faults across which there are contrasting alteration assemblages and associated mineralization characters. Offset Banco Porphyry and Mesozoic units are observable in figure 5.1.

Three structural sampling sites (22, 23 and 26) that are located between two of the NE-SW trending post-stockwork faults do not show the typical preferred orientations that other sites in the sector show (Fig. 7.2 compare to Fig 5.9 and 5.10). These sites indicate strong NW-SE trending veinlets whereas all other sites in the sector display NE-SW mineralized veinlet systems. Site 26 indicates the approximate limit of mineralized stockwork system and is dominated by chlorite-filled fractures with minor pyrite and chalcopyrite and no quartz-sulphide assemblages. If these faults were active prior to the stockwork mineralization, which is probable for at least one of these faults, then the orientation of the veinlets may be related to a strongly modified stress pattern around the faults. Another possibility is that deformation subsequent to veinlet mineralization along the faults has resulted in small block rotations. Assuming the veinlets were originally oriented parallel to the preferred NE-SW directional trend of the northeastern sector then the veinlets would have rotated clockwise about a vertical axis to maintain a SE dip direction. This contrasts with an expected counter-clockwise rotation associated with dextral faults. These veinlets systems are likely influenced by later faulting associated with the deposit-wide sinistral displacement event and may or may not have the same control on emplacement as the other veinlets of the sector.

Best estimates for displacement magnitudes along the north-east trending dextral fault structures are between 200 and 350 metres based on the offset Banco Porphyry, the stockwork system and individual blocks of Mesozoic stratigraphy. NNE trending structures, presented previously in Chapter 6, are suggested to have up to 1000 metres of dextral

displacement that is largely based on the displacement of Mesozoic units from outside of the open pit.

7.1.2 Post-Vein Array Displacements

Following the emplacement of vein array assemblages, Type#2 through Type#4, dextral displacements continued parallel to the veins generating breccia and foliated gouge seams. The lack of mineralization cementing the breccias and gouges suggests that at least their latest motion was post-mineralization. This of course does not suggest that the latest displacements along these structures are solely related to Oligocene activity as the West Fault System has experienced several episodes of displacement the latest of which may be mid-Pleistocene (Lindsay et al., 1997).

The presence of pervasively altered wall-rock fragments within fault breccias and gouges indicates that at least some of the dextral displacements were accommodated following the hydrothermal phase producing the sericitic alteration (~31 Ma). However, the NE-SW trending fault are not observed to displace the quartz-sericitic alteration zone. It is probable that the breccias and gouges along the numerous sub-parallel faults represent an accommodation of the dextral displacements by distributed slip. An alternative is that the observed dextral displacements took place prior to the hydrothermal alteration, which suggests that the West Fault has truncated and displaced a portion of the 33.4 Ma copper-bearing stockwork system.

7.1.3 Timing of Phase 1 Displacements

The timing of these dextral displacements is partially constrained by the massive quartz-sericitic alteration phase (~31 Ma) and the development of supergene enrichment (19-15 Ma, Sillitoe and McKee, 1996). In previous chapters, the fault and vein systems of Phase I were described as having quartz-sericitic alteration halos. This association establishes that the faults and veins were in existence by the time of the hydrothermal activity that produced the alteration. The presence of pervasively altered wall-rock fragments within fault breccias and gouges indicates that at least some of the dextral displacements were accommodated

following the hydrothermal phase producing the alteration (~31 Ma). As the core of the massive quartz-sericitic alteration zone is not displaced by the NE-SW trending faults suggesting that the displacement was accommodated by distributed slip across a larger number of faults, the slip was accommodated in the formation of the West Fault and megabreccia, or most of the dextral displacement took place prior to the conclusion of the hydrothermal activity that produced the alteration assemblage. Similarly, the basin of supergene enrichment (19-15 Ma) is continuous from south to north, showing no evidence of offset associated with the NE-SW trending faults (R. Freraut, J. Rojas, pers. comm., 1996).

These data indicate the dextral displacements observed on the NE-SW trending principal faults followed the emplacement of the Banco Porphyry and stockwork mineralization phase (Chapter 5) associated with potassic alteration that we estimate to be ~33.4 Ma in age (Reynolds et al., in press). These fault systems, although dominated by extension, were active during the emplacement of the large quartz-molybdenite (Type#2) vein array (Chapter 6). Continued dextral faulting activity is evidenced by the presence of breccia and foliated gouge parallel to the veins. Displacement continued following the quartz-sericitic alteration event (~31 Ma, Reynolds et al., in press) to account for the development of gouges but terminated before the supergene enrichment event (19-15 Ma, Sillitoe and McKee, 1996).

Fig. 7.1 Illustration of selected faults and their associations with apparent post-mineralization activity. Faults A through D are dextral faults of structural sectors A and B. Fault A, limits potassic and sericitic alteration to its SE side and propylitic to the NW. This fault has experienced a possible 1000 m of dextral displacement part of which may have juxtaposed alteration assemblages. Fault B, displaces Banco Porphyry and Mesozoic stratigraphy (see Fig 4.1 and 4.2). Similarly, fault C displaces Mesozoic stratigraphy that is not shown in this figure and appears to offset alteration assemblages. Fault D offsets alteration assemblages and appears to limit the stockwork system, possibly displacing the southern portion westward.

Fig. 7.1 (see caption on previous page)

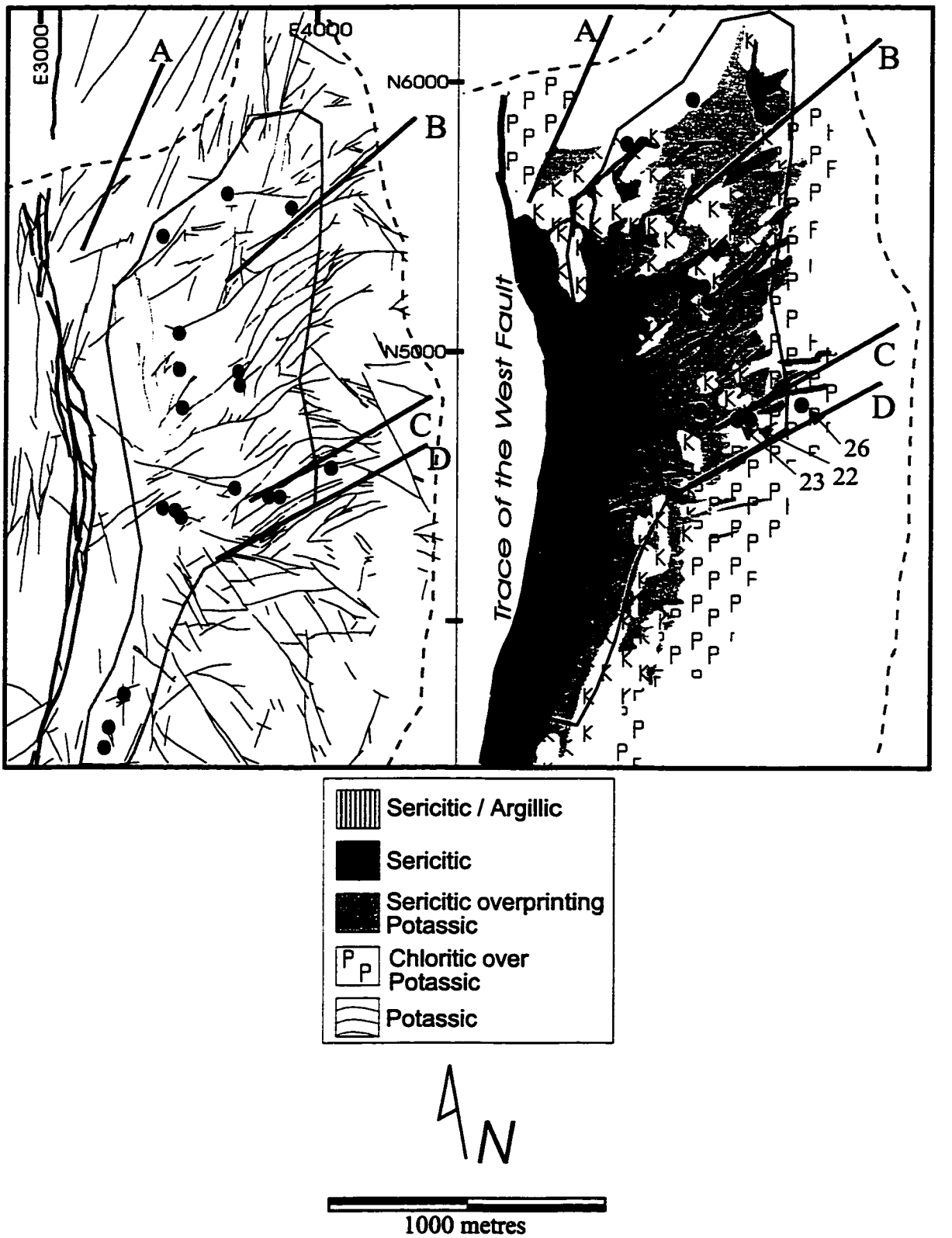

Fig. 7.2 Schmidt lower hemisphere stereoplots for structural sampling sites between principal NE-SW trending dextral faults. Plots on the lefthand side are for sites 22 and 23and those on the righthand side are for site 26. See figure 7.1 for site locations. These trends contrast with those NE-SW trends established for the northeastern sector within which these sites are located. Veinlet types v1, v2, v4, v5 and v6 are those described in Chapter 5, see Table 5.1.

Fig. 7.2 (see caption on previous page)

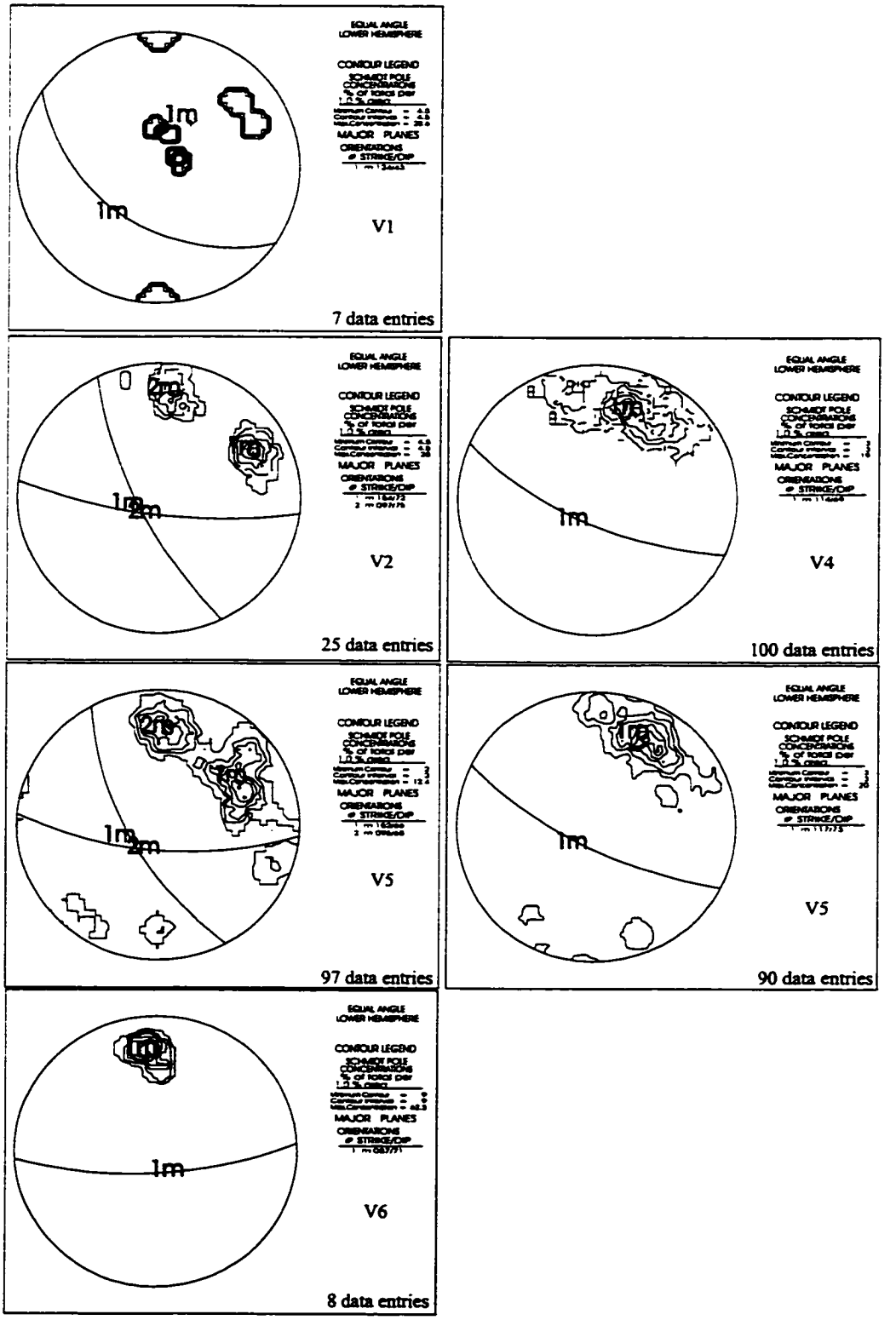

7.2 Phase Two : Brittle Faulting and the West Fault

The sinistral strike-slip character of Phase II was shown in Chapter 6.5.4 and is briefly summarized here with additional information on the timing of deformation. The domain D fault system displaces altered and mineralized faults of Phase I and the supergene enrichment basin (19-15 Ma, Sillitoe and McKee, 1996) by up to 50 metres along individual sinistral faults (Rojas and Lindsay, proprietary mapping, 1996). Domain F faults offset both the trace of the West Fault and the quartz-sericite alteration zone (~31 Ma) a maximum of 60 metres in a dextral sense. This relationship also indicates that a gouge-bearing West Fault existed prior to the dextral displacements of domain F. The West Fault bounds the quartz-sericite alteration zone to the west and shows sinistral kinematic indicators. These fault systems represent a sinistral district to regional scale strike-slip fault system (Fig. 6.17). A maximum age for Phase II deformation event is given by the West Fault that has generated foliated gouges from the ~31 Ma quartz-sericite alteration zone, which is related to the mineralization events of Phase I. Sinistral foliated gouge-bearing subsidiary faults to the West Fault anastomose through the pervasively sericitized megabreccia. Displacement of the supergene enrichment basin shows that sinistral fault activity postdated at least some portion of the 19-15 Ma supergene history. Activity concentrated along the West Fault continued until at least the Late Miocene-Pliocene based on a thrust fault described by Zamora (1979) which placed Eocene Fortuna Complex over Miocene gravel at the south end of Chuquicamata (Fig. 7.3). Preliminary Electron Spin Resonance (ESR) dating of quartz clasts from the foliated intra-fault material of the West Fault suggest that activity of the fault continued until at least the Middle Pleistocene (Lindsay et al.,1997).

Fig. 7.3 Sketch section of the southern exposure of the West Fault as interpreted from bench faces of the open pit from Zamora (1979). The Eocene Fortuna Granodiorite overlies Miocene gravels along a reverse fault contact.

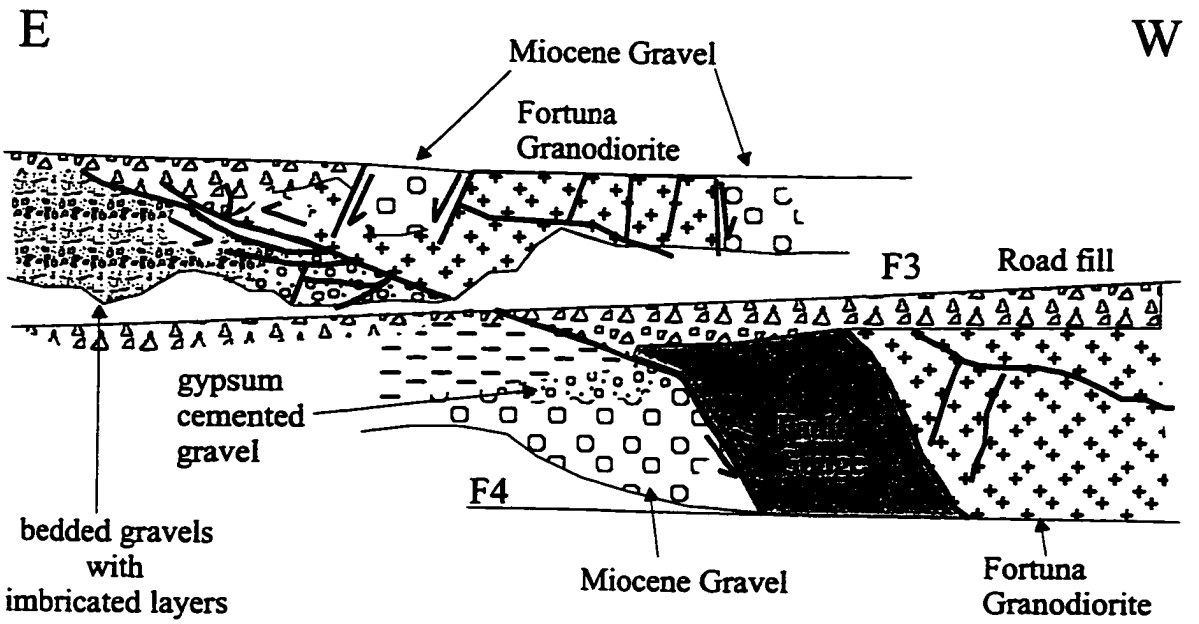

Fig. 7.4 Geometry of the plane of the West Fault showing in plan view (A) a northern section that bows eastward and a southern section that bows westward. The contour plot (B) of this plane indicates that the West Fault dips westerly in its southern section. The northern section appears more complex with the West Fault dipping eastwards from the surface but curving to vertical at depth. The N-S cross-section (C) shows the distribution of data points used in the contour plot and the open pit surface. Depth to the fault plane data has been incorporated from Ramierez (1993) to generate the contour plot.

Fig. 7.4 (see caption on previous page)

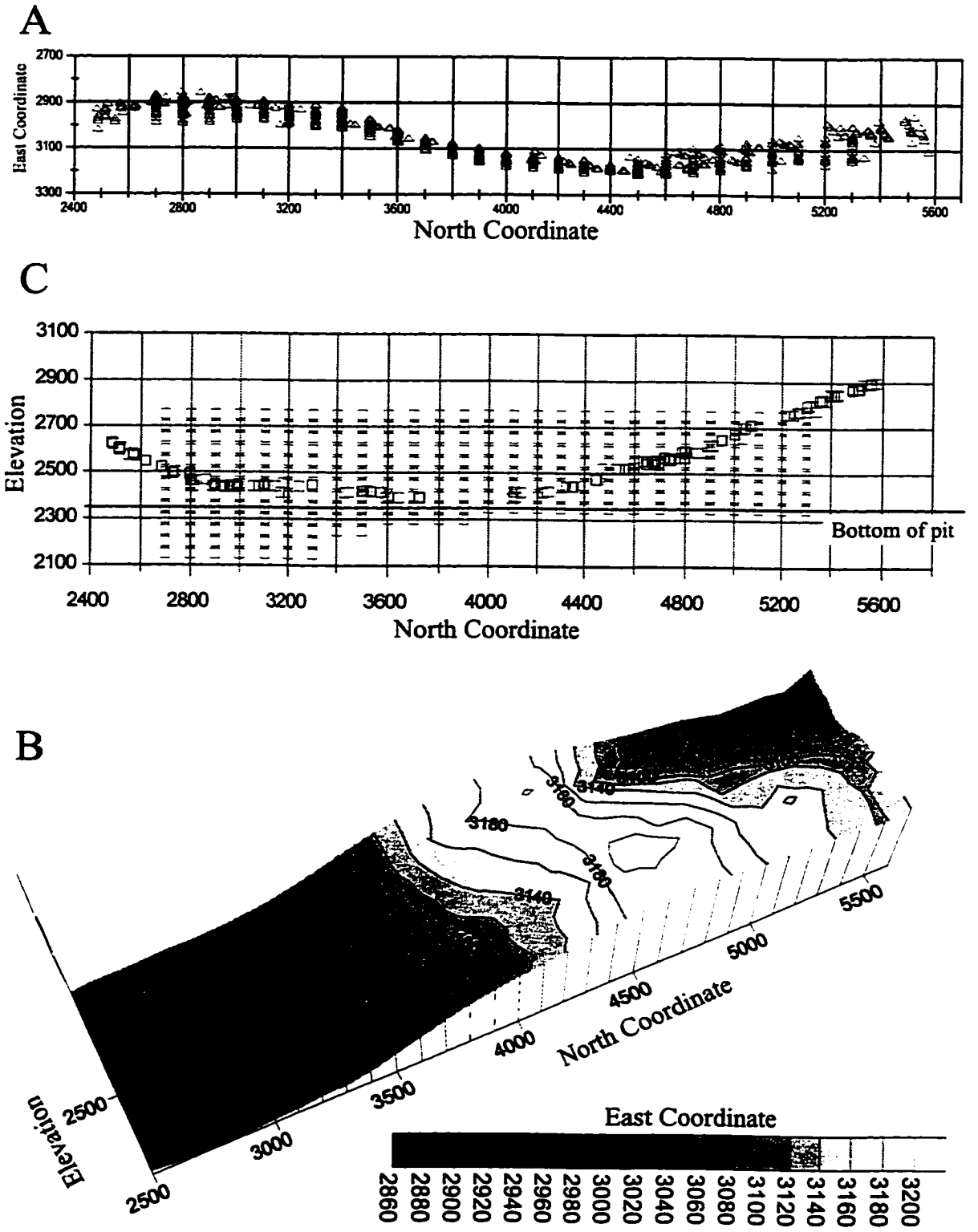

7.2.1 Displacement Activity of the West Fault

The West Fault, a N10°E striking fault zone, as exposed in the Chuquicamata open pit, has a concave form and outcrops over a horizontal extent of 3.3 kilometres and vertical extent of 0.55 kilometres. Drilling has encountered the fault zone an additional 0.56 kilometres below the bottom of the open pit, below which it is unexplored. At depth, the boundary is interpreted to be a single fault plane, based on lithological juxtaposition that in places is defined by <1 cm of cataclasite (J. Rojas, pers. comm., 1995). Ramirez (1993) determined the plane of contact to have a geometry such that the northern portion dips between vertical and 80° east and the southern portion between vertical and 70° west (Fig.7.4). Mapping completed during this study indicates that the West Fault is a series of gouge and cataclasite-bearing planes, 3 - 10 m in width, along which slip has concentrated. This fault constitutes the western economic limit of the mine, juxtaposing the strongly altered and mineralized Chuquicamata Complex and the non-mineralized Fortuna Complex. Previous discussions have suggested that the West Fault may have been active during the mineralization events of Chuquicamata. However, a younger, brittle, upper crustal, sinistral event, involving tens of kilometres of displacement along the West Fault, has obscured all evidence of an older dextral event and any syn-mineralization relationships within the present fault zone.

7.2.1.1 Eocene-Oligocene Activity

An early dextral displacement of approximately 2 km along the regional West Fault System has been quantified by Tomlinson and Blanco (1997a, b). This older dextral fault system is supported by plate tectonic reconstructions of Pilger (1984) and Pardo-Casas and Molnar (1987) that indicate an increased rate of convergence between the Nazca and South American plates in the Eocene at a strongly oblique angle. Strong coupling between the down-going slab and a forearc continental sliver of South America may have resulted in the formation of a lithospheric right-lateral transpressive system (Scheuber and Reutter, 1992; Reutter et al., 1996). Deformation away from the West Fault does provide local and regional evidence for an earlier dextral event (Reutter et al., 1991; Charrier and Reutter, 1994;

Tomlinson et al., in prep.). Radiometric $^{40}Ar/^{39}Ar$ dating of a mylonite zone in the East Porphyry of 32.8±0.2 Ma and a schist of the Messabi Fault at 33.4±0.2 Ma support an early dextral displacement. Due to their closeness to the porphyry deposit it is likely that the dates represent cooling ages following emplacement of the initial mineralization phase. Reutter et al. (1993, 1996) propose an inversion of the sense of shear of the fault system from dextral to sinistral at the time of hydrothermal alteration, approximately 33 Ma. However, the data presented here and the interpretation of the mineralization and deformation sequence show that dextral deformation continued until at least 31 Ma.

7.2.1.2 Middle Oligocene - lower Miocene Activity

The West Fault and fault systems parallel and subparallel to its main branches show kinematic evidence of sinistral displacement (Ambrus, 1979; Hunt et al., 1983; Baker and Guilbert, 1987; Lindsay et al., 1995; Reutter et al. 1993, 1996). Shear sense was determined from the presence of non-coaxial strain fabrics including: s-c fabrics and asymmetric tails on sigma and delta-type clasts observed in foliated gouge and cataclasite samples. The application of these fabrics to foliated cataclastites and gouges is discussed in Engelder (1974), Chester et al. (1985), Chester and Logan (1986), and Cladouhos (1996 a, b, in press). This sinistral displacement is proposed to have occurred during the mid-Oligocene to lower Miocene beginning between 31-25 Ma and ending between 19-15 Ma. Tomlinson and Blanco (1997b) discuss detailed regional correlations that confirm those relationships derived from the relationships observed at Chuquicamata.

Previous regional studies have discussed left-lateral displacement magnitudes for the West Fault (West Fault System) ranging from 7 to 45 kilometres (Thomas, 1978; Ambrus, 1979; Reutter et al., 1993, 1996). Recent detailed investigations indicate 35-37 km of sinistral displacement (Tomlinson and Blanco, 1997b; Dilles et al, 1997). Most of these authors only discuss a lateral component of displacement describing the fault plane striae as sub-horizontal. However, Tomlinson and Blanco (1997b) describe correlations, which indicate 500 to 600 metres or greater of down-on-the-west displacement. Cataclastic lineations (Tanaka, 1992) within the gouge of the West Fault, observed in the open pit,

indicate a variety of motions that include significant sub-horizontal and lesser abundant intermediate to vertical slip events. Lineation variations are indicative of multiple distinct fault displacements, or displacement partitioning of a single event onto various fault planes, suggesting a complex strain history for the West Fault.

7.2.1.3 Post-upper Miocene Activity

Post-upper Miocene activity is observed in a number of localities where the central branches of the West Fault are offset by low angle reverse faults and oblique-slip faults. The offsets are on the order of metres with the exception of an approximately 60 m right-lateral displacement by a fault in structural domain F. Zamora (1979) describes post- gravel reverse faulting along the West Fault, exposed in the southern end of the open pit, as a block of Eocene Fortuna Complex (Chapter 2.3.1.2) riding over a Chuquicamata block of Miocene gravels (Fig. 7.3). Estimates of displacement were 30 metres lateral and 16 metres vertical (east side down) that were confirmed in Mina Sur (4 km south) by a 13-19 metre difference in groundwater levels (Zamora, 1979).

Regionally, local folding between 6-7 m.y. and post-3 Ma have been identified in the Calama Basin (May et al., 1996; Tomlinson et al., in prep) indicating late Pliocene and /or Quaternary activity of the West Fault System. An ongoing attempt to date the most recent motion of the West Fault, using electron spin resonance dating techniques applied to quartz clasts of the intra-fault materials, indicates a mid-Pleistocene age for most recent movements (Lindsay et al., 1997).

7.3 Summary

Post-mineralization dextral deformation has been shown to take place after, cross-cut and displace the copper-bearing stockwork system. The displacements are suggested to have accompanied the emplacement of large fault-vein arrays which display crack-seal texture that indicates the veins where formed by a series of mineralizing fluid pulses. Slip along these same structural features generated fault gouges and breccias indicate that dextral slip continued after the 31 Ma quartz-sericitic alteration event. However, the quartz-sericitic

alteration zone and the supergene enrichment basin are not offset by these same faults suggesting that the majority of dextral slip terminated during or prior to the 31 Ma event. An inversion of the West Fault from a dextral slip to sinistral slip system occurred sometime after 31 Ma. The sinistral displacements foliated the quartz-sericite alteration zone and offset the supergene-enrichment basin by tens of metres. Sinistral displacements began between 31-25 Ma and continued until at least 19-15 Ma. This long-lasting brittle sinistral event overprints and obscures evidence of earlier dextral slip along the West Fault.

Chapter 8. Evolution of Structural Control at Chuquicamata

In Chapter 3, the Chuquicamata porphyry copper-molybdenum deposit was presented in terms of the geological characteristics of lithology, alteration and mineralization at their present level of knowledge. Chapters 4, 6 and 7 described and discussed a series of structural features that represent the pre-, syn- and post-mineralization stages of deformation, structural control of mineralization and deposit dissection. Chapters 5 and 6 described two distinct episodes and scales of mineralization, their mechanism of formation and their structural-tectonic settings. The influence of the preferred structural directions, presented in this thesis, on mineralization and ore grade is reflected in the analysis of ore grades by Krige and Dunn (1996), who in using the data described herein concluded an anisotropic distribution of ore exists at Chuquicamata. This chapter discusses the sequence of deformation events related to emplacement, mineralization, dissection and displacement of the deposit in light of available geochronology data and previously suggested regional geological models for the formation of Chuquicamata.

8.1 Host Porphyry Emplacement

The Chuquicamata deposit is hosted by a ca. 34-33 Ma, NNE-trending granodioritic stock that is 14 kilometres long, 1 kilometre wide (Alvarez et al, 1980) and buried beneath Miocene-Pliocene gravel. The location of the Chuquicamata deposit, a 4 kilometre by 2 kilometre outcrop, within the Domeyko Fault System has led many authors to use kinematic data and relationships between the outcropping fault patterns to infer the character of regional deformation (Maksaev and Zentilli, 1988; Maksaev, 1990; Reutter et al., 1991, 1993, 1996; Tomlinson and Blanco, 1997a, b). The fault patterns, which overprint the deposit, are comparable to natural, numerical and clay-box experiment fracture patterns for a variety of strike-slip extensional settings (Sanderson and Marchini, 1984; Hempton and Neher, 1986; Woodcock, 1986; Woodcock and Fisher, 1986; Deng et al., 1986; Gamond, 1987; Sibson, 1985, 1986, 1987; Sylvester, 1988; Woodcock and Schubert, 1994). These brittle fault patterns have been used to infer the emplacement of the Chuquicamata Intrusive

Complex into a dextral strike-slip transtensional setting (Lopez, 1939, 1942; Perry, 1952, Taylor, 1935; Hollister, 1978; Sibson, 1987; Maksaev and Zentilli, 1988; Maksaev, 1990; Reutter et al., 1991, 1993, 1996).

Structural fabrics found within the CIC at Chuquicamata, as described in Chapter 4, confirm that the Chuquicamata complex intruded a dextral strike-slip deformation environment. The low-angle reverse faults and high-angle dextral strike-slip faults are compatible with a dextral strike-slip deformation zone with the principal maximum stress axis oriented approximately NE-SW. Potassic alteration a high temperature alteration associated with the final stages of crystallization of the intrusion and therefore approximates the age of emplacement, crystallization and ductile deformation of the CIC. Geochronological data from potassic alteration assemblages constrain the timing of this series of events with cooling ages of 33.4±0.2 Ma (Reynolds et al., in press). Contrary to the long-lived dextral strike-slip Domeyko Fault System, proposed by Maksaev and Zentilli (1988), Maksaev (1990) and Reutter et al. (1991, 1993, 1996) as being associated with the Eocene Incaic tectonic phase, Tomlinson and Blanco (1997a) suggest that this Early Oligocene deformation is a short-lived event that is not likely associated with the earlier Eocene Incaic tectonic phase. From this early, pre-mineralization, deformation data, which support a dextral strike-slip deformational setting, we can hypothesise a mechanism of emplacement for the CIC that is consistent with this environment. Many authors have described and explained the synkinematic emplacement of plutons within extensional domains along transcurrent fault zones (Guineberteau et al., 1987; Hutton et al., 1990; Morand, 1992; D'Lemos et al., 1992; Renne et al., 1993). If Chuquicamata had a fault-controlled emplacement, then the bounding fault systems, the Messabi and West Faults, have assisted in creating an environment for emplacement (Fig. 8.1A,B) implying their existence at least by the time of emplacement. A rapid emplacement is necessary for the magma to reach upper crustal levels where porphyry-type deposits form before it crystallizes.. A mechanism that is compatible with rapid ascent and emplacement of magma into an extensional setting is one of "seismic", or "fluid-pumping" that Sibson et al. (1975) and Sibson (1987, 1986, 1987, 1996) describe for hydrothermal fluid systems and D'Lemos et

al. (1992) apply to the transport of magmas in strike-slip shear zones. This emplacement model is consistent with observations of arc volcanos, such as Mount St. Helens that occur in tensile zones above deep, seismically active fault zones that are oriented to accommodate strike-slip displacements within the magmatic arc (Weaver and Hill, 1978; Weaver et al., 1987). The driving forces for the emplacement of the Domeyko magmatic arc and the inferred shear-zone magma-pumping events are associated with plate tectonic activity during the Eocene-Oligocene. Plate tectonic reconstructions by Pardo-Casas (1987) and Pilger (1984) show the Eocene-Oligocene as a period of rapid and oblique, NE-SW, convergence between the South American and Farallon (Nazca) plates. Oblique convergence may partition into an arc-normal component, which results in strain at the plate boundary and perhaps enhances plate coupling, and an arc-parallel component, which concentrates shear stresses within the continental plate. The shear stresses localize in the thermally weakened lithosphere along the magmatic front generating a trench-linked strike-slip deformation zone (see Fig. 6.14)(Woodcock, 1986; Sylvester, 1988). Displacement within this zone produces zones of local transpression and transtension that may assist with the upwards transport of magmas into extensional zones of the upper crust (D'Lemos et al., 1992). This emplacement scenario is consistent with the plate tectonic interactions and the described early deformation fabrics of the CIC and is therefore considered a probable emplacement model for the CIC and the Chuquicamata deposit.

Fig. 8.1 Proposed model of emplacement, deformation and mineralization of the Chuquicamata porphyry copper-molybdenum complex within the Domeyko Fault System of northern Chile via localized extension and associate magma-pumping (see text). The schematic model represents a middle to upper crustal fault undergoing dextral strike slip displacement.
(A) The initiation of a fault jog, or stepover, begins create an extensional zone along the fault. This extension may draw magma from below into the opening.
(B) Continued deformation along the regional fault may develop fabrics internal to the intrusion consistent with the sense of fault slip.
(C) Cooling, consolidation, retrograde boiling followed by hydrofracturing events form a mineralized stockwork/veinlet system. The veinlets of this stockwork bear preferred trends in accordance with the ±NE-SW regional and district principle stress orientation.
(D) Uplift and exhumation of the region and possible renewed magmatic activity at depth accompanied by continued deformation result in deposit to district-scale fault systems that host molybdenum and copper-iron-sulphide mineralization. Spatially related to these N-S, NNE-SSW, NE-SW and ENE-WSW trending mineralized fault-vein arrays is a texture-destructive quartz-sericitic alteration phase. The fault system kinematics are compatible with a regional dextral fault zone.
(E) At some time following the emplacement of mineralized fault-vein arrays and associated quartz-sericitic alteration, the regional fault system inverted to regionally active sinistral strike-slip fault zone. This fault zone is characterised by the West Fault and a set of subsidiary NW-SE trending non-mineralized brittle faults.

Fig. 8.1 (See caption on previous page).

South North

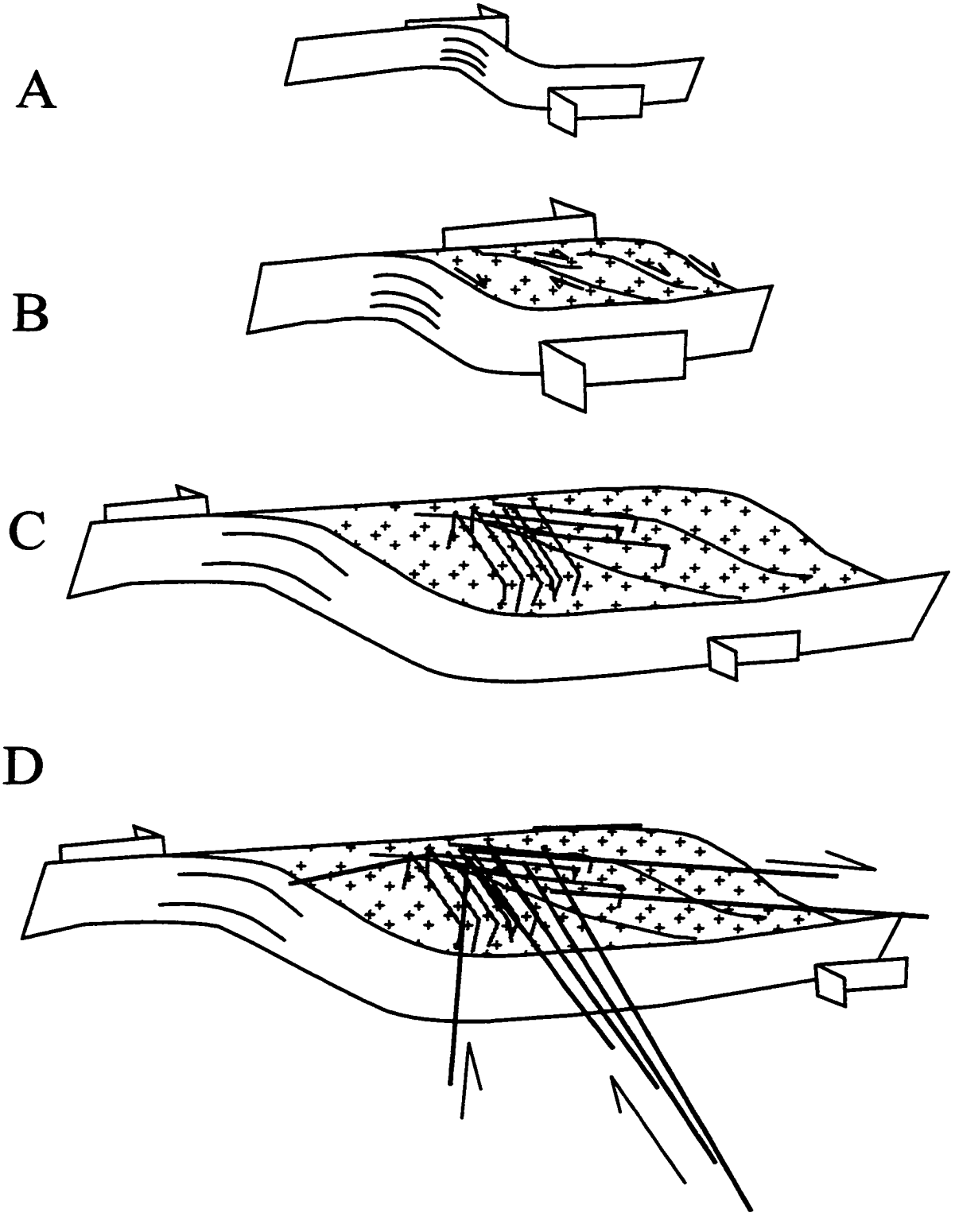

Fig. 8.1 Continued

(See caption on page 238).

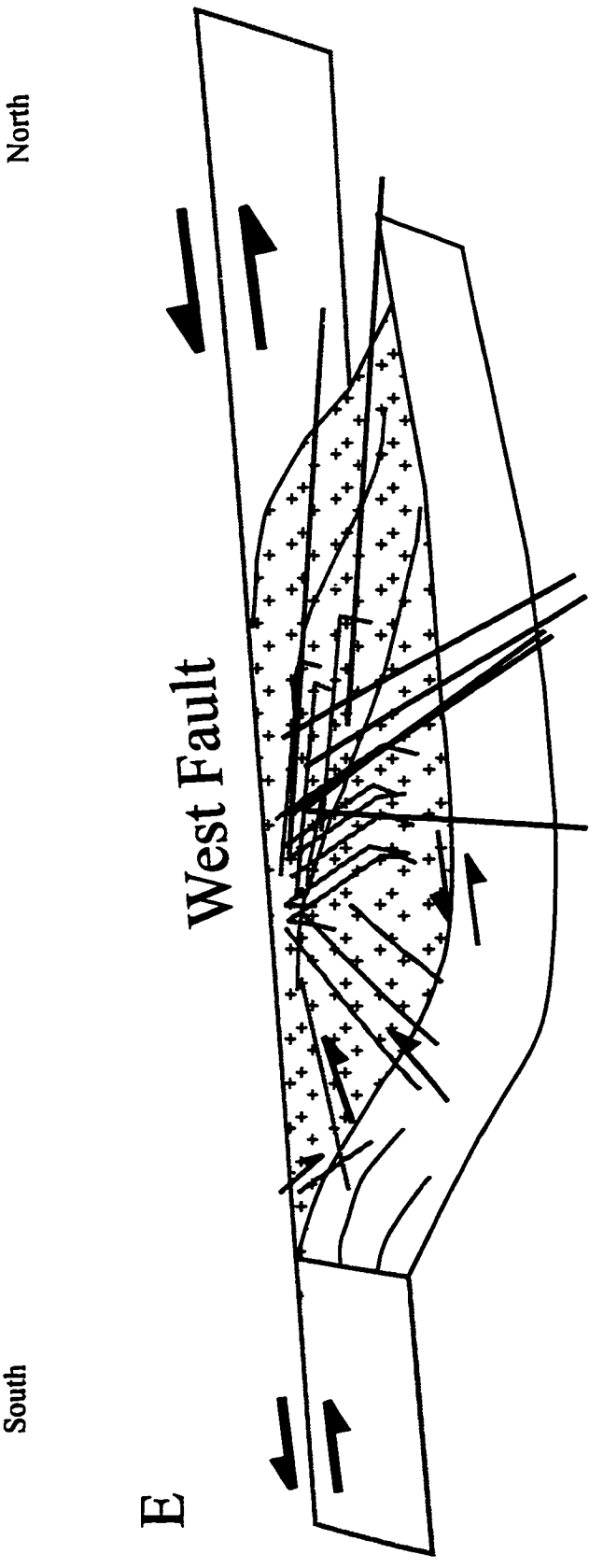

8.2 Mineralization

Mineralization outcropping at Chuquicamata was described at two scales: the first being a stockwork-veinlet system with individual veinlets having maximum widths of a couple of centimetres (Chapter 5), and the second, a vein array with individual vein widths ranging from tens of centimetres to several metres (Chapter 6). This leads to several possible interpretations of the alteration-mineralization sequence and associations. A preferred model is summarized in this section (Fig. 8.2).

8.2.1 Stockwork Mineralization

Stockwork formation is believed to be an end result of the emplacement of a fluid-saturated granodioritic stock into epizonal crustal levels. Sillitoe (1973) proposed that these late-stage stocks are subvolcanic in nature. At deeper erosional levels, stocks and their associated porphyry deposits are related to batholiths as cupolas (Dilles and Einaudi, 1992; Henley and McNabb, 1978). The formation of fracture systems within the environment of a shallowly emplaced pluton have been throughly presented by Burnham (1967, 1979), Koide and Bhattacharji (1975) and Knapp and Norton (1981), and are summarized here. As the stock cools and crystallizes the melt may become saturated with respect to fluid and crystalline phases. Volatile components concentrate in the fluid and in certain cases where this leads to an increase in vapour pressure within the fluid and this pressure is such that it exceeds the confining forces of the crystallizing magma retrograde or resurgent boiling may occur (Burnham, 1979, 1985; Phillips, 1973; Giggenbach, 1992). If the magma in which resurgent boiling occurs is largely consolidated and the vapour pressure overcomes the tensile strength of the rock then there will be rapid and extensive expansion through brecciation and fracturing. These fracture systems provide a permeability network for fluids rising from the consolidating melt. The release of the vapour/fluid pressure causes a relative decrease in the total pressure that further cools and crystallizes more melt, generating more fluids that result in a series of hydrofracturing events. These hydrothermal fluids pass through the hydrofractured permeability network precipitating minerals and altering wallrock. Both heat and mineralizing fluids escape to the fracture system, causing the

Fig. 8.2. Proposed relative timing sequence for main deformation, alteration and mineralization events observed at the Chuquicamata deposit. The time-frame is established using geochronological data of Reynolds et al. (in press) for potassic and quartz-sericitic principal alteration phases. Age data for supergene enrichment are from Sillitoe and McKee (1996). The black boxes represent ranges in age of geochronological data for specific events. Series of vertical lines indicate proposed timing for specific mineralizing events.

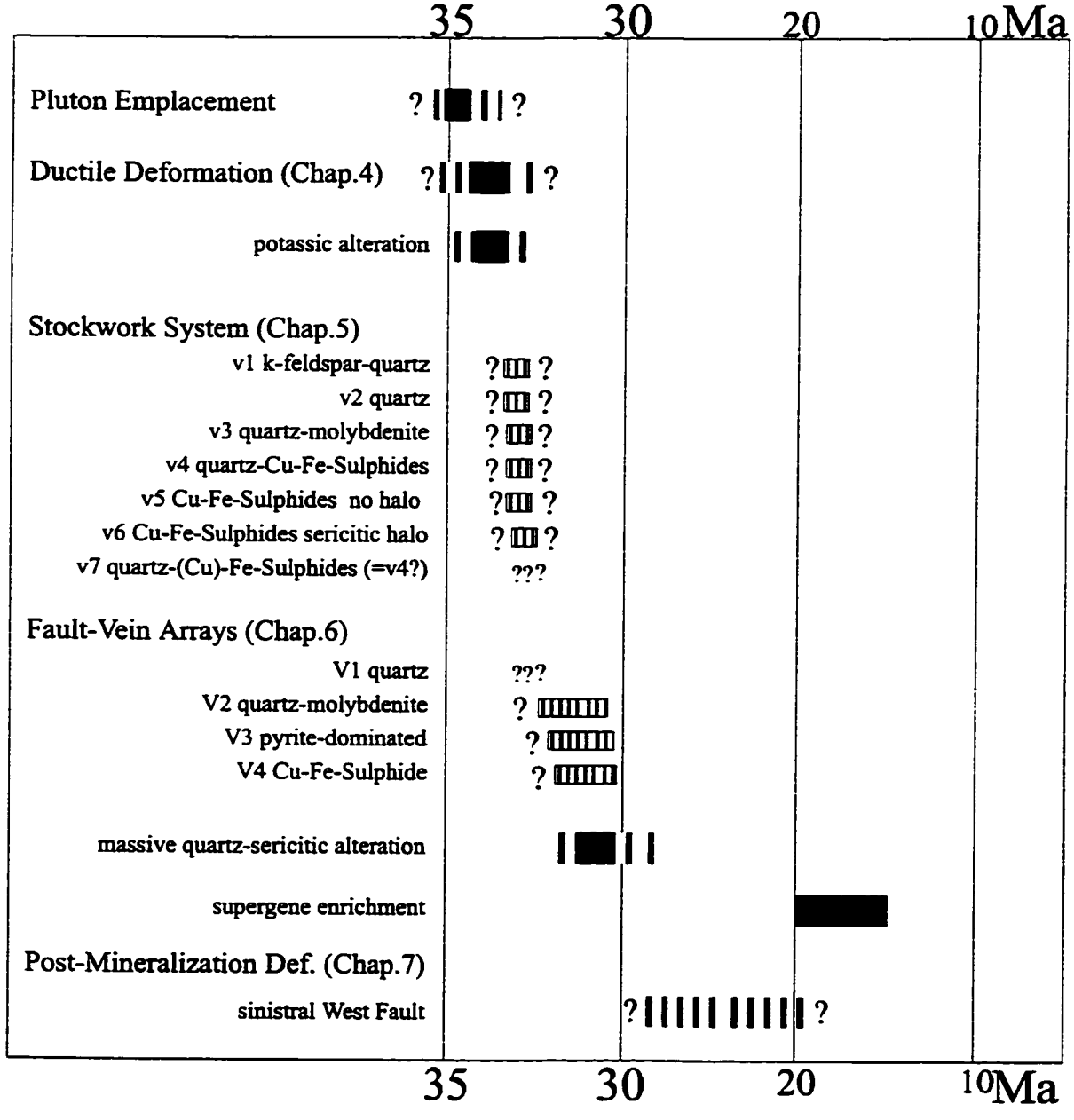

underlying magma to further cool, crystallize and segregate fluids until the fractures heal and thereby reclose the system. As the system cools further and the fluid saturated carapace retreats to deeper levels, a reactivation of these fracture mechanisms produce a vertical network of crosscutting veinlets with different alteration associations that narrow at depth (Burnham, 1979).

The fracture systems that form in the crystallized carapace and the surrounding country rocks are generally steep (Knapp and Norton, 1981) and may reflect the regional stress field or tectonic setting that existed during the magmato-hydrothermal fracturing events (Rehrig and Heidrick, 1972; Burnham, 1979). Knapp and Norton (1981) indicate that although fractures form simultaneously near the top of the pluton, at depth a maximum 0.2 m.y. lag may exist between earlier-formed fluid pressure enhanced fractures and fractures formed by thermal cooling. By way of numerical modelling, these authors also indicate that fracture dips would be intermediate to vertical, above and adjacent to the pluton and would become shallower at greater depth within the pluton. Although the models take place in isotropic stress fields, Burnham (1979) suggests that the orientation of the least principal stress depends on the regional stress field, as dictated by the tectonic setting. Directional trends in veinlet orientations have been described from a number of porphyry deposits and the districts which surround them (Haynes and Titley, 1980; Titley et al., 1986; Casselman et al. 1995; Heberlein 1995). For the porphyry systems of the American southwest, a correlation between the density of veinlets and mineralized centres was shown and related to regionally distributed fracture patterns, which were tectonically induced in upper crustal stress fields during and following porphyry emplacement (Rehrig and Heidrick, 1972; Heidrick and Titley, 1982; Titley et al., 1986).

The mineralized fracture pattern, or stockwork system, at Chuquicamata, as described in Chapter 5, is proposed to reflect those regional stress patterns that prevailed at the time of fracture formation and mineralization. The mineralized system that is being referred to is the stockwork system that formed upon the cooling of the CIC through the ductile conditions necessary to form the deformation fabrics discussed in Chapter 4, which the stockwork crosscuts. This stockwork is crosscut by later deposit-scale faults and vein structures (Fig.

8.1C, D). The details of the veinlet systems were described and discussed in Chapter 5, where they were summarized according to mine sector (northern, northeastern and southern). From these sectors it was concluded that preferred orientations for the veinlets systems exist in each of these areas. The overall NNE-trend of the northern sector veinlets and the NE-trend of the northeastern sector veinlets suggests either a domainal control to mineralization or the remnants of a radial fracture pattern around an intrusion centre whose southern portion was modified by brittle deposit-scale faulting. NNE, NE and NW orientations are consistent with shear fractures that may have developed in response to the magma cooling in a dextral strike-slip fault system. The mineralized fracture patterns are consistent with numerically modelled and clay-box experiment fracture patterns for strike-slip fault systems (compare Tchalenko, 1970; Sanderson and Marchini, 1984; Schreurs, 1994). These fractures would form or be reactivated as extensional or shear extensional fractures by fluid and vapour fracturing processes associated with an underlying, cooling and crystallizing magma. The sub-vertical character of the mineralized fractures indicate that they overlie, or are adjacent to the magmatic and mineralizing source (see Knapp and Norton, 1981). Alternatively, the fractures appear to have a sub-elliptical radial pattern with the long axis of the ellipse oriented NE-SW, which is also consistent with the proposed dextral strike-slip model and maximum principal stress orientation. Post-mineralization fault displacements have offset portions or this stockwork system making overall initial veinlet orientation patterns difficult to determine. However, both strike-slip zone and magmatic controls on the formation of the veinlets appear to have influenced their orientations. This mineralization phase is closely related to the rapid cooling of the magma and thus is closely associated with the "late-magmatic" potassic alteration of the crystallized host porphyry at about 33 Ma (Reynolds et al., in press). The generation of this stockwork mineralization phase likely occurred over a protracted time frame as indicated by the sequence of seven veinlet sets identified in Chapter 5. Quantifying a time length for the generation of this stockwork system would involve an extensive geochemical study of host rock and alteration phase geochemistry and the involvement of numerical modelling that would greatly aid the understanding of the formation of this deposit. However, the degree of involvement needed for such a study falls

outside of this present work. Knapp and Norton (1981) indicate for a cooling stock emplaced within the upper crust that fractures near the top of the intrusion form simultaneously and that at depth a maximum time lag of 0.2 m.y. may exist between earlier hydrofractures and later formed thermal fractures. These authors also suggests that this intrusion would also be completely crystallized within 0.5 m.y. This data suggest that geochronological dating using present technology might be able to distinguish between only those earliest and latest formed veinlets providing no thermal resetting has taken place. The modelling conclusion of Knapp and Norton (1981) also indicate that alteration and mineralization events associated with a shallowing emplaced intrusion are unlikely to span millions of years. For those intrusion-related deposits that do span several million years, such as Chuquicamata, a multiple-intrusion hypothesis is probably more appropriate.

8.2.2 Vein Array Mineralization

The fault pattern at Chuquicamata and the surrounding regional structural pattern have been used to infer tectonically driven models for the mineralization at the deposit, but without a direct examination of style and fault-vein mineralization associations at the deposit (eg. Boric et al., 1990; Reutter et al., 1996). In the previous section, an early, initial mineralization phase was outlined as a system of crosscutting veinlets that bear typical mineralization and associated alteration assemblages for porphyry copper type deposits (see above, Chapter 5). Although contact relationships are obscured by alteration and later brittle faulting, this stockwork system is suggested to be ***crosscut*** by deposit-scale mineralized vein arrays and is crosscut by reactivation of these vein systems as vein-parallel faults (Fig. 8.1D). The characteristics of these vein arrays and fault systems were described in Chapter 6, where they were grouped into domains and used to establish deformational phases. Of the two established phases the first, Phase I, is related to vein mineralization and the second, Phase II, is related to a period of brittle faulting that is closely associated with proposed large magnitude displacements along the West Fault.

Phase I is a significant contributor to the molybdenum mineralization at the Chuquicamata deposit. Of the molybdenite-bearing structures, the most spectacular are the

large quartz-molybdenite vein arrays that are parallel to and are parallelled by fault sets in individual structural domains. The patterns of these fault sets and vein arrays imply a structural setting of the Chuquicamata district at the time of their formation. From the observed geometries of the fault-veins, the quartz-molybdenite vein array and subsequent vein mineralization were proposed to have formed during a transtensional to simple shear deformation event.

The geometrical relationships of the observed fault-vein systems which are associated with the mineralization and deformation of Phase I, are similar to those which are predicted to form in strike-slip to transtensional deformation systems (Sanderson and Marchini, 1984; Woodcock and Schubert, 1994; Freund, 1974). These fault relationships have also been described from natural systems in Iran (Tchalenko, 1970), Sumatra and California (Tikoff and Teyssier, 1994); northern Chile (Lindsay et al., 1995; Reutter et al., 1996), in granitic rocks (Granier, 1985), and at a variety of scales (Tchalenko, 1970; Hempton and Neher, 1986; Bürgmann and Pollard, 1994; Arboleya and Engelder, 1995).

The vein array mineralization phase is associated with continued dextral deformation of the established strike-slip setting and the probable emplacement of an intrusion at depth within the extending zone. Mineralizing fluids that evolved from this magma used already established fracture systems to guide the associated mineralizing fluids. The preferred fracture planes are oriented NNE to NE in the northern half of the mine, trending parallel to the finer stockwork/veinlet systems of the initial mineralizing event (see above). Differing from the stockwork mineralizing phase, the vein arrays were seemingly formed by continuous hydraulic fracturing pulses, which would account for the observed crack-seal textures. The elliptical sub-radial pattern of these larger vein arrays mimics that of the finer veinlets and indicates a NW-SE to WNW-ESE extension direction. Dextral slip along fault systems associated with the vein arrays was suggested to have occurred based on the presence of low-angle shear veins along fault planes of domain B. This relationship is difficult to confirm due to later brittle faulting events. Fault slip during or following vein emplacement apparently offset the mineralized stockwork system and early formed alteration zones. A pervasive quartz-sericite-(kaolinite) alteration, ca. 31 Ma in age, parallels the

trends of the vein arrays and fault systems, crosscutting the inferred boundaries of potassic and propylitic alteration zones and the initial stockwork system. This alteration clearly postdates the stockwork and is possibly associated with the final stages of vein array formation, appearing related to the formation of a zone of megabreccia that is central to the open pit. The megabreccia is host to large blocks of quartz-molybdenite vein rock and blocks of host porphyry that are interpreted from ghost- rock textures and veinlet systems. The formation of the breccia and its associated alteration phase may be related to a fluid generated by a subsequent magma pulse, or a brecciation associated with fault motion and pumping of hydrothermal fluids. In any case, the vein arrays, fault systems and megabreccia were hydrothermally altered to quartz-sericite-(kaolinite) ca. 31 Ma (Reynolds et al., in press) in association with an established dextral strike-slip fault system.

8.2.3 Interpretation of the Alteration-Mineralization Sequence

The crosscutting and overprinting nature of mineralized veins and veinlets and the occurrence of alteration zones lead to several possible generalized mineralization models. Often these models are based solely on the deposit-scale map patterns (Reutter et al, 1993), or on the alteration zone which contains abundant mineralization (eg. Lopez, 1939, 1942; Perry, 1952, Ramirez, 1993). Of the several possible mineralization models that can be proposed for the Chuquicamata deposit, the most probable model is presented here, based on interpretations from this study and available geochronology.

The initial alteration phase of the mineralized system was K-metasomatism that is related to the latest stage of cooling, crystallization and deformation of the host porphyry. Our geochronological data shows this event to have occurred at about 33.4 Ma (Reynolds et al., in press). Approximately concurrent with this phase is the formation of a brittle fracture system that hosts a mineralized veinlet sequence that is typical of porphyry-copper-type deposits. This mineralization formed as the host porphyry cooled through plastic-brittle deformation conditions as shown by its crosscutting relationships with ductile-brittle shear zones, and is considered to be related to late stage magmatic processes associated with the rapid cooling of the host porphyry. Interpretations at this scale of mineralization are often

overlooked in place of the larger fault-vein array patterns (Ramirez, 1993; Reutter et al., 1996). This stockwork is representative of a relatively deep (3-5 km) and hot (>350°C) mineralization system that cooled, and in the process emplaced veinlets with sericitic halos, indicating relatively different fluid compositions and probable cooler (250°C?) fluid temperatures. The cooling of this system was probably accompanied by uplift and exhumation of the magmatic arc that may have been associated with the deepening of the magmatic system (Zentilli et al., 1995).

Subsequent mineralization, as represented by vein arrays, was probably associated with the emplacement of a yet unencountered magma body at depth. Observed mineralization at this stage of large vein arrays, includes spectacular quartz-molybdenite veins followed by pyrite and pyrite-enargite vein systems all of which represent a vertical zonation of a high-level vein system associated with an underlying porphyry system. This vein system is closely associated with an obvious deposit-scale fault pattern and an extensive quartz-sericitic alteration zone that formed at about 31 Ma. The high-level vein arrays, which crosscut the potassic alteration and associated stockwork system, are spatially associated with the quartz-sericitic alteration, whose extensiveness implies the circulation of large volumes of hydrothermal fluids through the permeability network provided by the vein arrays and fault systems. This phyllic alteration overprints the earlier potassic alteration and stockwork system. Concluding this 31 Ma mineralization phase are the enargite-pyrite veins, which appear closely associated with extension, normal to the West Fault. This mineralization is the subject of ongoing studies by Chuquicamata geologists.

Field evidence of crosscutting relationships between distinct styles and scales of mineralization, which are representative of their conditions and environments of formation, indicates at least two episodes of magmato-hydrothermal mineralization and alteration at Chuquicamata. Geochronology of alteration assemblages associated with each scale of mineralization corroborates this interpretation by indicating an earlier potassic alteration age of about 33.4 Ma and a later quartz-sericitic alteration age of about 31 Ma.

8.3 Dissection and Displacement

Regional studies have often been concerned with the possible displacement of the "other half of Chuquicamata"or its implications for other mineralized zones occurring along the West Fault (Ambrus, 1979, Reutter et al., 1991, 1993, 1995, 1996; Dilles et al., 1997; Tomlinson and Blancos, 1997a, 1997b). Post-stockwork mineralization dextral deformation on NE-striking faults at Chuquicamata appears to displace the copper-bearing stockwork system (Fig. 8.1E). The displacements may have accompanied the emplacement of the large fault-vein arrays, which have textures that indicate incremental formation. Slip along these same structural features generated fault gouges and breccias that suggest this dextral slip continued at least until the 31 Ma hydrothermal event that created the quartz-sericite alteration zone, which is not offset by dextral displacements. An inversion of the West Fault from a dextral-slip to sinistral-slip system occurred sometime after 31 Ma. The sinistral deformation foliated the quartz-sericite alteration zone immediately adjacent to the West Fault and offset the supergene enrichment basin by tens of metres along several NW-trending subsidiary faults. Sinistral displacements began between 31-25 Ma, a range constrained by the quartz-sericitic alteration phase (this work) and the development of a transtensional basin with interbedded 25 Ma tuffs north of Chuquicamata (Tomlinson and Blanco, 1997a), and continued until at least 19-15 Ma, which is the age range of supergene enrichment (Sillitoe and McKee, 1996). This long-lasting, brittle sinistral event, associated with displacements of ca. 35-37 kilometres, overprints and obscures evidence of any earlier association the West Fault may have had with dextral displacements and mineralization events.

8.4 Preferred Evolutionary Model for the Emplacement and Mineralization of Chuquicamata

The Domeyko Cordillera is a region that has at different times undergone orogen-normal and orogen-parallel deformation (Maksaev and Zentilli, 1988; Maksaev, 1990; Reutter et al., 1991; Tomlinson et al., 1994; Tomlinson and Blanco, 1997a, 1997b) and has been a locally transpressional to transtensional tectonic setting. The Chuquicamata district itself has undergone strike-slip deformation since the Eocene-Oligocene with the emplacement, mineralization and alteration of the Chuquicamata Intrusive Complex and the associated Chuquicamata and Radomiro Tomic porphyry copper deposits. Evidence from field mapping within the Chuquicamata deposit suggests that the host porphyry intruded an active dextral strike-slip fault zone to high crustal levels (epizonal). The rapid cooling and crystallization of the host porphyry and subsequent magmas at deeper levels resulted in the exsolution of volatile-rich aqueous fluids, which at supralithostatic pressures ruptured the confining crystalline host rock releasing mineralizing fluids into permeable fracture systems (see Burnham, 1979; Phillips, 1984). The mineralized fracture system at Chuquicamata is observed as a sequence of veinlets. From studies of the El Salvador deposit in northern Chile, Gustafson and Hunt (1975) have shown that there is a characteristic sequence of veinlet formation in porphyry-type deposits. A consistent veinlet sequence was also described from the porphyry deposits of the southwestern United States (Titley et al., 1986; Titley, 1993, 1994). The orientations of these veinlet systems around porphyry deposits have been shown to be influenced by the regional tectonic setting, where fractures are perpendicular to the minimum principal stress (Rehrig and Heidrick, 1972; Titley and Heidrick, 1978; Heidrick and Titley, 1982). The orientations of the veinlets in the sequence at Chuquicamata are consistent with the expected fracture orientations in dextral strike-slip fault zones (eg. Sanderson and Marchini, 1984; Woodcock and Schubert, 1994; Schreurs, 1994). Similarly, large-scale vein arrays that are not common in porphyry copper deposits, follow similar trends and appear to crosscut the finer mineralized stockwork system. The mineralized stockwork and vein arrays are interpreted as distinct mineralizing events occurring approximately 2 million years apart. These mineralizing events formed within a strike-slip

tectonic setting that was produced by Eocene-Oligocene plate tectonic activity along the South American margin (Pilger, 1984; Pardo-Casas and Molnar, 1987; Maksaev, 1990; Scheuber and Reutter, 1991). Inversion of this strike-slip fault system, during the Oligocene-Miocene displaced the supergene enrichment and earlier formed alteration-mineralization zones in a sinistral sense. This deformation and displacement was concentrated along and within the West Fault.

Chapter 9. Conclusions

Geological data from the Chuquicamata porphyry copper deposit has lead to the following conclusions concerning the structural control on the emplacement, sequences of alteration and associated scales of mineralization, and deformation exhibited by the current exposure of this deposit.

Shear zones internal to the Chuquicamata host rock and parallel to its eastern contact with Mesozoic country rocks display ductile to ductile-brittle deformation and are crosscut by mineralized fractures. The internal shear zones are composed of a set of low-angle NW-striking reverse faults and a series of high-angle NNE-SSW and NE-SW-trending dextral strike-slip faults. These and the dextral strike-slip shear fabrics associated with the contact zone indicate that the Chuquicamata complex has undergone deformation following and possibly during its emplacement and initial alteration, but prior to its mineralization. The kinematics and geometries of the observed ductile shear zones are consistent with those established through numerical and physical (claybox/sandbox) experimental models for strike-slip to transtensional fault systems. The Chuquicamata Complex is therefore proposed to have been emplaced within a strike-slip fault system that was active during the evolution of the Eocene-Oligocene magmatic arc.

The alteration configuration at Chuquicamata does not follow accepted model patterns where phyllic alteration zones occur between a core potassium silicate zone and a propylitic zone (eg. Lowell and Guilbert, 1970). Rather, the pattern at Chuquicamata results from the existence, or formation of permeability conduits during a hydrothermal event that produced a texture-destructive quartz-sericitic (phyllic) alteration phase. The distribution of this alteration phase highlights the areas of the deposit where greatest structural permeability existed, that is, along deposit-scale fault systems and internally-fractured large-scale vein arrays. These fault systems and vein arrays allow the quartz-sericitic alteration to crosscut the potassic and chloritic alteration zones that are related by a transitional contact. Quartz-sericitic alteration, radiometrically dated at about 31 Ma, establishes a relative temporal relationship between fault systems and vein arrays that existed prior to, or formed during this

hydrothermal event and those which formed following this event.

Mineralization within the deposit is observed as a stockwork or veinlet system, where individual veinlets are usually <5 mm in width, and as vein arrays, where individual veins are usually much greater than 10 cm in width. The stockwork system, which is emplaced within a host rock bearing potassic alteration that formed at about 33.4 Ma, is composed of a series of veinlets that based on crosscutting relationships have a definable emplacement sequence. Earliest veinlets are quartz±K-feldspar (A) followed in order by quartz (A), quartz+molybdenite (B), quartz+Cu-Fe sulphides (B), Cu-Fe sulphides (D) and Cu-Fe sulphides+sericitic alteration halo (D). As indicated, this sequence of veinlets may be classified into Gustafson and Hunt's (1975) A-, B- and D-type veinlet categorization. The veinlet sequence, which is typical of porphyry copper deposits, indicates an evolution of the mineralizing fluids through time that has been tentatively confirmed by a radiometric age of 32.1 Ma on a sericitic veinlet halo. Individual veinlets show preferred orientations that are spatially distinct within the open pit. The northern sector has veinlets that dominantly trend NNE to NE, the northeastern sector is dominated by NE-trending veinlets and the southern area shows NNW veinlet trends. The mineralized fractures formed as extensional (NE) and shear-extensional (NNE and NNW) fractures by way of hydrofracturing that was influenced by the regional stress field acting on the host rocks.

The larger-scale mineralized vein arrays are spatially associated with vein-parallel fault systems and texture-destructive quartz-sericitic alteration that is visually distinct (whitish-buff) from the sericitic alteration associated with the stockwork veinlet system. This mineralization sequence is dominated by quartz-molybdenite veins that are crosscut by enargite-rich +pyrite ±sphalerite veins and pyrite-dominated (+chalcopyrite ±chalcocite ±covellite) veins. The relationship between the latter vein types is unclear but a vertical relationship is probable, that is the enargite-rich veins may be emplaced at a higher level than the pyrite-dominated veins. Directional data for these vein types, as that of the veinlets, establish preferred orientations, or an anisotropy, of the contained mineralization. These orientations coincide with dominant fault trends within mining sectors, or structural domains.

Kinematic data and fault system relationships within the deposit define two major deformation events within the West Fault Zone. The first is associated with successive mineralization phases that occurred on distinct scales and provided permeability networks to hydrothermal fluids during alteration and mineralization. This deformation event is characterized by: dextral ductile deformation fabrics associated with the emplacement and subsequent deformation of the host intrusions, mineralized fracture systems whose preferred orientations indicate that regional stress patterns associated with a dextral fault systems influenced the mineralized hydrofracture system, and the kinematics of deposit-scale brittle fault systems (domains) that host the majority of molybdenum mineralization and indicate a that the fault-vein systems formed within a regional dextral strike-slip fault zone. It is the continued deformation along the regional fault system that has localized the emplacement and the multiple mineralization events that have been determined for Chuquicamata, making this one of the world's giant ore deposits. The second major deformation event resulted in the formation of brittle fault domains that are kinematically distinct and indicate a sinistral displacement within the same regional fault zone. This sinistral fault zone is best known as the West Fault, which is characterized by strongly foliated fault gouges that incorporate and deform a large volume of the laterally adjacent quartz-sericitic alteration zone.

The structural model proposed within this study involving a dextral simple shear to transtensional strike-slip fault system, during most if not all of the mineralization episodes, that was later reactivated as a brittle sinistral strike-slip fault system confirms other more regional scale geological studies and indicates a link between plate tectonic associated deformation and localized magmato-hydrothermal systems.

Appendix 1. Structural Sampling Database

This appendix lists the database constructed from the sampling of individual study sites. Veinlet types correspond to those listed in Table 5.1, mineral abbreviations and veinlet types not in Table 5.1 are listed below.

A = exposed fracture surface
x = XIS = unmineralized shear fracture
alun = alunite
py = pyrite
cc = chalcocite
cv = covellite
cp = cpy = chalcopyrite
hm = hematite
dg = digenite
gyp = gypsum
moly = mo = molybdenite
qmo = quartz-molybdenite
qtz = quartz
Kfld = K-feldspar
ser = sericite
sulf = sulphide
lim = limonite
qs = quartz-sericite
frac = fracture
wht = white
W = chlorite-gypsum
V = chlorite
U = chlorite-epidote
T = limonite

STRUCTURAL SAMPLING SITE DL94-A (SK) - 1994

N4957 E3748 c2618 I3N

No.	Strike	Dip	Width	Type	Note
1	66	46	10	v4	main vn,alun, pycc
2	55	40	10	v4	main vn
3	36	72	0.3	v6	halo no sulf??
4	42	60	0.5	v2	w/ gyp cut sulf stringer
5	75	66	0.2	v5	stringer cuts qtzeye
6	25	90	0.4	v4	channel
7	35	90	0.0	v2	late py cc
8	205	85	1.0	v4	central channel
9	356	62	0.3	v4	cc cut by qtzpy with vughs
10	190	82	1.0	v4	central pycccpy?vugs
11	185	80	1.0	v2	<3% sulf
12	227	86	1.0	v2	<3% sulf
13	358	53	0.3	v4	cc vnlt cut by qtzpy
14	107	55	0.0	v4	pycc red stain
15	50	80	0.3	v2	py <1%
16	16	88	1.0	v4	cc centre
17	90	85	0.2	v5	stringer
18	100	57	0.2	v5	stringer
19	50	86	0.2	v2	stringer cut by sulf
20	73	74	0.2	v5	stringer py cc
21	135	50	2.0	v6	pylimqs halo green
22	55	90	0.0	v6	py lim centre
23	352	58	0.1	v	stringer
24	349	57	0.1	v5	pycclim stringer
25	214	80	1.0	v2	late pycc
26	83	68	0.3	v2	mo??
27	35	84	0.0	v5	vein
28	160	75	0.0	A	
29	267	67	0.3	alun	frac in qtz vn
30	278	65	0.3	alun	frac in qtz vn
31	183	46	0.0	v4	central sulf wht qtz
32	55	46	0.0	v4	central sulf pycccv wht qtz
33	165	43	0.3	v2	wht qtz cpy?
34	58	50	0.0	v4	wht qtz sulf central
35	50	64	2.0	v6	qtz pycc
36	37	52	2.0	v6	qtz py cc
37	69	58	3.0	v6	wht qtz pycccpy vugh
38	53	54	1.0	v6	cuts megacrystals
39	116	70	0.0	v6	wht qtz py
40	65	50	0.1	v5	stringer
41	68	50	1.0	v6	wht qtz py
42	65	66	1.0	v5	py stringer
43	112	85	1.0	v6	pycc cut by halo(wht qtz)
44	73	60	2.0	v6	wht qtz sulf
45	96	44	2.0	v6	wht qtz pycc ribbon
46	70	72	0.1	v5	stringer
47	75	82	0.1	v5	stringer
48	60	55	0.0	v4	wht qtz pycccv centre

STRUCTURAL SAMPLING SITE DL94-A (SK) - 1994

No.	Strike	Dip	Width	Type	Note
49	72	30	0.3	v4	wht qtz py centre
50	156	38	0.3	alun	
51	63	50	1.0	v6	wht qtz pycc
52	70	55	0.2	v5	stringer
53	340	65	0.2	v5	stringer
54	65	62	0.0	v6	qtz pycc
55	51	65	1.0	v6	qtz sulf
56	66	52	2.0	v6	wht qtz sulf
57	63	54	2.0	v6	wht qtz sulf
58	68	44	2.0	v6	wht qtz sulf
59	64	46	0.3	v4	wht qtz pycc
60	82	37	0.3	v4	
61	45	37	0.1	v2	stringer
62	85	42	0.5	v2	sulf alun
63	90	40	0.2	v5	stringer halo??
64	80	55	0.1	v5	stringer
65	83	55	0.1	v5	stringer
66	87	41	0.3	v4	
67	108	90	0.2	v4	
68	65	33	0.2	v4	
69	208	72	3.0	v2	wht qtz
70	90	62	1.0	v6	stringer py cc
71	50	26	0.1	v2	stringer
72	56	48	0.3	v3	
73	164	83	0.0	A	
74	156	83	0.0	A	
75	205	53	0.0	A	
76	204	65	0.0	A	
77	195	80	0.0	A	
78	125	46	0.0	A	
79	161	79	0.0	A	
80	123	62	0.0	A	
81	345	78	0.0	A	
82	175	45	0.0	A	
83	109	40	0.0	A	
84	152	69	0.0	A	
85	156	77	0.0	A	
86	200	64	0.0	A	
87	183	50	0.0	A	
88	116	48	0.0	A	
89	54	72	0.0	A	
90	197	86	0.0	A	
91	170	82	0.0	A	
92	125	50	0.0	A	
93	300	88	0.0	A	

STRUCTURAL SAMPLING SITE DL94-B (SK) - 1994

N4918 E3753 c2621 I3N

No.	Strike	Dip	Width	Type	Note
1	214	68	2.0	v2	ribbon texture
2	95	71	0.5	v6	green halo wht qtz centre c
3	48	90	0.0	v6	appears cut by qtz rib????
4	97	68	0.4	v6	wht qtz centre cc cv?
5	72	75	0.3	v6	no qtz centre
6	64	82	0.3	v5	sulf veinlet
7	218	85	0.2	v4	sulphide fine grained black
8	82	65	0.4	v6	sulphide veinlet halo
9	68	68	0.4	v6	sulf wht qtz halo
10	67	74	0.5	v4	qtz central sulf
11	187	85	0.1	v5	veinlet
12	197	77	0.1	v5	stringer
13	84	70	0.4	v6	wht qtz cc cv halo
14	60	73	1.0	v6	wht qtz sulf halo cuts sulf
15	90	80	0.5	v6	sulf halo
16	87	70	0.5	v6	wht qtz sulf centre halo
17	103	80	0.0	v5	parallel qtz "sil"band
18	212	65	2.0	v3	qtzribbon lam Mo cut by all
19	100	66	0.5	v4	py cc cv sulf + qtz
20	43	66	0.0	v2	qtz +<1%sulf cc
21	208	65	2.0	v3	
22	80	74	0.5	v6	wht qtz sulf centre halo
23	205	72	0.0	v2	
24	86	56	0.2	v5	
25	15	68	0.4	v4	
26	80	61	0.1	v5	stringer
27	187	35	0.2	v2	
28	80	67	0.1	v5	
29	111	55	0.2	v5	
30	95	89	0.3	v5	
31	94	66	2.0	v6	qtz mo ??? halo
32	87	60	1.0	v6	qtz sulf halo
33	35	42	0.4	v6	sulf centre
34	2	30	0.2	v2	
35	93	65	0.4	v6	sulf centre
36	75	49	0.1	v5	stringer
37	72	56	0.1	v5	stringer
38	21	63	0.2	v2	
39	78	53	0.1	v5	
40	80	70	0.1	v5	
41	70	77	0.1	v5	
42	59	83	0.1	v5	
43	83	70	0.5	v6	qtz wht sulf chan halo
44	88	80	0.5	v6	wht qtz sulf centre halo
45	54	70	0.3	v5	py cccv
46	20	72	0.3	v4	

STRUCTURAL SAMPLING SITE DL94-B (SK) - 1994

No.	Strike	Dip	Width	Type	Note
47	100	64	0.3	v6	qtz sulf through megacrystal
48	98	43	0.1	v5	
49	35	45	0.2	v5	
50	10	85	0.5	v6	wht qtz sulf halo
51	235	90	0.5	v6	sulf
52	84	51	0.3	v4	wht qtz sulf centre
53	76	70	0.1	v5	
54	61	90	0.0	v3	ribbon texture lam mo?
55	85	68	0.3	v5	pycccv
56	10	85	0.3	v4	fine halo?
57	47	90	1.0	v3	
58	357	50	0.2	v2	
59	85	70	0.1	v5	
60	190	82	1.0	v3	
61	270	80	1.0	v6	wht qtz sulf halo
62	65	55	1.0	v6	sulf halo
63	85	77	4.0	v6	wht qtz py centre halo
64	112	70	0.5	v6	py gyp halo
65	200	70	4.0	v2	wht qtz
66	193	74	0.0	A	
67	107	70	0.0	A	
68	110	83	0.0	A	
69	98	75	0.0	A	
70	187	85	0.0	A	
71	110	75	0.0	A	
72	108	84	0.0	A	
73	105	70	0.0	A	
74	179	80	0.0	A	
75	215	46	0.0	A	
76	208	73	0.0	A	
77	201	70	0.0	A	
78	183	73	0.0	A	
79	81	50	0.0	A	
80	93	73	0.0	A	
81	195	80	0.0	A	
82	12	64	0.0	A	
83	182	90	0.0	A	

STRUCTURAL SAMPLING SITE DL94-C (K) - 1994
N5100 E3500 c2619 I3N

No.	Strike	Dip	Width	Type	Note
1	190	52	0.2	v2	qtz
2	196	57	0.1	v2	qtz stringer
3	195	63	0.2	v2	qtz through mega Kfd
4	275	71	1.0	v6	halo sulf w/ halo py (cc)
5	285	84	1.0	v6	halo pycc +-qtz halo
6	288	40	0.5	v5	sulf pycc ox brown lim cuts halo
7	196	54	0.3	v2	qtz
8	198	55	0.2	v3	qmo mo
9	95	86	0.4	v6	halo cc green yellow halo
10	95	80	0.1	v5	sulf discontinuous stringer
11	278	83	2.0	v6	halo series of stringers in halo
12	105	90	0.4	v5	sulf coarse py(cc) lim
13	197	59	1.0	v2	qtz
14	202	60	0.2	v3	qmo mo??
15	192	66	0.1	v5	sulf stringer
16	195	58	1.0	v2	qtz
17	203	50	0.3	v2	qtz
18	205	60	2.0	v6	halo dark green halo to sulf (py
19	190	52	3.5	v2	qtz
20	179	45	0.1	v5	sulf stringer
21	195	38	0.2	v2	qtz
22	90	90	0.1	v5	sulf stringer
23	180	50	0.2	v2	qtz
24	185	42	0.2	v2	qtz
25	188	56	1.0	v6	halo sulf halo
26	290	85	0.4	v6	halo pycc halo
27	262	60	0.2	v4	qtzpy
28	166	30	0.1	mo	other mo-cpy
29	180	46	1.0	v3	qmo mo edges?
30	120	67	1.0	v5	sulf py cc ox stain lim
31	195	55	0.5	v2	qtz
32	195	70	0.4	v3	qmo
33	290	80	0.5	v6	halo sulf stringer halo
34	10	90	0.2	v5	limonite?
35	20	82	0.3	v3	qmo
36	184	74	0.5	v2	qtz
37	97	83	1.5	v6	halo sulf halo
38	166	35	0.1	mo	other moly
39	175	45	0.2	v3	qmo
40	285	84	0.3	v6	halo pycc stringer halo
41	290	78	0.3	v6	halo sulf stringer halo
42	280	80	0.3	v6	halo sulf stringer halo
43	182	45	1.0	v3	qmo mo edges appears to cut halo
44	282	80	0.3	v6	halo py halo
45	174	57	0.5	v2	qtz
46	180	53	0.3	v2	qtz
47	233	62	0.2	v2	qtz

STRUCTURAL SAMPLING SITE DL94-C (K) - 1994

No.	Strike	Dip	Width	Type	Note
48	198	71	0.3	v2	qtz
49	275	88	0.1	v5	sulf stringer appears cut by qtz
50	280	88	1.0	v6	halo sulf halo
51	277	86	0.3	v6	halo sulf
52	288	84	0.2	v6	halo py
53	156	40	0.1	v2	qtz stringer
54	256	33	0.1	v2	qtz stringer
55	164	43	0.5	v2	qtz
56	286	90	0.2	v6	halo sulf stringer
57	190	54	0.3	v3	qmo
58	186	68	0.2	v3	qmo
59	287	90	0.2	v6	halo sulf stringer
60	293	85	0.2	v6	halo sulf stringer
61	285	80	0.4	v6	halo sulf halo limonitic dis py
62	284	90	1.0	v6	halo sulf with dis py?
63	274	90	0.3	v6	halo sulf halo dis py
64	272	90	0.5	v6	halo sulf halo dis py
65	276	88	1.0	v6	halo sulf halo dis py
66	172	46	4.0	v2	qtz
67	174	44	1.0	v3	qmo
68	257	90	0.5	v6	halo pycc halo
69	286	83	1.0	v5	sulf pycc lim cuts qmo
70	183	52	1.0	v3	qmo
71	285	85	1.0	v6	halo sulf
72	194	65	0.2	v3	qmo
73	173	47	0.1	v2	qtz
74	60	90	0.0	x	ductil biotite foliation
75	286	88	0.5	v6	halo sulf
76	95	82	1.0	v6	halo sulf
77	295	88	0.4	v6	halo sulf
78	278	72	0.4	v6	halo sulf
79	271	79	0.1	v5	sulf stringer
80	290	90	1.5	v6	halo sulf
81	292	82	2.0	v6	halo coarse pycc lim
82	258	90	0.0	x	ductile qtz eye elongation
83	97	28	0.1	mo	other mo cpy surface
84	158	43	0.4	v2	qtz
85	282	83	0.5	v6	halo sulf
86	285	75	0.5	v6	halo sulf
87	254	70	0.0	x	ductile foliation biotite-qtz eye
88	170	47	0.2	v2	qtz
89	282	82	1.0	v6	halo sulf
90	278	87	1.0	v6	halo sulf
91	278	90	1.0	v6	halo sulf
92	273	87	1.0	v6	halo sulf
93	265	70	0.0	x	ductile biotite foliation
94	170	44	1.0	v3	qmo
95	268	90	2.0	v6	halo sulf stringers series halo
96	190	57	0.2	v2	qtz

STRUCTURAL SAMPLING SITE DL94-C (K) - 1994

No.	Strike	Dip	Width	Type	Note
97	172	50	0.3	v3	qmo
98	275	88	0.2	v5	sulf py cc lim
99	288	43	0.5	v5	sulf late cuts halos pycc feox
100	287	78	0.4	v5	sulf late sulf cuts/joins #274
101	96	75	0.0	A	recent
102	43	35	0.0	A	recent
103	45	20	0.0	A	recent
104	43	80	0.0	A	recent
105	37	66	0.0	A	recent
106	203	77	0.0	A	recent
107	90	78	0.0	A	recent
108	35	85	0.0	A	recent
109	95	80	0.0	A	recent
110	325	15	0.0	A	recent
111	30	20	0.0	A	recent
112	5	78	0.0	A	recent
113	108	63	0.0	A	recent
114	111	65	0.0	A	recent
115	40	90	0.0	A	recent
116	260	78	0.0	A	recent
117	35	83	0.0	A	recent
118	100	84	0.0	A	recent
119	253	47	0.0	A	recent
120	37	77	0.0	A	recent
121	35	65	0.0	A	recent
122	100	88	0.0	A	recent
123	30	85	0.0	A	recent
124	340	90	0.0	A	recent
125	18	80	0.0	A	recent

STRUCTURAL SAMPLING SITE DL94-D (SK) - 1994
N4971 E3415 c2567 I3N

No.	Strike	Dip	Width	Type	Note
1	34	85	2.0	v3	qmo whtqtz ribbon mo lam displd
2	24	75	1.0	v2	qtz grey qtz finely disem mo ??
3	198	73	1.0	v3	qmo cuts qtz vein
4	308	46	0.4	v2	qtz
5	2	63	0.3	v2	qtz
6	277	74	0.5	v3	qmo
7	257	74	2.0	v3	qmo
8	5	72	0.4	v2	qtz
9	30	75	0.2	v3	moly moly veinlet
10	0	57	0.4	v2	qtz
11	83	83	0.2	v2	qtz
12	82	90	0.1	v3	moly moly veinlet
13	40	80	0.5	v3	qtz grey, finely dissem moly??
14	30	66	0.4	v2	qtz
15	18	60	0.4	v2	qtz
16	218	87	0.1	v5	sulf sulf stringer
17	25	79	1.0	v2	qtz
18	170	80	0.3	v3	qmo qtz with greyish core
19	259	22	0.2	v2	qtz
20	15	70	0.4	v2	qtz
21	65	90	0.1	v4	qsulf stringer
22	18	85	0.3	v5	sulf sulf stringer cutsarea vary
23	250	80	0.2	v4	qsulf cut mo
24	23	75	0.2	v4	qsulf
25	240	72	0.2	v4	qsulf
26	350	72	0.3	v2	qtz cutby qsulf
27	350	85	0.3	v2	qtz
28	24	75	0.1	v5	sulf stringer
29	197	76	0.1	v5	sulf stringer
30	0	85	0.3	x	shear mo shear, mo cv cc
31	178	81	0.2	x	shear mo shear
32	342	70	1.0	v2	qtz
33	16	50	0.3	v2	qtz
34	175	25	1.0	v2	qtz
35	12	84	1.0	v3	qmo
36	258	89	0.2	v4	qsulf
37	350	88	0.2	v5	sulf
38	245	85	0.1	v5	sulf
39	234	75	0.2	v3	qmo qtz mo center
40	0	57	0.4	v2	qtz
41	24	74	0.3	v2	qtz cut by qtzmo
42	15	54	0.2	v2	qtz
43	282	64	0.2	v5	sulf
44	329	40	0.2	v2	qtz
45	34	56	0.5	v3	qmo
46	236	75	0.2	v3	qmo cuts qmo
47	0	85	0.2	v3	qmo center

STRUCTURAL SAMPLING SITE DL94-D (SK) - 1994

No.	Strike	Dip	Width	Type	Note
48	20	72	0.4	v3	qmo lamin
49	10	55	0.2	v3	qmo lamin rect
50	90	80	0.2	v3	qmo center non-rect
51	15	34	0.1	v2	qtz rect
52	290	20	0.1	v2	qtz rect
53	345	65	0.4	v2	qtz
54	330	90	0.1	v5	sulf minor mo? cuts qtz
55	164	80	0.3	v2	qtz grey cut by wht
56	16	61	0.4	v2	qtz
57	355	53	0.4	v2	qtz
58	245	78	0.2	v4	qsulf
59	17	65	0.2	v4	qsulf minor mo?
60	25	48	1.0	v3	qmo
61	92	84	0.1	v5	sulf stringer
62	185	88	0.0	A	recent shatter zone shear?
63	92	84	0.0	v3	qmo qtzmo shear pitch 28w
64	0	80	0.3	v3	qmo center
65	25	76	0.2	v5	sulf shear??
66	10	36	0.4	v2	qtz grey
67	243	68	0.5	v2	qtz cuts qtzmo center
68	341	61	0.3	v2	qtz
69	236	88	0.3	v3	qmo center
70	104	60	0.0	v3	qmo cc shear leftsidesite pitch
71	68	77	0.0	x	shear shear
72	40	70	0.0	x	shear shear
73	248	90	0.0	x	shear shear
74	253	74	0.0	x	shear shear dextral

STRUCTURAL SAMPLING SITE DL94-E (SK) - 1994
N4481 E3674 c2541

No.	Strike	Dip	Width	Type	Note
1	45	73	3.0	v6	qtz vfine grain black cc?
2	48	79	2.0	v6	qtz cc dissem sulf in halo
3	230	40	1.0	v6	
4	228	30	1.0	v6	
5	248	82	0.2	v4	irreg diss cc?
6	60	75	0.1	v5	v fine black cc?
7	46	83	0.3	v4	central channel sulf cc
8	62	70	0.1	v4	
9	55	60	0.2	v4	
10	172	31	0.3	v2	
11	48	58	0.1	v5	
12	40	71	0.1	v5	
13	192	75	0.0	x	shear, sense?
14	197	68	0.0	x	shear, sense?
15	172	74	0.0	x	
16	51	72	1.0	v6	sulf disem cc qs halo
17	150	82	0.3	v4	central sulf channel
18	47	75	0.2	v4	sulf center of veinlet
19	45	65	0.2	v4	
20	48	80	0.1	v4	
21	90	76	0.2	v4	
22	164	42	0.3	v2	
23	104	85	1.0	v2	
24	195	78	0.3	v5	
25	71	60	0.2	v4	
26	57	83	0.2	v4	
27	66	84	0.2	v4	
28	43	76	1.0	v2	qtz with late sulf stringer
29	55	82	1.0	v2	cuts sulf dis halo and qtz
30	165	36	0.2	v2	
31	60	85	0.1	v5	stringer
32	225	90	2.0	v6	qtz disem sulf halo sil
33	95	55	0.2	v4	central sulf
34	92	68	0.2	v4	
35	95	56	0.3	v4	central sulf edge of halo /
36	95	80	0.3	v4	central channel
37	130	70	0.0	x	shear, pitch 28w SIN
38	220	30	0.0	v4	slip surf cccv? qtz
39	115	40	0.1	v5	stringer
40	98	85	0.2	v4	central sulf channel
41	145	61	0.1	v2	
42	176	70	0.2	v4	central sulf
43	73	61	0.5	v4	central
44	126	44	0.0	x	slip surface
45	159	85	0.2	v2	
46	45	70	0.1	v4	central sulf
47	41	68	0.1	v5	stringer

STRUCTURAL SAMPLING SITE DL94-E (SK) - 1994

No.	Strike	Dip	Width	Type	Note
48	56	82	0.2	v5	sulf strngr irreg qtz conc
49	63	85	0.1	v5	stringer
50	76	90	0.3	v2	
51	50	63	0.1	v2	
52	174	78	0.0	x	
53	92	85	1.0	v2	qtz rib late sulf
54	261	84	0.1	v5	stringer
55	76	80	0.5	v2	late sulf
56	131	45	0.0	x	black vfine grn sil? slip 2
57	135	50	0.1	v5	
58	75	35	0.1	v4	
59	75	30	0.3	v4	
60	86	52	0.3	v4	
61	74	55	0.4	v2	
62	60	62	1.0	v2	
63	140	38	0.5	v2	late sulf
64	220	90	1.0	v2	late sulf
65	54	77	0.3	v2	
66	73	80	0.3	v2	
67	64	58	5.0	v4	stringer zone
68	35	80	1.0	v4	
69	200	74	0.0	x	shear, pitch 20w

STRUCTURAL SAMPLING SITE DL95-G (K) - 1995
N4837 E3525 c2522 K3N

No.	Strike	Dip	Width	Type	Note
72	21	80	1	mo	
73	65	60	0.001	mo	frac surface mo rake 05NE
46	72	50	10	v1	aplite
15	65	50	12	v1	aplite
35	20	38	3	v1	qtz (aplite)
38	70	70	2	v1	qtz aplite
29	70	73	0.5	v1	qtz aplite
3	25	44	10	v1	qtz aplite cut by min
74	320	51	15	v1	kf cut by py qs halo, qtz(cppy)
1	70	59	30	v1	aplitic dike cut by veinlets
27	70	33	4	v2	qtz
26	100	59	4	v2	qtz
17	45	87	0.5	v2	qtz
14	85	62	5	v2	qtz discont. cut by min
42	38	51	5	v2	qtz
43	304	82	1	v2	qtz
94	201	24	1	v2	qtz
13	238	90	10	v2	qtz
88	324	68	1	v2	qtz
80	150	57	6	v2	qtz
81	169	70	4	v3	qtz mo cut by py qs halo, offset dextrally
84	168	80	1.5	v3	qtz mo
85	165	84	1	v3	qtz mo cut by qs halo (sulf)
59	172	81	3	v4	qtz pyhmmo
12	48	35	2.5	v4	qtz py
18	155	84	5	v4	qtz pycp
69	327	27	0.5	v4	qtz py sin displaced by qtz(cppy)
70	82	40	7	v4	qtz (cppy) cut by cppy qtz qs
45	84	55	2	v4	qtz py
76	48	69	3	v4	qtz (cppy)
39	60	74		v4	qtz pycp weak ser?
40	55	78		v4	qtz py ser
28	70	60	2	v4	qtz sulf?
25	54	34		v4	qtz py cuts all striae 15->254
57	152	54	0.001	v5	pycc surface disem py and soot
4	56	74	1	v5	py no halo
54	322	78	0.2	v5	py
65	60	76	1.5	v5	pycp weak halo
6	60	70	0.7	v5	py
48	105	87		v5	dg?cv striae 15->254, fracture surface
5	67	73	1	v5	pycp
9	65	80	0.5	v5	py ox no halo
16	62	87	3	v5	py(mo) weak halo
20	67	70	0.5	v5	py(cp) sil halo
19	237	87	0.4	v5	py weak halo
68	320	45	0.5	v5	py
10	62	75	3	v5	cppy

STRUCTURAL SAMPLING SITE DL95-G (K) - 1995

No.	Strike	Dip	Width	Type	Note
21	50	80	0.5	v5	py through mxx and aplite
71	67	74	10	v6	qtz cppy qs halo cuts qtz(cppy)
67	73	67	3	v6	py qs halo
66	60	74	4	v6	pycp qs white halo
86	75	78	2	v6	qs halo (sulf?)whitish halo
83	90	90	3	v6	py qs halo
82	60	75	3	v6	py qs halo
89	45	81	2	v6	py qs halo
90	78	76	4	v6	py qs halo
87	275	89	3	v6	halo
91	74	75	3	v6	py qs halo
78	70	62	2	v6	py white halo
77	55	76	8	v6	qtz py qs halo central channel
75	57	76	10	v6	py qs halo
92	114	16	2	v6	halo
79	70	69	3	v6	py white halo
93	71	60	2	v6	py qs halo
33	82	62	4	v6	qs
32	60	76	6	v6	pycp qs halo irreg halo cuts aplite
31	70	70	6	v6	pycp qs halo irreg halo
34	80	65	1	v6	py qs cc chalcocite =soot
41	73	70	1	v6	py qs halo
37	187	21	0.5	v6	qs py
36	75	58	3	v6	qs (py)
30	134	62	1	v6	py sil halo cc
8	58	60	3	v6	py qs halo
7	60	70	4	v6	py qs halo
2	45	90	10	v6	pycp qs halo min<1mm
11	64	80	3	v6	pycp qs halo
24	31	84	4	v6	py qs halo
23	50	79	5	v6	py qs halo
22	56	76	2.5	v6	py qs halo through mxx
60	75	70	2	v6	py qs halo
58	49	76	4	v6	py qs halo
56	80	76	3	v6	halo
61	67	69	6	v6	qtz py ser
64	71	73	3	v6	py qs halo
63	271	50	2	v6	halo cross cuts qshalo-py
62	65	65	2	v6	halo clay ??
55	48	79	4	v6	halo cut by late sulphide, halo of clay alt?
49	64	60	3	v6	py qs halo
47	73	70	3	v6	pycp qs halo
44	145	53	1	v6	py sil
50	89	44	10	v6	qtz py qs halo
53	70	79		v6	halo
52	65	65		v6	py cuts above halo
51	64	74		v6	py white halo

STRUCTURAL SAMPLING SITE DL95-H (SK-QS) - 1995
N4432 E3407 c2335 O1

No.	Strike	Dip	Width	Type	Note
1	57	78	10	v6	min 2mm halo 10mm
2	81	47	5	v6	halo 5mm, split from above
3	122	80	4	v2	cut by halo bearing veinlets
4	125	86	3	v2	
5	217	90	2.5	v4	no halo
6	313	65	0.8	v2	
7	127	72	10	v2	en echelon, bands
8	310	80	5	v2	
9	183	38	3	v2	
10	185	84	2	v2	cross cut by qtz trending e-w
11	346	68	1.5	v2	
12	335	45	2	v2	en echelon
13	300	72	2.5	v2	
14	313	76	3	v2	
15	24	65	1	v2	cuts 31376 offsets D doesnt offset pycc that crosses qtz
16	78	60	2	v5	cuts qtz
17	9	64	0.5	v2	
18	190	80	1.5	v5	cuts qtz post second qtz generation
19	210	87	10	v6	offsets qtz dex 1.5cm
20	50	68	10	v6	
21	118	85	10	v4	open channel qtz teeth
22	35	55	10	v6	
23	34	41	6	v6	
24	200	51	3	v4	central channel
25	66	54		v4	
26	220	85	0.5	v5	
27	24	66	4	v4	remobilized mo? cuts qtz
28	63	50	4	v4	central
29	52	76	7	v6	
30	56	66	3	v4	central
31	109	64	1.5	v2	between two larger
32	120	61	1	v2	
33	215	62	4	v2	banded
34	176	56		v2	striae on qtz 10->344
35	291	76	10	later	gyp sph en ga
36	185	60	15	v3	shattered
37	65	59	2	v5	through qtz no halo
38	190	75	2	v5	weak halo
39	184	75	3	v4	
40	50	90	2	v5	weak qs halo
41	214	88	10	v6	cc?
42	205	84	20	v3	
43	50	57	10	v6	
44	47	70	20	v3	late py and qs halo, appears cut by qtz
45	40	50	20	v6	cc?
46	297	81	1	v5	cuts all

STRUCTURAL SAMPLING SITE DL95-H (SK-QS) - 1995

No.	Strike	Dip	Width	Type	Note
47	310	74	3	v2	
48	338	42	3	v4	possibly qtz refractured then sulf
49	305	74	4	v2	
50	170	48	7	v2	
51	306	75	10	v2	
52	114	82	12	v2	
53	78	70	1	v5	discontinous
54	307	71	2	v2	
55	102	57	20	v1	
56	187	74	10	v6	weak halo
57	357	41	10	v6	cuts pyccqtz
58	340	56	3	v2	
59	164	60	3	v2	
60	65	70	2	v5	through qtz cuts north-south trend
61	320	20	10	v6	
62	60	62	20	v6	
63	56	34	3	v5	no halo appears to displace those pycc with halo
64	56	60	40	v4	central, internal slip
65	60	63	10	v6	
66	344	39	0.3	v5	discontinuous
67	300	57	8	v2	cuts and displaces dex 34958
68	349	58	6	v2	
69	305	58	2	v2	
70	340	54	2	v2	
71	306	50	2	v2	
72	355	45	1	v5	no halo
73	20	75	0.5	v5	discontinuous
74	218	82	0.5	v5	discont.
75	224	90	0.5	v5	
76	207	76	0.5	v5	
77	287	60	0.5	v5	
78	280	62	0.5	v5	
79	130	84	2	v2	
80	310	67	1	v2	
81	302	86	4	v2	
82	308	70	2	v2	
83	170	54	2	v2	
84	33	71	3	v2	
85	192	80	35	v2	diseminated mo flakes
86	343	32	30	v6	does not appear to cut through 19280 qtz
87	340	72	3	v6	weak halo
88	20	68	1	v2	
89	61	70	5	v6	no apparent min
90	63	61	1	v5	no halo
91	58	54	50	v6	halo green
92	60	66	1	v5	
93	48	68	2	v6	cuts qmo, remobilized mo?
94	43	52	10	v6	remobilized mo?

STRUCTURAL SAMPLING SITE DL95-I (K-SK) - 1995
N5434 E3489 c2778 F4N

No.	Strike	Dip	Width	Type	Note
1	0	86	20	v5	ccpy clay cc over py bounds site to east
2	171	87	4	v5	ccpy cc over py en echelon?
3	179	87	3	v5	ccpy irreg min pockets
4	208	54	1	v4	ccpy qtz
5	0	85	1	v5	ccpy discont min along fracture
6	245	84	3	v2	qtz central suture
7	80	85	2	v2	qtz
8	260	68	2	v2	qtz
9	55	51	0.5	v2	qtz cut by larger
10	103	56	1	v2	qtz cut by larger
11	253	85	0.5	v2	qtz through qtz eye
12	180	90	1	v5	ccpy discont min along trend
13	186	76	0.5	v5	limccpy
14	210	80	0.5	v5	lim ccpy
15	57	86	1	v5	lim ccpy
16	172	73	1	v5	lim ccpy
17	0	83	2	v5	ccpy
18	226	76	1	v5	ccpy
19	206	71	1	v5	ccpy
20	37	71	2	v5	ccpy
21	194	45	3	v5	ccpy
22	90	47	4	v2	qtz
23	76	64	4	v2	qtz
24	61	52	1	v2	qtz
25	173	72	0.5	v4	qtzcc cc late
26	167	75	0.5	v4	qtz cc cc late
27	184	54	2	v2	qtz
28	0	70	1	v4	qtz (cc)through qtz eyes
29	70	50	2	v4	qtz (cc)weak disemm cc
30	172	70	0.5	v5	cc discont along structure
31	172	77	0.5	v5	cc
32	190	66	0.5	v5	cc discont
33	48	64	3	v2	qtz
34	164	66	3	v6	pycc qs halo weak greenish halo
35	177	40	1	v4	qtz (cc) late cc?
36	23	85	2	v2	qtz
37	166	43	2	v2	qtz cut by pycc
38	184	90	4	v2	qtz
39	178	82	3	v5	pycc irreg wandering
40	182	42	4	v2	qtz
41	235	74	5	v2	qtz
42	212	74	5	v4	qtz (pycc) disem pycc
43	71	44	3	v4	qtz (cc) cc on fracture surface
44	40	90	1	v2	qtz
45	0	66	0.5	v5	cc discont
46	350	55	0.5	v5	cc
47	60	60	3	v2	qtz

STRUCTURAL SAMPLING SITE DL95-I (K-SK) - 1995

No.	Strike	Dip	Width	Type	Note
48	247	46	3	v2	qtz
49	32	62	3	v2	qtz cut by thinnest<<1m qtz
50	148	81	0.01	v2	qtz cuts wider
51	186	42	0.01	v2	qtz cuts wider
52	193	80	1.5	v4	qtz (py)cc weak green halo
53	164	72	0.01	v6	pycc halo
54	280	74	4	v2	qtz discontinuous
55	197	50	2	v2	qtz
56	196	78	2	v4	qtz (pycc) late sulphides refractured qtz
57	95	40	3	v2	qtz
58	268	76	2	v2	qtz
59	67	82	4	v2	qtz cuts thin set w-side down
60	187	84	10	v2	qtz dis cc in halo???
61	33	40	2	v2	qtz
62	224	56	3	v2	qtz
63	195	75	10	v6	pycc halo? central to qtz
64	220	35	3	v2	qtz cut by halo bearing
65	193	72	10	v6	qtz pycc halo
66	186	67	0.5	v5	cc discont
67	5	80	0.3	v2	qtz
68	5	80	0.3	v2	qtz
69	209	24	0.5	v5	cc
70	209	24	0.4	v5	cc
71	0	85	7	v2	qtz
72	180	90	6	v2	qtz central fracture
73	58	52	4	v2	qtz dis late cc?
74	71	57	2	v5	pycc
75	77	46	0.5	v5	cc fracture
76	204	31	2	v2	qtz
77	30	80	4	v5	pycclim irreg
78	25	70	4	v5	pycc lim
79	28	76	1	v5	pycc
80	25	86	2	v5	pycc
81	25	86	100	x	cata shear west down
82	76	34	1	v5	pycc lim cuts those of N-S trend
83	86	55	1	v5	pycc lim
84	60	47	3	v5	pycc lim
85	73	37	0.5	v5	pycc lim
86	243	25	2	v2	qtz
87	10	40	3	v2	qtz
88	32	72	0.5	v5	pycc lim
89	62	60	1	v5	pycc lim
90	52	75	1.5	v5	pycc lim
91	15	41	3	v2	qtz displaced sin 1cm by 23582qtz
92	235	82	3	v2	qtz
93	45	43	2	v2	qtz cuts 23582qtz offset .5cm
94	59	59	2	v2	qtz
95	80	60	0.5	v5	cc fracture
96	199	78	5	v6	pycc halo

STRUCTURAL SAMPLING SITE DL95-I (K-SK) - 1995

No.	Strike	Dip	Width	Type	Note
97	212	69	2	v5	pycc discont
98	175	73	2	v5	pycc possible weak halo?
99	190	64	50	v6	qtz pycc lim halo qtz-halo zone
100	242	71	1	v2	qtz
101	215	75	20	v4	qtz pycc lim
102	215	80	10	v2	qtz alt cata
103	46	60	2	v2	qtz cut by halo zones
104	235	87	1	v2	qtz
105	64	55	0.5	v5	cc on fracture surface
106	216	70	10	v6	qtz halo zone
107	126	57	2	v2	qtz
108	128	46	3	v2	qtz
109	42	39	0.5	v2	qtz
110	61	44	0.5	v2	qtz
111	55	71	0.5	v5	pycclim
112	52	71	0.5	v5	py cc lim
113	48	67	0.5	v5	py cc lim
114	168	75		v5	qtz py lim central channel
115	15	90	1	v2	qtz
116	187	60	2	v2	qtz
117	198	72	3	v4	qtzlim central channel
118	192	68	10	v6	qtz lim white halo
119	184	58	10	v6	qtz lim white halo
120	16	73	2	v2	qtz
121	356	82	1	v2	qtz
122	78	62	0.5	v5	cc on fracture surface rake 21w
123	60	45	0.5	v5	cc on fracture surface
124	55	45	0.5	v5	cc fracture surface
125	65	38	0.5	v5	cc fracture surface 21w
126	65	65	0.5	v5	cc fracture surface
127	72	64	0.5	v5	cc fracture surface
128	57	68	0.5	v5	cc fracture surface
129	55	70	1	v5	lim cc py
130	62	57	0.5	v5	cc slip surface rake 15w

STRUCTURAL SAMPLING SITE DL95-J (SK) - 1995
N3703 E3299 c2347 N4E

No.	Strike	Dip	Width	Type	Note
1	280	85	4	v5	pycchm cc film over py, ox stain
2	93	90	5	v5	pycchm cc film, hm stain, cuts/offset qtz06535
3	65	35	3	v2	qtz banded, displaced s-side down
4	275	83	0.5	v5	pycc ox
5	270	86	2	v5	pycc ox through qtz
6	269	86	0.5	v5	py
7	280	90	2	v5	py hmox
8	64	86	2	v5	pyhmcc
9	85	62	3	v5	pyhmcc
10	87	85	4	v5	pyhmcc
11	90	75	1.2	v6	pycc thin qtz, halo??
12	340	75	8	v3	qtzmo py late py, cut by all, small dex offsets
13	85	86	3	v5	pyhmcc
14	102	63	10	v6	py qs halo cut by pyox .5cm dex
15	130	90	2	v5	pycchmox through qshalo vein
16	105	79	5	v6	py qs halo
17	80	70	10	v6	py qs halo discont min within
18	79	39	2	v2	qtz banded grey
19	115	80	5	v6	py qs halo
20	310	90	3	v5	pycchm
21	320	90	2	v5	pycchm
22	289	84	3	v5	pycchm irregular min concentrations
23	123	84	0.5	v5	pycchm
24	60	49	1	v2	qtz lam?
25	278	85	3	v5	pyccox discontinuous
26	89	90	0.5	v6	py qs halo
27	75	26	2	v2	qtz
28	63	70	1	v2	qtz
29	102	90	1	v5	py no halo
30	290	90	1	v5	py no halo
31	285	76	2	v5	pyccox
32	301	73	4	v5	pyccox
33	104	80	4	v5	pyccox
34	48	14	3	v2	qtz grey banded, cut by all
35	96	74	5	v5	pyccox
36	316	75	2	v5	pyccox
37	75	74	50	v5	pycc sil zone stringers
38	38	58	4	v2	qtz
39	48	70	2	v2	qtz
40	110	90	10	v2	qtz lam shear!
41	334	76	2	v2	qtz grey banded
42	254	25	0.5	v5	pyccox surface
43	284	65	0.5	v2	qtz not observed cross cut
44	315	63	0.5	v5	pycc discont
45	118	82	10	v3	qtzmo py py is later
46	337	66	0.5	v5	pycc cross cuts qtzmo
47	96	90	0.5	v5	py? cpy??

STRUCTURAL SAMPLING SITE DL95-J (SK) - 1995

No.	Strike	Dip	Width	Type	Note
48	270	84	0.5	v5	py? cpy??
49	54	30	2	v4	qtz py parallel to each other
50	320	71	2	v2	qtz grey
51	342	60	1	v2	qtz
52	110	87	0.5	v4	qtz py cc pycc are late in refractured qtz
53	87	32	0.5	v2	qtz cuts thicker qtz veins
54	115	82	0.5	v5	pycc parallel fracture
55	81	84	0.5	v5	pycc parallel fracture
56	27	80	10	v2	qtz
57	59	84	10	v5	ccox(py) shear??
58	87	20	3	v2	qtz
59	337	84	3	v2	qtz
60	60	76	5	v5	pyccox sil zone ,min discont.
61	122	77	0.5	v5	pyccox in fracture
62	99	88	0.5	v5	pyccox fracture
63	110	78	0.5	v5	pyccox fracture
64	220	75	0.1	v5	ccox slip surface rake 18SW, frags qmo
65	87	15	2	v2	qtz
66	310	78	0.5	v5	pycc
67	355	68	0.5	mo	mo slip surface
68	330	82	15	v3	qtz mo vein fragment between 2 shears
69	54	85	0.5	x	fault slip surface
70	60	25	4	v2	qtz weak corragated
71	334	79	10	v3	qtzmo vein fragment??

STRUCTURAL SAMPLING SITE DL95-K (QS) - 1995
N3613 E3257 c2347 N4E

No.	Strike	Dip	Width	Type	Note
1	110	90	40	v3	qtz(mo)pycc late cc over py
2	304	60	2	v5	pycc
3	112	90	1	v5	pycc
4	355	55	0.5	v5	pycc
5	348	86	0.3	v5	pycc
6	337	90	1	v5	ccpy
7	280	80	3	v5	pycc
8	265	70	3	v5	pycc
9	320	68	4	v4	qtzpycc open central channel
10	290	66	0.3	v5	pycc
11	105	88	10	v4	qtz pycc qtz
12	317	54	2	v5	ccpy
13	301	64	0.3	v5	pycc
14	115	90	5	v6	pycc qtzhalo?
15	320	90	0.3	v5	pycc
16	282	78	2	v5	pycc
17	276	60	2	v5	pycc
18	146	42	3	v5	ccpy
19	134	84	3	v5	ccpy
20	308	65	3	v5	ccpy
21	302	84	3	v5	pycc
22	314	74	1	v5	pycc
23	146	60	2	v5	ccpy offset by 31474pycc steps s-side down
24	290	80	3	v5	pycc
25	278	78	10	v4	qtzpycc
26	136	88	0.3	v5	pycc
27	182	75	0.3	v5	pycc
28	295	85	0.3	v5	pycc
29	280	82	6	v5	cc parallel qtz vein
30	115	90	2	v5	pycc
31	310	61	2	v5	pycc
32	334	73	1	v5	pycc
33	320	80	1	v5	pycc
34	263	83	1	v5	pycc
35	114	85	2	v5	pycc cut by 33074pycc
36	330	74	3	v5	pycc
37	320	50	3	v5	pycc coarse granular
38	326	70	3	v5	pycc branches
39	345	86	4	v5	pycc assoc qtz???
40	330	70	1	v5	pycc
41	299	78	2	v6	pycc assoc qtz or in qtz/sil block
42	110	90	10	v6	pycc sil halo
43	326	64	0.3	v6	pycc associated with sil block
44	310	90	1	v5	pycc
45	316	85	1	v5	pycc
46	310	87	0.3	v5	pycc
47	8	85	10	v2	qtz

STRUCTURAL SAMPLING SITE DL95-K (QS) - 1995

No.	Strike	Dip	Width	Type	Note
48	10	72	10	v2	qtz
49	310	85	2	v5	pycc qtz through qtz
50	315	80	2	v6	cc ser
51	95	43	2	v5	pycc
52	310	90	2	v5	pycc
53	122	83	1	v5	pycc
54	310	73	2	v5	pycc
55	302	65	2	v5	pycc
56	299	72	2	v5	pycc
57	112	43	2	v5	pycc
58	20	78	10	v3	qtzmo
59	355	88	5	v4	qtzpycc sulphides central only py??
60	5	87	5	v2	qtz
61	333	50	1	v5	pycc
62	10	70	0.5	v5	cc on surface
63	89	84	0.5	v5	pycc
64	303	65	2	v5	pycc
65	326	71	1	v5	pycc
66	285	74	2	v5	pycc
67	282	89	1	v5	pycc
68	310	74	0.5	v5	pycc
69	314	58	2	v5	pycc
70	310	58	2	v5	pycc
71	208	42	1	v5	cc on surface
72	130	85	1	v5	cc
73	330	73	0.5	v5	pycc
74	350	74	1	v5	cc
75	325	69	0.5	v5	pycc

STRUCTURAL SAMPLING SITE DL95-L (SK) - 1995
N5619 E3705 c2770 F4N

No.	Strike	Dip	Width	Type	Note
1	267	66	3	alun	qtz alun later sheared
2	259	78	6	v2	qtz pinch swell
3	321	76	2	v2	qtz
4	165	80	0.5	alb	white fracture with albitic halo
5	135	86	1	v2	qtz
6	318	75	2	v2	qtz
7	173	90	0.5	alun	alun
8	328	65	0.7	v2	qtz
9	295	60	2	v2	qtz
10	166	80	0.5	alun	alun
11	271	78	3	v2	qtz
12	302	68	2	v2	qtz
13	264	70	3	v2	qtz spots of py
14	270	70	2	v2	qtz
15	268	76	4	v2	qtz
16	270	67	2	v2	qtz
17	308	85	2	v2	qtz
18	258	70	2	v2	qtz
19	310	83	3	v2	qtz
20	269	65	2	v2	qtz
21	280	75	5	v2	qtz
22	284	66	1	v2	qtz
23	280	84	2	v2	qtz
24	312	80	2	v2	qtz
25	304	80	10	v2	qtz
26	293	80	3	v2	qtz halo? silicious trend no min-vein
27	287	75	2	v2	qtz halo?
28	286	90	3	v1	qtz kf halo
29	295	70	1	v4	qtz py cc through kmega
30	268	69	3	v2	qtz
31	125	86	0.5	v5	cc on fracture
32	292	72	3	v6	qtz halo?
33	275	74	2	v2	qtz
34	267	68	2	v2	qtz
35	172	53	3	alb	white fracture albitic?halo
36	274	76	2	v2	qtz
37	274	83	3	v2	qtz
38	65	25	3	v1	kf
39	124	75	0.5	v5	cc on fracture
40	134	71	1	v5	pycc
41	138	80	0.5	v5	pycc
42	139	84	1	v5	pycc
43	135	84	0.5	v5	pycc
44	137	89	0.5	v5	pycc
45	130	90	2	v2	qtz
46	282	72	2	v2	qtz
47	127	85	0.5	v5	pycc

STRUCTURAL SAMPLING SITE DL95-L (SK) - 1995

No.	Strike	Dip	Width	Type	Note
48	267	90	3	v2	qtz
49	262	70	0.5	v2	qtz
50	327	75	2	v2	qtz
51	300	77	7	v2	qtz pinch swell
52	276	77	4	v2	qtz late pycc on vein fracture surface
53	300	71	3	v2	qtz
54	150	84	0.5	v5	pycc white halo
55	269	82	4	v2	qtz
56	340	65	3	v6	qtz halo silica trend
57	308	72	2	v6	qtz halo silicious trend
58	122	86	1	v2	qtz
59	285	70	3	v2	qtz cuts kmega
60	312	78	3	v2	qtz
61	105	85	0.5	v5	pycc white halo alb??20mm
62	264	74	0.5	v2	qtz
63	124	80	0.5	v6	pycc halo
64	164	78	2	v2	qtz
65	130	75	0.5	v6	pycc halo
66	138	90	0.5	v6	pycc halo
67	330	85	1	v2	qtz late py
68	304	90	2	v2	qtz late cc
69	132	70	2	v2	qtz
70	297	90	2	v6	pycc weak halo
71	124	85	1	v6	pycc weak halo
72	302	90	1	v6	pycc weak halo
73	290	84	4	v6	pycc halo
74	116	84	2	v6	qtz halo sil trend
75	300	90	2	v1	qtz kf trend
76	117	88	0.5	v6	pycc halo
77	94	87	3	v2	qtz
78	294	65	3	v2	qtz
79	104	84	4	v2	qtz sheared
80	285	74	3	v2	qtz
81	286	73	2	v2	qtz
82	322	80	2	v2	qtz
83	122	88	0.5	v6	pycc halo
84	304	80	0.5	v6	pycc halo
85	157	90	0.5	v5	pycc
86	272	80	2	v2	qtz
87	87	84	3	v2	qtz
88	144	90	1	v2	qtz
89	132	88	3	v1	kf trend
90	324	74	2	v2	qtz
91	260	81	2	v2	qtz
92	265	64	3	v2	qtz late py cc in fractured qtz
93	302	75	4	v2	qtz banded
94	269	76	2	v2	qtz
95	267	67	1	v2	qtz cut by 30572qtz offset 5mm
96	305	72	1	v2	qtz green

STRUCTURAL SAMPLING SITE DL95-L (SK) - 1995

No.	Strike	Dip	Width	Type	Note
97	310	80	0.5	v2	qtz
98	305	75	1	v2	qtz green
99	280	56	2	v2	qtz
100	302	75	3	v1	qtz kf halo cut by 28056qtz
101	265	57	3	v2	qtz banded, cut by 16080fraccc 1cm sin
102	160	80	0.3	v5	cc in fracture
103	303	58	2	v2	qtz
104	303	72	2	v2	qtz
105	243	83	1	v2	qtz
106	130	60	0.5	v5	cc in fracture
107	271	55	2	v2	qtz
108	272	45	1	v2	qtz
109	274	66	2	v2	qtz late cc in fractured qtz
110	260	70	1	v2	qtz
111	249	58	2	v2	qtz
112	255	54	3	v2	qtz late cc in fractured qtz
113	273	70	2	v2	qtz
114	249	77	3	v2	qtz
115	157	64	1	v2	qtz
116	310	72	2	v2	qtz sheared
117	260	56	2	v2	qtz
118	295	79	3	v6	qtz ccpy halo
119	248	67	0.5	v5	ccpy
120	130	84	0.5	v5	pycc
121	167	83	0.5	v5	pycc
122	158	76	0.5	v5	pycc
123	140	62	0.5	v5	pycc
124	144	80	0.5	v5	pycc

STRUCTURAL SAMPLING SITE DL95-M (SK) - 1995
N5490 E3945 c2773 F4N

No.	Strike	Dip	Width	Type	Note
1	70	70	2	v5	pycccv
2	94	80	2	v5	py
3	90	71	4	v4	py qtz
4	70	65	2	v5	py
5	40	54	1	v5	py
6	74	73	3	v4	qtz py
7	195	75	15	v6	qtz qs halo
8	216	75	2	v6	py qs halo
9	200	66	20	v6	py qs halo
10	205	77	2	v6	py qs halo
11	61	85	1	gyp	yeso
12	227	82	2	v6	py qs halo
13	204	72	2	v6	py qs halo
14	222	83	2	v6	py qs halo
15	196	68	3	v7	qtz pycc qs halo
16	190	78	2	v6	py qs halo
17	210	85	2	v7	qtz pycc qs halo
18	155	72	0.5	chl	chl
19	241	76	10	v2	qtz
20	95	75	1	v5	pycc
21	225	69	10	v2	qtz
22	200	76	2	v4	py qs halo
23	74	48	0.5	v5	py
24	61	67	0.5	v5	py
25	80	64	1.5	v5	py
26	65	77	1	v6	py qs halo
27	47	84	3	v4	py qtz?
28	85	70	3	v4	qtz pycccv
29	60	72	0.5	v6	py
30	56	62	0.5	v5	py
31	83	66	0.5	v5	py
32	235	68	10	v2	qtz
33	207	70	2	x	shear
34	250	82	10	v2	qtz
35	205	75	2	v6	py qs halo
36	210	66	0.5	v6	py
37	35	84	0.5	v5	pycc
38	54	73	0.5	v6	pycc
39	93	55	2	v4	qtz pycc yesp
40	196	60	2	v6	py qs halo
41	213	73	2	v6	py qs halo
42	193	72	2	v6	py qs halo
43	200	85	2	v6	py qs halo
44	199	70	2	v6	py qs halo
45	194	67	2	v6	py qs halo
46	204	80	1	v6	qs halo
47	213	82	2	v6	pycc qs halo

STRUCTURAL SAMPLING SITE DL95-M (SK) - 1995

No.	Strike	Dip	Width	Type	Note
48	210	80	2	v6	py qs halo
49	190	80	20	v7	qtz pycccv qs halo
50	192	73	2	v6	py qs halo
51	210	85	2	v6	py qs halo

STRUCTURAL SAMPLING SITE DL95-N (QS) - 1995
N3867 E3415 c2362 N3E

No.	Strike	Dip	Width	Type	Note
1	156	84	2	gyp	yeso
2	132	82	20	v6	cpy bn qs halo
3	111	90	2	v5	cpy bn
4	302	84	0.5	v4	qtz py central channel
5	126	70	0.5	v6	py cc qs halo
6	355	85	2	gyp	yeso
7	145	85	0.5	v5	cpy bn
8	150	90	1	v5	py cc irreg walls, cc coating
9	313	90	2	v5	cpy cc cc coating
10	344	88	10	v3	qtz mo py
11	335	90	2	v4	qtz cpy py?
12	155	85	10	v4	qtz py cpy central channel vuggy pockets
13	316	85	3	v5	py cc cc coating
14	140	85	10	v4	qtz py cc
15	305	84	10	v4	qtz cpy cc
16	295	83	0.5	mo	mo slip plane
17	125	84	30	v4	qtz py open channel, vug qtz
18	142	84	1	v5	py cpy
19	143	72	7	v4	qtz py parallels yeso
20	142	80	1	v5	py cpy
21	162	64	0.5	v4	qtz cpy bn cc
22	145	80	1	v5	cp cc
23	302	90	2	mo	mo remobilized
24	134	81	4	v5	py cpy cuts mo
25	130	86	10	v3	qtz mo latepycp
26	148	74	1	v5	py cc irreg
27	134	80	2	v5	cpy py cc irreg
28	142	82	1	v5	py cc irreg
29	152	80	2	v5	cpy
30	152	82	10	v6	py qs halo
31	161	84	2	mo	mo remobilized
32	163	76	0.5	mo	mo remobilized
33	138	83	2	v5	py cc assoc qtz??, cc coating
34	144	85	20	v6	py cc qs halo
35	165	80	0.5	v5	py cc surface
36	150	75	3	v2	qtz late cccv on fractured qtz
37	156	85	4	v4	qtz cp
38	168	82	10	v2	qtz banded grey
39	160	85	5	v3	qtz mo central
40	155	90	0.5	v6	qtz cp halo
41	5	70	3	v2	qtz
42	159	83	5	v6	cpy qs halo
43	158	84	10	v6	cpy dg? qs halo
44	312	90	2	v2	qtz
45	163	76	30	v6	cpy cc qs halo cuts kmega
46	135	82	3	v2	qtz
47	296	82	10	v3	qtz mo late pycp, deformed stlo mo

STRUCTURAL SAMPLING SITE DL95-N (QS) - 1995

No.	Strike	Dip	Width	Type	Note
48	285	76	2	v6	cpy cc s halo
49	322	90	2	v6	cpy cc s halo
50	184	82	0.3	v2	qtz
51	345	90	1	vv2	qtz
52	5	90	3	v3	qtz mo
53	150	83	2	v5	cpy cc
54	152	75	20	v2	qtz sheared late py
55	339	89	5	v4	qtz cpy py cc
56	135	66	0.5	v5	cpy cc
57	143	81	0.5	v5	cpy cc
58	308	85	1	v4	qtz cpy cc
59	345	74	15	v4	qtz py banded central channel
60	161	84	2	v6	cpy cc qs halo
61	315	87	1	v5	cpy cc
62	129	75	10	v4	qtz py feox late py ox
63	300	80	6	v2	qtz white, some py
64	320	87	1	v5	cpycc
65	322	86	1	v5	cpy cc
66	150	44	0.5	v5	cpy cc cuts 32286cpcc
67	150	44	0.5	v5	cpy cc
68	150	83	1	v5	cpy cc
69	140	90	10	v6	py cc qs halo
70	128	23	0.5	v5	py cc cuts all
71	175	78	2	v3	qtz mo remobilized
72	153	83	1	v5	py feox
73	330	90	1	v5	cpy py feox halo qs?
74	305	58	1	v6	py cc qs halo
75	335	87	2	v6	py qs halo
76	162	82	2	v3	qtz mo remobilized
77	148	79	2	v4	qtz py cpy white qtz

STRUCTURAL SAMPLING SITE DL93-22 (K) - 1993
N E c I1E

No.	Strike	Dip	Width	Type	Note
1	5	34	0	LIN	LIN
2	46	41	0	LIN	
3	14	21	0	LIN	LIN
4	105	7	0	LIN	LIN
5	47	34	0	LIN	LIN
6	41	41	0	LIN	LIN
7	92	9	0	LIN	LIN ON QTZ
8	141	66	0	A	RECENT
9	138	68	0	A	RECENT
10	244	69	0	A	RECENT
11	195	73	0	A	RECENT
12	226	24	0	A	RECENT
13	193	30	0	A	RECENT
14	38	62	0	A	RECENT
15	108	76	0	A	RECENT
16	21	71	0	A	RECENT
17	254	43	0	A	RECENT
18	40	48	0	A	RECENT
19	188	75	0	A	RECENT
20	73	80	0	A	RECENTRUST
21	160	63	0	A	RECENT
22	30	70	0	A	RECENT
23	255	54	0	A	RECENT
24	20	77	0	A	RECENT
25	13	87	0	A	RECENT
26	35	78	0	A	RECENT
27	105	84	0	A	RECENT
28	36	74	0	A	RECENT
29	163	75	0	A	RECENT
30	119	34	0	A	RECENT
31	206	31	0	A	RECENT
32	168	39	0	A	RECENT
33	99	79	0	A	RECENT
34	176	40	0	A	RECENT
35	185	58	0	A	RECENT
36	198	87	0	A	RECENT
37	18	71	0	A	RECENT
38	228	74	0	A	RECENT
39	79	31	0	A	RECENT
40	83	78	0	A	RECENT
41	217	31	0	A	RECENT
42	110	69	0	A	RECENT
43	192	40	0	A	RECENT
44	16	64	0	A	RECENT
45	207	31	0	A	RECENT
46	185	84	0	A	RECENT
47	237	76	0	A	RECENT

STRUCTURAL SAMPLING SITE DL93-22 (K) - 1993

No.	Strike	Dip	Width	Type	Note
48	204	57	0	A	RECENT
49	210	62	0	A	RECENT
50	203	57	0	A	RECENT
51	247	64	0	A	RECENTQLIN
52	250	61	0	A	RECENTQlin
53	16	25	0	A	RECENT
54	225	55	0	A	RECENT
55	354	56	0	A	RECENT
56	230	84	0	A	RECENT
57	246	40	0	A	RECENT
58	5	64	0	A	RECENT
59	9	73	0	A	RECENT
60	248	56	0	A	RECENT
61	240	78	0	A	RECENT
62	150	70	0	A	RECENT
63	148	60	0	A	RECENT
64	228	69	0	A	RECENT
65	130	32	0	A	RECENT
66	159	64	0	A	RECENT
67	164	68	0	A	RECENT
68	326	89	0	A	RECENT
69	87	20	0	A	RECENT
70	297	71	0	A	RECENT
71	345	18	0	A	RECENT
72	142	57	0	A	RECENT
73	333	87	0	A	RECENT
74	237	90	0	A	RECENT
75	40	12	0	A	RECENT
76	350	28	0	A	RECENT
77	143	73	0	A	RECENT
78	285	85	0	A	RECENT
79	154	58	0	A	RECENT
80	161	71	0	A	RECENT
81	78	23	0	A	RECENT
82	141	70	0	A	RECENT
83	110	55	0	A	RECENT
84	116	71	0	A	RECENT
85	130	84	0	F	FAULT main fault
86	34	12	0	F	FAULT rel mnfault?
87	50	32	0	F	FAULT rel mnfault?
88	40	35	0	A	RECENT
89	132	82	0	F	FAULT main fault
90	133	78	0	F	FAULT fault sin
91	178	90	0	A	RECENT
92	153	75	0	A	RECENT
93	147	78	0	A	RECENT
94	214	23	0	A	RECENT
95	227	24	0	A	RECENT
96	32	37	0	A	RECENT

STRUCTURAL SAMPLING SITE DL93-22 (K) - 1993

No.	Strike	Dip	Width	Type	Note
97	73	74	0	A	RECENT
98	52	36	0	A	RECENT
99	147	79	0	A	RECENT
100	133	58	0	A	RECENT
101	97	76	0	A	RECENT
102	19	71	0	A	RECENT
103	20	79	0	A	RECENT
104	196	78	0	A	RECENT
105	294	84	0	F	FAULT
106	110	89	0	A	RECENT
107	159	33	0	A	RECENT
108	163	30	0	A	RECENT
109	20	71	0	A	RECENT
110	335	38	0	A	RECENT
111	145	18	0	A	RECENT
112	116	67	0	A	RECENT
113	110	74	0	A	RECENT
114	182	25	0	A	RECENT
115	208	27	0	A	RECENT
116	123	63	0	A	RECENT
117	115	70	0	A	RECENT
118	135	52	0	A	RECENT
119	114	60	0	A	RECENT
120	155	66	0	A	RECENT
121	134	70	0	A	RECENT
122	244	59	0	A	RECENT
123	235	66	0	A	RECENT
124	107	81	0	A	RECENT
125	105	83	0	A	RECENT
126	20	40	0	A	RECENT
127	110	90	0	A	FRACZ
128	215	61	0	A	FRACZ
129	101	82	0	A	FRACZ
130	136	43	0	A	FRACZ
131	124	71	0	A	FRACZ
132	102	75	0	A	FRACZ
133	130	70	0	A	FRACZ
134	225	84	0	A	RECENT
135	115	62	0	A	RECENT
136	155	70	0	A	RECENT
137	348	84	0	A	RECENT
138	289	87	0	A	RECENT
139	90	84	0	A	RECENT
140	83	61	0	X	SHEARS
141	94	82	0	A	RECENT
142	30	60	0	A	RECENT
143	182	47	0	A	RECENT
144	5	68	0	A	RECENT
145	84	77	0	A	RECENT

STRUCTURAL SAMPLING SITE DL93-22 (K) - 1993

No.	Strike	Dip	Width	Type	Note	
146	40	60	0	A	RECENT	
147	103	83	0	A	RECENT	
148	135	88	0	A	RECENT	
149	105	28	0	v1	QUARTZ	Sin disp by pyvl
150	138	72	0	v1	QUARTZ	
151	84	33	0	v1	QUARTZ	
152	155	73	0	v1	QUARTZ	
153	147	18	0	v1	QUARTZ	
154	173	18	0	v1	QUARTZ	
155	90	90	0	v1	QUARTZ	qtz lin 09->092
156	145	78	0	v4	QSULF	
157	90	68	0	v4	QSULF	wad?(black- green)stain
158	68	87	0	v4	QSULF	wad?(black- green)stain
159	137	72	0	v4	QSULF	qtz py cv
160	170	74	0	v4	QSULF	py cc qtz
161	161	79	0	v4	QSULF	py cc qtz
162	111	22	0	v4	QSULF	
163	156	68	0	v4	QSULF	main vein
164	154	70	0	v4	QSULF	main vein
165	149	69	0	v4	QSULF	main vein
166	150	64	0	v4	QSULF	
167	149	75	0	v4	QSULF	
168	138	68	0	gyp		
169	140	75	0	gyp		
170	155	62	0	gyp		
171	133	78	0	gyp		
172	95	80	0	gyp		
173	109	70	0	gyp		
174	94	84	0	gyp		
175	292	83	0	gyp		
176	145	62	0	gyp		
177	168	57	0	v5	SULF	py cv
178	315	81	0	v5	SULF	
179	265	81	0	v5	SULF	hem cu-sulf?
180	91	60	0	v6	HALO	py cv? w/green halo
181	70	52	0	v5	SULF	py cv? Sin disp by sim
182	146	76	0	v5	SULF	py cv
183	127	53	0	v5	SULF	
184	294	86	0	v5	SULF	py cv
185	200	77	0	v5	SULF	py cv
186	300	74	0	v5	SULF	cv
187	132	83	0	v5	SULF	py cv cp
188	102	75	0	v5	SULF	cc
189	301	83	0	v5	SULF	py cc
190	83	75	0	v5	SULF	rel mnfault py cv
191	86	70	0	v5	SULF	py cv rel mainfault
192	94	57	0	v5	SULF	rel main fault
193	87	72	0	v5	SULF	py cv rel mainfault?
194	273	78	0	v5	SULF	pycc

STRUCTURAL SAMPLING SITE DL93-22 (K) - 1993

No.	Strike	Dip	Width	Type	Note				
195	204	80	0	v5	SULF	cc and black stain?, series veinlets	196	1	8	4
	85	0	v5	SULF	black stain?				
197	113	69	0	v5	SULF	black stain?				
198	153	64	0	v5	SULF	py black stain				
199	155	56	0	v5	SULF	py black stain				
200	147	62	0	v5	SULF	series 6-8 py				
201	147	62	0	v5	SULF	py black recent				
202	141	65	0	v5	SULF	recent py black				
203	136	60	0	v5	SULF	py black				
204	126	60	0	v5	SULF	black stain?				
205	171	55	0	v5	SULF	spotty py				
206	180	58	0	v5	SULF	black stain?				
207	140	83	0	v5	SULF	py black				
208	158	69	0	v5	SULF	py black				
209	160	68	0	v5	SULF	py black				
210	162	68	0	v5	SULF	py black				
211	159	61	0	v5	SULF	py black				
212	154	68	0	v5	SULF	black				
213	151	64	0	v5	SULF	chl? lin 26->168				
214	135	70	0	v5	SULF	black stain?				
215	148	69	0	v5	SULF	py black				
216	143	76	0	v5	SULF	py black				
217	138	59	0	v5	SULF	py black				
218	143	78	0	v5	SULF	py black				
219	165	53	0	v5	SULF	py black cuts Kfeld xtal				
220	117	24	0	v5	SULF	py black				
221	170	57	0	v5	SULF	py cv				
222	106	62	0	v5	SULF	py cv				
223	180	56	0	v5	SULF	rec py cv				
224	146	56	0	v5	SULF	py wad?cc?en?				
225	145	49	0	v5	SULF	py wad?cc?en?				
226	208	81	0	v5	SULF	black stain?				
227	195	86	0	v5	SULF	black stain?				
228	42	54	0	v5	SULF	black				
229	97	65	0	v5	SULF	cut DUCTILE				
230	87	55	0	v5	SULF	cut DUCTILE				
231	170	67	0	v4	SULF	py black qtz?				
232	196	85	0	v5	SULF	black stain?				
233	192	71	0	v5	SULF	black stain?				
234	172	74	0	v5	SULF	black stain?				
235	155	69	0	v5	SULF	black stain?				
236	142	63	0	v5	SULF	black stain?				
237	140	78	0	v5	SULF	black stain?				
238	160	64	0	v5	SULF	py black				
239	175	77	0	v5	SULF	py black				
240	161	74	0	v5	SULF	py black				
241	159	84	0	v5	SULF	py black				
242	156	65	0	v5	SULF	black stain?				
243	133	83	0	v5	SULF	py cv				

STRUCTURAL SAMPLING SITE DL93-22 (K) - 1993

No.	Strike	Dip	Width	Type	Note	
244	170	65	0	v5	SULF	py
245	136	75	0	v5	SULF	py +cpy?
246	93	64	0	v5	SULF	cpy +py?
247	128	54	0	v5	SULF	py? +?
248	105	76	0	v5	SULF	py?+?
249	315	77	0	v5	SULF	py?+?
250	98	63	0	v5	SULF	spotty xtiline py
251	126	70	0	v5	SULF	py?+?
252	87	63	0	v5	SULF	py +?
253	87	66	0	v5	SULF	py+?
254	84	75	0	v6	HALO	py+? w/ 3mm halo
255	96	79	0	v5	SULF	cpy
256	95	72	0	v5	SULF	cpy
257	98	75	0	v5	SULF	cpy
258	88	82	0	v5	SULF	cpy
259	97	84	0	v5	SULF	cpy
260	96	64	0	v5	SULF	cpy
261	114	57	0	v5	SULF	cpy
262	77	72	0	v5	SULF	cpy
263	85	83	0	v5	SULF	cpy
264	105	69	0	v5	SULF	cpy
265	144	85	0	v5	SULF	cpy
266	175	90	0	v5	SULF	cpy
267	103	68	0	v5	SULF	py+ black?
268	137	58	0	v5	SULF	py +black
269	87	74	0	v5	SULF	black +py?
270	104	66	0	v5	SULF	py+black
271	272	73	0	v5	SULF	py
272	267	71	0	v5	SULF	py
273	165	70	0	v5	SULF	py
274	167	59	0	v5	SULF	py
275	86	76	0	v5	SULF	py?+?
276	115	59	0	v5	SULF	py +? black green
277	9	76	0	x	SHEAR	
278	0	73	0	x	SHEAR	
279	355	78	0	x	SHEAR	c-plane
280	208	90	0	x	SHEAR	s-plane
281	152	80	0	v4	QTZPY	qtz py
282	157	76	0	v4	QTZPY	qtz py
283	110	77	0	v4	QTZPY	qtz py mo?
284	105	48	0	v4	QTZPY	grey(mo?) qtz py
285	96	72	0	v4	QTZPY	grey ?qtz mo? py
286	97	68	0	v4	QTZPY	grey mo?qtz py
287	93	79	0	v4	QTZPY	py qtz +?
288	92	72	0	v6	QTZPY	py grey? qtz
289	85	76	0	v6	QTZPY	py grey qtz?
290	76	76	0	v6	QTZPY	greyqtz? py
291	82	72	0	v6	QTZPY	py grey qtz?
292	94	63	0	v6	QTZPY	py grey qtz?

STRUCTURAL SAMPLING SITE DL93-22 (K) - 1993

No.	Strike	Dip	Width	Type	Note	
293	90	76	0	v6	QTZPY	py grey qtz?
294	80	81	0	v4	QTZPY	py
295	95	88	0	v4	QTZPY	qtz w/ py center
296	97	83	0	v4	QTZPY	qtz w/ py center
297	102	70	0	v4	QTZPY	qtz w/ py center+cv?
298	110	66	0	v4	QTZPY	
299	124	56	0	v2	KFELD	Kalt1cmsidescutbylargemin
300	0	72	0	v2	KFELD	post alt pre min
301	188	75	0	x	SHEAR	UNKNOWN
302	255	54	0	x	SHEAR	UNKNOWN
303	13	87	0	x	SHEAR	UNKNOWN
304	99	79	0	x	SHEAR	UNKNOWN
305	247	64	0	x	SHEAR	UNKNOWN
306	250	61	0	x	SHEAR	UNKNOWN
307	90	90	0	x	SHEAR	UNKNOWN

STRUCTURAL SAMPLING SITE DL93-23 (K) - 1993
N4446 E3799 c2593 I3E

No.	Strike	Dip	Width	Type	Note
1	70	68	0	LI-SS	LI-SS
2	78	76	0	LI-MIN	LI-MIN
3	145	16	0	LI-SS	LI-SS
4	128	12	0	LI-SS	LI-SS
5	35	24	0	LI-SS	LI-SS
6	35	28	0	LI-SS	LI-SS
7	242	60	0	LI-SS	LI-SS
8	189	90	0	A	JI-FRAC
9	318	76	0	A	JI-FRAC
10	219	72	0	A	JI-FRAC
11	205	65	0	A	JI-FRAC
12	221	76	0	A	JI-FRAC
13	172	72	0	A	JI-FRAC
14	30	90	0	A	JI-FRAC
15	190	70	0	A	JI-FRAC
16	10	88	0	A	JI-FRAC
17	20	82	0	A	JI-FRAC
18	200	81	0	A	JI-FRAC
19	122	65	0	A	JI-FRAC
20	209	83	0	A	JI-FRAC
21	205	76	0	A	JI-FRAC
22	260	72	0	A	JI-FRAC
23	179	57	0	A	JI-FRAC
24	245	66	0	A	JI-FRAC
25	260	62	0	A	JI-FRAC
26	201	83	0	A	JI-FRAC
27	250	69	0	A	JI-FRAC
28	203	75	0	A	JI-FRAC
29	16	90	0	A	JI-FRAC
30	20	84	0	A	JI-FRAC
31	195	74	0	A	JI-FRAC
32	210	84	0	A	JI-FRAC
33	338	80	0	A	JI-FRAC
34	342	84	0	A	JI-FRAC
35	224	68	0	A	JI-FRAC
36	331	88	0	A	JI-FRAC
37	174	30	0	A	JI-FRAC
38	231	67	0	A	JI-FRAC
39	28	67	0	A	JI-FRAC
40	86	64	0	A	JI-FRAC
41	185	74	0	A	JI-FRAC
42	205	85	0	A	JI-FRAC
43	197	75	0	A	JI-FRAC
44	239	62	0	A	JI-FRAC
45	205	79	0	A	JI-FRAC
46	151	66	0	A	JI-FRAC
47	198	76	0	A	JI-FRAC

STRUCTURAL SAMPLING SITE DL93-23 (K) - 1993

No.	Strike	Dip	Width	Type	Note
48	340	84	0	A	JI-FRAC
49	349	81	0	A	JI-FRAC
50	206	81	0	A	JI-FRAC
51	356	80	0	A	JI-FRAC
52	228	68	0	A	JI-FRAC
53	225	73	0	A	JI-FRAC
54	61	80	0	A	JI-FRAC
55	246	84	0	A	JI-FRAC
56	350	79	0	A	JI-FRAC
57	260	49	0	A	JI-FRAC
58	146	84	0	A	JI-FRAC
59	135	74	0	A	JI-FRAC
60	318	77	0	A	JI-FRAC
61	319	65	0	A	JI-FRAC
62	321	75	0	A	JI-FRAC
63	317	84	0	A	JI-FRAC
64	30	74	0	A	JI-FRAC
65	45	86	0	A	JI-FRAC
66	308	81	0	A	JI-FRAC
67	15	80	0	A	JI-FRAC
68	350	85	0	A	JI-FRAC
69	323	82	0	A	JI-FRAC
70	332	86	0	A	JI-FRAC
71	10	58	0	A	JI-FRAC
72	130	71	0	A	JI-FRAC
73	115	52	0	A	JI-FRAC
74	333	82	0	A	JI-FRAC
75	21	72	0	A	JI-FRAC
76	120	59	0	A	JI-FRAC
77	317	82	0	A	JI-FRAC
78	293	33	0	A	JI-FRAC
79	119	58	0	A	JI-FRAC
80	100	83	0	A	JI-FRAC
81	315	69	0	A	XIS
82	38	23	0	A	JI-FRAC
83	142	79	0	A	JI-FRAC
84	70	79	0	A	JI-FRAC
85	327	79	0	A	JI-FRAC
86	125	69	0	A	JI-FRAC
87	116	74	0	A	JI-FRAC
88	151	90	0	A	JI-FRAC
89	327	81	0	A	JI-FRAC
90	120	76	0	A	JI-FRAC
91	330	62	0	A	JI-FRAC
92	105	72	0	A	JI-FRAC
93	72	19	0	A	JI-FRAC
94	17	56	0	A	JI-FRAC
95	11	62	0	A	JI-FRAC
96	56	69	0	A	JI-FRAC

STRUCTURAL SAMPLING SITE DL93-23 (K) - 1993

No.	Strike	Dip	Width	Type	Note
97	21	65	0	A	JI-FRAC
98	98	57	0	A	JI-FRAC
99	11	60	0	A	JI-FRAC
100	90	57	0	A	JI-FRAC
101	108	89	0	A	JI-FRAC
102	143	73	0	A	JI-FRAC
103	122	67	0	A	JI-FRAC
104	227	74	0	A	JI-FRAC
105	224	72	0	A	JI-FRAC
106	232	84	0	A	JI-FRAC
107	75	68	0	v2	VI
108	90	63	0	v2	VI
109	92	75	0	v2	VI
110	290	86	0	v4	VI
111	75	69	0	v4	VI
112	86	76	0	v4	VI
113	110	82	0	v4	VI
114	154	68	0	v4	VI
115	101	75	0	v4	VI
116	116	66	0	v4	VI
117	146	80	0	v4	VI
118	114	75	0	v4	VI
119	115	70	0	v4	VI
120	150	80	0	v4	VI
121	123	75	0	v4	VI
122	115	70	0	v4	VI
123	98	85	0	v4	VI
124	130	72	0	v4	VI
125	109	70	0	v4	VI
126	110	45	0	v4	VI
127	90	40	0	v4	VI
128	85	68	0	v4	VI
129	144	68	0	v4	VI
130	114	64	0	v4	VI
131	302	85	0	v4	VI
132	307	78	0	v4	VI
133	111	70	0	v4	VI
134	80	51	0	v4	VI
135	131	60	0	v4	VI
136	130	71	0	v4	VI
137	130	66	0	v4	VI
138	295	90	0	v4	VV
139	110	74	0	v4	VI
140	114	63	0	v4	VI
141	135	74	0	v4	VI
142	330	90	0	v4	VV
143	130	81	0	v4	VI
144	142	74	0	v4	VI
145	130	78	0	v4	VI

STRUCTURAL SAMPLING SITE DL93-23 (K) - 1993

No.	Strike	Dip	Width	Type	Note
146	125	66	0	v4	VI
147	141	76	0	v4	VI
148	129	60	0	v4	VI
149	121	65	0	v4	VI
150	84	60	0	v4	VI
151	75	88	0	v4	VI
152	124	81	0	v4	VI
153	116	55	0	v4	VI
154	125	69	0	v4	VI
155	131	66	0	v4	VI
156	129	66	0	v4	VI
157	138	70	0	v4	VI
158	103	70	0	v4	VI
159	132	84	0	v4	VI
160	135	71	0	v4	VI
161	123	84	0	v4	VI
162	104	70	0	v4	VI
163	112	73	0	v4	VI
164	125	56	0	v4	VI
165	125	62	0	v4	VI
166	135	55	0	v4	VI
167	125	72	0	v4	VI
168	102	75	0	v4	VI
169	172	85	0	v4	VI
170	90	65	0	v4	VI
171	105	65	0	v4	VI
172	102	67	0	v4	VI
173	96	62	0	v4	VI
174	95	62	0	v4	VI
175	94	74	0	v4	VI
176	109	76	0	v4	VI
177	136	66	0	v4	VI
178	117	75	0	v4	VI
179	95	59	0	v4	VI
180	107	68	0	v4	VI
181	104	74	0	v4	VI
182	68	68	0	v4	VI
183	88	84	0	v4	VI
184	72	82	0	v4	VI
185	55	72	0	v4	VI
186	80	66	0	v4	VI
187	67	70	0	v4	VI
188	98	77	0	v4	VI
189	75	78	0	v4	VI
190	151	58	0	v4	VI
191	141	83	0	v4	VI
192	76	61	0	v4	VI
193	71	64	0	v4	VI
194	55	85	0	v4	VI

STRUCTURAL SAMPLING SITE DL93-23 (K) - 1993

No.	Strike	Dip	Width	Type	Note
195	65	82	0	v4	VI
196	109	64	0	v4	VI
197	234	90	0	v4	VI
198	157	68	0	v4	VI
199	68	83	0	v4	VI
200	103	69	0	v4	VI
201	91	64	0	v4	VI
202	75	70	0	v4	VI
203	113	81	0	v4	VI
204	82	63	0	v4	VI
205	105	51	0	v4	VI
206	103	71	0	v4	VI
207	117	77	0	gyp	VI
208	70	88	0	gyp	VI
209	74	90	0	gyp	VI
210	65	81	0	gyp	VI
211	69	88	0	gyp	VI
212	45	66	0	gyp	VI
213	55	74	0	gyp	VI
214	59	81	0	gyp	VI
215	108	87	0	v5	VI
216	155	80	0	v5	VI
217	75	38	0	v5	VI
218	155	55	0	v5	VI
219	170	55	0	v5	VI
220	250	80	0	v5	VI
221	102	63	0	v5	VI
222	275	88	0	v5	VI
223	109	86	0	v5	VI
224	87	82	0	v5	VI
225	72	88	0	v5	VI
226	248	80	0	v5	VI
227	122	72	0	v5	VI
228	160	78	0	v5	VI
229	245	78	0	v5	VI
230	132	75	0	v5	VI
231	130	65	0	v5	VI
232	112	74	0	v5	VI
233	95	85	0	v5	VI
234	115	74	0	v5	VI
235	122	75	0	v5	VI
236	120	51	0	v5	VI
237	150	60	0	v5	VI
238	130	66	0	v5	VI
239	122	68	0	v5	VI
240	123	78	0	v5	VI
241	141	74	0	v5	VI
242	293	81	0	v5	VI
243	62	55	0	v5	VI

STRUCTURAL SAMPLING SITE DL93-23 (K) - 1993

No.	Strike	Dip	Width	Type	Note
244	62	72	0	v5	VI
245	90	82	0	v5	VI
246	131	71	0	v5	VI
247	147	62	0	v5	VI
248	121	79	0	v5	VI
249	159	90	0	v5	VI
250	122	68	0	v5	VI
251	135	70	0	v5	VI
252	115	68	0	v5	VI
253	150	80	0	v5	VI
254	135	70	0	v5	VI
255	116	75	0	v5	VI
256	146	74	0	v5	VI
257	123	55	0	v5	VI
258	310	83	0	v5	VI
259	96	84	0	v5	VI
260	118	81	0	v5	VI
261	124	72	0	v5	VI
262	110	83	0	v5	VI
263	123	69	0	v5	VI
264	103	78	0	v5	VI
265	166	83	0	v5	VI
266	324	67	0	v5	VI
267	308	75	0	v5	VI
268	111	72	0	v5	VI
269	125	78	0	v5	VI
270	300	78	0	v5	VI
271	168	65	0	v5	VI
272	120	80	0	v5	VI
273	126	78	0	v5	VI
274	100	66	0	v5	VI
275	163	67	0	v5	VI
276	118	87	0	v5	VI
277	133	69	0	v5	VI
278	130	54	0	v5	VI
279	136	70	0	v5	VI
280	112	61	0	v5	VI
281	105	60	0	v5	VI
282	93	76	0	v5	VI
283	101	80	0	v5	VI
284	99	75	0	v5	VI
285	109	67	0	v5	VI
286	111	71	0	v5	VI
287	113	74	0	v5	VI
288	155	55	0	v5	VI
289	139	72	0	v5	VI
290	90	84	0	v5	VI
291	251	85	0	v5	VI
292	48	84	0	v5	VI

STRUCTURAL SAMPLING SITE DL93-23 (K) - 1993

No.	Strike	Dip	Width	Type	Note
293	125	84	0	v5	VI
294	133	75	0	v5	VI
295	80	77	0	v5	VI
296	305	71	0	v5	VI
297	42	68	0	v5	VI
298	270	82	0	v5	VI
299	190	72	0	v5	VI
300	102	71	0	v5	VI
301	110	26	0	v5	VI
302	90	83	0	v5	VI
303	110	72	0	v5	VI
304	119	71	0	v5	VI
305	89	81	0	v4	VI
306	85	59	0	v4	VI
307	106	74	0	v4	VI
308	300	78	0	v1	VI
309	338	79	0	v1	VI
310	229	62	0	v1	VI
311	73	72	0	v1	VI
312	318	77	0	x	XIU
313	315	69	0	x	XIU
314	143	73	0	x	XIU
315	122	67	0	x	XIU
316	227	74	0	x	XIU
317	224	72	0	x	XIU
318	232	84	0	x	XIU

STRUCTURAL SAMPLING SITE DL93-24 (QS) - 1993
N4400 E3474 c2411 M3

No.	Strike	Dip	Width	Type	Note
1	101	60	0	v7	VI
2	88	54	0	v7	VI
3	90	64	0	v7	VI
4	83	56	0	v7	VI
5	56	40	0	v7	VI
6	78	63	0	v7	VI
7	85	65	0	v7	VI
8	65	68	0	v7	VI
9	270	72	0	v2	VI
10	30	84	0	v2	VI
11	101	60	0	v2	VI
12	50	88	0	v2	VI
13	40	84	0	v2	VI
14	35	71	0	v2	VI
15	255	88	0	v2	VI
16	50	81	0	v2	VI
17	27	50	0	v2	VI
18	40	33	0	v2	VI
19	2	78	0	v2	VI
20	21	63	0	v2	VI
21	63	35	0	v2	VI
22	66	86	0	v2	VI
23	64	86	0	v2	VI
24	65	80	0	v2	VI
25	33	64	0	v2	VI
26	103	64	0	v2	VI
27	161	70	0	v2	VI
28	240	58	0	v2	VI
29	52	54	0	v2	VI
30	60	75	0	v2	VI
31	51	75	0	v2	VI
32	50	82	0	v2	VI
33	46	80	0	v2	VI
34	225	73	0	v2	VI
35	37	85	0	v2	VI
36	58	87	0	v2	VI
37	31	70	0	v2	VI
38	137	46	0	v2	VI
39	75	50	0	v2	VI
40	41	84	0	v2	VI
41	44	42	0	v2	VI
42	52	50	0	v2	VI
43	54	62	0	v2	VI
44	49	72	0	v2	VI
45	102	70	0	v2	VI
46	47	84	0	v2	VI
47	88	82	0	v2	VI

STRUCTURAL SAMPLING SITE DL93-24 (QS) - 1993

No.	Strike	Dip	Width	Type	Note
48	147	83	0	v2	VI
49	60	76	0	v2	VI
50	104	73	0	v2	VI
51	255	88	0	v2	VI
52	74	74	0	v2	VI
53	52	25	0	v4	VI
54	267	27	0	v4	VI
55	300	25	0	v4	VI
56	332	63	0	v4	VI
57	43	41	0	v4	VI
58	25	33	0	v4	VI
59	90	46	0	v4	VI
60	72	74	0	v4	VI
61	350	57	0	v4	VI
62	243	75	0	v4	VI
63	341	32	0	v4	VI
64	86	46	0	v4	VI
65	290	54	0	v4	VI
66	54	53	0	v4	VI
67	60	38	0	v4	VI
68	88	60	0	v4	VI
69	67	68	0	v4	VI
70	300	57	0	v4	VI
71	231	22	0	v4	VI
72	118	25	0	v4	VI
73	329	54	0	v4	VI
74	324	54	0	v4	VI
75	302	42	0	v4	VI
76	355	14	0	v4	VI
77	351	40	0	v4	VI
78	100	37	0	v4	VI
79	174	56	0	v4	VI
80	150	52	0	v4	VI
81	160	55	0	v4	VI
82	168	49	0	v4	VI
83	35	64	0	v4	VI
84	31	74	0	v4	VI
85	83	83	0	v4	VI
86	105	77	0	v4	VI
87	119	75	0	v4	VI
88	73	68	0	v4	VI
89	22	44	0	v5	VI
90	20	46	0	v5	VI
91	20	75	0	v5	VI
92	340	60	0	v5	VI
93	80	66	0	v5	VI
94	230	72	0	v5	VI
95	229	71	0	v5	VI
96	53	59	0	v5	VI

STRUCTURAL SAMPLING SITE DL93-24 (QS) - 1993

No.	Strike	Dip	Width	Type	Note
97	222	50	0	v5	VI
98	84	76	0	v5	VI
99	267	84	0	v5	VI
100	91	73	0	v5	VI
101	30	84	0	v5	VI
102	57	33	0	v5	VI
103	241	76	0	v5	VI
104	220	74	0	v5	VI
105	95	77	0	v5	VI
106	72	29	0	v5	VI
107	50	36	0	v5	VI
108	49	55	0	v5	VI
109	319	79	0	v5	VI
110	155	46	0	v5	VI
111	279	78	0	v5	VI
112	76	87	0	v5	VI
113	77	90	0	v5	VI
114	43	87	0	v5	VI
115	73	60	0	v5	VI
116	88	10	0	v5	VI
117	96	67	0	v5	VI
118	86	62	0	v5	VI
119	91	65	0	v5	VI
120	61	74	0	v5	VI
121	147	70	0	v5	VI
122	92	42	0	v5	VI
123	66	71	0	v5	VI
124	65	84	0	v5	VI
125	81	88	0	v5	VI
126	106	78	0	v5	VI
127	31	45	0	v5	VI
128	97	73	0	v5	VI
129	313	65	0	x	XIU
130	330	73	0	x	XIU
131	71	25	0	v3	VI
132	298	71	0	v3	VI
133	110	57	0	v3	VI
134	108	62	0	v3	VI
135	92	37	0	v3	VI
136	2	84	0	v7	VI
137	40	66	0	v7	VI
138	26	38	0	v7	VI
139	30	35	0	v7	VI
140	46	42	0	v7	VI
141	337	49	0	v7	VI
142	57	80	0	v7	VI
143	56	79	0	v7	VI
144	48	78	0	v7	VI
145	56	70	0	v7	VI

STRUCTURAL SAMPLING SITE DL93-24 (QS) - 1993

No.	Strike	Dip	Width	Type	Note
146	51	79	0	v7	VI
147	51	77	0	v7	VI
148	63	80	0	v7	VI
149	73	30	0	v7	VI
150	72	28	0	v7	VI
151	80	28	0	v7	VI
152	45	24	0	v7	VI
153	58	67	0	v7	VI

STRUCTURAL SAMPLING SITE DL93-25 (QS) - 1993
N4418 E3463 c2411 M3

No.	Strike	Dip	Width	Type	Note
1	231	39	0	v7	VI
2	286	44	0	v7	VI
3	141	78	0	v7	VI
4	243	71	0	v7	VI
5	239	76	0	v7	VI
6	244	90	0	v7	VI
7	240	61	0	v7	VI
8	298	77	0	v7	XID
9	305	79	0	v7	XIS
10	252	61	0	v7	VI
11	240	77	0	v7	VI
12	265	80	0	v7	VI
13	335	90	0	v7	VI
14	258	33	0	v2	XID
15	302	85	0	v2	XID
16	132	74	0	v2	VI
17	355	65	0	v2	VI
18	286	44	0	v2	VI
19	152	40	0	v2	VI
20	208	48	0	v2	VI
21	290	34	0	v2	VI
22	131	89	0	v2	VI
23	260	54	0	v2	VI
24	311	77	0	v2	VI
25	356	68	0	v2	VI
26	213	50	0	v2	VI
27	44	37	0	v2	VI
28	233	83	0	v2	VI
29	2	20	0	v2	VI
30	42	45	0	v2	VI
31	141	79	0	v2	VI
32	25	60	0	v2	VI
33	234	52	0	v2	VI
34	271	40	0	v2	VI
35	239	45	0	v2	VI
36	256	33	0	v2	VI
37	311	84	0	v2	VI
38	335	90	0	v2	VI
39	127	79	0	v2	VI
40	230	58	0	v2	VI
41	294	25	0	v2	VI
42	339	31	0	v2	VI
43	27	74	0	v2	VI
44	35	54	0	v2	VI
45	246	31	0	v2	VI
46	355	38	0	v2	VI
47	253	75	0	v2	VI

STRUCTURAL SAMPLING SITE DL93-25 (QS) - 1993

No.	Strike	Dip	Width	Type	Note
48	30	80	0	v2	VI
49	353	65	0	v2	VI
50	206	85	0	v2	VI
51	34	55	0	v2	VI
52	27	45	0	v2	VI
53	80	68	0	v2	VI
54	31	44	0	v2	VI
55	36	42	0	v4	VI
56	112	65	0	v4	VI
57	150	55	0	v4	VI
58	110	69	0	v4	VI
59	133	65	0	v4	VI
60	130	54	0	v4	VI
61	105	84	0	v5	VI
62	138	56	0	v5	VI
63	122	86	0	v5	VI
64	222	51	0	v5	VI
65	108	61	0	v5	VI
66	294	86	0	v5	VI
67	354	90	0	v5	VI
68	287	84	0	v5	VI
69	43	88	0	v5	VI
70	47	38	0	v5	VI
71	185	36	0	v5	VI
72	134	72	0	v5	VI
73	133	60	0	v5	VI
74	117	51	0	v5	VI
75	264	15	0	v5	VI
76	141	53	0	v5	VI
77	124	63	0	v5	VI
78	326	82	0	v5	VI
79	90	44	0	v5	VI
80	31	48	0	v5	VI
81	274	77	0	v5	VI
82	119	57	0	v5	VI
83	108	59	0	v5	VI
84	280	82	0	v5	VI
85	238	90	0	v5	VI
86	31	40	0	v5	VI
87	9	46	0	v5	VI
88	143	61	0	v5	VI
89	210	50	0	v5	VI
90	224	54	0	v5	VI
91	223	45	0	v5	VI
92	222	51	0	v5	VI
93	112	60	0	v5	VI
94	115	57	0	v5	VI
95	93	61	0	v5	VI
96	109	37	0	v5	VI

STRUCTURAL SAMPLING SITE DL93-25 (QS) - 1993

No.	Strike	Dip	Width	Type	Note
97	275	46	0	v5	VI
98	221	51	0	v3	VI
99	225	56	0	v3	VI
100	223	58	0	v3	VI
101	226	56	0	v3	VI
102	249	54	0	v3	VI
103	8	25	0	v3	VI
104	250	32	0	v3	VI
105	224	41	0	v3	VI
106	243	45	0	v3	VI
107	222	50	0	v3	VI
108	219	48	0	v3	VI
109	194	44	0	v3	VI
110	10	20	0	v3	VI
111	238	48	0	v3	VI
112	237	63	0	v3	VI
113	225	50	0	v3	VI
114	247	55	0	v3	VI
115	228	49	0	v3	VI
116	223	47	0	v3	VI
117	294	20	0	v3	VI
118	358	21	0	v3	VI
119	291	87	0	v3	VI
120	296	73	0	v3	VI
121	228	54	0	v3	VI
122	223	56	0	v3	VI
123	260	58	0	v3	VI
124	235	68	0	v3	VI
125	225	50	0	v3	VI
126	231	52	0	v3	VI
127	325	57	0	v3	VI
128	226	58	0	v3	VI
129	233	44	0	v3	VI
130	220	51	0	v3	VI
131	248	77	0	v3	VI
132	337	25	0	v3	XID
133	341	34	0	v3	VI
134	216	54	0	v3	VI
135	220	53	0	v3	VI
136	225	51	0	v3	VI
137	216	36	0	v3	VI
138	185	36	0	v3	VI
139	217	52	0	v3	VI
140	208	50	0	v3	VI
141	218	56	0	v3	VI
142	0	32	0	v3	VI
143	221	48	0	v3	VI
144	224	54	0	v3	VI
145	222	48	0	v3	VI

STRUCTURAL SAMPLING SITE DL93-25 (QS) - 1993

No.	Strike	Dip	Width	Type	Note
146	222	37	0	v3	VI
147	200	50	0	v3	VI
148	156	55	0	v3	VI
149	160	59	0	v3	VI
150	207	50	0	v3	VI
151	298	77	0	v7	VI
152	305	79	0	v7	XIS
153	290	54	0	v7	VI
154	265	89	0	v7	VI
155	335	90	0	v7	VI
156	284	83	0	v7	VI
157	283	89	0	v7	VI

STRUCTURAL SAMPLING SITE DL93-26 (Chloritic) - 1993
N4527 E4075 c2773 F4

No.	Strike	Dip	Type	Note
1	275	14	XIS	XIS
2	264	3	XIS	XIS
3	270	16	XIS	XIS
4	180	0	LI-MIN	LI-MIN 185/60
5	33	24	LI-MIN	LI-MIN 344/37
6	74	36	A	JI-FRAC
7	111	77	A	JI-FRAC
8	325	35	A	JI-FRAC
9	40	89	A	JI-FRAC
10	116	70	A	JI-FRAC
11	308	32	A	JI-FRAC
12	52	64	A	JI-FRAC
13	297	86	A	VI
14	301	82	A	VI
15	296	72	A	JI-FRAC
16	199	74	A	JI-FRAC
17	301	74	A	JI-FRAC
18	134	50	A	JI-FRAC
19	153	85	A	JI-FRAC
20	335	38	A	JI-FRAC
21	348	39	A	JI-FRAC
22	140	48	T	JI-FRAC
23	138	47	T	JI-FRAC
24	115	62	T	JI-FRAC
25	127	48	T	JI-FRAC
26	257	30	T	JI-FRAC
27	276	27	T	JI-FRAC
28	116	59	T	JI-FRAC
29	112	62	T	JI-FRAC
30	116	57	T	JI-FRAC
31	114	60	T	JI-FRAC
32	140	58	T	JI-FRAC
33	131	63	T	JI-FRAC
34	264	41	T	JI-FRAC
35	116	60	T	JI-FRAC
36	104	88	U	VI
37	310	46	U	VI
38	108	69	U	VI
39	298	72	U	VI
40	298	83	U	VI
41	285	84	U	VI
42	304	84	U	VI
43	301	78	U	VI
44	277	90	U	VI
45	196	69	U	VI
46	106	57	V	VI
47	112	71	V	VI

STRUCTURAL SAMPLING SITE DL93-26 (Chloritic) - 1993

No.	Strike	Dip	Type	Note	
48	211	72	V	VI	
49	216	69	V	VI	
50	193	60	V	VI	
51	204	66	V	VI	
52	217	70	V	VI	
53	203	68	V	VI	
54	195	68	V	VI	
55	193	70	V	VI	
56	290	78	V	VI	
57	319	34	V	VI	
58	203	66	V	VI	
59	200	75	V	VI	
60	207	62	V	VI	
61	289	78	V	VI	
62	120	62	V	VI	
63	125	64	V	VI	
64	125	66	V	VI	
65	122	60	V	VI	
66	126	85	V	VI	
67	135	66	V	VI	
68	113	84	V	VI	
69	121	90	V	VI	
70	125	58	V	VI	
71	287	90	V	VI	
72	120	85	V	VI	
73	135	75	V	VI	
74	122	48	V	VI	
75	112	74	V	VI	
76	213	63	W	VI	
77	205	68	W	VI	
78	204	69	W	VI	
79	203	67	W	VI	
80	200	72	W	VI	
81	204	72	W	VI	
82	200	75	W	VI	
83	205	71	W	VI	
84	197	75	W	VI	
85	198	75	W	VI	
86	267	77	X	VI	14->275
87	262	76	X	VI	03->264
88	269	80	X	VI	16->270
89	185	60	X	VI	00->180
90	344	37	X	VI	24->033

Appendix 2. Open Pit Surface Mapping Database

Structural database for project : "Actualization of Principal Fault Structures"

A digital database containing data from open-pit bench-face mapping was constructed from information contained on the individual map sheets that were used to consruct a 1:2000 principal fault structures map of the Chuquicamata deposit. This database, in both digital and field map sheets forms, is maintained by the geological department of CODELCO-Chuquicamata.

This appendix is an excerpt from that database used in concert with notes from appropriate field mapping sheets to describe and classify the fault systems and vein arrays presented in Chapter 6. Methodology and results of this project are discussed in Chapter 6.

Database Key :

black \ bed = sedimentary layering
blue = fault type # 3
brown = fault type # 2
contact = lithological contact
folia / mylonite = fault type # 1
green = vein type #2
orange = vein type #1
red = vein type # 4
yellow = vein type # 3

STRUCTURAL SECTOR A - ZARAGOZA

North	East	Elev	Strike	Dip	Width	Type
5195	3404	2624	5	82	0.010	blue
5132	3612	2595	60	60	99.000	blue
5082	3444	2591	280	90	99.000	blue
5105	3558	2595	60	60	99.000	blue
5166	3696	2628	180	82	99.000	blue
5229	3258	2702	359	61	99.000	blue
5399	3277	2773	20	85	0.030	blue
5185	3611	2625	145	50	0.050	blue
5342	3128	2776	246	38	0.010	blue
5155	3331	2636	326	79	0.700	blue
4995	3114	2652	37	90	0.010	blue
4977	3151	2618	40	90	0.030	blue
4793	3416	2468	169	87	0.100	blue
4984	3137	2640	25	85	0.000	blue
4972	3134	2638	205	85	0.050	blue
5175	3364	2634	52	65	0.050	blue
5038	3369	2593	205	84	0.050	blue
4988	3287	2592	56	90	0.010	blue
4831	3269	2542	273	86	0.100	blue
5242	3272	2698	339	75	0.030	blue
5431	3467	2773	180	84	0.010	blue
5437	3714	2712	270	65	0.100	blue
5454	3221	2819	210	70	2.000	blue
5429	3438	2773	205	87	0.010	blue
5706	3902	2800	174	67	0.010	blue
5668	3831	2772	195	70	0.200	blue
5621	3807	2757	210	65	0.400	blue
5742	3875	2803	95	75	0.010	blue
5611	3835	2754	80	72	0.100	blue
5537	3232	2851	40	90	0.010	blue
5251	3525	2644	45	55	0.050	blue
5256	3718	2657	158	61	0.010	blue
5219	3308	2677	10	63	0.050	blue
5219	3581	2625	73	66	0.010	blue
5268	3720	2660	174	71	0.010	blue
5254	3694	2655	36	90	0.500	blue
5371	3719	2690	186	73	0.750	blue
5308	3740	2676	130	63	0.010	blue
5339	3736	2682	135	66	0.010	blue
4790	3438	2470	65	82	0.050	blue
4666	3217	2520	334	88	0.010	blue
4734	3202	2542	3	88	0.010	blue
4777	3374	2468	123	81	0.010	blue
4693	3229	2517	5	74	0.010	blue
4743	3325	2467	26	82	0.010	blue
4786	3285	2523	120	80	0.030	blue
4728	3318	2467	288	83	0.050	blue
4622	3200	2525	349	71	0.010	blue

STRUCTURAL SECTOR A - ZARAGOZA (Continued)

North	East	Elev	Strike	Dip	Width	Type
4655	3212	2524	330	77	0.010	blue
4678	3224	2518	255	73	0.010	blue
4793	3411	2470	270	76	0.010	blue
4753	3211	2542	297	83	0.000	blue
4785	3227	2541	224	80	0.010	blue
4795	3232	2541	341	75	0.010	blue
5780	3901	2825	160	73	1.200	blue, green
4806	3519	2525	95	60	0.010	blue green
5121	3288	2621	355	87	0.010	blue green
5220	3561	2624	50	62	0.200	brown
5328	3509	2706	70	70	0.200	brown
5257	3498	2644	60	65	0.100	brown
5289	3414	2678	25	90	0.100	brown
5232	3499	2627	50	70	0.200	brown
5290	3538	2678	50	60	1.000	brown
5292	3469	2676	120	73	1.000	brown
5332	3457	2705	40	73	2.000	brown
5337	3551	2700	60	75	1.000	brown
5291	3511	2675	120	75	1.000	brown
5293	3428	2679	130	65	0.500	brown
5246	3413	2648	30	90	0.500	brown
5279	3595	2664	60	70	1.000	brown
5348	3598	2701	60	75	0.500	brown
4758	3261	2521	269	86	0.100	brown
4771	3360	2467	334	83	0.100	brown
4779	3225	2541	92	87	0.050	brown
4723	3244	2521	309	71	0.050	brown
5073	3509	2593	115	82	0.500	brown
5047	3212	2632	50	90	2.500	brown
5168	3670	2628	230	90	0.200	brown
5086	3472	2593	115	82	0.500	brown
5204	3294	2675	94	56	0.050	brown
5268	3301	2700	225	72	0.300	brown
5317	3393	2699	110	80	0.300	brown
5262	3355	2677	350	70	1.500	brown
5399	3277	2773	67	76	0.500	brown
5215	3360	2647	350	75	0.100	brown
5300	3361	2700	273	60	0.050	brown
5251	3281	2698	242	62	0.300	brown
5373	3216	2774	5	60	0.300	brown
5331	3421	2706	40	80	2.000	brown
5437	3557	2776	96	82	0.700	brown
5422	3591	2754	70	70	0.500	brown
5481	3644	2753	260	90	0.050	brown
5542	3686	2754	260	90	0.050	brown
5432	3483	2774	210	75	0.050	brown
5429	3401	2776	45	60	0.050	brown
5402	3476	2755	50	70	0.300	brown
5412	3532	2755	15	80	0.200	brown

STRUCTURAL SECTOR A - ZARAGOZA (Continued)

North	East	Elev	Strike	Dip	Width	Type
5460	3627	2756	240	90	0.300	brown
5503	3749	2733	195	64	0.200	brown
5603	3738	2752	230	65	0.500	brown
5464	3745	2721	195	64	0.800	brown
5589	3717	2753	260	90	0.100	brown
5469	3634	2755	240	90	0.050	brown
5661	3858	2772	35	90	0.300	brown
5424	3690	2713	185	75	0.100	brown
5763	3847	2803	175	75	0.500	brown
5312	3680	2672	15	90	0.100	brown
5386	3691	2699	180	75	0.100	brown
5323	3709	2676	75	75	0.500	brown
5345	3738	2683	76	56	0.200	brown
5693	3825	2779	175	55	2.500	brown
5256	3582	2648	40	65	4.000	brown
4768	3221	2541	270	85	0.020	brown
4709	3336	2445	60	72	0.020	brown
5418	3311	2772	30	90	0.010	brown
5574	3104	2897	200	50	0.700	brown
5546	3258	2849	41	90	1.000	brown
5660	3873	2773	180	65	0.500	brown
5286	3615	2678	40	73	1.000	brown
5752	3849	2800	177	64	0.500	brown
5420	3124	2821	217	46	0.100	brown
5455	3109	2844	48	88	0.020	brown
4972	3404	2569	320	65	0.100	brown
5124	3288	2636	5	84	0.100	brown
5158	3220	2676	239	62	0.100	brown
5133	3304	2635	320	80	0.100	brown
5025	3353	2591	0	90	0.100	brown
4971	3412	2568	320	65	0.100	brown
4893	3434	2541	170	78	0.030	brown
4961	3464	2572	95	70	0.030	brown
5102	3262	2635	46	90	0.350	brown
4820	3477	2516	30	70	0.100	brown
4934	3420	2555	42	90	0.050	brown
4933	3456	2554	50	90	0.050	brown
5026	3184	2635	224	77	0.150	brown
5186	3275	2674	320	70	99.000	brown
5187	3276	2675	89	84	0.010	brown
5165	3157	2707	19	74	0.010	brown
5170	3167	2706	10	68	0.010	brown
5102	3111	2707	19	72	0.020	brown
5175	3364	2634	326	76	0.050	brown
5094	3222	2646	310	74	0.050	brown
4933	3467	2555	50	74	0.100	brown
5091	3217	2647	247	72	0.010	brown
4806	3491	2515	25	90	0.300	brown
5180	3265	2673	2	80	0.030	brown

STRUCTURAL SECTOR A - ZARAGOZA (Continued)

North	East	Elev	Strike	Dip	Width	Type
4841	3280	2543	273	85	0.200	brown
4835	3275	2542	102	85	0.700	brown
4809	3240	2541	285	90	0.700	brown
4825	3339	2519	110	68	0.100	brown
4992	3144	2638	282	34	2.500	brown
4823	3266	2542	328	85	0.050	brown
4999	3161	2621	304	57	0.200	brown
4984	3154	2618	273	34	0.100	brown
4969	3148	2619	92	52	0.020	brown
4992	3144	2638	270	45	99.000	brown
5130	3616	2596	170	75	0.800	brown, green
5113	3688	2613	212	36	0.500	brown, green
5058	3400	2592	10	90	1.500	brown, green
4972	3134	2638	289	57	0.400	brown, orange
4852	3401	2523	145	72	0.100	brown, red
5149	3326	2634	0	90	0.300	brown, red
5248	3547	2644	200	90	0.400	brown, yellow
5401	3725	2700	55	67	99.000	brown, yellow
4950	3222	2593	355	75	0.300	brown, yellow
5185	3388	2622	42	65	2.500	brown, green
5433	3496	2778	219	70	4.000	brown, green
5348	3597	2701	254	77	0.010	folia
5254	3694	2655	224	75	99.000	green
4788	3393	2468	342	84	0.500	green
4893	3363	2542	350	90	1.000	green
4739	3322	2468	325	82	0.400	green
4950	3477	2570	230	84	0.700	green
4935	3440	2554	5	90	1.000	green
5430	3413	2774	146	40	0.400	green
4964	3250	2592	355	90	1.000	green
4946	3350	2565	20	90	3.000	green
5388	3699	2698	227	68	0.400	green
5365	3742	2688	205	86	0.300	green
5229	3664	2649	18	90	0.500	green
4855	3418	2522	130	75	0.200	green
4969	3416	2568	240	70	0.300	green
4934	3416	2556	345	90	0.400	green
4935	3424	2555	0	90	0.100	green
5229	3676	2647	205	82	2.000	green
4940	3277	2573	80	87	0.050	green
5206	3595	2625	70	80	1.500	green
5167	3349	2636	20	84	0.300	green
4747	3330	2466	4	72	0.350	green
5185	3611	2625	187	76	0.200	green
4798	3296	2525	294	72	0.300	green
5216	3589	2627	45	55	0.100	green
5184	3381	2635	347	82	0.300	green
5102	3262	2635	10	47	0.150	green
4684	3226	2518	264	86	0.200	green

STRUCTURAL SECTOR A - ZARAGOZA (Continued)

North	East	Elev	Strike	Dip	Width	Type
4698	3232	2518	314	71	0.200	green
5149	3331	2620	5	90	0.500	green
5089	3535	2594	18	90	2.000	green
5018	3341	2593	345	90	0.300	green
5061	3399	2597	186	85	2.000	green
5169	3635	2623	216	76	0.700	green
4828	3473	2518	25	90	4.000	green
5222	3540	2623	198	70	0.600	green
4964	3424	2567	220	80	1.500	green
5728	3883	2798	194	86	2.000	green, blue
5027	3351	2594	5	90	0.400	green, brown
4999	3307	2592	5	90	0.400	green, brown
5835	3863	2824	175	72	0.010	green, brown
5595	3761	2747	105	70	0.100	green, brown
5789	3891	2822	195	76	0.400	green, brown
5155	3331	2636	32	72	0.400	green, brown
5219	3581	2625	188	75	1.700	green blue
5205	3420	2623	38	68	0.350	green blue
5219	3577	2624	10	55	0.100	green yellow
5422	3326	2773	13	75	0.600	green yellow
5389	3256	2772	315	53	0.200	green yellow
5283	3325	2699	40	90	0.020	orange
5177	3617	2624	221	87	0.200	orange
5291	3339	2700	338	75	0.500	orange
4855	3420	2522	355	80	0.300	orange
4962	3444	2569	160	74	0.300	orange
4971	3409	2568	185	90	0.450	orange
4961	3453	2569	15	90	0.100	orange
5167	3635	2618	205	75	0.500	orange, brown
4897	3409	2541	350	90	0.500	orange, green
4934	3403	2558	350	90	0.200	orange, green
4717	3311	2469	320	80	0.300	red
4769	3268	2520	180	79	0.400	red
4752	3338	2467	3	73	0.400	red
4795	3292	2526	270	88	0.600	red
4679	3298	2467	110	85	0.200	red
4753	3259	2520	352	80	2.000	red
4619	3271	2468	118	80	0.350	red
4715	3239	2520	117	71	0.050	red
4849	3436	2521	15	90	0.200	red
5260	3474	2650	10	90	0.200	red
4712	3237	2521	260	74	0.100	red, brown
5193	3397	2634	65	87	0.050	red, brown
4895	3427	2542	10	90	0.200	red, green
5633	3895	2773	183	85	0.300	yellow
5345	3716	2682	10	90	99.000	yellow
4717	3240	2520	170	88	0.030	yellow
5306	3749	2676	130	54	0.200	yellow
5175	3255	2674	298	70	5.000	yellow

STRUCTURAL SECTOR A - ZARAGOZA (Continued)

North	East	Elev	Strike	Dip	Width	Type
4784	3280	2524	52	78	0.020	yellow
5306	3366	2701	315	60	0.300	yellow
4745	3254	2519	236	76	0.010	yellow
5165	3656	2620	210	70	0.400	yellow
5291	3338	2698	325	88	0.300	yellow
5117	3280	2634	65	90	0.400	yellow
5258	3346	2678	348	86	0.300	yellow
5245	3340	2676	354	88	0.200	yellow, brown
4955	3364	2566	15	90	0.100	yellow, green
4718	3342	2441	20	74	0.200	yellow, orange
5430	3428	2774	240	87	0.010	yellow red
5431	3419	2773	228	88	0.400	yellow red

STRUCTURAL SECTOR B - ESTANQUES BLANCOS

North	East	Elev.	Strike	Dip	Width	Type
4540	3597	2516	80	70	99.000	blue
4568	3454	2416	164	90	99.000	blue
4474	3574	2469	100	40	0.010	blue
4454	3578	2463	165	90	0.010	blue
4555	3596	2518	45	90	99.000	blue
5092	3967	2786	67	82	0.010	blue
4570	3989	2700	120	73	0.050	blue
4540	3597	2516	300	85	99.000	blue
5159	3993	2794	210	88	0.010	blue
4467	3409	2391	234	80	0.100	blue
4420	3857	2618	235	88	0.002	blue
4979	3860	2707	36	90	0.010	blue
4449	3800	2592	282	67	99.000	blue
4593	3442	2413	105	64	0.050	blue
4407	3869	2623	150	63	0.010	blue
5095	3746	2624	45	38	0.300	blue
4416	3911	2652	140	76	0.010	blue
5006	3779	2650	194	75	0.010	blue
4497	3309	2389	70	84	99.000	blue
4497	3309	2389	70	84	99.000	blue
4433	3317	2362	50	90	0.010	blue
4408	3307	2361	50	90	0.010	blue
4656	4169	2795	120	55	0.010	blue
4665	4134	2774	120	33	0.010	blue
5208	3855	2700	214	78	0.010	blue
4503	3931	2673	100	87	0.100	blue
4650	4064	2724	220	72	0.010	blue
5055	3969	2789	66	82	0.300	blue
5035	3994	2794	41	90	0.350	blue
4706	3554	2522	40	90	0.010	blue
4537	3947	2674	250	87	0.050	blue
4526	3399	2399	40	40	0.100	blue
4488	3886	2649	105	74	0.100	blue
5053	3883	2745	70	65	0.400	blue
4570	3351	2396	35	77	0.050	blue
4593	3320	2415	63	90	0.050	blue
4762	3960	2702	90	86	0.010	blue
4767	3955	2701	122	80	0.010	blue
4784	3798	2619	125	71	0.010	blue
4751	3478	2470	109	80	0.010	blue
4499	3613	2516	115	75	99.000	blue
4732	4037	2724	100	64	0.010	blue
4981	3779	2649	204	74	0.010	blue
4791	3977	2720	116	65	0.010	blue
4757	3972	2704	96	75	0.200	blue
4751	3716	2567	70	58	0.010	blue
4546	3752	2567	130	80	0.050	blue
4529	3697	2542	270	83	0.050	blue

STRUCTURAL SECTOR B - ESTANQUES BLANCOS (Cont.)

North	East	Elev.	Strike	Dip	Width	Type
4488	3675	2543	90	90	0.050	blue
4469	3727	2570	92	66	0.050	blue
4543	3751	2568	132	72	0.040	blue
4523	3736	2568	125	84	0.040	blue
4788	3757	2594	126	63	0.010	blue
4488	3713	2567	124	79	0.050	blue
4921	3862	2709	130	80	99.000	blue
4921	3862	2709	194	90	0.010	blue
4975	3644	2584	89	67	2.000	blue
4445	3860	2618	73	86	99.000	blue
4998	3922	2774	210	85	0.010	blue
4993	3860	2707	218	86	0.010	blue
4991	3860	2706	110	70	0.010	blue
4908	3874	2714	106	78	0.010	blue
4939	3862	2707	190	90	0.010	blue
4741	3986	2706	113	62	0.010	blue
4732	3803	2595	116	67	0.020	blue
4978	3748	2619	20	75	0.010	blue
4908	3755	2621	20	80	0.100	blue
4934	3786	2650	75	36	0.200	blue
4418	3803	2593	60	88	99.000	blue
4407	3804	2593	83	82	99.000	blue
4910	3754	2620	82	40	0.300	blue
4747	3942	2691	150	60	0.010	blue
4384	3858	2621	55	74	0.300	blue
5505	3940	2773	187	58	0.010	blue
5561	3886	2751	54	52	0.030	blue
4632	3747	2541	120	70	0.010	blue
5561	3886	2751	127	40	99.000	blue
5550	3962	2796	56	70	0.200	blue
4657	3568	2521	120	68	99.000	blue
4691	3760	2568	166	64	0.010	blue
4658	3730	2541	70	57	0.010	blue
4590	3819	2593	60	63	0.400	blue
5353	4015	2795	187	70	0.010	blue
4606	3785	2570	243	77	0.100	blue
4640	3787	2571	108	64	0.010	blue
4608	3749	2543	38	90	0.010	blue
5302	4007	2793	50	70	0.300	blue
5361	4014	2795	50	90	0.200	blue
5342	4013	2794	40	76	0.200	blue
4451	4088	2773	270	85	0.010	blue
4505	4140	2794	102	57	0.300	blue
4405	4067	2773	227	76	0.010	blue
4438	4121	2794	100	68	0.010	blue
4898	4030	2795	50	86	0.200	blue
4876	4047	2794	80	70	0.300	blue
4333	3306	2350	40	82	99.000	blue
3895	4227	2829	153	68	99.000	blue

STRUCTURAL SECTOR B - ESTANQUES BLANCOS (Cont.)

North	East	Elev.	Strike	Dip	Width	Type
4328	3619	2468	185	66	0.010	blue
5476	4029	2802	172	74	0.010	blue
4630	3369	2391	259	81	0.150	blue
4370	3613	2471	140	68	0.010	blue
4356	3469	2389	46	70	0.400	blue
4422	3245	2415	68	90	0.050	blue
5604	3859	2750	65	85	0.050	blue
4477	3207	2468	340	87	99.000	blue
5389	3752	2697	110	69	0.200	blue
4671	3882	2620	116	71	0.010	blue
4364	3939	2701	65	78	99.000	blue
5271	3800	2678	103	68	0.010	blue
4529	3979	2697	315	75	0.200	blue
4328	3863	2625	115	80	0.030	blue
4302	3864	2626	240	40	0.050	blue
5261	3973	2776	45	90	0.010	blue
5249	3846	2698	132	60	0.010	blue
4357	3875	2628	110	90	0.100	blue
5230	3973	2776	102	50	0.040	blue
5223	3853	2699	140	60	0.010	blue
5233	4005	2795	220	80	0.050	blue
5393	3750	2698	160	82	0.010	blue
5214	3974	2779	65	90	0.300	blue
4359	3857	2622	40	85	0.200	blue
4399	3941	2699	55	75	99.000	blue
5024	3746	2621	48	90	0.300	blue, green
4568	3454	2416	115	75	0.100	blue, green
4907	3790	2650	20	90	0.600	blue, green?
4951	4006	2798	85	90	0.700	blue, orange
5448	3916	2758	60	90	0.400	blue, yellow
5194	3966	2779	60	90	0.600	blue, yellow
4996	3993	2795	327	70	0.150	blue brown
4436	3588	2465	148	60	0.010	blue green
4370	4092	2795	91	44	0.010	blue orang
4344	3307	2349	52	85	0.250	blue red?
5427	3883	2747	75	70	4.000	blue yellow
5207	3903	2747	75	85	1.500	blue yellow
4708	4129	2775	90	90	1.000	blue yellow
4359	3325	2349	70	85	0.010	blue yellow
4782	3527	2518	25	57	0.100	brown
4651	4133	2771	90	90	0.100	brown
4576	4052	2729	95	90	1.500	brown
4429	4120	2795	250	86	1.000	brown
4715	4001	2708	80	78	0.300	brown
4622	3889	2620	222	77	1.000	brown
4593	4160	2795	250	78	3.000	brown
4438	4121	2794	40	87	1.000	brown
4713	4049	2723	90	77	0.600	brown
4460	4088	2772	68	83	0.700	brown

STRUCTURAL SECTOR B - ESTANQUES BLANCOS (Cont.)

North	East	Elev.	Strike	Dip	Width	Type
4735	3738	2572	98	52	0.200	brown
4706	3748	2568	66	64	1.000	brown
4677	3772	2575	64	74	0.600	brown
4667	4016	2713	280	71	0.300	brown
4639	4036	2722	115	84	0.400	brown
4682	3769	2572	170	57	0.030	brown
4688	3717	2542	32	74	0.200	brown
4643	3784	2568	35	61	0.500	brown
4746	3688	2544	75	65	1.000	brown
4732	3700	2542	86	78	0.700	brown
4678	3876	2619	46	78	0.500	brown
4669	3968	2683	73	90	0.400	brown
4620	3300	2443	275	90	0.100	brown
4469	4089	2769	110	90	4.000	brown
4708	3817	2596	90	34	0.400	brown
4682	3498	2470	45	67	0.400	brown
4600	4032	2721	82	70	0.200	brown
4669	3559	2519	110	65	0.200	brown
4637	3310	2441	50	70	0.100	brown
4615	3963	2676	106	44	0.300	brown
4781	3527	2518	25	40	0.100	brown
5243	3845	2696	232	70	0.300	brown
5357	3803	2700	85	65	0.400	brown
5324	3815	2697	62	75	0.300	brown
5333	3973	2773	57	90	0.300	brown
5258	4006	2795	64	55	0.600	brown
5580	3876	2750	75	70	0.040	brown
5334	3945	2768	90	85	1.500	brown
5280	4004	2794	64	65	0.250	brown
5385	3756	2697	60	85	0.050	brown
5295	3782	2678	72	87	1.000	brown
5212	3808	2677	99	80	0.300	brown
5203	4004	2794	45	78	0.450	brown
5244	3974	2776	76	85	0.100	brown
5294	3826	2697	210	80	0.200	brown
5250	3846	2699	78	84	0.050	brown
5311	3821	2697	58	85	0.100	brown
5535	3895	2753	45	78	0.100	brown
4853	3762	2620	67	66	0.400	brown
4812	3783	2620	70	60	0.700	brown
4438	3251	2416	68	90	0.200	brown
4807	3654	2542	70	53	0.100	brown
4843	3921	2720	93	82	0.200	brown
4889	3977	2771	70	90	0.300	brown
4815	3649	2542	58	64	0.700	brown
4803	3788	2621	45	75	0.800	brown
5415	3955	2771	110	65	0.400	brown
5575	3946	2794	75	90	0.700	brown
5524	3935	2774	50	71	0.150	brown

STRUCTURAL SECTOR B - ESTANQUES BLANCOS (Cont.)

North	East	Elev.	Strike	Dip	Width	Type
5454	3876	2749	62	65	0.200	brown
4563	3246	2467	100	85	0.050	brown
4423	3279	2388	25	90	0.050	brown
5561	3920	2774	83	75	0.800	brown
5603	3996	2821	60	90	5.000	brown
4961	3780	2649	47	72	0.500	brown
4968	3717	2589	58	60	0.800	brown
4941	3750	2620	55	43	0.200	brown
4967	3670	2586	263	90	0.500	brown
4955	3862	2708	49	50	0.400	brown
4918	3958	2771	60	90	0.400	brown
4948	3688	2593	75	60	3.000	brown
4975	3934	2773	35	55	0.200	brown
4753	3788	2596	96	60	0.400	brown
4775	3670	2542	44	68	0.600	brown
4763	3537	2522	300	84	0.400	brown
4750	3681	2543	22	60	0.050	brown
4774	3997	2722	78	84	0.700	brown
4903	3724	2594	87	44	0.150	brown
4768	3815	2621	53	67	0.050	brown
4799	3923	2697	275	68	0.300	brown
5007	3717	2584	85	50	0.020	brown
5178	3811	2677	43	90	0.400	brown
5130	3879	2743	52	90	0.500	brown
5179	3860	2705	53	87	0.200	brown
5081	3838	2697	46	72	0.300	brown
5127	3810	2680	202	90	1.000	brown
5222	3713	2647	48	90	0.100	brown
5073	3808	2675	104	69	0.600	brown
5114	3994	2795	90	65	1.000	brown
5063	3747	2621	105	40	0.200	brown
5023	3715	2584	80	50	0.500	brown
5043	3707	2583	11	76	0.040	brown
5050	3779	2652	90	90	0.050	brown
5105	3809	2679	71	56	0.150	brown
5170	3854	2699	82	78	0.200	brown
5072	3847	2700	116	65	0.100	brown
5156	3853	2698	110	90	0.100	brown
4379	3874	2626	135	75	0.300	brown
4358	3803	2594	60	70	0.350	brown
4319	3837	2618	50	76	0.200	brown
4359	3884	2646	40	90	0.050	brown
4393	3803	2593	114	73	0.100	brown
4526	3978	2696	130	85	0.050	brown
4449	3385	2364	228	84	0.200	brown
4400	3379	2362	55	90	0.200	brown
4552	3387	2393	40	50	0.040	brown
4363	3871	2625	30	62	0.500	brown
4355	3943	2701	154	90	0.700	brown

STRUCTURAL SECTOR B - ESTANQUES BLANCOS (Cont.)

North	East	Elev.	Strike	Dip	Width	Type
4310	3669	2517	90	75	0.150	brown
4314	3616	2467	116	83	0.300	brown
4469	3955	2697	120	90	0.150	brown
4303	3708	2540	120	72	0.100	brown
4303	3765	2579	95	90	0.100	brown
4425	3951	2698	275	85	0.150	brown
4370	3889	2650	60	76	0.020	brown
4341	3864	2626	85	79	0.050	brown
4577	3991	2701	45	75	0.100	brown
4418	3911	2672	55	80	0.100	brown
4303	3614	2469	280	87	0.600	brown
4452	3670	2540	115	60	0.010	brown
4454	3640	2517	115	75	0.010	brown
4457	3729	2568	130	61	0.020	brown
4400	3702	2541	195	90	0.020	brown
4431	3559	2438	188	84	0.200	brown
4442	3728	2569	56	52	0.010	brown
4441	3413	2391	57	78	0.500	brown
4510	3406	2400	60	90	0.700	brown
4541	3505	2437	283	80	0.400	brown
4536	3462	2415	71	90	0.250	brown
4593	3514	2467	65	75	0.400	brown
4452	3475	2390	78	72	0.020	brown
4423	3686	2540	50	90	0.100	brown
4441	3681	2541	55	65	0.300	brown
4406	3857	2619	48	73	0.020	brown
4407	3600	2468	90	77	0.400	brown
4435	3503	2413	60	47	0.030	brown
4426	3417	2391	65	75	0.050	brown
4474	3799	2592	242	82	0.020	brown
4400	3427	2391	52	80	0.030	brown
4429	3484	2391	102	88	0.030	brown
4435	3482	2390	13	62	0.030	brown
4336	3735	2568	57	77	0.050	brown
4585	4028	2721	205	90	0.050	brown
4564	3988	2699	70	85	1.000	brown
4464	3859	2618	25	65	0.400	brown
4362	3766	2582	130	65	0.040	brown
4383	3703	2540	203	80	0.010	brown
4572	4156	2793	110	65	0.300	brown
4372	3404	2368	52	68	0.300	brown
4403	4108	2795	64	78	0.500	brown
4448	3956	2698	172	72	0.700	brown
4584	4121	2771	258	86	0.200	brown
4597	4126	2774	68	84	0.600	brown
4301	3737	2567	89	78	0.050	brown
4316	3705	2541	45	75	0.050	brown
4371	3534	2413	105	70	0.030	brown
4416	3911	2652	244	90	0.250	brown

STRUCTURAL SECTOR B - ESTANQUES BLANCOS (Cont.)

North	East	Elev.	Strike	Dip	Width	Type
4598	3995	2704	97	75	0.300	brown
4491	3871	2620	245	85	0.350	brown
4529	3804	2592	95	85	1.000	brown
5534	4000	2808	67	62	0.400	brown, blue
5457	4032	2804	58	66	0.400	brown, blue
5023	3782	2652	52	55	0.300	brown, green
4518	3473	2422	148	82	0.100	brown, green
4497	3309	2389	164	80	0.100	brown, red
4674	3443	2419	200	84	0.600	brown, red
4570	3371	2397	280	90	0.500	brown, red
4415	3383	2363	58	90	0.020	brown, red
4405	3516	2413	252	70	0.050	brown, red
4465	3799	2592	98	80	0.050	brown, yellow
4597	3960	2675	60	58	1.000	brown, yellow
4556	3455	2414	109	90	0.400	brown, yellow
4634	4006	2709	73	56	0.500	brown, yellow
5656	3920	2795	52	60	0.350	brown, yellow
5227	3804	2675	204	74	0.700	brown, yellow
5294	3972	2774	65	60	0.700	brown, yellow
4593	3995	2704	112	50	0.150	brown, yellow
5398	3965	2772	60	65	0.800	brown, yellow
4349	3766	2580	35	82	0.100	brown, yellow
4398	3888	2647	80	60	0.350	brown, yellow
5516	3899	2754	65	65	0.500	brown
4537	3328	2391	275	90	1.500	brown green
4677	3560	2519	112	75	0.200	brown green
4561	3433	2389	96	90	0.050	brown green
4632	3573	2519	67	63	0.350	brown green yellow
4373	4049	2777	56	80	0.600	brown red
4473	4134	2794	92	90	3.000	brown yellow
4470	3464	2389	5	75	0.300	brown yellow
4383	3516	2389	70	55	0.050	brown yellow
4708	3552	2522	42	40	0.600	brown yellow
4381	3606	2466	112	90	1.000	brown yellow
4426	3914	2652	55	75	2.500	folia
4339	3838	2619	45	64	99.000	folia
4453	3495	2414	208	50	0.200	green
4934	3720	2591	47	80	0.400	green
5089	3746	2623	32	75	99.000	green
4851	3633	2542	76	62	2.000	green
4376	3390	2364	188	64	2.500	green
4988	3780	2649	30	77	0.300	green
4387	3296	2362	255	76	0.020	green
4558	3454	2414	255	65	0.600	green
5080	3809	2677	210	77	1.000	green
4388	3524	2414	115	83	0.450	green
4575	3250	2467	153	75	0.020	green
4360	3544	2414	50	70	0.200	green
4460	3386	2363	168	67	0.200	green

STRUCTURAL SECTOR B - ESTANQUES BLANCOS (Cont.)

North	East	Elev.	Strike	Dip	Width	Type
4374	3580	2443	60	70	0.500	green
4359	3671	2517	230	85	0.350	green
5394	3935	2766	90	60	0.600	green
4366	3614	2470	75	90	1.500	green
4375	3581	2443	72	75	0.800	green
4367	3450	2389	30	80	2.000	green
4488	3276	2412	280	90	1.000	green
4320	3579	2439	120	72	0.100	green
5139	3720	2623	92	70	0.200	green
5041	3778	2650	60	80	0.200	green
4880	3728	2596	30	90	0.500	green
4833	3731	2595	182	74	0.300	green
4453	3260	2413	268	85	2.000	green
4526	3399	2399	246	73	0.600	green
4409	3382	2363	135	80	0.250	green
4443	3254	2414	340	88	1.000	green
5149	3709	2624	92	60	0.300	green
5034	3781	2651	82	62	0.300	green
4760	3536	2520	235	70	0.400	green
4773	3530	2518	230	57	1.300	green
4693	3472	2438	215	69	0.400	green
4427	3685	2540	80	75	0.200	green
4768	3459	2474	40	88	1.500	green
4497	3404	2395	191	70	5.000	green
4585	3488	2442	122	72	3.000	green
4774	3530	2518	205	65	1.500	green
4780	3767	2595	213	82	1.000	green
4747	3482	2467	47	84	0.350	green
4627	3451	2417	73	90	3.000	green
4650	3780	2569	61	58	0.200	green
4729	3545	2521	125	65	0.100	green
4739	3438	2443	215	82	4.000	green
4701	3713	2540	43	60	2.000	green
4632	3483	2443	60	87	0.500	green
4630	3475	2439	244	77	2.000	green
4742	3729	2570	46	58	0.600	green
4419	3419	2392	187	52	3.000	green
4574	3489	2442	220	75	2.500	green
4988	3614	2583	263	90	99.000	green
4400	3427	2391	220	58	3.000	green
4469	3539	2443	165	62	1.500	green
4653	3504	2474	83	72	1.500	green brown
4959	3937	2771	284	62	0.300	green, blue
4830	3770	2619	176	80	0.010	green, blue
4503	3283	2412	230	75	0.400	green, blue
4330	3548	2411	70	73	2.000	green, blue
4686	3764	2569	51	78	0.100	green, brown
4689	3558	2520	80	82	0.400	green, brown
5107	3741	2623	30	90	0.800	green, orange

STRUCTURAL SECTOR B - ESTANQUES BLANCOS (Cont.)

North	East	Elev.	Strike	Dip	Width	Type
4537	3328	2391	275	90	1.500	green, orange
4570	3371	2397	200	84	1.000	green, red
4465	3490	2416	60	90	99.000	green, red
4413	3567	2438	260	84	0.800	green, yellow
4322	3381	2352	65	90	0.400	green red
4369	3516	2388	56	70	0.300	green red
4401	3494	2389	242	70	0.550	green yellow
4408	3597	2466	58	90	2.000	green yellow
4343	3514	2390	32	88	0.200	green yellow
4423	3589	2464	84	90	0.700	green yellow
4565	3434	2390	130	82	99.000	green yellow
4594	3428	2391	68	90	0.300	green yellow
4512	3547	2463	208	78	0.400	green yellow
4489	3558	2466	235	53	0.500	green yellow
4557	3434	2391	258	66	0.850	green yellow
5445	3878	2748	234	77	0.150	mylonite
5627	3933	2796	50	90	1.000	orange
5326	4010	2794	67	80	0.300	orange
4423	3279	2388	305	85	99.000	orange
5319	4010	2795	60	63	0.500	orange
4656	4169	2795	120	76	0.010	orange
4447	3550	2440	220	75	0.350	orange
4945	3750	2619	112	30	0.020	orange
5678	3954	2823	110	56	0.500	orange
4415	3863	2611	165	20	0.050	orange
4693	3496	2468	67	82	1.000	orange
4990	3993	2795	288	57	0.500	orange
4559	3766	2569	101	60	0.350	orange
4371	3287	2362	240	90	0.010	orange
4373	3801	2592	60	80	0.250	orange
4934	3786	2650	90	90	0.400	orange
5580	3876	2750	90	80	1.000	orange
5512	3937	2772	20	90	0.200	orange
4677	3501	2472	63	73	0.100	orange red
4650	3972	2682	84	38	0.050	orange, blue
5456	3916	2759	232	86	0.800	orange, red
5479	3949	2774	240	85	0.250	orange, yellow
5682	3953	2825	60	66	0.350	orange, yellow
4637	3572	2519	67	90	0.400	orange green
4639	3397	2392	128	74	3.500	orange red
4356	3338	2327	165	70	0.200	orange red
4531	3444	2390	280	86	0.300	orange red
4684	4170	2795	105	69	0.010	orange yellow
4678	4133	2775	92	60	0.400	orange yellow
4756	3474	2474	80	73	0.150	red
4658	3318	2440	330	78	0.100	red
4494	3218	2468	304	90	2.000	red
4605	3481	2442	110	82	0.200	red
4739	3733	2572	41	45	0.800	red

STRUCTURAL SECTOR B - ESTANQUES BLANCOS (Cont.)

North	East	Elev.	Strike	Dip	Width	Type
5314	3974	2775	50	66	1.500	red, green
4379	3668	2519	50	65	0.150	yellow
4357	3707	2542	60	90	0.150	yellow
4682	3966	2684	100	57	0.200	yellow
5416	3930	2763	77	56	0.100	yellow
4501	3972	2697	140	85	0.150	yellow
4366	3701	2539	65	80	0.150	yellow
4334	3673	2519	90	80	0.100	yellow
4693	3829	2597	54	90	0.600	yellow
4317	3738	2568	325	62	0.250	yellow
5257	3839	2696	220	76	1.000	yellow
5680	3918	2803	238	88	0.250	yellow
4327	3767	2580	35	85	0.200	yellow
4514	3972	2696	140	78	0.150	yellow
5664	3963	2825	57	70	0.450	yellow
4392	3665	2518	40	80	0.200	yellow
4804	3958	2719	133	58	0.300	yellow
4488	3886	2649	67	50	0.400	yellow
4556	3984	2699	65	77	0.500	yellow
5405	3930	2763	74	82	0.500	yellow
5422	3952	2771	45	90	0.600	yellow
4559	3868	2619	120	90	0.400	yellow
5572	3947	2794	237	84	1.500	yellow
5645	3976	2824	234	83	0.500	yellow
4378	3290	2363	85	80	0.030	yellow
4645	3571	2520	80	90	0.500	yellow
5495	4024	2805	237	75	0.600	yellow
4334	3673	2519	90	80	0.070	yellow
4673	3882	2620	100	60	0.100	yellow
4473	3894	2651	265	70	1.000	yellow
4437	3888	2647	72	83	1.000	yellow
4565	3953	2672	85	42	0.400	yellow
4872	3756	2619	80	47	0.200	yellow
4425	3887	2649	58	77	0.700	yellow
5583	3943	2794	52	78	0.200	yellow
4402	3655	2516	40	80	0.050	yellow
4396	3874	2626	66	75	2.000	yellow
4430	3560	2438	105	50	0.100	yellow
5126	3842	2699	65	76	0.400	yellow
4508	3798	2592	45	82	0.100	yellow
4748	3799	2595	85	75	0.300	yellow
4410	3653	2518	105	75	0.100	yellow
4705	3554	2522	50	90	0.400	yellow
4993	3921	2773	74	90	0.150	yellow
4665	4061	2725	104	62	1.000	yellow
4606	4000	2705	135	57	0.500	yellow
5049	3815	2683	30	82	2.000	yellow
4492	3797	2592	142	61	0.050	yellow
4386	3874	2626	99	64	0.450	yellow

STRUCTURAL SECTOR B - ESTANQUES BLANCOS (Cont.)

North	East	Elev.	Strike	Dip	Width	Type
4715	3494	2467	63	77	0.200	yellow
4476	3671	2541	220	85	0.400	yellow
5136	3971	2784	235	78	0.050	yellow
5096	3996	2794	248	67	0.100	yellow
4434	3647	2518	110	90	0.150	yellow
4747	4025	2724	105	70	0.400	yellow
4738	3989	2706	111	70	0.400	yellow
5012	3780	2651	81	46	0.600	yellow
5152	3992	2794	253	85	0.100	yellow
5166	3810	2677	94	75	0.200	yellow
4401	3871	2623	95	65	0.030	yellow
5163	3972	2783	275	77	0.300	yellow
4457	3862	2619	165	75	0.020	yellow
4441	3645	2517	50	83	0.750	yellow
4597	3782	2567	252	87	0.100	yellow
5128	3971	2784	85	75	0.200	yellow
5328	3814	2697	110	53	0.150	yellow
4957	3748	2618	46	55	0.300	yellow
4629	4019	2717	84	76	0.300	yellow
4605	4057	2727	87	76	0.300	yellow
4337	3863	2626	45	80	0.030	yellow
4504	3873	2620	75	70	0.100	yellow
4327	3889	2647	82	64	99.000	yellow
5258	3805	2677	234	77	0.600	yellow
5340	3807	2698	71	78	0.800	yellow
4424	3801	2591	117	65	0.150	yellow
4449	3860	2618	42	65	0.100	yellow
4632	4063	2726	117	60	0.200	yellow
4603	4057	2727	84	62	0.200	yellow
4329	3735	2568	47	85	0.350	yellow
4312	3863	2625	40	63	0.050	yellow
4432	3800	2591	75	70	0.070	yellow
4308	3801	2593	50	78	0.070	yellow
5296	3777	2675	86	80	0.100	yellow
4399	3804	2593	60	80	0.100	yellow
4324	3862	2624	60	70	0.150	yellow
4778	3946	2700	111	45	0.200	yellow
4318	3802	2594	51	66	0.150	yellow
5378	3778	2699	69	58	0.300	yellow
4972	3746	2618	65	65	0.500	yellow
4378	3857	2622	48	73	0.050	yellow
4676	4057	2722	144	77	0.300	yellow
5375	3793	2699	34	76	0.200	yellow
4336	3800	2593	50	88	0.050	yellow
5274	3798	2677	56	82	0.200	yellow
4886	4039	2794	80	70	0.300	yellow, blue
5370	4013	2795	56	72	0.400	yellow, blue
5152	3810	2677	48	83	0.600	yellow, blue
5086	3786	2651	200	84	0.700	yellow, blue

STRUCTURAL SECTOR B - ESTANQUES BLANCOS (Cont.)

North	East	Elev.	Strike	Dip	Width	Type
4671	4016	2713	111	67	0.500	yellow, brown
4641	4018	2716	90	90	1.500	yellow, brown
4413	3567	2438	250	75	0.800	yellow, brown
4570	4024	2722	266	85	1.500	yellow, brown
4345	3708	2541	115	80	0.100	yellow, brown
4581	3879	2621	115	80	0.500	yellow, brown
5039	3851	2700	44	84	0.400	yellow, brown
5036	3852	2702	90	90	0.300	yellow, brown
4452	3889	2648	100	90	1.000	yellow, brown
4777	3705	2569	33	65	0.300	yellow, green
4701	3416	2413	217	86	1.500	yellow, green
5350	3972	2773	70	65	0.350	yellow, orange
5032	3917	2774	61	58	0.150	yellow, orange
4612	3326	2416	108	90	2.000	yellow, red

STRUCTURAL SECTOR C - BALMACEDA

North	East	Elev.	Strike	Dip	Width	Type
3970	4135	2776	200	52	0.010	bed
3958	3678	2519	95	87	0.500	black
4064	3616	2467	120	77	0.010	blue
4122	3810	2595	115	84	0.100	blue
4212	3605	2470	258	82	0.200	blue
4200	3608	2468	110	90	0.150	blue
4188	3609	2468	152	69	0.010	blue
4022	4031	2705	296	80	99.000	blue
4171	4007	2703	135	77	99.000	blue
3974	4039	2703	153	83	99.000	blue
4109	3664	2517	255	81	99.000	blue
4187	3661	2515	138	74	99.000	blue
4294	3801	2592	46	83	99.000	blue
4284	3976	2698	265	75	99.000	blue
4211	3998	2701	118	65	99.000	blue
4136	3928	2648	125	66	0.050	blue
4285	3803	2593	72	86	99.000	blue
4216	3810	2596	74	85	99.000	blue
4261	3540	2411	215	75	0.100	blue
4223	3597	2465	105	72	0.150	blue
4220	3509	2391	164	82	0.050	blue
4296	3971	2699	220	80	99.000	blue
4265	3803	2592	60	83	99.000	blue
3937	3990	2678	70	85	0.100	blue
4156	4011	2705	140	85	0.050	blue
4011	4159	2800	190	90	2.500	blue
4267	3740	2567	132	86	99.000	blue
4017	4091	2752	160	75	0.010	blue
4102	4022	2706	250	85	0.400	blue
3983	3981	2679	140	77	99.000	blue
3947	3986	2678	198	60	0.020	blue
3949	3951	2650	94	54	99.000	blue
4066	4152	2798	125	83	0.300	blue
4163	4008	2706	145	58	0.300	blue
3991	3790	2596	185	82	99.000	blue
3969	3784	2595	116	84	99.000	blue
4025	2779		140	90	0.010	blue
4184	4003	2701	105	86	99.000	blue
4283	3665	2517	80	85	99.000	blue
3999	3603	2464	150	57	0.010	blue
4271	3739	2567	95	81	99.000	blue
3975	3617	2492	270	82	0.200	blue
3943	3712	2542	125	86	0.100	blue
4265	3768	2578	290	90	99.000	blue
3960	3615	2492	68	78	0.100	blue
4030	3523	2413	205	85	0.010	blue
4063	3528	2414	160	70	0.010	blue
4015	4156	2798	330	65	99.000	blue

STRUCTURAL SECTOR C - BALMACEDA (Continued)

North	East	Elev.	Strike	Dip	Width	Type
4015	4156	2798	228	60	99.000	blue
4031	4162	2801	95	60	99.000	blue
4047	4189	2825	140	66	99.000	blue
4101	3968	2675	100	85	99.000	blue
4031	3606	2464	133	87	2.000	blue
4013	3487	2391	158	87	99.000	blue
4025	4128	2779	305	85	0.300	blue
4104	3494	2387	36	86	0.050	blue
4175	3409	2361	45	81	0.010	blue
4069	3491	2387	178	90	0.050	blue
4108	4148	2800	213	77	99.000	blue
4056	3563	2443	340	85	0.010	blue
4041	3525	2413	225	65	0.010	blue
4011	3520	2413	190	85	0.050	blue
4110	3536	2414	150	90	0.050	blue
4104	3494	2387	155	78	0.050	blue
4089	3534	2414	85	70	0.050	blue
4120	4150	2804	195	66	99.000	blue
3963	4112	2754	160	75	0.010	blue
4013	3487	2391	120	86	0.500	blue
4163	3922	2646	102	83	0.030	blue
4001	3896	2621	140	71	0.010	blue
3976	3514	2415	260	75	0.010	blue
4002	3760	2576	46	70	0.100	blue
4225	3808	2593	113	85	0.150	blue
4203	3876	2633	300	70	0.100	blue
4087	3968	2677	143	70	0.050	blue
3956	4160	2796	93	90	99.000	blue
4237	3908	2648	140	64	0.050	blue
3979	4137	2779	225	75	0.010	blue
4060	3970	2676	140	77	99.000	blue
4061	3615	2466	104	90	0.250	blue
3970	3549	2441	252	70	0.050	blue
3991	4166	2800	195	84	99.000	blue
3968	4166	2800	33	76	99.000	blue
4256	3806	2593	28	85	0.200	blue, yellow
4250	3807	2593	56	81	0.200	blue, yellow
4274	3601	2466	93	75	0.600	blue yellow
4229	3410	2348	83	76	0.050	blue yellow
4028	4162	2801	284	79	0.300	brown
4036	3829	2594	164	80	0.400	brown
4103	3932	2647	109	90	0.500	brown
4194	3921	2646	287	81	0.050	brown
4158	3809	2595	79	74	0.050	brown
4168	3853	2619	57	90	1.000	brown
4098	3619	2469	175	75	1.000	brown
4038	3608	2465	87	73	1.000	brown
4082	3871	2619	75	76	2.000	brown
4118	3614	2468	305	85	2.000	brown

STRUCTURAL SECTOR C - BALMACEDA (Continued)

North	East	Elev.	Strike	Dip	Width	Type
4212	3809	2595	120	90	0.400	brown
4284	3838	2618	41	60	0.400	brown
4233	3844	2619	55	90	0.700	brown
4250	3871	2630	65	80	0.500	brown
4292	3607	2466	250	83	0.400	brown
4257	3770	2578	320	70	0.300	brown
4293	3837	2618	43	80	0.300	brown
4269	3893	2646	54	66	0.050	brown
4098	4174	2824	286	65	99.000	brown
3965	4203	2826	30	90	99.000	brown
4070	4177	2822	10	45	99.000	brown
4015	4197	2830	170	85	99.000	brown
3953	4117	2755	268	86	0.050	brown
3974	4199	2826	11	70	99.000	brown
3964	4137	2776	132	74	2.000	brown
3932	4145	2776	173	76	0.400	brown
4288	3666	2517	105	77	0.030	brown
4223	3770	2573	120	90	0.010	brown
4209	3662	2517	110	85	0.050	brown
4288	3666	2517	105	77	0.030	brown
4116	4020	2704	36	78	2.500	brown
4065	4027	2706	105	80	1.000	brown
4232	3720	2543	105	90	0.010	brown
4161	4009	2705	86	84	4.000	brown
4293	3713	2541	265	70	0.100	brown
4224	3718	2541	105	90	0.100	brown
4252	3601	2465	144	87	0.300	brown
4219	3661	2517	90	90	0.150	brown
4249	3662	2517	135	80	0.050	brown
4294	3767	2579	50	72	0.050	brown
4214	3720	2541	105	90	0.070	brown
4284	3739	2567	48	86	0.070	brown
4063	3666	2516	120	88	0.500	brown
3968	3653	2515	112	85	1.500	brown
3983	3657	2515	65	86	1.500	brown
3975	3655	2515	90	75	1.500	brown
3968	3748	2571	70	70	0.400	brown
3988	3789	2596	134	82	0.500	brown
3918	3896	2621	97	90	0.050	brown
3957	3817	2624	140	65	1.500	brown
4010	3554	2440	324	76	0.150	brown
3955	3817	2623	140	65	1.500	brown
3983	3981	2679	260	83	0.150	brown
3936	3991	2680	255	80	0.600	brown
4147	3577	2440	110	88	0.200	brown
4292	3542	2410	210	78	0.200	brown
4053	3490	2386	131	90	0.700	brown
4237	3538	2412	135	70	0.050	brown
4305	3576	2439	245	82	0.100	brown

STRUCTURAL SECTOR C - BALMACEDA (Continued)

North	East	Elev.	Strike	Dip	Width	Type
4217	3541	2413	140	70	0.100	brown
4132	3468	2367	294	78	0.700	brown
4167	3544	2413	287	83	0.300	brown
3998	3692	2522	244	80	0.100	brown
4293	3486	2389	80	81	0.400	brown
4127	3538	2414	150	80	0.400	brown
4310	3488	2386	48	71	0.300	brown
3912	3851	2597	129	88	2.000	brown
4142	3577	2442	170	85	0.010	brown
4025	3665	2516	90	75	0.400	brown
4023	3760	2570	57	51	0.100	brown
4151	3662	2514	332	85	0.100	brown
4060	3666	2516	145	77	0.100	brown
4108	3665	2517	247	78	0.300	brown
4084	3617	2465	117	76	0.300	brown
4081	4116	2781	124	56	2.500	brown
3980	3598	2465	279	84	0.600	brown
4160	3610	2469	110	77	0.200	brown
3977	3477	2385	148	85	0.200	brown
3966	4040	2703	285	76	0.700	brown
4126	3567	2440	120	80	0.150	brown
4170	3609	2469	85	90	0.500	brown
3991	3887	2652	56	81	4.000	brown
4160	3543	2412	155	79	0.100	brown
4197	3659	2514	140	82	0.050	brown
4059	3464	2386	111	84	0.100	brown
4178	3543	2416	145	70	0.100	brown
4229	3808	2593	65	75	0.200	brown, red
4069	3814	2598	76	85	3.000	brown, red
4147	3611	2467	100	85	0.200	brown red
4010	4132	2777	12	70	0.100	folia
3979	4137	2779	245	60	0.010	folia
4265	3663	2516	70	83	0.200	green
4140	3492	2385	310	70	0.400	green
4146	3468	2363	95	90	0.500	green
4190	3461	2363	95	90	2.000	green
4196	3452	2359	47	90	2.000	green
4310	3488	2386	178	90	2.000	green
4059	3464	2386	180	87	0.200	green
4318	3546	2410	105	70	0.800	green
4224	3571	2438	230	86	0.450	green
4183	3413	2361	52	77	0.150	green
4128	3501	2390	209	64	0.300	green
4154	3404	2362	122	76	0.300	green
4312	3511	2391	90	76	0.200	green red
4253	3410	2349	230	76	0.200	green red
4280	3406	2349	205	80	0.300	green yellow
4272	3507	2388	142	83	0.500	green yellow
4300	3510	2391	115	65	0.600	green yellow

STRUCTURAL SECTOR C - BALMACEDA (Continued)

North	East	Elev.	Strike	Dip	Width	Type
3984	3550	2439	239	80	0.200	orange
3988	4134	2777	105	74	0.050	orange
4111	3614	2467	70	78	0.300	orange
4207	3772	2573	70	85	0.150	orange
4228	3539	2412	215	90	0.300	orange
4206	3541	2413	245	85	0.400	orange
4166	3406	2361	72	87	1.000	orange, green
4128	3612	2466	256	82	0.200	orange yellow
4016	3606	2467	102	78	0.100	orange yellow
4264	3601	2465	237	80	1.000	orange yellow
4125	3916	2648	107	85	0.500	red
4185	3921	2647	97	90	2.000	red
3945	3611	2490	70	88	0.400	red
4229	3410	2348	310	35	0.010	red
4202	3721	2542	95	85	1.000	yellow, brown
4135	3723	2543	270	82	0.400	yellow, brown
4050	3735	2542	260	87	0.300	yellow brown
4105	3569	2442	255	60	0.150	yellow
3917	3703	2544	272	84	0.150	yellow
4000	3758	2576	97	72	0.600	yellow
4281	3714	2541	120	80	0.050	yellow
4121	3537	2414	296	87	0.200	yellow
4207	3574	2439	246	90	1.000	yellow
4139	3846	2620	135	83	0.100	yellow
4165	3842	2618	76	83	0.100	yellow
4192	3507	2386	125	61	0.080	yellow
4023	3520	2412	320	87	0.100	yellow
4071	3831	2617	55	70	2.500	yellow
4118	3932	2648	150	75	0.800	yellow
4088	3457	2390	146	87	0.100	yellow
4133	3464	2388	130	90	1.000	yellow
4295	3738	2567	53	77	0.150	yellow
4262	3767	2577	275	85	0.150	yellow
4222	3769	2573	150	90	0.150	yellow
4054	3478	2390	55	78	0.700	yellow
4277	3767	2578	50	70	0.250	yellow
4289	3738	2567	98	87	0.400	yellow
4223	3770	2572	146	90	0.300	yellow
4286	3575	2439	150	45	0.100	yellow
4223	3770	2572	71	85	0.500	yellow
4284	3714	2541	210	86	0.500	yellow
4233	3770	2575	85	86	0.100	yellow
4141	3465	2388	137	82	0.400	yellow
4124	3462	2388	256	74	0.300	yellow
4265	3895	2647	35	67	0.600	yellow
4207	3574	2439	65	75	0.400	yellow
4205	3542	2412	221	79	0.300	yellow
4224	3571	2438	235	80	0.300	yellow
4141	3465	2388	137	82	0.400	yellow

STRUCTURAL SECTOR C - BALMACEDA (Continued)

North	East	Elev.	Strike	Dip	Width	Type
4236	3660	2516	60	75	0.100	yellow
4103	3459	2389	140	82	0.400	yellow
4287	3838	2618	18	65	0.200	yellow
4040	3487	2386	186	90	0.050	yellow, blue
4055	3765	2568	61	86	0.500	yellow, brown
3955	3713	2543	250	85	1.500	yellow, brown
3958	3745	2569	82	85	0.400	yellow, brown
4260	3716	2541	210	86	99.000	yellow, brown
4190	3771	2571	73	86	1.000	yellow, brown
4147	3769	2568	250	88	0.500	yellow, brown
4176	3405	2350	51	88	0.010	yellow red

STRUCTURAL SECTOR D - SOUTHEASTERN

North	East	Elev.	Strike	Dip	Width	Type
3110	3722	2650	300	62	0.010	bed /folia
3876	3658	2517	236	80	0.050	black
3781	3620	2520	278	85	0.050	black
3719	3592	2516	250	80	0.010	black
3740	3599	2518	105	77	0.010	black
3791	3619	2516	118	80	0.050	black
3205	3761	2680	80	58	0.100	blue
3304	3777	2678	330	78	0.100	blue
3690	3699	2596	136	90	99.000	blue
3375	3683	2596	115	84	0.010	blue
3060	3746	2653	130	90	3.000	blue
3651	3590	2542	270	90	0.400	blue
2609	3134	2545	280	85	99.000	blue
3319	3779	2676	280	65	0.150	blue
3110	3750	2657	215	66	0.010	blue
3684	3761	2647	140	60	99.000	blue
3530	3999	2726	180	88	0.010	blue
3089	3747	2675	133	83	0.100	blue
3089	3808	2704	230	74	0.050	blue
3043	3804	2708	245	73	0.010	blue
3085	3848	2726	185	75	0.010	blue
3144	3816	2701	126	82	0.100	blue
3296	3742	2647	120	75	0.010	blue
3114	3812	2702	152	60	0.100	blue
3131	3813	2701	250	63	99.000	blue
3308	3746	2647	194	80	0.010	blue
3244	3712	2624	335	90	0.010	blue
3081	3843	2725	174	74	0.010	blue
3014	3835	2726	92	50	0.010	blue
3010	3953	2798	175	65	99.000	blue
3593	3975	2698	165	90	99.000	blue
3205	3824	2700	265	64	99.000	blue
3294	3816	2691	173	75	99.000	blue
3339	3784	2676	300	83	0.300	blue
3210	3765	2656	165	90	0.300	blue
3307	3648	2595	18	90	3.000	blue
3775	3979	2656	117	63	99.000	blue
3077	3414	2546	158	82	99.000	blue
3067	3513	2597	220	70	99.000	blue
3693	3879	2647	5	88	99.000	blue
3112	3425	2500	187	75	0.010	blue
3194	3451	2499	212	80	0.010	blue
3108	3695	2627	340	85	0.010	blue
3160	3752	2675	282	70	99.000	blue
3029	3768	2698	250	75	99.000	blue
3160	3751	2653	275	71	0.010	blue
3075	3746	2654	173	90	0.010	blue
3016	3743	2655	178	90	0.010	blue

STRUCTURAL SECTOR D - SOUTHEASTERN (Continued)

North	East	Elev.	Strike	Dip	Width	Type
3232	3767	2654	318	75	0.150	blue
3438	3941	2724	168	85	0.010	blue
3410	3931	2726	260	75	0.010	blue
3062	3744	2678	140	83	99.000	blue
2692	3185	2519	170	80	0.050	blue
3686	3696	2594	170	90	0.050	blue
3706	3583	2516	155	90	0.020	blue
3748	3541	2491	291	83	0.020	blue
3289	3537	2570	223	70	0.050	blue
3728	4233	2821	195	74	99.000	blue
3334	3590	2601	237	65	0.100	blue
3708	3559	2501	290	87	0.020	blue
3654	3566	2516	173	68	0.050	blue
3769	3438	2412	175	88	0.050	blue
3300	3475	2501	8	75	0.010	blue
3322	3549	2571	46	88	0.050	blue
3303	3454	2525	260	80	0.050	blue
3268	3524	2582	167	65	0.050	blue
3311	3583	2601	310	90	0.400	blue
3594	3976	2699	165	85	4.000	blue
3561	4046	2752	150	65	1.000	blue
3512	4031	2750	150	75	0.010	blue
3494	4146	2822	215	60	99.000	blue
3236	3458	2499	178	88	1.000	blue
3654	3566	2516	35	90	99.000	blue
3728	4233	2821	110	80	2.000	blue
3330	3586	2600	340	74	0.100	blue
3343	3554	2571	148	90	0.200	blue
3285	3575	2602	125	80	0.200	blue
3704	3596	2517	110	90	99.000	blue
3277	3255	2414	268	74	0.050	blue
3204	3238	2419	182	90	0.050	blue
3233	3253	2415	236	82	0.010	blue
3215	3520	2576	105	90	99.000	blue
3234	3277	2436	200	90	0.100	blue
3277	3262	2413	135	90	0.050	blue
3319	3725	2624	200	90	0.010	blue
3759	3549	2492	159	85	0.100	blue
3102	3847	2727	140	90	0.400	blue
3233	3253	2415	189	90	0.010	blue
3204	3238	2419	232	90	99.000	blue
3169	3819	2700	259	78	1.000	blue
3264	3411	2517	147	86	0.010	blue
3321	3479	2501	230	84	0.010	blue
3250	3443	2529	105	90	2.000	blue
3205	3452	2498	188	68	0.010	blue
3234	3402	2517	186	64	0.010	blue
3406	3889	2699	195	70	2.000	blue
3709	3523	2490	329	52	0.100	blue

STRUCTURAL SECTOR D - SOUTHEASTERN (Continued)

North	East	Elev.	Strike	Dip	Width	Type
3538	3996	2726	143	76	0.200	blue
3210	3518	2576	255	65	99.000	blue
3382	3494	2500	233	78	0.010	blue
3214	3520	2576	105	90	99.000	blue
3350	3523	2573	295	80	99.000	blue
3142	3443	2546	270	73	99.000	blue
3440	3780	2645	140	90	0.010	blue
2832	3299	2549	270	75	99.000	blue
2947	3329	2541	136	90	99.000	blue
2808	3253	2503	195	75	0.010	blue
2974	3354	2501	210	65	0.010	blue
3484	3502	2516	295	87	0.050	blue
3839	3681	2545	268	78	99.000	blue
2789	3914	2801	180	70	99.000	blue
2708	3221	2544	252	78	99.000	blue
2835	3302	2550	190	85	99.000	blue
3511	3521	2517	225	80	0.010	blue
2848	3356	2576	190	64	0.050	blue
3425	3480	2527	135	75	99.000	blue
2789	3267	2542	123	85	99.000	blue
3417	3480	2530	145	88	99.000	blue
2645	3222	2574	120	90	99.000	blue
2891	3300	2500	175	75	0.020	blue
2974	3354	2501	273	72	0.050	blue
2873	3246	2534	245	70	0.050	blue
2885	3387	2578	183	70	0.050	blue
3502	3512	2517	120	78	0.050	blue
3881	4194	2799	195	75	99.000	blue
2795	3325	2578	235	68	0.050	blue
3432	3606	2596	305	80	99.000	blue
2732	3242	2545	250	64	0.050	blue
2749	3251	2544	130	75	0.050	blue
2759	3252	2542	250	74	99.000	blue
2616	3239	2596	178	75	0.040	blue
3917	3502	2414	138	70	0.150	blue
3835	4164	2781	180	70	0.010	blue
3864	4128	2750	156	80	0.010	blue
3814	3966	2655	193	60	99.000	blue
3868	3906	2622	144	76	0.010	blue
3819	3637	2515	105	88	2.000	blue
3548	3789	2620	205	70	0.010	blue
2747	3220	2499	243	77	0.200	blue
2747	3220	2499	164	75	0.010	blue
2714	3226	2545	265	74	0.050	blue
3877	3999	2677	0	88	0.050	blue
3496	3764	2619	167	57	0.010	blue
3530	3779	2620	147	73	0.010	blue
2785	3265	2541	123	85	99.000	blue
2607	3229	2599	265	70	99.000	blue

STRUCTURAL SECTOR D - SOUTHEASTERN (Continued)

North	East	Elev.	Strike	Dip	Width	Type
2730	3240	2546	250	64	99.000	blue
2620	3243	2597	180	67	99.000	blue
3288	3884	2723	191	73	0.010	blue
3466	3707	2594	98	90	0.300	blue
3107	3362	2516	190	84	0.010	blue
3116	3368	2519	217	76	0.010	blue
3188	3391	2518	196	74	0.010	blue
3126	3372	2519	239	67	0.010	blue
2697	3312	2604	130	85	99.000	blue
3647	3941	2676	330	70	99.000	blue
3745	3977	2678	333	74	99.000	blue
3141	3239	2437	275	70	1.000	blue
3040	3434	2565	145	87	99.000	blue
3040	3434	2565	155	87	99.000	blue
3678	3948	2657	150	90	0.010	blue
3692	3848	2620	163	72	0.010	blue
3284	3844	2697	270	75	0.010	blue
3698	3964	2676	15	70	99.000	blue
2655	3265	2596	270	60	99.000	blue
3675	4014	2699	120	76	99.000	blue
2844	3409	2601	160	65	99.000	blue
3330	4064	2824	328	69	99.000	blue
3397	3971	2747	175	73	1.000	blue
2973	3435	2575	235	60	0.050	blue
3854	3442	2389	265	75	99.000	blue
3864	3518	2442	175	85	0.050	blue
3828	3504	2440	146	82	0.050	blue
3806	3455	2411	136	86	0.050	blue
3885	3486	2413	144	88	0.010	blue
3805	3565	2490	113	82	0.020	blue
2790	3369	2599	257	65	99.000	blue
2874	3426	2599	295	90	0.200	blue
2964	3827	2728	143	82	0.200	blue
3094	3358	2520	265	75	99.000	blue
2987	3832	2724	147	90	0.200	blue
2690	3292	2595	235	60	99.000	blue
2990	3445	2575	140	85	0.150	blue
3307	3546	2572	134	80	0.200	blue, brown
3799	3653	2543	203	90	0.030	blue, yellow
3612	3808	2621	115	90	0.100	blue contact
3805	3927	2645	335	67	99.000	blue contact
3444	3570	2574	60	82	0.300	brown
3428	3503	2498	140	84	0.300	brown
3508	3634	2596	75	74	0.100	brown
3480	3622	2594	132	88	0.060	brown
3594	3661	2594	146	76	0.050	brown
3492	3629	2598	253	70	0.100	brown
3402	3769	2646	150	84	0.600	brown
3482	3764	2619	113	82	0.200	brown

STRUCTURAL SECTOR D - SOUTHEASTERN (Continued)

North	East	Elev.	Strike	Dip	Width	Type
3569	3656	2600	153	80	0.200	brown
3468	3614	2594	256	83	0.030	brown
3569	3825	2649	313	85	0.700	brown
3416	3499	2498	250	77	1.000	brown
3496	3514	2517	137	60	0.300	brown
3417	3894	2699	190	70	0.100	brown
3535	3640	2595	240	74	0.030	brown
3575	3658	2598	135	89	0.030	brown
3573	3657	2598	135	89	0.030	brown
3715	3968	2675	188	90	0.500	brown
3738	3964	2653	155	80	0.400	brown
3770	3911	2645	132	70	0.400	brown
3615	3962	2656	280	86	0.600	brown
3884	3529	2441	132	87	0.100	brown
3870	3575	2465	230	86	0.100	brown
3850	3513	2441	305	84	0.100	brown
3707	3808	2602	130	80	0.100	brown
3762	3875	2620	155	75	0.100	brown
3781	3916	2645	100	25	0.010	brown
3646	3941	2656	324	82	0.100	brown
3786	3950	2653	334	90	0.400	brown
3634	3932	2655	310	76	0.300	brown
3756	3985	2676	170	83	0.200	brown
3934	3586	2464	260	72	0.350	brown
3891	3931	2645	156	90	0.050	brown
3867	3857	2597	190	84	0.010	brown
3806	4127	2754	145	90	0.400	brown
3924	3583	2464	110	70	0.100	brown
3918	3582	2464	190	79	0.050	brown
3902	3579	2463	205	73	0.050	brown
3829	3431	2387	112	90	0.200	brown
3882	3452	2387	306	76	0.200	brown
3899	3579	2464	145	85	0.150	brown
3888	3577	2464	200	88	0.200	brown
3869	3679	2543	61	82	0.100	brown
3946	3474	2390	161	85	0.400	brown
3829	3431	2387	112	90	0.200	brown
3781	3916	2645	63	76	0.010	brown
3668	3506	2489	288	88	0.100	brown
3785	3485	2441	225	73	0.100	brown
3726	3569	2506	145	85	0.100	brown
3709	3507	2468	232	83	0.150	brown
3683	3489	2466	251	62	0.300	brown
3608	3540	2516	80	79	0.200	brown
3781	3483	2441	130	88	0.200	brown
3534	4166	2821	205	60	0.500	brown
3593	4193	2821	175	65	0.400	brown
3448	4123	2823	225	58	0.300	brown
3422	4107	2823	5	90	1.000	brown

STRUCTURAL SECTOR D - SOUTHEASTERN (Continued)

North	East	Elev.	Strike	Dip	Width	Type
3639	3528	2497	120	83	0.100	brown
3742	3539	2490	122	80	0.100	brown
3657	3541	2502	320	75	0.100	brown
3699	3619	2542	280	87	0.200	brown
3667	3605	2541	320	84	0.100	brown
3678	3609	2541	240	81	0.100	brown
3662	3604	2542	162	84	0.200	brown
3791	3621	2515	125	90	0.700	brown
3755	3609	2515	345	68	0.300	brown
3782	3617	2516	294	80	0.200	brown
3607	3764	2598	145	76	0.020	brown
3690	3591	2518	330	85	0.600	brown
3719	3596	2516	260	90	0.400	brown
3947	3589	2463	50	90	1.000	brown
3776	3645	2542	64	83	0.100	brown
3706	3623	2542	215	81	0.100	brown
3759	3693	2581	300	87	0.050	brown
3173	3260	2436	165	70	0.100	brown
3154	3213	2425	192	85	0.200	brown
3037	3392	2503	66	90	0.050	brown
3047	3503	2497	120	90	0.350	brown
3168	3221	2413	330	75	0.200	brown
3148	3539	2599	145	80	0.020	brown
3148	3539	2599	145	80	0.020	brown
3008	3373	2501	105	90	0.200	brown
3168	3441	2501	192	75	0.010	brown
2900	3442	2603	334	72	0.100	brown
2992	3406	2560	185	80	0.100	brown
2905	3447	2605	35	60	0.010	brown
2855	3415	2600	155	75	0.100	brown
2998	3447	2576	170	90	0.500	brown
3159	3252	2437	240	85	0.010	brown
3138	3376	2516	310	86	0.050	brown
3032	3388	2502	133	90	0.010	brown
3102	3203	2437	150	90	0.010	brown
3126	3533	2599	145	86	0.040	brown
3149	3747	2653	196	90	0.400	brown
3138	3719	2652	140	70	0.400	brown
3074	3745	2674	338	68	99.000	brown
3016	3709	2651	178	90	0.100	brown
3153	3722	2650	174	90	0.500	brown
3110	3750	2657	147	88	1.000	brown
3075	3746	2654	149	83	4.000	brown
3060	3717	2652	165	76	0.600	brown
3040	3770	2699	308	70	0.750	brown
3181	3512	2576	215	85	0.100	brown
3189	3547	2598	130	89	0.150	brown
3116	3488	2569	206	80	0.050	brown
3057	3462	2567	260	73	0.050	brown

STRUCTURAL SECTOR D - SOUTHEASTERN (Continued)

North	East	Elev.	Strike	Dip	Width	Type
3139	3436	2499	155	67	0.200	brown
3148	3436	2498	280	85	0.600	brown
3079	3408	2502	235	85	0.700	brown
3006	3500	2600	350	75	0.200	brown
3084	3519	2598	125	90	0.200	brown
2758	3307	2577	115	90	0.050	brown
2748	3296	2572	64	64	0.050	brown
2610	3276	2622	122	84	0.050	brown
2676	3206	2546	273	65	0.050	brown
2679	3209	2547	180	75	0.050	brown
2791	3272	2545	110	90	0.150	brown
2714	3202	2523	265	80	0.200	brown
2696	3260	2573	170	80	0.100	brown
2750	3340	2600	147	77	0.100	brown
2706	3190	2519	145	85	0.500	brown
2793	3205	2523	270	80	0.020	brown
2690	3184	2522	270	76	99.000	brown
2654	3144	2518	250	60	0.200	brown
2736	3330	2597	180	82	0.030	brown
2727	3285	2577	125	90	0.050	brown
2610	3276	2622	122	84	0.050	brown
2756	3225	2499	92	79	0.030	brown
2725	3323	2597	240	75	0.030	brown
2709	3269	2577	257	75	0.200	brown
2855	3280	2499	357	85	1.000	brown
2896	3391	2573	145	90	1.000	brown
2805	3204	2523	100	80	0.300	brown
2821	3217	2527	120	80	0.400	brown
2894	3390	2572	145	90	1.000	brown
2921	3361	2554	130	90	1.500	brown
2958	3469	2599	20	60	99.000	brown
2820	3284	2544	135	90	1.000	brown
2941	3334	2502	134	84	1.250	brown
2743	3215	2522	260	66	0.300	brown
2787	3241	2501	251	90	0.300	brown
2765	3211	2522	112	90	0.200	brown
2741	3341	2605	310	85	0.300	brown
2796	3252	2507	140	77	2.000	brown
2908	3347	2553	160	74	0.200	brown
2814	3213	2527	260	75	0.300	brown
2919	3360	2554	130	90	99.000	brown
2909	3313	2501	187	66	0.050	brown
3274	3445	2525	257	75	1.000	brown
3350	3558	2572	212	55	1.000	brown
3264	3532	2570	153	80	1.000	brown
3214	3518	2569	118	90	0.800	brown
3399	3566	2571	258	80	1.000	brown
3398	3603	2597	247	86	0.150	brown
3214	3735	2650	150	83	0.200	brown

STRUCTURAL SECTOR D - SOUTHEASTERN (Continued)

North	East	Elev.	Strike	Dip	Width	Type
3357	3684	2597	328	82	0.100	brown
3244	3456	2498	284	83	2.000	brown
3206	3758	2676	198	75	99.000	brown
3347	3558	2591	158	82	0.100	brown
3229	3401	2517	277	82	0.200	brown
3321	3479	2501	13	75	0.100	brown
3221	3557	2599	125	90	0.100	brown
3260	3411	2517	295	80	0.100	brown
3212	3519	2581	110	90	0.500	brown
3383	3564	2571	265	80	0.600	brown
3365	3561	2572	295	84	0.500	brown
3250	3443	2529	180	80	0.300	brown
3353	3591	2597	121	90	0.400	brown
3511	3521	2517	115	90	0.050	brown
3510	3515	2517	95	90	0.050	brown
3477	3505	2496	239	74	0.020	brown
3351	4076	2824	194	64	0.300	brown
3559	3415	2437	335	65	0.010	brown
3537	3531	2518	214	80	0.200	brown
3557	3525	2516	244	82	0.200	brown
3573	3496	2491	140	85	0.150	brown
3508	3472	2493	110	80	0.050	brown
3548	3489	2494	120	90	0.100	brown
3243	3828	2697	330	80	0.100	brown
3274	3842	2697	180	72	0.150	brown
3310	3853	2700	175	80	0.050	brown
3362	3866	2698	125	87	0.010	brown
3379	3868	2697	325	63	0.010	brown
3320	3896	2723	145	72	0.800	brown
3306	4055	2823	180	86	0.100	brown
3217	3870	2725	306	82	0.600	brown
3384	3832	2683	317	57	0.400	brown
3274	3812	2693	335	83	0.500	brown
3226	3560	2601	145	74	0.020	brown
3186	3867	2727	143	90	0.700	brown
3133	3855	2724	180	85	0.500	brown
3002	3832	2724	115	90	0.100	brown
3370	3596	2598	270	82	0.040	brown
3387	3534	2581	120	90	0.010	brown
3376	3562	2570	205	90	99.000	brown
3303	3454	2525	270	84	99.000	brown
3245	3280	2437	146	90	0.020	brown
3239	3562	2599	145	70	0.010	brown
3369	3492	2499	155	80	0.010	brown
3062	3690	2622	4	76	10.000	brown
3349	3485	2499	230	90	0.050	brown
3006	3686	2624	180	79	10.000	brown
3208	3554	2600	264	70	0.070	brown
3642	3585	2543	80	67	0.400	brown, red

STRUCTURAL SECTOR D - SOUTHEASTERN (Continued)

North	East	Elev.	Strike	Dip	Width	Type
3779	3646	2542	103	86	0.150	brown, red
3167	3384	2517	140	81	0.030	brown, red
3746	3470	2443	202	85	0.010	brown, yellow
3677	3439	2440	224	83	0.010	brown, yellow
3794	3652	2543	83	90	2.000	brown, yellow
2957	3341	2500	213	80	0.100	brown mylonite
3857	3569	2466	210	78	0.200	brown red
3745	3520	2468	230	78	0.200	brown red
3765	3530	2467	252	64	0.150	brown red
3577	3445	2468	147	85	0.200	brown red
3803	3546	2465	240	79	0.250	brown red
3825	3555	2464	230	74	0.400	brown red
3629	3467	2466	195	65	1.000	brown red
3663	3481	2466	330	90	0.400	brown red
3752	3521	2466	238	58	0.150	brown red
3657	3478	2465	249	86	0.500	brown yellow
3848	4127	2749	250	85	0.400	cataclasite
3676	3786	2596	153	85	0.600	cataclasite
3692	3878	2647	163	73	99.000	contact blue
3183	3730	2653	303	85	0.010	folia
3693	3879	2647	140	83	99.000	folia
3870	3930	2644	210	70	99.000	folia
3612	3808	2621	130	83	99.000	folia
2675	3140	2500	30	84	99.000	folia
3746	3978	2657	305	80	99.000	folia
3647	3941	2656	316	80	0.100	folia
3781	3916	2645	345	56	0.010	folia
3569	3825	2649	124	66	0.010	folia
3444	3941	2724	200	72	0.500	folia
3200	3764	2654	326	84	3.000	folia
3775	3979	2656	155	74	99.000	folia / bed
3660	3832	2620	195	75	0.010	folia blue
3878	3484	2413	146	86	0.100	green
3676	3486	2466	315	90	2.500	green yellow
3931	3585	2463	158	85	0.070	mylonite
3498	3514	2517	80	73	1.000	mylonite
3512	3871	2653	294	68	1.000	mylonite
2682	3172	2499	116	75	0.050	mylonite
3761	3435	2411	189	90	99.000	mylonite
3836	3642	2515	278	85	0.050	red
3740	3608	2517	235	86	1.000	red
3821	3552	2464	320	89	0.200	red
3126	3372	2519	300	82	0.050	red
3663	3543	2502	250	83	0.200	red
3623	3519	2494	280	87	0.050	red
3601	3509	2492	240	80	0.150	red
3182	3388	2516	310	85	0.020	red
3658	3598	2542	100	70	0.600	cataclasite
3803	3454	2411	162	88	0.100	yellow

STRUCTURAL SECTOR D - SOUTHEASTERN (Continued)

North	East	Elev.	Strike	Dip	Width	Type
3692	3553	2501	250	75	0.150	yellow
3924	3539	2441	238	73	0.200	yellow
3868	3481	2414	302	88	0.100	yellow
3731	3571	2506	260	80	0.300	yellow
3891	3532	2440	235	63	0.200	yellow
3791	3448	2411	229	75	0.200	yellow
3813	3570	2491	241	86	0.200	yellow
3681	3548	2499	290	78	0.400	yellow
3528	3515	2517	120	86	0.300	yellow
3833	3642	2515	233	88	0.100	yellow
3759	3717	2595	95	73	0.200	yellow

STRUCTURAL SECTOR E - EASTERN

North	East	Elev	Strike	Dip	Width	Type
2961	3732	2658	151	86	0.010	blue
2961	3732	2658	242	75	0.010	blue
2855	3704	2659	98	90	0.010	blue
2995	3727	2678	247	70	99.000	blue
2988	3718	2676	10	63	99.000	blue
2865	3736	2704	175	83	99.000	blue
2906	3744	2700	180	83	99.000	blue
2987	3707	2652	350	80	0.050	blue
2803	3693	2697	310	85	0.500	blue
2839	3720	2703	300	65	0.500	blue
2987	3707	2652	145	90	0.050	blue
2839	3697	2657	190	90	0.010	blue
2993	3736	2655	177	90	0.010	blue
2950	3701	2650	195	80	0.010	blue
2942	3695	2675	270	70	99.000	blue
2775	3675	2702	185	80	99.000	blue
2745	3656	2699	185	85	99.000	blue
2659	3568	2700	187	90	99.000	blue
2608	3464	2658	165	70	0.300	blue
2729	3641	2700	170	86	99.000	blue
2728	3602	2657	290	76	0.050	blue
2961	3684	2624	30	80	10.000	brown
2529	3408	2703	180	75	0.040	brown
2560	3442	2701	20	75	0.050	brown
2973	3733	2657	155	90	0.700	brown
2809	3679	2656	182	87	2.000	brown
2579	3460	2702	200	87	0.020	brown
2766	3642	2659	175	85	0.400	brown
2766	3642	2659	155	90	0.400	brown
2784	3658	2657	185	80	1.000	brown
2534	3414	2703	175	70	0.050	brown
2672	3544	2660	180	82	0.300	brown
2950	3701	2650	223	75	0.010	folia

STRUCTURAL SECTOR F - SOUTHERN

North	East	Elev	Strike	Dip	Width	Type
2452	3326	2701	265	67	99.000	blue
2449	3322	2701	225	50	99.000	blue
2574	3239	2622	240	70	0.010	blue
2438	3307	2701	225	50	99.000	blue
2518	3068	2596	216	76	0.020	blue
2512	3039	2598	165	60	0.020	blue
2475	3318	2678	240	68	99.000	blue
2526	3369	2679	211	54	0.050	blue
2507	3348	2678	230	70	0.300	blue
2574	3239	2622	285	85	0.200	blue
2574	3239	2622	285	85	0.200	blue
2411	3270	2703	80	90	0.200	blue
2452	3274	2674	170	73	0.050	blue
2452	3274	2674	288	74	0.050	blue
2512	3350	2678	160	75	0.200	blue
2370	3156	2701	270	80	99.000	blue
2379	3191	2700	270	70	99.000	blue
2486	3035	2625	266	85	0.010	blue
2362	3078	2703	275	65	0.200	blue
2360	3030	2699	74	90	99.000	blue
2370	3019	2678	250	60	0.050	blue
2392	3118	2679	230	82	0.050	blue
2486	3035	2625	266	85	0.010	blue
2364	3096	2701	270	75	99.000	blue
2389	3137	2679	245	66	99.000	blue
2497	3101	2626	233	60	0.010	blue
2532	3111	2603	280	53	0.010	blue
2486	3016	2627	200	60	0.020	blue
2486	3016	2627	200	60	0.020	blue
2497	3101	2626	233	60	0.010	blue
2363	3058	2701	265	68	99.000	brown
2410	3204	2678	264	73	0.300	brown
2495	3339	2679	264	73	0.200	brown
2464	3344	2704	190	60	0.020	brown
2525	3167	2627	260	70	0.030	brown
2525	3167	2627	260	70	0.030	brown
2458	3337	2703	250	70	0.020	brown
2414	3287	2708	263	84	0.100	brown
2486	3367	2703	264	75	0.050	brown
2500	3376	2703	152	65	0.050	brown

STRUCTURAL SECTOR G - WEST FAULT/AMERICANA

North	East	Elev.	Strike	Dip	Width	Type
3411	3057	2386	245	90	0.050	blue
3560	3046	2388	156	85	0.010	blue
3183	3139	2387	300	80	99.000	blue
2946	3089	2416	185	80	0.010	blue
3439	3028	2412	20	70	0.200	blue
3444	3056	2388	310	61	0.050	blue
3185	3140	2387	265	86	99.000	blue
3174	3132	2388	170	58	99.000	blue
3189	3145	2387	280	85	99.000	blue
3502	2999	2419	121	70	99.000	blue
3411	3057	2386	336	90	99.000	blue
3180	3136	2387	360	83	99.000	blue
3166	3126	2388	180	70	99.000	blue
2957	3094	2415	165	86	0.010	blue
4092	3147	2390	175	80	99.000	blue
2610	3031	2521	215	70	0.200	blue
3897	3043	2423	194	60	1.500	blue
4156	3165	2392	10	90	0.300	blue
4110	3151	2396	186	74	0.300	blue
4111	3110	2418	209	73	99.000	blue
3802	3052	2410	260	73	99.000	blue
2913	3058	2413	355	83	99.000	blue
2946	3119	2438	185	72	99.000	blue
3420	3029	2416	55	70	0.200	blue
3891	3047	2418	310	79	99.000	blue
3725	3068	2392	205	88	1.200	blue
3708	3118	2367	35	86	0.010	blue
3072	3187	2439	270	80	99.000	blue
3102	2990	2421	335	75	0.020	blue
3115	2915	2442	10	78	99.000	blue
3176	2966	2414	30	90	99.000	blue
3130	3087	2389	210	85	99.000	blue
3132	3067	2388	175	75	99.000	blue
3138	3048	2391	350	77	99.000	blue
3115	3184	2415	170	90	0.020	blue
3076	2915	2440	352	55	99.000	blue
3051	2912	2442	30	85	99.000	blue
3073	2916	2439	297	43	99.000	blue
3020	2987	2415	340	75	0.020	blue
3054	2957	2421	345	90	0.010	blue
3074	2957	2420	50	90	0.010	blue
3189	3010	2418	60	80	99.000	blue
3302	3039	2390	260	90	99.000	blue
3284	3000	2412	5	79	99.000	blue
3257	3019	2415	68	84	99.000	blue
3313	3040	2389	270	90	0.300	blue
3315	3025	2415	330	70	0.200	blue
3348	3044	2389	10	90	0.050	blue

STRUCTURAL SECTOR G - WEST FAULT/AMERICANA (Cont.)

North	East	Elev.	Strike	Dip	Width	Type
3195	3149	2386	117	73	99.000	blue
3130	3093	2391	210	83	99.000	blue
3247	2970	2414	222	88	99.000	blue
3204	2962	2415	214	75	99.000	blue
3003	3151	2438	154	82	99.000	blue
3131	3095	2391	215	85	99.000	blue
3244	2927	2441	335	90	99.000	blue
4617	3198	2523	212	87	0.010	blue
5301	2996	2798	165	55	0.010	blue
5303	2997	2799	190	67	0.010	blue
4650	3118	2553	190	67	0.200	blue
4756	3081	2594	337	90	0.050	blue
4728	3199	2541	315	65	0.010	blue
5301	2934	2819	0	90	0.010	blue
4798	3102	2595	78	75	99.000	blue
4653	3166	2542	0	90	99.000	blue
5378	3064	2819	212	48	0.010	blue
4798	3102	2595	343	81	99.000	blue
5314	3023	2799	185	70	0.010	blue
5356	3015	2821	120	60	0.010	blue
5058	3169	2650	14	72	0.050	blue
5072	3079	2711	340	75	99.000	blue
5068	3074	2712	350	57	99.000	blue
4947	3086	2647	100	83	99.000	blue
5047	3073	2699	355	80	99.000	blue
4942	3044	2675	354	87	0.010	blue
4951	3086	2647	30	64	99.000	blue
4947	3086	2647	340	84	99.000	blue
4885	3039	2654	45	90	99.000	blue
4806	3108	2595	155	80	99.000	blue
5002	3169	2620	7	72	0.010	blue
4950	3087	2646	356	87	99.000	blue
5037	3065	2701	193	86	99.000	blue
4868	3152	2593	30	80	0.050	blue
5378	3064	2819	328	90	0.010	blue
4327	3172	2444	152	78	0.050	blue
4293	3186	2415	22	80	0.010	blue
2762	3064	2439	170	82	99.000	blue
4537	3164	2520	325	90	99.000	blue
4319	3168	2443	85	77	0.050	blue
4347	3183	2442	78	80	0.050	blue
2609	3055	2522	210	90	99.000	blue
4250	3167	2418	190	79	99.000	blue
2626	3100	2518	250	65	0.010	blue
2632	3035	2494	272	80	0.010	blue
4223	3151	2416	174	43	99.000	blue
4248	3165	2420	70	75	99.000	blue
2623	3091	2518	190	90	99.000	blue
4543	3167	2521	325	70	99.000	blue

STRUCTURAL SECTOR G - WEST FAULT/AMERICANA (Cont.)

North	East	Elev.	Strike	Dip	Width	Type
5404	3008	2843	343	82	0.010	blue
5505	3003	2870	60	90	0.010	blue
5428	3043	2846	197	72	0.020	blue
5267	3014	2771	12	70	0.010	blue
5486	2970	2867	334	65	0.010	blue
5509	3012	2871	0	81	0.010	blue
4598	3084	2553	352	90	99.000	blue
4492	3026	2544	215	77	99.000	blue
4566	3175	2521	315	86	99.000	blue
2583	3054	2546	280	85	99.000	blue
4464	3011	2545	20	90	99.000	blue
4458	3009	2544	341	90	99.000	blue
4519	3043	2544	198	42	99.000	blue
3113	3125	2412	310	65	0.100	blue
3411	3115	2365	0	88	0.010	blue
2487	2968	2621	140	84	0.200	blue
3712	3302	2365	180	80	0.010	blue
3494	3127	2364	212	90	0.010	blue
3785	3338	2362	200	85	0.010	blue
3856	3340	2350	170	88	0.400	blue
2487	2968	2621	140	84	0.200	blue
3590	3287	2389	222	75	99.000	blue
3410	3282	2412	83	81	99.000	blue
3392	3275	2412	210	76	0.050	blue
3314	3259	2412	186	90	0.050	blue
3295	3288	2437	160	85	0.010	blue
3372	3276	2414	192	83	0.030	blue
3374	3268	2412	58	90	0.050	blue
3596	3143	2364	21	90	0.010	blue
3494	3127	2364	7	90	0.010	blue
3371	3215	2389	255	70	0.500	blue
3562	3138	2364	14	90	0.010	blue
3564	3311	2402	230	72	0.020	blue
3662	3352	2392	260	80	5.000	blue
3596	3243	2365	170	90	0.010	blue
2745	2947	2466	282	57	0.010	blue
3579	3351	2412	209	78	0.050	blue
2739	2950	2466	355	72	0.020	blue
3545	3337	2412	27	90	0.050	blue
3545	3337	2412	266	70	0.050	blue
3499	3318	2411	20	90	0.050	blue
3882	3383	2363	172	60	0.010	blue
2788	2923	2465	210	80	0.200	blue
3555	3410	2441	175	90	99.000	blue
3572	3279	2388	240	84	99.000	blue
3472	3348	2438	260	85	99.000	blue
2788	2923	2465	190	80	0.010	blue
3525	3399	2439	182	88	99.000	blue
3864	3378	2359	55	76	0.010	blue

STRUCTURAL SECTOR G - WEST FAULT/AMERICANA (Cont.)

North	East	Elev.	Strike	Dip	Width	Type
3879	3350	2351	135	90	99.000	blue
2907	2896	2440	135	67	99.000	blue
4269	3289	2348	130	83	0.050	blue
3750	3319	2364	64	71	0.010	blue
2512	2939	2601	230	83	99.000	blue
4299	3219	2392	42	90	0.050	blue
3390	3113	2365	163	86	0.010	blue
3380	3113	2363	23	88	0.010	blue
2972	2878	2440	190	78	99.000	blue
3127	3138	2414	220	65	0.100	blue
4136	3393	2327	140	85	0.010	blue
3208	3161	2386	200	85	0.100	blue
4209	3271	2347	224	90	0.010	blue
4221	3275	2348	342	88	0.010	blue
3242	3033	2389	0	90	1.000	blue
2914	2893	2441	173	62	0.020	blue
3698	3295	2366	265	90	0.010	blue
2784	2931	2464	360	75	99.000	blue
3356	3209	2387	185	90	99.000	blue
3331	3292	2437	200	80	99.000	blue
2701	2936	2495	288	90	99.000	blue
2971	2954	2431	220	22	99.000	blue
3295	3284	2436	160	85	99.000	blue
3379	3220	2388	360	70	99.000	blue
3148	3159	2413	220	65	0.100	blue
3333	3272	2413	200	90	0.010	blue
3235	3138	2364	337	79	0.010	blue
2923	2888	2441	340	90	99.000	blue
3382	3176	2363	204	78	0.010	blue
3327	3199	2386	40	90	0.100	blue
4083	3240	2348	227	78	0.010	blue
3371	3171	2362	210	87	0.010	blue
4375	3221	2419	345	86	0.050	blue red
4266	3175	2416	65	90	99.000	blue red
4098	3380	2347	10	80	0.010	blue green
4154	3398	2327	54	90	0.010	blue yellow?
5300	3054	2773	330	90	0.030	brown
5314	3013	2800	23	47	0.400	brown
5364	3025	2821	184	76	0.100	brown
5363	3023	2822	184	76	0.100	brown
3673	3284	2363	202	62	0.020	brown
3664	3353	2392	150	87	0.150	brown
5401	2997	2846	182	80	2.000	brown
5425	3036	2848	188	65	0.150	brown
5401	3001	2844	355	75	0.150	brown
5413	3027	2844	187	62	0.150	brown
3610	3254	2366	172	72	0.200	brown
5272	3034	2769	342	56	3.000	brown
5354	3007	2822	353	75	0.500	brown

STRUCTURAL SECTOR G - WEST FAULT/AMERICANA (Cont.)

North	East	Elev.	Strike	Dip	Width	Type
5519	2951	2892	343	80	0.700	brown
5543	2995	2892	182	73	0.500	brown
5501	2986	2870	185	70	0.300	brown
5087	3094	2709	16	70	0.020	brown
5033	3147	2647	25	65	0.020	brown
5064	3070	2712	350	84	99.000	brown
5016	3137	2647	35	90	0.300	brown
5035	3142	2654	345	50	0.100	brown
5011	3127	2647	242	65	0.100	brown
3832	3363	2360	60	90	2.000	brown
5036	3064	2701	197	78	99.000	brown
4099	3244	2348	76	80	2.000	brown
5046	3072	2700	174	81	99.000	brown
3927	3410	2376	330	83	0.200	brown
5046	3072	2700	355	82	99.000	brown
5029	3059	2701	45	90	99.000	brown
3807	3352	2363	246	73	0.200	brown
5366	3031	2821	350	90	0.010	brown
3608	3409	2439	190	87	0.050	brown
3707	3409	2412	170	87	0.200	brown
3799	3347	2364	12	69	0.200	brown
3739	3388	2388	346	80	0.400	brown
3625	3303	2385	190	75	1.000	brown
3868	3380	2359	140	75	99.000	brown
5002	3080	2673	345	88	2.000	brown
3892	3354	2351	112	82	0.050	brown
3965	3370	2360	160	88	0.100	brown
5363	2943	2845	190	74	1.000	brown
5257	2997	2769	18	90	0.500	brown
3902	3353	2351	295	65	0.010	brown
5550	3021	2891	198	79	0.200	brown
2832	3044	2414	0	90	1.000	brown
2811	3027	2412	198	90	0.400	brown
2987	3073	2415	25	67	0.100	brown
2836	3075	2440	340	75	2.000	brown
2964	3133	2439	140	75	0.030	brown
3506	3129	2364	33	85	0.030	brown
3458	3122	2365	135	78	0.030	brown
2846	3078	2441	350	70	0.030	brown
2746	3096	2466	5	66	2.500	brown
2648	3004	2493	360	83	2.000	brown
3499	3317	2411	287	83	99.000	brown
2891	3060	2414	5	83	0.030	brown
2845	3045	2414	0	83	0.030	brown
2880	3086	2440	145	85	0.030	brown
2842	3076	2440	225	70	0.030	brown
3068	3186	2439	160	82	99.000	brown
3108	3176	2429	285	90	0.150	brown
3017	3068	2412	192	80	0.200	brown

STRUCTURAL SECTOR G - WEST FAULT/AMERICANA (Cont.)

North	East	Elev.	Strike	Dip	Width	Type
3127	3138	2411	10	85	0.250	brown
3122	3133	2411	190	83	0.100	brown
3085	3102	2414	292	70	0.050	brown
3185	3034	2386	345	90	0.050	brown
3002	3071	2413	195	87	0.050	brown
3133	3142	2412	270	86	0.030	brown
3331	3167	2363	253	86	0.200	brown
3334	3162	2362	45	90	0.200	brown
3319	3197	2385	217	85	0.250	brown
3068	3186	2439	6	64	99.000	brown
3206	3122	2365	189	87	0.600	brown
3271	3187	2385	15	90	1.000	brown
3235	3175	2385	15	90	1.000	brown
2564	3110	2577	220	68	99.000	brown
3587	3242	2367	325	70	1.500	brown
3554	3221	2362	15	70	2.000	brown
2552	3074	2574	250	70	99.000	brown
3499	3318	2411	339	86	0.400	brown
2582	3004	2546	5	90	10.000	brown
3560	3221	2361	17	73	1.000	brown
2581	3026	2548	5	90	99.000	brown
5510	3019	2871	354	90	1.000	brown
3685	3363	2390	216	76	99.000	brown
5550	3021	2891	345	60	0.200	brown
3530	3401	2439	182	88	0.010	brown
4354	3247	2396	228	80	0.050	brown
5556	3051	2896	36	90	1.000	brown
5415	3021	2848	10	50	1.000	brown
3463	3301	2412	192	81	0.100	brown
2687	3067	2466	190	63	0.100	brown
2633	3044	2493	227	76	0.050	brown
3501	3251	2385	140	90	0.010	brown
2645	3093	2484	240	75	0.200	brown
2732	3005	2443	360	90	1.000	brown
2636	3055	2492	215	87	0.500	brown
2615	3021	2518	30	83	0.250	brown
2677	3100	2493	330	68	0.020	brown
3440	3294	2413	142	70	0.050	brown
3456	3295	2412	183	84	0.050	brown
2638	3074	2494	250	75	99.000	brown
2755	3057	2438	190	90	99.000	brown
3556	3269	2387	290	90	0.020	brown
3468	3302	2412	255	80	0.050	brown
2650	3099	2504	235	70	0.020	brown
5047	3073	2700	346	88	99.000	brown
2801	2910	2464	175	90	99.000	brown
2800	2911	2465	152	90	99.000	brown
2925	2888	2441	358	80	99.000	brown
2802	2910	2464	183	90	99.000	brown

STRUCTURAL SECTOR G - WEST FAULT/AMERICANA (Cont.)

North	East	Elev.	Strike	Dip	Width	Type
2887	2915	2439	183	79	99.000	brown
2968	2913	2438	174	70	99.000	brown
2982	2878	2443	185	77	99.000	brown
2811	2948	2439	282	50	0.050	brown
2987	2914	2438	153	84	0.200	brown
2898	2900	2441	310	85	0.200	brown
2959	2877	2443	10	80	99.000	brown
2819	2895	2466	205	75	99.000	brown
2800	2956	2438	290	55	0.050	brown
2807	2904	2465	335	80	99.000	brown
2619	2996	2518	350	80	3.000	brown
2621	2989	2519	195	64	3.000	brown
2621	2911	2546	157	85	3.000	brown
2615	2896	2559	205	65	1.000	brown
2795	2853	2490	193	64	1.500	brown
2654	2989	2496	360	83	1.500	brown
2685	2897	2523	10	87	3.000	brown
2802	2909	2465	254	59	99.000	brown
2894	2905	2440	310	82	99.000	brown
2813	2898	2466	287	60	99.000	brown
2731	2905	2494	360	90	3.000	brown
2729	2899	2499	353	85	4.000	brown
2803	2908	2464	160	90	99.000	brown
3204	2962	2415	283	90	0.020	brown
3506	2998	2421	5	90	99.000	brown
3447	2993	2417	195	90	99.000	brown
3174	2915	2453	192	78	2.000	brown
3244	2927	2441	192	72	99.000	brown
3298	2940	2446	190	75	99.000	brown
3431	2991	2414	214	65	0.010	brown
3572	3009	2417	192	68	99.000	brown
3590	3047	2393	65	75	0.010	brown
3483	3031	2414	50	90	0.100	brown
3502	2999	2419	194	75	0.500	brown
3434	2991	2414	10	90	3.000	brown
3568	3009	2417	203	68	99.000	brown
3164	2995	2412	220	90	0.150	brown
2935	2920	2437	175	60	0.700	brown
2938	2918	2438	180	65	0.700	brown
2868	2808	2490	195	46	1.000	brown
2898	2900	2441	165	85	0.200	brown
2894	2905	2440	135	68	0.200	brown
2915	2952	2435	155	81	0.400	brown
2992	2876	2445	6	90	1.500	brown
3095	2914	2441	20	60	0.600	brown
3146	2923	2441	5	70	99.000	brown
3190	2994	2412	355	85	0.150	brown
2865	2856	2467	198	75	4.500	brown
3098	2935	2442	180	90	99.000	brown

STRUCTURAL SECTOR G - WEST FAULT/AMERICANA (Cont.)

North	East	Elev.	Strike	Dip	Width	Type
3080	2954	2440	40	90	99.000	brown
2728	2904	2496	20	82	1.000	brown
2489	2958	2620	186	88	0.800	brown
2571	2920	2575	177	83	1.500	brown
2404	2936	2679	186	68	3.000	brown
2568	2902	2581	190	78	0.400	brown
2482	2927	2627	198	70	0.400	brown
2482	2927	2627	198	70	0.400	brown
2549	2983	2571	20	70	3.000	brown
2679	2901	2522	0	0	99.000	brown
2682	2898	2523	15	86	99.000	brown
2681	2900	2522	20	85	99.000	brown
2521	2903	2605	188	67	3.000	brown
2511	2930	2603	185	86	4.000	brown
2402	2933	2682	185	64	>5	brown
2513	2927	2605	180	65	0.300	brown
2515	2963	2594	12	75	0.030	brown
2577	2943	2569	2	71	0.050	brown
2486	2981	2621	183	80	0.050	brown
2380	2988	2675	188	82	0.300	brown
2549	2972	2573	235	90	99.000	brown
2571	2908	2576	335	80	99.000	brown
2486	2981	2621	183	80	0.050	brown
2513	2958	2596	187	37	0.200	brown
2512	2930	2603	189	90	0.200	brown
2570	2926	2574	195	80	0.300	brown
2591	2969	2548	345	70	0.100	brown
2411	2949	2678	185	82	0.100	brown
2583	2999	2546	170	70	0.150	brown
2660	2808	2552	260	60	0.150	brown
2609	2938	2551	170	90	0.200	brown
2661	2821	2549	220	70	0.200	brown
2628	2976	2518	322	90	0.100	brown
2674	2969	2496	263	75	0.100	brown
2664	2922	2501	170	71	0.100	brown
2729	2828	2531	230	70	0.200	brown
2693	2988	2470	349	78	0.500	brown
2799	2907	2467	360	83	0.700	brown
2703	2987	2465	340	70	1.000	brown
2617	2924	2548	151	90	0.200	brown
2760	2976	2441	341	55	0.300	brown
2712	2919	2498	202	66	0.300	brown
2738	2876	2503	190	65	0.050	brown
2683	2898	2524	16	86	99.000	brown
2685	2896	2525	183	70	99.000	brown
2687	2893	2526	0	0	99.000	brown
2618	2920	2547	145	85	99.000	brown
2621	2914	2546	163	82	99.000	brown
2620	2914	2546	158	81	99.000	brown

STRUCTURAL SECTOR G - WEST FAULT/AMERICANA (Cont.)

North	East	Elev.	Strike	Dip	Width	Type
2798	2957	2443	265	60	99.000	brown
2666	2973	2500	275	84	0.020	brown
2689	2953	2496	270	70	0.020	brown
2745	2944	2467	70	63	0.020	brown
2659	2932	2518	195	83	0.020	brown
2715	2917	2494	200	77	0.020	brown
2671	2917	2517	360	83	0.020	brown
3474	3031	2414	65	80	0.200	brown
4408	3130	2501	325	60	99.000	brown
4471	3132	2522	200	60	99.000	brown
4454	3192	2474	25	82	0.020	brown
4683	3179	2542	377	69	0.600	brown
4597	3189	2526	5	87	99.000	brown
4636	3109	2552	350	55	0.400	brown
4444	3001	2543	0	87	0.150	brown
4527	3156	2523	180	80	0.200	brown
4446	3191	2474	165	80	0.400	brown
4449	3189	2477	324	62	0.020	brown
4450	3189	2476	22	88	0.020	brown
4449	3191	2475	355	90	0.100	brown
4599	3190	2525	112	80	99.000	brown
4347	3183	2442	355	90	0.500	brown
4352	3184	2444	6	87	0.500	brown
4441	3160	2495	195	55	99.000	brown
4250	3165	2420	80	90	99.000	brown
4670	3125	2555	348	80	2.000	brown
4242	3157	2421	123	86	0.030	brown
4402	3155	2479	195	75	99.000	brown
4444	3190	2474	163	80	99.000	brown
4523	3191	2500	195	87	99.000	brown
4400	3151	2482	200	80	99.000	brown
4796	3157	2568	147	65	1.500	brown
4734	3160	2560	310	45	0.800	brown
4504	3033	2545	195	72	0.700	brown
4680	3178	2542	352	62	99.000	brown
4740	3163	2560	330	78	99.000	brown
4744	3165	2561	147	36	99.000	brown
4720	3117	2568	343	84	99.000	brown
4680	3179	2542	300	65	99.000	brown
4694	3185	2541	349	61	99.000	brown
4785	3095	2595	335	72	99.000	brown
4788	3096	2594	145	85	99.000	brown
4719	3116	2568	335	90	99.000	brown
4799	3104	2595	350	75	99.000	brown
4715	3113	2568	6	57	99.000	brown
4720	3116	2569	330	81	99.000	brown
4676	3178	2541	310	40	99.000	brown
4737	3162	2560	160	84	99.000	brown
4772	3143	2568	315	90	99.000	brown

STRUCTURAL SECTOR G - WEST FAULT/AMERICANA (Cont.)

North	East	Elev.	Strike	Dip	Width	Type
4721	3120	2568	90	90	99.000	brown
4582	3194	2519	340	85	1.000	brown
4798	3158	2569	334	78	99.000	brown
4798	3158	2568	321	84	99.000	brown
4668	3124	2555	0	90	99.000	brown
4721	3119	2568	186	65	99.000	brown
4740	3131	2568	162	73	99.000	brown
4683	3179	2542	265	74	0.300	brown
4645	3165	2541	280	44	0.100	brown
4698	3035	2599	10	80	0.100	brown
4250	3165	2420	180	75	99.000	brown
3880	3047	2419	257	77	2.000	brown
4851	3145	2593	326	30	0.400	brown
3818	3038	2417	265	80	1.000	brown
3949	3051	2420	147	45	0.500	brown
3902	3049	2418	155	54	0.600	brown
3660	3061	2416	200	90	0.100	brown
3641	3053	2393	25	85	0.030	brown
4914	3108	2621	328	60	0.020	brown
3721	3069	2395	210	90	0.020	brown
3907	3094	2397	196	80	8.000	brown
3777	3033	2417	262	80	0.200	brown
3725	3069	2392	26	88	0.200	brown
4955	3115	2642	20	90	99.000	brown
4907	3102	2622	350	75	99.000	brown
3764	3032	2420	236	84	0.050	brown
3725	3125	2364	270	74	0.020	brown
3721	3069	2395	37	86	0.020	brown
4885	3039	2654	349	87	0.400	brown
4889	3093	2622	357	85	0.500	brown
3723	3068	2395	210	90	0.400	brown
3907	3094	2397	194	73	8.000	brown
4132	3124	2417	183	76	3.000	brown
4353	3184	2444	334	80	99.000	brown
4093	3147	2391	184	75	0.500	brown
4951	3086	2647	2	85	0.300	brown
4104	3107	2418	161	73	0.150	brown
4338	3178	2442	0	0	99.000	brown
4245	3132	2445	192	52	99.000	brown
4843	3141	2593	92	74	99.000	brown
4351	3183	2443	25	90	99.000	brown
3454	3031	2413	240	90	0.200	brown
3519	3000	2422	5	90	1.000	brown
4131	3123	2417	190	78	99.000	brown
3530	3004	2419	195	70	0.250	brown
3460	3058	2388	275	90	0.400	brown
2810	3080	2441	190	70	1.500	brown, green
2637	3028	2495	170	83	3.000	brown, green
3028	3071	2416	186	68	0.100	brown, green

STRUCTURAL SECTOR G - WEST FAULT/AMERICANA (Cont.)

North	East	Elev.	Strike	Dip	Width	Type
3635	3310	2387	225	80	0.150	brown, green
2840	3073	2440	170	90	2.000	brown, green
3867	3378	2359	152	72	1.200	brown, green
3574	3278	2387	204	75	1.000	brown, green
2926	3027	2413	210	90	0.500	brown, green
3636	3310	2386	250	78	0.500	brown, orange
5007	3125	2647	2	88	0.020	brown, orange
5047	3161	2649	36	82	0.050	brown, orange
2591	3090	2547	190	85	0.150	brown, orange
2489	2958	2620	186	88	0.800	brown, red
3261	2967	2416	10	65	0.200	brown, red
3953	3373	2359	170	82	0.200	brown, red
3069	3082	2413	170	60	0.500	brown, red
4326	3232	2392	240	90	0.100	brown, red
2971	2954	2431	326	80	0.020	brown, red
2515	2971	2594	220	85	0.400	brown, red
2680	3011	2466	182	90	1.000	brown, yellow
2680	3011	2466	205	25	1.000	brown, yellow
4356	3214	2415	63	87	0.010	brown, yellow
3805	3311	2347	96	80	0.300	brown, yellow
4037	3378	2366	86	83	0.100	brown, yellow
3685	3363	2390	216	76	0.400	green
3723	3277	2347	315	85	0.400	green
3982	3367	2359	210	82	0.400	green
3936	3414	2378	20	90	0.400	green
4064	3368	2349	115	90	2.000	green
3688	3289	2364	53	63	2.500	green
4112	3395	2361	57	78	4.000	green
4098	3380	2349	135	86	2.000	green
4073	3237	2349	88	70	0.300	green
4024	3390	2371	198	77	0.100	green
3989	3368	2361	285	82	0.200	green
3989	3368	2361	176	30	0.200	green
3593	3323	2399	160	90	0.300	green
3542	3263	2386	160	87	0.300	green
3442	3229	2384	260	70	1.000	green
3350	3169	2361	35	90	0.100	green
2546	3058	2576	220	55	1.000	green
3580	3282	2387	225	82	0.150	green
3562	3138	2364	254	82	4.000	green
3550	3136	2366	55	90	2.000	green
3516	3130	2365	240	53	0.100	green
3411	3319	2439	190	90	99.000	green
2747	2990	2442	170	90	1.000	green
2898	3053	2418	190	82	0.200	green
3172	3112	2387	190	65	4.000	green
2613	3025	2519	5	86	3.000	green
2672	3033	2473	180	90	2.000	green
2669	3043	2469	155	55	1.500	green

STRUCTURAL SECTOR G - WEST FAULT/AMERICANA (Cont.)

North	East	Elev.	Strike	Dip	Width	Type
3220	3030	2389	253	75	0.700	green
3675	3164	2347	322	80	0.010	green
3221	3131	2364	175	68	0.200	green brown
3209	3110	2363	200	80	0.400	green brown
2697	3068	2469	162	65	0.100	green, blue
3053	3074	2412	30	90	0.500	green, brown
3368	3211	2390	170	90	1.500	green, brown
4390	3229	2415	62	90	0.300	green, orange
4303	3273	2366	305	90	0.400	green, yellow
3956	3410	2360	160	75	0.010	green blue
3542	3263	2386	180	90	0.020	green blue
4056	3365	2347	100	65	0.500	green blue yellow
4098	3380	2349	135	86	99.000	green red
4035	3357	2347	330	80	0.010	green red
4140	3395	2327	115	88	0.400	green yellow
4146	3396	2327	64	80	0.500	green yellow
5392	2973	2847	352	76	0.010	mylonite blue
3596	3243	2365	140	68	2.000	orange
4243	3251	2360	176	88	0.050	orange
3620	3334	2396	150	90	0.500	orange
4113	3245	2348	80	77	0.200	orange
3725	3277	2346	295	85	1.500	orange
4057	3360	2350	92	84	0.250	orange
4072	3372	2349	349	80	0.030	orange blue
4121	3249	2347	45	86	0.400	orange red
3611	3333	2397	205	82	0.400	orange, red
3676	3254	2348	165	84	1.000	orange, yellow
4065	3238	2347	330	85	0.300	orange yellow
2745	2947	2466	185	70	99.000	red
2514	3001	2604	220	79	0.500	red
4058	3365	2350	143	90	0.050	red
4287	3267	2364	275	90	0.400	red
2687	2958	2495	242	83	99.000	red
4233	3244	2363	74	76	0.100	red
2515	2980	2594	161	79	0.400	red
4182	3263	2348	350	88	0.500	red blue
2733	2958	2464	200	90	0.400	red, brown
4260	3256	2363	70	80	0.400	red, orange
4023	3353	2347	100	70	0.010	yellow green
3748	3285	2347	112	84	0.250	yellow
3735	3281	2347	145	88	0.400	yellow
3820	3320	2347	82	78	0.100	yellow
3247	2970	2414	95	48	99.000	yellow
2922	3059	2415	145	70	0.200	yellow
3902	3353	2351	18	75	0.200	yellow
3830	3326	2347	82	78	0.200	yellow
4322	3231	2392	310	86	0.500	yellow
4057	3383	2364	276	86	0.200	yellow
3909	3348	2350	14	90	0.400	yellow

STRUCTURAL SECTOR G - WEST FAULT/AMERICANA (Cont.)

North	East	Elev.	Strike	Dip	Width	Type
3867	3345	2351	169	88	1.000	yellow
3850	3336	2350	149	85	0.450	yellow
4383	3260	2393	255	90	0.400	yellow
3834	3328	2348	138	74	2.000	yellow
3714	3273	2346	70	83	0.100	yellow
4011	3400	2372	24	80	0.300	yellow
3823	3322	2347	280	80	0.100	yellow
4062	3386	2364	251	88	0.400	yellow
3953	3373	2359	274	88	0.400	yellow
3535	3134	2364	198	90	0.050	yellow red
3305	3194	2385	110	90	2.000	yellow, brown
3743	3188	2346	350	86	0.050	yellow, brown
3732	3281	2347	275	87	2.000	yellow, orange
3826	3325	2348	57	85	0.100	yellow, red
4277	3289	2348	60	84	0.010	yellow orange
4112	3386	2347	280	75	0.010	yellow red

Resume

Name: Darryl Desment Lindsay

Date of Birth : 16 Feb. 1968

Languages : English, Spanish

Education:

Doctorate of Philosophy in Earth Sciences
Dalhousie University, Halifax, NS, Canada (Sept. 1992-1997)

Bachelor of Science Honours Degree - Geological Science
Carleton University, Ottawa, ON, Canada (Sept.1986-1991)

Geological Experience:

Consulting Geologist, Sept. 1994 to March 1995 and July 1995 through Dec. 1996
Reporting to Guillermo Ossandón C. and Roberto Fréraut,
Superintendencia de Geologia, Codelco-Chile, Division Chuquicamata, Chuquicamata, Chile

Geological Assistant, July 1992 through September 1992.
Reporting to Dr. Mike McDonough,
Geological Survey of Canada - Calgary, 3303-33rd St. SW, Calgary, AB, Canada.

Geological Assistant, May 1991 through December 1991.
Reporting to Dr. Jack Henderson,
Geological Survey of Canada- Ottawa, 601 Booth Street, Ottawa, ON, Canada.
Regional

Field Assistant, May through August 1990 and 1989.
Reporting to Dr. Trygve Hoy and Kathryn Dunne,
EMPR - British Columbia - Geological Survey Branch, 5-1810 Blanshard St, Victoria, BC, Canada.

Professional Development:

Volcanic associated Massive Sulphide Deposits : Processes and Examples, 1997.
Low Temperature Thermochronology, Geological Association of Canada, 1992.
Canadian mining districts: Sudbury, Timmins and south central British Columbia, 1996.
Serrinha Greenstone Belt and gold deposits (Salitre, Brasileiro, Jacobina), Brazil, 1996.

Associations / Organizations :

Geological Association of Canada : Mineral Deposit Division
Canadian Institute of Mining, Metallurgy and Petroleum : Mineral Economics Society
Colegio de Geologos de Chile, A.G.

Awards:

Dalhousie Graduate Scholarship, September 1992 through August 1997.
The Hugh E. McKinstry Fund of the Society of Economic Geologists Foundation, Inc. November 1993.

Publications:

Reynolds, P. R., Ravenhurst, C., Zentilli, M., and **Lindsay, D.D.**, in press. High-precision $^{40}Ar/^{39}Ar$ dating of two consecutive hydrothermal events in the Chuquicamata porphyry copper system, Chile. Isotope Geoscience.

Lindsay, D.D., Zentilli, M. and Rojas, J., 1995. Evolution of permeability in an active ductile to brittle shear system controlling the mineralization at the Chuquicamata porphyry copper deposit, northern Chile. International Geology Review, v. 37, p.945-958.

McDonough, M.R., Grover, T.W., McNicoll, V.J., **Lindsay, D.D.**, 1993. Preliminary report of the geology of the southern Taltson magmatic zone, northeastern Alberta; *in* Current Research, Part C; Geological Survey of Canada, Paper 93-1C, p. 221-232.

Presented Abstracts:

Lindsay, D.D., Zentilli, M., and Godfrey-Smith, D. 1996. Age Determinations on the West Fissure, Chuquicamata, Chile : Integration of FT, TL, ESR, K/Ar and $^{40}Ar/^{39}Ar$ techniques (Extended Abstract). 39th Congresso Geologico Brasilero, Sept. 1-7, 1996; V. , p.

Lindsay, D.D., Zentilli, M. and Ossandon, G., 1996. Falla Oeste fault system : Record of its regional significance as exposed in the Chuquicamata open pit, northern Chile. (Extended Abstract) 3rd International Symposium on Andean Geodynamics, St.Malo, France, September 17-19, 1996; p.427-430.

Lindsay, D.D., Zentilli, M. and Rojas, J., 1995. Evolution of permeability in an active ductile to brittle shear system at the Chuquicamata porphyry copper deposit, northern Chile.(Extended Abstract) Giant Ore Deposits 2, Queen's University, Kingston, ON, p. 57-85.

Lindsay, D.D. and Zentilli, M. 1995. Formation of a Stockwork System : Structural Control of Mineralization in the Chuquicamata Porphyry Copper Deposit, Northern Chile. (Abstract) GAC/MAC Annual Meeting, v. 20, p. A-61.
Lindsay, D.D. and Zentilli, M. 1995. A ductile through brittle structural sequence : emplacement and mineralization of a porphyry copper deposit, northern Chile. (Abstract) GAC/MAC Annual Meeting, v. 20, p. A-61.

Lindsay, D.D., 1994. Structural Control and Anisotropy of Mineralization at Chuquicamata. (Abstract) in 7th Congresso Geologico Chileno, Volume 2, pp. 1510-1515.

Lindsay, D.D., 1994. Anisotropy of ore-stage fracture permeability in a porphyry copper system : A response to regional shear. (Abstract) Atlantic Geology, v. 30(1), p. 75.

Open File Map Sheets:

McDonough, M.R., Grover, T.W., McNicoll, V.J., **Lindsay, D.D.**, Kelly, K.L., and Guerstein, P.G., 1994. Revised Geology, Andrew Lake, Alberta (74M/16). Geological Survey of Canada, Open File 2905, scale 1:50 000.

McDonough, M.R., Grover, T.W., McNicoll, V.J., **Lindsay, D.D.**, Kelly, K.L., and Guerstein, P.G., 1993a. Geology, Tulip Lake, Alberta (East-Half 74M/14). Geological Survey of Canada, Open File, scale 1:50 000.

McDonough, M.R., Grover, T.W., McNicoll, V.J., **Lindsay, D.D.**, Kelly, K.L., and Guerstein, P.G., 1993b. Geology, Mercredi Lake, Alberta (74M/15). Geological Survey of Canada, Open File, scale 1:50 000.

McDonough, M.R., Grover, T.W., McNicoll, V.J., **Lindsay, D.D.**, Kelly, K.L., and Guerstein, P.G., 1993a. Geology, Andrew Lake, Alberta (74M/16). Geological Survey of Canada, Open File 2664, scale 1:50 000.

References

Ague, J.J. and Brimhall, G.H., 1989. Geochemical modelling of steady state fluid flow and chemical reaction during supergene enrichment of porphyry copper deposits. Economic Geology, v. 84, pp. 506-528.

Akande, S. and Zentilli, M., 1982. Genesis of the Gays River lead-zinc mineralization reconsidered in the light of geologic and fluid inclusion studies. In: GAC-MAC Annual Meeting. Program with Abstracts, 7, p. 35.

Alpers, C.N. and Brimhall, G.H., 1988. Middle Miocene climatic change in the Atacama Desert, northern Chile: Evidence from supergene mineralization at La Escondida. Geological Society of America Bulletin, v. 100, p. 1640-1656.

Alvarez, C.O. and Aracena, P.I., 1985. Algunas consideraciones de la petrologia y alteracion del complejo plutonico de Chuquicamata, Chile. Translated Title: Some considerations on the petrology and alteration of the Chuquicamata plutonic complex. Actas Congreso Geologico Chileno, v. 4, p 4.1-4.30.

Alvarez, O. and Flores, R. 1985. Alteracion y mineralizacion hipogena en el yacimiento de Chuquicamata, Chile. Translated Title: Alteration and hypogene mineralization in the Chuquicamata Mine, Chile. Actas, 4th Chilean Geological Congress, Antofagasta, v. 2-3, p. 78-100.

Alvarez, O., Miranda, J., and Guzman, P., 1980. Geologia del complejo Chuquicamata. Translated Title: Geology of the Chuquicamata Complex. In Minera de cobres porfidicos: Instituto de Ingenieros de Minas de Chile, Santiago, v2, p. 314-363.

Ambrus, W.J., 1979. Emplazamiento y mineralizacion de los porfidos cupriferos de Chile. Translated Title: Emplacement and mineralization of the porphyry copper deposits of Chile. Unpublished Ph.D. Thesis, Universidad de Salamanca, Spain, 313p.

American Geological Institute, 1966. Glossary of Geology and Related Sciences. American Geological Institute, Washington, D.C., 325 p.

Anderson, J.L., Osborne, R.H., and Palmer, D.F., 1983. Cataclastic rocks of the San Gabriel fault - an expression of deformation at deeper crustal levels in the San Andreas fault zone. Tectonophysics, 98, pp. 209-251.

Applegate, B., 1966. Compilation map of the distribution of lithological units of the Chuquicamata deposit. Archives of the Superintendencia de Geologia, Codelco-Chuquicamata, Chuquicamata, Chile.

Aracena, I., 1981. Geologia y alteracion del sector norte del yacimiento de Chuquicamata. Translated Title: Geology and alteration in the northern sector of the Chuquicamata mine. Unpublished Memoria, Universidad de Chile, 94 pages.

Araneda, R., 1978. Marco geologico de la region Chuquicamata-El Abra. Translated Title: Geological aspects of the Chuquicamata-El Abra region. Codelco-Chuquicamata, Chuquicamata, Chile. Internal Report CGN-27.

Arboleya, M.L. and Engelder, T., 1995. Concentrated slip zones with subsidiary shears: their development on three scales in the Cerro Brass fault zone, Appalachian valley and ridge. Journal of Structural Geology, v. 17, p. 519-532.

Aydin, A. and Page, B.M., 1981. Quaternary structural domains in a dominant strike-slip environment, west-central California. Geological Society of America, Abstracts with Programs, v. 13, p. 399.

Aydin, A. and Page. B.M., 1984. Diverse Pliocene-Quaternary tectonics in a transform environment, San Francisco Bay region, California. Geological Society of America Bulletin, v. 95, p. 1303-1317.

Bahlburg, H., Breitkreuz, C. and Zeil, W., 1988. The middle to late Paleozoic evolution of northern Chile (21o-27o): Geotectonic implications for the east Pacific margin of Gondwana. V Congreso Geologico Chileno, Santiago, Tomo 1, p. A1-A17.

Baker, M.C.W., 1977. Geochronology of Upper Tertiary volcanic activity in the Andes of northern Chile. Geol. Rundsch., v. 66, pp. 455-465.

Baker, R.C. and Guilbert, J.M., 1987. Regional structural control of porphyry copper deposits in northern Chile. Abstracts with Programs - Geological Society of America, v. 19, p. 578.

Baldwin, J.T., Swain, H.D. and Clark, G.H., 1978. Geology of the Panguna porphyry copper deposit, Bougainville, Papua New Guinea. Economic Geology, v. 73, p. 690-702.

Beane, R.E. and Titley, S.R., 1981. Porphyry copper deposits; Part II, Hydrothermal alteration and mineralization. Economic Geology, Seventy-fifth anniversary volume; 1905-1980, p. 235-269.

Berggren, W.A., Kent, D.V., Swisher, C.C. and Aubry, M-P., 1995a. A revised Cenozoic geochronology and chronostratigraphy. In Geochronology, Time Scales and Stratigraphic Correlation, Berggren, W.A., Kent, D.V., Aubry, M-P. And Hardenbol, J. (Editors), Society for Sedimentary Geology, Special Publication, 54, p. 129-212.

Berggren, W.A., Kent, D.V., Aubry, M-P. and Hardenbol, J., 1995b. Geochronology, Time

Scales and Stratigraphic Correlation. Society for Sedimentary Geology, Special Publication, 54.

Berthé, D., Choukroune, P. and Jegouzo, P., 1979. Orthogneiss, mylonite and non-coaxial deformation of granites: the example of the South Armoricain shear zone. Journal of Structural Geology, v. 1, p. 31-42.

Best. M.G., 1982. Igneous and Metamorphic Petrology. W.H. Freeman and Company, New York, New York, pp. 630.

Bodnar, R.J., 1995. Fluid-inclusion evidence for a magmatic source for metals in porphyry copper deposits, in Thompson ,J.F.H., ed., Magmas, Fluids, and Ore Deposits, Mineralogical Association of Canada, Short Course, v. 23, pp. 139-152.

Boggs Jr., S., 1987. Principles of Sedimentary and Stratigraphy. Merrill Publishing Company, Columbus, Ohio, 784 p.

Boric, R., Diaz, F., and Maksaev, V., 1990. Geologia y yacimientos metaliferos de la region de Antofagasta. Translated Title: Geology and metaliferous deposits of the Antofagasta Region. Servico Nacional de Geologia y Mineria, Santiago, Chile, Boletin No. 40, 246 pages.

Brace, W.F., 1980. Permeability of crystalline and argillaceous rocks: status and problems. International Journal of Rock Mechanics in Mineral Sciences and Geomechanical Abstracts, v. 17, p. 876-893.

Brown, M., 1994. The generation, segregation, ascent and emplacement of granite magma: the migmatite-to-crustally-derived granite connection in thickened orogens. Earth Science Reviews, v. 36, p. 83-130.

Buddin, T.S., Stimpson, I.G. and Williams, G.D., 1993. Northern Chilean fore-arc tectonics and Cenozoic plate kinematics. Tectonophysics, v. 220, p. 193-203.

Bürgmann, R. and Pollard, D.D., 1994. Strain accommodation about strike-slip fault discontinuities in granitic rock under brittle to ductile conditions. Journal of Structural Geology, v. 16, p. 1655-1674.

Burnham, C.W., 1979. Magmas and hydrothermal fluids, in Barnes, H.L., ed., Geochemistry of Hydrothermal Ore Deposits, 2nd edition, New York, John Wiley and Sons, pp. 71-136.

Bursnall, J.T., 1989. Introduction: Review of mechanical principles, deformation mechanisms and shear zone rocks. In Mineralization and Shear Zones, J.T. Bursnall (editor), Geological Association of Canada Short Course Notes Volume 6, p. 1-28.

Caine, J.S., Evans, J.P and Forester, C.B., 1996. Fault zone architecture and permeability structure. Geology, v. 24, p. 1025-1028.

Campos, O.A., Mercado, J.M. and Vivanco, P.G., 1979. Geologia del complejo Chuquicamata. Translated Title: Geology of the Chuquicamata Complex. Codelco-Chuquicamata, Chuquicamata, Chile. Internal Report CGN-33.

Casselman, M.J., McMillan, W.J., and Newman, K.M., 1995. Highland Valley porphyry copper deposits near Kamloops, British Columbia: a review and update with emphasis on the Valley deposit. In Porphyry Deposits of the Northwestern Cordillera of North America. T.G. Schroeter (ed.), Canadian Institute of Mining, Metallurgy and Petroleum Special volume 46, pp. 161-191.

Charrier, R. and Reutter, K. J., 1994. The Purilactis Group of northern Chile: Boundary between arc and backarc from Late Cretaceous to Eocene. In: K.J. Reutter, E. Scheuber and P. Wigger (editors), Tectonics of the Southern Central Andes; Springer-Verlag, p. 189-202.

Chester, F.M. and Logan, J.M., 1986. Composite planar fabric of gouge from the Punchbowl fault, California. Journal of Structural Geology, v. 9, p. 621-634.

Chester, F.M., Friedman, M. and Logan, J.M., 1985. Foliated Cataclasites. Tectonophysics, v. 111, p. 139-146.

Chivas, A.R. and Wilkins, W.T., 1977. Fluid incusion studies in relation to hydrothermal alteration and mineralization at the Koloula porphyry copper prospect, Guadalcanal, Economic Geology, v. 72, pp. 153-169.

Chong, G. and Pardo, R., 1993. Geologia del distrito de Chuquicamata, Segunda region de Antofagasta (documento en trabajo). Translated Title: Geology of the Chuquicamata District, Antofagasta Region (preliminary working document). Internal report, Codelco-Exploration (Calama), Calama, Chile, 141 pages.

Cladouhos, T.T., 1996a. Shape preferred orientations of survivor grains in fault gouge. Journal of Structural Geology, in review.

Cladouhos, T.T., 1996b. A kinematic model for deformation within brittle shear zones. Journal of Structural Geology, in review.

Clark, A.H., 1993. Are outsize porphyry copper deposits either anatomically or environmentally distinctive ? In B.H. Whiting, C.J. Hodgson, and R. Mason (Editors), Giant Ore Deposits, Society of Economic Geologists, Special Publication 2, p.213-283.

Coira, B., Davidson, J., Mpodozis, C and Ramos, V., 1982. Tectonic and magmatic evolution

of the Andes of northern Argentina and Chile. Earth Science Reviews, v. 18, p. 303-332.

Cox, R.A., Dempster, T.J., Bell, B.R. and Rogers, G., 1996. Crystallization of the Shap Granite: evidence from zoned K-feldspar megacrysts. Journal of the Geological Society, London, v. 153, p. 625-635.

Deng, Q., Wu, D., Zhang, P. and Chen, S., 1986. Structure and deformational character of strike-slip fault zones. In Internal Structure of Fault Zones, C. Wang (editor), Birkhäuser Verlag, Basel. Pure and Applied Geophysics, v. 124, p. 203-223.

Dilles, J.H., 1987. Petrology of the Yerington Batholith, Nevada: Evidence for evolution of porphyry copper ore fluids. Economic Geology, v. 82, p. 1750-1789.

Dilles, J.H. and Einaudi, M.T., 1992. Wall-rock alteration and hydrothermal flow paths about the Ann-Mason porphyry copper deposit, Nevada - A 6-km vertical reconstruction. Economin Geology, v. 87, p. 1963-2001.

Dilles, J.H., Tomlinson, A.J., Martin, M. and Blanco, N., 1997. El Abra and Fortuna Complexes: A porphyry copper batholith sinistrally displaced by the Falla Oeste. In 8th Congresso Geologico Chileno, in press.

D'Lemos, R.S., Brown, M. and Strachan, R.A., 1992. Granite magma generation, ascent and emplacement within a transpressional orogen. Journal of the Geological Society of London, v. 149, p. 487-490.

Eastoe, C.J., 1983. Sulfur isotope data and the nature of the hydrothermal systems at the Panguna and Frieda porphyry copper deposits, Papua New Guinea. Economic Geology, v.78, p. 201-213.

Engelder, J.T., 1974. Cataclasis and the generation of fault gouge. Geological Society of America Bulletin, v. 85, p. 1515-1522.

Fitch, T.J., 1972. Plate convergence, transcurrent faults, and internal deformation adjacent to southeast Asia and the western Pacific. Journal of Geophysical Research, v. 77, p. 4432-4460.

FitzGerald, J.D. and Stunitz, H., 1993. Deformation of granitoids at low metamorphic grade. I: Reactions and grain size reduction. Tectonophysics, v. 221, p. 269-297.

Flint, S., Hartley, A.J., Rex, D.C., Guise, P., and Turner, P., 1983. Geochronology of the Purilactis Formation northern Chile, An insight into the late Cretaceous / Early Tertiary basin dynamics of the central Andes. Revista Geologica de Chile, v. 16(2), p. 241-246.

Flores, R. 1985. Control del enriquecimiento supergeno en el yacimiento Chuquicamata, Chile. Translated Title: Controls on the supergene enrichment in the Chuquicamata deposit, Chile. Actas 4th Congreso Geologico Chileno, Antafagasta, Chile, p. XX

Fossen, H. and Tikoff, B., 1993. The deformation matrix for simultaneous simple shearing, pur shearing and volume change, and its application to transpression-transtension tectonics. Journal of Structural Geology, v. 15, p. 413-422.

Freund, R., 1974. Kinematics of transform and transcurrent faults. Tectonophysics, v. 21, p. 93-134.

Gamond, J.F., 1987. Bridge structures as sense of displacement criteria in brittle fault zones. Journal of Structural Geology, v. 9, p. 609-620.

Gapais, D., 1989. Shear structures within deformed granites: mechanical and thermal indicators. Geology, v. 17, p. 1144-1147.

Giggenbach, W.F., 1992. Magma degassing and mineral deposition in hydrothermal systems along convergent plate boundaries. Economic Geology, v. 87, pp. 1927-1944.

Glazner, A.F., 1991. Plutonism, oblique subduction and continental growth : An example from the Mesozoic of California. Geology, v. 19, p. 784-786.

Gradstein, F.M. and Ogg, J., 1996. A Phanerozoic time scale. Episodes, v. 19, p. 3-5.

Graney, J.R. and Kesler, S.E., 1995. Gas composition of inclusion fluid in ore deposits : Is there a relation to magmas ?, in Thompson ,J.F.H., ed., Magmas, Fluids, and Ore Deposits, Mineralogical Association of Canada, Short Course, v. 23, pp. 221-246.

Granier, T., 1985. Origin, damping and pattern of development of faults in granite. Tectonics, v. 4, p. 721-737.

Grocott, J., Brown, M., Dallmeyer, R.D., Taylor-Graeme, K. and Treloar, P.J., 1994. Mechanisms of continental growth in extensional arcs; an example from the Andean plate-boundary zone. Geology, v. 22, pages 391-394.

Grocott, J., Taylor, G.K. and Treloar, P.J., 1993. Mesozoic extensional and strike-slip fault systems in magmatic arc rocks of the Andean plate boundary zone, northern Chile. *In* Second International Symposium on Andean Geodynamics, Oxford, U.K. , p. 187-190.

Grocott, J., Taylor, G.K., Treloar, P.J., and Wilson, J., 1994. Magmatic arc fault systems and the emplacement of Mesozoic plutonic complexes in northern Chile. *In* Actas 7th Congreso Geologico Chileno, v. 2, p. 1360-1364.

Guilbert, J.M., 1981. A plate tectonic-lithotectonic classification of ore deposits. In Relations of tectonics to ore deposits in the southern Cordillera. W.R. Dickenson and W.D. Payne (eds).Arizona Geological Society Digest v. 14, pp.1-10.

Guilbert, J.M. and Park Jr, C.F., 1986. The Geology of Ore Deposits. W.H. Freeman and Company, New York, 985 p.

Guilbert, J.M. and Lowell, J.D., 1974. Variations in zoning patterns in porphyry ore deposits. Canadian Mining and Metallurgical Bulletin, v. 67, pages 99-109.

Guineberteau, B., Bouchez, J-L, and Vigneresse, J-L, 1987. The Mortagne granite pluton (France) emplaced by pull-apart along a shear zone: Structural and gravimetric arguments and regional implication. Geological Society of America Bulletin, v. 99, p. 763-770.

Gustafson, L.B. and Hunt, J.P., 1975. The Porphyry Copper Deposit at El Salvador, Chile. Economic Geology, vol. 70, pp. 857-912.

Gustafson, L.B. and Quiroga G., J., 1995. Patterns of mineralization and alteration below the porphyry copper orebody at El Salvador, Chile. Economic Geology, v. 90, p. 2-16.

Guzman, P., 1983. Geologia y evaluacion del yacimiento del tipo porfido cuprifero de Chuqui norte, II Region de Antofagasta. Translated Title: Geology and evaluation of a porphyry copper deposit in the Antofagasta region of northern Chile. Memoria, Universidad de Chile, 186 pages.

Haynes, F.M., 1984, Vein densities in drill core, Sierrita Porphyry Copper deposit, Pima County, Arizona: Economic Geology, v.79, pp. 755-758.

Haynes, F.M. and Titley, S.R., 1980. The evolution of fracture-related permeability within the Ruby Star Granodiorite, Sierrita porphyry copper deposit, Pima County, Arizona. Economic Geology, v. 75, p. 673-683.

Hanmer, S. and Passchier, C., 1991. Shear-sense indicators: A review. Geological Survey of Canada, Paper 90-17. 72 pages.

Heberlein, D.R., 1995. Geology and supergene processes: Berg copper-molybdenum porphyry, west central, British Columbia. In Porphyry Deposits of the Northwestern Cordillera of North America. T.G. Schroeter (ed.), Canadian Institute of Mining, Metallurgy and Petroleum Special volume 46, pp. 304-312.

Hedenquist, J.W., 1995. The ascent of magmatic fluid : Discharge versus mineralization, in Thompson ,J.F.H., ed., Magmas, Fluids, and Ore Deposits, Mineralogical Association of Canada, Short Course, v. 23, pp. 263-290.

Heidrick, T.L. and Titley, S.R., 1982. Fracture and dike patterns in Laramide plutons and their structural and tectonic implications. In, Titley, S.R. (Editor),Advances in geology of the porphyry copper deposits, southwestern North America. Tuscon, University of Arizona Press, p.73-91.

Hempton, M.R. and Neher, K., 1986. Experimental fracture, strain and subsidence patterns over en échelon strike-slip faults: implications for the structural evolution of pull-apart basins. Journal of Structural Geology, v. 8, p. 597-605.

Henley, R.W. and McNabb, A., 1978. Magmatic vapour plumes and ground-water interaction in porphyry copper emplacement. Economic Geology, v. 73, no. 1, p. 1-20.

Hollister V.F. and Bernstein, M., 1975. Copaquire, Chile: Its geologic setting and porphyry copper deposit. Society of Mining Engineers, AIME, Transactions, v. 258, p. 137-142.

Hollister, V.F., 1978. Geology of the porphyry copper deposits of the western hemisphere. AIME, New York, NY, 219p.

Hubbert, M.K. and Rubey, W.W., 1959. Role of fluid pressure in mechanics of overthrust faulting. Geological Society of America Bulletin, v. 70, p. 115-166.

Hubbert, M.K. and Willis, D.G., 1957. Mechanics of hydraulic fracturing. Trans. American Institute of Mining Engineers, v. 210, 153-168.

Hunt, J.P., 1991. Porphyry Copper Deposits. In Huchison, R., (editor) Historical Perspectives of Geologic Concepts and Case Histories of Famous Discoveries. Economic Geology Monograph 8, p. 192-206.

Hutton, D.H.W., Dempster, T.J., Brown, P.E. and Becker, S.D., 1990. A new mechanism of granite emplacement: intrusion in active extensional shear zones. Nature, v. 343, p. 452-455.

Jarrell, O.W., 1944. Oxidation at Chuquicamata, Chile. Economic Geology, v 39, p. 215-286.

Karlstrom, K.E., Miller, C.F., Kingsbury, J.A., Wooden, J.L., 1993. Pluton emplacement along an active ductile thrust zone, Piute Mountains, southeastern California: Interaction between deformational and solidification processes. Geological Society of America Bulletin, v. 105, p. 213-230.

Kay, S., Ramos, V., Mpodozis, C. and Sruoga, P., 1989. Late Paleozoic to Jurassic silicic magmatism at the Gondwana margin: Analogy to the Middle Proterozoic in North America? Geology, v. 17, p. 324-328.

Kirkham, R.V., 1971. Intermineral intrusions and their bearing on the origin of porphyry

copper and molybdenum deposits. Economic Geology, v. 66, pp. 1244-1249.

Knapp, R.B. and Norton, D., 1981. Preliminary numerical analysis of processes related to magma crystallization and stress evolution in cooling pluton environments. American Journal of Science, v. 281, p. 35-68.

Knipe, R.J., 1989. Deformation mechanisms - recognition from natural tectonites. Journal of Structural Geology, v. 11, p. 127-146.

Koide, H. and Bhattacharji, S., 1975. Formation of fractures around magmatic intrusions and their role in ore localization. Economic geology, v. 70, p. 781-799.

Kontak, D., Clark, A.H., Farrer, E. and Strong, D.F., 1985.The rift-associated Permo-Triassic magmatism of the Eastern Cordillera: a pre-cursor to the Andean orogeny. In Pitcher, W.S., Atherton, M.P., Cobbing, E.J. and Beckinsale, R.D. (Editors). Magmatism at a plate edge - The Peruvian Andes. John Wiley and Sons, New York, Glasglow and London, p.36-44.

Krige, D.G. and Dunn, P.G., 1995. Some practical aspects of ore reserve estimation at Chuquicamata Copper Mine, Chile. APCOM XXV Conference, Brisbane, Australia, p. 125-133.

Langerfeldt, H., 1964. Preliminary survey of rock problems at Chuquicamata. Internal report, Superintendencia de Geologia, Codelco-Chile, 48 p.

Laubach, S.E., 1988. Subsurface fractures and their relationship to stress history in East Texas Basin sandstone. Tectonophysics, v. 156, p. 37-49.

Lewis, M.H., 1996. Characterisation of hypogene covellite assemblages at the Chuquicamata porphyry copper deposit, Chile, section 4500N. Unpublished MSc. thesis, Dalhousie University. 223 p.

Lindsay, D.D., Zentilli, M. 1997. Successive stages of fracture controlled mineralization, Chuquicamata porphyry copper deposit, Chile. Abstract Volume, GAC/MAC Annual Meeting, Ottawa, Canada, p. A-91.

Lindsay, D.D., Zentilli, M. and Rojas de la Rivera, J., 1995. Evolution of an active ductile to brittle shear system controlling mineralization at the Chuquicamata porphyry copper deposit, northern Chile. International Geology Review, v. 37, p. 945-958.

Lindsay, D.D., Zentilli, M. and Ossandon C., G., 1996. Falla Oeste fault system: Record of its regional significance as exposed in the Chuquicamata open pit, northern Chile. In Third International Symposium on Andean Geodynamics (Extended Abstracts), St.Malo, France, p. 427-430.

Lister, G.S. and Snoke, A.W., 1984. S-C mylonites. Journal of Structural Geology, v. 6, p. 617-638.

Lopez, V.M., 1939. The primary mineralization at Chuquicamata, Chile. Economic Geology, v 34, p. 674-711.

Lopez, V.M., 1942. Chuquicamata, Chile. In W.H. Newhouse (ed.), Ore Deposits as Related to Structural Features, Princeton University Press, Princeton, New Jersey, p. 126-128, 280p.

Lowell, J.D., 1968. Geology of the Kalamazoo orebody, San Manuel district, Arizona. Economic Geology, v. 63, p. 645-654.

Lowell, J.D. and Guilbert, J.M., 1970. Lateral and vertical alteration / mineralization zoning in porphyry ore deposits. Economic Geology, v 65, p. 378-408.

Lowenstern, J.B., 1995. Applications of silicate-melt inclusions to the study of magmatic volatiles, in Thompson ,J.F.H., ed., Magmas, Fluids, and Ore Deposits, Mineralogical Association of Canada, Short Course, v. 23, pp. 71-100.

Mackin, J.H., 1968. Iron ore deposits of the Iron Springs district, southwestern Utah. In, Ore Deposits of the United States (L.C. Graton- R. Sales Memorial Volume), J.D. Ridge (ed.), American Institute of Mining Engineers, v. 2, p. 992-1019.

Maksaev, V., 1979. Las fases tectónicas Incaica y Quechua en la Cordillera de los Andes del Norte Grande de Chile. Translated Title: The Incaic and Quechua tectonic phases in the Andean Cordillera of northern Chile. Actas II Congresso Geológico Chileno, Arica, v., 1, p. B63-77.

Maksaev, V., 1990. Metallogeny, Geological Evolution and Thermochronology of the Chilean Andes Between Latitudes 21° and 26° South, and the Origin of Major Porphyry Copper Deposits. Unpublished PhD thesis, Dalhousie University. 544 p.

Maksaev, V. and Zentilli, M., 1988, Marco metalogenico regional de los megadepositos de tipo porfido cuprifero del norte grande de Chile. Translated Title: The regional metalogenic mark of the porphyry copper megadeposits of northern Chile. 5th Congresso Geologico Chileno, v. 1, p. B181-B212.

Maksaev, V., Zentilli, M., and Reynolds P.H., 1988a. ^{40}Argon-^{39}Argon geochronology of porphyry copper deposits of the northern Chilean Andes. 5th Congresso Geologico Chileno, v 1, B109-B133.

Maksaev, V., Boric, R., Zentilli, M., and Reynolds P.H., 1988b. Metallogenic implications of K-Ar, ^{40}Ar/^{39}Ar and fission track dates of mineralized areas in the Andes of Northern

Chile. 5th Chilean Geological Congress, v 1, p. B65-B86.

Marcosson, I.F., 1957. Anaconda. Kingsport Press, Inc. Tennessee, USA, 370 p.

Marinovic, N. and Lahsen, A., 1984. Hoja Calama, Region de Antofagasta. Carta Geologico de Chile 58, 1:250000, Servicio Nacional Geologia Mineria, Santiago, Chile.

Martel, S.J., Pollard, D.D. and Segall, P., 1988. Development of simple strike slip fault zones, Mount Abbot quadrangle, Sierra Nevada, California. Geological Society of America Bulletin, v. 100, pp. 1451-1465.

Martin, W., Leiva, G. and Rojas, J., 1993. Inventorio del conocimiento geologico del yacimiento Chuquicamata. Translated Title: Inventory of the state of geological knowledge of the Chuqucamata Mine. Unpublished report. Chuquicamata, Codelco-Chile, 26 p.

May, G., Hartley, A.J. and Stuart, F.M., 1996. Oligocene-Recent sedimentary and tectonic evolution of the Calama Basin, northern Chilean forearc. In third International Symposium on Andean Geodynamics, St. Malo, France, p. 435-437.

McKenzie, D. and Jackson, J., 1986. A block model of distributed deformation by faulting. Journal of the Geological Society London, v. 143, p. 349-353.

McMillan, W.J., Thompson, J.F.H., Hart, C.J.R. and Johnston, S.T., 1995. Porphyry deposits of the Canadian Cordillera. Geoscience Canada, v. 23, p. 125-134.

McMillan, W.J. and Panteleyev, A., 1980?. Porphyry copper deposits. In Ore Deposit Models, R.G. Roberts and P.A. Sheahan (editors), Geoscience Canada Reprint Series 3, p.45-58.

Meyer, C. and Hemley, J.J., 1967. Wall rock alteration. In Geochemistry of Hydrothermal Ore Deposits. Barnes, H.L. (editor),Holt, Rinehart and Winston, New York, p. 166-235.

Moore, D.E., Lockner, D.A., Summers, R. and Byerlee, J.D., 1995. Permeability changes in intact, fractured, and crushed granite under hydrothermal conditions. Geological Society of America, Abstracts with Programs, Spring Meeting, T12B-20, p. 5301.

Moore, W.J. and Nash, J.T., 1974. Alteration and fluid inclusion studies of the porphyry copper ore body at Bingham, Utah. Economic Geology, v. 69, p. 631-645.

Morand, V.J., 1992. Pluton emplacement in a strike-slip fault zone: the Doctor's Flat Pluton, Victoria, Australia. Journal of Structural Geology, v. 14, p. 205-213.

Mpodozis, C., Tomlinson, A.J., and Cornejo, P.C., 1994. Acerca del control estructural de

intrusivos eocenos y porfidos cupriferos en la region de Potrerillos-El Salvador. Translated Title: Towards the structural control of Eocene intrusives and porphyry copper deposits in the Potrerillos-El Salvador region. In 7th Congreso Geologico Chileno, v. 2, pp. 1596-1600.

Mpodozis, C. and Ramos, V., 1989. The Andes of Chile and Argentina. In Eriksen, G.E, Canas-Pinochet, M.T. and Reinemund, J.A. (Editors), Geology of the Andes and its relation to hydrocarbon and mineral resources: Houston, Texas, Circum -Pacific Council for Energy and Mineral Resources, Earth Science Series, v.11, p.59-90.

Munchmeyer, F.C. and Urqueta, D.I., 1974. Geologia del yacimiento Exotica. Translated Title: Geology of the Exotica deposit. Communicacion - Departamento de Geologia, Facultad de Ciencias Fisicas y Matematicas, Universidad de Chile, v. 41, p. 213-253.

Munizaga, F., 1976, Determinacion de edades radiometricas de rocas de Chuquicamata y El Abra. Translated Title: Determination of radiometric ages for rocks from Chuquicamata and El Abra. Informe Departamento de Geologia, Universidad de Chile. Laboratorio de Geocronologia, Universidad de Sao Paulo, Brazil.

Munoz, M. and Araneda, M., 1980. Physical properties of rocks of the Chuquicamata mine. Tralka, 1(2), p. 119-142.

Murrell, S.A.F.,1970. Global tectonics, rock mechanics, and the mechanism of volcanic intrusions. In Symposium on Mechanism of Igneous Intrusion, G.Newall and N. Rast (editors), Seel House Press, Liverpool, UK, p. 231-244.

Naranjo, J.A. and Paskoff, R.P., 1982. Estratigrafia de las unidades sedimentarias Cenozoicas de la cuenca del Rio Loa en la pampa del Tamarugal, Region de Antofagasta, Chile. Translated Title: The stratigraphy of Cenozoic sedimentary units of the Loa River Basin, Tamarugal plains, Antofagasta Region, Chile. Revista Geologica de Chile, v. 15, p. 49-57.

Naranjo, J.A. and Paskoff, R.P., 1981. Estratigrafia de los depositos Cenozoicas de la Region de ChiuChiu-Calama, Desierto de Atacama. Translated Title: Stratigraphy of the Cenozoic deposits in the ChiuChiu-Calama region, Atacama Desert. Revista Geologica de Chile, v. 13-14, p. 79-85.

Norton, D. and Cathles, L.M., 1979. Thermal aspects of ore deposition, in Barnes, H.L., ed., Geochemistry of Hydrothermal Ore Deposits, 2nd edition, New York, John Wiley and Sons, pp. 611-631.

Norton, D. and Knight, J., 1977. Transport phenomena in hydrothermal systems: cooling plutons. American Journal of Science, v. 277, p. 937-981.

Nur, A., Ron, H. and Scotti, O., 1989. Mechanics of distributed fault and block rotation. In Paleomagnetic Rotations and Continental Deformation, C. Kissel and C. Laj (editors), Kluwer Academic Publishers, p. 209-228.

Odé, H., 1957. Mechanical analysis of the dike pattern of the Spanish Peaks area, Colorado. Bulletin of the Geological Society of America, v. 68, p. 567-576.

Pallauta, J., 1982. Analisis de estabilidad y desarrollo de los taludes del sector suroriental, Mina Chuquicamata. Translated Title: Analyese of slope stability and development in the southeastern sector of the Chuquicamata Mine. Unpublished Memoria, Facultad de Ciencias Fisicas y Matematicas, Departtamento de Geologia, Universidad de Chile, Santiago. 94 pages.

Parada, M.A., Aracena, I. and Tanaka, H., 1987. The petrology of the Chuquicamata Plutonic Complex, Chile. Journal of the Japanese Association of Mineralogy, Petrology and Economic Geology, v. 82, p. 177-188.

Pardo-Casas, F. and Molnar, P., 1987. Relative motion of the Falleron (Nazca) and South American plates since late Cretaceous time. Tectonics, v. 6, p. 233-248.

Park, C.F. and MacDiarmid, R.A. 1975. Ore Deposits. W.H. Freeman and Company, San Francisco, 529 p.

Passchier, C.W. and Simpson, C., 1986. Porphyroclast systems as kinematic indicators. Journal of Structural Geology, v. 8, p 831-844.

Passchier, C.W. and Trouw, R.A.J., 1996. Microtectonics. Springer-Verlag, Berlin, Germany, pp.289.

Perry, V.D., 1952. Geology of the Chuquicamata ore body. Mining Engineering, v 4(12), p. 1166-1168.

Petit, J.P., 1987. Criteria for the sense of movement on fault surfaces in brittle rocks. Journal of Structural Geology, v. 9, p. 597-608.

Phillips W.J., 1972. Hydraulic fracturing and mineralization. Journal of the Geological Society of London, v. 128, p. 337-359.

Phillips, W.J., 1973. Mechanical effects of retrograde boiling and its probable importance in the formation of some porphyry ore deposits. Institute of Mining and Metallurgy Transactions, section B, v. 82, pp. B90-B98.

Pilger, R.H., 1984.Cenozoic plate kinematics, subduction and magmatism: South American

Andes. Journal of the Geological Society of London, v. 141, p.793-802.

Pryer, L.L., 1993. Microstructures in feldspars from a major crustal thrust zone: the Grenville Front, Ontario, Canada. Journal of Structural Geology, v. 15, p. 21-36.

Quirt, G.S., 1972. A potassium -argon geochronological investigation of the Andean mobile belt of north-central Chile. Ph.D. Thesis, Queen's University, Kingston, Canada, 240 p.

Ramirez, F., 1993. Estudio estructural-geomechánico del yacimiento Chuquicamata, II Region, Chile. Translated Title: Structural and geomechanical study of the Chuquicamata Mine. Unpublished Memoria de Geologo, Universidad Catolica del Norte, Antofagasta, Chile. 89 pages.

Ramirez, C. and Gardewag, M., 1982. Hoja Toconao, Región de Antofagasta. Carta Geológica de Chile, SERNAGEOMIN, Santiago, No. 54, 121 p.

Ramos, V., Jordan, T.E., Allemdinger, R.W., Mpodozis, C., Kay, S.M., Cortes, J.M. and Palma, M.A., 1986. Paleozoic terranes of the Central Argentine-Chilean Andes. Tectonics, v. 5, p. 855-880.

Ramsay, JG., 1980. The crack-seal mechanism of rock deformation. Nature, v.284, p. 135-139.

Ramsey, J.G. and Huber, M.I., 1987. The Techniques of Modern Structural Geology, Volume 2: Folds and Fractures. Academic Press, London, 391 p.

Rehrig, W.A. and Heidrick, T.L., 1972. Regional fracturing in Laramide stocks of Arizona and its relationship to porphyry copper mineralization. Economic Geology, vol. 67, p. 198-213.

Renzetti, B.L., 1957. Geology and petrogenesis at Chuquicamata, Chile. Unpublished Ph.D. Thesis, Indiana University, 71 pages.

Reutter, K., Scheuber, E., and Helmcke, D., 1991. Structural evidence of origin-parallel strike-slip displacements in the North Chilean Precordillera. Geologische Rundschau, v. 80, p. 135-153.

Reutter K.J., Chong, G., and Scheuber, E., 1993, The "West Fissure" and the Precordilleran fault system of northern Chile: In Andean Geodynamics, ISAG 1993, ORSTROM/Oxford University, Oxford, U.K., p 237-240.

Reutter, K-J., Scheuber, E., and Chong, G., 1996. The Precordilleran fault system of Chuquicamata, northern Chile: evidence for reversals along arc parallel strike-slip faults.

Tectonophysics, v. 259, p. 213-228.

Reutter, K.J., Scheuber, E. and Wigger, P.J. (Editors) 1994. Tectonics of the Southern Central Andes: Structure and evolution of an Active Continental Margin. Springer-Verlag, Berlin, 333 pages.

Reynolds, P., Ravenhurst, C., Zentilli, M. and Lindsay, D.D., in press. High-precision $^{40}Ar/^{39}Ar$ dating of two consecutive hydrothermal events in the Chuquicamata porphyry copper system, Chile. Isotope Geoscience, in press.

Robertson, E.C., 1982. Continuous formation of gouge and breccia during fault displacement. In, Issues in Rock Mechanics, Proceedings 23rd Symp. Rock Mechanics, R.E Goodman and F.E. House (eds.), Am. Inst. Mining Metall. Petrol. Eng., New York, pp. 397-403.

Roedder, E., 1971. Fluid inclusion studies on the porphyry-type ore deposits at Bingham, Utah; Butte, Montana; and Climax, Colorado, Economic Geology, v. 66, pp. 98-120.

Rojas, J. and Lindsay, D.D., 1997.Evolucion Estructural de Chuquicamata. Extended Abstract, Chilean Geological Congress, in press.

Rutter, E.H., Maddock, R.H., Hall, S.H. and White, S.H., 1986. Comparative microstructures of natural and experimentally produced clay-bearing fault gouges. In: International structure of fault zones, Wang, C-Y. (editor). Pure and Applied Geophysics, v. 124, pp. 3-30.

Sanderson, D.J. and Marchini, W.R.D., 1984. Transpression. Journal of Structural Geology, v. 6, p. 449-458.

Sasso, A.M., Clark, A.H., and Farrar, E., 1995. Tectonic controls on scale of upper Miocene Cu-Au mineralization centres 250 km to the east of coeval mineralization in the Chilean Andes: preliminary results from the Farallon Negro Project, Catamarca, Argentina (extended abstract). In Giant Ore Deposits 2, Proceedings of the second giant ore deposits workshop, A.H. Clark (ed). Kingston, Ontario, pp. 38-56.

Scheuber, E. and Reutter, K.J., 1992, Magmatic arc tectonics in the Central Andes between 21° and 25° South: Tectonophysics, v.205, p. 127-140.

Scheuber, E., Bogdanic, T., Jensen, A., and Reutter, K.-J., 1994. Tectonic development of the North Chilean Andes in relation to plate convergence and magmatism since the Jurassic. In: Tectonics of the Southern Central Andes: Structure and evolution of an active continental margin, K.-J. Reutter, E. Scheuber and P.J. Wigger (editors), Springer-Verlag, Berlin, p. 121-139.

Schmid, S.M. and Haas, R. 1989. Transition from near surface thrusting to intrabasement decollement, Schlinig thrust, Eastern Alps. Tectonics, v. 8, p. 697-718.

Scholz, C.H., 1987. Wear and gouge formation in brittle faulting. Geology, v. 15, p. 493-495.

Schreurs, G., 1994. Experiments on strike-slip faulting and block rotation. Geology, v.22, p. 567-570.

Secor, D.T., 1965. Role of fluid pressure in jointing. American Journal of Science, v. 263, p.633-646.

Seraphim, R.H. and Hollister, V.F., 1976. Structural Settings. In Porphyry deposits of the Canadian Cordillera, A. Sutherland Brown (ed). Canadian Institute of Mining and Metallurgy, Special Volume 15, pp.30-43.

Sibson, R.H., Moore, J.McM. and Rankin, A.H., 1975. Seismic pumping- a hydrothermal fluid transport mechanism. Journal of the Geological Society of London, v. 131, p. 653-659.

Sibson, R.H. 1977. Fault rocks and fault mechanisms. Journal of the Geological Society of London, v. 133, p.191-213.

Sibson, R.H., 1986. Brecciation processes in fault zones: Inferences from earthquake rupturing. Pure and Applied Geophysics, v. 124, p. 159-175.

Sibson, R.H., 1987. Earthquake rupturing as a mineralizing agent in hydrothermal systems. Geology, v. 15, p. 701-704.

Sibson, R.H., 1990. Conditions for fault-valve behaviour. In Knipe, R.J. and Rutter, E.H.(eds.), Deformation Mechanisms, Rheology and Tectonics, Geological Society Special Publication No. 54, p. 15-28.

Sibson, R.H., 1996. Structural permeability of fluid-driven fault-fracture meshes. Journal of Structural Geology, v. 18, p. 1031-1042.

Sillitoe, R.H., 1972. A plate tectonic model for the origin of porphyry copper deposits. Economic Geology, v 67, p. 184-197.

Sillitoe, R.H., 1973. The tops and bottoms of porphyry copper deposits. Economic Geology, v 68, p. 799-815.

Sillitoe, R.H., 1981a. Ore deposits in cordilleran and island arc settings. In: Relations of tectonics to ore deposits in the southern Cordillera. W.R. Dickenson and W.D. Payne (eds).Arizona Geological Society Digest v. 14, pp. 49-69.

Sillitoe, R.H., 1981b. Regional aspects of the Andean porphyry copper belt in Chile and Argentina. Institute Mining and Metallurgy Transactions, v 90, p. B15-B36.

Sillitoe, R.H., 1988. Epochs of intrusion-related copper mineralization in the Andes. Journal of South American Earth Science, v 1, p.89-108.

Sillitoe, R.H. and Bonham Jr., H.F., 1984. Volcanic landforms and ore deposits. Economic Geology, 79, pp. 1286-1298.

Sillitoe, R.H. and McKee, E.H., 1996. Age of supergene oxidation and enrichment in the Chilean porphyry copper province. Economic Geology, v. 91, p. 164-179.

Simpson, C. 1985. Deformation of granitic rocks across the brittle-ductile transition. Journal of Structural Geology, v. 7, p.503-511.

Simpson, C., 1986. Fabric development in brittle-to-ductile shear zones. In Internal Structure of Fault Zones, C. Wang (editor), Birkhäuser Verlag, Basel. Pure and Applied Geophysics

Simpson, C. and Schmidt, S.M., 1983. An evaluation of criteria to deduce the sense of movement in sheared rocks. Bulletin of the Geological Society of America, v. 94, p. 1281-1288.

Skewes, M.A. and Stern, C.R., 1995. Genesis of the giant late Miocene to Pliocene Cu deposits of central Chile in the context of Andean magmatic and tectonic evolution (extended abstract). In Giant Ore Deposits 2, Proceedings of the second giant ore deposits workshop, A.H. Clark (ed). Kingston, Ontario, pp. 38-56.

Soto P., H.M., 1979. Alteracion y mineralization primaria en Chuquicamata. Unpublished Ph.D. Thesis, Universidad de Salamanca, Spain, 243p.

Sylvester, A.G., 1988. Strike-slip faults. Geological Society of America Bulletin, v. 100, p. 1666-1703.

Sylvester, H. and Palacios, C.M., 1992. Transpressional structures in the Andes between the Atacama Fault Zone and the West Fissure System at 27°S, northern Chile. Zentr. Geol. Palaontol., v. 6, p. 1645-1658.

Tanaka, H., 1992. Cataclastic lineations. Journal of Structural Geology, v 14, p. 1239-1252.

Tapia, J. 1980. XXXX. Unpublished Memoria, Universidad de Catolica del Norte.

Taylor, A.V., 1935. Ore deposits at Chuquicamata, Chile. XVI International Geological Congress, Washington, v. 2, p. 473-484.

Tchalenko, J.S., 1970. Similarities between shear zones of different magnitudes. Geological Society of America Bulletin, v. 81, p. 1625-1640.

Teyssier, C., Tikoff, B. and Markley, M., 1995. Oblique plate motion and continental tectonics. Geology, v. 23, p. 447-450.

Thomas, A., 1978. Geologia de la zona El Inca, Chuquicamata. Internal report, CODELCO-Chuquicamata, Chuquicamata, Chile.

Thompson, J.F.H., 1995. Exploration and research related to porphyry deposits. In Porphyry deposits of the northwestern cordillera of North America, T. Schroeter (ed.) Canadian Institute of Mining, Metallurgy and Petroleum, Special Volume 46, pp.857-870.

Tikoff, B. and Teyssier, C., 1992. Crustal-scale, en echelon "P-shear" tensional bridges: A possible solution to the batholithic room problem. Geology, v. 20, p. 927-930.

Tikoff, B. and Teyssier, C., 1994. Strain modelling of displacement-field partitioning in transpressional orogens. Journal of Structural Geology, v. 16, p. 1575-1588.

Titley, S.R., 1993. Characteristics of porphyry copper occurrences in the American southwest. In Mineral Deposit Modeling, R.V. Kirkham, W.D. Sinclair, R.I. Thorpe and J.M. Duke (editors), Geological Association of Canada Special Paper 40, p. 433-464.

Titley, S.R., 1994. Evolutionary habits of hydrothermal and supergene alteration in intrusion-centred ore systems, southwestern North America, in Lentz, D.R., ed., Alteration and Alteration Processes Associated with Ore-forming Systems. Geological Association of Canada, Short Course Notes, v. 11, p. 237-260.

Titley, S.R. and Beane, R.E., 1981. Porphyry copper deposits. Part 1. Geologic settings, petrology, and tectogenesis: Part 2. Hydrothermal alteration and mineralization. Economic Geology, 75th anniversary volume, pp. 214-269.

Titley, S.R., Fleming, A.W. and Neale, T.I., 1978. Tectonic evolution of the porphyry copper system at Yandera, Papua New Guinea. Economic Geology, v. 73, p. 810-828.

Titley, S.R. and Heidrick, T.L., 1978. Intrusion and fracture styles of some mineralized porphyry systems of the southwestern Pacific and their relationship to plate interactions. Economic Geology, v. 73, 891-903.

Titley, S.R., Thompson, R.C., Haynes, F.M., Manske, S.L., Robison, L.C., and White, J.L., 1986. Evolution of fractures and alteration in the Sierrita-Esperanza hydrothermal system, Pima County, Arizona. Economic Geology, vol. 81, p. 343-370.

Tomlinson, A.J. and Blanco, N., 1997a. Structural evolution and displacement history of the West Fault System, Precordillera, Chile: Part 1, synmineral history. Actas 8th Congresso Geologico Chileno, in press.

Tomlinson, A.J. and Blanco, N., 1997b. Structural evolution and displacement history of the West Fault System, Precordillera, Chile: Part 1, postmineral history. Actas 8th Congresso Geologico Chileno, in press.

Tomlinson, A.J., 1994. Relaciones entre el porfido cuprifero y la falla inversa de la mina de Potrerillos: un caso de intrusion sintectonica. Translated Title: Relations between the porphyry copper deposit and reverse fault of the Potrerillos Mine: A case of syntectonic intrusion. Actas 7th Congreso Geologico Chileno, v. 2, pp. 1629-1633.

Tomlinson, A., Mpodozis, C., Cornejo, P., Ramirez, C., and Dumintru, T., 1994, El sistema de fallas Sierra Castillo- Agua Amarga : transpresion sinestral Eocena en la Precordillera de Potrerillos, El Salvador. Translated Title: The Sierra Castillo-Agua Amarga fault system: Eocene sinistral transpression in the Potrerillos Precordillera, El Salvador, Chile. Actas 7th Congreso Geologico Chileno, v. 2, p. 1459-1463.

Tomlinson, A.J., Mpodozis, C., Cornejo, P.C., Ramirez, C.F., 1993. Structural geology of the Sierra Castillo-Agua Amarga Fault Sysem, Precordillera of northern Chile, El Salvador-Potrerillos. Second ISAG, Oxford University, London, p. 259-262.

Tullis, J., Snoke, A.W., and Todd, V.R., 1982. Penrose Conference report; Significance and petrogenesis of mylonitic rocks. Geology, v. 10, p. 227-230.

Vega, J. and Borones, L., 1981. Geologia del cuadrangulo Cerros de Paqui y parte oeste del cuadrangulo Conchi, Provincia El Loa - II region de Antofagasta, Chile. Translated Title: Geology of the Paqui Hills quadrangle and the west part of the Conchi quadrangle, El Loa Province, Antofagasta Region, Chile. Unpublished Memoria de Titulo, Universidad de Catholica del Norte, 169 pages.

Vega, M. 1982. Estudio y caracterizacion de vetas de cuarzo en un sector del yacimiento Chuquicamata. Translated Title: Study and Characterization of quartz veins in a sector of the Chuquicamata Mine.Unpublished Memoria de Titulo, Universidad del Norte, Antofagasta, Chile, 77 p.

Wallace, R.E. and Morris, H.T., 1986. Characteristics of faults and shear zones in deep mines. In: Internal Structure of Fault Zones, C. Wang (editor), Birkhäuser Verlag, Basel. Pure and Applied Geophysics, vol. 124, No. 1/2, pp. 107-125.

Walsh, J.J. and Watterson, J., 1988. Analysis of the relationship between displacements and dimensions of faults. Journal of Structural Geology, v. 10, pp. 239-247.

Waterman, G.C., 1951. Geology of the Chuquicamata drainage tunnel. Internal report, Anaconda Copper Mining Company, Chuquicamata, Chile, X pages.

Weaver, C.S. and Hill, D., 1978. Earthquake swarms and local crustal spreading along major strike-slip faults in California. Pure and Applied Geophysics, v. 117, p. 51-64.

Weaver, C.S., Grant, W.C. and Shemeta, J.E., 1987. Local crustal extension at Mount St. Helens, Washington. Journal of Geophysical Research, v. 92, B-10, p. 10170-10178.

Weihed, P. and Fallick, A.E., 1994. A stable isotope study of the Palaeoproterozoic Tallberg porphyry-type deposit, northern Sweden. Mineral Deposita, v. 29, p. 128-134.

White, D.E., 1968. Environments of generation of some base-metal ore deposits, Economic Geology, v. 63, pp. 301-335.

White, D.E., 1974. Diverse origins of hydrothermal ore fluids, Economic Geology, v. 69, pp. 954-973.

Williams, W., 1994. Structural metallogeny of northern Chile : a relationship to plate tectonics? *In* Actas 7th Congreso Geologico Chileno, v. 2, p. 931-935.

Wise, D.U., Dunn, D.E., Engelder, J.T., Geiser, P.A., Hatcher, R.D., Kish, S.A., Odom, A.L. and Schamel, S., 1984. Fault-related rocks: Suggestions for terminology. Geology, v. 12, p. 391-394.

Wollard, G.P., 1973. Geological and geophysical setting of the Nazca Plate. Abstract, Geological Society of America, p. 123.

Woodcock, N.H., 1986. The role of strike-slip fault systems at plate boundaries. Philosophical Transactions of the Royal Society of London, A317, 13-2, p. 13-29.

Woodcock, N.H. and Fischer, M., 1986. Strike-slip duplexes. Journal of Structural Geology, v.8, p. 725-735.

Woodcock, N.H. and Schubert, C., 1994. Continental strike-slip tectonics. In Continental Deformation, P. Hancock editor. Pergamon Press, New York, pp. 251-263.

Wroth, J.S., 1917. Report on the vein mines of Chuquicamata, Chuquicamata, Chile, S.A. Internal report, CGN-2, Chile Exploration Company, Chuquicamata, Chile

Yeatman, P., 1916. Mine of Chile Exploration Company, Chuquicamata, Chile. Engineering and Mining Journal, v 101-7, p. 307-314.

Zamora, J., 1979. Desplazamiento inverso de la Falla Oeste. Translated title: Reverse displacemsnts of the West Fault. Breves Geologicas #3. 3 paginas.

Zentilli, M., Graves, M., Lindsay, D., Ossandon, G. and Camus, F., 1995. Recurrent mineralization in the Chuquicamata porphyry copper system: Restrictions on genesis from mineralogical, geochronological and isotopic studies. In Proceedings of Conference on Giant Ore Deposits : Controls on the Scale of Orogenic Magmatic-Hydrothermal Mineralization, A.H. Clark, ed., Queen's University, Kingston, Canada, April 25-27, 1995, pp. 86-100.

Zentilli, M., Leiva, G., Rojas, J. and Graves, M.C., 1994a. The Chuquicamata system revisited. 7th Congresso Geologico Chileno (Extended abstract). Conception, Chile, October 17-18, 1994. Proceedings, v. 2, p.1647-1651.

Zentilli, M., Krough, T.E., Maksaev, V., and Alpers, C.E., 1994b. Uranium-lead dating of zircons from the Chuquicamata and La Escondida porphyry copper deposits, Chile : inherited zircon cores of Paleozoic age with Tertiary overgrowths. Comunicaciones, Universidad de Chile, July 1994, 12 p.

Zentilli, M., Doe, B.R., Hedge, C.E., Alvarez, O., Tidy, E., and Daroca, J.A., 1988. Isotopos de plomo en yacimientos de tipo porfido cuprifero comparados con otros depositos metaliferos en los Andes del norte de Chile y Argentina. Translated Title: Lead isotopes in porphyry copper-type deposits compared with other metalliferous deposits in the Andes of northern Chile and Argentina. Actas, 5th Chilean Geological Congress, v 1, p. B331-B369.

Zvezdov, V.S., Migachev, I.F. and Girfanov, M.M., 1993. Porphyry copper deposits of the CIS and the models of their formation. Ore Geology Reviews, v. 7, p. 511-549.

IMAGE EVALUATION
TEST TARGET (QA-3)

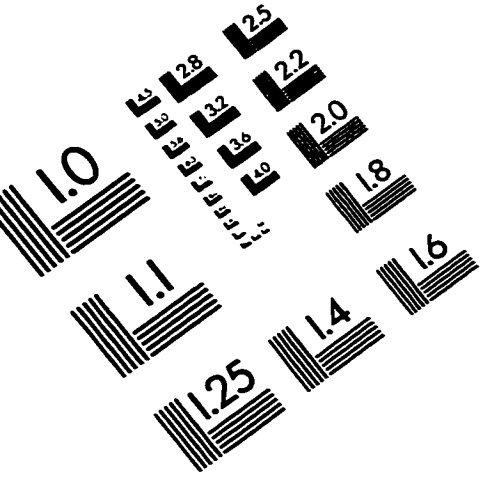

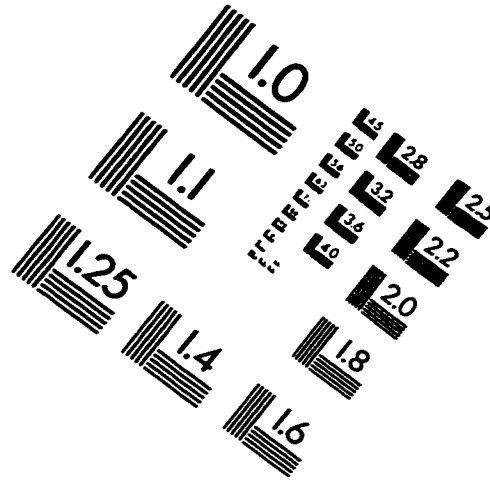

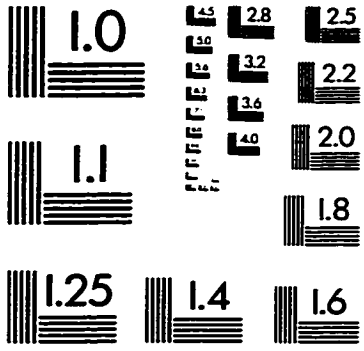

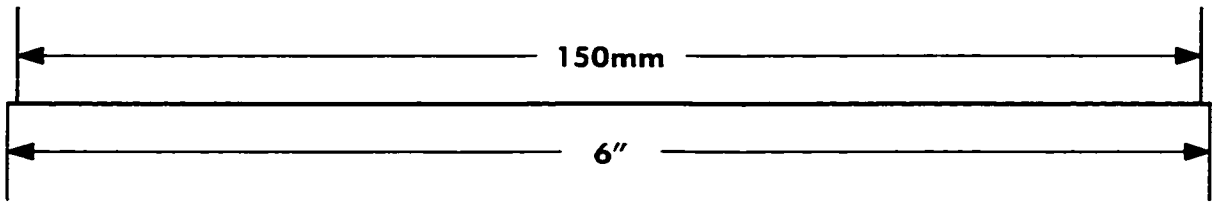

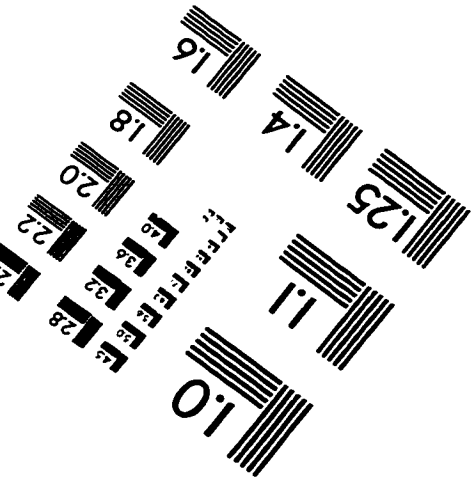

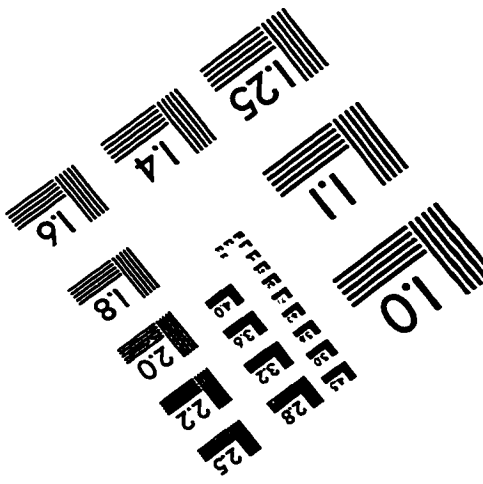

APPLIED IMAGE, Inc
1653 East Main Street
Rochester, NY 14609 USA
Phone: 716/482-0300
Fax: 716/288-5989